Title:
Phase transformations in nickel-rich nickel-titanium alloys : influence of strain-rate, temperature, thermomechanical treatment and nickel composition on the shape memory and superelastic characteristics

Author:
Adharapurapu, Raghavendra R.

Acceptance Date:
2007

Series:
UC San Diego Electronic Theses and Dissertations

Degree:
Ph. D., UC San Diego

Permalink:
http://escholarship.org/uc/item/7dt6n9p8

Local Identifier:
b6635759

Abstract:
Nearly four decades of academic research and industrial interest on Nitinol has largely focused on the superelastic applications in the bio-medical sector and in the development of 'smart' shape-memory based sensors involving the low-strain rate (0.001/s) response of NiTi. It is only within the last decade that there has been a growing interest in the exploitation of Nitinol towards high-strain rate applications such as seismic damping, blast-mitigation or energy-absorbing applications. However, a systematic study of the influence of high-strain rate and temperature on the shape memory characteristics of NiTi is severely lacking. The current research program reports the findings on: (1) The phase-transformation mechanisms in Ni-rich Ni-Ti alloys. These include (a) diffusionless multiple-stage martensitic transformations and (b) diffusion-based phase transformations that govern the precipitation reactions in Ni-rich alloys and the overall time-temperature-transformation (TTT) curves. (2) The systematic study of the high-strain rate response of Ni-rich NiTi alloys as a function of temperature (between -196□C and 400□C) and thermomechanical treatment, viz., fully annealed, work-hardened and precipitation hardened conditions. Two Ni-rich Nitinol alloys, a commercial 50.8- NiTi (at.%) and a new 55-NiTi (at.%), were selected for the study, since the Ni composition determines the precipitation processes and, critically, the transformation temperatures in NiTi alloys. It was observed that the presence of dislocations (through work- hardening) and the presence of Ni-rich precipitates (through age-hardening) contribute to a more complex two- stage or multiple-stage transformations and also improve the overall strength of the NiTi alloy. Based on the microstructural changes, such as recovery, recrystallization and precipitation formation in 50.8-NiTi alloys, the current work uniquely provides a unified and general understanding of the various multiple-stage transformations

reported in the literature, specifically providing the transition between two main transformation sequence mechanisms rationalized on the basis of partial differential scanning calorimetry (DSC) studies. Additionally, the work also identified unusual multiple- stage transformations in 55-NiTi. Aging in Ni-rich 55NiTi elicited precipitation reactions with the formation of Ti□Ni□, Ti□Ni□ and TiNi□ in sequence. A time-temperature- transformation diagram for 55NiTi was constructed, as well as the upper temperature limit of formation for several precipitates has been estimated for Ni-rich NiTi alloys system as a function of Ni concentration between 50.6-56 at.%. Superelasticity and shape memory characteristics in Ni-rich 55NiTi, thought to be unfeasible, have been successfully demonstrated with recoverable strains up to ~4-6%

UNIVERSITY OF CALIFORNIA, SAN DIEGO

Phase Transformations in Nickel-rich Nickel-Titanium Alloys: Influence of Strain-rate, Temperature, Thermomechanical Treatment and Nickel Composition on the Shape Memory and Superelastic Characteristics

A dissertation submitted in partial satisfaction of the

requirements for the degree Doctor of Philosophy

in

Materials Science and Engineering

by

Raghavendra R. Adharapurapu

Committee in charge:

Professor Kenneth S. Vecchio, Chair
Professor Prabhakar R. Bandaru
Professor Sungho Jin
Professor John B. Kosmatka
Professor Robert O. Ritchie

2007

The dissertation of Raghavendra R. Adharapurapu is approved,

and it is acceptable in quality and form for publication on microfilm:

_____

_____

_____

_____

_____

Chair

University of California, San Diego

2007

DEDICATION

Dedicated to

My Parents, who taught me how to speak

My Guru, who taught me how to be silent

TABLE OF CONTENTS

LIST OF FIGURES

LIST OF TABLES

ACKNOWLEDGEMENTS

- Foremost, I would like to express my sincere gratitude to my advisor, Prof. Kenneth S. Vecchio, for his effort to get me admitted at UCSD and giving me the opportunity to conduct research in his group. It has been a memorable learning experience from Dr. V; especially, his 'just-do-it' attitude has kept me constantly motivated. All the lost opportunities and failings are, however, solely mine.
- I would like to thank my committee members: Prof. Prabhakar Bandaru for his timely support and extensive feedback, Prof. Sungho Jin for his counsel and approving the generous scholarship without which this dissertation would not have been completed, Prof. John B. Kosmatka, and Prof. Robert Ritchie (UCB) for their time, patience and accommodation.
- I would like to sincerely acknowledge Dr. Sheldon Cytron from the US Army Picatinny Arsenal for the financial support for this project, and Jerry Julien of Nitinol Technologies for his cooperation and assistance.
- I would also like to express my gratitude to Dr. Fengchun Jiang for helping me through many pitfalls of dynamic testing and especially for his invaluable friendship. For contributions and fruitful discussions by Dr. 'Rusty' Gray (LANL) on high-strain rate testing, and Dr. John Bingert (LANL) on X-ray diffraction texture measurements, I am greatly indebted.
- Prof. Kaushik Bhattacharya (Caltech) has been of immense help, both through his book and through personal communication, in guiding me through many 'tricky' aspects of shape-memory alloys.

- I would like to extend a special thanks to Dr. Jim Mabe (Boeing) for the insightful discussions on 60Nitinol.
- Many useful discussions with the SMST-2006 conference (Monterey, CA) attendees, particularly, Dr. Tom Duerig, Dr. Gunther Eggeler, Dr. Petr Sittner, Dr. Neil Morgan and Dr. Kenneth Gall, are greatly appreciated.
- I am very grateful to Jason Flowers for his timely help with the thermal measurements on Nitinol alloys. A very special thanks to my peers, fellow Materials Science graduate students, and especially my group members, Rob Kulin, Eric McKee, Christian Deck, Justin Cheney, Hesham Khalifa and Zhang, for their friendship and, particularly, the distractions they provided.
- A special thanks is extended to 'Big' Bob, Don, Tom Chalfant and Dave Lischer for patiently tolerating many machining demands over the years.
- Sincere appreciation is also extended to Charlotte Lauve for diligently keeping track of my progress, Andre Burgos and Alan Moxley for their assistance with various computational needs, and Deborah Kegel (S&E library) for her assistance in searching and retrieving shape-memory literature/documents.

I am forever indebted to my parents and family for their support and faith in me, who have tolerated my protracted absences from home, especially during the past six years. I am particularly grateful for the friendship and counsel of many people who are now a part of my extended family in San Diego and elsewhere.

Chapter 3, in full, is a reprint of the material (under preparation) to appear as Raghavendra R. Adharapurapu, Kenneth S. Vecchio, "Evolution of Multiple-Stage Transformations (MST) in Ni-rich 50.8-NiTi: Effects of Aging and Cooling Rate on

the Shape Memory Characteristics". The dissertation author was the primary investigator and author of this paper.

Chapter 4, in full, is a reprint of the material as it appears in Acta Materialia as Raghavendra R. Adharapurapu, Fengchun Jiang, Kenneth S. Vecchio, George T. Gray III, "Response of NiTi Shape Memory Alloy at High Strain Rate: A Systematic Investigation of Temperature Effects on Tension-Compression Asymmetry", Acta Materialia, Vol. 54, pp. 4609-4620, 2006. The dissertation author was the primary investigator and author of this paper.

Chapter 5, in full, is a reprint of the material (under preparation) to appear as Raghavendra R. Adharapurapu, Fengchun Jiang, Kenneth S. Vecchio, John F. Bingert, "High-Strain Rate Response of 50.8-NiTi: Influence of Thermomechanical Treatment and Texture". The dissertation author was the primary investigator and author of this paper.

Chapter 6, in full, is a reprint of the material (under preparation) to appear as Raghavendra R. Adharapurapu, Kenneth S. Vecchio, "Microstructure Development in Ni-rich 60NiTi (wt.%) Alloy: Aging Studies on Precipitation Reactions and Shape Memory Characteristics", submitted to Metallurgical and Materials Transactions. The dissertation author was the primary investigator and author of this paper.

Chapter 7, in full, is a reprint of the material as it appears in Experimental Mechanics as Raghavendra R. Adharapurapu, Kenneth S. Vecchio, "Superelasticity in a New BioImplant Material: Ni-rich 55NiTi Alloy", Experimental Mechanics, Vol. 47, pp.365-371, 2007. The dissertation author was the primary investigator and author of this paper.

CURRICULUM VITAE

Education

2001	Bachelor of Technology (B.Tech) in Mechanical Engineering Indian Institute of Technology, Madras (IIT-M), Chennai, India
2003	Master of Science (M.S.) in Materials Science and Engineering University of California, San Diego, U.S.A
2007	Doctor of Philosophy (Ph.D.) in Materials Science and Engineering University of California, San Diego, U.S.A

Ph.D. Dissertation: Phase Transformations in Nickel-rich Nickel-Titanium Alloys: Influence of Strain-rate, Temperature, Thermomechanical Treatment and Nickel Composition on the Shape Memory and Superelastic Characteristics
Advisor: Prof. Kenneth S. Vecchio

The dissertation work focuses on the characterization of several thermoelastic martensitic phase transformations occurring in two Ni-Ti alloys: near-equiatomic 50.8-NiTi and a new Ni-rich 55-NiTi. The emphasis is on (i) Determining the nature and the sequence of multiple-stage transformations, (ii) the effects of temperature and strain-rate, (iii) the effect of texture and thermomechanical treatment on the phase transformations and the concomitant dynamic mechanical behavior. Since aging in Ni-rich NiTi alloys, such as 55NiTi, leads to the precipitation of intermetallic phases Ti_3Ni_4, Ti_2Ni_3 and $TiNi_3$ in sequence, the present investigation studies the precipitation processes to establish time-temperature-transformation (T-T-T) curves for 55NiTi and optimize its superelastic and shape-memory properties. The motivation for the present work on 55-NiTi is due to its promising bio-medical and actuator related properties such as high strength, very high hardness, low thermal conductivity, corrosion resistance and non-magnetic behavior. There is also a drive governed by a growing interest in various impact related applications for these materials and hence the present work is a preliminary step in ascertaining the applicability of Ni-Ti shape memory alloys under impact loading conditions.

M.S. Thesis: Fracture and Fatigue in Metal-Intermetallic Laminate (MIL) Composites
Advisor: Prof. Kenneth S. Vecchio

A new class of material Ti-Al_3Ti termed Metal-Intermetallic Laminate (MIL) composite was developed at Prof. Kenneth Vecchio's Research Group in the 1990's. The composite was initially developed as a light-weight armor material that exhibited optimal combination of high-strength and toughness due to its layered architecture of hard (but brittle) intermetallic (Al_3Ti) and tough metallic layers (Ti). The thesis work

involved appraising the feasibility of these lightweight MIL composites towards structural and aerospace applications by quantifying its damage critical properties, viz. fracture and fatigue, as a function of laminate layer architecture, such as layer thickness and/or volume percent. Particularly, fatigue crack propagation and modeling the 'bridging' contributions of the ductile Ti layer to the R-curve behavior were quantified. The attractive feature of these laminate composites is that with just 20% addition of ductile Ti phase (i.e. 80% brittle intermetallic), the MIL composites exhibit fracture and fatigue properties on par with many conventional alloys (viz. Ti-6Al-4V, high strength steel, superalloys like Inconel etc.) with the added advantage of optimization in weight due to their low density (~4 - 5 g/cc).

Fields of Study

Major Field: Engineering (Materials Science)

Academic Honors

- Recipient of Cal Research Assistant Fellowship at UCSD, 2001
- Recipient of Materials Science Fellowship (UCSD), 2007

Full Journal publications

1. Raghavendra R. Adharapurapu, Kenneth S. Vecchio, Fengchun Jiang, Aashish Rohatgi, "*Effect of Ductile Laminate Thickness, Volume Fraction and Orientation on Fatigue-Crack Propagation in Ti-Al_3Ti Metal-Intermetallic (MIL) Laminate Composites*", Metallurgical and Materials Transactions A, 2005, vol. 36A, pp. 1595-1608

2. Raghavendra R. Adharapurapu, Kenneth S. Vecchio, Aashish Rohatgi, Fengchun Jiang, "*Fracture of Ti-Al_3Ti Metal-Intermetallic Laminate (MIL) Composites: Effects of Lamination on R-curve Behavior*", Metallurgical and Materials Transactions A, 2005, vol. 36A, pp. 3217-3236

3. Raghavendra R. Adharapurapu, Fengchun Jiang, Kenneth S. Vecchio, "*Dynamic Fracture of Bovine Bone*", Materials Science and Engineering C, Vol. 26 (8), 1325-1332, 2006.

4. Raghavendra R. Adharapurapu, Fengchun Jiang, Kenneth S. Vecchio, George T. Gray III, "*Response of NiTi Shape Memory Alloy at High Strain Rate: A Systematic Investigation of Temperature Effects on Tension-Compression Asymmetry*", Acta Materialia, Vol. 54, pp. 4609-4620, 2006.

5. Raghavendra R. Adharapurapu, Kenneth S. Vecchio, "*Superelasticity in a New BioImplant Material: Ni-rich 55NiTi Alloy*", Experimental Mechanics, Vol. 47, pp. 365-371, 2007.

6. Raghavendra R. Adharapurapu, Kenneth S. Vecchio, "*Microstructure Development in Ni-rich 60NiTi (wt.%) Alloy: Aging Studies on Precipitation Reactions and Shape Memory Characteristics*", submitted to Metallurgical and Materials Transactions.

7. Raghavendra R. Adharapurapu, Kenneth S. Vecchio, "*Evolution of Multiple-Stage Transformations (MST) in Ni-rich 50.8-NiTi: Effects of Aging and Cooling Rate on the Shape Memory Characteristics*", to be submitted.

8. Raghavendra R. Adharapurapu, Fengchun Jiang, Kenneth S. Vecchio, John F. Bingert, "*High-Strain Rate Response of 50.8-NiTi: Influence of Thermomechanical Treatment and Texture*", to be submitted

9. Raghavendra R. Adharapurapu, Fengchun Jiang, Kenneth S. Vecchio, "*Phase Transformations in Ni-rich 55-NiTi: Influence of Aging and Strain-Rate on the Shape Memory Characteristics*", to be submitted.

10. J. Richeton, S. Ahzi, K. S. Vecchio, F. Jiang, R. R. Adharapurapu, "*Influence of temperature and strain rate on the mechanical behavior of three amorphous polymers: characterization and modeling of the compressive yield stress*", International Journal of Solids and Structures, 2006, vol.43, 2318-2335

11. Fengchun Jiang, Aashish Rohatgi, Kenneth S. Vecchio, Raghavendra. R. Adharapurapu, "*Crack length calculation for bend specimens under static and dynamic loading*", Engineering Fracture Mechanics, 71 (2004), 1971-1985.

Conference Presentations

1. Raghavendra R. Adharapurapu, Aashish Rohatgi, Kenneth S. Vecchio, Fengchun Jiang, "*Fatigue Behavior of Ti/Al_3Ti Metallic-Intermetallic Laminate (MIL) Composites*", in Processing – Structure – Property - Performance Relationships: TMS, Chicago '03, Orgs.:Luis Ruiz-Aparicio, George T. Gray III. (Invited)

2. Kenneth S. Vecchio, Fengchun Jiang and Raghavendra R. Adharapurapu, "*A Novel Three-Point Bend Test for Dynamic Fracture Toughness Measurement*", TMS' September 2004.

3. Raghavendra R. Adharapurapu, Fengchun Jiang, Kenneth S. Vecchio, "*Dynamic Fracture of Bovine Cortical Bone: A Systematic Study of Strain Rate Effects*", presented at TMS '05, Feb.13-17, San Francisco.

4. Kenneth S. Vecchio, Uday Deshmukh, R. R. Adharapurapu, F. Jiang, "*Dynamic Response of β-Ti alloys*", presented at TMS '05, Feb.13-17, San Francisco.

5. Raghavendra R. Adharapurapu, Jiang Fengchun, Kenneth S. Vecchio, "*Dynamic Response of NiTi Shape Memory Alloys: Influence of Temperature and Strain-rate on Tension-Compression Asymmetr*y", TMS'06 Annual Meeting, Wechsler Symposium on Radiation Effects, Deformation and Phase Transformations in Metals and Ceramics, San Antonio, Texas.

6. Raghavendra R. Adharapurapu, Kenneth S. Vecchio "*On the High strain-rate Response of Ni-rich NiTi Shape Memory Alloy as a function of Aging Temperature*", TMS'06 Annual Meeting, Wechsler Symposium on Radiation Effects, Deformation and Phase Transformations in Metals and Ceramics, San Antonio, Texas.

7. Raghavendra R. Adharapurapu, Jiang Fengchun, Kenneth S. Vecchio, "*Effect of Product Form on the Dynamic Response of 50NiTi: Sheet vs. Rod Textures*", TMS'07 Annual Meeting, Symposium on Dynamic Behavior of Materials, Orlando, Florida.

8. Raghavendra R. Adharapurapu, Jiang Fengchun, Kenneth S. Vecchio, "*Dissimilar Dynamic Response of Two Nitinol Alloys: 50NiTi vs. 55NiTi (at.%)*", TMS'07 Annual Meeting, Symposium on Dynamic Behavior of Materials, Orlando, Florida.

9. Raghavendra R. Adharapurapu, Kenneth Vecchio, "*Superelasticity and Shape Memory in a New Ni-Rich 55NiTi Bio-Implant Material: An Appraisal*", TMS'07 Annual Meeting, Symposium on Biological Materials Science, Orlando, Florida.

10. Jiang Fengchun, Kenneth S. Vecchio, Raghavendra R. Adharapurapu, Justin Cheney, "*Comparison of Quasi-Static and Dynamic Fracture of Nitinol*", TMS'07 Annual Meeting, Symposium on Dynamic Behavior of Materials, Orlando, Florida.

11. Kenneth S. Vecchio, Jiang Fengchun, Justin Cheney, Raghavendra R. Adharapurapu, "*Evaluation of a Hopkinson Bar Loaded Four-point Bend Fracture Test*", TMS'07 Annual Meeting, Symposium on Dynamic Behavior of Materials, Orlando, Florida.

ABSTRACT OF THE DISSERTATION

Phase Transformations in Nickel-rich Nickel-Titanium Alloys:

Influence of Strain-rate, Temperature, Thermomechanical Treatment and

Nickel Composition on the Shape Memory and Superelastic Characteristics

by

Raghavendra R. Adharapurapu

Doctor of Philosophy in Materials Science and Engineering

University of California, San Diego, 2007

Professor Kenneth S. Vecchio, Chair

Nearly four decades of academic research and industrial interest on Nitinol has largely focused on the superelastic applications in the bio-medical sector and in the development of 'smart' shape-memory based sensors involving the low-strain rate (~0.001/s) response of NiTi. It is only within the last decade that there has been a growing interest in the exploitation of Nitinol towards high-strain rate applications such as seismic damping, blast-mitigation or energy-absorbing applications. However, a systematic study of the influence of high-strain rate and temperature on the shape memory characteristics of NiTi is severely lacking. The current research program reports the findings on: (1) The phase-transformation mechanisms in Ni-rich Ni-Ti alloys. These include (a) diffusionless multiple-stage martensitic transformations and (b) diffusion-based phase transformations that govern the

precipitation reactions in Ni-rich alloys and the overall time-temperature-transformation (TTT) curves. (2) The systematic study of the high-strain rate response of Ni-rich NiTi alloys as a function of temperature (between -196^{o}C and 400^{o}C) and thermomechanical treatment, viz., fully annealed, work-hardened and precipitation hardened conditions. Two Ni-rich Nitinol alloys, a commercial 50.8-NiTi (at.%) and a new 55-NiTi (at.%), were selected for the study, since the Ni composition determines the precipitation processes and, critically, the transformation temperatures in NiTi alloys. It was observed that the presence of dislocations (through work-hardening) and the presence of Ni-rich precipitates (through age-hardening) contribute to a more complex two-stage or multiple-stage transformations and also improve the overall strength of the NiTi alloy. Based on the microstructural changes, such as recovery, recrystallization and precipitation formation in 50.8-NiTi alloys, the current work uniquely provides a unified and general understanding of the various multiple-stage transformations reported in the literature, specifically providing the transition between two main transformation sequence mechanisms rationalized on the basis of partial differential scanning calorimetry (DSC) studies. Additionally, the work also identified unusual multiple-stage transformations in 55-NiTi. Aging in Ni-rich 55NiTi elicited precipitation reactions with the formation of Ti_3Ni_4, Ti_2Ni_3 and $TiNi_3$ in sequence. A time-temperature-transformation diagram for 55NiTi was constructed, as well as the upper temperature limit of formation for several precipitates has been estimated for Ni-rich NiTi alloys system as a function of Ni concentration between 50.6–56 at.%. Superelasticity and shape memory characteristics in Ni-rich 55NiTi, thought to be unfeasible, have been successfully demonstrated with recoverable strains up to ~4-6%.

1 INTRODUCTION

1.1 General introduction

The development of novel materials is critical for the advancement of materials science/engineering and is often the vanguard for many progressive innovative applications. Shape memory alloys (SMA) epitomize such "new-age" materials, where the functional characteristics, such as shape memory and superelasticity, are exploited through the interplay of structure and properties. Shape memory alloys represent only one subset of a vaster class of materials called '*smart/active materials*', where, their functional capabilities arise due to distinctive multi-physics coupling (see Figure 1.1) of various physical parameters, such as mechanical, thermal, optical, electro-magnetic, and are usually accompanied by a change in crystal structure [1, 2].

For example, a coupling between stress and electric field leads to the manifestation of *piezoelectric* effect in Pb(Zr, Ti)O_3, commonly known as PZT. Similarly, *electrostrictive* Pb(Mg, Nb)O_3 materials exhibit coupling between electric and stress fields, *magnetostrictive* (Tb, Dy)Fe_2 materials exhibit coupling between magnetic and stress fields and, finally *shape memory* NiTi alloys are sensitive to both stress and temperature fields [1]. Active materials usually have one or more novel properties that can be dramatically altered and this particular aspect typically dictates or forms the basis of a 'smart' structure, thus leading to an innovative application.

Shape memory effect and superelasticity are unique properties of certain alloys systems that arise from a (reversible) thermo-elastic behavior of the alloy that has its basis in temperature-induced diffusionless, solid-solid, first-order transformation

(high-temperature austenite $\rightarrow$ low-temperature martensite) involving a change in crystalline symmetry [3]; detailed discussion will follow in Chapter 2. Figure 1.2 schematically illustrates the superelastic (SE) and the shape memory effect (SM) observed in NiTi shape memory alloys.

Above the austenite finish temperature (A_f), the parent material is called austenite and has a cubic structure. Upon cooling below the martensite start temperature (M_s), the crystal structure changes to a low-symmetry, monoclinic martensite structure; this martensitic transformation is reversible upon heating. Below the martensite finish temperature (M_f), the alloy is completely martensitic and is termed as thermally-induced martensite (TIM). When the thermally-induced martensite is deformed by an external stress, the shape of the alloy changes to accommodate the loading strains. However, upon heating above the austenite finish temperature, A_f, the alloy 'remembers' its original austenite phase structure and the reverse transformation occurs; thus the material exhibit shape memory effect. By contrast, when the austenite phase is deformed by external stress within the temperature range $A_f < T < M_d$, the austenite undergoes a stress-induced martensite (SIM) transformation. Upon removal of the load, however, the martensite structure reverts back to the austenite phase, since austenite is the more stable phase within this temperature 'window'. This is termed as the superelasticity if the specimen recovers all of the loading strains; partial unloading is termed pseudoelasticity. These phenomenons are discussed in Chapter 2 in more detail. The superelastic, shape memory and pseudoelastic stress-strain responses are shown in Figure 1.3.

1.2 Motivation and Purpose of the study

The current work focuses on three main problems, namely:

(1) To study the high-strain rate response of Ni-rich NiTi alloys as a function of temperature, texture and thermomechanical treatment (fully annealed or cold-worked or precipitation hardened).

(2) To understand the phase-transformations in Ni-rich Ni-Ti alloys.

The phase transformations include (a) diffusionless martensitic transformations that are observed as multiple-peaks during heating and cooling cycles of the NiTi alloys in a differential scanning calorimeter (DSC), and (b) diffusion-based phase transformations that govern the precipitation reactions in Ni-rich alloys and hence the overall time-temperature-transformation (TTT) curves.

(3) To demonstrate and optimize superelasticity and shape-memory in a new Ni-rich 55-NiTi (at.%) and study the influence of aging and strain-rate on the overall mechanical behavior.

The motivation for the study of the above three problems is proposed, followed by the outline of specific research objectives.

(1) Since the discovery of shape-memory effect (SME) in Au-Cd alloys more than 50 years ago [4], numerous alloy systems have been reported to exhibit shape memory effect behavior [5, 6]. However, after more than a decade of relative dormancy, research on shape memory alloys underwent a revival with the discovery of shape memory effect in NiTi alloys; these alloys promised significant engineering applications due to their superior “smart” properties. The alloys that exhibit shape memory function can generally be classified into noble metal-based, Fe-based and

NiTi-based alloys systems, and nonmetallic shape memory alloys [7]. Despite the efforts by the research community to develop shape memory alloys for commercial applications, only a few alloys like NiTi, NiTi-Cu/Nb, Cu-Al-Ni and Fe-Mn-Si have found a niche in commercial markets. Among these, NiTi is considered to be a favorable shape memory material for practical applications due to its superior memory and structural properties. The commercial success of 'superelastic' Nitinol was essentially triggered by the medical industries' drive towards minimally invasive procedures that demanded non-conventional materials [8]. Indeed, the success of superelastic Nitinol alloys was due to the ability to optimize the superelastic 'window' around the constant body temperature of 37^{o}C [8, 9].

NiTi shape memory alloys display an intricate non-linear deformation behavior that is dependent on temperature, stress state (compression or tension), strain-rate (quasi-static versus high-strain rate), texture and prior thermo-mechanical deformation history [3, 5, 6, 9-17]. Although, the fundamental (atomic) mechanisms that lead to shape memory and superelasticity in NiTi have been solved in the early 1970's [6, 18, 19], and the superiority of NiTi alloys in terms of their strength, ductility, corrosion resistance and biocompatibility, was established, the industry's effort in engineering NiTi alloys sauntered behind. This stagnation was due to the difficulty in working with some unusual properties of NiTi, such as, sigmoid stress-strain (non-linear) response, hysteresis, fatigue, high-sensitivity of transformation temperatures to Ni-composition, adiabatic heating and cooling, etc., which led to unavoidable delays in the burgeoning of engineering applications [20]. Furthermore, the unreliability in alloy melting procedures and material processing led to high production costs and

hence relatively few bulk Nitinol products were made available, until recently [8, 12]. To date, the largest employment of superelastic NiTi has been in various applications in the bio-medical industry [7, 8, 20-30] or as shape-memory actuators and sensors in the micro-electronic mechanical systems (MEMS) [2, 12, 31-38]. Therefore, the high processing costs of bulk products, the engineering difficulties in exploiting reliably the unique properties of NiTi and a large demand for novel medical devices (for e.g., the notable self-expanding stent [8, 28, 29]) have largely focused the research efforts on non-structural applications where dynamic properties of the alloy do not play any significant role. It is only in the past decade that these alloys have been critically assayed as structural elements in earthquake engineering [35-37, 39, 40] or energy absorbing applications [37, 41], where high-strain rate or dynamic loading conditions assume a critical function.

While the influence of temperature and thermomechanical-treatment (such as cold-work and annealing) on the overall superelastic and shape-memory stress-strain behavior at low strain-rates has been studied exhaustively in the past four decades [3, 9-14, 16, 17, 42], the literature on the dynamic stress-strain responses of NiTi is limited, with most of the high-strain rate studies conducted only recently, refer to the introduction in [43]. Unfortunately, the lack of material properties at high-strain rates curtails the widespread use of NiTi in a number of aerospace and defense applications. A systematic study of the interplay or interaction between temperature and high-strain rate is, therefore, warranted.

(2) The current industry standard Nitinol alloy is the near-equiatomic 50.8 at.% NiTi alloy (henceforth designated as 50.8-NiTi) that has become the workhorse of

most superelastic medical applications [9, 44, 45]. It is known that Ni-rich NiTi alloys with Ni composition greater than 50.6 at.% undergo precipitation reactions, where metastable phases such as Ti_3Ni_4, Ti_2Ni_3 and $TiNi_3$ precipitate in seriatim during aging between 300^{o}C and 800^{o}C [17, 46, 47]. The nature of the phases that precipitate is a strong function of Ni composition and aging parameters (temperature and time) [47, 48]. However, the most important impact of the Ni composition on the usage of a particular Ni-Ti alloy is its influence on the transformation temperatures; it is known that an increase in Ni composition by 1% from 50.5 to 51.5 at.% decreases the M_s (martensite start temperature) to below 100 K (in solution treated condition) [49, 50].

Since the transformation temperatures (especially A_f, the austenite finish temperature) are an important indicator for the type of application of a certain Ni-Ti alloy, several studies on the influence of thermomechanical treatments, specifically, either cold work or aging, or a combination of both, are extant in the literature [51] . While the traditional simplified view of phase transformations occurring in Ni-Ti alloys involves only one-stage cubic austenite (B2) to monoclinic (B19') martensite transformation (transformation strains ~ 6-10%), the influence of cold work, i.e., high density of dislocations [53-55] and the presence of Ni-rich precipitates in Ni-rich (Ni > 50.6at.%) Ni-Ti alloys contribute to a more complex two-stage, three-stage or even four-stage transformations, collectively termed 'multiple stage transformation' (MST) [17, 50, 51, 55-67]. It is now known that the introduction of a dislocation network/substructures or precipitates into the Ni-Ti matrix can act as obstacles to the direct B2→B19' transformation [55, 59, 61, 65]. As a result of this barrier, a competing martensitic transformation, B2→R-phase that involves lower

transformation strains (~1-2%), becomes feasible and dominant. Further transformation occurs as R-phase converts to B19', thus leading to a two-step process that is seen as a double peak (two-stage) on the differential scanning calorimetry (DSC) trace. The heating cycle however, involved only one large peak indicating that the B19'→B2 transformation occurred in one step. Yet, it was observed that aged Ni-rich NiTi alloys exhibited three DSC peaks during cooling from austenitic phase, instead of a two-stage transformation [53, 54, 68-72]. Since the Ni-Ti alloy did not exhibit any competing martensitic transformation, other than to R-phase and B19' phase, there was uncertainty with regards to the correct interpretation of the multiple-stage transformation (MST).

Thus, that the occurrence of multiple-stage transformations has been rationalized through several theories. Carroll *et al.* [59] have recently reviewed that the multiple-stage transformations are governed by (i) local or small-scale inhomogeneity (coherency stress fields, compositional fluctuation, precipitation with a critical interparticle spacing) associated with the precipitation of metastable phases such as Ti_3Ni_4, (ii) large-scale inhomogeneity characterized by preferential grain-boundary precipitation and precipitate free matrix, presence of single crystal defects such as dendrites and low-angle boundaries, and (iii) the thermomechanical process that cause heterogeneity of both dislocations and precipitate distribution.

Thus, the above discussion points out that there exists no uniform description of the causes of MST observed in several Ni-Ti alloys. Furthermore, as Fan *et al.* point out [60], the sequence of the transformations may vary with composition, aging temperature and time and prior thermomechanical treatment. Carroll *et al.* [59]

summarize that it is a challenging task to differentiate between the relative importance or degree of influence of each of the above mechanisms on the multiple phase transformations. In all likelihood, the multiple mechanisms could be concomitantly affecting the MST; but whether the multiple transformations occurring concurrently are synergistic or independent, or if they are interfering with each other is still unclear. Thus, the importance of understanding the underlying mechanisms that are responsible for the observed multiple-stage transformation is paramount.

(3) The early investigations at the Naval Ordnance Laboratory (NOL) by Buehler and his colleagues [73-76] focused on a series of non-magnetic Ni-Ti alloys based on the ductile intermetallic compound NiTi that displayed two distinct sets of properties as a function of Ni composition and heat treatment. [76]. This division was initially based upon hardness measurements over a range of Ni composition, viz., 50 to 64 weight % (~ 47 to 57 atomic %). It was seen that equiatomic and near-equiatomic (or near 55 weight % Ni) alloys exhibit minimum hardness and are relatively unaffected by cooling rates when cooled from 950°C. By contrast, the alloys composed of Ni in excess of 50-atomic percent exhibit increasing hardness under quenched conditions. A further mark of distinction was revealed in the microstructural differences during metallographic studies. While 50-Nitinol (atomic percent) was found to be single-phase alloy of NiTi (oxide and nitride impurities were present in minute quantities), Ni-rich NiTi alloys were found to contain $TiNi_3$ phase (in the form of precipitates) in equilibrium with the NiTi matrix phase. It has been shown that a series of thermomechanical treatments, i.e., various combinations of solution-treatments combined with cold work and/or anneal heat-treatments etc., are

required to optimize the superelastic and shape-memory properties of equiatomic alloys [9, 17, 52, 76-79]. However, departure from the 50-Nitinol (atomic %), i.e. near stoichiometric NiTi, towards the Ni-rich alloys leads to the second group of Nitinol alloys that are also non-magnetic, but are at variance with the former alloys in that the latter group can be thermally hardened by aging heat treatments to high hardness levels, viz., ~60 - 70 R_C [76, 80-82]. The latter group, i.e., NiTi alloys spanning the composition range from 56 to 62 weight % Ni (51 to 56 atomic %) were generically designated as 60-Nitinol alloys (designated by weight %) [76]. While both the 50-NiTi (atomic %) and 55-Nitinol (atomic %) possessed common unusual properties such as non-magnetic character, marine corrosion resistance, due to the difference in hardness, microstructural features and the general effect of heat treatment on their properties, 50-NiTi (atomic %) and 55-Nitinol (atomic %) were considered as separate and distinct alloy types [76].

Furthermore, an additional divergence was seen among the 55-NiTi (atomic %) alloys, namely, between the 'quenched' and 'furnace cooled' alloys. While it was pointed out by Buehler and Wang [76] that not only the high hardness 'quenched' or low hardness 'furnace cooled' 55-NiTi (atomic %) alloys could be produced, but also indicated the possibility of attaining alloys with any desired intermediate hardness accomplished by either intermediate cooling rates or by utilizing some sort of 'overaging' or pseudo-tempering' post-quench heat treatment. Later investigations by Nitinol Technology Inc., Mountain View, WA, have attributed the superelasticity and shape-memory behavior in 55-NiTi (atomic %) alloys as directly resulting from this crucial difference in cooling rate, viz., quenching vs. furnace cooling, respectively [80,

83, 84]) . In spite of many promising properties of 55-NiTi (atomic %) alloys, such as high hardenability, ability to tailor hardness through aging heat-treatments only, high corrosion resistance, low susceptibility to stress corrosion failure, '*they exhibited the most noteworthy engineering weakness, viz., notch sensitivity*' [76].

Due to the difficulties in forming and hot-working, machining and forming these materials into near-net shapes for practical applications became difficult and impractical [83]. Therefore, 50-NiTi or 50.8-NiTi (atomic %) was eventually preferred over 55-NiTi (atomic %), as evidenced by the numerous products in bio-medical and sensor applications. However, since the development of hot rolling methods for 55-NiTi (atomic %) and special fabrication techniques (by Nitinol Technologies Inc., Mountain View, WA) [80, 83], a number of patents have emerged that exploit some of the afore-mentioned unique properties of the alloys [80, 84-101]. A decade ago, it was shown that under special heat treatment conditions, both the shape-memory and superelasticity effects could be produced in the alloy from the same ingot without any additional mechanical processing [80, 83, 84]. Since then, the interest in the development of Ni-rich 55-NiTi (atomic %) alloys has seen a resurgence, although very little work exists on the mechanical properties of these alloys [81-83, 102-104]. The motivation for the present work on 55NiTi is due to its promising bio-medical and actuator related properties such as high strength, very high hardness, low thermal conductivity, corrosion resistance and non-magnetic behavior. There is also a commercialization drive governed by a growing interest in various impact related applications for these materials, and hence the present work is a

preliminary step in ascertaining the applicability of Ni-Ti shape memory alloys under impact loading conditions.

1.3 Objectives

Based on the discussion in Section 1.2, the objectives of the current work are:

(1) *Characterization of multiple-stage transformations (MST) in 50.8-NiTi*

The study is focused on the *evolution* of the multiple-stage transformations in 50.8-NiTi alloy (cold-worked sheet) under aging at low (300-400^{o}C) and intermediate temperatures (500-700^{o}C) by varying the aging times (0.5, 1, 5hrs). The evolution of the martensitic transformation was investigated through a series of partial transformation cycles using differential scanning calorimetry (DSC) methods. Additionally, the influence of cooling rate, viz., air-cooled, furnace-cooled and water-quenched, on the multiple-stage transformation and on the transformation temperatures are investigated. Finally, the effects of aging temperature, time and the rate of cooling on the *superelastic* properties, such as plateau stress, and on the *mechanical* properties, such as tensile strength and ductility, are examined; the time-temperature-transformation (TTT) curves for 50.8-NiTi was determined and compared with earlier studies.

(2) *Response of 50.8-NiTi at high-strain rates: Influence of temperature on the compression-tension asymmetry*

Although, 50.8-NiTi exhibits precipitation hardening upon aging, this preliminary investigation focuses on the high-strain rate deformation (~1200/s) of a fully annealed (solution-treated at 800^{o}C for 1-hr) 50.8-NiTi rod under both

compression and tension between -196^{o}C (liquid nitrogen temperature) and 400^{o}C. The high-strain rate stress-strain behavior and the attendant compression-tension asymmetry are also compared with the quasi-static strain-rate (~0.001/s) studies. In both cases, i.e., high- and low-strain rates, the variation of the critical stress (0.2% strain offset) with temperature and the influence of strain-rate on the presence/absence of the stress-induced martensite (SIM) transformation plateau is analyzed.

(3) *High-strain rate response of 50.8-NiTi: Influence of texture and thermomechanical treatment (cold-work + annealing versus solution-treated)*

In order to study the influence of texture and the thermomechanical treatment on the high-strain rate behavior, two sets of experiments were conducted. The first set consisted of high-strain rate testing of fully-annealed 50.8-NiTi alloy in sheet and rod geometries that differed in their recrystallized texture, but possessed nearly similar grain size and transformation temperatures. The results from the high-strain rate experiments based on *objective (2)* were utilized here. The second set of experiments involved the comparison of high-strain rate response of fully-annealed 50.8-NiTi sheet and cold-worked (~30%) + annealed (at 510^{o}C for 10 minutes) sheet. The difference in superelasticity and the overall stress-strain response is analyzed at both quasi-static and high-strain rates. Furthermore, the relative degree of influence between texture and thermomechanical treatment on the overall mechanical behavior is analyzed.

(4) *Aging studies on the precipitation reactions in Ni-rich 55-NiTi*

The current work investigates the influence of aging on the microstructural evolution of a new Ni-rich 55-NiTi (atomic %). It is demonstrated that this alloy is capable of exhibiting shape memory (SM) and superelasticity (SE). During aging

heat-treatments at higher temperatures or, longer aging times, Ti_3Ni_4, Ti_2Ni_3 and $TiNi_3$ precipitates formed in sequence, with $TiNi_3$ being the only stable phase. Since precipitates in Ni-rich NiTi alloys greatly affect the shape memory properties, initial investigation was focused on precipitation studies using conventional metallographic techniques and a TTT (Time-Temperature-Transformation) diagram was obtained for the composition Ti-55 at.% Ni (or 60 wt.% Ni). Additionally, the transformation temperatures and the hardness were measured as a function of both aging temperature and time.

(5) *Superelasticity in 55-NiTi*

Subsequent to the study of the diffusional phase transformations and the concomitant precipitation reactions in Ni-rich 55-NiTi, the influence of aging on the overall quasi-static stress-strain response was investigated. Essentially, the aging temperature and time 'window' for tailoring the strength, ductility, recoverable strains and the overall mechanical response was evaluated for the Ni-rich 55-NiTi.

1.4 Significance of the study

Nearly four decades of academic research and industrial interest on Nitinol has focused primarily on the superelasticity (medical devices being the primary driving force) and shape memory (high energy density actuators in various active feedback sensors) behavior at low deformation rates, ~0.001/s. It is only in the last decade that Nitinol alloys have been approached with the intent of understanding and exploiting dynamic properties in various seismic, blast-mitigation or energy-absorbing

applications. Therefore, the current study on the high-strain rate response of NiTi alloys is significant in the following ways:

(1) Primarily, it reports at an accurate, reliable and systematic study of the high-strain rate behavior of NiTi alloys under both tension and compression. The reliability of the high-strain rate behavior is established by the proposal of pulse-shaping experiments that allow constant strain-rate throughout the high-strain rate compression tests in NiTi alloys that exhibit complex sigmoid-type stress-strain behavior. This sets a common ground for the comparison of high-strain rate data in NiTi alloys, since constant high-strain rates are maintained throughout the test, i.e., up to 25% total strains.

(2) Since the high-strain rate tests are conducted over a wide range of temperature spanning -196^{o}C and 400^{o}C, the dynamic response of thermally-induced martensite (TIM) at low temperatures ($T < M_f$), superelastic austenite ($A_f < T < M_d$) and stable austenite at high temperatures ($T > M_d$) are studied in a systematic manner.

(3) Typically, rolled sheet/plate, drawn rod and extruded tube represent the most common products of NiTi alloys. While, the influence of rolling texture and cold-work on the overall shape memory characteristics, under quasi-static strain rates, have been investigated exhaustively in the past, most of the high-strain rate investigations in the literature have been conducted on solution-treated near-equiatomic NiTi alloys. Therefore, the current study is significant, in that, it compares the dynamic response of fully-annealed and cold-worked NiTi alloys with different textures and systematically analyzes the relative degree of influence between texture and thermomechanical treatment on the overall high-strain rate response.

(4) Multiple-stage transformations (MST) in NiTi alloys have received considerable scrutiny in recent years primarily to understand the physics of multiple-peak formation during the differential scanning calorimetry (DSC) heating and cooling studies. In addition, there has also been an attempt to characterize the transformations in terms of the transformation sequence(s) and the role of the microstructure in inducing the MST. The current work systematically analyses the formation of MST in cold-worked and aged Ni-rich NiTi in a wide range of temperatures, viz., 300^{o}C to 700^{o}C and specifically studies the evolution of the multiple-peaks through different aging times.

Based on the microstructural changes, such as recovery, recrystallization and precipitation formation in Ni-rich NiTi alloys, the current work uniquely provides a unified and general understanding of the various MST reported in the literature, specifically providing the transition between two main transformation sequence mechanisms rationalized on the basis of partial DSC studies. In addition, the current work also includes a systematic evaluation of the effects of cooling rate (water-quenched vs. air-cooled vs. furnace cooled) over the wide range of temperature on both the MST sequence and the superelastic characteristics.

(5) The current study also presents a detailed primary study of the martensitic (diffusionless) and the diffusion-based (precipitation reactions) phase-transformations in a new Ni-rich 55-NiTi (atomic %). The time-temperature-transformation (TTT) and the multiple-stage transformations (MST) are studied for the first time in these Ni-rich alloys.

1.5 Relevance to practical applications

The unique properties of superelasticity and shape memory of NiTi alloys have made them very attractive to innumerable applications in almost all areas of engineering and medical sciences. They include: couplings and fasteners, actuators, electrical connectors, circuit breakers, adaptive materials and reinforced composites, smart-materials, high-capacity dampeners, heat engines, wear resistant materials, even arts, fashion, decoration, toys and gadgets, eyeglass frames, cellular phone antennas, MEMS devices, valves, robotics; orthodontic dental arch wires, blood clot filters (vena cava filter), intracranial aneurism clips, artificial hearts, orthopedic devices, bio-implants, self-expanding stents in gastroenterology, radiology, urology, cardiovascular devices [2, 7, 10-13, 16, 21-27, 29-38]. The roster of innovative applications of near-equiatomic NiTi shape memory alloys is ever expanding and will not be discussed further here. However, the promising applications of 55-NiTi will be briefly mentioned. In the recent years, a number of patents have emerged that exploit some of the unique properties of the 55-NiTi alloys, like high-hardness, non-magnetic character, immunity to most corrosive agents [80, 84]. These include high-precision actuator, vibration dampener, seals, high-security locks, gun barrels, rotary actuators, high-hardness cutting instruments, horse-shoes, heater elements, impact absorbers, projectiles, liquid-jet nozzles, ball bearing elements, ski-structures [80, 84-101]. One of the most promising applications is the cutting edge smart material actuator developed by Boeing [103, 104]; it is described below.

In a typical high-bypass ratio engines, the turbulent mixing of the hot exhaust stream, fan stream and the surrounding air stream leads to high noise levels during

take off. One possible noise reduction method involves the usage of serrated chevrons along the trailing edge of the jet engines exhaust nozzles. These serrated chevrons were shown to be aerodynamic and very efficient in reducing the jet noise through optimal mixing of the exhaust streams and ambient air. However, the geometric arrangement of the exhaust nozzles with respect to the air flow resulted in drag and, hence, thrust reduction. In order to achieve a fair trade-off, Boeing devised a unique morphing technology involving Variable Geometry Chevrons (VGC) that utilizes light-weight, thermally activated shape memory alloy actuators made of 55-NiTi. Its basic principle involves the movement of the VGCs in and out of the flow during take-off and cruise, respectively, actuated by the 55-NiTi shape-memory actuator. Thus, noise reduction during take-off and optimal thrust during cruising is achieved successfully. The Boeing program have confirmed stable two-way shape memory and cyclic stability of 55-NiTi [83, 104] that provides remarkable morphing control over the VGCs and hence attest to the promising potential of 55-NiTi. Therefore, there is considerable motivation to study and understand the shape-memory properties of 55-NiTi in order to exploit them for further novel applications.

1.6 Arrangement of the thesis

Chapter 2 presents a summary of various aspects of NiTi alloys gleaned from the literature and establishes a background for understanding, relating and finally comparing the present work. Beginning with the basic phenomena of superelasticity and shape-memory effect and their origin, martensitic transformations and its crystallography and twinning are summarized. Subsequently, the physical metallurgy

of NiTi alloys and the deformation behavior of NiTi alloys with emphasis on the temperature, and thermo-mechanical treatment effects are dealt with. While NiTi alloys have been under study for the past half-century, indicating thus to a cornucopia of literature, only the relevant terms, concepts and phenomena that are necessary or useful in the current study and those that form a basis of our current understanding are included.

Chapter 3 presents the evolution of the multiple-stage transformations (MST) in Ni-rich 50.8-NiTi alloy as a function of aging temperature and time. The influence of cooling-rate on the phase transformations and the overall mechanical behavior is also discussed.

Chapter 4 provides a systematic study of the effect of strain-rate (0.001/s and 1200/s) on the fully-annealed 50.8-NiTi drawn rod stock as a function of temperature. The main study involves the variation of the critical stress and the evolution of the compression-tension asymmetry with varying temperature.

Chapter 5 examines the effect of texture (rolled sheet versus drawn rod geometries) on the stress-strain response of 50.8-NiTi (in fully-annealed condition) as a function of temperature and strain-rate. The chapter also presents a similar comparison between fully-annealed and cold-worked+annealed 50.8-NiTi sheet, thus studying the effects of thermomechanical treatment on the quasi-static and dynamic response of 50.8-NiTi.

Chapter 6 presents the time – temperature - transformation (TTT) data as a function of aging temperature and time in the Ni-rich 55-NiTi (atomic %) along with the microstructures that are formed during the precipitation of several phases. It is

shown that this new Ni-rich alloys is capable of both shape-memory and superelasticity. In Chapter 7, the range of mechanical behavior possible in 55-NiTi through aging heat-treatments at quasi-static strain rates is discussed. Chapter 8 summarizes the important conclusions gleaned from the present study.

1.7 Figures

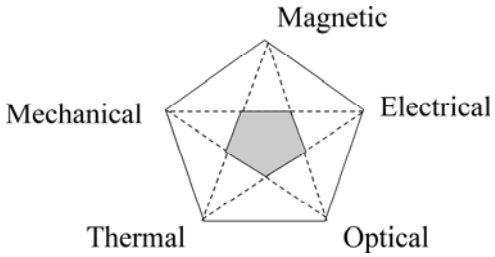

Figure 1.1 Schematic to illustrate multi-physics coupling between various physical parameters in active materials, thus leading to functionality or smartness in their properties.

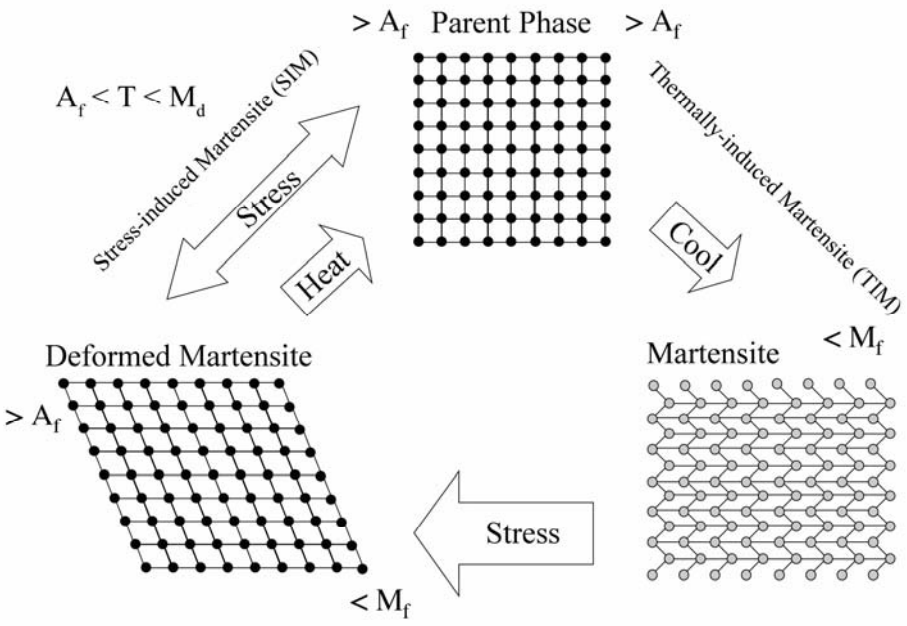

Figure 1.2 Schematic illustration of shape memory effect. A_f and M_f are austenite and martensite finish temperatures.

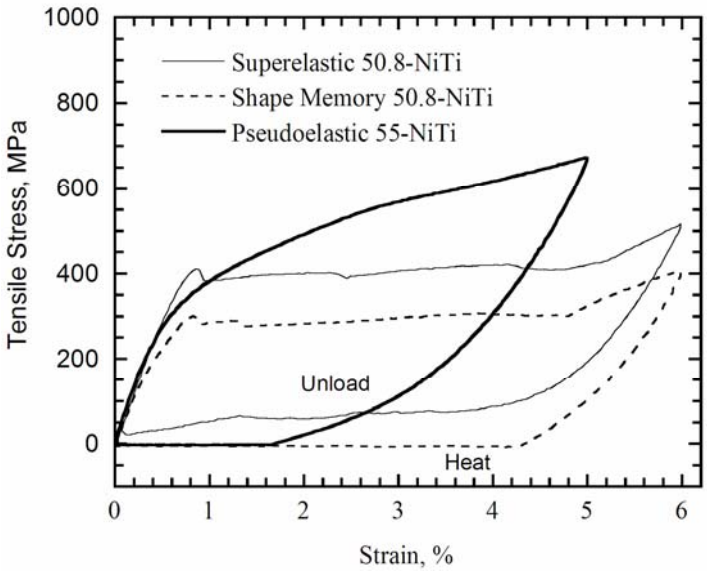

Figure 1.3 Superelastic (SE), Shape memory (SM) and pseudoelastic (PSE) stress-strain response in NiTi alloys.

1.8 References

1. Newham, R.E., *Phase Transformation in Smart Materials.* Acta Cryst. A, 1998. **54**: p. 729-737.

2. Wang, Z.-l. and Z.C. Kang, *Functional and Smart Materials: Structural Evolution and Structural Analysis*. 1998: Springer.

3. Bhattacharya, K., *Microstructure of martensite: why it forms and how it gives rise to the shape-memory effect*. Oxford series on materials modeling, ed. A.P. Sutton and R.E. Rudd. 2003: Oxford University Press.

4. Chang, L.C. and R.A. Read, *Plastic deformation and diffusionless phase changes in metals - The gold-cadmium beta phase.* Trans. AIME, 1951. **189**: p. 47-52.

5. Tadaki, T., K. Otsuka, and K. Shimizu, *Shape Memory Alloys.* Ann. Rev. Mater. Sci., 1988. **18**: p. 25-45.

6. Wayman, C.M., *Shape memory and related phenomena.* Progress in Materials Science, 1992. **36**: p. 203-224.

7. Humbeeck, J.V., *Shape memory alloys: A material and a technology.* Advanced Engineering Materials, 2001. **3**(11): p. 837-850.

8. Duerig, T.W. and A.R. Pelton, *An overview of superelastic stent design.* Materials Science Forum, 2002. **394-395**: p. 1-8.

9. Pelton, A., J. DiCello, and S. Miyazaki. *Optimization of processing and properties of medical-grade nitinol wire*. in *Proceedings of the International Conference on Shape Memory and Superelastic Technologies (SMST)*. 2000. Pacific Grove, CA.

10. *Shape Memory Effects in Alloys*. in *Proceedings of the International Symposium on Shape Memory Effects and Applications*. 1975. Toronto, Canada: Plenum Press, NY.

11. Funakubo, H., *Shape memory alloys*. 1987: Gordon & Breach Science Publishers, New York.

12. Duerig, T.W., K.N. Melton, D. Stockel, and C.M. Wayman, *Engineering aspects of shape memory alloys*. 1990: Butterworth-Heinemann, London.

13. Eucken, S., ed. *Progress in Shape Memory Alloys*. 1992, DGM Informationsgesellschaft Verlag.

14. Fremond, M. and S. Miyazaki, *Shape Memory Alloys*. 1996: CISM courses and lectures, No:351.

15. Berveiller, M. and F.D. Fischer, eds. *Mechanics of Solids with phase changes*. 1997, Springer Wien.

16. Otsuka, K. and C.M. Wayman, eds. *Shape memory materials*. 1998, Cambridge University Press. 284.

17. Otsuka, K. and X. Ren, *Physical metallurgy of Ti-Ni based shape memory alloys.* Progress in Materials Science, 2005. **50**: p. 511-678.

18. Wayman, C.M. and K. Shimizu, *Shape memory ('marmem') effect in alloys.* Metal Science Journal, 1972. **6**: p. 175-183.

19. Wayman, C.M. and J.D. Harrison, *The origins of the shape memory effect.* The Journal of Minerals, Metals and Materials (JOM), 1989. **41**(9): p. 26-28.

20. Duerig, T.W., A.R. Pelton, and D. Stoeckel. *The use of superelasticity in medicine*. in *Metall (Heidelberg)*. 1996: Sonderdruck aus Heft.

21. Duerig, T.W. *Present and future applications of shape memory and superelastic materials*. in *Materials Research Society Symposium Proceedings, Materials for Smart Systems*. 1995: Materials Research Society (MRS).

22. Duerig, T.W., D. Stoeckel, and A.R. Pelton, *An overview of nitinol medical applications.* Materials Science and Engineering A, 1999. **273-275**: p. 149-160.

23. Ryhanen, J., *Biocompatibility evaluation of nickel-titanium shape memory alloy*, in *Department of Surgery*. 1999, University of Oulu.

24. Frank, T.G., W. Xu, and A. Cuschieri, *Instruments based on shape memory alloy properties for minimal access surgery: interventional radiology and*

flexible endoscopy. Journal of Minimally Invasive Therapy and Allied Technologies (MITAT), 2000. **9**(1).

25. Pelton, A.R., D. Stoeckel, and T.W. Duerig, *Medical uses of nitinol.* Materials Science Forum, 2000. **327-328**: p. 63-70.

26. Stoeckel, D., *Nitinol medical devices and implants.* Minimally Invasive Therapy and Allied Technologies, 2000. **9**(2): p. 81-88.

27. Duerig, T., D. Stoeckel, and D. Johnson. *SMA-smart materials for medical applications*. in *Proceedings of SPIE 4763*. 2002. European Workshop on Smart Structures in Engineering and Technology.

28. Stoeckel, D., C. Bonsignore, and S. Duda, *A survey of stent designs.* Minimally Invasive Therapy and Allied Technologies, 2002. **11**(4): p. 137-147.

29. Stoeckel, D., A. Pelton, and T. Duerig, *Self-expanding nitinol stents : material and design considerations.* European Radiology, 2003(1-12).

30. Pelton, A.R., T.W. Duering, and D. Stockel, *A guide to shape memory and superelasticity in nitinol medical devices.* Minimally Invasive Therapy and Allied Technologies, 2004. **13**(4): p. 218-221.

31. Wayman, C.M., *Some applications of shape-memory alloys.* Journal of Metals, 1980. **June**: p. 129-137.

32. Duerig, T.W., *Applications of shape memory.* Materials Science Forum, 1990. **56-58**: p. 679-692.

33. Humbeeck, J.V., *Non-medical applications of shape memory alloys.* Materials Science and Engineering A, 1999. **273-275**: p. 134-148.

34. Schetky, L.M., *The industrial applications of shape memory alloys in North America.* Materials Science Forum, 2000. **327-328**: p. 9-16.

35. Saadat, S., J. Salichs, M. Noori, Z. Hou, H. Davoodi, I. Bar-on, Y. Suzuki, and A. Masuda, *An overview of vibration and seismic applications of NiTi shape memory alloy.* Smart Materials and Structures, 2002. **11**: p. 218-229.

36. Fugazza, D., *Shape-memory alloy devices in earthquake engineering: Mechanical properties, constitutive modelling and numerical simulations*, in *Earthquake Engineering*. 2003, Universita degli Studi di Pavia: Pavia. p. 141.

37. Humbeeck, J.V., *Damping capacity of thermoelastic martensite in shape memory alloys.* Journal of Alloys and Compounds, 2003. **355**: p. 58-64.

38. Schetky, L.M. and M.H. Wu. *Issues in the further development of nitinol properties and processing for medical device applications*. in *ASM Materials and Processes for Medical Devices Conference*. 2003. Anaheim, CA.

39. Dolce, M. and D. Cardone, *Mechanical behavior of shape memory alloys for seismic applications. 1. Martensite and austenite NiTi bars subjected to torsion.* International Journal of Mechanical Sciences, 2001. **43**: p. 2631-2656.

40. Dolce, M. and D. Cardone, *Mechanical behavior of shape memory alloys for seismic applications. 2. Austenite NiTi wires subjected to tension.* International Journal of Mechanical Sciences, 2001. **43**: p. 2657-2677.

41. Zhao, Y., M. Taya, and H. Izui, *Study on energy absorbing composite structure made of concentric NiTi spring and porous NiTi.* International Journal of Solids and Structures, 2006. **43**: p. 2497-2512.

42. Warlimont, H. and J. Delaey, *Martensitic transformations in Cu-, Ag-, and Au-based alloys.* Progress in Materials Science, 1974. **18**.

43. Adharapurapu, R.R., F. Jiang, K.S. Vecchio, and G.T. GrayIII, *Response of NiTi shape memory alloy at high strain rate: A systematic investigation of temperature effects on tension-compression asymmetry.* Acta Materialia, 2006. **54**: p. 4609-4620.

44. Yeung, K.W.K., K.M.C. Cheung, W.W. Lu, and C.Y. Chung, *Optimization of thermal treatment parameters to alter austenitic phase transition temperature of NiTi alloy for medical implant.* Materials Science and Engineering A, 2004. **383**: p. 213-218.

45. Favier, D., Y. Liu, L. Orgeas, A. Sandel, L. Debove, and P. Comte-Gaz, *Influence of thermomechanical processing on the superelastic properties of a Ni-rich Nitinol shape memory alloy.* Materials Science and Engineering A, 2006. **429**: p. 130-136.

46. Nishida, M., C.M. Wayman, and T. Honma, *Precipitation processes in near-equiatomic TiNi shape memory alloys.* Metallurgical Transactions A, 1986. **17**: p. 1505-1515.

47. Adharapurapu, R.R. and K.S. Vecchio, *Microstructure development in Ni-rich 60NiTi (wt.%) alloy: Aging studies on precipitation reactions and shape memory characteristics.* submitted to Metallurgical Transactions A, 2007.

48. Kainuma, R., M. Matsumoto, and T. Honma, *Metallographic study of precipitation processes in Ni-rich TiNi alloys.* Tohoku Daigaku Senko Seiren Kenkyujo iho, 1987. **43**(2): p. 149-158.

49. Tang, W., *Thermodynamic study of the low temperature phase B19' and the martensitic transformation in near-equiatomic Ti-Ni shape memory alloy.* Metallurgical Transactions A, 1997. **28**: p. 537-544.

50. Allafi, J.K., X. Ren, and G. Eggeler, *The mechanism of multistage martensitic transformations in aged Ni-rich NiTi shape memory alloys.* Acta Materialia, 2002. **50**: p. 793-803.

51. Otsuka, K. and X. Ren, *Factors affecting the Ms temperature and its control in shape memory alloys.* Materials Science Forum, 2002. **394-395**: p. 177-184.

52. Otsuka, K. and C.M. Wayman, eds. *Shape memory materials*. 1998, Cambridge University Press.

53. Morawiecz, H., D. Stroz, and D. Chrobak, *Effect of deformation and thermal treatment of NiTi alloy on transition sequence.* Journal de Physique IV, 1995. **5-C2**: p. 205-210.

54. Morawiecz, H., D. Stroz, T. Goryczka, and D. Chrobak, *Two-stage martensitic transformation in a deformed and annealed NiTi alloy.* Scripta Materialia, 1996. **35**(4): p. 485-490.

55. Chrobak, D., D. Stroz, and H. Morawiec, *Effect of early stages of precipitation and recovery on the multi-step transformation in deformed and annealed near-equiatomic NiTi alloy.* Scripta Materialia, 2003. **48**: p. 571-576.

56. Khalil-Allafi, J., A. Dlouhy, and G. Eggeler, *Ni_4Ti_3-precipitation during aging of NiTi shape memory alloys and its influence on martensitic phase transformations.* Acta Materialia, 2002. **50**: p. 4255-4274.

57. Liu, Y., H. Yang, and A. Voigt, *Thermal analysis of the effect of aging on the transformation behavior of Ti-50.9at.%Ni.* Materials Science and Engineering A, 2003. **360**: p. 350-355.

58. Stroz, D., *TEM studies of the R-phase transformation in a NiTi shape memory alloy after thermo-mechanical treatment.* Materials Chemistry and Physics, 2003. **81**: p. 460-462.

59. Carroll, M.C., C. Somsen, and G. Eggeler, *Multiple-step martensitic transformations in Ni-rich NiTi shape memory alloys.* Scripta Materialia, 2004. **50**: p. 187-192.

60. Fan, G., W. Chen, S. Yeng, J. Zhu, X. Ren, and K. Otsuka, *Origin of abnormal multi-stage martensitic transformation behavior in aged Ni-rich Ti-Ni shape memory alloys.* Acta Materialia, 2004. **52**: p. 4351-4362.

61. Khalil-Allafi, J., G. Eggeler, A. Dlouhy, W.W. Schmahl, and C. Somsen, *On the influence of heterogeneous precipitation on martensitic transformations in a Ni-rich NiTi shape memory alloy.* Materials Science and Engineering A, 2004. **378**: p. 148-151.

62. Michutta, J., M.C. Carroll, A. Yawny, C. Somsen, K. Neuking, and G. Eggeler, *Martensitic phase transformation in Ni-rich NiTi single crystals with one family Ni_4Ti_3 precipitates.* Materials Science and Engineering A, 2004. **378**: p. 152-156.

63. Johnson, A.J.W., R.F. Hamilton, H. Sehitoglu, G. Biallas, H.J. Maier, Y.I. Chumlyakov, and H.S. Woo, *Analysis of multistep transformations in single-crystal NiTi.* Metallurgical and Materials Transactions A, 2005. **36**: p. 919.

64. Wang, Z.G., X.T. Zu, and Y.Q. Fu, *Study of incomplete transformations of near equiatomic TiNi shape memory alloys by DSC methods.* Materials Science and Engineering A, 2005. **390**: p. 400-403.

65. Khalil-Allafi, J., G. Eggeler, W.W. Schmahl, and D. Sheptyakov, *Quantitative phase analysis in microstructures which display multiple step martensitic transformations in Ni-rich NiTi shape memory alloys.* Materials Science and Engineering A, 2006. **438-440**: p. 593-596.

66. Michutta, J., C. Somsen, A. Yawny, A. Dlouhy, and G. Eggeler, *Elementary martensitic transformation processes in Ni-rich NiTi single crystal with Ni_4Ti_3 precipitates.* Acta Materialia, 2006.

67. Chiang, L.J., C.H. Li, Y.F. Hsu, and W.H. Wang, *Age-induced four-stage transformation in Ni-rich NiTi shape memory alloys.* Journal of Alloys and Compounds, 2007. **doi:10.1016/j.jallcom.2007.04.006**.

68. Todoriki, T. and H. Tamura, Trans Jpn Inst Met, 1987. **28**: p. 83.

69. Stroz, D., J. Kwarciak, and H. Morawiec, *Effect of aging on martensitic transformation in nickel-titanium (NiTi) shape memory alloy.* Journal of Materials Science, 1988. **23**(11): p. 4127-4131.

70. Zhu, J.S. and R. Gotthardt, *New phase transition peak in nickel-titanium (NiTi) alloy.* Physics Letters A, 1988. **132**(5): p. 279-282.

71. Favier, D., Y. Liu, and P.G. McCormick, Scripta Metall Mater, 1992. **28**: p. 669-672.

72. Bataillard, L. and R. Gotthardt, *Influence of thermal treatment on the appearance of a three step martensitic transformation in NiTi.* J. Phys IV, 1995. **5-C8**: p. 647-652.

73. Buehler, W.J. and R.C. Wiley, *The properties of TiNi and associated phases*. 1961, U. S. Naval Ordnance Laboratory Report 61-75. p. 1-91.

74. Buehler, W.J. and R.C. Wiley, *TiNi: Ductile intermetallic compound.* Trans. Quart Am. Soc. Metals., 1962. **55**: p. 269-276.

75. Buehler, W.J. and R.C. Wiley, *Nickel-base Alloys*, in *United States Patent Office # 3174851*. 1965.

76. Buehler, W.J. and F.E. Wang, *A summary of recent research on the nitinol alloys and their potential application in ocean engineering.* Ocean Engineering, 1968. **1**: p. 105-120.

77. Saburi, T., T. Tatsumi, and S. Nenno, *Effects of heat treatment on mechanical behavior of titanium-nickel alloys.* Journal de Physique, Colloque, 1982. **C-4**: p. 261-266.

78. Saburi, T., S. Nenno, Y. Nishimoto, and M. Zeniya, *Effects of thermomechanical treatment on the shape-memory effect and pseudoelasticity of Ti-50.2Ni and Ti-47.5Ni-2.5Fe at. pct alloys.* J. Iron and Steel Inst. Japan (Tetsu to Hagane), 1986. **72**(6): p. 571-578.

79. Hornbogen, E., *Microstructure and thermo-mechanical properties of NiTi shape memory alloys.* Materials Science Forum, 2004. **455-456**: p. 335-341.

80. Julien, G.J., *Manufacturing of Nitinol parts and forms*, in *US Patent# 6422010*. 2002, Nitinol Technologies, Inc. (Edgewood, WA): United States. p. 1-15.

81. Adharapurapu, R.R. and K.S. Vecchio, *Superelasticity in a new bioimplant material: Ni-rich 55NiTi alloy.* Experimental Mechanics, 2006. **In Press**.

82. Adharapurapu, R.R. and K.S. Vecchio, *Microstructure development in Ni-rich NiTi alloys: Aging studies on precipitation reactions.* Work in Progress, 2007.

83. Clingman, D.J., F.T. Clalkins, and J.P. Smith. *Thermomechanical properties of 60-Nitinol*. in *SPIE Smart Structures and Materials*. 2003. San Diego CA.

84. Julien, G.J., *Shape memory parts of 60 Nitinol*, in *US Patent# 7005018*. 2006, Nitinol Technologies, Inc. (Edgewood, WA): United States. p. 1-15.

85. Julien, G.J., *Shape memory metal precision actuator*, in *US Patent#4932210*. 1990, Nitinol Technologies, Inc. (Edgewood, WA): United States.

86. Julien, G.J., *Method and apparatus for sensing and damping vibration*, in *US Patent#5005678*. 1991, Nitinol Technologies, Inc. (Edgewood, WA): United States.

87. Julien, G.J., *Method for producing an elongate passage within a component*, in *US Patent#5013507*. 1991, Nitinol Technologies, Inc. (Edgewood, WA): United States.

88. Julien, G.J., *Reusable metallic seal using memory metal*, in *US Patent#5226683*. 1993, Nitinol Technologies, Inc. (Edgewood, WA): United States.

89. Julien, G.J., *High security lock*, in *US Patent#5868013*. 1999, Nitinol Technologies, Inc. (Edgewood, WA): United States.

90. Julien, G.J., *Gun barrel*, in *US Patent#5856631*. 1999, Nitinol Technologies, Inc. (Edgewood, WA): United States.

91. Julien, G.J., *Shape memory rotary actuator*, in *US Patent#6065934*. 2000, Nitinol Technologies, Inc. (Edgewood, WA): United States.

92. Julien, G.J., *Plasma spraying of nickel-titanium compound*, in *US Patent#6043451*. 2000, Nitinol Technologies, Inc. (Edgewood, WA): United States.

93. Julien, G.J., *Post processing for nitinol coated articles*, in *US Patent#6254458*. 2001, Nitinol Technologies, Inc. (Edgewood, WA): United States.

94. Julien, G.J., *Cutting instruments*, in *US Patent#6293020*. 2001, Nitinol Technologies, Inc. (Edgewood, WA): United States.

95. Julien, G.J., *Nitinol horseshoes*, in *US Patent#6454016*. 2002, Nitinol Technologies, Inc. (Edgewood, WA): United States.

96. Julien, G.J., *Nitinol heater elements*, in *US Patent#6410886*. 2002, Nitinol Technologies, Inc. (Edgewood, WA): United States.

97. Julien, G.J., *Nitinol impact absorbers*, in *US Patent#6530564*. 2003, Nitinol Technologies, Inc. (Edgewood, WA): United States.

98. Julien, G.J., *Projectile*, in *US Patent#6581522*. 2003, Nitinol Technologies, Inc. (Edgewood, WA): United States.

99. Julien, G.J., *Liquid jet nozzle*, in *US Patent #6715701*. 2004, Nitinol Technologies, Inc. (Edgewood, WA): United States. p. 1-9.

100. Julien, G.J., *Nitinol ball bearing element and process for making*, in *USPTO*. 2005, Nitinol Technologies, Inc. (Edgewood, WA): United States. p. 1-17.

101. Julien, G.J., *Nitinol ski structures*, in *US Patent#6267402*. 2001, Nitinol Technologies, Inc. (Edgewood, WA): United States.

102. Mabe, J.H., R.T. Ruggeri, E. Rosenzweig, and C.-J.M. Yu. *Nitinol performance characterization and rotary actuator design*. in *SPIE 5388-11, Smart Structures and Materials Conference*. 2004. San Diego, CA.

103. Mabe, J.H., R.H. Cabell, and G.W. Butler. *Design and control of a morphing chevron for takeoff and cruise noise reduction*. in *11th AIAA/CEAS Aeroacoustics Conference*. 2005. Monterey, California: AIAA-2005-2889.

104. Calkins, F.T., J.H. Mabe, and G.W. Butler. *Boeing's variable geometry chevron: morphing aerospace structures for jet noise reduction*. in *13th SPIE Smart Structures and Materials Conference*. 2006. San Diego, CA.

2 BACKGROUND

2.1 Basic Phenomenon

2.1.1 What is unique about NiTi alloy?

The development of novel materials is critical for the advancement of materials engineering and is often the vanguard for many progressive innovative applications. From an engineering point of view, NiTi, popularly known as Nitinol, is an avant-garde alloy. The distinctiveness stems from its unique ability to 'memorize' pre-determined shape(s): even after severe deformation of several percent (strain), they are capable of returning spontaneously to their original, pre-deformed shape under certain thermal conditions. This phenomenon is termed as *shape memory behavior (SM)* and is both thermal and mechanical in nature. Additionally, the alloy also exhibits another remarkable property, namely, *superelasticity (SE)*. Superelasticity is the ability of the material to deform reversibly to very high strains of ~ 6-10% and recover the original pre-deformed shape spontaneously upon unloading. Unlike shape memory behavior, materials exhibiting superelasticity do not require any thermal changes to display superelasticity, *i.e.*, it is temperature independent. However, the test temperature can affect superelasticity. The physical manifestation of both the phenomena, viz., SM and SE, can be observed in their unusual stress-strain curves in Figure 2.1 when compared to other conventional alloys like steel, titanium, and Ni-based superalloys. Figure 2.2(a-b) also compare various mechanical properties such as elastic modulus, yield stress and reversible elastic strains observed in Ni-Ti alloys with other common

alloys used in the medical applications. The following sections introduce the concepts of SM and SE and try to explain the physical origin of this phenomenon and the concomitant observations.

2.1.2 Brief History

The genesis toward the eventual discovery of the shape memory behavior was laid down with the preliminary reports of shape memory-related phenomenon in Au-47.5Cd alloy system by Ölander [1, 2] in 1932 who noted a rubber-like behavior* (see section 2.1.9 for its description); it is now known that the Au-Cd alloys exhibit rubber-like behavior only upon aging of the martensite, freshly transformed specimen display only the shape memory effect (SME) [3]. This was followed by an observation by Greninger and Mooradian (in 1938) of the temperature dependent formation of the martensitic phase in a Cu-Zn alloy [4]. Within a decade, Kurdyumov and Khandros (1949) discovered the thermoelastic behavior of martensites that gave a crystallographic and kinetic basis for the thermal reversibility of the martensitic transformations, and which forms the basis of the shape memory effect [5]. Soon after, in 1950, twinned lamellar structures were observed in martensites of several alloys, including In-Tl and Au-Cd [6].

Chang and Read (1951), subsequently performed remarkable experiments on banded martensite and showed that by applying shear forces, the twin layers could be forced all to one "hand" (as described by [7]), thus providing a crystallographic

* Some authors quote pseudoelasticity instead of rubber-like behavior. Pseudoelasticity is a more generic term that encompasses both superelastic and rubber like behavior and hence an ambiguous term since it does not emphasize the phase (i.e., superelastic martensite or martensite) that is under investigation. Refer to section 2.1.9 for more description.

explanation of the "rubbery" phenomena of Au-Cd martensite first described by Ölander [1, 2]. Additionally, they demonstrated that if a shear-deformed Au-Cd martensite (unaged) was heated to a critical temperature, it recovered its original shape, which was due to the reverse transformation from orthorhombic to parent cubic phase. Analogous thermoelastic behavior was revealed in In-Tl [8] followed by the demonstration of shape memory in Cu-Zn (1953) (see [7] for a brief historical trace) and CuAlNi (1957), both of which vied for prospective engineering applications.

Since the discovery of shape-memory effect (SME) in Au-Cd alloys more than 50 years ago [1, 2], numerous alloy systems have been reported to exhibit SME behavior [9, 10]. However, after more than a decade of relative dormancy, research on SMA underwent a revival with the discovery of SME in NiTi by Buehler and his colleagues (in 1961) at the U. S. Naval Ordnance Laboratory (NOL) [11-14]. During an appraisal of different intermetallic materials as thermal shields that mandated stringent thermal property requirements, the oddity of NiTi exhibiting temperature dependent acoustic damping properties, surface relief, unusual micro-hardness indentation behavior, substantial ductility combined with high strength, good corrosion resistance and low density fostered further inquiries into its atypical properties. Subsequently, shape memory was discovered when a bent corrugated strip of NiTi straightened out by heating it with a pipe lighter during a project review; this serendipitous discovery of shape memory and subsequently other related phenomenon in NiTi are described vividly in [15]. It was the ensuing efforts by Buehler and his colleagues, who coined the term "shape memory" and Nitinol (Ni+Ti+NOL), now ubiquitous, that propelled NiTi as an avant-garde engineering material.

Since then, there has been tremendous growth in investigations aimed at elucidating the basic mechanics of its behavior. By the 1970s, the fundamental understanding of the origin of SME and the shape memory mechanism [16-19] followed by the crystallography of the stress-induced martensitic transformation (SIM) [20, 21] was ascertained for Cu-based alloys [10]. Due to the ease of processing single crystals of Cu-based alloys and also their relative low-cost, most of findings were based on these alloys. However, due to the brittleness of Cu-based alloys, like Cu-Zn-Al and Cu-Al-Ni, in their polycrystalline state [22-24] and due to the superiority of Ni-Ti alloys in terms of their strength and ductility, corrosion resistance and biocompatibility, Nitinol alloys have been the chief materials for many shape memory applications.

Notwithstanding the insight into the microstructural mysteries of shape memory effect in its minute details, the industry's effort of engineering the Ni-Ti alloy sauntered behind. Primarily, the unusual properties, such as sigmoid stress-strain curve (i.e., high non-linear), hysteresis, fatigue, adiabatic heating and cooling, confounded the product designers [25]. In addition, alloy melting procedures and subsequent processing steps posed a steep challenge in terms of overall economics compounded by the problem of reliability, resulting in the development of only a few products. Duerig *et al.* [25] point out that by the 1980's, despite its allure and promise as a panacea in many applications due to its added functionalities, it was precisely these properties that have baffled the design engineers with the result that, by the 1990s, many big companies had rescinded from investing in Nitinol based technologies due to a flagging economic recompense. However, as they further point

out, Nitinol has reinvented itself as a household name in the medical community as a result of ever-growing roster of medical devices and applications. To the question, 'what mobilized such a reversal?' Duerig *et al*. [3, 25] advance, among many possible reasons, the medical community's drive towards minimally invasive medical procedures. A shift towards minimally invasive medical procedures necessitated the availability of novel medical instruments (with unconventional properties) and Nitinol was well suited for this task. Compared to the cryogenic alloys required in couplings and fasteners, or high-M_s alloys necessary in actuator applications, the medical applications were based on implants that demanded optimal performance at/around the body temperature (37°C), the temperature window where the Nitinol alloys excelled. Additionally, instead of dealing with the complicated shape memory effect, interest was diverted towards superelasticity, a property that forms the basis of many medical devices. As early as the 1970s, reports of NiTi use as an implant material were burgeoning [26-28] and by the early 1980s orthodontic and orthopedic applications were realized [29-31]; however, it was only in the 1990's that NiTi applications proliferated with the commercial breakthrough of stents that revolutionized the medical industry [25, 31-43] (also refer to the thesis [44]). Availability of microtubing and precision laser cutting of tubing also aided in the promulgation of the Nitinol superelastic technology [25].

Given the importance of NiTi over Cu-based alloys, the basic understanding of the thermomechanical treatment [23, 45-47], deformation behavior [48-52], shape memory mechanisms [53-57], the occurrence of R-phase [58-64] (and its crystallography [65-69]) in Ni-Ti alloys were established in the 1980s [10].

Subsequently, the controversies associated with the Ni-Ti phase diagram were also eventually clarified [47, 70-73] and the crystal structure of metastable as well as the stable precipitates were obtained [70, 73-75] (section 2.3 discusses these issues in more detail).

The alloys that exhibit shape memory function can generally be classified into Fe-based, non-ferrous and particularly NiTi-based, noble-metal based alloy systems and nonmetallic shape memory alloys like SM ceramics and polymers [23]. Despite the efforts by the research community to develop SMA for commercial applications, only a few alloys have found a niche in commercial markets; in 2001, 90% of all SMA-applications were based on NiTi or ternary NiTi-Cu/Nb alloys and other alloys like Cu-Al-Ni, Fe-Mn-Si, NiTi-Zr, Cu-Zr, Ni-Al were either being introduced into the market or promised interesting, but limited potentials [76]. While Copper based alloys like Cu-Zn-Al and Cu-Al-Ni are commercially available, these alloys exhibit less stability and are brittle in nature when compared with Ni-Ti and therefore, although less expensive, have been minimally accepted [23]. Some other ternary alloys like Ni-Ti-Pd/Hf/Zr are being investigated as potential shape memory alloys for high-temperature applications (that require higher transformation temperatures, >100°C), since Ni-Ti and Cu-based SMA exhibit transformation temperatures between –100°C and 100°C. However due to the lack of minimum quality standards for stability, ductility, functional behavior and reliability issues, successful applications appear distant [77]. More recently, various Ni-free β-Ti alloys, such as Ti-Nb-X and Ti-Mo-X (where X is a ternary additive) have been under consideration as non-toxic alternatives in bio-medical applications, since β-Ti alloys also exhibit biocompatibility

[78]. There has also been a moderate drive towards processing and studying the relevant SM and SE effects in nano-grain-sized Ni-Ti alloys [79-84].

While the development of NiTi in bio-medical applications such as stents and other implants, where its superelastic behavior is of primary importance, and the utilization of shape memory property in the advancement of smart actuators and other non-medical applications has occurred in large strides in the past two-decades. More recent investigations (within the last decade) have looked at seismic protections of structures [85-88] and there is a growing interest in the exploitation of Nitinol towards high-strain rate applications such as energy-absorbing structures [89-91].

While the origin and the development of Nitinol have been briefly recounted in the preceding paragraphs, an important auxiliary was delayed until now. The early investigations at the NOL by Buehler and his colleagues [11-14] focused on a series of non-magnetic Ni-Ti alloys based on the ductile intermetallic compound NiTi that displayed two distinct sets of properties as a function of Ni composition and heat treatment. [13]. This division was initially based upon hardness measurements over a range of Ni composition, viz., 50 to 64 weight pct (remainder being titanium, see Figure 2.3). It can be seen that equitomic and near-equiatomic (i.e., near 55 weight pct Ni) alloys exhibit minimum hardness and are relatively unaffected by cooling rates when cooled from 950°C. By contrast, the alloys composed of Ni in excess of 55 weight pct exhibit increasing hardness under quenched conditions. A further mark of distinction was revealed in the microstructural differences during metallographic studies. While 55-Nitinol (wt pct) was found to be single-phase alloy of NiTi (oxide and nitride impurities were present in minute quantities), Ni-rich NiTi alloys were

found to contain $TiNi_3$ phase (in the form of precipitates) in equilibrium with the NiTi matrix phase. It has been shown that a series of thermomechanical treatments, i.e., various combinations of solution-treatments combined with cold work and/or anneal heat-treatments etc., are required to optimize the SE and SM properties of equiatomic alloys [13, 23, 39, 46, 47, 92, 93]. However, departure from the 55-Nitinol (wt pct), i.e. near stoichiometric NiTi, towards the Ni-rich alloys leads to the second group of Nitinol alloys that are also non-magnetic, but are at variance with the former alloys in that the latter group can be thermally hardened by aging heat treatments to high hardness levels, viz., ~60 - 70 R_C [13, 94-96]. The latter group, i.e., NiTi alloys spanning the composition range from 56 to 62 wt pct Ni (remainder being titanium) were generically designated as 60-Nitinol alloys (designated by wt pct) [13]. While both the 55-nitnol and 60-Nitinol possessed common unusual properties such as non-magnetic character, marine corrosion resistance due to the difference in hardness, microstructural features and the general effect of heat treatment on their properties, 55-Nitinol and 60-Nitinol were considered as separate and distinct alloy types [13]. Furthermore, an additional divergence was seen among the 60-Nitinol alloys, namely, between the ‘quenched’ and ‘furnace cooled’ alloys, as shown in Figure 2.3. While it was pointed out by Buehler and Wang [13] that not only the high hardness ‘quenched’ or low hardness ‘furnace cooled’ 60-Nitinol alloys could be produced, but also indicated the possibility of attaining alloys with any desired intermediate hardness accomplished by either intermediate cooling rates or by utilizing some sort of ‘overaging’ or pseudo-tempering’ post-quench heat treatment, later investigations by Nitinol Technology Inc., Mountain View, WA, have attributed the SE and SM

behavior in 60-Nitnol alloys as directly resulting from this crucial difference in cooling rate, viz., quenching vs. furnace cooling, respectively [94, 97, 98]) . In spite of many promising properties of 60-Nitinol alloys, such as high hardenability, ability to tailor hardness through aging heat-treatments only, high corrosion resistance, low susceptibility to stress corrosion failure, '*they exhibited the most noteworthy engineering weakness, viz., notch sensitivity*' [13]. Due to the difficulties in forming and hot-working, machining and forming these materials into near-net shapes for practical applications became difficult and impractical [97]. Therefore, 55-Nitinol was eventually preferred over 60-Nitinol, as evidenced by the numerous products in bio-medical and sensor applications. However, since the development of hot rolling methods for 60-Nitinol and special fabrication techniques (by Nitinol Technologies Inc., Mountain View, WA) [94, 97], a number of patents have emerged that exploit some of the afore-mentioned unique properties of the alloys [94, 98-115]. A decade ago, it was shown that under special heat treatment conditions, both the SM and SE effects could be produced in the alloy from the same ingot without any additional mechanical processing [94, 97, 98]. Since then, the interest in the development of Ni-rich 60-Nitinol alloys has seen a resurgence, although very little work exists on the mechanical properties of these alloys [95-97, 116-118].

With regards to the development and progress in understanding the behavior of Ni-Ti alloys, the current work finds its place in two significant ways. The primary aim of the current work is the investigation of dynamic or high-strain rate behavior of equiatomic (or 55-Nitinol wt pct) alloys. As pointed out in the preceding paragraphs, the interest in the dynamic response of Ni-Ti alloys has been gaining momentum

during the last decade and the current study involves a systematic evaluation of the dynamic properties in Ni-Ti alloys as a function of temperature, strain-rate and texture (see [89] for a perusal at the limited literature on the high-strain rate response of Ni-Ti alloys). Additionally, with the significant development of methods to produce SE and SM 60-Nitinol products from the same ingot that obviates the need for cold-work in these alloys, the current work evaluates and assesses this alloy's potential as a SE and SM material towards bio-medical and actuator applications and also investigates its dynamic mechanical properties that seeks to exploit them towards defense platforms.

2.1.3 Thermoelasticity and Martensitic Transformations

(a) General introduction

The shape memory effect (SME) and superelasticity (SE) are unique properties of certain alloys systems that arise from a (reversible) *thermo-elastic behavior* of the alloy that has its basis in temperature-induced *diffusionless, solid-solid first-order* transformation (high-temperature austenite $\rightarrow$ low-temperature martensite), involving a *change in crystalline symmetry* [119]. The *italicized* terms will be discussed in sequence in the following paragraphs.

Similar to the phase transformations occurring during melting of ice or evaporation of water[†], these '*first-order phase transformations*' lie at the core of the unique behaviors of SMA. The first-order phase transitions are defined by the

[†] A phase transition/transformation is the transformation of a (thermodynamically defined) system from one phase to another due to the variation in a thermodynamic parameter (such as temperature) and it is usually accompanied by an abrupt change in one or more physical properties of the system; for e.g., variation of heat capacity or lattice parameter with temperature changes. Many transformations such as solid $\leftrightarrow$ liquid $\leftrightarrow$ gases, amorphous $\leftrightarrow$ crystalline $\leftrightarrow$ different crystal structures, magnetic states (ferromagnetic $\leftrightarrow$ paramagnetic), even superconductivity, illustrate some common examples.

characteristic presence of latent heat of the transformation that expresses the amount of (heat) energy required for a material to undergo a phase change.

This is a *solid-solid transformation* in that, upon cooling, the crystal lattice structure changes abruptly from a high-temperature cubic *austenite* phase to a low-temperature monoclinic *martensite* phase at some critical temperature (see Figure 2.4). The phase transition or the change in the lattice structure is quite abrupt and is accompanied by a considerable amount of unit cell distortion; however, there is no diffusion of the atoms involved and there is no change in the relative positions of the atoms during the transformation (refer to Bhattacharya [119] for an excellent introduction on the microstructures of martensite and their origin).

These solid-solid phase transformations introduced in the preceding paragraph are known as *martensitic phase transformations* (after the German Scientist Adolf Martens, 1890) [120]. According to Wayman and Harrison [7],

"The world's most economically important metallurgical transformation is that of austenite to martensite during the quenching of steel. So important is this process that hundreds of man-years of sophisticated study have been devoted to its understanding…"

Martensitic phase transformations have been observed in various metals, alloys, ceramics [23, 120, 121] and even biological systems [122], but the most significant understanding of martensitic transformations have come from the iron-carbon (Fe-C) system and, by the 1930s, many basic features of the transformation were already understood (see [121] for an interesting synopsis of the history and numerous scientific studies of the martensitic phase transformations). Hitherto,

martensitic transformations, that were largely observed in the Fe-C system, were presumed to be irreversible (refer to Table 2.1 for a qualitative comparison between ferrous and non-ferrous martensites), however, thermally reversible martensitic transformations were first observed in Cu-Zn and Cu-Al-Ni alloys (during late 1930's) [5, 123]. Thus, the concept of *thermoelastic martensite* gave a crystallographic and kinetic basis for understanding these phenomena [7]. A *thermoelastic martensitic transformation* is realized if the martensite nucleates and grows continuously in tandem with the lowering of the temperature and, per contra, shrinks and disappears as the temperature is raised [124-127]. There are no sudden appearances or disappearances of large groups of plates ("burst"), the transformation essentially proceeds in equilibrium between the 'chemical driving energy' (the difference between the free energies of austenite and martensite phases) and the 'resistive elastic energy' (due to the transformation) and often exhibits small local discontinuities or jumps during the growth of a martensite plate (termed as 'degenerate elastic transformation' by [125]). Evidently, when the chemical driving force greatly exceeds the resistive elastic forces, the transformations are termed as 'spontaneous' or 'burst' [125]. A thermodynamic analysis of these transformations will be attempted shortly. Delaey [128] makes a distinction between the kinetics of a single martensite plate and the global kinetics, i.e., the volume fraction of the parent phase that is transformed: martensitic transformations can be either athermal, where the transformation proceeds with decreasing temperature; or isothermal, where the transformation proceeds with time at a constant temperature (refer to Figure 2.5), and, as alluded earlier, the growth

may be 'thermoelastic' or of the 'burst' type[‡]. The unique behavior observed in NiTi is typically a *thermoelastic martensitic transformation*.

Table 2.1 A brief qualitative comparison between martensites formed in ferrous and non-ferrous alloys [128].

Property	**Ferrous martensite**	**Non-ferrous martensite**
Nature of alloying	Interstitial and/or substitutional	Substitutional
Hardness	Martensitic state in interstitial ferrous alloys is much harder than the austenite state	Martensitic state is not much harder and may even be softer than the austenite state
Transformation hysteresis	Large	Small to very small
Transformation strain	Relatively large	Relatively small
Elastic constants of the parent phase	High values near the M_s	Low values near the M_s
Transformation enthalpy	High	Low to very low
Transformation entropy	Large	Small
Chemical driving force	Large	Small
Growth character	Self accommodation is not obvious	Well developed self accommodating variants
Kinetics	High rate, "burst", athermal and/or isothermal transformation	Slower rate, no "burst", no isothermal transformation, thermoelastic balance
Growth front	No single interface transformation observed	Single interface possible
Interface mobility	Low and non-reversible	High and reversible
Damping capacity of martensite	Low	High

[‡] In the non-thermoelastic martensitic transformation, the martensite phase, after nucleation, grows instantaneously to their final size and do not grow further as the temperature decreases. However, during the reverse transformation, the martensitic phase does not shrink and revert back to the austenite phase (as it occurs in thermoelastic transformation); rather, the austenite phase is nucleated within the martensite phase and grows, similar to the martensite phase that nucleated and grew within the austenite phase. Thus, reverse transformation is not reversible.

(b) Thermodynamics

The thermoelastic martensitic transformations observed in NiTi are not associated with any compositional changes (since diffusionless), therefore, the free energy curves of both austenite and the martensite phases may be represented schematically as a function of temperature in the manner shown in Figure 2.6 (the discussion here will follow in the vein of [124, 130]. T_o represents the thermodynamic equilibrium temperature between the two phases, viz., martensite and austenite; $\Delta G^{a\to m}|_{M_s} = G^m - G^a$ is the driving force for the martensite nucleation, where G^a and G^m represent the Gibbs free energy of the austenite and the martensite phases, respectively.

For a thermoelastic transformation, all the transforming interfaces necessarily reach equilibrium between the opposing forces at a given temperature (during cooling). The driving force during martensite formation, as noted above, results from the lower energy of the martensite phase; this is opposed by the accompanying increase in elastic strain energy, interfacial energy and the resistive forces against interfacial motion. During its reverse transformation to austenite, the stored elastic energy provides the impetus along with the reverse transformation driving force; these are balanced by the resistive forces. The total change in the free energy accompanying these forward (assuming an oblate-spheroid martensite particle of radius *r* and semi-thickness *c* [131]) and reverse transformations can be written, respectively, as:

$$\Delta G(T)^{m\to a} = \Delta G_{ch}^{m\to a}(T) + \Delta G_{el}^{m\to a} + \Delta G_s^{m\to a} \qquad \text{Equation 2.1}$$

$$\begin{aligned}\Delta G(T)^{a\to m} &= \Delta G_{ch}^{a\to m}(T) + (\Delta G_{el}^{a\to m} + \Delta G_{s}^{a\to m}) \\ &= \frac{4}{3}\pi r^2 c\Delta g_{ch} + (\frac{4}{3}\pi r^2 c(A\frac{c}{r}) + 2\pi r^2\sigma) \\ &= \Delta G_{ch}^{a\to m}(T) + \Delta G_{nc}^{a\to m}\end{aligned} \qquad \text{Equation 2.2}$$

where, *a* and *m* represent the austenite and martensite phase, $\Delta G_{ch}^{a\to m}$ is the change in the chemical free energy ($\Delta g_{ch}^{a\to m}$ is calculated per unit volume)); $\Delta G_{el}^{a\to m}$ is the elastic strain energy (equals elastic strain energy per unit volume times the particle volume; $\Delta g_{el}^{a\to m} V_m = (Ac/r)(4\pi r^2 c/3))$), $\Delta G_{s}^{a\to m}$ corresponds to the interfacial energy between the two phases (these forces resist either the growth and shrinkage of existing martensite crystals or the creation and annihilation of new martensite crystals). The elastic strain energy term implicitly assumes an elastic accommodation of the martensite. Usually, the elastic energy and the interfacial energy terms are combined to represent the non-chemical free energy, $\Delta G_{nc}^{a\to m}$ [130]. In most martensitic transformations, $\Delta G_{nc}^{a\to m}$ is as large as $\Delta G_{ch}^{a\to m}$, and because of this, supercooling and superheating is necessary for the martensitic or the reverse transformation, respectively. Due to similar reasons, M_s is not the same as M_f, since the elastic energy around the martensite phase resists any further growth of martensite unless the driving force is increased by further cooling. In both the forward and the reverse transformations, a change in temperature alters the driving force and thus the equilibrium point is displaced resulting in the growth or shrinkage of the martensite phase. For thermoelastic alloys, the driving force for the transformation is usually small since the interface between the austenite parent phase and the martensite phase is mobile during heating or cooling and the transformation itself is crystallographically

reversible, i.e., the martensite reverts back to the parent austenite in the original orientation. From Equation 2.1, considering that the thermoelastic equilibrium is reached at a given temperature when the rate of growth of the martensite particle reaches zero, Kaufman and Cohen [132] derived that this occurs when the elastic strain energy balances the chemical driving force as:

$$\Delta g_{ch} + 2\Delta g_{el} = 0 \qquad \text{Equation 2.3}$$

i.e., when the elastic strain energy per unit volume of the particle (stored in the matrix and the particle) approaches half the magnitude of the chemical driving force. When the temperature is decreased at such an equilibrium, Δg_{ch} increases relative to Δg_{el} and hence the martensite grows and vice versa. Further, if $(A_f - M_s)$ is small and the degree of supercooling and superheating are very similar, then one can derive that $T_o = (M_s + A_f)/2$ [124].

The DSC thermal measurements of exothermic, Q_M and endothermic, Q_A heats can be related to the thermodynamics of the thermally induced thermoelastic martensitic transformations as follows [133, 134]:

$$-Q_m = -\Delta H_{ch}^{a\to m} + \Delta H_{el}^{a\to m} + W_{fr}^{a\to m} \qquad \text{Equation 2.4}$$

$$Q_a = \Delta H_{ch}^{m\to a} - \Delta H_{el}^{m\to a} + W_{fr}^{m\to a} \qquad \text{Equation 2.5}$$

where ΔH_{ch} is the change in chemical enthalpy due to structure, ΔH_{el} is the elastic strain enthalpy stored in the specimen that accommodates the transformational shape and volume changes and W_{fr} is the work done to overcome frictional resistive forces opposing the motion of the interfaces. Equation 2.5 has been modified to accommodate the influence of cold-rolling in martensitic NiTi alloys that leads to a

substantial decrease in the ΔH value of the first reverse martensitic transformation (and also between the first and second DSC runs) and further with increase in the degree of cold rolling [133, 134]:

$$Q_a = \Delta H_{ch} - \Delta H_{el} + W_{fr} - \Delta H_{CR} \qquad \text{Equation 2.6}$$

where ΔH_{CR} is an extra term that takes into consideration defect recovery for cold-rolled samples. In NiTi alloys, factors such as work hardening [135-137], rolling temperatures, thickness reduction and heat treatment history [138, 139], were found to have significant impact on the heat of transformation [133]. The effect of the applied stress on the martensitic transformation and the effect of cold-work and thermo-mechanical history on the phase transformation will be dealt in section 2.1.5 and section 2.4.2, respectively.

(c)Transformation kinetics

While the 'burst' type martensitic transformations are characterized by an autocatalytic nucleation and rapid growth (speeds can be greater than 10^3 m/s, about 1/3 the speed of elastic waves in solids [124]) of a large number of martensite plates, typical 'thermoelastic' martensites exhibit parallel-sided or wedge-shaped pairs of plates that grow progressively as the temperature is lowered below M_s. This type of behavior is observed when the matrix accommodates the shape deformation of the martensite plate elastically in such a way that, at a given temperature, the transformation front of the martensite plate and the austenite matrix are in thermodynamic equilibrium. Any variation in the temperature alters the plate growth, i.e., either grows or shrinks [124]. While, during non-thermoelastic transformations, new martensite crystals, once nucleated, grow almost instantaneously to their final size

and further growth does not occur upon decreasing the temperature or waiting longer times, during the thermoelastic transformations, the nucleated martensite crystals were found to grow at a velocity proportional to the cooling rate, some growth rates are even detectable with the naked eye [124]. In thermoelastic transformations, it was shown that the martensite plates that first formed when cooled near M_s are the last to reverse transform at A_f [124]. Particularly, in Ni-Ti SMAs, the rate of transformation of austenite into martensite has been quantitatively described by empirical relations, such as [140]:

$$f = 1 - \left(\frac{T - M_f}{M_s - M_f} \right)^n \qquad \text{Equation 2.7}$$

where f is the volume fraction of the transformed martensite and n is a material dependent exponent, n = 3 for NiTi alloys.

(d) Microstructure

So far, only the thermodynamic and the kinetic aspects of the martensitic transformation have been introduced without any specific reference to the microstructure that is produced by the transformation. As Bhattacharya [119] emphasizes, the characteristic observable feature of the martensitic transformation is the microstructure that it generates. Typically, the high-temperature austenite phase has a greater *crystallographic symmetry* (with reference to the unit cell) than that of the low-temperature martensite phase, Figure 2.7(a) illustrates this by contrasting the square unit cell of the austenite versus the less symmetric rectangular unit cell of the martensite, Figure 2.7(b,c), (the discussion here follows in the vein of Bhattacharya [119]). This transition suggests that multiple *symmetry-related martensite variants* are

possible. Upon cooling, the square lattice transforms into the rectangular lattice, and since the latter lattice exhibits two variants, i.e., either is equally likely to be the transformation product, the transformed crystal is made up of a mixture of numerous variants. Depending on the nucleation kinetics and the ability to form different shapes, different parts of the parent phase may transform into different variants.

However, in the formation of the variant mixtures, the material cannot tear itself and, necessarily, the interfaces between the variants must maintain *coherency* with unbroken rows of atoms across the interface. This unique combination of the tendency to form variant mixtures in the *martensite microstructure* combined with the necessity to impose coherency across the variant interfaces leads to the formation of complex and characteristic patterns at a very small length-scale (from a few nm to tenths of mm). It is precisely this ability of a material to form unique *martensite microstructures* and their ability to transform it lends the martensitic materials their exclusive properties.

(e) Hysteresis

A corollary to the thermoelastic martensitic transformation observed in NiTi is the development of *hysteresis*. As discussed previously, during the cooling and heating cycle, changes in the lattice parameter can be observed as a result of the martensitic transformation. However, there is a difference between the temperature where austenite transforms to martensite and martensite transforms to austenite. The temperature difference between the forward transformation and the reverse transformation is known as hysteresis and it may vary between a few to hundreds of degrees Celsius [23, 141], depending on the material type; shape memory alloys

typically have small hysteresis (also refer to Table 2.1). In the athermal mode of transformation, the amount of martensite formed is a function of only the temperature (i.e., an incremental change in temperature produces a proportionate change in the phase) to which the alloy is cooled and not the time of holding at that particular temperature. When the austenite NiTi is cooled, it starts to transform at the *martensite start temperature* (M_s) and ends at the *martensite finish temperature* (M_f). Typically, the entire austenite phase has transformed to martensite. Upon heating, analogously, the martensite begins to transform into austenite at the *austenite start temperature* (A_s) and the transformation is complete at the *austenite finish temperature* (A_f) [142], as indicated in Figure 2.8. Typically, Ni-Ti based shape memory alloys have a hysteresis width of 30^oC-50°C [143].

One caveat should be noted: Not all diffusionless transformations can be termed as martensitic. The term *martensitic* is reserved for transformation involving sufficiently large strains that the product domain structure must form by nucleation and growth [144]. Thus, martensitic transformations are: (i) *shear-dominant* i.e., the deviatoric/shear strain components are larger than the dilatational strain components. In the former case no undistorted line is seen and, in the latter case, an undistorted line exists. *(ii) Lattice-distortive* (i.e., such displacements contribute to a homogeneous strain in the lattice). (iii) D*iffusionless* transformations occurring by nucleation and growth. See Figure 2.9 for the classification scheme of diffusionless/displacive phase transformations as proposed by Cohen [128, 144].

2.1.4 Martensitic transformation in Ni-Ti alloys

2.1.4.1 Crystal Structures of the austenite and the martensite phases

(a) NiTi B2 austenite phase: NiTi is a B2 (cubic) type ordered structure [145] that undergoes an order-disorder transition from B2 to BCC at 1090°C. Upon quenching or slow cooling to room temperature, the phase is retained, and it is this phase that undergoes the martensitic transformation and the concomitant SM or SE effects.

(b) NiTi B19' martensite phase: Nitinol, NiTi, undergoes martensitic transformation to any of the following phases: trigonal R-phase or monoclinic B19' phase or orthorhombic B19 phase [23, 47]. Both Michal and Sinclair (1981) [67, 146] and Kudoh *et al.* (1985) [67, 146] arrived at the correct space group $P2_1/m$ monoclinic structure for NiTi martensite and the resulting crystal structure is schematically shown in Figure 2.10.

(c) NiTi R-phase: In 1985, Goo and Sinclair [147] arrived at the space group of R-phase as $P\bar{3}1m$ using convergent beam electron diffraction (CBED); however, they did not arrive at any definite atomic positions. By 1989, Wu and Wayman [148] suggested a trigonal distortion of the cubic structure such that the R-phase could be obtained by elongating the B2 cube along the body diagonal, see Figure 2.11. About a decade ago (1997), Hara *et al.* [149] studied the R-phase structure using electron-diffraction and powder x-ray diffraction and concluded that the crystal structure is *P3*. Recently, in 2003, Schryvers and Potapov [150] proposed yet another crystal structure for the R-phase, namely, $P\bar{3}$ based on dynamic nanoprobe electron diffraction and

least-squares minimization analysis. Apparently, the difference between the two proposed structures, viz., *P3* and $P\bar{3}$ is very minimal in that the former does not posses a center of symmetry. Around the same time, Sitepu *et al.* [151, 152] combined refinements of the R-phase formed in $Ti_{50.75}Ni_{47.75}Fe_{1.50}$ alloy using both neutron and diffraction data were carried out using three space groups, viz. P31, P3 and $P\bar{3}$. Their results indicated that the reasonable space group for R-phase is $P\bar{3}$. More recently, in 2006, Gong *et al.* [153] suggested that the P31m space group is the correct crystalline ground state of R-phase. They based their conclusions on *ab-initio* calculation of the electronic and crystal structure for the R-phase using the density functional theory (DFT) with plane-wave pseudopotentials. Their calculations of geometry optimization between *P3* and $P\bar{3}$ indicated that *P3* structure changes to *P31m* structure and that it possesses a lower energy than that of $P\bar{3}$. Based on the lattice parameters computed from their calculations, the XRD spectrum corroborated well with the experimental XRD values. Around the same time, Khalil-Allafi *et al.* [154] used neutron diffraction studies to redetermine the crystal structure parameters of the R-phase in a binary $Ni_{50.8}Ti_{49.2}$ shape memory alloy. Several models with different space group symmetries such as $P\bar{3}$, P3 and $P\bar{3}$1m were refined against their neutron diffraction data and their results favored the $P\bar{3}$ symmetry, confirming the results of electron and X-ray diffraction studies [151, 152, 155, 156]. Due to the growing evidence for the support of $P\bar{3}$ symmetry of the R-phase, the crystal structure parameters calculated by Khalil-Allafi *et al.* [154] will be used to index the XRD patterns in the present work.

2.1.4.2 Twinning

(a) General Introduction:

When the martensite phase nucleates and grows during a thermoelastic martensitic transformation, it was stipulated that the microstructure so formed is actually a mixture of different symmetry-related variants of martensite that maintain a coherency across their interfaces; unique in terms of its complexity and fine length-scale features [119]. However, while considering the unique microstructure of these martensites, two important features of the microstructure must be noted: what is the nature of this coherent interface between the variants, i.e., what is the mode of *self-accommodation?* and what is the nature of the interface between the martensite and the parent austenite phases? It has been conclusively shown, based on continuum theories of crystalline solids [158] that the resulting martensitic microstructure is a result of energy minimization of the specimen that undergoes the martensitic transformation (the discussion henceforth will follow in the vein of Bhattacharya [119]). Since the martensitic transformations observed in NiTi alloys is a lattice-distortive and shear-dominant one, and since the driving force is essentially governed by the difference in free energy as a function of temperature, the total energy of a specimen subjected to a deformation **y** at a temperature T may be expressed as:

$$\int_{\Omega} \varphi(\nabla \mathbf{y}, T) dV \qquad \text{Equation 2.8}$$

where φ is the stored energy density (or the Helmholtz free energy) ∇**y,** the deformation gradient (measures the local distortion in the lattice). The basic premise is that the specimen undergoing the martensitic transformation will occupy a state that

minimizes this total energy, and therefore, the microstructure and the concomitant behavior of the specimen is completely determined by this energy density. It was found that the energy density has multiple minima (*multi-well structure*) that are related to the crystal structures of the austenite and the martensite. Most importantly, it was shown that the consequence of the energy well structure leads to twinning in the martensite. In other words, the twinning deformation mode arises out of the necessity to satisfy the energy minimization conditions; as a result, the martensite that forms during the transformation is internally twinned. In order to arrive at this conclusion, a few preliminary results, gleaned from Bhattacharya [119], will be utilized.

Result 1: The Cauchy-Born Hypothesis [159]

The Cauchy-Born hypothesis essentially links the lattice deformation to the continuum deformation. Consider a crystalline solid occupying a region Ω in a reference configuration where at each point $\mathbf{x} \in \Omega$, a Bravais lattice with lattice vectors $\{\mathbf{e}_i^o(\mathbf{x})\}$ may be constructed. Now, if the solid undergoes some deformation $\mathbf{y}(\mathbf{x})$ due to the decrease in temperature (such that the deformation gradient is given by $\mathbf{F}(\mathbf{x}) = \nabla\mathbf{y}(\mathbf{x})$), and at the same point $\mathbf{x}$ the distorted lattice is now spanned by the lattice vectors $\{\mathbf{e}_i(\mathbf{x})\}$, the Cauchy-Born hypothesis essentially states that the deformation of the lattice vectors is governed by the deformation gradient as:

$$\mathbf{e}_i(\mathbf{x}) = \mathbf{F}(\mathbf{x})\,\mathbf{e}_i^o(\mathbf{x}) \qquad \text{Equation 2.9}$$

In other words, the lattice vectors behave like infinitesimal line elements of the continuum. Therefore, for a Bravais lattice $\Im(\mathbf{e}_i, \mathbf{o})$, the energy density of the lattice at

a given temperature T may be rewritten as $\hat{\varphi}(\mathbf{e}_i, T)$ i.e., the energy density depends on the lattice vectors and the temperature.

Result 2: Symmetry group of the lattice

If two Bravais lattices $\Im(\mathbf{e}_i, \mathbf{o})$ and $\Im(\mathbf{f}_i, \mathbf{o})$ spanned by the lattice vectors $\{\mathbf{e}_i\}$ and $\{\mathbf{f}_i\}$, respectively, exist, then there exists a matrix **F** (det **F** ≠ 0) such that

$$\mathbf{f}_i = \mathbf{F}\mathbf{e}_i \qquad \text{Equation 2.10}$$

then we may regard the $\Im(\mathbf{f}_i, \mathbf{o})$ as a deformation of the lattice $\Im(\mathbf{e}_i, \mathbf{o})$ through the deformation gradient **F**. Furthermore, if the deformation **F** maps the lattice back to itself, then the following relation holds true:

$$\mathbf{f}_i = \alpha_i^j \mathbf{e}_i \qquad \text{Equation 2.11}$$

for some 3 x 3 integer matrix α_i^j such that det $[\alpha_i^j] = 1$. Thus, a matrix **M** maps a Bravais lattice $\Im(\mathbf{e}_i, \mathbf{o})$ back to itself if and only if

$$M e_i = \alpha_i^j \mathbf{e}_j \qquad \text{Equation 2.12}$$

such that det $[\alpha_i^j] = 1$. Therefore,

$$\Gamma(\mathbf{e}_i) = \{\mathbf{H}: \mathbf{H}\mathbf{e}_i = \alpha_i^j \mathbf{e}_j, \text{ such that det } [\alpha_i^j] = 1\} \qquad \text{Equation 2.13}$$

represents a set of deformations that map a lattice back into itself and is termed a *symmetry group of the lattice*. This set $\Gamma(\mathbf{e}_i)$ contains both shears and rotations (i.e., it can be decomposed into a pure distortion and rotation, according to Polar Decomposition theorem [160]). Whereas, shears typically cause large distortions of

the lattice and are usually associated with plasticity (or slip), rotations do not lead to any distortions or strains in the lattice. Since in martensitic phase transformations observed in SMAs, plasticity is very limited, a smaller group $\wp(\mathbf{e}_i)$ may be defined that includes only the rotations, but excludes any distortive large shears:

$$\wp(\mathbf{e}_i)=\{\mathbf{R} \mid \mathbf{R} \text{ is a rotation and } \mathbf{Re}_i = \alpha_i^j \mathbf{e}_j, \text{ such that det } [\alpha_i^j] = 1\} \quad \text{Equation 2.14}$$

$\wp(\mathbf{e}_i)$ is called the point group of a lattice and is defined as a set of rotations that map a lattice back to itself. It can be shown that there are seven groups that arise in Bravais lattices (i.e., they describe seven different symmetries) and there are fourteen distinct Bravais lattices types. The relationship between the seven point groups is shown in Figure 2.12 and the total number of elements within each point group is indicated in the parenthesis.

Corollary: If we assume that the point group of the austenite phase is $\wp_a$ and the martensite point group is $\wp_m$, then $\wp_m$ is a subgroup of the austenite point group $\wp_a$, i.e., the austenite lattice has greater symmetry than the martensite lattice. Moreover, the number of variants of martensite that form upon transformation from austenite phase is given by:

$$N = \frac{\#\text{rotations in } \wp_a}{\#\text{ rotations in } \wp_m} \quad \text{Equation 2.15}$$

where the # rotations in either lattice are given in Figure 2.12. Consequently, the number of variants formed in the transformation from cubic B2 NiTi to monoclinic B19' NiTi are 24/2 = 12 variants. It should be noted that the 12 variants have the same crystal structure, i.e., B19' monoclinic ($P2_1/m$), but they are all oriented

differently with respect to the austenite lattice and hence called *correspondence variants of martensite* or simply *variants of martensite*. Also, each variant exhibits a specific *lattice correspondence,* which expresses the relationship between the unit cells (in terms of corresponding directions or planes) that describe the two lattices B2 and B19' (see section 2.1.4.3).

Result 3: Kinematic Compatibility

If we consider the deformation shown in Figure 2.13, where the lower portion of the body (Ω_2) is sheared in the opposite way compared to the upper portion (Ω_1) in such a way that the body remains unbroken, a straight reference line is kinked but remains unbroken. This is an example of continuous deformation, where the deformation gradient suffers a jump across the interface. Such deformations have been shown to describe coherent interfaces and hence are invaluable in studying martensitic transformations. If the deformation is a continuous one, Bhattacharya [119] argues that the deformation gradient jump cannot be arbitrary, since, if the body should not tear itself, then the interfacial plane should suffer the same deformation with respect to both portions of the body (i.e., Ω_1 and Ω_2), and this restricts the deformation gradient from being arbitrary.

If the deformation of the body in Ω_1 and Ω_2 is given by:

$$\begin{aligned} y &= \mathbf{F}\mathbf{x} + \mathbf{c} \qquad \mathbf{x} \in \Omega_1 \\ y &= \mathbf{G}\mathbf{x} + \mathbf{d} \qquad \mathbf{x} \in \Omega_2 \end{aligned} \qquad \text{Equation 2.16}$$

where **F**, **G** are constant matrices and define the deformation gradient in Ω_1 and Ω_2, respectively, and **c**, **d** are constant vectors, then **F** and **G** must satisfy [119]:

$$\mathbf{F} - \mathbf{G} = \mathbf{a} \otimes \hat{\mathbf{n}} \qquad \text{Equation 2.17}$$

where $\mathbf{a}$, $\hat{\mathbf{n}}$ are some vectors. Moreover, the interface must be a plane with a reference normal $\hat{\mathbf{n}}$ and this condition is known as *kinematic compatibility condition*. This is also known as the *invariant plane condition*, since for any vector $\mathbf{v}$ lying on the interface (i.e., on the invariant plane), thus satisfying $\mathbf{v} \cdot \hat{\mathbf{n}} = 0$, we see that:

$$\mathbf{Fv} - \mathbf{Gv} = (\mathbf{a} \otimes \hat{\mathbf{n}})\mathbf{v} = \mathbf{a}(\mathbf{v}.\hat{\mathbf{n}}) = 0 \Rightarrow \mathbf{Fv} = \mathbf{Gv} \qquad \text{Equation 2.18}$$

which suggests that the vector $\mathbf{v}$ is deformed equally by $\mathbf{F}$ and $\mathbf{G}$, i.e., the plane $\hat{\mathbf{n}}$ is an *invariant plane*.

Result 4: Martensitic phase transformation: Bain or Transformation matrix

As specified earlier, the martensitic transformation involves a diffusionless solid-solid phase transformation where the austenite lattice stable at high temperature changes its structure to a martensitic lattice stable at low temperature; one can obtain this transformation by deformation only without any rearrangement of the atoms. If $\{\mathbf{e}_1^a, \mathbf{e}_2^a, \mathbf{e}_3^a\}$ and $\{\mathbf{e}_1^m, \mathbf{e}_2^m, \mathbf{e}_3^m\}$ represent the lattice vectors of the austenite and the martensite lattices, respectively, we can describe the transformation between the lattices using a matrix $\mathbf{U_1}$ (also called *Bain* or *transformation matrix)* such that it describes a homogenous deformation that maps the martensite lattice to the austenite lattice as:

$$\mathbf{e}_i^m = \mathbf{U}_1 \mathbf{e}_i^a \qquad \text{Equation 2.19}$$

Thus, $\mathbf{U_i}$ (I = 1 - 12) describe the transformation matrices of the variants of martensite.

2.1.4.3 Twinning and Twins in NiTi

The Bain transformation matrices $\mathbf{U}_i$ (for all the 12 martensite variants) are given in Figure 2.14, assuming that the lattice constants are a = 2.889 Å, b = 4.12 Å, c = 4.622; β = 96.8° [161]. The variables α, γ, δ, and ε depend on the lattice geometry as follows [119]:

$$\alpha = \frac{1}{2\sqrt{2}a_0}\left(\frac{c(c+\sqrt{2}a\sin\beta)}{\sqrt{2a^2+c^2+2\sqrt{2}ac\sin\beta}}+b\right);\quad \gamma = \frac{1}{a_0}\left(\frac{a(c\sin\beta+\sqrt{2}a)}{\sqrt{2a^2+c^2+2\sqrt{2}ac\sin\beta}}\right)$$
$$\delta = \frac{1}{2\sqrt{2}a_0}\left(\frac{c(c+\sqrt{2}a\sin\beta)}{\sqrt{2a^2+c^2+2\sqrt{2}ac\sin\beta}}-b\right);\quad \varepsilon = \frac{1}{\sqrt{2}a_0}\left(\frac{ac\cos\beta)}{\sqrt{2a^2+c^2+2\sqrt{2}ac\sin\beta}}\right) \qquad \text{Equation 2.20}$$

It should be noted that one can rotate the parent austenite lattice through some rotation **R** and then transform it to any one of the 12 martensite variants by applying the corresponding *Bain transformation matrix,* $\mathbf{U_i}$. Since all the 12 variants are related by symmetry, they all possess the same energy:

$$\varphi(\mathbf{U_1},\theta) = \varphi(\mathbf{U_2},\theta) = \ldots = \varphi(\mathbf{U_N},\theta) \qquad \text{Equation 2.21}$$

Given that there are 12 variants possible when the austenite transforms to martensite upon cooling, we will first study a deformation involving only two variants (since an interface is necessarily formed between two surfaces only), i.e., we seek to find a deformation **y** such that the deformation gradient in one part of the body Ω_1 (martensite *I*) and the deformation gradient in the other part of the Ω_2 (martensite *J*) is given as follows:

$$\begin{aligned} \nabla \mathbf{y} &= \mathbf{Q_1 U_1} \qquad in \quad \Omega_1 \\ \nabla \mathbf{y} &= \mathbf{Q}_2 \mathbf{U}_2 \qquad in \quad \Omega_2 \end{aligned} \qquad \text{Equation 2.22}$$

where $\mathbf{Q_1}$ and $\mathbf{Q_2}$ are constant rotations, and $\mathbf{U_I}$ and $\mathbf{U_J}$ are given in Figure 2.14. Although the deformation gradient suffers a discontinuity across the interface, it has to satisfy the kinematic compatibility condition:

$$\mathbf{Q_1 U_1} - \mathbf{Q_2 U_2} = \mathbf{b} \otimes \hat{\mathbf{n}} \qquad \text{Equation 2.23}$$

where $\mathbf{b}$ and $\hat{\mathbf{n}}$ are some vectors, and the interface between the two martensite variants is a plane described by the normal $\hat{\mathbf{n}}$. This can be rewritten as:

$$\mathbf{Q U_1} - \mathbf{U_2} = \mathbf{a} \otimes \hat{\mathbf{n}} \qquad \text{Equation 2.24}$$

where $\mathbf{Q} = \mathbf{Q_2}^{\mathbf{T}} \mathbf{Q_1}$ and $\mathbf{a} = \mathbf{Q_2}^{\mathbf{T}} \mathbf{b}$, and the above equation is called the *twinning equation* [119], since it can be shown that the above equation describes a deformation where the lattice on one side can be obtained by either a *simple shear* or *rotation* of the lattice on the other side, and this planar defect in the crystal is termed as a *twin* [119]. Thus, the twinning elements with respect to the martensite lattice, viz., *twinning shear s, shear direction* η_1 and the *twin plane* K_1, are given by:

$$s = |\mathbf{a}| \left| \mathbf{U}_\mathbf{J}^{-1} \hat{\mathbf{n}} \right| \qquad \eta_1 = \frac{\mathbf{a}}{|\mathbf{a}|} \qquad K_1 = \frac{\mathbf{U}_\mathbf{J}^{-1} \hat{\mathbf{n}}}{\left| \mathbf{U}_\mathbf{J}^{-1} \hat{\mathbf{n}} \right|} \qquad \text{Equation 2.25}$$

When the twinning Equation (2.22) is solved completely (for certain conditions discussed in [119]), i.e., for each given $\mathbf{U_I}$ and $\mathbf{U_J}$, solving for $\mathbf{Q}$, $\mathbf{a}$, $\hat{\mathbf{n}}$ that satisfy Equation (2.22), one obtains two distinct solutions, i.e., if the variants *I* and *J* form a twin, they form two different kinds of twins. In other words, according to Bhattacharya [119], for every twin, there is a reciprocal twin that connects the same

set of variants. These solutions also lead to the classification of twins into three types, namely: *Type I* (where the twinning plane is rational and the shearing direction has irrational indices), *Type II* (where the twinning plane is irrational and the shearing direction has rational indices) and *Compound twins* (where both the twinning plane the shearing directions have rational indices). In this manner, one can choose different combinations of variants and solve the twinning Equation (2.22) and calculate all the (theoretically) possible twins and twinning elements.

For example, in the Ni-Ti system, if we solve the twinning Equation (2.22) to compute the possible twins between variant 1 and the remaining variants 2 through 12 that may arise during a cubic – monoclinic transformation, we find that four distinct twinning modes are possible, as shown in Figure 2.16. Each mode consists of a *Type I* and *Type II* twin or two *Compound twins*. Among the eight possible twins (or four twinning modes) and the corresponding twinning elements listed in Figure 2.16 and Figure 2.17, only the twins that are listed in Table 2.2 have been observed experimentally to date (refer also to [47, 119, 163]. Additionally, the *lattice correspondence* between each of the 12 B19' martensite variants and the B2 matrix is given in Figure 2.15.

Based on the calculations of Equation (2.24), it has been shown that variant 1 can form twins with variants 2, 3, 4, 5, 8, 9 and 11; however, it cannot form twins with variants 6, 7, 10 and 12 unless the lattice constants satisfy some stringent conditions:

$$\delta(\gamma - \alpha + \delta) - \varepsilon^2 = 0 \qquad \text{Equation 2.26}$$

which is a very special criterion that is typically not satisfied by many materials. Special materials that do exhibit such twins are termed *non-generic* twins [170]. If one repeats the above calculations beginning with different variants, the various twinning possibilities that arise from such computations are listed in Figure 2.18.

Table 2.2 Twins observed experimentally in B19' martensite [119].

Mode	Twin type	Observed in experiments
Mode A	(001) Compound (100) Compound	**Yes** [65, 164-169]
Mode B	{011} Type I	**Yes** [164, 165, 168, 169]
	<011> Type II	**Yes** [55, 56, 65, 67, 165, 166, 168, 169]
Mode C	{111} Type I	**Yes** [67, 68, 168, 169]
	<211> Type II	*No*
Mode D	{-111} Type I	**Yes** [161, 164-166, 168, 169]
	<-211>Type II	*No*

The twins obtained by solving the twinning equations considered only a single twin interface; however, in materials such as NiTi [168, 169] and Cu-Al-Ni [119]., many parallel twin planes that separate alternating regions of two variants are observed; these microstructures are termed as *twin laminates* or *fine twins* (see also Figure 2.19).

Additionally, *crossing twins*, such as those illustrated in Figure 2.20 [119], are observed in NiTi (see also Figure 2.19) ; they are formed when a twin plate zigzags through a region of *twin laminates* (see Table 2.3). The important features of this microstructure are its four-fold corner, where four interfaces that separate four variants meet. The entire microstructure can be reproduced by replicating such a four-fold

corner. This type of *crossing twins* have been incontrovertibly verified in NiTi by Nishida *et al.* [168, 169]. In their high-resolution TEM images, Nishida *et al.* [168, 169] shows that the twin boundaries are sharp and remain straight even at the corner. Figure 2.19 also shows that the interface alternates between *Type I* and *Type II* twins (either can be substituted with a *compound twin*) as shown in Figure 2.20.

Table 2.3 Twin crossings in NiTi B19' [119, 168, 169].

Type I twin	Type II twin
{100} Compound	<011>
{011}	{001} Compound
{111}	<011>
{-111}	<011>

2.1.4.4 Classification of twin types

When one cools the austenite B2 phase past the M_f temperature, the martensite that forms is self-accommodated (discussed subsequently), i.e. no shape-change occurs. However, at a microstructural level and at the atomic level, the structure has undergone a tremendous change. The crystal structure has changed from B2 cubic to B19' monoclinic structure; B19' is a distorted orthorhombic B19 structure. The martensite now consists of all the 12 variants of martensite that can form from austenite due to group-sub-group symmetry considerations. These 12 variants are arranged in such a way that each variant of a group of variants accommodate the large strains due to the other variants and in total effect, the net macroscopic strain is zero, i.e., no shape change. The variants themselves are not simply arranged, they bear twin relationship between different variants, i.e., a set or sets of variants are related by

different modes of twins. Each of the four twinning modes, briefly named A, B, C and D, is made of either Type I twin or Type II twin or compound twins. Based on their physical origin, these twins are further subject to classification as listed in Figure 2.21 [158]; the relevant ones being: (a) *lattice-invariant twin*, (b) v*ariant accommodation twin* and (c) *deformation twin*.

Lattice-invariant twin forms without any change in the crystal structure of the martensite. When the variants of martensite are accommodated in such a way that the elastic strain due to one set of variants is accommodated by the other set, then the twinning plane is a *accommodation twin*. *Deformation twins* have no solution in the phenomenological theory of twinning and form only upon deformation. If the stress for yielding is greater than the stress for twinning under deformation, then the material deforms by deformation twinning.

2.1.4.5 Austenite-martensite interface

When the martensite phase forms or grows within the austenite matrix, the austenite-martensite interface, also known as *habit plane*, is typically an irrational or high index plane that is dependent on material. It should be noted at the outset that the notion of *habit plane* is adopted from the steel literature, where the martensitic transformation is accompanied by considerable plastic deformation and the microstructure (including *habit plane*) is frozen intact [119]. The austenite-martensite interface is not reversible upon unloading or removal of external stress. Transposing this notion to Ni-Ti shape memory alloys that exhibit thermoelastic martensitic transformation can be very misleading for many reasons [119]:

(a) The martensitic transformation is not accompanied by plastic deformation and, subsequent to the transformation, the newly formed "microstructure" can change freely, since the interfaces are mobile.

(b) austenite-martensite interfaces are therefore transient or metastable states and thus the concept of *habit plane* is irrelevant.

(c) As will be discussed later, either during the deformation of thermally-induced martensite (TIM, that forms when the material is cooled below M_f) or stress-induced martensite (martensite formed when external stress is applied on austenite), only single-variants are preferred states either due to detwinning of TIM or due to the growth of single-variant martensite that accommodates the maximum shape change accompanying the external stress.

(d) As will be discussed shortly, Ni-Ti theoretically has 192 austenite-martensite interfaces and not 24 as many assume in the literature [119]; notwithstanding, only 24 interfaces have been identified to date.

Materials where a planar interface separate the austenite phase and exactly one variant of martensite phase are very rare; only Ti-29%Ta [171] and Ti-Ni-Cu [119] alloys have this exact austenite-martensite interfaces. Typically, the interface is between austenite on one side and fine twins of two variants of martensite on the other, the interface being not atomically sharp, as shown in Figure 2.22 [119].

The twins produce a uniform deformation gradient on an average with a continuous deformation across the interface. These conditions can be represented mathematically as below [119]:

$$(a)\mathbf{A}-\mathbf{B}=\mathbf{a}\otimes\hat{\mathbf{n}}$$
$$(b)(\lambda\mathbf{A}+\mathbf{(1}-\lambda\mathbf{)B)}-\mathbf{C}=\mathbf{b}\otimes\hat{\mathbf{m}} \qquad \text{Equation 2.27}$$

where **A** and **B** are deformation gradient in martensite variants *I* and *J*, respectively, that can form an interface, and **a**, **b** and $\hat{\mathbf{m}}$ are some vectors, and $0 \le \lambda \le 1$. Equation (2.27) can be rewritten as follows [119]:

$$(a)\mathbf{QU_J}-\mathbf{U_I}=\mathbf{a}\otimes\hat{\mathbf{n}}$$
$$(b)\mathbf{Q}'\mathbf{(}\lambda\mathbf{QU_J}+\mathbf{(}1-\lambda\mathbf{)U_I)}=\mathbf{I}+\mathbf{b}\otimes\hat{\mathbf{m}} \qquad \text{Equation 2.28}$$

where **Q'**, **Q** are rotation matrices, $\mathbf{U_I}$ and $\mathbf{U_J}$ are Bain matrices given in Figure 2.14, **a**, **b**, $\hat{\mathbf{n}}$ and $\hat{\mathbf{m}}$ are some vectors. Equation 2.28 (a) is the familiar twinning equation, while Equation 2.28 (b) is called the *austenite-martensite interface equation* [119]. It can be shown [119] that Equation 2.28 (b) simplifies as:

$$\mathbf{RSB}=\mathbf{I}+\mathbf{p}\otimes\mathbf{d} \qquad \text{Equation 2.29}$$

where **B** is the Bain distortion, **S** is a lattice-invariant shear and **R** is a rotation; which is in essence the statement of the phenomenological theory of martensite (PTM) [172-175]. Equation (2.28) can be solved to calculate the *austenite-martensite interfaces* and it is shown by [119] that for each pair of variants *I* and *J*, it is possible to form up to *eight* austenite-martensite interfaces. It can be further shown that it is not possible to form the austenite-martensite interface using twins of Mode A and D (Figure 2.16), whereas, 96 austenite-martensite interfaces can be formed using twins of Mode B and an additional 96 using twins of Mode C. Thus, there are 192 distinct austenite-martensite interfaces that can form theoretically, in particular Ti-49.8 at.% Ni [119,

162, 163, 176]. As alluded earlier, while 192 *habit planes* can be found for a particular Ti-49.8 at.% Ni alloy, only 24 have been unambiguously observed in experiments. Hane and Shield [162] further point out that while Ti-49.8 at.% Ni theoretically exhibits only 192 *habit planes*, for other choices of lattice parameters, a general Ti-Ni alloy may possess as many as 528 *habit plane* solutions. Since one of the reasons that Ti-Ni is a good contender as a shape memory material is the large number of variants, i.e., more number of ways available for deformation, they recommend further studies to find out the lattice parameter(s) that may allow more *habit planes* and hence better shape memory properties.

As indicated above, the austenite-martensite transformation creates a shape-memory material where the martensite variants arrange themselves in such a fashion that no macroscopic change in shape of the specimen occurs. However, at a microstructural level, the structure has undergone a tremendous change, i.e., it exhibits deformation. However, these 12 variants are arranged in such a way that each variant of a group of variants accommodate the large strains due to the other variants in such a way that there is no shape change at a macroscopic level. This is known as *self-accommodation*. A *self-accommodating microstructure* is a coherent arrangement of martensitic variants occupying a region whose boundary suffers no displacement with respect to the austenite; a material forming such a microstructure is called a *self-accommodating material* [177]. It should be noted that not every material that undergoes martensitic transformation is self-accommodating. Saburi and Wayman [178] have emphasized the importance of self-accommodation to the SME and noted that it plays a crucial role in rendering the transformation thermoelastic or reversible.

Specifically, they argue that only in a self-accommodating material, martensite can nucleate in the interior of a specimen (surrounded by a sea of austenite) in a coherent, stress-free manner. Bhattacharya [177] shows that the necessary and sufficient condition for a material to exhibit self-accommodation is dependent on the symmetry of the parent lattice, although it is the martensite variants that participate in forming the microstructure. It is further shown that for cubic materials the requirement is simply volume preservation. In Ni-Ti, the volume decreases by a very small amount during the martensitic transformation from austenite, ~0.023% (calculated) [177].

A clarification is due with regards to the literature pertaining to self-accommodating structures proposed by various authors in Ni-Ti alloys. These structures include *wedge*, *triangle*, and *diamond* (which is nothing but two wedges back to back), and are shown in Figure 2.23. However, calculations by Bhattacharya [177] and James and Hane [176] show that wedges and diamond structures are not possible in Ni-Ti.

Saburi and Wayman [178] have proposed a diamond microstructure in Ni-Ti and call this morphology a *self-accommodating plate group*. According to them, a *plate group* is formed by four *habit planes* symmetrically arranged about a pole (typically around {110} family of planes in cubic austenite) , i.e., $\hat{\mathbf{m}}$ in Equation (2.28) is close to some permutation of {1, ±1, 0}(there are six permutations possible in cubic austenite) in such a manner that the average shape deformation is nearly equal to the identity matrix [176, 177]. Additionally, James and Hane [176] point out that often in the literature a micrograph of certain martensitic microstructure is described by corresponding strain matrices and the argument of self-accommodation is justified

on the basis that the weighted average (with respect to four variants of a plate group) of the respective strain matrices sums to nearly zero. They argue that the diamond morphology is possible only for very special lattice parameters and that "*the strains listed in the literature do not correspond to the picture that is drawn*" [176]. According to their calculations, these strains would necessarily represent a microstructure that required either gaps or exhibit interpenetration of matter and hence incompatible. Bhattacharya [177] and James and Hane [176] also point out that the analysis of *self-accommodating plate group* verifies only the first of the three compatibility conditions and suggest that there is no necessity for these special microstructures to satisfy the remaining two. Miyazaki *et al.* [55, 56] similarly propose triangle morphology to model microstructures in Ti-Ni SMA. However, Hane and Shield [162] show that the proposed microstructure is not an energy minimizing structure. Evidently, the observed microstructures may be more complicated than those analyzed in the literature. So, the argument that these special microstructures are desirable for the manifestation of shape-memory effect should be taken with a certain caution, since there is compelling evidence that such structures are not possible in Ni-Ti alloys. Further clarification on these complicated microstructures remains to be solved.

Summary: Martensitic transformations were described as being displacive solid state transformations requiring no long range atom movements, in contrast to long range diffusional transformations that require atomic migration that is dependent on both time and temperature. In displacive transformations the atoms rearrange into a stable crystal lattice structure in a cooperative manner without changing the

chemical nature of the matrix; this displacive reaction is a time-independent transformation with the motion of the interface limited only by the speed of sound in the solid. These transformations are athermal due to their time-independent nature, but are typically dependent on the temperature in a linear fashion. While the terms austenite and martensite originally referred to the high-temperature parent phase and low temperature transformed product phase in steels, they are now generalized to identify phases participating in a specific class of transformation rather than the material itself. Martensitic transformations are first order transformations, in that they are exothermic reactions, which release heat when martensite forms as a result of the transformation. Moreover, materials undergoing these transformations exhibit hysteresis behavior and there is a temperature range within which both austenite and martensite phases co-exist. The martensitic phase volume fraction increases as the temperature is reduced and vice versa, with the volume fraction being independent of time. The martensite phase inherits the composition and the atomic order of the parent phase, and in fact, austenite-martensite maintains a certain group-subgroup point symmetry relationship.

At the microscale, the transformation crystallography may be envisioned as a combination of Bain strain and lattice-invariant shear. Bain stain is the lattice deformation necessary to produce the new crystal lattice structure from the parent lattice and the lattice invariant shear is an accommodation process, as explained in what follows. While martensite in steel undergoes both volumetric and shape changes, the martensite in SMA like Ni-Ti undergoes only shape change (the volume changes are extremely low, -0.003%) and the martensite accommodates this shape

change without either tearing the matrix or interpenetrating it by introducing either internal slip or twinning. While slip is a permanent process, twinning accommodates shape changes (it cannot accommodate volume changes) in a reversible manner, thus being the dominant accommodation process in shape memory effect as discussed in the next section.

Until now, the nature of thermoelastic martensitic transformations, its thermodynamics, and its kinetics have been discussed. This was followed by the introduction of *martensite microstructure* that is a consequence of energy minimization of the austenite-to-martensitic transformation. Thereupon, twinning and twins in Ni-Ti SMA were shown to be the dominant deformation mode as an outcome of energy minimization. Finally, the internally twinned martensite interface, the austenite-martensite interface (*habit plane*) and the concept of self-accommodation was highlighted. All of these features were discussed with respect to the B2 (austenite) to B19' (martensite) transformations only. As pointed out earlier, in some cases, B2→R-phase martensitic transformation also occurs. However, before discussing the B2→R-phase transformation, based on the above concepts, the main properties of Ni-Ti materials such as shape memory and superelasticity will be dealt with.

2.1.5 Effect of stress on the martensitic transformation

It has been shown that the martensitic transformations can be induced at temperatures greater than M_s by applying stress to the material [23, 141]. As early as 1932, it was pointed out by Scheil [179] that the stress required to induce a martensitic

transformation decreased with decreasing temperature until none is needed at M_s. Later, Burkart and Read [8] and Patel and Cohen [180] tried to quantify the effects of the stress on the martensitic transformation. The effects of an applied stress aids in elucidating additional information on the nucleation kinetics in martensitic transformations. External applied stress typically can affect the nucleation in several ways [181]:

(a) hydrostatic pressure alters the equilibrium temperature T_o according to the Clausius-Clapeyron relation,

(b) shear stress interacts with the stress fields of the sub-critical nuclei and may either favor or impede their subsequent growth, and

(c) plastic deformation due to the applied stress may introduce extra nucleation sites or even destroy the existing ones.

Patel and Cohen have extensively considered (a, b) cases in their now famous work [180], where they have considered both the cases of uniaxial tension and compression stress that induce shear as well as volume stresses in the specimen. They essentially equate the work done by an external stress on the system to the change of the free energy of the system. The work done on a system by an applied stress that produces shape strain is a function of stress and the orientation of the transforming martensite plate, and is given by [127]:

$$W = \Delta G_{\sigma}^{a \to m} = \tau \gamma_0 + \sigma \varepsilon_0 \qquad \text{Equation 2.30}$$

where τ is the shear stress (resolved along the transformation shear direction in the martensite habit plane) and σ is the normal stress (resolved perpendicular to the habit

plane), and ε_o and γ_o are the dilatational component of the transformation shape strain and the transformation shear strain (along the transformation shear direction in the habit plane), respectively. For uniaxial tension and compression, one can derive (using Mohr circle calculations or otherwise) the resolved shear and normal stresses in terms of the angle between the specimen axis and the normal to any potential habit plane (θ), given by:

$$\tau = \frac{1}{2}\sigma_a \sin 2\theta, \qquad \sigma = \pm\frac{1}{2}\sigma_a(1+\cos 2\theta) \qquad \text{Equation 2.31}$$

where σ_a is the absolute value of the applied stress (tension or compression). Thus,

$$W = \Delta G_{\sigma}^{a\to m} = \frac{1}{2}\sigma_a[\gamma_0 \sin 2\theta \pm \varepsilon_0(1+\cos 2\theta)] \qquad \text{Equation 2.32}$$

When a martensitic transformation begins by stressing a polycrystalline parent austenite phase (with random texture), a martensite plate whose orientation maximizes '*W*' forms first [182]. The maximum orientation effect is obtained for the transformation shear system for which $dW/d\theta$ vanishes, thus giving the condition for the direction of the applied stress to the shear system that is most prone to transformation:

$$\tan 2\theta = \pm\frac{\gamma_0}{\varepsilon_0} \qquad \text{Equation 2.33}$$

Analyzing Equation (2.30), we find that by convention, σ is positive for tensile stress and negative for compressive stress, $\varepsilon_0 = \Delta V/V$ is negative in most martensitic transformations (except for typical ferrous martensites). Thus, the second term $\sigma\varepsilon_0$ depends upon the sign of the stress, while the sign of the first term $\tau\gamma_0$ is always

positive, since when stress is applied to the specimen, the habit plane that is optimally oriented (i.e., that best accommodates for relieving the stress) is selectively formed throughout the specimen regardless of the sign of the applied stress. This implies that the shear stress component always aids the transformation, whereas the normal component may aid or hinder the transformation. For the case of hydrostatic pressure p ($p > 0$), $\Delta G_{\sigma}^{a \to m} = -p\,\varepsilon_0$, and thus the sign of ΔG depends on ε_0, volume change. To date, there have been restricted studies on the effect of hydrostatic pressure on the transformation behavior in SM alloys [183-185], especially Ni-Ti [186-189]. Jacobus *et al.* [188] studied the effect of stress state (or hydrostatic pressure, see Figure 2.24) on the character and extent of the stress-induced martensitic transformation in polycrystalline Ni-Ti shape memory alloy and calculated the volume change as being between -0.0037 and –0.0031. This result agrees exceptionally well with the theoretical value of –0.0034 calculated from the lattice constants.

(a) Clausius-Claperyon Equation

Thermodynamically, alloy phases undergoing diffusionless transformations may be considered as one-component systems and the free energies of the martensite and the austenite phases can be schematically represented by Figure 2.25a.

While the individual free energies as a function of temperature G(T) are not known, the change in free energy, $\Delta G^{a \to m}$(T) can be derived as follows [127]:

$$\Delta G^{a \to m} = G^m - G^p = \Delta H^{a \to m} - T\Delta S^{a \to m} \qquad \text{Equation 2.34}$$

where $\Delta H^{a\to m}$ and $\Delta S^{a\to m}$ are the enthalpy and entropy of the transformation. At equilibrium temperature T_o, $\Delta G^{a\to m} = 0$. $\Delta H^{a\to m}$ is typically measured using calorimetric methods, and T_o is estimated using the following [190, 191]:

$$T_o = \frac{M_s + A_s}{2} \quad or \quad T_o = \frac{M_s + A_f}{2} \qquad \text{Equation 2.35}$$

However, there has been sufficient controversy on the calculation of T_o with regards to whether T_o is greater or less than A_f [127, 190-193], also see [124]. Hence, it is possible to compute [127]:

$$\frac{\partial \Delta G^{a\to m}}{\partial T} = \frac{\Delta H^{a\to m}}{T_0} = \Delta S^{a\to m} \qquad \text{Equation 2.36}$$

The change in entropy, $\Delta S^{a\to m}$, is an important term, since it gives the rate of change of free energy as one deviates from the equilibrium temperature T_o and, additionally, it is every useful in quantifying the transformation behavior when an applied stress acts on the specimen. At the critical stress, σ_c, the parent austenite will begin to transform to martensite in order to accommodate the strain and this is represented as the equality between the Gibbs free energy per unit volume of the austenite (G_A) and the martensite (G_M) phases. Assuming that $\Delta G^{a\to m}(T)$ and $\Delta G_\sigma{}^{a\to m}(T)$ are linear functions, we can assume that the slopes of these functions are equal [127]:

$$\frac{\partial \Delta G_\sigma^{a\to m}}{\partial T} = \frac{\partial \Delta G^{a\to m}}{\partial T} = \frac{\Delta H^{a\to m}}{T_o} = \Delta S^{a\to m} \qquad \text{Equation 2.37}$$

Also, from Equation 2.32 ,

$$\frac{\partial \Delta G_\sigma^{a\to m}}{\partial \sigma_a} = \frac{1}{2}[\gamma_0 \sin 2\theta \pm \varepsilon_0(1+\cos 2\theta)] = \varepsilon_{a\to m} \qquad \text{Equation 2.38}$$

where $\varepsilon_{a\to m}$ is the total strain of the transformation. Thus, we have [127]:

$$\frac{\partial T_o}{\partial \sigma_a} = \frac{\partial T}{\partial \Delta G^{a\to m}} \frac{\partial \Delta G_\sigma^{a\to m}}{\partial \sigma_a}$$
$$= \frac{T_o}{\Delta H^{a\to m}} \frac{\partial \Delta G_\sigma^{a\to m}}{\partial \sigma_a} \frac{1}{2} [\gamma_0 \sin 2\theta \pm \varepsilon_0 (1+\cos 2\theta)] \varepsilon_{a\to m} \qquad \text{Equation 2.39}$$
$$= \frac{T_o \varepsilon_{a\to m}}{\Delta H^{a\to m}} = \frac{\varepsilon_{a\to m}}{\Delta S^{a\to m}}$$

Thus, we see that $\Delta G^{a\to m}$ is displaced as a function of stress to produce $\Delta G_\sigma{}^{a\to m}$, as shown in Figure 2.25b; its magnitude (of displacement) is inversely proportional to the transformational entropy. Thus, from a knowledge of $\Delta S^{a\to m}$, it is possible to calculate the stress effects on the transformation characteristics. Equation 2.39 may be rewritten as [127]:

$$\frac{\partial \sigma^{a\to m}{}_a}{\partial T_0} = \frac{\rho}{\varepsilon_{a\to m}} \frac{\Delta H^{a\to m}}{T_0} = \rho \frac{\Delta S^{a\to m}}{\varepsilon_{a\to m}} \qquad \text{Equation 2.40}$$

where the equation has been corrected for density (ρ) to maintain consistent units, while adapting the DSC measurements, which measures energy/mass, instead of energy/volume. This is the well known Clausius-Claperyon equation that quantifies the effect of stress on the martensitic transformation for an uniaxial stress loading condition. It has been used, particularly, to calculate the magnitude of reversible strains accompanying the superelastic Nitinol. However, using the T_o values given by Equation (2.35) in Equation (2.40) has led to large errors (60%) in the estimation of enthalpies [190, 194]. Recently, McKelvey and Ritchie [194] have provided an alternative approach in estimating the reversible transformation strains of a uniaxially

loaded specimen in tension using the Clausius Claperyon equation by avoiding the calculation of the equilibrium temperature, T_o:

Assuming that at some critical stress, σ_c, the parent austenite will begin to transform to martensite in order to accommodate the strain, and this is represented by Equation (2.41a) below. At equilibrium, Equation (2.41b) is valid.

$$(a) \quad G_A = G_B; \qquad (b) \quad \partial G_A = \partial G_B \qquad \text{Equation 2.41}$$

By utilizing the Gibbs-Duhem equation, the partial Gibbs free energies are given by:

$$\begin{aligned} &-S^a dT - \varepsilon^a \, d\sigma = -S^m dT - \varepsilon^m \, d\sigma \\ &\Rightarrow \frac{d\sigma}{dT} = \frac{-\Delta S}{\varepsilon^{a\to m}} = \frac{-1}{\varepsilon^{a\to m}} \frac{\Delta H}{T} \end{aligned} \qquad \text{Equation 2.42}$$

where S, H are the molar entropy and enthalpy per unit volume, respectively, ε^i is the strain in either phase, and $d\sigma/dT$ is called the *stress rate*, a very important descriptor of superelastic behavior and typically varies between 3 to 20 MPa/°C [195]. At constant pressure, utilizing the relationship between the enthalpy and entropy leads to the last line in Equation (2.42). McKelvey and Ritchie [194] call this an alternative expression for the Clausius-Claperyon equation, where the conventional pressure and volume terms are replaced with the conjugated variables stress and strain. Again, correcting for the units (for using the enthalpy values from the DSC) and integrating the Equation (2.42):

$$\frac{d\sigma}{dT} = \frac{-\rho}{\varepsilon^{a\to m}} \frac{\Delta H}{T} \Rightarrow \sigma_c - \sigma_0 = \frac{-\rho \Delta H}{\varepsilon^{a\to m}} \ln\left(\frac{T}{T_0}\right) \qquad \text{Equation 2.43}$$

(b) Orientation dependence of the transformation: The transformation strain alluded to earlier also depends on the orientation of the specimen. Otsuka *et al.* [196] give the following relationship for the transformation strain [124, 197, 198]:

$$\varepsilon_c = \sqrt{(m_1^p \sin\chi)^2 + 2m_1^p \sin\chi\cos\lambda + 1} - 1 + m_1^n \sin^2\chi \qquad \text{Equation 2.44}$$

where m_1^p and m_1^n are the shear (γ_0) and dilatational component (ε_0), respectively, of the transformation strain (also called as invariant plane strain) included in Equation (2.30), see Figure 2.26. The angles χ and λ are the angles between the tensile axis and the habit plane (p_1), and the shape strain direction (d_1), respectively. In thermoelastic alloys, typically $m_1^n << m_1^p$ and $(m_1^p \sin\chi)^2 << 1$; thus yielding:

$$\varepsilon_c \sim m_1^p \sin\chi\cos\lambda \qquad \text{Equation 2.45}$$

2.1.6 Pseudoelasticity and Superelasticity

The discussion on pseudoelasticity will follow that of Duerig and Zadno [195]. Duerig and Zadno define that any non-linearity in the unloading portion of the stress-strain curve is termed *pseudoelasticity*, see Figure 2.27.

The curve in Figure 2.27 for 50.8-NiTi indicates that the material recovers completely a total strain of nearly 6% upon unloading, whereas, the curve for 55-NiTi recovers only 3.5% upon unloading. This second case of pseudoelasticity is termed as *superelasticity* and is perhaps the most useful manifestation of pseudoelasticity that has been exploited to date in a variety of applications [25, 31, 36, 38, 200]. Specifically, any pseudoelastic material that shows a plateau during unloading is termed *superelastic*. Pseudoelasticity may be caused through twinning or by stress-induced martensitic (SIM) transformation.

(a) Superelasticity

Wasilwski and Honma [201-204] were among the early workers who observed superelasticity in Ni-Ti alloys. Superelasticity typically occurs when a material is deformed above A_s, where external applied stress induces the transformation of the parent austenite phase to a martensitic phase. Normally, austenite is the stable phase under stress-free conditions, however upon the application of a critical stress, the austenite yields and starts transforming to the martensite phase at a constant stress (this 'plateau' stress is a strong function of temperature), thus producing a stress plateau. The plateau is a consequence of the martensite phase's ability to form variants during the transformation. The selection of the variants essentially depends on the loading direction and the crystal orientation or the texture (in the case of a polycrystalline specimen). Specifically, the particular variant of martensite activated is stress-induced based on which variant is oriented to accommodate the maximum strain due to the applied stress. At a certain strain value, the stress plateau terminates, and the new martensitic phase now elastically deforms according to the martensite modulus. However, this martensite becomes unstable upon the removal of the stress; hence during unloading, the martensite phase reverse transforms to the austenite phase and at zero load the material should be entirely austenitic with the specimen recovering its original undeformed shape (see Figure 2.28). Superelasticity typically occurs if the specimen temperature is between $A_f < T < M_d$. If the temperature is above M_d, the stress level needed to induce martensite is greater than the stress required to introduce slip in austenite and hence SIM does not occur. By contrast, if the temperature is below A_s, the SIM remains stable since austenite is not the stable

phase and hence, above A_f, the unloading plateau will not be observed. The temperature dependency of superelasticity is schematically shown in Figure 2.29. Between A_f and M_d, the yield stress to induce martensite (or the plateau stress) increases linearly with temperature, and the slope, $d\sigma/dT$ (*stress rate*) is given by the Clausius-Claperyon equation introduced earlier.

It should be noted that it is nearly impossible to observe SE in Ni-Ti single crystal alloys under solution-treated (ST) condition since the critical stress for slip is lower than the critical stress for SIM transformation [47]. Therefore, superelasticity is typically observed in single crystals for aged Ni-rich Ni-Ti alloys, where the critical stress for slip is increased due to precipitation hardening or by cold working (or proper thermomechanical treatment) of Ni-Ti alloys that introduce sufficient dislocation density and increase the critical stress for slip. The largest recoverable strains (elastic + SE) observed in polycrystalline Ni-Ti alloys to date is 11% and are typically less than 8%. Clearly, if the material is strained beyond a critical strain limit (beyond SE limit), slip will be introduced into the material, thus leading to unrecoverable plastic strains. While the effect of temperature on SE will be discussed in section 2.4.1, it should be noted that the total plastic strain (say after 8% tensile deformation of 50.8Ni-Ti cold worked to 40% and annealed at 375°C for 30 minutes) is dependent on the temperature, and it is a minimum within a narrow window of 60°C (10^oC to 70°C). While this 'useful' SE window may be raised using many thermomechanical treatments, the maximum range observed so far in Ni-Ti alloys has been less than 80°C [195].

(b) Pseudoelasticity by twinning

Reversible motion of twin boundaries leads to *twinning pseudoelasticity* [195]. In some materials, deformation of the austenite phase well above M_d (where SIM is not possible) leads to the formation of twins that are unstable and hence there is a driving force to return to the original condition by the shrinking or disappearance of the twins during unloading. This type of mechanical twinning perturbs the lattice ordering and is therefore different from conventional twinning; it is termed *pseudotwinning*. Upon unloading, the material attempts to return to the preferred lattice ordering by shrinking of the twins. This is depicted by the non-linear unloading of the stress-strain curve in Figure 2.27. Few other materials that are in their martensitic state also exhibit twinning pseudoelasticity (*martensitic pseudoelasticity*), where the deformation occurs by the motion of the martensite twin boundaries. Unlike the above case, conventional twin motion does not cause disorder. Nonetheless some driving force impels the twins to return to their original position upon unloading; the mechanism was not clear until recently (see the discussion in section 2.1.9) [3]. Both kinds of twinning pseudoelasticity appear to be minor effects that have little engineering value [195].

2.1.7 Shape memory effect: Origin and mechanisms

Otsuka and Ren [16, 47, 125, 205, 206] point out that both superelasticity and shape memory effect are characteristic of thermoelastic alloys. When the parent cubic austenite is cooled below M_f, the entire specimen undergoes martensitic transformation without any shape change that is achieved through self-accommodation

(as discussed in section 2.1.4.5 earlier). When such a self-accommodated martensite is deformed by an external stress, the material deforms through the motion of the twin boundaries, where one particular martensite variant, that is most favorably oriented to the applied stress, grows at the expense of other variants. If sufficient strain is introduced into the specimen, it is possible to produce a single crystal of the most favorably oriented variant of martensite; such deformation mechanism where several variants coalesce into a single variant is termed *detwinning* (see Figure 2.30). The twins here refer to both the boundaries between the martensite plates (habit plane variants, h.p.v) and the boundaries (correspondent variants, c.v.) within individual martensite plates. Subsequent heating of the specimen above A_f temperature transforms the material back to the original austenite phase due to lattice correspondence. Since the martensite can be transformed to a single crystal of the most favorably oriented variant with respect to the applied stress, the maximum recoverable strain is the same as that observed in the superelastic condition [18].

It has been proposed [16, 17] that the basic requirements for shape memory effect and superelasticity are: (a) the thermoelastic nature of the martensitic transformation, (b) ordering and (c) group-subgroup relationship between the parent austenite and the martensite (this condition leads to twinning) [119, 207]. The thermoelastic nature (as discussed in section 2.1.3) leads to a mobile boundary between the austenite and the martensite phases, small temperature hysteresis, and avoiding the introduction of irreversible slip, thus leading to a crystallographic reversibility of the transformation. It was argued that ordering or unique lattice correspondence confines the reverse transformation uniquely, thus guaranteeing the

reversibility of the thermoelastic transformation. Bhattacharya *et al.* [119, 207], propose a general group-subgroup relationship (see Figure 2.12) between the two phases as a condition for the transformation to be reversible. Otsuka and Ren [47] point out that while this is a necessary condition, it is not sufficient, since no SE and poor SME is observe in solutionized (ST) 50-NiTi, unless the material is thermomechanically treated; since slip is easily introduced in the ST condition, as discussed earlier.

The foregoing explanation of the shape memory effect may be summarized as shown in Figure 2.31. Figure 2.31a shows the behavior of a typical metal/alloy upon cooling or deformation, where irreversible slip is introduced after the initial Hookian elasticity of few percent (<1%); further heating does not result in a 'remembering' of the original shape. Figure 2.31b schematically illustrates the shape memory effect, where upon cooling, the self-accommodated twinned martensite variant structure is formed; further deformation leads to the formation of a 'single crystal' of the favorably oriented martensite variant through the movement of twin boundaries. Upon subsequent heating, the material 'remembers' the original shape and returns to the original austenite parent phase through lattice correspondence. Figure 2.32 schematically captures both the superelastic effect and the shape memory effect in Ni-Ti alloys in a stress-strain-temperature space [24, 208].

2.1.8 One-way, Two-way and All-round shape memory effect

The shape memory effect introduced in the previous subsection can also be termed '*one-way*' *shape memory effect*, since it spontaneously 'remembers' its original

parent shape when heated above a critical temperature, A_f. However, the material has to be deformed first to a new shape and the component recovers its original shape on heating; hence in order to start a new shape memory cycle, the materials should be deformed again. '*Two-way*' *shape memory* (TWSM) effect occurs when there is a spontaneous shape change of a material on both heating and cooling; i.e., the material remembers both the high temperature and the low temperature shape (as well as all the shapes in between these two extremes) [209]. In TWSM, no external force is required to achieve any shape change, and the specimen simply bends in two different ways upon heating or cooling. Notwithstanding its usefulness, TWSM strains are significantly less (~2-4%) compared to the 'one-way' shape-memory effect. Additionally, TWSM is not a natural behavior of the material; rather the material should be 'trained' to exhibit the TWSM through special thermomechanical processes. Perkins and Hodgson enumerate various applications of the TWSM in [209]. The first report of TWSM was by Wang and Buehler [210]. Subsequent reports [211, 212] described the phenomenon in more details for Ti-Ni and other SM alloys, where TWSM (also called as *reversible SME*) is obtained when the specimen is deformed severely below the M_s temperature. Later on, various processes were described to induce TWSM in the alloys, such as: plastic deformation, constraint aging, thermal cycling, etc. [213-215]. The idea is straightforward [47]: in order to train the material to remember the martensitic phase shape, certain martensite variants need to be selected, and since the martensitic transformation strongly interacts with stress, the external applied stress automatically selects specific variants that contributes a specific shape of the martensite. In other words, the fully self-accommodated martensite

selects specific variants upon loading; cycling through this process a few times repeatedly introduces the low temperature shape into the specimen and the alloy learns the microstructural pattern during the TWSM "training" [209]. Perkins and Hodgson [209] list five methods to leave some "reminders" of the deformed low temperature conditions (deformed martensite):

(a) Over-deformation while in martensitic condition: Cool the alloy below M_f and bend (or deform) it severely beyond the shape memory recoverable strain limit. When the specimen is heated above A_f, the material will not recover the original shape completely, however, if cooled below M_f again, the component moves partly toward the over-deformed shape.

(b) Shape memory (SME) cycling (Cool-Deform-Heat): Cool the alloy below M_f, deform below SM strain limit, heat to recover the parent phase shape – repeating this cycle for 5-10 times, the specimen begins to spontaneously change shape on cooling to trained, deformed geometry. The TWSM strain is ~ 1/4 or 1/5 (1-2%) of the training shape strain (6%).

(c) Pseudoelastic (PE) cycling (Load-Unload): Repeatedly load and unload the austenite phase at a temperature above A_f, but below M_d.

(d) Combined SME+PE cycling: Combining (b) and (c) above has been shown to be a very effective training schedule. It consists in deforming the parent austenite by introducing SIM, followed by a cooling cycle below M_f at constant strain induced in the sample. Subsequently, the specimen is heated to recover the original shape and this cycle is repeated a few times until TWSM behavior is manifested in the material upon cooling and heating.

(e) Constrained thermal cycling of deformed martensite: This is the most common and effective method used in training a SMA to exhibit TWSM and is relatively less elaborate than training (d). The sample is typically deformed below M_f leading to the development of stress-*biased* martensite due to the reorientation of several martensite variants. Subsequently, the sample is constrained in the deformed condition and heated to $T > A_f$ followed by thermal cycling between M_f and A_f several times. The sample is constrained in the original deformed configuration throughout the cycling schedule. Perkins and Hodgson [209] highlight that TWSM application has four intrinsic limitations: the typical reversible strain limit has a low bound (maximum observed for NiTi is ~4%), temperature hysteresis between heating and cooling transformation cycles, low transformation forces on cooling (more efficient in pushing during heating than cooling cycles), and a upper temperature limit where higher temperature application may eliminate the training memory through an 'all-out' annealing treatment.

Similar to the TWSM, another unique SM behavior termed '*all-round*' *shape memory effect* (ARSME) was discovered by Nishida *et al.* [216-218] in 1984; it is reported to be a particular case of TWSM effect. The similarity is with respect to the deflection in different directions upon heating and cooling cycling; however, the physical basis and the training schedule have been shown to be different from that of TWSM. The ARSME is achieved in Ni-Ti alloys with Ni concentration greater than 50.5 at.%, i.e., those alloys susceptible to precipitation upon aging. A typical cycling routine consists of aging the sample around 400°C (~ 50 hours) or 500°C (for 1 hr) in a constrained geometry (that is usually the high temperature shape). Upon aging,

coherent Ti_3Ni_4 intermetallic phase precipitates along the {111} plane of the parent phase creating a tensile stress normal to the habit plane as shown in Figure 2.42b. When a specimen of Ni-rich NiTi alloy is constrained in a bent geometry, tensile and compressive stresses arise on the outer and the inner surfaces, respectively. The bending stresses are thus relieved only when the precipitates form parallel and normal to the tensile and compressive stress, respectively. Such an arrangement was indeed confirmed by TEM studies [219-221] and is schematically shown in Figure 2.33. These precipitates create sufficient back-stress to create a deflection in the opposite direction when the specimen is released and cooled.

It should be noted that maximum reversible strains in ARSME are limited to ~1% and the higher Ni composition in Ni-Ti alloys utilized to precipitate Ti_3Ni_4 lowers the M_s and hence not particularly attractive for many applications.

2.1.9 Rubber-like effect and Pseudoelasticity

Although rubber-like behavior (RLB) is not found in Ni-Ti alloys, for the sake of completeness, it will be discussed in this section. This RLB is a type of *pseudoelasticity,* introduced in Section 2.1.6 and has been given several others names in the literature, such as *ferroelasticity* (due to some similarities with magnetism) or *twinning pseudoelasticity*. It should be duly noted that RLB is different from the two other kinds of pseudoelasticity: SIM transformation and pseudo-twinning (see Section 2.1.7). Even though RLB has been known since 1932 in many alloys such as Au-Cd, Au-Cu-Zn, Cu-Zn-Al, Cu-Al-Ni, the origin of such behavior and the influence of aging remained unsolved until a decade ago [2, 3, 9, 206, 213, 222-231].

It has been discussed in Section 2.1.7, that upon deformation of a thermally-induced martensite (whose microstructure is made up of several twin-related martensite domains exhibiting self-accommodation) and subsequent unloading to a stress-free state, the original domains do not revert back, thus leading to an irreversible strain that may be recovered completely only by heating the specimen above A_f. However, certain shape memory alloys in their stable or equilibrium martensitic state are known to exhibit strain recovery of a few percent upon unloading, even though no martensitic transformations have occurred, i.e., they can be deformed like a soft and pseudo-elastic rubber and hence a *rubber-like behavior* (RLB). Such phenomenon usually occurs in alloy martensites that are aged, although some alloys exhibit RLB without any need for aging. Martensite aging is also known to cause martensite stabilization (increase in A_s) that may be detrimental in actuator applications that depend on the SME. The puzzling questions naturally were: why should there be a restoring force if there is no phase transformation involved, and what is the role of aging that leads to martensite stabilization and RLB even though the average martensite structure (as revealed by XRD results) does not show any detectable changes? Ren and Otsuka [3], based on sensitive electrical resistivity measurements, proposed that this behavior does not involve any long-range order (LRO) changes, rather, it arises due to the atomic rearrangements at a sub-lattice level of the imperfectly order alloy during martensite aging. They based their conclusions on the principle of symmetry-conforming short-range ordering (SRO), which requires that the symmetry of the configuration of lattice imperfections in equilibrium conform to the symmetry of the crystal.

In essence, when the higher symmetry austenite phase of an imperfectly ordered A-B alloy transforms to a lower symmetry martensite phase, the stable SRO of the austenite lattice that is inherited by the martensite lattice becomes an unstable configuration for the martensite, since it does not satisfy the martensitic symmetry. This results in an atomic rearrangement during aging that alters the inherited SRO to a stable SRO that satisfies the symmetry conditions of the martensite. These changes in SRO affect the deformation process of martensite in such a way that, upon the removal of the external stress, a restoring force tends to revert the deformed martensite domain back into the pre-deformed state through de-twinning. This symmetry-conforming SRO theory also provides a way, from a thermodynamic viewpoint, to account for the martensite stabilization, i.e. increase reverse transformation temperature (A_s). Refer to Otsuka and Ren [3, 232] for further details.

2.2 R-phase Transition

In Ni-Ti alloys under certain conditions, a competing martensitic transformation occurs prior to the B2 $\rightarrow$ B19' martensitic transformation; it is termed the R-phase transition [233]. This B2 $\rightarrow$ R-phase transformation is characterized by a small temperature hysteresis (1-10^{o}C) compared to the B2 $\rightarrow$ B19' (typically 20-50^{o}C) and also a very sharp increase in the electrical resistivity [47, 234]. The noticeable feature in the electron diffraction pattern of the R-phase is the appearance of sharp superlattice reflections at 1/3 positions along <110> and <111> directions of the parent phase in reciprocal space [149], see Figure 2.34. The appearance of the R-phase also leads to the (110) peak splitting of the B2 lattice upon cooling [59, 60]; it is

observable on a X-ray diffraction (XRD) scan, as shown in Figure 2.35 [235]. The R-phase lattice may be visualized as a B2 cubic lattice by stretching its unit cell along one of the body diagonals; the cube angle (α) was found to decrease with temperature indicating that the lattice distortion increases as temperature decreases [59, 60, 233].

For a long time, the R-phase phenomenon was considered to be a precursor/ pre-martensitic and even a distinct second-order transformation [236-238]; however, it is now confirmed that the formation of R-phase from B2 is a distinct martensitic transformation; furthermore, the shape memory and superelastic effects are observed in the R-phase, thus confirming the B2→R-phase transformation as thermoelastic in nature [58, 64]. This implies that the B2→R-phase transformation is a competing transformation that appears before the transformation into B19' martensite, i.e., the complete transformation is B2→R→B19'. A detailed crystallographic analysis of the B2→R→B19' phase transformations has been presented elsewhere in the literature [163] and will not be considered here.

The R-phase can be realized by several methods, which would suppress the formation of B19' martensite directly from B2 austenite, see Figure 2.36 [47]. They include [233]:

(a) Introduction of dislocations through cold-working + 400^{o}C-500^{o}C aging,

(b) Introduction of precipitates in Ni-rich NiTi by aging (400^{o}C-500^{o}C), or

(c) Ternary alloying with elements such as Fe, Al, etc.

Thus, the stress fields of the defects or the secondary phases interfere with the direct B2→B19' transformation, since it involves larger transformation strains (~ 6-

10%) compared to the B2→R-phase (~1-2%). The presence of the R-phase can be detected as a double-peak in the cooling cycle of a DSC scan, see Figure 2.37.

Figure 2.37 shows two DSC scans identifying the R-phase: (a) Asymmetric DSC trace, where the forward transformation sequence is B2→R→B19', and the reverse transformation sequence is B19'→B2, and (b) Symmetric DSC trace with forward and reverse transformations B2↔R↔B19'. As mentioned above, the thermoelastic nature of the transformation gives rise to shape memory and superelastic properties [60-63, 239], as observed from the stress-strain behavior shown in Figure 2.38 [63]; the dashed lines indicates that the specimen recovers the loading strains upon heating. The recoverable strains are of the order 0.5-1%, much smaller than the B2↔B19' transformation strains. Since the shape memory strains are a function of the angle α, which decreases with decreasing temperatures, the recovery strains are also temperature dependent [63, 163, 233]. It has been shown that thermomechanical treatment affects the shape memory and superelasticity associated with the R-phase [64]: (a) ST at 1000^{o}C + age at 400^{o}C leads to lower critical stresses (i.e., transformation stresses) compared to (b) cold-worked and annealed (400^{o}C) alloy. Cold-working not only increases the resistance to slip deformation, but also resists the twin boundary motion. This indicates that dislocations have a greater impact on functional properties associated with the R-phase transformation compared to simple aging heat-treatments [64, 233].

Even though the transformation strains involved in the R-phase transformation are small, they have been successfully used in actuator applications, especially those

requiring high cyclic loading stability. Indeed, it has been shown that the deflection vs. temperature response is nearly unchanged, even after 0.5 million cycles [58].

2.3 Physical Metallurgy and Processing of NiTi alloys

2.3.1 Phase diagram

The phase diagram is critical for understanding the microstructure-properties of alloys, especially, if one desires to tune the properties of the alloy through heat-treatment procedures towards specific applications (e.g. SM in actuators vs. SE in biomedical stents). The phase diagram of NiTi has been controversial for nearly three decades before some consensus was established (the discussion here will follow that of Otsuka and Ren [47]). The Ni-rich solid solutions were initially studied by Hunter and Bacon [240] who measured the conductivity of some Ni-Ti alloys. Later, Ni-rich alloys in the range 70-100 wt.% Ni, were studied in terms of their microstructure constitution, and Vogel and Wallbaum [241] reported that Ni-rich solid solutions form eutectic with the compound $TiNi_3$. It was Laves and Wallbaum [242, 243] who first reported through X-ray investigations that, besides $TiNi_3$, additional compounds of TiNi (55.06 wt.% Ni) and Ti_2Ni (38 wt.% Ni) were also present in the Ni-Ti system. Particularly, they recognized that TiNi was single phase near the equiatomic composition. However, numerous controversies transpired, largely regarding the presence [244-248] or absence [70, 71, 249-253] of an eutectoid reaction $TiNi \rightarrow Ti_2Ni + TiNi_3$. Duwez and Taylor [245] initially reported the decomposition of TiNi into Ti_2Ni and $TiNi_3$ at 800°C and Poole and Hume-Rothery [244] made a thorough study of the solubility limits of TiNi above 900°C using metallographic techniques.

They concluded that the boundary on the Ti-rich side close to 50:50 NiTi ratio is quite steep, while on the Ni-rich side, the solubility decreases rapidly as temperature drops.

Based on these works [244, 245], the first phase-diagram of Ni-Ti binary alloy system was prepared by Hansen [254]. Margolin *et al.* [249] and Purdy and Parr [246] however have not found any evidence corroborating the proposed eutectoid reaction. Furthermore, Purdy and Parr [246] corroborated the solubility limits computed by Poole and Hume-Rothery [244] and found that the NiTi phase transforms at a low temperature (and hence diffusionless transformation) to a π phase (indexed as a hexagonal phase at 36°C) in a reversible manner. This was basically the first observation of martensitic transformation in Ni-Ti, although the authors did not quote the term. Almost a decade after the discovery of SME in 1963, Wasilewski *et al.* [252] re-examined the Ni-Ti phase diagram and using metallography, XRD and electron probe micro analysis (EPMA), identified a new phase Ti_2Ni_3 and proposed the inclusion of a peritectoid reaction at 625°C. They also established the presence of a near vertical boundary on the Ti-rich side for the solubility range of NiTi, and a large solubility limit on Ni-rich side that reduces rapidly to an insignificant amount below 500°C [252, 253]. However, the proposed peritectoid reaction was never confirmed by other researchers.

Around the same time, Koskimaki *et al.* [248] observed plate-shaped precipitates (using an electron microscope) in a Ni-Ti specimen aged below 625°C, and incorrectly indexed it as a FCC structure; this "X-phase" would later be identified as $Ti_{11}Ni_{14}$ (actually Ti_3Ni_4) [74, 216, 255, 256]. So, different phases such as Ti_2Ni,

$TiNi_3$ (1938), Ti_2Ni_3 (1971), X-phase (Ti_3Ni_4) (1969), and 'π'-phase have been identified over many decades and were inducted into the Ni-Ti phase-diagram as constituents of various phase reactions (such as eutectoid and peritectoid).

However, it was not until the work of Nishida *et al.* [70] and Kainuma *et al.* [71], that many of the afore-mentioned inconsistencies were resolved; their investigations are detailed in the following section. Regarding the important properties of interest (SM and SE) in Ni-Ti alloy system, the region of interest in its phase diagram is bounded by the phases Ti_2Ni and $TiNi_3$, especially between 55 wt.% and 65 wt.% Ni composition, since alloys with these range of composition exhibit promising SM and SE phenomenon that can be tailored by various thermo-mechanical procedures, such as cold (or hot)-rolling, solution-treatment (ST), aging, etc.

2.3.2 Precipitation in NiTi alloys

Nishida *et al.* [70] performed aging heat-treatment studies on Ni-rich Ti-52Ni alloy to investigate the diffusion-controlled transformations using metallographic, TEM, SEM and EDS techniques. Their observations suggested that three phases, viz., Ti_3Ni_4, Ti_2Ni_3 and $TiNi_3$, precipitate in sequence, depending on the aging temperature and time. In other words, at low temperature and shorter aging time, Ti_3Ni_4 phase precipitates, while at higher aging temperature and longer aging times $TiNi_3$ phase appears and at intermediary aging temperatures and time, Ti_2Ni_3 phase precipitates. Additionally, upon continual aging, the prior-formed Ti_3Ni_4 dissolves into the matrix, and the Ti_2Ni_3 phase increases in both percentage and the of the precipitates. Continuing the aging further, Ti_2Ni_3 is reabsorbed by the matrix and is replaced by

$TiNi_3$ precipitates. These observations debunk many of the earlier observations or suggestions regarding the nature of various phases identified in the Ni-Ti alloy system, and indicate that Ti_3Ni_4 and Ti_2Ni_3 are only intermediary phases with $TiNi_3$ being the equilibrium phase:

$$\text{NiTi B2 parent phase} \rightarrow \alpha_1 + Ti_3Ni_4 \rightarrow \alpha_2 + Ti_2Ni_3 \rightarrow \alpha_3 + TiNi_3,$$

where α_1, α_2, α_3 are matrices with different Ni concentration. Nishida *et al.* [70] summarized the aging studies using a time-temperature-transformation (TTT) diagram, as reproduced in Figure 2.39. Further corroborative work was accomplished by Kainuma *et al.* [71] who provided the TTT diagrams for Ti-(52, 54, 56)Ni, these are recomputed and plotted in Figure 2.40.

In the light of all the above investigations the most reliable Ni-Ti phase diagram, according to Otsuka and Ren [47], is shown in Figure 2.41; it is similar to Massalski *et al.* [257] except that in the latter, a possible eutectoid reaction at 630°C is included. Additionally, a possible (unconfirmed) order-disorder transition from B2 to BCC at 1090°C is included by Otsuka and Ren [47].

2.3.3 Crystal structure of different precipitates

There are several phases that are observed in the Ni-Ti system; three of the phases are formed through martensitic transformation from the parent cubic austenite phase, viz. monoclinic B19' martensite, trigonal R-phase and orthorhombic B19 phase. In addition, several other phases are formed during the aging processes in Ni-rich alloys as a result of precipitation. The crystal structure and relevant crystallographic information of various precipitates encountered during the aging of

Ni-rich Ni-Ti alloys are summarized in Table 2.4; refer to [23, 47] for additional details.

Table 2.4 Summary of the crystallographic information on various phases found in Ni-Ti alloy system [47]

Phase	**Crystal structure**	**SG (atoms/ Unit cell)**	**Lattice parameters**	**Ref.**
NiTi Austenite	Cubic B2	Pm-3m	a = 3.015 Å	[145]
NiTi Martensite	Monoclinic B19'	$P2_1/m$	a = 2.898 Å, b = 4.108 Å, c = 4.646, β = 97.78°	[67, 146]
$Ni_{40.5}Ti_{49.5}Cu_{10}$	Orthorhombic B19	Pmma	a = 2.881 Å, b = 4.279 Å, c = 4.514	[258]
NiTi R-phase	Trigonal	P3 or P-3		[154]
Ti_2Ni	Cubic	Fd-3m	a = 11.32 Å	[259]
Ti_3Ni_4	Rhombohedral	R3	a = 6.70 Å, α = 113.8°	[255, 256]
Ti_2Ni_3	Tetragonal, Orthorhombic	I4/mmm Bbmm	a = 3.095 Å, c = 13.585 Å a = 4.398 Å, b = 4.370 Å, c = 13.544 Å	[72, 73]
$TiNi_3$	Hexagonal DO_{24}	$P6_3/mmc$	a = 5.1010 Å, c = 8.3067 Å	[145]

(a) Ti_3Ni_4: Ti_3Ni_4 is a very important phase since it affects the shape memory characteristics in Ni-rich Ni-Ti alloys [64, 216, 219, 220, 235, 260, 261]. The shape of Ti_3Ni_4 is typically lenticular, as shown in Figure 2.42(c). While Nishida *et al.* [255] and Saburi *et al.* [256] calculated the lattice parameters for a rhombohedral Ti_3Ni_4 (a = 6.70 Å, α = 113.8°), Tadaki *et al.* [74] and Saburi *et al.* [256] determined the crystal structure as *R3*. The atomic arrangement in the until cell may be described by

utilizing the hexagonal axes, according to Saburi *et al.* [256]. In the B2 cubic austenite, the (111) planes consist of alternating Ti and Ni hexagonal layers and a set of six layers define one period. In Ti_3Ni_4, however, the excess Ni atoms are distributed in each original Ti layers leading to a sequence as shown in Figure 2.42a. Accordingly, the orientation relationship between the matrix and the precipitate is given as $(001)_h \parallel (111)_{B2}$, $<010>_h \parallel <-2\ -1\ 3>_{B2}$, and the habit plane of the precipitate is given as $\{111\}_{B2}$, see Figure 2.42(b,c) [256]. Using this structure and atomic stacking, Tadaki *et al.* [74] calculated the lattice strain that accompanies the precipitation of Ti_3Ni_4 in the surrounding NiTi B2 matrix. In the direction of the habit plane normal, the strain is –2.3% and –0.5% in the habit plane.

(b) Ti_2Ni_3: As discussed above, Ti_2Ni_3 is the second metastable precipitate that forms at intermediate temperatures or at low temperatures for longer aging times. Nishida and Wayman [72] studied the phase transformations associated with Ti_2Ni_3 precipitates in an aged 52-NiTi alloy using in-situ TEM with a heating specimen holder; they reported two main findings: (i) The precipitate shows two step transformation; tetragonal high temperature phase to a orthorhombic intermediate phase and finally to a monoclinic low-temperature phase. (ii) These phases differed in their morphologies; the intermediate orthorhombic phase exhibited an antiphase-like contrast and the monoclinic phase exhibited a needle-like domain contrast; the needle-like domain contrast is apparently caused by twins. However, they do not provide any crystal structure lattice parameters, instead they report that the diffraction patterns for the tetragonal high-temperature Ti_2Ni_3 phase were similar to $Ti_2(Ni, Cu)_3$ patterns (as reported by Van Loo *et al.* [262]) and that the lattice parameters of the latter could be

used to index the patterns from the former. Therefore, they concluded that the crystal structures of both the above phases are identical. A decade later, Hara *et al.* [73] studied the structure of Ti_2Ni_3 precipitate in detail along with $Ti_2(Ni, Cu)_3$ by utilizing various diffraction techniques in order to determine its crystal structure and the nature of the transformation in the precipitate from a crystallographic point of view and also examine the similarity between Ti_2Ni_3 and $Ti_2(Ni, Cu)_3$. They reported that the precipitate has two phases as a function of temperature, and that the phase transformation occurs martensitically through the formation of an intermediate phase, similar to the R-phase transition observed between the transformation from B2 NiTi austenite to B19' NiTi martensite. The higher temperature phase (stable above 100°C) was found to exhibit a tetragonal structure with space group *I4/mmm* and lattice parameters a = 3.095 Å, c = 13.585 Å (at 100°C); the lower phase has an orthorhombic structure with space group *Bbmm* and lattice parameters a = 4.398 Å, b = 4.370 Å, c = 13.544 Å (at 25°C) [73]. However, they do not report the structure of the low temperature monoclinic phase.

(c) $TiNi_3$: Taylor and Floyd investigated the structure of $TiNi_3$ and reported a hexagonal DO_{24} type ordered structure with space group $P6_3/mmc$. The lattice constants are a = 5.1010 Å, c = 8.3067 Å [145].

2.3.4 Processing of Ni-Ti alloys: Effect of Ni composition

Since the binary Ni-Ti alloys are overwhelmingly the preferred material choice for many medical devices, it is important to understand the challenges in alloy

fabrication. The distinction presented here will be in terms of a comparison between near equiatomic alloys and Ni-rich (56 wt.% - 62wt.%) Ni-Ti alloys.

(a) Melting practices and contaminants

A précis from Schetky and Wu [263] and Otsuka and Wayman [264] will be provided here. Typical fabrication route involves melting and casting followed by primary metal working (forging and hot rolling), secondary metal working (cold working and forming) and finally a heat-treatment (solution-treatment, annealing, aging etc.) that imparts the Ni-Ti alloy with its SE or SM properties. The melting and casting of NiTi ingots is frequented by the following challenges: Ni/Ti ratio, interstitial contamination by oxygen and carbon requiring solidification conditions to minimize segregation at both microscale and macroscale and finally avoidance of non-metallic inclusions. Since molten Ti is extremely reactive to oxygen, the most successful melting procedures used for the production of NiTi are: vacuum induction melting (VIM) for the primary alloy preparation followed by vacuum arc melting (VAR) that imparts microstructural homogeneity. The segregation characteristics are a function of solidification rate; smaller dendrite arm spacing is favored by faster cooling rates and is responsible for minimum segregation. Faster cooling rates also promote particulate (such as carbides and other intermetallic compounds) dispersion. Since VIM uses graphite crucibles, oxygen contamination is negligible, but carbon ties up Ti preferentially in the form of TiC inclusions. This selective leaching of Ti leads to a Ni-rich matrix and, as will be discussed in the next section, leads to a lowering or suppressing of M_s; a one percent deviation in Ni content results in a decrease of M_s by nearly 100°C. It is not clear whether carbon has any proven detrimental effect on the

properties. Earlier melting procedures required that the melt temperature should be maintained below 1450°C and the carbon levels achieved were in the range of 200 – 500 ppm. Oxygen also ties up Ti in a similar, but disproportionate manner (especially with Ti_2Ni, which has a high solubility for oxygen and forms Ti_4Ni_2O inclusions), thus leading to a depression in M_s (NiTi however does not have any solubility for oxygen at 900°C). The stoichiometry of the oxide is such that a relatively small amount of oxygen forms a large weight of oxide, with the oxide to oxygen weight being ~20:1. The current state of art Ni-Ti alloy melting procedures typically achieve less than 30 ppm of carbon and less than 300 ppm of oxygen (more recent standards achieve even lower oxygen content); the general requirements on Nitinol chemistry and trace elements (contaminants) are delineated in the ASTM standard, F2063-00 [265]. Another advantage of induction melting is the reliable control of chemical composition, and in a small VIM ingot, the transformation temperature variation (due to Ni composition variation) can be held to ±5 °C. Segregation problems compound with increasing ingot size, and usually for larger ingots, multiple VAR melting practices have achieved more homogeneous chemistry distribution along the ingot. Schetky *et al.* [263] point out that the benefits of high purity Nitinol are yet to be proven. Notwithstanding the evidence that subsurface inclusions promote fatigue crack nucleation, the purity levels with respect to carbon between VIM-VAR and multiple VAR processes do not result in a measurable difference in fatigue resistance.

(b) Primary and secondary metal working

Most medical devices are fabricated from wire, strip or tube; investment casting is used for implantable orthopedic devices. The primary metal working

involves a hot break down through hot forging or hot rolling; the hot working breaks down the cast structure and provides a usable size/shape (such as a bar or a slab) for subsequent cold drawing. Based on the high-temperature tensile strength of NiTi, the optimal hot working is carried out a temperature of 800°C, a temperature that enables good workability and also minimizes oxide buildup, thus avoiding severe oxidation. Subsequent to the hot working, the rod is cold-worked to the final dimension followed by a suitable heat treatment to achieve the desired mechanical and physical properties. However, compared to the hot-working, cold-working Ni-Ti is very difficult due to its high work hardening coefficient, thus limiting the cold reduction achievable in one pass: yield strength of fully annealed NiTi is less than 100MPa, after deformation, tensile stresses rise rapidly beyond the stress plateau to a high value of 1-1.5GPa at ~ 40% strain. Hence, interpass annealing at 600°C – 800°C is typically performed. Nitinol tube and sheet morphologies have become the most sought after product due to its use for the production of stents. Currently, tubes with outer diameters ranging between 0.25 mm and 5 mm are being produced; the problems often encountered include tube concentricity and surface finish. Due to rapid work hardening of the alloy, machining of Nitinol is extremely difficult; stent manufacturing typically utilizes Nd:YAG laser cutting and machining.

(c) Ni-rich Ni-Ti alloys

The processing specifications for 55 at.% NiTi (60 wt.%) are summarized from Buehler and Wang [13] and Julien [94], see Table 2.5. The melting practices for 60-Nitinol (wt.%) is similar to 55-Nitinol (wt.%), where the Ni-rich alloys are melted in a draw-down graphite crucible vacuum furnaces for casting into a billet or ingot suitable

for hot working. Buehler and Wang [13] note that, "*60-Nitinol alloys have been found to be more difficult to hot work directly from the cast ingot; however, a long time high temperature soaking treatment leaves the ingot much more amenable to the initial stages of hot working*". Hence, the ingots are soaked in a furnace to a working temperature of nearly 900^{o}C – 950°C for at least one hour until the heat has penetrated the work piece. Subsequently, the work piece is subjected to hot working by rolling, forging etc. "It has been observed that once the cast structure of a 60-Nitinol ingot has been 'broken down', little if any further cracking (hot tearing) is encountered" [13]. It is necessary that the ingot work piece temperature be maintained above 900°C while it is being worked, since otherwise, it would lose malleability thereby increasing the susceptibility to cracking.

Table 2.5 Primary working characteristics of various Ni-Ti alloys as a function of Ni composition [266, 267].

Ni Composition, at.% (wt.%)	**Working parameters**
50 - 51 (55 – 56)	Hot working through rolling, forging, etc., possible directly from vacuum melted ingot. Hot working Temperature ~ 700–900 °C. Working at room temperature is possible with intermediate anneals at 800 °C.
51 – 52.5 (56 – 57.5)	(transitional composition range) Some forms of hot working possible directly from the melted ingot. Hot working temperature ~ 800-950 °C. Limited room temperature working.
53 – 56 (58 – 62)	Thorough homogenization of chemical composition through thermal treatment prior to any break down of the cast structure is mandated. The ingot structure needs to be broken down by hot extrusion or press forging. Hot working temperature ~ 900-950 °C. Several cycles of high temperature soaking followed by hot rolling is recommended.

Additionally, the strain rate of the hot working should be maintained moderate to slow, since 60-Nitinol ingots, being a strain rate sensitive material, has been observed to shatter catastrophically upon impact, thus posing a safety concern. Julien [94] suggests that optimum rolling conditions typically limit the thickness reduction to about 0.1 – 0.5 mm (5 – 20 mils), preferably 5 mils per roller pass. After the initial hot working, the plate is reheated to the working temperature of 900°C – 950°C in a furnace for a second hot-rolling pass. Subsequent to a few rolling and reheating cycles, the plate can be soaked at lower temperatures, viz. 800°C – 900°C. These lower temperature passes seem to proceed without any cracking, and the rolling is repeated until the plate is reduced to the desired dimensions. It should be noted that the afore-mentioned heating and hot rolling cycles produce a very hard and brittle 60-Nitinol. Subsequent heat-treatment is necessary to impart the important SE or SM properties, this will be discussed below.

(d) Heat Treatment

Optimal superelastic properties are typically achieved through a combination of cold work and ageing heat treatments for equiatomic and near equiatomic Nitinol alloys [195, 268]. A thorough understanding of the effects of various factors involved in thermomechanical treatments allow the engineer to exercise precise control over the reproducibility of mechanical properties and transformation temperatures in Nitinol alloys.

Typical thermomechanical history for most medical devices that use SE Nitinol involves 30-40% cold work followed by heat treatment at 500°C and for shape memory, the preferred heat treatment range is 350^{o}C – 450°C (the influence of cold

work, annealing heat treatments on the transformation temperature will be presented in Section 2.4.2). It should be emphasized that the thermomechanical routes a particular Nitinol alloy is subjected to is dependent on the Ni composition since aging of Ni-rich alloys (Ni > 50.6 at.%) causes precipitation of Ni-rich intermetallic compounds [70] that usually harden the matrix and make primary or secondary working difficult at lower temperatures. An excellent case study on the optimization of processing and properties of a medical grade 50.8 at.% Nitinol wire is presented by Pelton *et al.* [39].

For Ni-rich alloys, such as 55-NiTi investigated in the current thesis, Julien [94] recommends the following heat treatment schedule. As mentioned above, the hot rolled plate produced by a series of heating and rolling cycles is extremely hard and brittle. To impart superelastic properties, the work piece is then heated in an oven between 500^{o}C and 700°C for a period of 15min to several hours and subsequently quenched to room temperature. An optimal hardness (50-55R_C), strength (~900MPa – 1050MPa), and elastic strains between 3-6% can be achieved using this heat treatment. To obtain the shape memory effect, the hot rolled plate is heated in a furnace to a temperature between 500^{o}C and 800°C, until thermal equilibrium is attained, and subsequently the work piece is furnace cooled (a full anneal) at a slow rate (~1-2 °C/min) so that the work piece cools down to room temperature over a period of 10-15 hours. The shape memory alloy thus obtained has low hardness (25-35R_C) and low yield strength (~300-400 MPa) and a reasonable tensile strength (~800-950 MPa). The transition temperatures for the shape memory parts range between 25^{o}C and 85°C and the material exhibits high ductility. The transition temperature can be altered by cooling the work piece from different temperatures.

2.3.5 Tailoring transformation temperatures: Effect of various parameters

Since superelastic and shape memory behaviors typically occur within a temperature 'window' dictated by the transformations temperatures (like R_s, M_s, A_f, etc.), control over these transformation temperatures is very crucial in the application of Ni-Ti alloys. Over the decades, several factors were found to influence the transformation temperatures [269]. Among them, the most important ones are: (1) Ni-composition, (2) ternary alloying elements, (3) precipitation in Ni-rich NiTi alloys, (4) aging heat-treatments, and (5) point defects and dislocations

The effect of Ni composition on the martensite start temperature (M_s) is shown in Figure 2.44 [270]; it can be seen that M_s is very sensitive to the Ni content. A change in Ni concentration from 50.5 to 51.5 at.% reduces the M_s from room temperature (20^oC) to below -173^oC [47, 270, 271] for a fully homogenized alloy (solution treated, ST). This suggests that the most effective way of changing M_s is through Ni composition changes. Figure 2.44 also indicates that the transformation temperature on the Ti-rich side is nearly constant ($\sim 50^oC$), probably due to the limited solubility of NiTi on the Ti-rich side (the solvus line is near vertical).

Another method to vary the Ni-content is through tertiary alloying elements, as shown in Figure 2.45. Among the elements that increase the transformation temperature, Pt, Zr, Hf, Pd and Au are the prominent ones. In fact, Ti-Ni-(Hf, Zr, Pd) are considered as probable candidates for high-temperature shape memory applications [47, 76, 272-277].

Since the transformation temperatures are very sensitive to the Ni-composition and furthermore, since the Ni-rich NiTi alloys exhibit precipitation of Ni-rich phases

such as Ti_3Ni_4 with aging, another way to manipulate the transformation temperature is through the control of aging parameters (temperature and time) of different Ni-rich alloys.

Figure 2.46 shows the effects of aging on the transformation temperatures of a Ni-rich 51-NiTi alloy fully annealed at 800^{o}C for 2hrs followed by a water quench [234]. In Figure 2.46(a, b), the aging temperature is maintained constant at 500^{o}C and 400^{o}C, and the aging duration is varied between 0.1hr and 250 hrs (~10 days). It can be seen that within the first 15-min, there is a rapid increase in the M_s with the appearance of an intermediate phase (R-phase) identified by its start transformation temperature M_s'; thus indicating a 2-stage transformation. The reason behind the formation of multiple transformation stages will be discussed in the following section. The transformation temperatures M_s and A_s increase until 10-hrs of aging before they saturate.

By contrast, the aging effects at 400^{o}C, shown in Figure 2.46(b) indicate that, after an initial drop, the transformation temperatures continue to increase up to 100 hours of aging and beyond [234]. This may be explained by the formation of hardening Ti_3Ni_4 precipitates that siphon excess Ni from the matrix, thus reducing the overall Ni content of the matrix. Since the transformation temperatures are very sensitive to the Ni content, as indicated in Figure 2.44, the formation of precipitates is accompanied by a corresponding increase in the transformation temperatures [39].

While the controlled aging of Ni-rich NiTi is plausible, it is desirable for many applications to use an alloy whose transformation temperatures are made insensitive to the composition after the initial aging heat-treatment. It has been reported that an

alternating aging between 440°C and 550°C leads to an alternating change in the transformation temperatures, as shown in Figure 2.47 [269]. Furthermore, the transformation temperatures were governed by the aging temperatures and not the number of aging cycles.

The nature of the phenomenon was clarified by Zhang *et al.* [278], who suggested that the behavior is dictated by the equilibrium between the stable NiTi phase and the metastable Ni-rich precipitate Ti_3Ni_4. Aging between 440°C and 550°C leads to an alternating variation of Ni composition between 50.13 and 50.33 atomic percent; which in turn influences the variation in the transformation temperatures between set values [278]. Therefore, Otsuka and Ren [47] note that, although the shape memory properties are due to the diffusionless martensite transformation, the control over it can be achieved through diffusional precipitation reactions.

The traditional view of the martensitic transformations occurring in NiTi alloys involves only 1-stage (B2→B19') transformation or 2-stage transformation involving the intermediate R-phase. However, over the past decade, multiple-stage transformations (MST) have been reported quite frequently; the mechanisms behind these MST are now discussed.

2.3.6 Multiple-stage Transformations (MST)

While the traditional simplified view of phase transformations occurring in Ni-Ti alloys involves only one-stage cubic austenite (B2) to monoclinic (B19') martensite transformation (transformation strains ~ 6-10%), the influence of cold work, i.e., high density of dislocations [279-281] and the presence of Ni-rich precipitates in Ni-rich

(Ni > 50.6at.%) Ni-Ti alloys contribute to a more complex two-stage, three-stage or even four-stage transformations, collectively termed 'multiple stage transformation' (MST) [47, 270, 281-294]. It is now known that the introduction of a dislocation network/substructures or precipitates into the Ni-Ti matrix can act as obstacles to the direct B2-B19' transformation [281, 286, 288, 292]. As a result of this barrier, a competing martensitic transformation, B2→R-phase that involves lower transformation strains (~1-2%), becomes feasible and dominant. Further transformation occurs as R-phase converts to B19', thus leading to a two-step process, that is seen as a double peak (two-stage) on the differential scanning calorimetry (DSC) trace. The heating cycle however, involved only one large peak indicating that the B19'→B2 transformation occurred in one step. Yet, it was observed that aged Ni-rich NiTi alloys exhibited three DSC peaks during cooling from austenitic phase, instead of a two-stage transformation [279, 280, 295-299]. Since the Ni-Ti alloy did not exhibit any competing martensitic transformation, other than to R-phase and B19' phase, there was uncertainty with regards to the correct interpretation of the multiple-stage transformation (MST). Furthermore, according to Carroll *et al.* [286], the DSC peaks evolve from one or two peaks after short aging times to three peaks after intermediate aging times and back again to two peaks or one peak after long term aging, a behavior termed as '2-3-2' transformation by Allafi *et al.* [282].

Bataillard *et al.* [299, 300] cite the influence of local coherency stress fields around the Ni-rich Ti_3Ni_4 precipitates on the transformation sequence in such a way that the B2 matrix initially transforms to R-phase near the regions affected by the coherency stresses followed by the second transformation R-phase→B19'. This

second transformation occurs in two steps, one near the precipitate and the other in the Ni-Ti matrix volume unaffected by the coherency. Subsequently, Allafi *et al.* [282] have proposed that the 3-stage transformation was due to localized composition inhomogeneity in the austenite due to the precipitation of Ni-rich Ti_3Ni_4 precipitates that deplete Ni from the surrounding matrix, see Figure 2.48. They implied that since the transformation temperatures depend strongly on the Ni composition of the matrix, the composition (chemical) inhomogeneity in the volume surrounding the precipitates would result in a single B2→R transformation followed by two R→B19' transformations occurring near and away from the precipitates, respectively [286].

Recently, in situ TEM studies [282, 301] of transformations occurring in aged Ni-rich Ni-Ti alloys suggested that, due to the preferential precipitation of lenticular Ti_3Ni_4 at the grain boundaries, the first DSC peak corresponds to the B2→R-phase transformation near the grain boundary (GB) followed by the R-phase→B19' transformation. Furthermore, the third peak then corresponds to the direct B2→B19' transformation in the precipitate free grain interior (GI) region. Thus, a large scale inhomogeneity in the microstructure due to preferential precipitation of phases near the grain boundary was suggested as the main cause behind the multiple-stage transformations.

All of the above theories, i.e., local-scale inhomogeneity in either coherency stress fields and chemical composition, or the large-scale microstructural inhomogeneity (due to preferential GB precipitation) indicate that the 3-stage transformation is the norm rather than the exception [47]. However, Fan *et al.* [287] point out that, typically, single crystals of Ni-rich NiTi alloys with different Ni

compositions and Ni-rich (e.g., 51.5Ni-Ti) polycrystalline alloys exhibit the normal 2-stage transformation, whereas only the near equiatomic polycrystalline alloys capable of undergoing precipitation reactions (e.g. 50.6-NiTi), exhibit 3-stage transformations.

Their study suggested that, while the presence of grain boundaries is a necessary condition to create microstructural inhomogeneity due to preferential precipitation, it is not a sufficient condition for the 3-stage transformation. Instead, they invoke that it is the degree of supersaturation, which is high in Ni-rich alloys such as 51.5-NiTi, that governs the nucleation kinetics of the Ti_3Ni_4 precipitation and thus the MST. In particular, if the degree of supersaturation is high, as in the case of 51.5-NiTi, the precipitation process is less sensitive to the presence of grain boundaries, and thus results in a homogeneous precipitation and only a 2-stage transformation. If the degree of supersaturation is low, as in the case of 50.6-NiTi, the precipitation is severely affected by the presence of grain boundaries (GB), since the GB nucleation rate is substantially greater than in the grain interior. This leads to large-scale heterogeneity in microstructure and chemical composition between the grain boundaries and the grain interior [287]. Thus, they conclude the two opposing factors, viz., presence of grain boundaries that instigate preferential precipitation due to favorable energetics and the Ni supersaturation level that dictates the nucleation rate, govern the distribution of the precipitates and thus the nature of MST, i.e., 2-stage vs. 3-stage. They also exclude the possibility of 3-stage transformations in single crystals devoid of GBs or in microstructures with small-scale heterogeneities.

More recently, Michutta *et al.* [293] studied the transformations in aged single crystals of 51.3-NiTi and observed that 3-stage transformations can indeed occur in

aged Ni-rich single crystals that exhibit homogeneous distribution of the metastable Ti_3Ni_4 precipitates provided that the interparticle spacing is greater than a critical value (~ 200 nm). The three peaks on the DSC trace correspond to the formation and growth of R-phase from all the precipitate/matrix interfaces, followed by the formation and growth of B19' phase along the same interfaces. The final transformation peak corresponds to the B2-B19' transformation. Thus, Michutta *et al.* [293] put forward a general proposal regarding the MST: (a) MST occur in Ni-rich NiTi alloys that exhibit large scale (10μm) microstructural heterogeneities (due to preferential precipitation near GBs in polycrystalline Ni-Ti, differences between the dendritic and inter-dendritic regions in cast single crystals, heterogeneous distribution of oxide and carbide inclusions and variable grain sizes across the specimen cross section). (b) MST can also occur in the absence of large-scale microstructural heterogeneities, for example in aged Ni-rich NiTi single crystals with a homogeneous distribution of the precipitates, provided that the interparticle spacing is greater than a threshold value (~ 200 nm).

In the above discussion, whether the microstructure is heterogeneous (due to preferential GB precipitation) or homogeneous (with interparticle spacing greater than 200 nm), the 3-stage transformation was identified as the B2→R phase transformation near the precipitates followed by the R→B19' transformation, and the final peak was identified as B2→B19' transformation in the precipitate free matrix [281, 282, 284, 287, 288, 290, 293, 301]. Additionally, as mentioned earlier, Bataillard *et al.* [300] suggested an alternative sequence for the 3-stage transformation based on the effect of coherency stresses around Ti_3Ni_4 precipitates: the first step consists of B2→R phase

transformation nucleating at the precipitate/matrix interfaces and growing into the matrix. The second peak corresponds to the transformation of R→B19' near the precipitate region affected by the coherency stresses followed by the R→B19' peak representing the transformation in the matrix; thus totaling one B2→R and two R→B19' (1R-2M) transformations. More recently, it has also been reported that 3-step transformations in deformed and low-temperature (200^{o}C-300^{o}C) aged (i.e., with prior thermomechanical history) 50.6-NiTi alloy may consist of two B2→R phase transformation followed by one R-phase→B19' transformation (2R-1M) [302-304] or even two B2→R-phase and two R→B19' phase transformations (2R, 2M) (in total, 4-stage transformation) [303, 305] that was rationalized by invoking the inhomogeneous distribution of dislocations or grain size, as discussed below.

Chrobak *et al.* [303] considered a cold-rolled (15% cold-work) 50.6-NiTi aged at 400^{o}C for very short times (0.25-0.5hrs); they explain the 3-stage transformation based on the heterogeneous distribution of dislocations in a cold-rolled NiTi: The first R-phase forms in low dislocation density regions followed by the R-phase in high dislocation density before finally transforming into B19' (see Figure 2.49). In another study, Chrobak *et al.* [281] examined cold-rolled 50.6-NiTi for shorter aging times between 5-15 min at 400^{o}C and proposed that a combined influence of two intertwined processes of dislocation density and precipitate growth influences the MST. Aging influences both the processes of dislocation annihilation (recovery during annealing) and precipitate growth. Aging heat treatment of a cold-rolled sheet material is likely to produce a complex microstructure containing relatively large densities of dislocations and precipitates that are interwoven in such a way that precipitation may

occur mainly on dislocations, act as obstacles for dislocation movement, and may hinder the recovery process (see Figure 2.50). This scenario is indeed supported by some studies in the literature [281, 303, 306], which showed intricate microstructures containing dislocations decorated with precipitates. Thus, the heterogeneity of both the dislocations and precipitate distribution leads to the inhomogeneity of Ni composition in the matrix and lead to two R→M (M1, M2) transformations [281].

More recent results have also indicated additional complexity in the transformation sequence: Neutron and X-ray diffractions studies indicate that in some alloys, the first DSC peak corresponds to the formation of both the R-phase and the B19' martensitic transformation; thus a single DSC peak is not necessarily tied to a single martensitic transformation event [307, 308]. In another study of MST in single crystal NiTi alloys with compositions: 50.1, 50.4, 50.8 and 51.5 at.% Ni, Johnson *et al.* [290], first reported the occurrence of an unprecedented MST in 50.1-NiTi alloys and suggest that they are associated with single crystal defects such as dendrites and low-angle boundaries. They observe, in addition to the 2/2-stage B2→R→B19' transformations, the 3/2-stage, 3/3-stage and even 4/4-stage transformations. Furthermore, the presence of the same defects in higher Ni content single crystals does not elicit similar MST.

Thus it can be summarized [286] that the occurrence of MST is governed by local or small-scale inhomogeneity (coherency stress fields, compositional fluctuation, precipitation with a critical interparticle spacing) associated with the precipitation of metastable phases such as Ti_3Ni_4, large-scale inhomogeneity characterized by preferential grain-boundary precipitation and precipitate free matrix, presence of

single crystal defects such as dendrites and low-angle boundaries, and the thermomechanical process that cause heterogeneity of both dislocations and precipitate distribution.

2.4 Deformation behavior of NiTi alloys

The origin and the characteristics of the phase transformations observed in NiTi alloys have been discussed so far. This section will discuss the deformation behavior of NiTi alloys with particular emphasis on temperature effects. Further, the influence of thermomechanical treatment on the overall mechanical behavior and the superelastic and shape-memory characteristics will be discussed in section 2.4.2.

2.4.1 Effect of temperature

The stress-strain curves of NiTi alloys are dependent on the relation between the test temperature (T) and the transformation temperatures. Typically, the stress-strain behavior has been classified into five types, as shown in Figure 2.51 [234].

(1) $\mathbf{T < M_f}$ (Martensite finish temperature): Below the martensite finish temperature (M_f), the NiTi alloy is entirely in the martensitic phase. Typically, the thermally-induced martensite (formed when cooled below M_s) in NiTi is made of twinned martensite variants with <011> type II, {11-1} type I and (001) compound twins co-existing in the microstructure; among these the <011> type II twin is more frequently observed [56, 65, 164, 166, 169, 309].

The tensile deformation of the twinned martensite proceeds through (a) elastic deformation of the martensite, (b) plateau region corresponding to martensite reorientation and detwinning process, (c) elastic deformation of reoriented martensite

and further detwinning, and finally (d) plastic deformation. Liu *et al.* [309] (who studied NiTi bar annealed at 600^{o}C for 0.5-hr) have shown that during stage (a), the martensite deforms uniformly along the gage length with the inelastic arrangement of some martensite twins and the generation of dislocations within the (11-1) type I twins. Stage (b), which corresponds to the constant-stress plateau region, involves the martensite reorientation and detwinning of <011> type II twins following the formation of mobile (100) compound twins between the type-II twins, in addition to the rearrangement of dislocation substructures. During stage (c), further reorientation and detwinning of unfavorably oriented martensite twins occur with increasing stress along with the generation of high density of dislocations [309]; concluding with the plastic deformation of unfavorably oriented martensite plates [309-312]. Zheng and Liu [310] have suggested two detwinning mechanisms, namely, domino and assisted detwinning. They argued that the domino detwinning, once initiated in a finite volume, proceeds at a constant external stress in a self-propagation manner, whereas the assisted detwinning necessitated increasing loading to trigger further detwinning. Furthermore, they suggested that the end of the plateau region corresponds to the cessation of the domino detwinning mechanisms, while assisted detwinning occurs beyond the plateau region. At $T << M_f$, under tensile deformation, the martensite would deform elastically followed by work-hardening plastic deformation without the reorientation of martensite plates due to the immobility of the martensite interfaces at low temperatures [313].

(2) $\mathbf{M_f < T < M_s}$: The overall deformation of the alloy now proceeds through the deformation of existing martensite, as explained above, and the formation and growth of new stress-induced martensite.

(3) $\mathbf{M_s < T < A_f}$: Deformation in this temperature range leads to the irreversible stress-induced martensite; although the overall stress-strain curve would be similar to the stress-induced martensite (SIM), the specimen will not recover the loading strain upon unloading. However, the transformation strain can be recovered upon heating above a certain temperature, which is due to the shape memory effect [313].

(4) $\mathbf{A_f < T < M_d}$: This is the superelastic range, where the material can exhibit reversible stress-induced martensitic phase transformation. The material is thus termed superelastic austenite; superelasticity occurs only between a narrow window of temperatures ($A_f < T < M_d$) with the variation of the superelastic plateau stress with respect to the temperature (also termed stress-rate, $d\sigma/dT$) ranging between 3 and 20MPa/^oC [195]. The superelastic window is typically about ~50-80^oC for the NiTi alloys.

Generally, it is agreed that the elastic deformation of austenite (stage a) is followed by the stress-induced martensitic transformation (SIM) (stage b) represented by the flat plateau. Subsequently, the SIM reorients (stage III) before plastic deformation of martensite begins (stage c) [314]. The stress-induced martensitic (SIM) transformation that is responsible for the plateau region, and hence superelasticity, occurs through the formation of martensitic variant(s) [119]. It was suggested that the formation of SIM during uniaxial tension is governed by the variant

group(s) that will accommodate the largest tensile strains for a given loading direction [315] and that this variant(s) will then grow during subsequent loading. It is known that the largest recoverable strains in single crystals are possible due to SIM formation when the loading directions are parallel to $<111>_{B2}$ followed by $<110>_{B2}$ and $<100>_{B2}$. Furthermore, different variants recover different transformation strains [133, 316]. The degree of the role of intergranular constraint on the properties of polycrystalline SMA has also been invoked by several investigators to explain the observed SE strains [119, 133, 316, 317].

(5) $\mathbf{M_d < T}$: Above a certain temperature, M_d, the stress to induce martensite transformation is greater than the stress to introduce slip in to the austenite matrix and hence, the specimen deforms as a stable austenite, i.e. in a fully austenitic condition. Funakubo [234] report the superelastic stress-strain behavior of three near equi-atomic alloys, viz., 50-NiTi, 50.5-NiTi and 51-NiTi, solution treated at 800^{o}C; the behaviors of 50-NiTi and 51-NiTi are shown in Figure 2.52 and Figure 2.53, respectively. All the specimens were loaded to 5% strains and unloaded and heated above A_f temperature to recover the strains.

In Figure 2.52, the minimum yield stress can be found near 66^{o}C, consistent with the martensite start temperature, M_s = 69^{o}C. The yield stress increases above 66^{o}C, with recovery of strains above 84^{o}C being incomplete, i.e., permanent plastic deformation has been introduced into the specimen. Above 125^{o}C, there is no recovery with specimen exhibiting only pseudoelastic behavior.

Figure 2.53 shows the stress-strain curves for 51-NiTi that exhibits superelasticity between -44^{o}C and -21^{o}C, with complete recovery of the 5% loading

strains; the specimen also recovered the loading strains between -74^{o}C and -49^{o}C upon heating [234]. The variation of the yield stress with temperature for these three alloys is summarized in Figure 2.54.

It can be seen that variation of Ni by 0.5 at.%, changes the superelastic window towards the body temperature (37^{o}C) or greater (especially, for the 51-NiTi); thus Nitinol alloys with Ni content between 50.5 and 51 are widely commercialized, particularly 50.8-NiTi [39], although the alloys undergo prior thermomechanical treatment to fine-tune the transformation temperatures and the overall mechanical properties. A collage of the stress-strain curves for the popular 50.8-NiTi alloy is shown in Figure 2.55; the temperature is varied between -100^{o}C and 150^{o}C, with the superelastic window between 0^{o}C and 60^{o}C centered on the body temperature (37^{o}C), which is ideal for biomedical applications. The A_f temperature is 11^{o}C and M_d temperature is between 100^{o}C-150^{o}C; the stress-rate calculated between these two temperatures is 6.1MPa/^{o}C [39]. As shown in Figure 2.56, the tensile strength (UTS) decreases from -100^{o}C to 150^{o}C, with the plateau stress and the UTS curves meeting around ~150^{o}C, suggesting that the M_d ~ 150^{o}C.

2.4.2 Effect of thermomechanical treatment

It has been indicated in the previous section that the fully-annealed 50-NiTi alloy does not exhibit fully recoverable superelastic strains, i.e. it exhibits irreversible slip that cannot be recovered either by unloading or heating. This has been shown to be due to the ease of introducing slip into the austenite [47] that leads to partial pseudoelasticity. Thus, in order to improve the SE and SM properties, the critical

stress for slip has to be increased through any of the following methods: (i) work-hardening, (ii) grain-refinement (iii) precipitation-hardening, or a combination of these. The influence of cold-work on the pseudoelasticity and the grain-refinement is shown in Figure 2.57(a) and Figure 2.57(b), respectively. It can be seen that increasing cold-work from 6% to 25% improves the pseudoelastic strains and approaches ideal superelastic 'flag' for large cold-working [92]. Figure 2.57(b) shows the grain-size effect on the pseudoelastic behavior of 50.5-NiTi fully-annealed at 800^{o}C (1hr) followed by water quench; the tensile tests are conducted at 40^{o}C (10^{o}C greater than A_f). It is clear that refining the grain size improves the pseudoelasticity [318, 319].

(a) Cold-work + Annealing: Figure 2.58 shows the influence of thermomechanical treatment on the stress-strain behavior of 49.8-NiTi as a function of temperature [45]. Figure 2.58(a) shows a series of stress-strain curves for a fully-annealed alloy (800^{o}C) followed by a low temperature anneal (400^{o}C) for 1hr. Since this alloy does not exhibit any precipitation hardening, the low temperature anneal would not alter the ST microstructure. This specimen shows permanent strains during tensile testing at all temperatures; it does not exhibit superelasticity in any temperature range since the resistance to slip is low in the ST material.

By contrast, Figure 2.58(b) shows a second series of stress-strain curves for a cold-worked + annealed (400^{o}C for 1hr) without any homogenizing heat-treatment [45]. It can be seen that the specimens not only exhibit large superelastic strains, but also the best SE and SM characteristics. This has been explained by Otsuka and Ren [47], who report different thermomechanical treatments on the NiTi alloys. They

argue, based on the TEM micrographs shown in Figure 2.59, that the cold-worked alloy exhibits large amount of tangled dislocation networks. The specimen annealed at 400^{o}C exhibited re-arranged dislocations, i.e., it is recovered.

However, the annealing treatment at 400^{o}C did not recrystallize the alloy. The specimens in this heat-treatment condition not only exhibit a clean martensitic transformation, but also maintain sufficient strength due to the re-arranged dislocations. Figure 2.59(c) shows the TEM image annealed at 500^{o}C; recrystallization is now evident. The specimens annealed at 400^{o}C exhibited superior superelasticity than the specimens annealed at 500^{o}C. The specimens annealed at 600^{o}C exhibited grain growth following recrystallization, and the superelastic behavior was inferior [47].

(b) Precipitation-hardening: Age-hardening by Ti_3Ni_4 precipitates has been shown to affect the shape memory and superelastic properties [45, 46]. Figure 2.60 shows the stress-strain behavior of 50.6-NiTi alloy, solution-treated at 1000^{o}C for 1hr followed by an intermediate temperature aging at 500^{o}C, as a function of test temperature. This behavior is compared with the corresponding observations for the same alloy aged at a lower temperature of 400^{o}C, as shown in Figure 2.61. In the specimens aged at 500^{o}C, although superelasticity is observed, it is in a very narrow temperature 'window'; shape memory effect is also incomplete due to the permanent residual strains even after heating. By contrast, the specimen aged at 400^{o}C exhibits superior SM and SE characteristics, with a large superelastic temperature 'window'. This can be rationalized from the observation that high-density precipitate formation increases the critical stress for slip considerably.

As the TEM micrographs, shown in Figure 2.62, indicate, aging at 400°C produces high density of small sized Ti_3Ni_4 precipitates, whereas at 500°C, the precipitates are larger and density is lower. At 600°C, the precipitates are not observed at all [47]. This is confirmed by the TTT data reported by [39, 268], where the optimal precipitation kinetics are exhibited at 400°C. Aging at 300°C, however, does not improve the SE characteristics since the precipitation kinetics are sluggish at this temperature, thus requiring longer aging times for high-density of precipitate formation and thus high-resistance for slip.

(c) Work-hardening + precipitation-hardening: Both work-hardening and precipitation hardening has been shown to improve the SE and SM characteristics. It has been further shown that combined usage of both types of hardening mechanisms is more effective to improve the critical stress for slip, thus making it possible to achieve SE at higher stress levels compared to that achievable with either work-hardening or age-hardening alone [47]. Indeed, as Figure 2.63 shows, complete and stable SE is observed for a cold-worked and aged 50.6-NiTi alloy; even at high stress levels of ~800MPa.

Thus, thermomechanical treatment is very useful in improving the overall SE and SM characteristics of the NiTi alloys. Typically, the recovery temperature for cold-worked NiTi alloys is between 400°C and 500°C. Aging heat treatment of a cold-worked Ni-rich NiTi alloy is likely to produce a complex microstructure containing relatively large densities of dislocations and precipitates that are interwoven in such a way that precipitation may occur mainly on dislocations, act as obstacles for

dislocation movement, and may hinder the recovery process (see Figure 2.50); thus the recovery temperature is likely to be ~500^{o}C.

2.5 Summary of Objectives

The preceding sections introduced various concepts concerning diffusionless (martensitic) and diffusion-based phase transformations in NiTi alloys. Additionally, the quasi-static response of NiTi in shape-memory (martensite) and superelastic (austenite) conditions were discussed. For further development of Ni-Ti based shape memory alloys in structural and impact related fields, two Ni-rich NiTi alloys are systematically investigated in this study. The objectives of the current work are summarized in Figure 2.64.

2.6 Figures

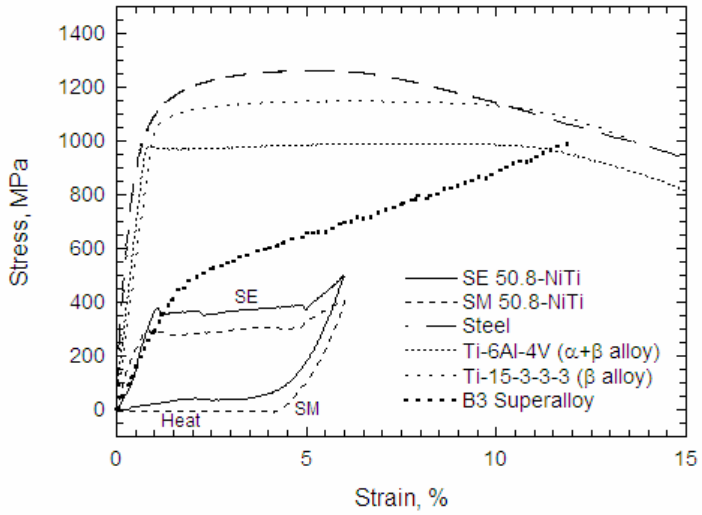

Figure 2.1 Stress-strain curves of superelastic (SE) and shape-memory (SM) NiTi alloys juxtaposed with the corresponding curves of conventional alloys of Ti, Ni-based superalloys and steels. The SM alloy recovers the apparent permanent strain of 6% upon heating beyond 60°C.

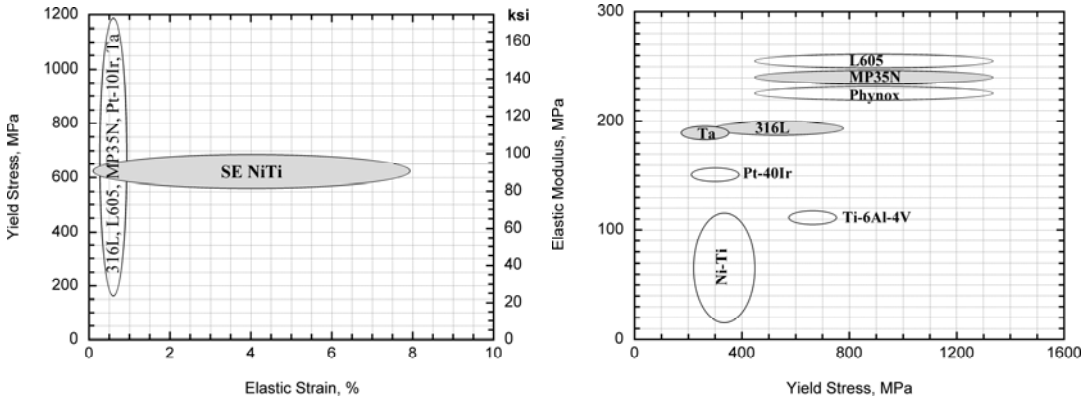

Figure 2.2 (a) Yield stress vs. Elastic strain and (b) Elastic modulus vs. yield stress comparison between Ni-Ti alloy and various common medical alloys[§] (Redrawn, courtesy Neil Morgan).

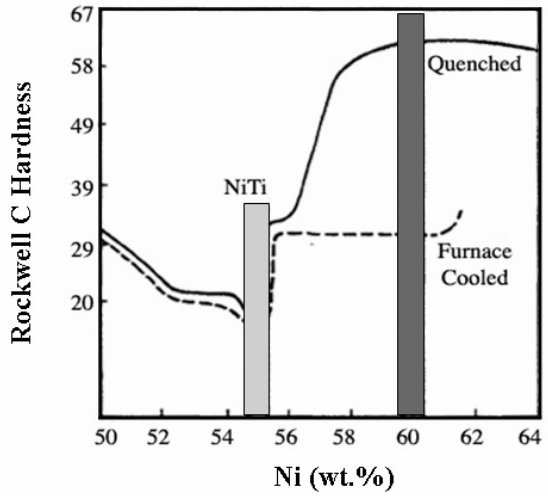

Figure 2.3 Variation of hardness in Ni-Ti alloys as a function of Ni composition in furnace cooled and quenched conditions (from 950°C). Adapted from [13].

[§] L605 is a solid-solution strengthened Co-base alloy (Co-Cr-Ni-W-3% Fe); MP35N is a nonmagnetic, ultra high strength, corrosion resistant Ni-Co-Cr-Mo alloy; Phynox is a age hardenable Co-Cr-Ni alloy with a good combination of high strength, ductility, corrosion resistant, excellent fatigue life and nonmagnetic properties; 316LVM is a Cr-Ni stainless steel alloy with 8% Ni and 2-3% Mo addition to improve corrosion resistance in human body. Ti-6Al-4V is a $\alpha+\beta$ alloy known for its biocompatibility and good combination of mechanical properties, such as high strength and ductility.

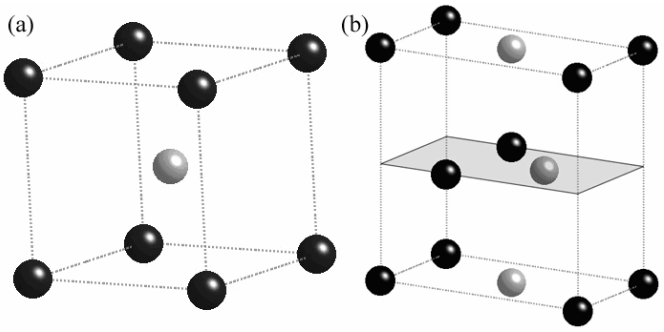

Figure 2.4 Crystal structure of (a) cubic parent austenite phase (after the British scientist Sir W. C. Roberts-Austen, 1898) and (b) monoclinic low temperature martensite phase (after the German Scientist Adolf Martens, 1890).

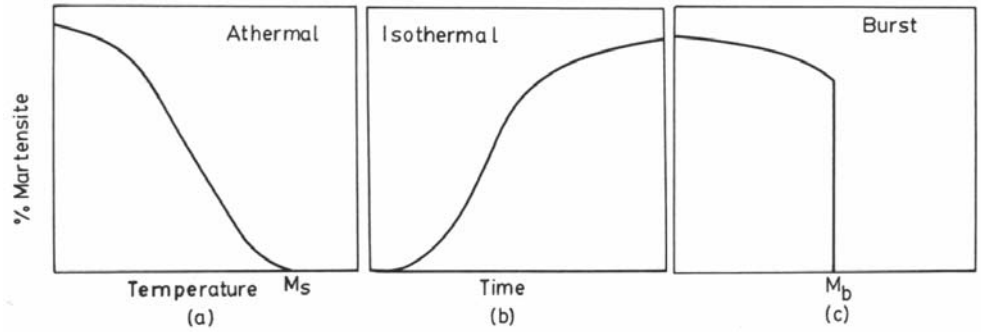

Figure 2.5 Kinetic modes of martensite growth: (a) athermal, (b) isothermal and (c) burst [129].

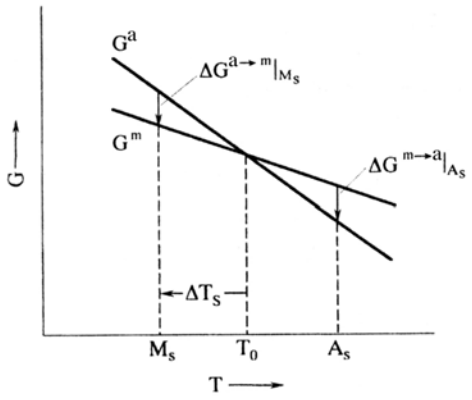

Figure 2.6 Schematic representation of free energy curves for austenite and martensite phases. ΔT_s is the supercooling required for the martensitic transformation [125].

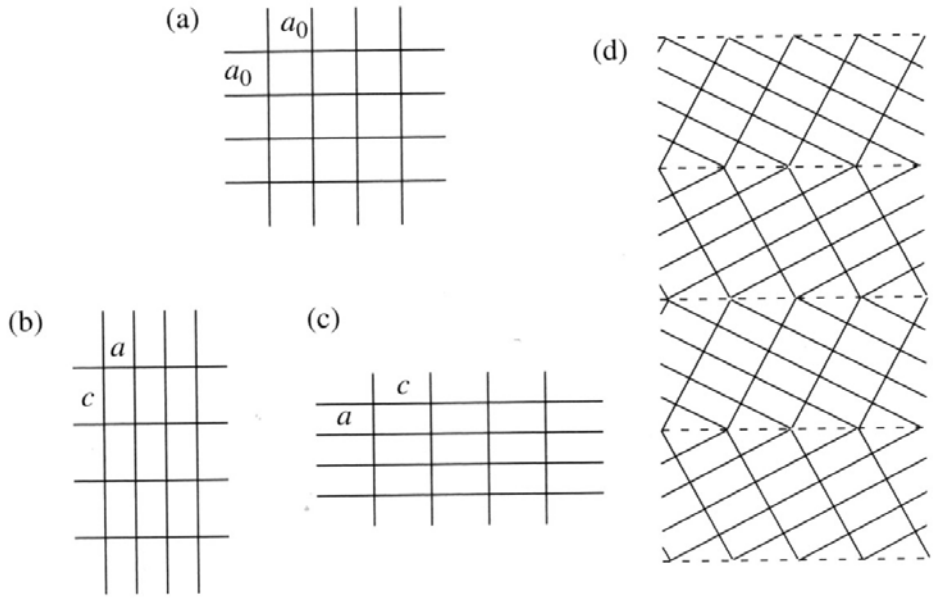

Figure 2.7 Schematic illustration of the martensitic phase transformation: (a) austenite unit cell and (b,c) variants of the martensite phase. (d) Alternating variants of the martensite are arranged coherently resulting in no net shape change [119].

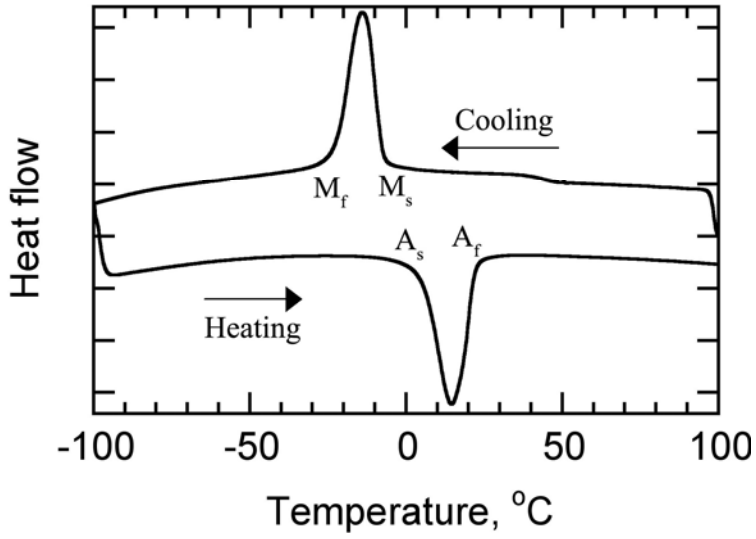

Figure 2.8 DSC trace of fully annealed (800°C, 0.5-hr) 50.8-NiTi and the corresponding transformation temperatures, M_s, M_f, A_s and A_f.

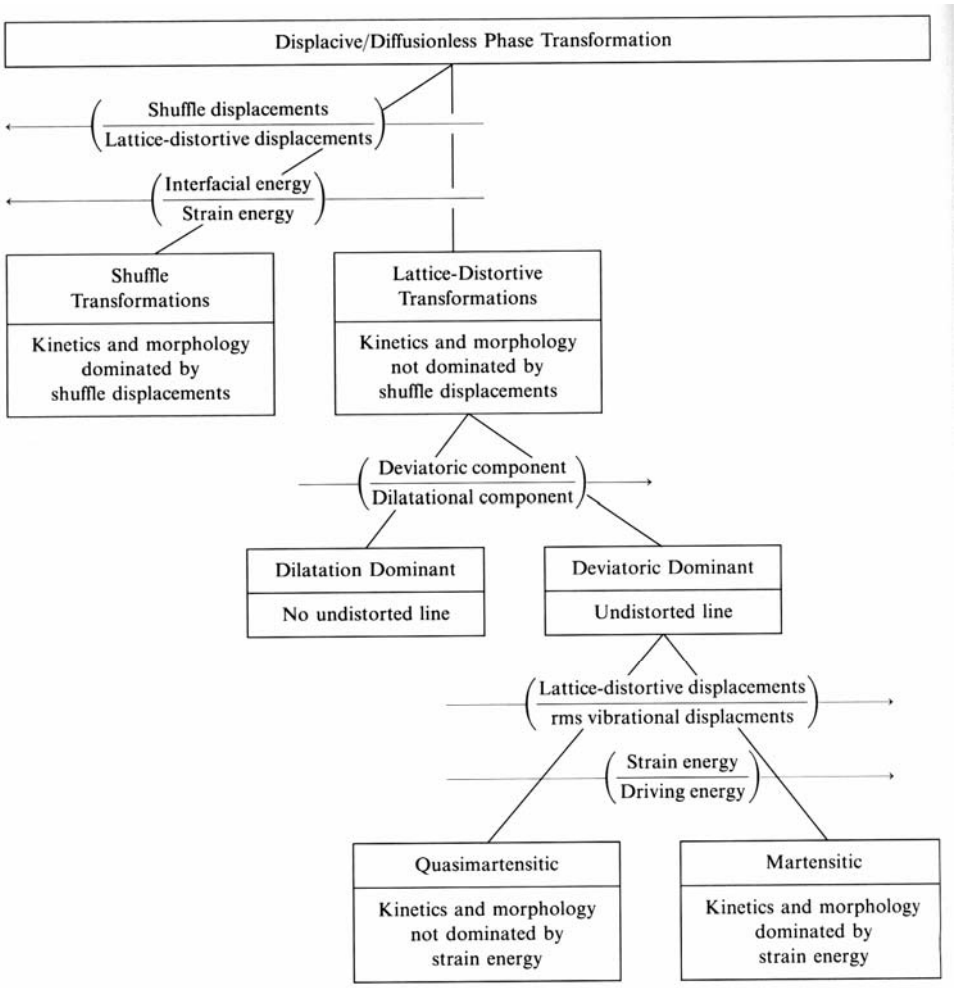

Figure 2.9 Classification scheme/criteria for diffusionless phase transformations proposed by Cohen *et al.* [128, 144].

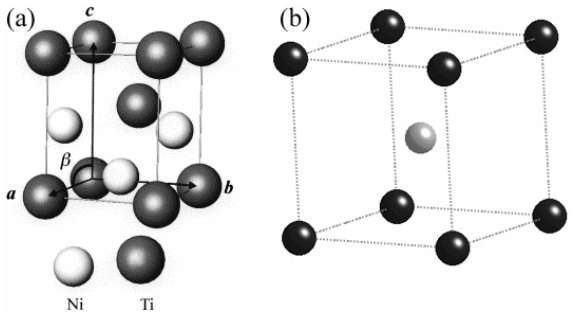

Figure 2.10 Schematic illustration of the crystal structure of NiTi (a) B19' monoclinic unit cell (adapted from [47]) and (b) B2 cubic unit cell of NiTi austenite.

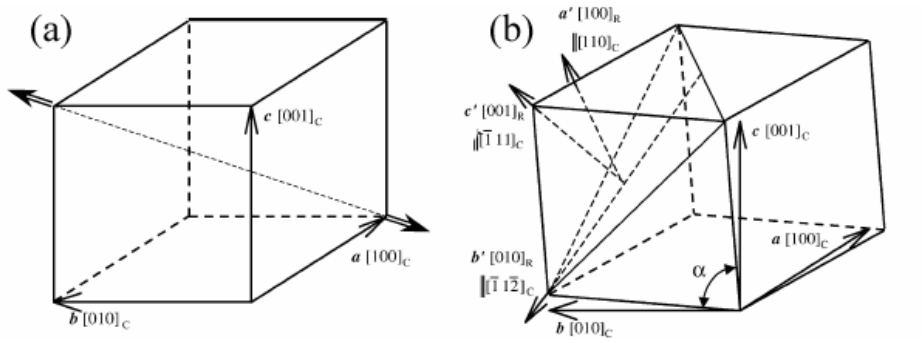

Figure 2.11 Lattice distortion from B2 to R-phase. The axes *a'*, *b'*, *c'* represent the principal axes in the lattice distortion [157].

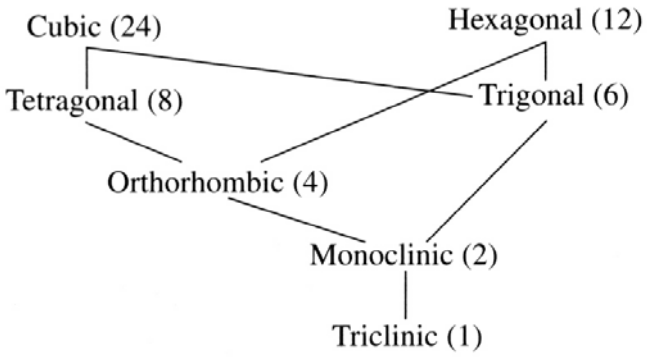

Figure 2.12 The seven symmetries with the total number of elements within each point group is indicated in the parenthesis. The group at the bottom of a connecting line is a subgroup of that on the top [119].

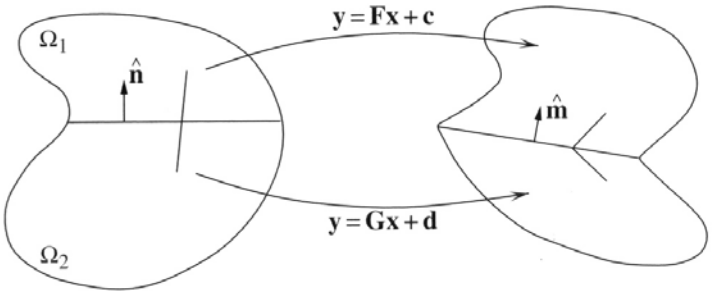

Figure 2.13 Schematic illustration of kinematic compatibility [119].

$$\mathbf{U}_1=\begin{pmatrix}\gamma & \varepsilon & \varepsilon\\ \varepsilon & \alpha & \delta\\ \varepsilon & \delta & \alpha\end{pmatrix} \quad \mathbf{U}_2=\begin{pmatrix}\gamma & -\varepsilon & -\varepsilon\\ -\varepsilon & \alpha & \delta\\ -\varepsilon & \delta & \alpha\end{pmatrix} \quad \mathbf{U}_3=\begin{pmatrix}\gamma & -\varepsilon & \varepsilon\\ -\varepsilon & \alpha & -\delta\\ \varepsilon & -\delta & \alpha\end{pmatrix}$$

$$\mathbf{U}_4=\begin{pmatrix}\gamma & \varepsilon & -\varepsilon\\ \varepsilon & \alpha & -\delta\\ -\varepsilon & -\delta & \alpha\end{pmatrix} \quad \mathbf{U}_5=\begin{pmatrix}\alpha & \varepsilon & \delta\\ \varepsilon & \gamma & \varepsilon\\ \delta & \varepsilon & \alpha\end{pmatrix} \quad \mathbf{U}_6=\begin{pmatrix}\alpha & -\varepsilon & \delta\\ -\varepsilon & \gamma & -\varepsilon\\ \delta & -\varepsilon & \alpha\end{pmatrix}$$

$$\mathbf{U}_7=\begin{pmatrix}\alpha & -\varepsilon & -\delta\\ -\varepsilon & \gamma & \varepsilon\\ -\delta & \varepsilon & \alpha\end{pmatrix} \quad \mathbf{U}_8=\begin{pmatrix}\alpha & \varepsilon & -\delta\\ \varepsilon & \gamma & -\varepsilon\\ -\delta & -\varepsilon & \alpha\end{pmatrix} \quad \mathbf{U}_9=\begin{pmatrix}\alpha & \delta & \varepsilon\\ \delta & \alpha & \varepsilon\\ \varepsilon & \varepsilon & \gamma\end{pmatrix}$$

$$\mathbf{U}_{10}=\begin{pmatrix}\alpha & \delta & -\varepsilon\\ \delta & \alpha & -\varepsilon\\ -\varepsilon & -\varepsilon & \gamma\end{pmatrix} \quad \mathbf{U}_{11}=\begin{pmatrix}\alpha & -\delta & \varepsilon\\ -\delta & \alpha & -\varepsilon\\ \varepsilon & -\varepsilon & \gamma\end{pmatrix} \quad \mathbf{U}_{12}=\begin{pmatrix}\alpha & -\delta & -\varepsilon\\ -\delta & \alpha & \varepsilon\\ -\varepsilon & \varepsilon & \gamma\end{pmatrix}$$

Figure 2.14 Bain transformation matrix for 12 martensite variants theoretically possible in Ni-Ti. α = 1.0243, γ = 0.9563, δ = 0.058, and ε = -0.0427 [65, 162]

LCVs	Basis of martensite cell		
	$[1\,0\,0]_m$	$[0\,1\,0]_m$	$[0\,0\,1]_m$
1	$[1\,0\,0]_p$	$[0\,1\,1]_p$	$[0\,1\,1]_p$
2	$[\bar{1}\,0\,0]_p$	$[0\,\bar{1}\,1]_p$	$[0\,\bar{1}\,1]_p$
3	$[1\,0\,0]_p$	$[0\,\bar{1}\,1]_p$	$[0\,\bar{1}\,\bar{1}]_p$
4	$[\bar{1}\,0\,0]_p$	$[0\,1\,\bar{1}]_p$	$[0\,\bar{1}\,\bar{1}]_p$
5	$[0\,1\,0]_p$	$[1\,0\,1]_p$	$[1\,0\,\bar{1}]_p$
6	$[0\,\bar{1}\,0]_p$	$[\bar{1}\,0\,\bar{1}]_p$	$[1\,0\,\bar{1}]_p$
7	$[0\,1\,0]_p$	$[1\,0\,\bar{1}]_p$	$[\bar{1}\,0\,\bar{1}]_p$
8	$[0\,\bar{1}\,0]_p$	$[\bar{1}\,0\,1]_p$	$[\bar{1}\,0\,\bar{1}]_p$
9	$[0\,0\,1]_p$	$[1\,1\,0]_p$	$[\bar{1}\,1\,0]_p$
10	$[0\,0\,\bar{1}]_p$	$[\bar{1}\,\bar{1}\,0]_p$	$[\bar{1}\,1\,0]_p$
11	$[0\,0\,1]_p$	$[\bar{1}\,1\,0]_p$	$[\bar{1}\,\bar{1}\,0]_p$
12	$[0\,0\,\bar{1}]_p$	$[1\,\bar{1}\,0]_p$	$[\bar{1}\,\bar{1}\,0]_p$

Figure 2.15 The lattice correspondence variants (LCVs) for B2-B19' in NiTi [163].

a	$\hat{\mathbf{n}}$	Twinning elements
Twinning mode A, variants 1–2		
Compound		
$\begin{pmatrix} -0.01263 \\ 0.16020 \\ 0.16020 \end{pmatrix}$	$\begin{pmatrix} 1 \\ 0 \\ 0 \end{pmatrix}$	$s = 0.2385$ $\eta_1 = [001]$ $K_1 = (100)$
$\begin{pmatrix} 0.25619 \\ -0.01143 \\ -0.01143 \end{pmatrix}$	$\frac{1}{\sqrt{2}}\begin{pmatrix} 0 \\ 1 \\ 1 \end{pmatrix}$	$s = 0.2385$ $\eta_1 = [100]$ $K_1 = (001)$
Twinning mode B, variants 1–3 (also 1–4)		
Type I		
$\begin{pmatrix} 0.1709 \\ -0.0197 \\ -0.2274 \end{pmatrix}$	$\begin{pmatrix} 0 \\ 1 \\ 0 \end{pmatrix}$	$s = 0.2804$ $\eta_1 = [\overline{1.572}, 1, \bar{1}]$ $K_1 = (011)$
Type II		
$\begin{pmatrix} -0.01204 \\ 0.28900 \\ 0.01638 \end{pmatrix}$	$\begin{pmatrix} 0.5846 \\ 0. \\ -0.8113 \end{pmatrix}$	$s = 0.2804$ $\eta_1 = [011]$ $K_1 = (0.7206, \bar{1}, 1)$
Twinning mode C, variants 1–5 (also 1–9)		
Type I		
$\begin{pmatrix} 0.0814 \\ 0.1161 \\ 0.2835 \end{pmatrix}$	$\frac{1}{\sqrt{2}}\begin{pmatrix} 1 \\ -1 \\ 0 \end{pmatrix}$	$s = 0.3096$ $\eta_1 = [1.176, 1, \overline{2.1764}]$ $K_1 = (111)$
Type II		
$\begin{pmatrix} 0.2131 \\ -0.2276 \\ -0.0215 \end{pmatrix}$	$\begin{pmatrix} 0.2975 \\ 0.2975 \\ 0.9072 \end{pmatrix}$	$s = 0.309637$ $\eta_1 = [211]$ $K_1 = (\overline{0.2470}, \overline{0.5060}, 1)$
Twinning mode D, variants 1–8 (also 1–11)		
Type I		
$\begin{pmatrix} 0.08814 \\ -0.09450 \\ -0.03755 \end{pmatrix}$	$\frac{1}{\sqrt{2}}\begin{pmatrix} 1 \\ 1 \\ 0 \end{pmatrix}$	$s = 0.1423$ $\eta_1 = [2.954, 1, 1.954]$ $K_1 = (\bar{1}11)$
Type II		
$\begin{pmatrix} 0.1037 \\ 0.1114 \\ 0.0017 \end{pmatrix}$	$\begin{pmatrix} 0.6674 \\ -0.6674 \\ -0.3305 \end{pmatrix}$	$s = 0.1423$ $\eta_1 = [\bar{2}11]$ $K_1 = (0.6686, 0.3376, 1)$

Figure 2.16 Twinning modes and twinning elements theoretically possible in a B2-B19' transformation in NiTi [119].

Twinning mode	K_1		η_1		K_2	η_2	s	Sol.
$\{\bar{1}\,\bar{1}\,1\}$	$(\bar{1}\,\bar{1}\,1)$	$(\bar{1}\,\bar{1}\,0)_p$	$[0.540430.459571]$		$(0.246950.506111)$	$[\bar{2}\,\bar{1}\,1]$	0.30961	Yes
Type I	$(\bar{1}\,1\,1)$	$(\bar{1}\,0\,1)_p$	$[0.540430.459571]$		$(0.246950.506111)$	$[\bar{2}\,1\,1]$	0.30961	Yes
$\{1\,1\,1\}$	$(1\,1\,1)$	$(1\,0\,1)_p$	$[\overline{1.511720}.511721]$		$(\overline{0.66875}0.337501)$	$[2\,1\,1]$	0.14222	No
Type I	$(1\,\bar{1}\,1)$	$(1\,\bar{1}\,0)_p$	$[\overline{1.511720.511721}]$		$(\overline{0.66875}0.337501)$	$[2\,\bar{1}\,1]$	0.14222	No
$\{0\,1\,1\}$	$(0\,1\,1)$	$(0\,0\,1)_p$	$[1.572711\,\bar{1}]$		$(0.720531\,\bar{1})$	$[0\,1\,1]$	0.28040	Yes
Type I	$(0\,1\,\bar{1})$	$(0\,1\,0)_p$	$[\overline{1.572711}\,1]$		$(\overline{0.72053}\,1\,1)$	$[0\,1\,\bar{1}]$	0.28040	Yes
$\langle 0\,1\,1\rangle$	$(0.720531\,\bar{1})$		$[0\,1\,1]$	$[0\,0\,1]_p$	$(0\,1\,1)$	$[1.572711\,\bar{1}]$	0.28040	Yes
Type II	$(\overline{0.72053}\,1\,1)$		$[0\,1\,\bar{1}]$	$[0\,1\,0]_p$	$(0\,1\,\bar{1})$	$[\overline{1.57271}\,1\,1]$	0.28040	Yes
Compound	$(0\,0\,1)$	$(0\,\bar{1}\,1)_p$	$[1\,0\,0]$	$[1\,0\,0]_p$	$(1\,0\,0)$	$[0\,0\,1]$	0.23848	No
	$(1\,0\,0)$	$(1\,0\,0)_p$	$[0\,0\,1]$	$[0\,\bar{1}\,1]_p$	$(0\,0\,1)$	$[1\,0\,0]$	0.23848	No
$\{2\,0\,\bar{1}\}$	$(2\,0\,\bar{1})$	$(4\,1\,\bar{1})_p$	$[\bar{1}\,0\,\bar{2}]$	$[\bar{1}\,\bar{2}\,\bar{2}]_p$	$(0\,0\,\bar{1})$	$[1\,0\,0]$	0.4250	No

Figure 2.17 Twinning modes of B19' martensite [47]. All indices without subscript are indexed in the martensite lattice, while those with subscript p are indexed in austenite lattice; they can be related through the lattice correspondence. The column under 'sol.' Indicates whether a solution as a lattice invariant shear exists under the phenomenological crystallographic theory.

Variant	1	2	3	4	5	6	7	8	9	10	11	12
1		A	B	B	C	N	N	D	C	N	D	N
2	A		B	B	N	D	C	N	N	D	N	C
3	B	B		A	N	C	D	N	D	N	C	N
4	B	B	A		D	N	N	C	N	C	N	D
5	C	N	N	D		A	B	B	C	N	N	D
6	N	D	C	N	A		B	B	N	D	C	N
7	N	C	D	N	B	B		A	D	N	N	C
8	D	N	N	C	B	B	A		N	C	D	N
9	C	N	D	N	C	N	D	N		A	B	B
10	N	D	N	C	N	D	N	C	A		B	B
11	D	N	C	N	N	C	N	D	B	B		A
12	N	C	N	D	D	N	C	N	B	B	A	

Figure 2.18 The various twinning modes possible between different combinations of 12 variants taken in pairs. A, B, C and D represent the twinning modes as indicated in Figure 2.16 and N represents a *non-generic twin* [119], although none have been observed to date.

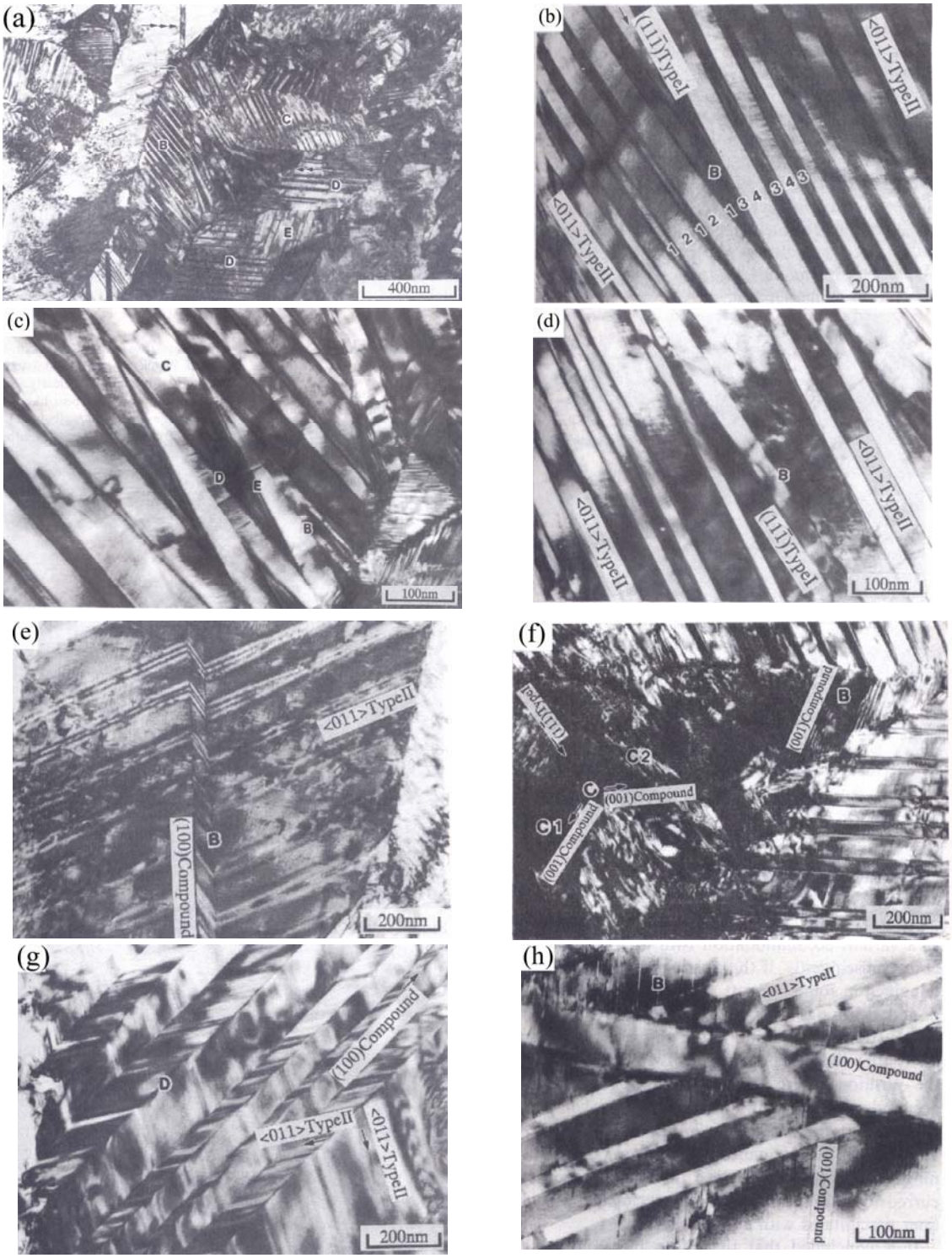

Figure 2.19 Various twins observed in B19' martensite upon transformation from B2 – B19' [168, 169].

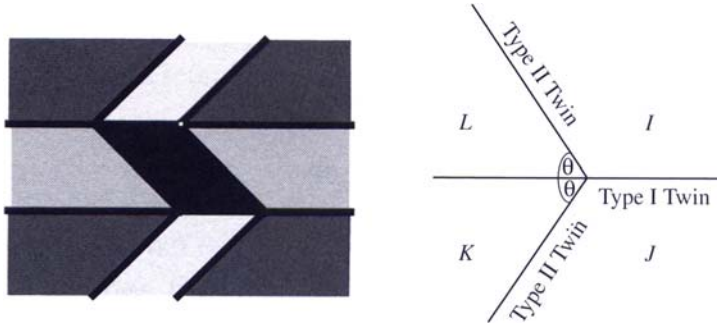

Figure 2.20 Schematic illustration of crossing twins (reproduced from [119]).

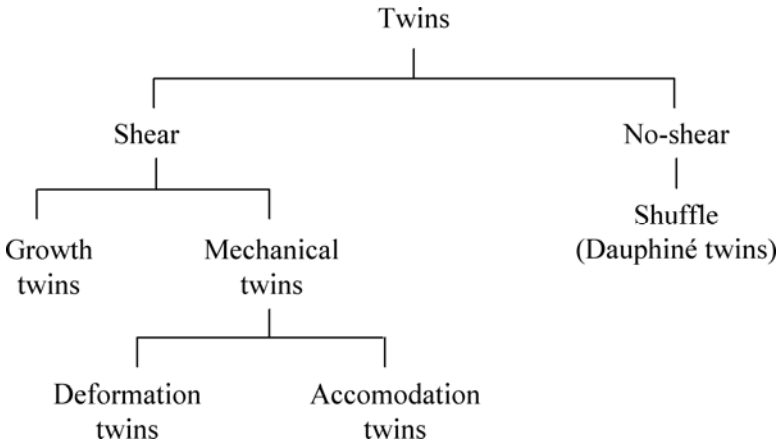

Figure 2.21 Classification of twins based on their physical origin [158].

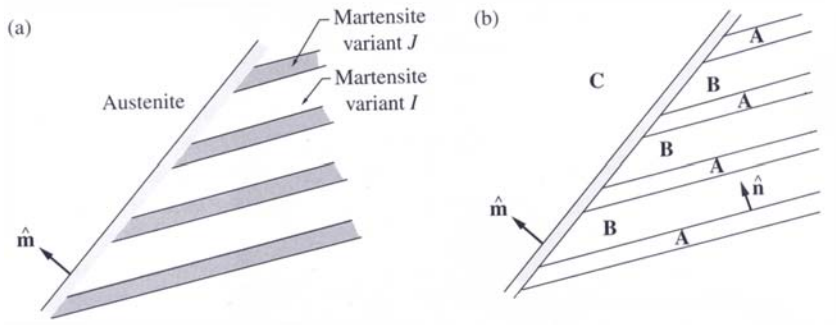

Figure 2.22 (a) Schematic illustration of austenite-martensite interface (*habit plane)* showing the twin relationship of variants *I* and *J* (b) **A**, **B** are the deformation gradients (reproduced from [119]).

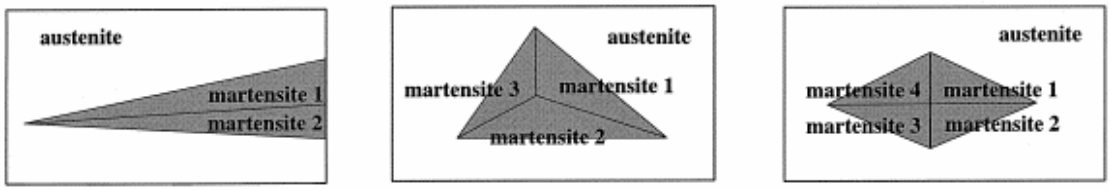

Figure 2.23 Schematic illustration of wedge, triangle and diamond microstructures. The grey areas may be internally twinned also [176].

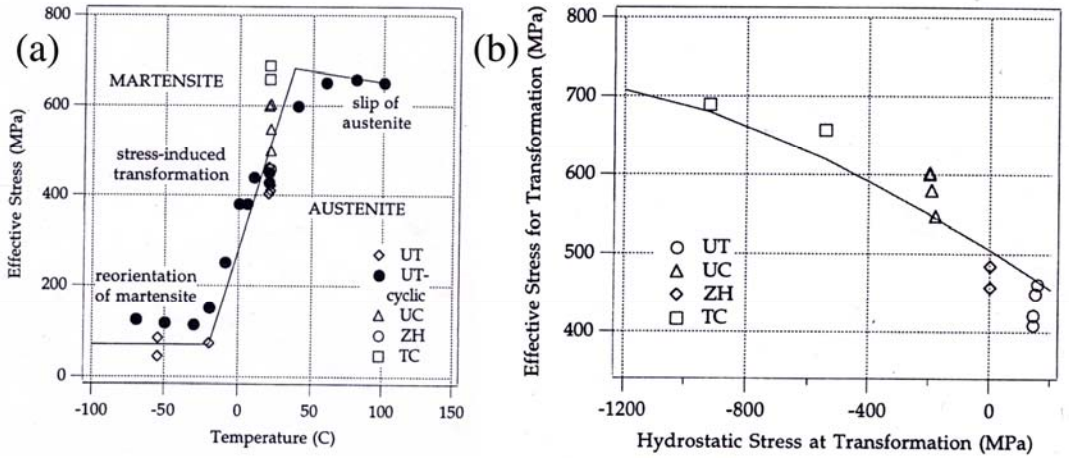

Figure 2.24 Variation of effective stress for transformation as a function of (a) temperature and (b) hydrostatic stress component at transformation for differing stress states at 20 °C [188].

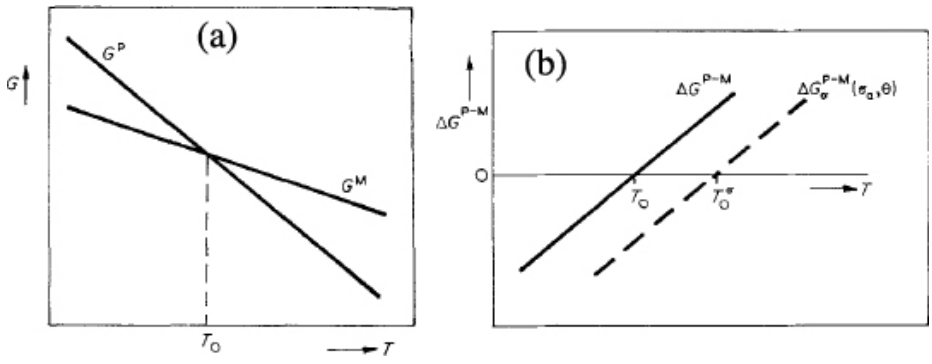

Figure 2.25 Free energies of the austenite and martensite phases as a function of temperature (a) in the absence of stress and (b) in the presence of an applied stress [127].

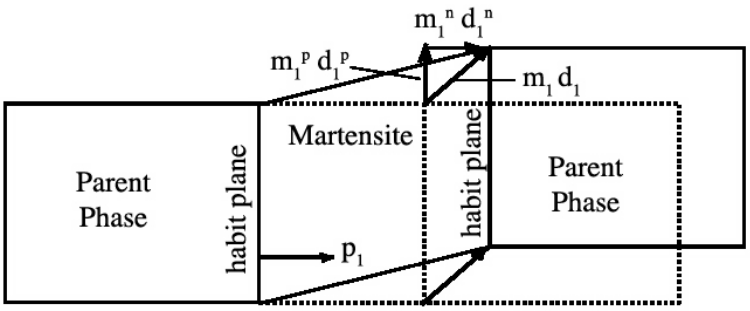

Figure 2.26 Schematic illustration of the transformation (or invariant plane) strain into its components. P_1 is the habit normal, m_1 is the magnitude of shape strain, d_1 is the shape strain direction (redrawn from [199]) .

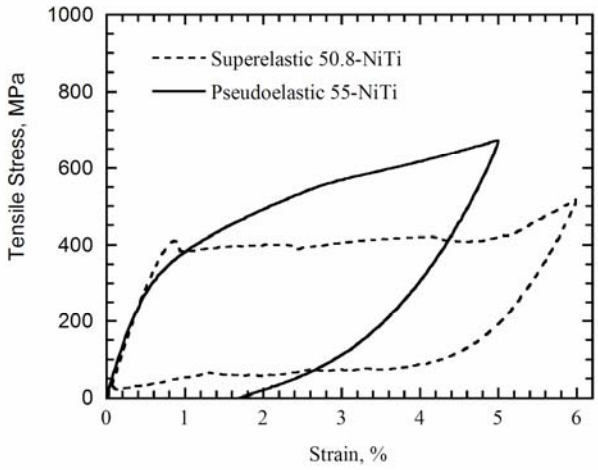

Figure 2.27 Pseudoelasticity in Ni-Ti alloys

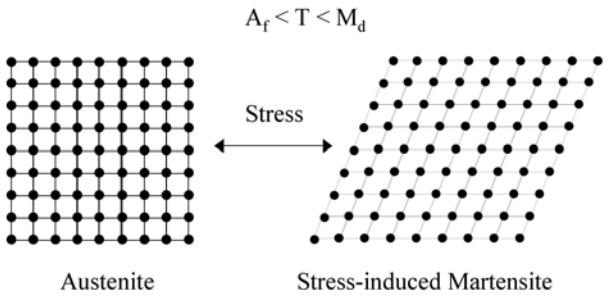

Figure 2.28 Schematic illustration of superelastic effect.

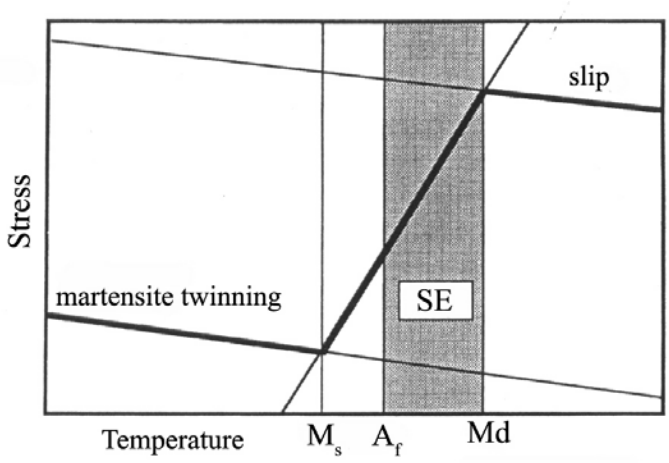

Figure 2.29 σ-T phase diagram of Ni-Ti indicating the SE window [195].

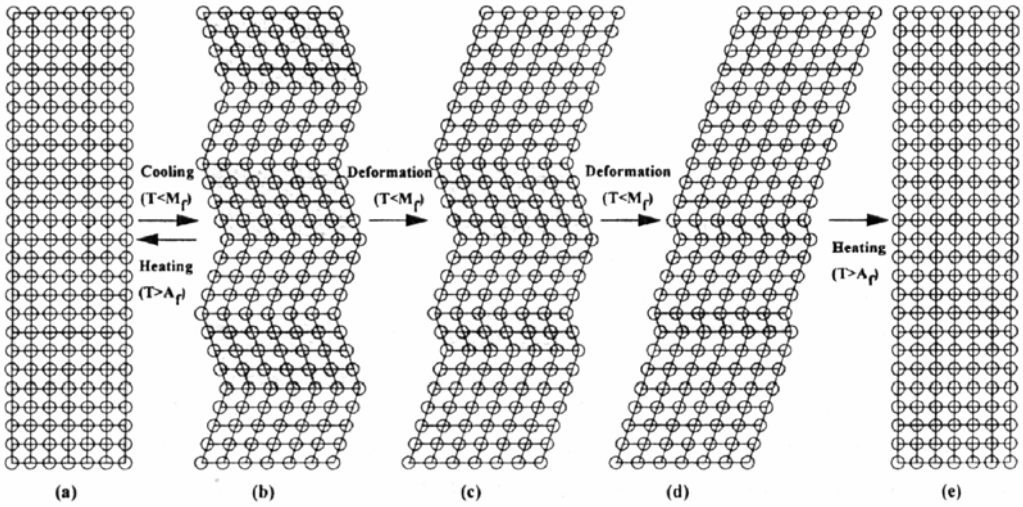

Figure 2.30 Mechanism of shape-memory effect (SME). (a) austenite, (b) self-accommodated martensite, (c-d) deformation of martensite through variant coalescence, (d) reverse transformation [198].

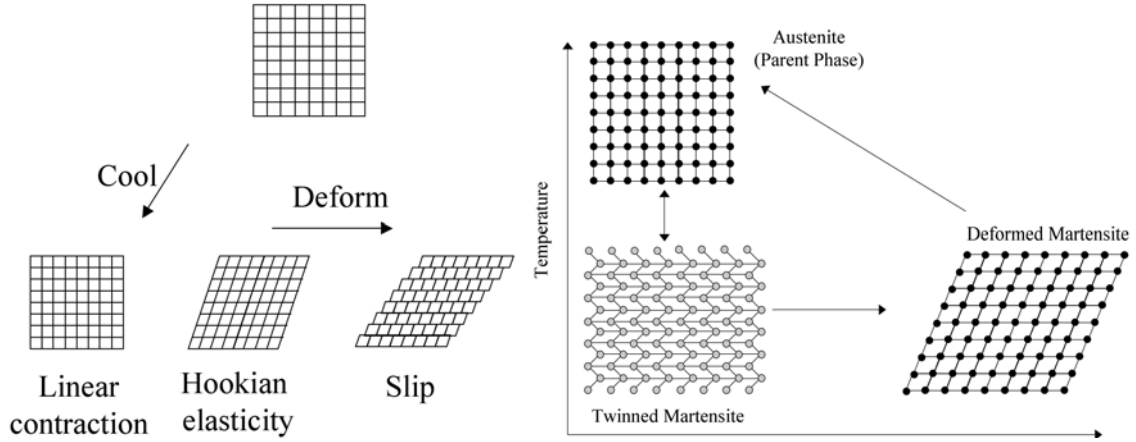

(a) (b)

Figure 2.31 (a) Deformation of conventional alloy vs. (b) shape memory alloy [119].

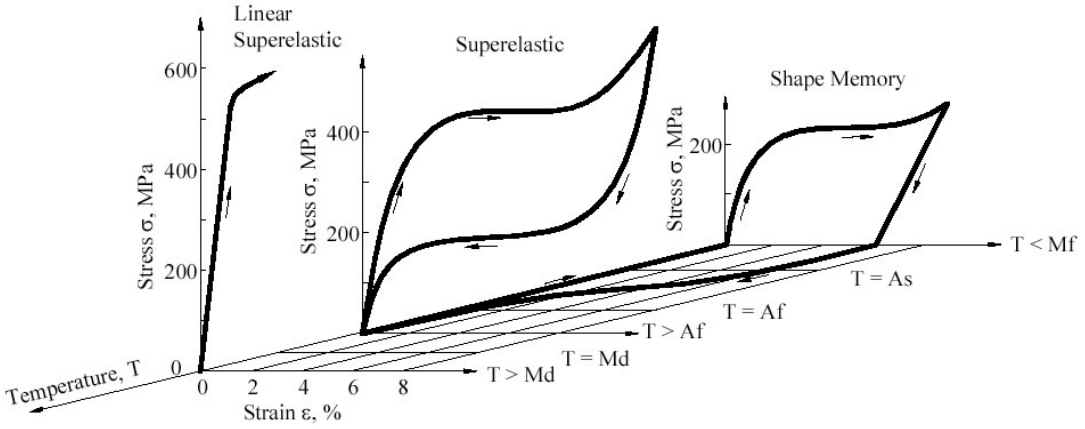

Figure 2.32 Three dimension stress-strain-temperature schematic for shape memory alloys (adapted and reproduced from Duerig *et al.*, and Ryhänen [24, 208]).

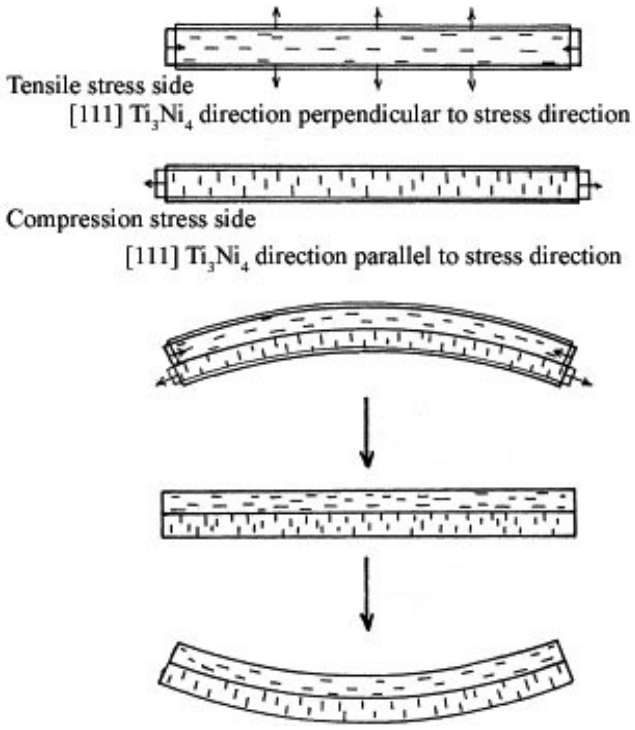

Figure 2.33 Mechanism of *all-round shape memory effect* (ARSME) [219-221].

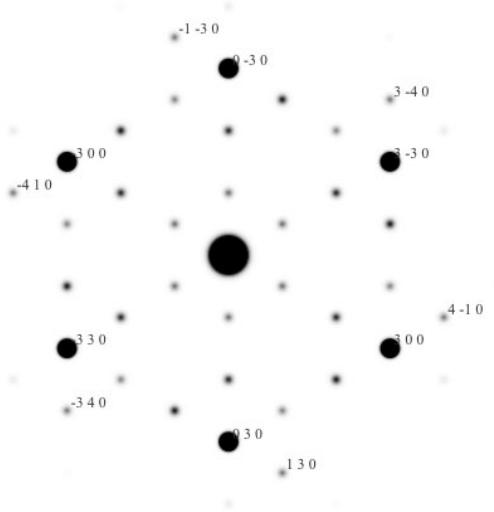

Figure 2.34 Simulated electron diffraction pattern of R-phase (space group *P*-3). Pattern indexing is with respect to <001> zone. The pattern is calculated using Crystal Maker's Single Crystal software program. Compare the pattern with that of Hara reproduced in [47].

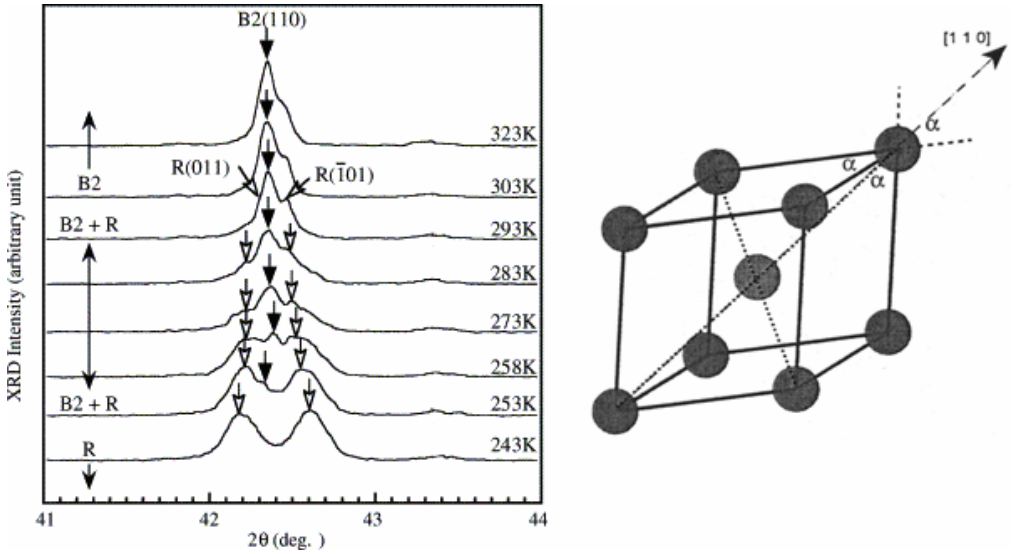

Figure 2.35 X-ray peak splitting due to the transformation from B2 - R-phase [235].

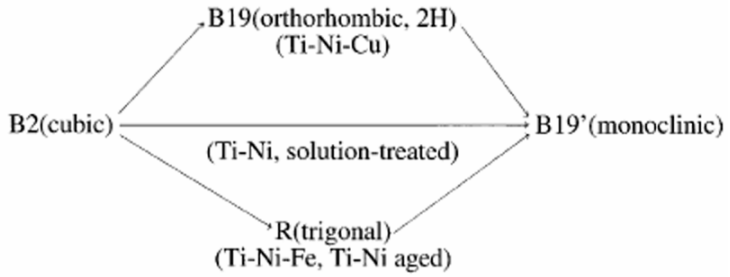

Figure 2.36 Transformation path for martensitic transformations possible in NiTi alloys [47].

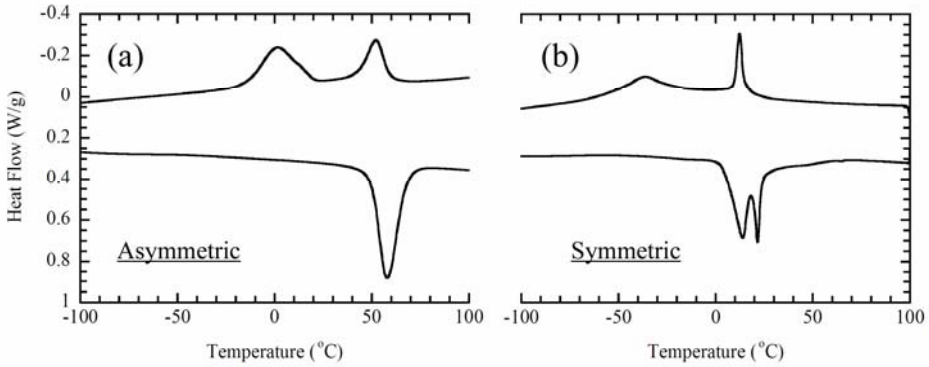

Figure 2.37 R-phase transformation identified on a DSC scan : (a) Asymmetric 2-peak/1-peak transformation and (b) Symmetric 2-peak/2-peak transformation.

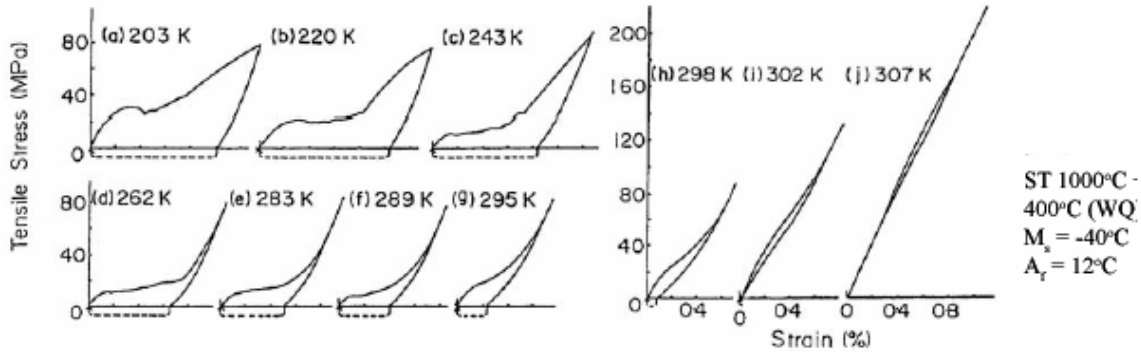

Figure 2.38 Stress-strain curves of 50.5-NiTi single crystals aged at 400°C (1-hr) after solution-treatment (ST). The alloy exhibits both shape memory and superelasticity [63].

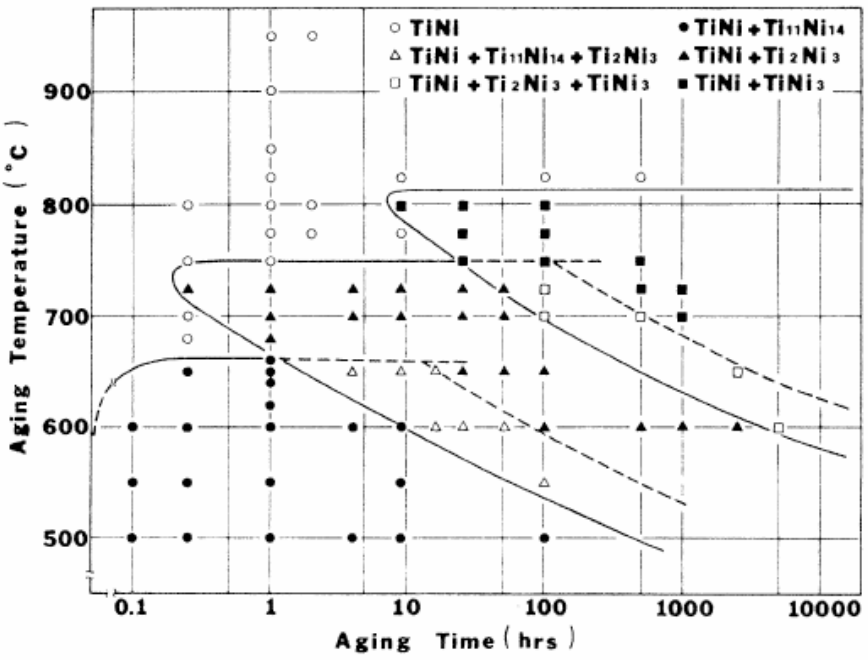

Figure 2.39 TTT diagram computed after the aging behavior of Ti-52Ni at.% (reproduced from Nishida *et al.* [70])

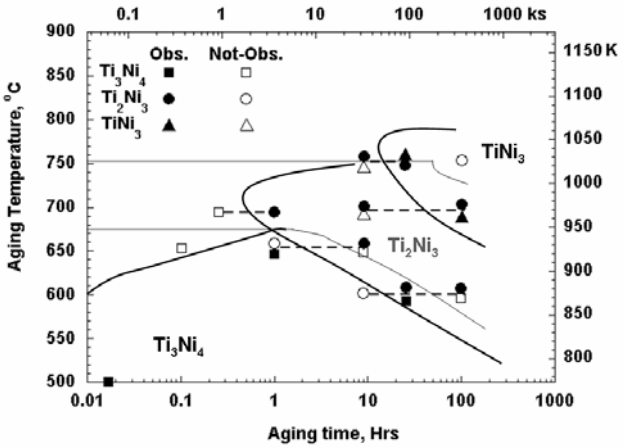

(a)

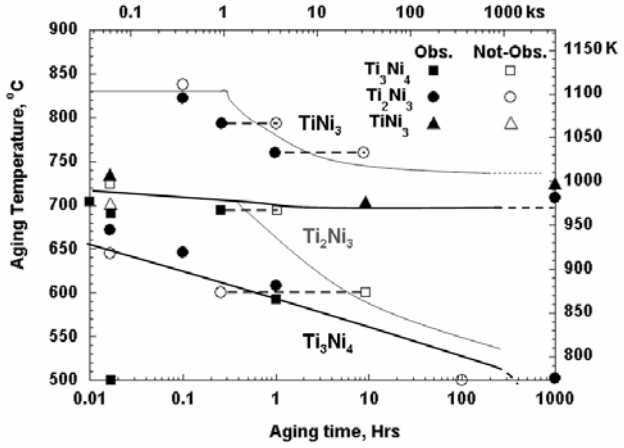

(b)

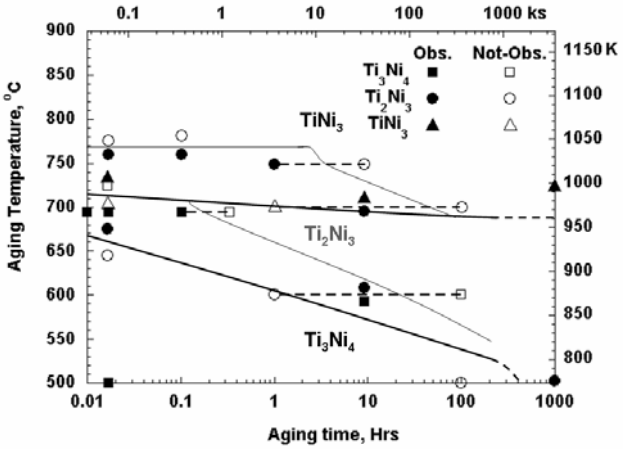

(c)

Figure 2.40 TTT diagram computed after the aging behavior of Ti-(52, 54, 56 at.%) Ni (adapted and redrawn from Kainuma *et al.* [71]).

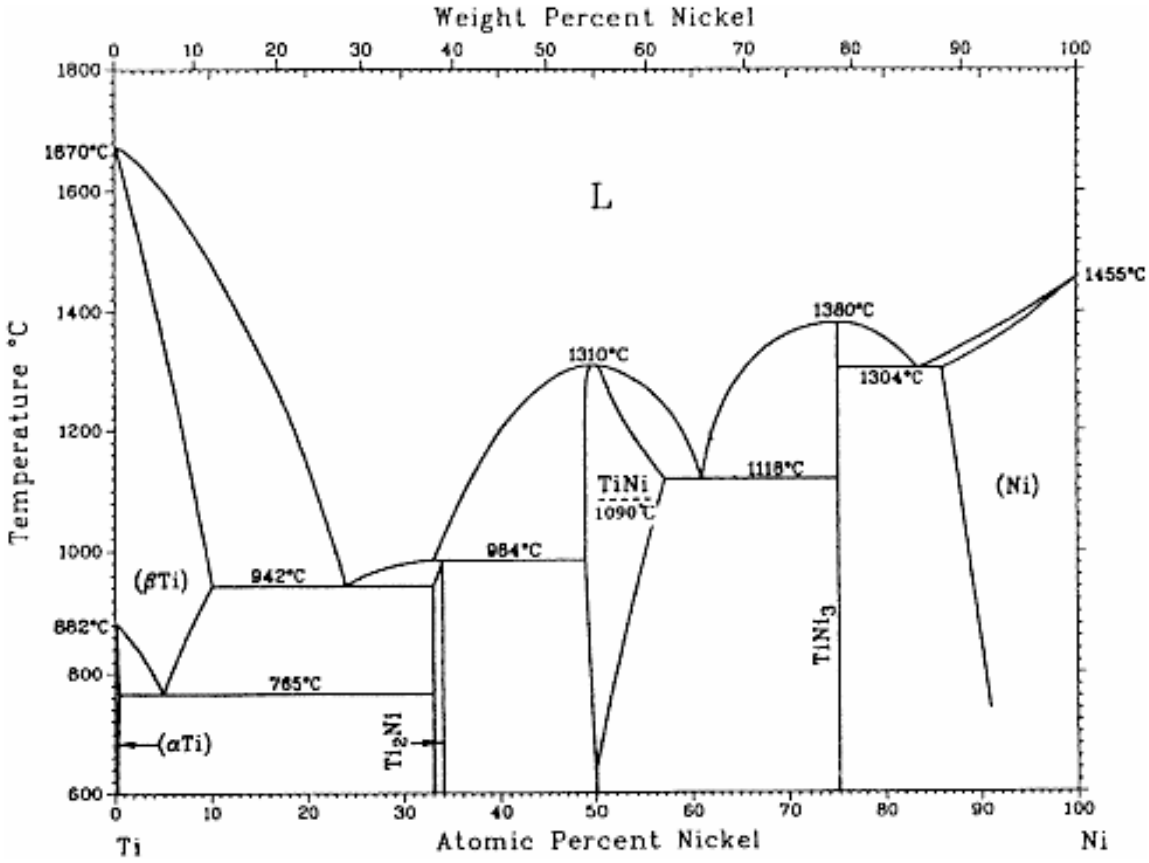

Figure 2.41 Phase diagram of Ni-Ti binary alloy [47, 257].

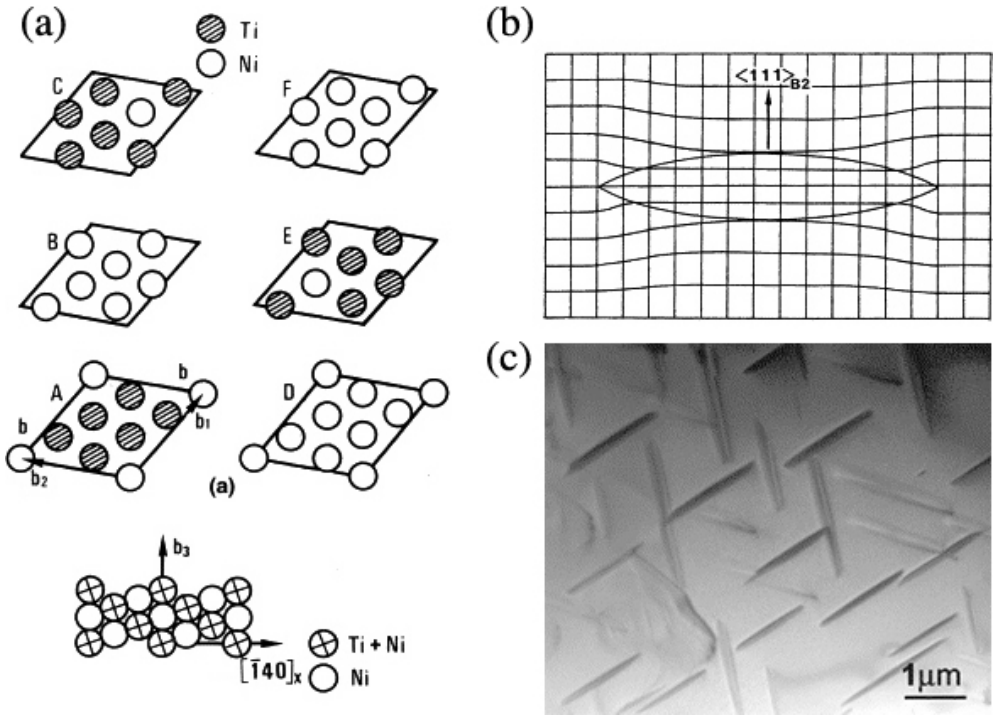

Figure 2.42 (a) The atomic arrangement of Ni and Ti atoms in a single unit cell of Ti_3Ni_4 precipitate composed of six layers, (b) lattice distortion of the matrix surrounding the precipitate, (c) TEM micrograph of Ti_3Ni_4 formed during the aging of Ti-51Ni at 500°C for 150 hrs [256].

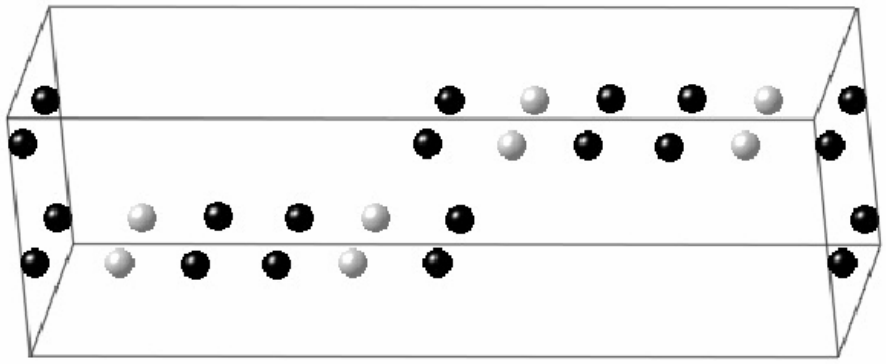

Figure 2.43 Crystal structure of orthorhombic Ti_2Ni_3 (at 20°C). Space group is *Bbmm* and the lattice parameters are a = 4.398 Å, b = 4.370 Å, c = 13.544 Å (at 25 °C) [73].

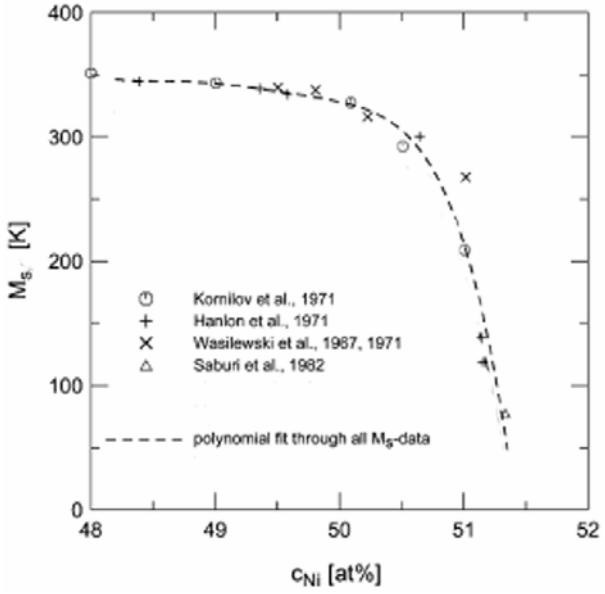

Figure 2.44 Effect of Ni concentration of the martensite start temperature, M_s [270].

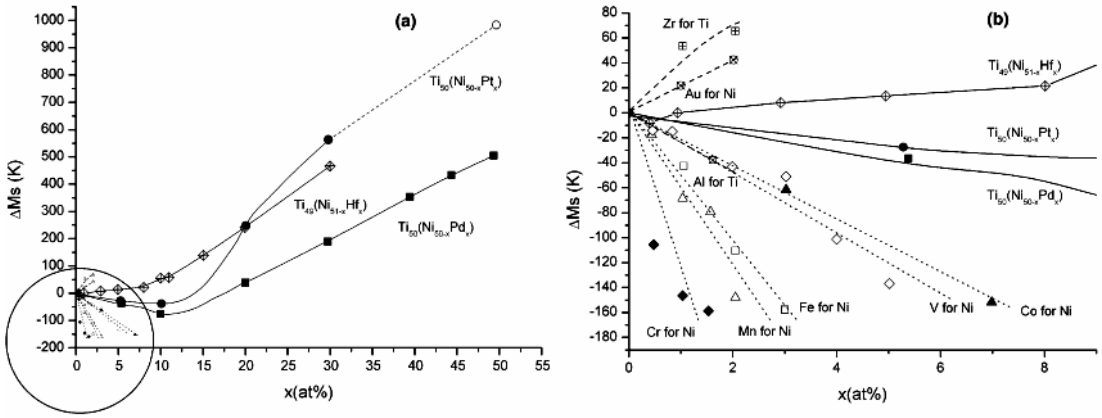

Figure 2.45 Effect of different alloying elements on the martensite start temperature in NiTi alloys: Al, Au, Co, Cr, Fe, Hf, Mn, Pd, Pt, V, Zr. Adapted from [47].

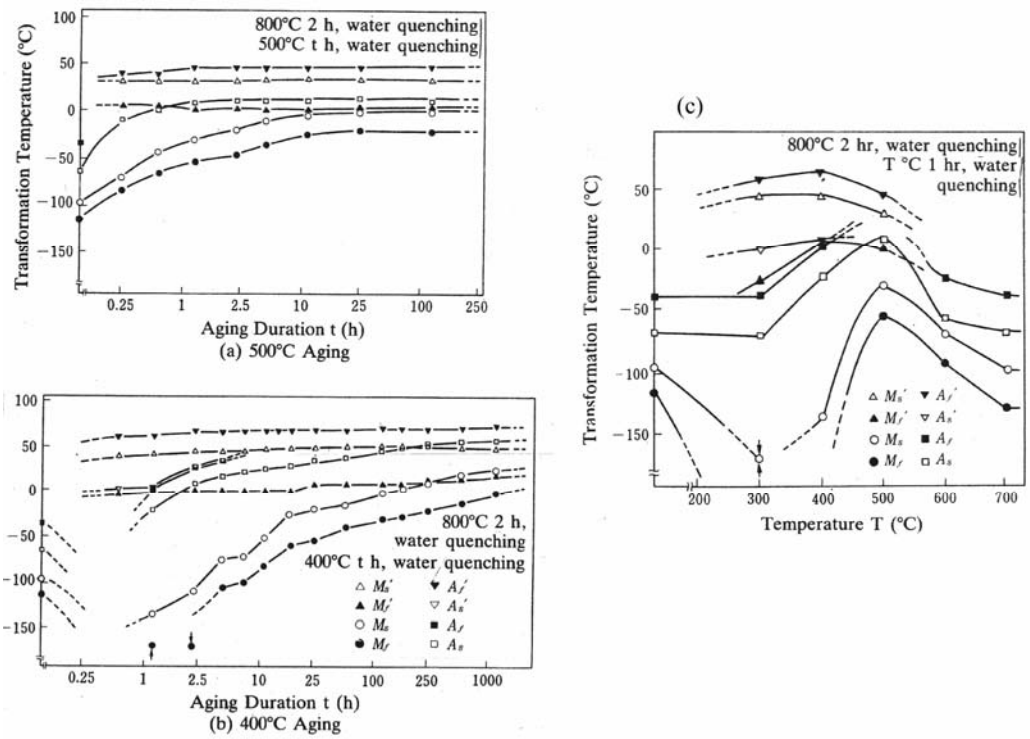

Figure 2.46 Effects of aging time on the transformation temperatures of 51-NiTi (a) aging at 500°C, (b) aging at 400°C. (c) Effect of aging temperature on the transformation temperatures of 51-NiTi (aged for 1hr) [234].

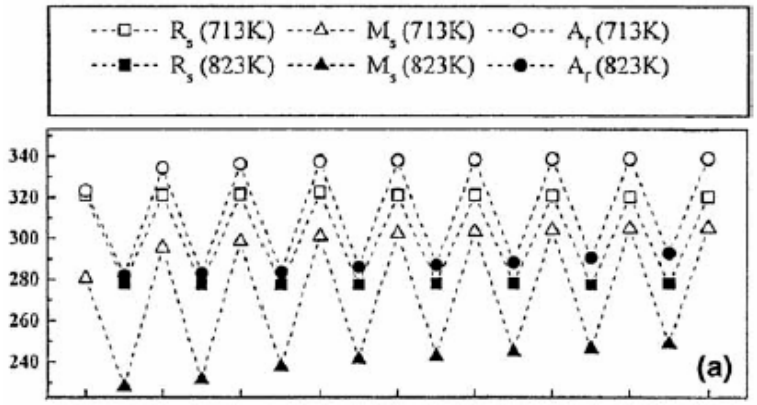

Figure 2.47 Variation of transformation temperatures with number of aging cycles between 440°C and 550°C for 51-NiTi alloy. The aging time at 440°C is 24hrs and at 550°C is 10min/1hr/24hrs/48hrs [47, 269, 278].

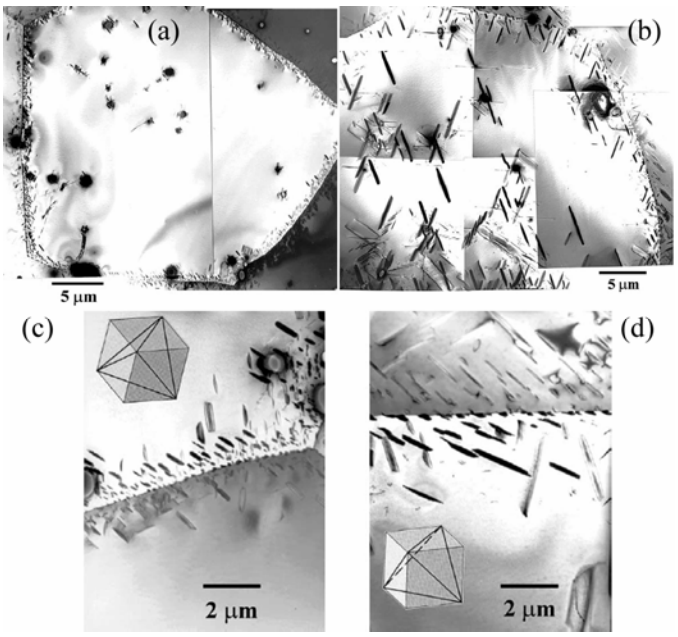

Figure 2.48 Preferential precipitation of Ti_3Ni_4 phases at the grain boundary (GB) and near the Ti_4Ni_2O in the grain interior (GI) after aging for (a) 1hr, (b) 10hrs. Heterogeneous precipitation magnified near the grain boundary after aging for (a) 1hr, (b) 10hrs [270].

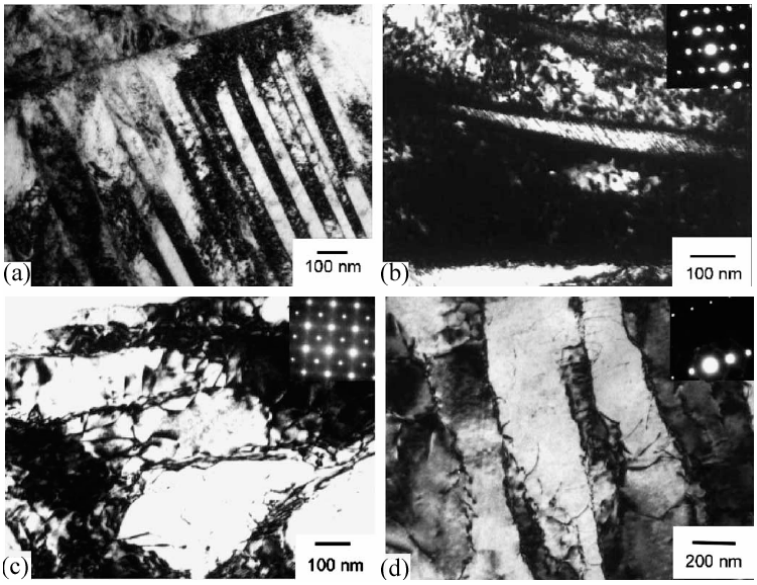

Figure 2.49 Cold rolled (15%) 50.6-NiTi exhibiting (a) slip bands and (b) martensite plate along with high dislocation density. Annealing at 400^{o}C for (c) 15 min and (d) 20 min leads to the formation of well developed dislocations cells that grow with increasing annealing time [303].

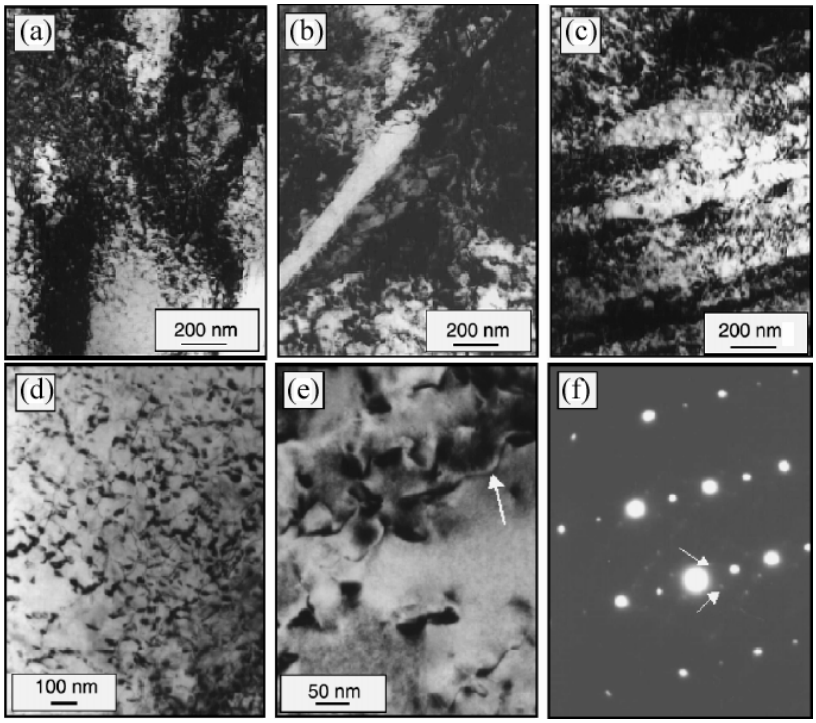

Figure 2.50 Cold-worked (10%) + annealed (400°C) 50.6-NiTi alloy structure after (a) 0.5hr, (b) 2hrs and (c) 4hrs. The Ti_3Ni_4 precipitates decorate the dislocations in the alloy after annealing at 400°C for (d) 2hrs and (e) 4hrs, the dislocations can be seen to bend at the precipitates. The selected area diffraction in (f) shows the extra sports from the precipitates [281].

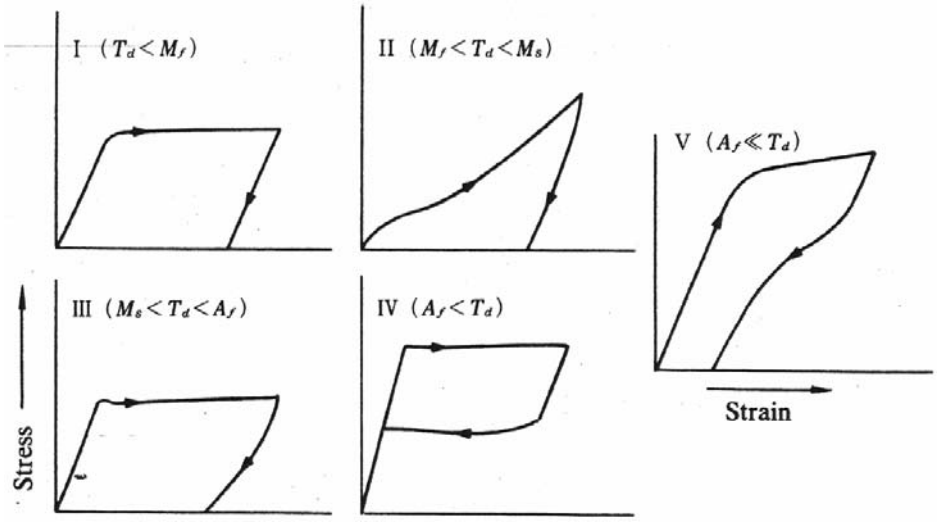

Figure 2.51 Different types of stress-strain curves observed in NiTi alloys [234].

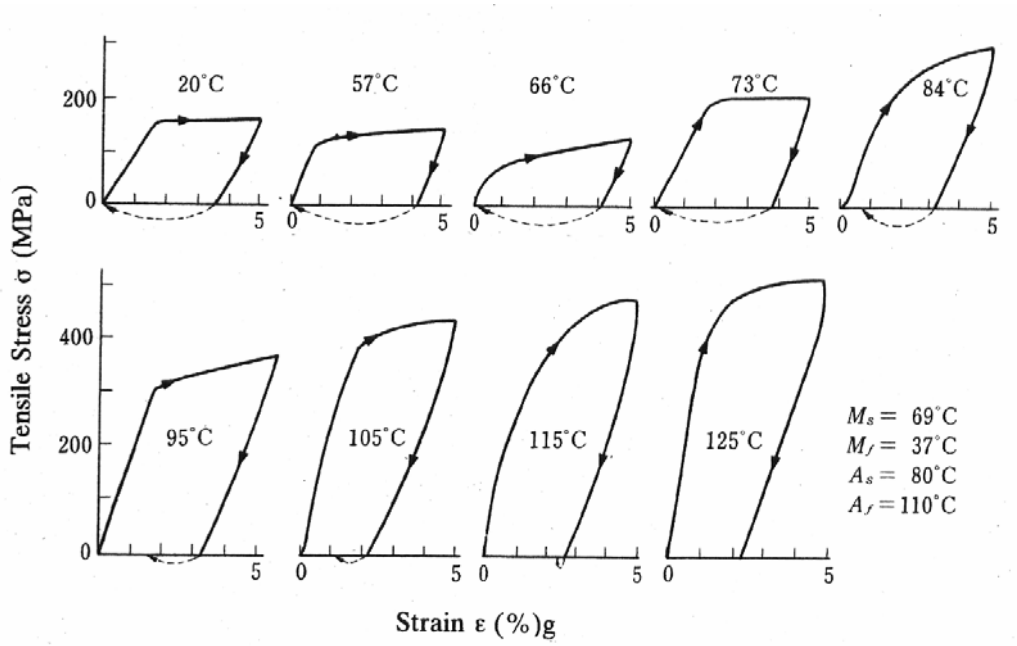

Figure 2.52 Stress-strain curves for 50-NiTi as a function of temperature [234].

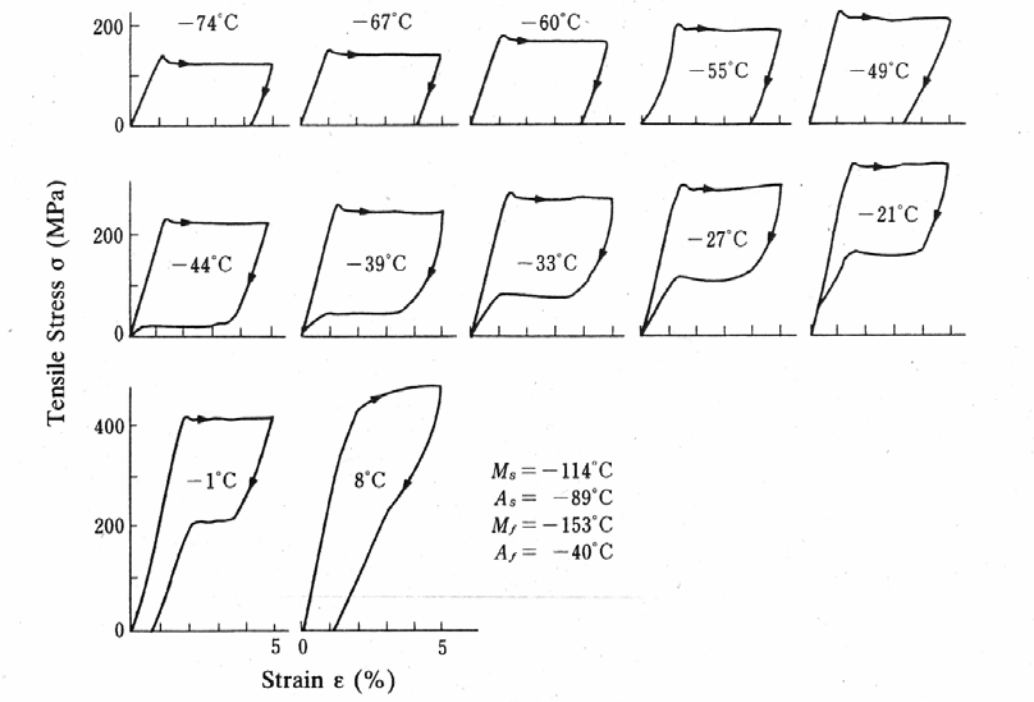

Figure 2.53 Stress-strain curves for 51-NiTi as a function of temperature [234].

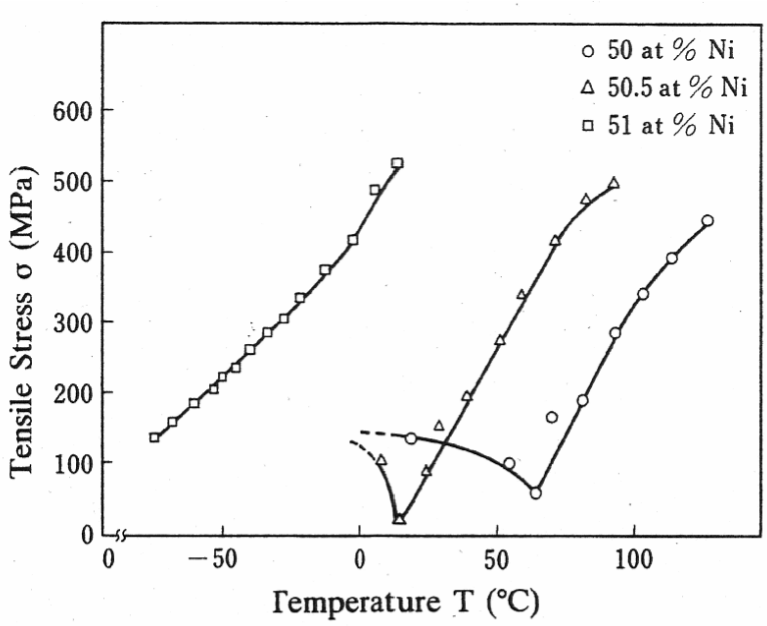

Figure 2.54 Yield stress versus temperature for 50-NiTi, 50.5-NiTi and 51-NiTi [234].

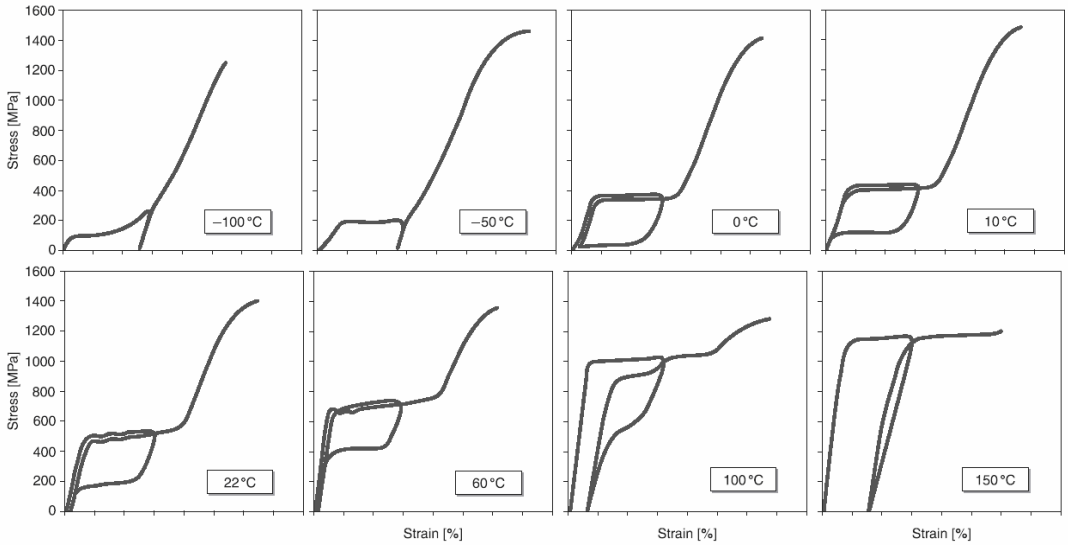

Figure 2.55 Temperature effects on the SE behavior of commercial 50.8-NiTi [39]

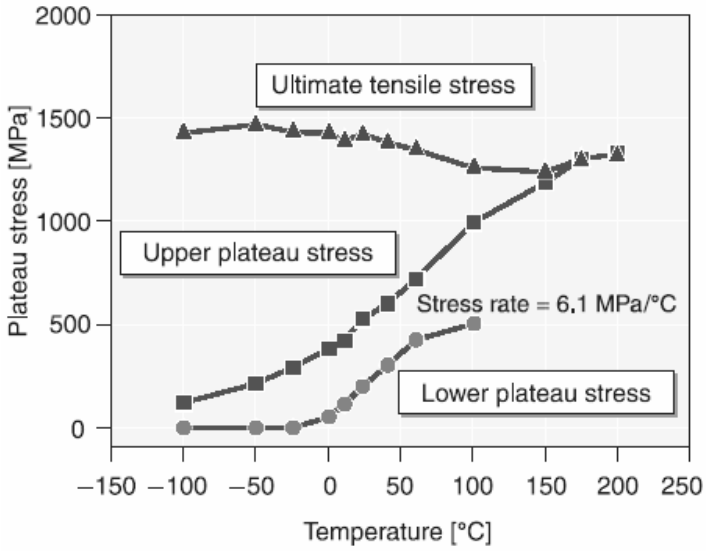

.Figure 2.56 Variation of the superelastic characteristics such as plateau stress and the tensile strength of 50.8-NiTi as a function of temperature [39].

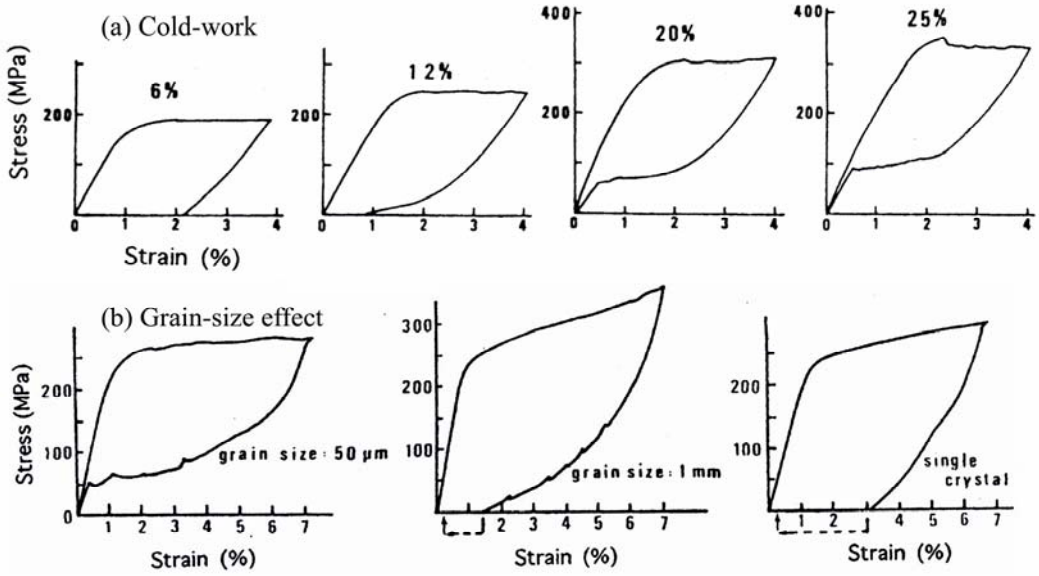

Figure 2.57 (a) Improvement in pseudoelasticity with work-hardening followed by annealing at 400°C for 1hr (tests were conducted at 50°C). [92]. (b) Effect of grain size on the pseudoelasticity of 50.5-NiTi [318].

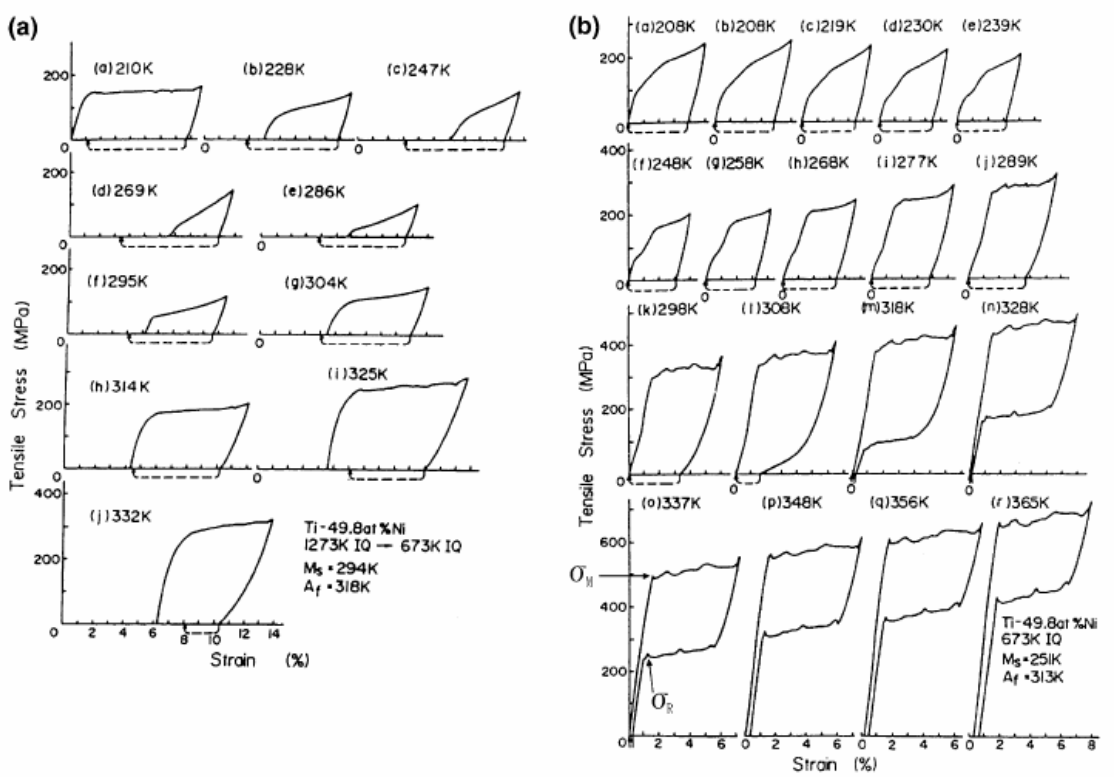

Figure 2.58 Influence of thermomechanical treatment on the mechanical behavior of 49.8-NiTi as a function of temperature: (a) ST at 1000°C (1hr) + annealing at 400°C (1hr). (b) Cold-work + annealing at 400°C (1hr) [45].

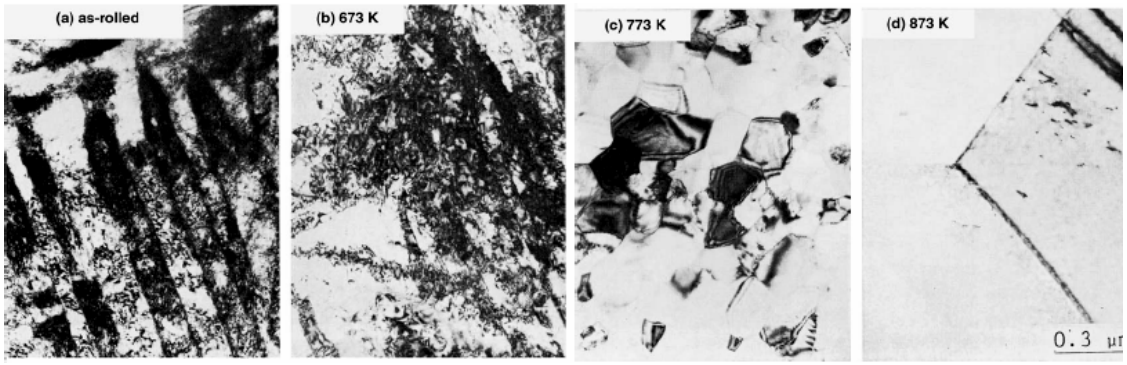

Figure 2.59 TEM images of 49.8-NiTi as a function of annealing temperature for 1hr: (a) cold-rolled, (b) 400°C, (c) 500°C, (d 600°C [47]

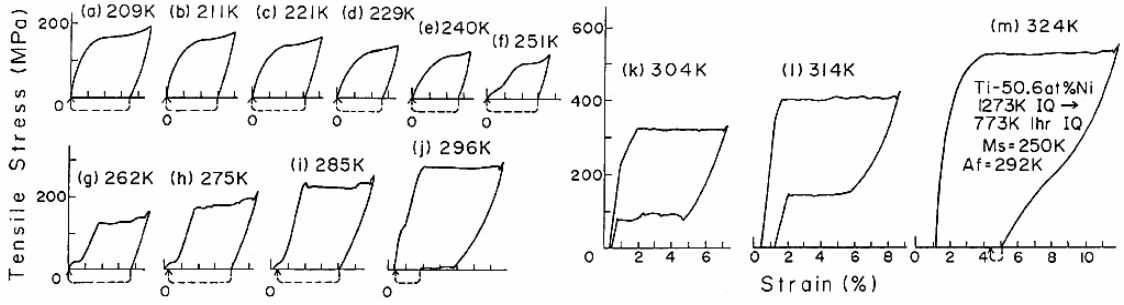

Figure 2.60 Stress-strain curves of 50.6-NiTi alloy aged at 500°C for 1hr after 1000°C solution-treatment for 1hr [47].

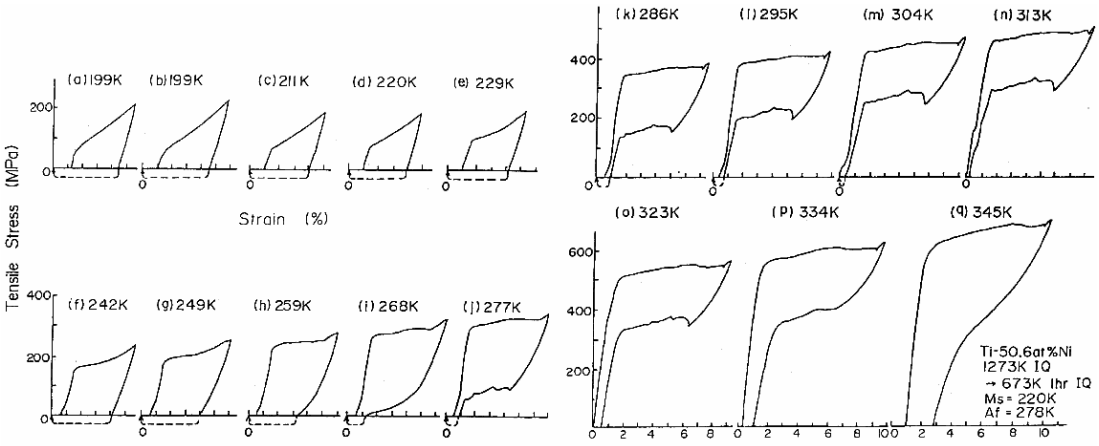

Figure 2.61 Stress-strain curves of 50.6-NiTi alloy aged at 400°C for 1hr after 1000°C solution-treatment for 1hr [47].

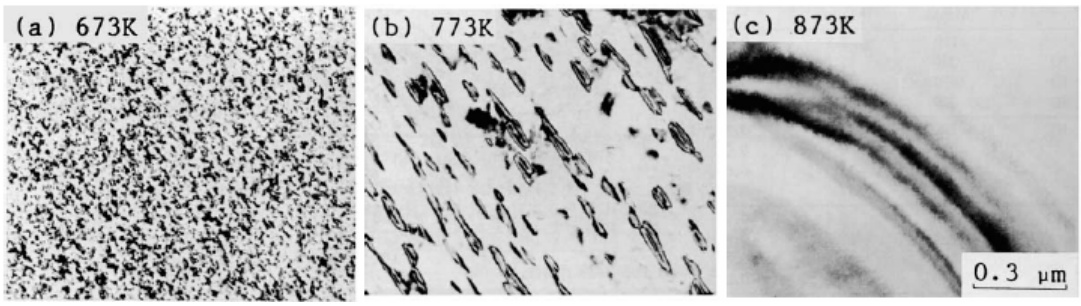

Figure 2.62 TEM images of 50.6-NiTi solution-treated at 1000°C for 1hr followed by a second aging treatment at (a) 400°C, (b) 500°C and (c) 600°C [47].

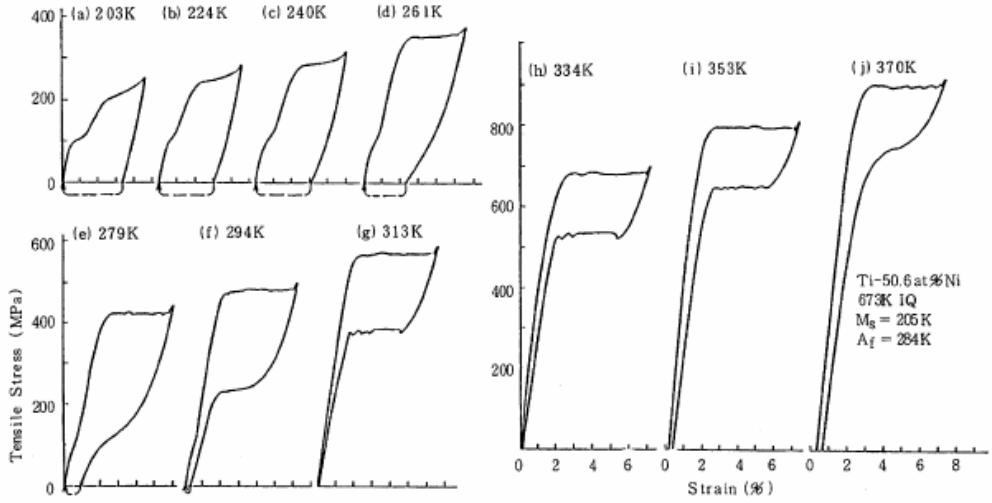

Figure 2.63 Stress-strain curves of 50.6-NiTi alloy cold-worked + aged at 400°C for 1hr [47].

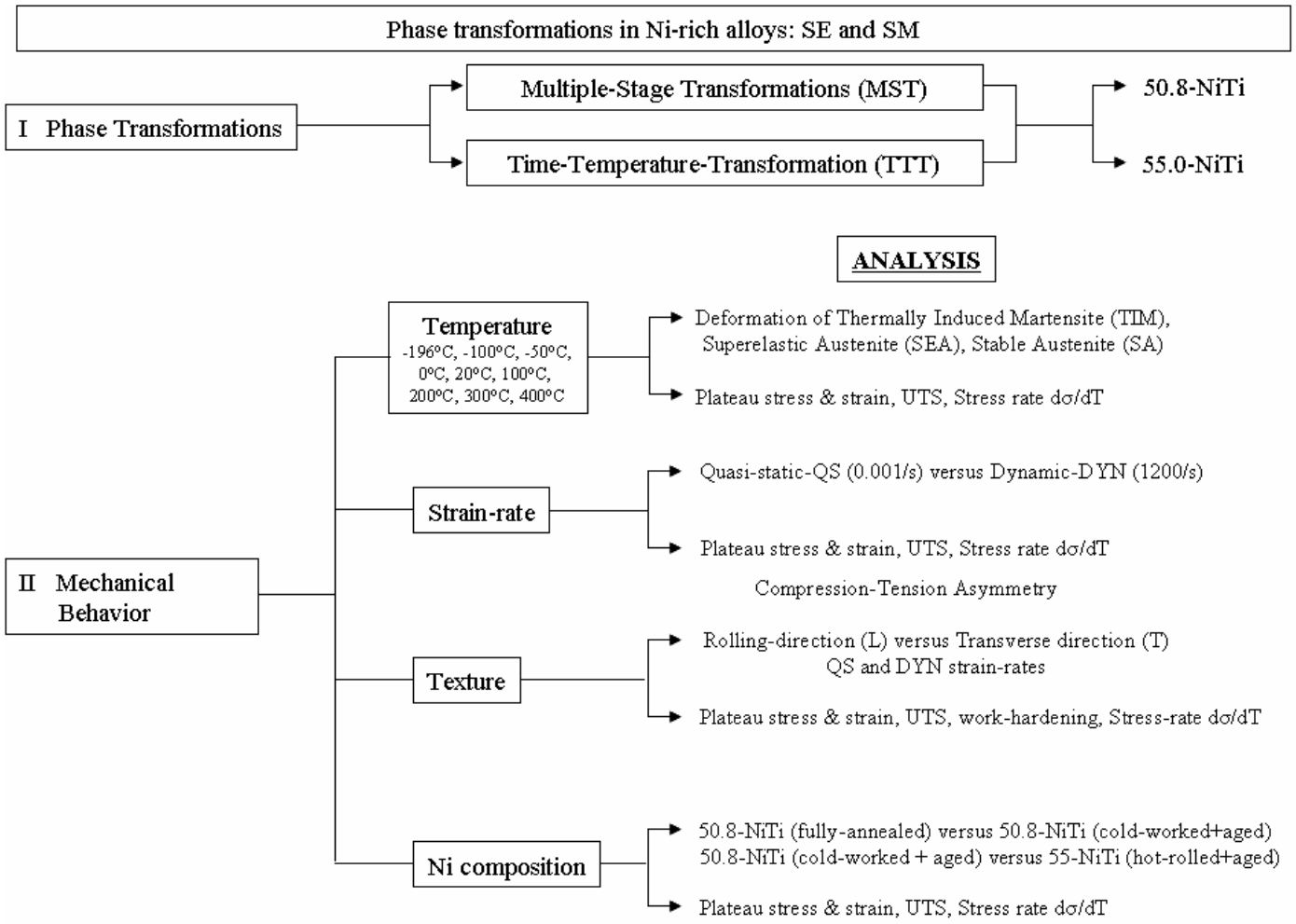

Figure 2.64 Schematic overview of the overall objectives for the current work.

2.7 References

1. Olander, A., *The crystal structure of AuCd.* Zeitschrift fuer Kristallographie, Kristallgeometrie, Kristallphysik, Kristallchemie, 1932. **83**: p. 145-148.

2. Olander, A., An electrochemical investigation of solid cadmium-gold alloys. J. Am. Chem. Soc., 1932. **54**: p. 3819-3833.

3. Ren, X. and K. Otsuka, *Origin of rubber-like behavior in metal alloys.* Nature, 1997. **389**(579-582).

4. Greninger, A.B. and V.G. Mooradian, *Strain transformation in metastable β Cu-Zn and β Cu-Tl.* Trans. Met. Soc. AIME, 1938. **128**: p. 337-369.

5. Kurdyumov, G.V. and L.G. Khandros, *On the thermoelastic equilibrium in martensitic transformations.* Dokiady Akademii Nauk SSSR, 1949. **66**: p. 211-214.

6. Bowles, J.S., C.S. Barrett, and L. Guttman, *Crystallography of the cubic-tetragonal transformation in the indium-thallium system.* J. Metals, Trans. AIME, 1950. **191**(47): p. 47-52.

7. Wayman, C.M. and J.D. Harrison, *The origins of the shape memory effect.* The Journal of Minerals, Metals and Materials (JOM), 1989. **41**(9): p. 26-28.

8. Burkart, M.W. and T.A. Read, *Diffusionless phase change in Indium-thallium system.* J. Metals, Trans. AIME, 1953(1516-1524).

9. Tadaki, T., K. Otsuka, and K. Shimizu, *Shape Memory Alloys.* Ann. Rev. Mater. Sci., 1988. **18**: p. 25-45.

10. Miyazaki, S. and K. Otsuka, *Development of shape memory alloys.* ISIJ International, 1989. **29**(5): p. 353-377.

11. Buehler, W.J. and R.C. Wiley, Nickel-base Alloys, in United States Patent Office # 3174851. 1965.

12. Buehler, W.J. and R.C. Wiley, *The properties of TiNi and associated phases*. 1961, U. S. Naval Ordnance Laboratory Report 61-75. p. 1-91.

13. Buehler, W.J. and F.E. Wang, A summary of recent research on the nitinol alloys and their potential application in ocean engineering. Ocean Engineering, 1968. **1**: p. 105-120.

14. Buehler, W.J. and R.C. Wiley, *TiNi: Ductile intermetallic compound.* Trans. Quart Am. Soc. Metals., 1962. **55**: p. 269-276.

15. Kauffman, G.B. and I. Mayo, The story of Nitinol: The serendipitous discovery of the memory metal and its applications. The Chemical educator, 1997. **2**(2): p. 1-21.

16. Otsuka, K. and K. Shimizu, *Memory effect and thermoelastic martensite transformation in Cu-Al-Ni alloy.* Scripta Metallurgica, 1970. **4**(6): p. 469-472.

17. Otsuka, K., *Origin of memory effect in copper-aluminum-nickel alloy.* Japanese Journal of Applied Physics, 1971. **10**(5): p. 571-579.

18. Saburi, T. and S. Nenno. The shape memory effect and related phenomena. in Proc. Int. Conf. Solid-Solid Phase Transformations. 1981 (1982): Metall. Soc. AIME, Warrendale, PA.

19. Saburi, T., C.M. Wayman, K. Takata, and S. Nenno, *The shape memory mechanisms in 18R martensitic alloys.* Acta Metallurgica, 1976. **28**(1): p. 15-32.

20. Otsuka, K., C.M. Wayman, K. Nakai, H. Sakamoto, and K. Shimizu, *Superelasticity effects and stress-induced martensitic transformation in Cu-Al-Ni alloys.* Acta Metallurgica, 1976. **24**(3): p. 207-226.

21. Otsuka, K., H. Sakamoto, and K. Shimizu, Successive stress-induced martensitic transformations and associated transformation pseudoelasticity in Cu-Al-Ni alloys. Acta Metallurgica, 1979. **27**(4): p. 585-601.

22. Miyazaki, S. and K. Otsuka, eds. *Shape memory alloys*. ed. H. Funakubo. 1987, Gordon and Breach Sci. Publ., New York.

23. Otsuka, K. and C.M. Wayman, eds. *Shape memory materials*. 1998, Cambridge University Press.

24. Duerig, T.W., K.N. Melton, D. Stockel, and C.M. Wayman, *Engineering aspects of shape memory alloys*. 1990: Butterworth-Heinemann, London.

25. Duerig, T.W., D. Stoeckel, and A.R. Pelton, *An overview of nitinol medical applications.* Materials Science and Engineering A, 1999. **273-275**: p. 149-160.

26. Castleman, L.S., S.M. Motzkin, F.P. Alicandri, and V.L. Bonawit, *Biocompatibility of nitinol alloy as an implant material.* J. Biomed. Mater. Res., 1976. **10**: p. 695-731.

27. Cutright, D.E., S.N. Bhaskar, B. Perez, R.M. Johnson, and G.S. Cowan, *Tissue reaction to nitinol wire alloy.* Oral Surg. Oral Med. Oral Pathol., 1973. **35**: p. 578-584.

28. Simon, M., r. Kaplow, E. Salzman, and D. Freiman, *A vena cava filter using thermal shape memory alloy-experiments aspects.* Radiology, 1977. **125**: p. 87-94.

29. Cragg, A., G. Lund, J. Rysavy, F. Castaneda, W. Castaneda-Zuniga, and K. Amplatz, *Nonsurgical placement of arterial endoprostheses: a new technique using nitinol wire.* Radiology, 1983. **147**: p. 261-263.

30. Dotter, C.T., R.W. Buschmann, M.K. McKinney, and J. Rosch, *Transluminal expandable nitinol coil stent grafting: preliminary report.* Radiology, 1983. **147**: p. 259-260.

31. Duerig, T.W. Present and future applications of shape memory and superelastic materials. in Materials Research Society Symposium Proceedings, Materials for Smart Systems. 1995: Materials Research Society (MRS).

32. Pelton, A.R., T.W. Duering, and D. Stockel, *A guide to shape memory and superelasticity in nitinol medical devices.* Minimally Invasive Therapy and Allied Technologies, 2004. **13**(4): p. 218-221.

33. Stoeckel, D., A. Pelton, and T. Duerig, *Self-expanding nitinol stents : material and design considerations.* European Radiology, 2003(1-12).

34. Duerig, T.W. and A.R. Pelton, *An overview of superelastic stent design.* Materials Science Forum, 2002. **394-395**: p. 1-8.

35. Stoeckel, D., C. Bonsignore, and S. Duda, *A survey of stent designs.* Minimally Invasive Therapy and Allied Technologies, 2002. **11**(4): p. 137-147.

36. Duerig, T., D. Stoeckel, and D. Johnson. *SMA-smart materials for medical applications*. in *Proceedings of SPIE 4763*. 2002. European Workshop on Smart Structures in Engineering and Technology.

37. Pelton, A.R., D. Stoeckel, and T.W. Duerig, *Medical uses of nitinol.* Materials Science Forum, 2000. **327-328**: p. 63-70.

38. Stoeckel, D., *Nitinol medical devices and implants.* Minimally Invasive Therapy and Allied Technologies, 2000. **9**(2): p. 81-88.

39. Pelton, A., J. DiCello, and S. Miyazaki. Optimization of processing and properties of medical-grade nitinol wire. in Proceedings of the International Conference on Shape Memory and Superelastic Technologies (SMST). 2000. Pacific Grove, CA.

40. Duerig, T.W., A.R. Pelton, and D. Stoeckel. *The use of superelasticity in medicine*. in *Metall (Heidelberg)*. 1996: Sonderdruck aus Heft.

41. Stoeckel, D., New developments in superelastic instrumentation for minimally invasive surgery, in Presentation for "Changing surgical markets - Increasing efficiency and reducing cost through new technology and procedure innovation". October 12, 1993: San Francisco, CA.

42. Melzer, A. and D. Stoeckel. Performance improvement of surgical instrumentation through the use of nitinol materials. in The 1st International Conference on shape memory and superelastic technologies. 1994.

43. Melzer, A., M.O. Schurr, M.M. Lirici, B. Klemm, D. Stoeckel, and G. Buess, *Future trends in endoscopic suturing.* Endoscopic surgery and allied technologies, 1994. **2**(1): p. 78-82.

44. Ryhanen, J., Biocompatibility evaluation of nickel-titanium shape memory alloy, in Department of Surgery. 1999, University of Oulu.

45. Miyazaki, S., Y. Ohmi, K. Otsuka, and Y. Suzuki, *Characteristics of deformation and transformation pseudoelasticity in titanium-nickel alloys.* Journal de Physique, Colloque, 1982. **C-4**: p. 255-60.

46. Saburi, T., T. Tatsumi, and S. Nenno, *Effects of heat treatment on mechanical behavior of titanium-nickel alloys.* Journal de Physique, Colloque, 1982. **C-4**: p. 261-266.

47. Otsuka, K. and X. Ren, *Physical metallurgy of Ti-Ni based shape memory alloys.* Progress in Materials Science, 2005. **50**: p. 511-678.

48. Miyazaki, S., T. Imai, K. Otsuka, and Y. Suzuki, *Luders-like deformation observed in the transformation pseudoelasticity of a titanium-nickel alloy.* Scripta Metallurgica, 1981. **15**(8): p. 853-856.

49. Miyazaki, S., K. Otsuka, and Y. Suzuki, *Transformation pseudoelasticity and deformation behavior in titanium-50.6 at. nickel alloy.* Scripta Metallurgica, 1981. **15**(3): p. 287-292.

50. Miyazaki, S., S. Kimura, F. Takei, T. Miura, K. Otsuka, and Y. Suzuki, *Shape memory effect and pseudoelasticity in a titanium-nickel single crystal.* Scripta Metallurgica, 1983. **17**(9): p. 1057-1062.

51. Takei, F., T. Miura, S. Miyazaki, S. Kimura, K. Otsuka, and Y. Suzuki, *Stress-induced martensitic transformation in a titanium-nickel single crystal.* Scripta Metallurgica, 1983. **17**(8): p. 987-992.

52. Miyazaki, S., T. Imai, Y. Igo, and K. Otsuka, *Effect of cyclic deformation on the pseudoelasticity characteristics of titanium-nickel alloys.* Metallurgical Transactions A, 1986. **17**(1): p. 115-120.

53. Miyazaki, S., K. Otsuka, and C.M. Wayman, Proc. MRS Int. Meeting on Advanced Materials, 1989.

54. Miyazaki, S. and C.M. Wayman, The R-phase transition and associate shape memory mechanism in titanium-nickel single crystals. Acta Metallurgica, 1988. **36**(1): p. 181-192.

55. Miyazaki, S., K. Otsuka, and C.M. Wayman, The shape memory mechanism associate with the martensitic transformation in titanium-nickel alloys - I. Self Accommodation. Acta Metallurgica, 1989. **37**(7): p. 1873-1884.

56. Miyazaki, S., K. Otsuka, and C.M. Wayman, The shape memory mechanism associate with the martensitic transformation in titanium-nickel alloys - II. Variant coalescence and shape recovery. Acta Metallurgica, 1989. **37**(7): p. 1885-1890.

57. Miyazaki, S., K. Otsuka, and C.M. Wayman, Morphological changes associated with the R-phase and martensitic transformations in titanium-nickel single crystals. ISIJ International, 1989. **29**(5): p. 423-429.

58. Hwang, C.M., M. Meichle, M.B. Salamon, and C.M. Wayman, *Transformation behavior of a titanium-nickel-iron alloy - II. Subsequent premartensitic behavior and the commensurate phase.* Philosophical Magazine A: Physics of Condensed Matter, Structure, Defects and Mechanical Properties, 1983. **47**(1): p. 31-62.

59. Salamon, M.b., M.e. Meichle, and C.M. Wayman, *Premartensitic phases of titanium-nickel-iron (Ti50Ni47Fe3).* Physical Reveiew B: Condensed Matter and Materials Physics, 1985. **31**(11): p. 7306-7315.

60. Ling, H.C. and R. Kaplow, *Phase transitions and shape memory in nickel-titanium (NiTi).* Metallurgical Transactions A: Physical Metallurgy and Materials Science, 1980. **11**(1): p. 77-83.

61. Ling, H.C. and R. Kaplow, Stress-induced shape changes and shape memory in the R-phase and martensite transformations n equiatomic nickel-titanium (NiTi). Metallurgical Transactions A: Physical Metallurgy and Materials Science, 1981. **12**(12): p. 2101-2111.

62. Miyazaki, S. and K. Otsuka, Mechanical behavior associate with the premartensitic rhombohedral-phase transition in a titanium-nickel-iron (Ti50Bi47Fe3) alloy. Philosophical Magazine A: Physics of Condensed Matter, Structure, Defects and Mechanical Properties, 1984. **50**(3): p. 393-408.

63. Miyazaki, S., S. Kimura, and K. Otsuka, *Shape-memory effect and pseudoelasticity associated with the R-phase transition in titanium-50.5 at%*

nickel single crystals. Philosophical Magazine A: Physics of Condensed Matter, Structure, Defects and Mechanical Properties, 1988. **57**(3): p. 467-78.

64. Miyazaki, S. and K. Otsuka, *Deformation and transition behavior associated with the R-phase in titanium-nickel alloys.* Metallurgical Transactions A: Physical Metallurgy and Materials Science, 1986. **17**(1): p. 53-63.

65. Knowles, K.M. and D.A. Smith, The crystallography of the martensitic transformation in equiatomic nickel-titanium. Acta Metallurgica, 1981. **29**: p. 101-110.

66. Miyazaki, S., S. Kimura, K. Otsuka, and Y. Suzuki, The habit plane and transformation strain associated with the martensitic transformation in Ti-Ni single crystals. Scripta Metallurgica, 1984. **18**: p. 883-888.

67. Kudoh, Y., M. Tokonami, S. Miyazaki, and K. Otsuka, Crystal structure of the martensite in Ti-49.3at.%Ni alloy analyzed by the single crystal x-ray diffraction method. Acta Metallurgica, 1985. **33**(11): p. 2049-2056.

68. Matsumoto, O., S. Miyazaki, K. Otsuka, and H. Tamura, *Crystallography of martensitic transformation in Ti-Ni single crystals.* Acta metall., 1987. **35**(8): p. 2137-2144.

69. Shaw, J.A. and S. Kyriakides, *Thermomechanical aspects of NiTi.* Journal of the Mechanics and Physics of Solids, 1995. **43**(8): p. 1243-81.

70. Nishida, M., C.M. Wayman, and T. Honma, *Precipitation processes in near-equiatomic TiNi shape memory alloys.* Metallurgical Transactions A, 1986. **17**: p. 1505-1515.

71. Kainuma, R., M. Matsumoto, and T. Honma, *Metallographic study of precipitation processes in Ni-rich TiNi alloys.* Tohoku Daigaku Senko Seiren Kenkyujo iho, 1987. **43**(2): p. 149-158.

72. Nishida, M. and C.M. Wayman, *Phase transformation in Ti_2Ni_3 precipitates formed in aged Ti-52 at. pct Ni.* Metallurgical Transactions A, 1987. **18A**: p. 785-799.

73. Hara, T., T. Ohba, K. Otsuka, and M. Nishida, *Phase transformation and crystal structures of Ti_2Ni_3 precipitates in Ti-Ni alloys.* Materials Transactions, JIM, 1997. **38**(4): p. 277-284.

74. Tadaki, T., Y. Nakata, K. Shimizu, and K. Otsuka, *Crystal structure, composition and morphology of a precipitate in an aged titanium-51 at.% nickel shape-memory alloy.* Transactions of the Japan Institute of Metals, 1986. **27**(10): p. 731-740.

75. Saburi, T., S. Nenno, and T. Fukuda, Crystal structure and morphology of the metastable X phase in shape memory Ti-Ni alloys. J. Less-Common Met., 1986. **125**: p. 157-166.

76. Humbeeck, J.V., *Shape memory alloys: A material and a technology.* Advanced Engineering Materials, 2001. **3**(11): p. 837-850.

77. Firstov, G.S., J.V. Humbeeck, and Y.N. Koval, *High-temperature shape memory alloys. Some recent developments.* Materials Science and Engineering A, 2004. **378**: p. 2-10.

78. Miyazaki, S., H.Y. Kim, and H. Hosoda, *Development and characterization of Ni-free Ti-base shape memory and superelastic alloys.* Materials Science and Engineering A, 2006. **In Press**.

79. Pushin, V.G., R.Z. Valiev, and L.I. Yurchenko, Processing of nanostructured TiNi-shape memory alloys: Methods, structures, properties, application. J. Phys. IV France, 2003. **112**: p. 659-662.

80. Pushin, V.G., V.V. Stolyarov, R.Z. Valiev, N.I. Kourov, N.N. Kuranova, E.A. Prokofiev, and L.I. Yurchenko, *Features of structures and phase transformations in shape memory TiNi-based alloys after severe plastic deformation.* Ann. Chim. Sci. Mat., 2002. **27**(3): p. 77-88.

81. Crone, W.C., A.N. Yahya, and J.H. Perepezko. Influence of grain refiement on superelasticity in NiTi. in Proceedings of the SEM Annual Conference on Experiemental Mechanics. 2001. Portaland, OR.

82. Crone, W.C., A.N. Yahya, and J.H. Perepezko, *Bulk shape memory NiTi with refined grain size synthesized by mechanical alloying.* Materials Science Forum, 2002. **386-388**: p. 597-602.

83. Waitz, T., V. Kazykhanov, and H.P. Karnthaler, *Martensitic phase transformations in nanocrystalline NiTi studied by TEM.* Acta Materialia, 2004. **52**: p. 137-147.

84. Waitz, T., The self-accommodated morphology of martensite in nanocrystalline NiTi shape memory alloys. Acta Materialia, 2005. **53**(8): p. 2273-2283.

85. Dolce, M. and D. Cardone, Mechanical behavior of shape memory alloys for seismic applications. 1. Martensite and austenite NiTi bars subjected to torsion. International Journal of Mechanical Sciences, 2001. **43**: p. 2631-2656.

86. Dolce, M. and D. Cardone, Mechanical behavior of shape memory alloys for seismic applications. 2. Austenite NiTi wires subjected to tension. International Journal of Mechanical Sciences, 2001. **43**: p. 2657-2677.

87. Fugazza, D., Shape-memory alloy devices in earthquake engineering: Mechanical properties, constitutive modelling and numerical simulations, in Earthquake Engineering. 2003, Universita degli Studi di Pavia: Pavia. p. 141.

88. Saadat, S., J. Salichs, M. Noori, Z. Hou, H. Davoodi, I. Bar-on, Y. Suzuki, and A. Masuda, *An overview of vibration and seismic applications of NiTi shape memory alloy.* Smart Materials and Structures, 2002. **11**: p. 218-229.

89. Adharapurapu, R.R., F. Jiang, K.S. Vecchio, and G.T. GrayIII, Response of NiTi shape memory alloy at high strain rate: A systematic investigation of temperature effects on tension-compression asymmetry. Acta Materialia, 2006. **54**: p. 4609-4620.

90. Zhao, Y., M. Taya, and H. Izui, *Study on energy absorbing composite structure made of concentric NiTi spring and porous NiTi.* International Journal of Solids and Structures, 2006. **43**: p. 2497-2512.

91. Adharapurapu, R.R., F. Jiang, and K.S. Vecchio, Texture effects on the dynamic response of NiTi at various temperatures: Rod vs. Sheet products. In preparation, 2007.

92. Saburi, T., S. Nenno, Y. Nishimoto, and M. Zeniya, Effects of thermomechanical treatment on the shape-memory effect and pseudoelasticity of Ti-50.2Ni and Ti-47.5Ni-2.5Fe at. pct alloys. J. Iron and Steel Inst. Japan (Tetsu to Hagane), 1986. **72**(6): p. 571-578.

93. Hornbogen, E., Microstructure and thermo-mechanical properties of NiTi shape memory alloys. Materials Science Forum, 2004. **455-456**: p. 335-341.

94. Julien, G.J., *Manufacturing of Nitinol parts and forms*, in *US Patent# 6422010*. 2002, Nitinol Technologies, Inc. (Edgewood, WA): United States. p. 1-15.

95. Adharapurapu, R.R. and K.S. Vecchio, *Superelasticity in a new bioimplant material: Ni-rich 55NiTi alloy.* Experimental Mechanics, 2006. **In Press**.

96. Adharapurapu, R.R. and K.S. Vecchio, Microstructure development in Ni-rich NiTi alloys: Aging studies on precipitation reactions. Work in Progress, 2007.

97. Clingman, D.J., F.T. Clalkins, and J.P. Smith. *Thermomechanical properties of 60-Nitinol*. in *SPIE Smart Structures and Materials*. 2003. San Diego CA.

98. Julien, G.J., *Shape memory parts of 60 Nitinol*, in *US Patent# 7005018*. 2006, Nitinol Technologies, Inc. (Edgewood, WA): United States. p. 1-15.

99. Julien, G.J., *Shape memory metal precision actuator*, in *US Patent#4932210*. 1990, Nitinol Technologies, Inc. (Edgewood, WA): United States.

100. Julien, G.J., *Method and apparatus for sensing and damping vibration*, in *US Patent#5005678*. 1991, Nitinol Technologies, Inc. (Edgewood, WA): United States.

101. Julien, G.J., *Method for producing an elongate passage within a component*, in *US Patent#5013507*. 1991, Nitinol Technologies, Inc. (Edgewood, WA): United States.

102. Julien, G.J., *Reusable metallic seal using memory metal*, in *US Patent#5226683*. 1993, Nitinol Technologies, Inc. (Edgewood, WA): United States.

103. Julien, G.J., *High security lock*, in *US Patent#5868013*. 1999, Nitinol Technologies, Inc. (Edgewood, WA): United States.

104. Julien, G.J., *Gun barrel*, in *US Patent#5856631*. 1999, Nitinol Technologies, Inc. (Edgewood, WA): United States.

105. Julien, G.J., *Shape memory rotary actuator*, in *US Patent#6065934*. 2000, Nitinol Technologies, Inc. (Edgewood, WA): United States.

106. Julien, G.J., *Plasma spraying of nickel-titanium compound*, in *US Patent#6043451*. 2000, Nitinol Technologies, Inc. (Edgewood, WA): United States.

107. Julien, G.J., *Post processing for nitinol coated articles*, in *US Patent#6254458*. 2001, Nitinol Technologies, Inc. (Edgewood, WA): United States.

108. Julien, G.J., *Cutting instruments*, in *US Patent#6293020*. 2001, Nitinol Technologies, Inc. (Edgewood, WA): United States.

109. Julien, G.J., *Nitinol horseshoes*, in *US Patent#6454016*. 2002, Nitinol Technologies, Inc. (Edgewood, WA): United States.

110. Julien, G.J., *Nitinol heater elements*, in *US Patent#6410886*. 2002, Nitinol Technologies, Inc. (Edgewood, WA): United States.

111. Julien, G.J., *Nitinol impact absorbers*, in *US Patent#6530564*. 2003, Nitinol Technologies, Inc. (Edgewood, WA): United States.

112. Julien, G.J., *Projectile*, in *US Patent#6581522*. 2003, Nitinol Technologies, Inc. (Edgewood, WA): United States.

113. Julien, G.J., *Liquid jet nozzle*, in *US Patent #6715701*. 2004, Nitinol Technologies, Inc. (Edgewood, WA): United States. p. 1-9.

114. Julien, G.J., *Nitinol ball bearing element and process for making*, in *USPTO*. 2005, Nitinol Technologies, Inc. (Edgewood, WA): United States. p. 1-17.

115. Julien, G.J., *Nitinol ski structures*, in *US Patent#6267402*. 2001, Nitinol Technologies, Inc. (Edgewood, WA): United States.

116. Mabe, J.H., R.T. Ruggeri, E. Rosenzweig, and C.-J.M. Yu. Nitinol performance characterization and rotary actuator design. in SPIE 5388-11, Smart Structures and Materials Conference. 2004. San Diego, CA.

117. Mabe, J.H., R.H. Cabell, and G.W. Butler. Design and control of amorphing chevron for takeoff and cruise noise reduction. in 11th AIAA/CEAS Aeroacoustics Conference. 2005. Monterey, California: AIAA-2005-2889.

118. Calkins, F.T., J.H. Mabe, and G.W. Butler. Boeing's variable geometry chevron: morphing aerospace structures for jet noise reduction. in 13th SPIE Smart Structures and Materials Conference. 2006. San Diego, CA.

119. Bhattacharya, K., *Microstructure of martensite: why it forms and how it gives rise to the shape-memory effect*. Oxford series on materials modelling, ed. A.P.S.a.R.E. Rudd. 2003: Oxford University Press.

120. Nishiyama, Z., *Martensitic transformations*. 1978: Materials Science and Technology Series. 496.

121. Olson, G.B. and W.S. Owen, eds. *Martensite, A tribute to Morris Cohen*. 1992, ASM International.

122. Olson, G.B. and H. Hartman, *Martensite and life: displacive transformation as biological processes.* Journal de Physique, Colloque, 1982. **C4**: p. 855-865.

123. Isaitschev, I., E. Kaminsky, and G.V. Kurdyumov, *Strain transformation in metastable copper alloys.* Trans. AIME, 1938. **128**: p. 365-367.

124. Funakubo, H., *Shape memory effect: mechanism*, in *Shape memory alloys*. 1987, Gordon & Breach Science Publishers, New York. p. 9.

125. Delaey, L., R.V. Krishnan, H. Tas, and H. Warlimont, Thermoelasticity, pseudoelasticity and the memory effects associated with martensitic transformations. Part 1. Structural and microstructural changes associated with the transformations. Journal of Materials Science, 1974. **9**: p. 1521-1535.

126. Krishnan, R.V., L. Delaey, H. Tas, and H. Warlimont, Thermoplasticity, pseudoelasticity and the memory effects associated with martensitic transformations. Part 2. The macroscopic mechanical behavior. Journal of Materials Science, 1974. **9**: p. 1536-1544.

127. Warlimont, H., L. Delaey, R.V. Krishnan, and H. Tas, Thermoelasticity, pseudoelasticity and the memory effects associated with martensitic transformations. Part 3. Thermodynamics and kinetics. Journal of Materials Science, 1974. **9**: p. 1545-1555.

128. Delaey, L., Diffusionless transformations, in Materials Science and Technology, A comprehensive Treatment, Volume 5: Phase transformations in materials, R.W. Cahn, P. Haasen, and E.J. Kramer, Editors. 1990, VCH, New York. p. 339-404.

129. Raghavan, V., *Kinetics of Martensitic transformations*, in *Martensite, A tribute to Morrish Cohen*, G.B. Olson and W.S. Owen, Editors. 1992, ASM International. p. 197-225.

130. Otsuka, K. and C.M. Wayman, *Shape memory materials: Introduction*, in *Shape memory materials*, K. Otsuka and C.M. Wayman, Editors. 1998, Cambridge University Press. p. 21-25.

131. Olson, G.B. and M. Cohen, *Thermoelastic behavior in martensitic transformations.* Scripta Metallurgica, 1975. **9**(11): p. 1247-1254.

132. Kaufman, L. and M. Cohen, *Thermodynamics and kinetics of martensitic transformations.* Prog. Met. Phys., 1975. **7**: p. 169-246.

133. Zhao, L., Texture development and anisotropic behavior in a Ti-45Ni-5Cu (at. %) shape memory alloy, in Materials Science and Engineering. 1997, University of Twente: Enschede, Netherlends.

134. Ortin, J. and A. Planes, Thermodynamic analysis of thermal measurements in thermoelastic martensitic transformations. Acta Metallurgica, 1988. **36**(8): p. 1873-1889.

135. Tsuji, K. and K. Nomura, *The influence of cold working on transformation properties of nickel-titanium-copper alloys.* Scripta Metallurgica et Materialia, 1990. **24**(11): p. 2037-2042.

136. Filip, P., J. Rusek, and K. Mazanec, Effects of work hardening and heat treatment on the phase transformation behavior of titanium-50.6at.% nickel alloys. Materials Science and Engineering A, 1991. **A141**(2): p. L5-L8.

137. Jean, R.D. and J.C. Tsai, *Effects of hot working on the martensitic transformation of Ni-Ti alloy.* Scripta Metallurgica et Materialia, 1994. **30**(8): p. 1027-1030.

138. Todoroki, T. and H. Tamura, Trans. JIM, 1987. **28**(2): p. 83-.

139. Tsuji, K. and K. Nomura, Effects of nickel-titanium-copper alloy composition and heat treatment temperature after cold working on phase transformation characteristics. Journal of Materials Science, 1992. **27**(8): p. 2199-2204.

140. Skrotzki, B., *The course of the volume fraction of martensite vs. temperature function $M_x(T)$.* Journal de Physique IV: Proceedings, Eur. Symp. Martensitic Transfom. Shape Mem. Prop., 1991. **C4**(1): p. 367-372.

141. Funakubo, H., *Shape memory alloys*. 1987: Gordon & Breach Science Publishers, New York.

142. Standard Terminology for nickel-titanium shape memory alloys. ASTM Standard F2005-00: p. 1-2.

143. Melton, K.N., ed. *Ni-Ti based shape memory alloys*. Engineering aspects of shape memory alloys, ed. T.W. Duerig, K.N. Melton, D. Stockel, and C.M. Wayman. 1990, Butterworth-Heinemann, London. 21-35.

144. Olson, G.B., *Introduction: Martensite in perspective*, in *Martensite, A tribute to Morris Cohen*, G.B. Olson and W.S. Owen, Editors. 1992, ASM International. p. 1-10.

145. Taylor, A. and R.W. Floyd, *Precision measuremets of lattice parameters of non-cubic crystals.* Acta Crystallographica, 1950. **3**(4): p. 285-289.

146. Michal, G.M. and R. Sinclair, *The structure of TiNi Martensite.* Acta Cryst., 1981. **B37**: p. 1803-1807.

147. Goo, E. and R. Sinclair, *The B2 to R transformation in $Ti_{50}Ni_{47}Fe_3$ and $Ti_{49.5}Ni_{50.5}$ alloys.* Acta Metall., 1985. **33**: p. 1717-1723.

148. Wu, S.K. and C.M. Wayman, On the reciprocal lattice of the 'premartensitic' R-phase in TiNi shape memory alloys. Acta Metall., 1989. **37**: p. 2805-2813.

149. Hara, T., T. Ohba, E. Okunishi, and K. Otsuka, *Structural study of R-phase in Ti-50.23 at.% Ni and Ti-47.75 at. % Ni-1.50 at. %Fe alloys.* Materials Transactions, JIM, 1997. **38**(1): p. 11-17.

150. Schryvers, D. and P.L. Potapov, *R-phase structure refinement using electron diffraction data.* Mater. Trans. (Japan), 2002. **43**: p. 774-779.

151. Sitepu, H., Use of synchrotron diffraction data for describing crystal structure and crystallographic phase analysis of R-phase NiTi shape memory alloy. Textures and Microstructures, 2003. **35**: p. 185-195.

152. Sitepu, H., J.P. Wright, T. Hansen, D. Chateigner, H.-G. Brokmeier, C. Ritter, and T. Ohba, *Combined synchrotron and neutron structural refinement of R-*

phase in Ti 50.75-Ni 47.75- Fe1.50. Materials Science Forum, 2005. **495-497 (Pt. 1, Textures of Materials)**: p. 255-260.

153. Gong, C., Y. Li, Y. Wang, and D. Yang, *Ab initio study for electronic and crystal structure of NiTi R-phase.* Modelling and Simulation in Materials Science and Engineering, 2006. **14**: p. 33-39.

154. Khalil-Allafi, J., W.W. Schmahl, and D.M. Toebbens, *Space group and crystal structure of the R-phase in binary NiTi shape memory alloys.* Acta Materialia, 2006. **54**: p. 3171-3175.

155. Goryczka, T. and H. Morawiec, *Structure studies of the R-phase using the X-ray and electron diffraction methods.* Journal de Physique IV, 2003(112): p. 693-696.

156. Goryczka, T. and H. Morawiec, *Structure studies of the R-phase using X-ray diffraction methods.* Journal of Alloys and Compounds, 2004. **367 (1-2)**: p. 137-141.

157. Zhang, X. and H. Sehitoglu, *Crystallography of the B2-R-B19' phase transformations in NiTi.* Materials Science and Engineering A, 2004. **374**: p. 292-302.

158. Pitteri, M. and G. Zanzatto, Continuum theories for phase transitions and twinning in crystals. 2003: Chapman and Hall.

159. Ericksen, J.L., The Cauchy and Born hypothesis for crystals, in Phase Transformations and Material Instabilities in Solids, M.E. Gurtin, Editor. 1984, Academic Press. p. 61-78.

160. Gurtin, M.E., *An Introduction to continuum mechanics*. 1981, Academic Press. p. 17.

161. Otsuka, K., T. Sawamura, and K. Shimizu, *Crystal structure and internal defects of equiatomic TiNi martensite.* Phys. Stat. Sol., 1971. **5**: p. 457-.

162. Hane, K.F. and T.W. Shield, Microstructure in the cubic to monoclinic transition in titanium-nickel shape memory alloys. Acta Mater., 1999. **47**: p. 2603-2617.

163. Zhang, X. and H. Sehitoglu, *Crystallography of the B2-R-B19' phase transformation in NiTi.* Materials Science and Engineering A, 2004. **374**: p. 292-302.

164. Gupta, S.P. and A.A. Johnson, *Morphology and crystallography of β^{3} martensite in TiNi alloys.* Trans. JIM, 1973. **14**: p. 292-302.

165. Madangopal, K. and R. Banerjee, *The lattice invariant shear in Ni-Ti shape memory alloy martensites.* Scripta Metall. Mater., 1992. **27**: p. 1627-1632.

166. Onda, T., Y. Bando, T. Ohba, and K. Otsuka, *Electron-microscopy study of twins in martensite in a Ti-50.0 at. percent Ni alloy.* Mat. Trans. Jap. Inst. Metals, 1992. **33**: p. 354-359.

167. Nishida, M., C.M. Wayman, and A. Chiba, Electron-microscopy studies of the martensitic-transformation in an aged Ti-51 at. %Ni shape memory alloy. Metallography, 1988. **21**: p. 275-291.

168. Nishida, M., H. Ohgi, I. Itai, and A. Chiba, Electron-microscopy studies of twin morphoolgies in B19' martensite in th eTi-Ni shape memory alloy. Acta Metall. Mater., 1995. **43**: p. 1219-1227.

169. Nishida, M., K. Yamauchi, I. Itai, H. Ohgi, and A. Chiba, High resolution electron-microscopy studies of twin boundary structures in B19' martensite in the Ti-Ni shape-memory alloy. Acta Metall. Mater., 1995. **43**: p. 1229-1234.

170. Pitteri, M. and G. Zanzotto, Generic and non-generic cubic to monoclinic transitions and their twins. Acta Mater., 1997. **46**: p. 225-237.

171. Bywater, K.A. and J.W. Christian, *Martensitic transformation in Ti-Ta alloys.* Phil. Mag. A, 1972. **25**: p. 1249-1274.

172. Wechler, M.S., D.S. Lieberman, and T.A. Read, *On the theory of the formation of martensite.* Trans AIME J. Metals, 1953. **197**: p. 1503-1515.

173. Bowles, J.S. and J.K. MacKenzie, *The crystallography of martensite transformations 1.* Acta metall., 1954. **2**: p. 129-137.

174. Bowles, J.S. and J.K. MacKenzie, *The crystallography of martensite transformations 2.* Acta metall., 1954. **2**: p. 138-147.

175. Bhadeshia, H.K.D.H., *Worked examples in geometry of crystals*. 1987: Institute of Metals.

176. James, R.D. and K.F. Hane, *Martensitic transformations and shape memory materials.* Acta mater., 2000. **48**: p. 197-222.

177. Bhattacharya, K., *Self-accommodating in martensite.* Arch. rational Mech. Anal., 1992. **120**: p. 201-244.

178. Saburi, T. and C.M. Wayman, *Crystallographic similarities in shape memory martensites.* Acta Metall., 1979. **27**: p. 979-995.

179. Scheil, E., Transformation of austenite into martensite in iron-nickel alloys under stress. Z. anorg. allgem. Chem, 1932. **207**: p. 21-40.

180. Patel, J.R. and M. Cohen, *Criterion for the action of applied stress in the martesitic transformation.* Acta Metallurgica, 1953. **1**(1953): p. 531-538.

181. Warlimont, H. and J. Delaey, *Martensitic transformations in Cu-, Ag- and Au-based alloys.* Progress in Materials Science, 1974. **18**: p. 1-.

182. Tamura, I., *Martensitic transformations and mechanical effects*, in *Martensite, A tribute to Morrish Cohen*, G.B. Olson and W.S. Owen, Editors. 1992, ASM International. p. 227-242.

183. Gefen, Y., A. Halwany, and M. Rosen, Effect of hydrostatic pressure onthe cubic-orthorhombic phase transformation in Au-47.5at % Cd alloy. Philosophical Magazine, 1973. **28**(1): p. 1-9.

184. Kakeshita, T., K. Shimizu, Y. Akahama, S. Endo, and F.E. Fujita, *Effect of hydrostatic pressure on martensitic transformation in Fe-Ni and Fe-Ni-C alloys.* Transactions of the Japan Institute of Metals, 1988. **29**(2): p. 109-115.

185. Kakeshita, T., Y. Yoshimura, K.i. Shimizu, S. Endo, Y. Akahama, and F.E. Fujita, *Effect of hydrostatic pressure on martensitic transformation in Cu-Al-Ni shape memory alloys.* Transactions of the Japan Institute of Metals, 1988. **29**(10): p. 781-789.

186. Kakeshita, T., K. Shimizu, S. Nakamichi, R. Tanaka, S. Endo, and F. Ono, Effect of hydrostatic pressures on thermoelastic martensitic transformation in aged Ti-Ni and ausaged Fe-Ni-Co-Ti shape memory alloys. Materials Transc, 1992. **33**(1): p. 1-6.

187. Johari, G.P., J.G. McAnanama, and G. Sartor, Effect of hydrostatic pressure on the thermoelastic transformation of Ni-Ti alloy and the entropy transformation. Philosophical Magazine B, 1996. **74**(3): p. 243-257.

188. Jacobus, K., H. Sehitoflu, and M. Balzer, *Effect of stress state on the stress-induced martensitic transformation in polycrystalline Ni-Ti alloy.* Metallurgical and Materials Transactions A, 1996. **27**: p. 3066-3073.

189. Daroczi, L., D.L. Beke, C. Lexcellent, and V. Mertinger, *Effect of hydrostatic pressure on the martensitic transformation in near equiatomic Ti-Ni alloys.* Philosophical Magazine B, 2002. **82**(1): p. 105-120.

190. Melton, K.N. and O. Mercier, *The mechanical properties of nickel-titanium (NiTi)-based shape memory alloys.* Acta Metallurgica, 1981. **29**(2): p. 393-398.

191. Wayman, C.M. and H.C. Tong, *On the equilibirum temperature in thermoelastic martensitic transformations.* Scripta Metallurgica, 1977. **11**(5): p. 341-343.

192. Tong, H.C. and C.M. Wayman, Characteristic temperatures and other properties of thermoelastic martensites. Acta Metallurgica, 1974. **22**(7): p. 887-896.

193. Olson, G.B. and M. Cohen, Reply to "On the equilibrium temperature in thermoelastic martensitic transformations. Scripta Metallurgica, 1977. **11**(5): p. 345-347.

194. McKelvey, A.L., Fatigue-crack Propagation behavior in the Shape-Memory and Superelastic Alloy Nitinol, in Materials Science and Mineral Engineering. 1999, Universtiy of California, Bekeley: Berkeley. p. 23-38.

195. Duerig, T.W. and T. Zadno, eds. *An engineer's perspective of pseudoelasticity*. Engineering aspects of shape memory alloys, ed. T.W. Duerig, K.N. Melton, D. Stockel, and C.M. Wayman. 1990, Butterworth-Heinemann, London. 394-413.

196. Otsuka, K., C.M. Wayman, K. Nakai, H. Sakamoto, and K. Shimizu, *Superelasticity effects and stress-induced martensitic transformations in copper-aluminum-nickel alloys.* Acta Metallurgica, 1976. **24**(3): p. 207-226.

197. Otsuka, K. and K. Shimizu, *Pseudoelasticity and shape memory effects in alloys.* International Metal Reviews, 1986. **31**(3): p. 93-114.

198. Otsuka, K. and C.M. Wayman, *Mechanism of shape memory and superelasticity*, in *Shape memory materials*, K. Otsuka and C.M. Wayman, Editors. 1998, Cambridge University Press. p. 27-45.

199. Zhao, L., Texture development and anisotropic behavior in a Ti-45Ni-5Cu (at.%) shape memory alloys, in Materials Science and Engineering. 1997, University of Twente, Enschede, the Netherlands: Enschede. p. 1-35.

200. Frank, T.G., W. Xu, and A. Cuschieri, Instruments based on shape memory alloy properties for minimal access surgery: interventional radiology and flexible endoscopy. Journal of Minimally Invasive Therapy and Allied Technologies (MITAT), 2000. **9**(1).

201. Rozner, A.G. and R.J. Wasilewski, *Tensile properties of NiAl and NiTi.* J. Inst. Metals, 1966. **94**(5): p. 169-175.

202. Wasilewski, R.J., *Stress-assisted martensite formation in titanium-nickel.* Scripta Metallurgica, 1971. **5**(2): p. 127-130.

203. Wasilewski, R.J., *Effects of applied stress on the martensitic transformation in TiNi.* Metallurgical Transactions A, 1971. **2**(11): p. 2973-2981.

204. Honma, T., *Tensile properties and hardness of nonstoichiometric TiNi compounds at room temperature.* Bull Res Inst Mineral Dressing and Metallurgy (Tohoku Daigaku Senko Seiren Kenkyusho Iho, In Japanese), 1971. **27**(1-2): p. 245-252.

205. Wayman, C.M. and K. Shimizu, *Shape memory ('marmem') effect in alloys.* Metal Science Journal, 1972. **6**: p. 175-183.

206. Christian, J.W., *Deformation by moving interfaces.* Metallurgical Transactions A, 1982. **13**(4): p. 509-538.

207. Bhattacharya, K., S. Conti, G. Zanzotto, and J. Zimmer, *Crystal symmetry and the reversibility of martensitic transformations.* Nature, 2004. **428**(6978): p. 55-59.

208. Bernal, L.I.B., Cyclic behavior of superelastic nickel-titanium and nickel-titanium-chromium shape memory alloys, in Civil Engineering. 2004, Georgia Institute of Technology: Georgia.

209. Perkins, J. and D. Hodgson, eds. *An engineer's perspective of pseudoelasticity*. Engineering aspects of shape memory alloys, ed. T.W. Duerig, K.N. Melton, D. Stockel, and C.M. Wayman. 1990, Butterworth-Heinemann, London. 195-206.

210. Wang, F.E. and W.J. Buehler, *Additional unique property changes observed during TiNi transition.* Applied Physics letters, 1972. **21**(3): p. 105-106.

211. Nagasawa, A., K. Enami, Y. Ishino, Y. Abe, and S. Nenno, *Reversible shape memory effect.* SCripta Metallurgica, 1974. **8**(9): p. 1055-1060.

212. Saburi, T. and S. Nenno, *Reversible shape memory in Cu-Zn-Ga.* Scripta Metallurgica, 1974. **8**(12): p. 1363-1367.

213. Schroeder, T.A. and C.M. Wayman, The two-way shape memory effect and other 'training' phenomena in copper-zinc single crystals. Scripta Metallurgica, 1977. **11**(3): p. 225-230.

214. Nishida, M. and T. Honma, *Effect of external stress on the microstructure of martensite in titanium nickel (TiNi).* Science Reports of the Research Institutes, Tohoku University, Series A, 1981. **29 (Suppl. 1)**: p. 79-84.

215. Ren, X. and K. Otsuka, *Universal symmetry property of point defects in crystals.* Physical Review Letters, 2000. **85**(5): p. 1016-1019.

216. Nishida, M. and T. Honma, All-round shape memory effect in Ni-rich TiNi alloys generated by constrained aging. Scripta Metallurgica, 1984. **18**(11): p. 1293-1298.

217. Nishida, M. and T. Honma, *Effect of heat treatment on the all-round shape memory effect in Ti-51at.%Ni.* Scripta Metallurgica, 1984. **18**(11): p. 1299-1302.

218. Nishida, M., C.M. Wayman, and T. Honma, *Electron microscopy studies of the all-round shape memory effect in a Ti-51at.%Ni alloy.* Scripta Metallurgica, 1984. **18**(12): p. 1389-1394.

219. Kainuma, R., M. Matsumoto, and T. Honma. in *Int. Conf. on Martensitic Transformation (ICOMAT-86)*. 1987. Sendai: Japan Institute of Metals.

220. Fukuda, T., A. Deguchi, T. Kakeshita, and T. Saburi, *Two-way shape memory properties of a Ni-rich Ti-Ni alloy aged under tensile-stress.* Materials Transactions, JIM, 1997. **38**(6): p. 514-520.

221. Malygin, G., Mechanism for the bidirectional shape memory effect in titanium nickelide crystals. Physics of the Solid State, 2003. **45**(9): p. 1784-1789.

222. Miura, S., S. Maeda, and N. Nakanishi, *Pseudoelasticity in Au-Cu-Zn thermoelastic martensite.* Philosophical Magazine, 1974. **30**(3): p. 565-581.

223. Rapacioli, R., M. Chandrasekaran, M. Ahlers, and L. Delaey, eds. *The rubberlike behavior in Cu-Zn-Al martensite single crystals*. Shape Memory Effects in Alloys, ed. J. Perkins. 1975, Plenum, NY. 385-388.

224. Ahlers, M., G. Barcelo, and R. Rapacioli, *A model for the rubber-like behavior in Cu-Zn-Al.* Scripta Metall., 1978. **12**: p. 1075-1078.

225. Zangwill, A. and R. Bruinsma, *Origin of martensitic pseudoelasticity.* Phys. Rev. Lett., 1984. **53**: p. 1073-1076.

226. Arab, A.A. and M. Ahlers, *The stabilization of martensite in Cu-An-Al alloys.* Acta Metall., 1988. **36**: p. 2627-2638.

227. Tadaki, T., H. Okazaki, Y. Nakata, and K. Shimizu, Atomic configuration studies by ALCHEMI and X-ray diffraction of a stabilized M18R martensite in a β phase Cu-Au-Zn alloy. Mater. Trans. Japan Institute of Metals, 1990. **31**: p. 941-947.

228. Nakajima, Y., S. Aoki, K. Otsuka, and T. Ohba, *The rubber-like behavior of ζ' (trigonal) martensite in Au-49.5 to 50.0 at. % Cd alloys.* Mater. Lett., 1994. **21**: p. 271-274.

229. Cahn, R.W., *Metalllic rubber bounces back.* Nature, 1995. **374**: p. 120-121.

230. Murakawa, K. and K. Tsuchiya, Short-range ordering as the cause of the rubber-like behavior in alloy martensites. Scripta Metall., 1995. **32**: p. 77-72.

231. Suzuki, T., T. Tonokawa, and T. Ohba, *Role of short-range order in martensitic transformation.* J. Phys. III, 1995. **5-C8**: p. 1065-1070.

232. Otsuka, K. and X. Ren, *Martensitic transformations in nonferrous shape memory alloys.* Materials Science and Engineering A, 1999. **273-275**: p. 89-105.

233. Otsuka, K., ed. *Introduction to the R-phase transition*. Engineering aspects of shape memory alloys, ed. T.W. Duerig, K.N. Melton, D. Stockel, and C.M. Wayman. 1990, Butterworth-Heinemann, London. 36-45.

234. Funakubo, H., *Types and mechanical characteristics of Shape Memory Alloys*, in *Shape memory alloys*. 1987, Gordon & Breach Science Publishers, New York. p. 64-70.

235. Kim, J.I., Y. Liu, and S. Miyazaki, *Ageing-induced two-stage R-phase transformation in Ti-50.9 at.%Ni.* Acta Materialia, 2004. **52**: p. 487-499.

236. Hehemann, R.F. and G.D. Sandrock, Relations between the premartensitic instability and the martensite structure in titanium-nickel. Scripta Metallurgica, 1971. **5**(9): p. 801-805.

237. Sandrock, G.D., A.J. Perkins, and R.F. Hehemann, *Premartensitic instability in near-equiatomic TiNi.* Metallurgical Transactions, 1971. **2**(10): p. 2769-2681.

238. Shindo, D., Y. Murakami, and T. Ohba, Understanding precursor phenomena for the R-phase transformation in Ti-Ni-based alloys. MRS Bulletin, 2002. **27**(2): p. 121-127.

239. Khachin, V.N., Y.I. Paskal, V.E. Gyunter, A.A. Monasevich, and V.P. Sivokha, *Structural transformations, physical properties, and memory effects in titanium nickelide and its alloys.* Fizika Metallov i Metallovedenie, 1979. **46**(3): p. 511-520.

240. Hunter, A.M. and J.W. Bacon, *Some electrical properties of titanium alloys.* Transactions of the American Electrochemical Society, 1920. **37**: p. 520-.

241. Vogel, R. and H.J. Wallbaum, *The system iron-nickel - nickel titanide - iron titanide.* Archiv fuer das Eisenhuettenwesen, 1938. **12**: p. 299-304.

242. Laves, F. and H.J. Wallbaum, *The crystal chemistry of titanium alloys.* Naturwissenschaften, 1939. **27**: p. 674-675.

243. Laves, F. and H.J. Wallbaum, *The crystal structure of Ni_3Ti and Si_2Ti.* Zeir. fur Kristal., 1939. **101**: p. 78-93.

244. Poole, D.M. and W. Hume-Rothery, *The equilibrium diagram of the system nickel-titanium.* Journal of the Institute of Metals, 1954-1955. **83**: p. 473-480.

245. Duwez, P. and J.L. Taylor, The structure of intermediate phases in alloys of titanium with iron, cobalt and nickel. Transactions AIME, 1950. **188**: p. 1173-1176.

246. Purdy, G.R. and J.g. Parr, *A study of the titanium-nickel system between Ti_2Ni and TiNi.* Transactions of the Metallurgical Society of AIME, 1961. **221**: p. 636-639.

247. Marcinkowski, M.J., A.S. Sastri, and D. Koskimaki, *Martensitic behavior in the equiatomic Ni-Ti alloy.* Phil. Mag. A, 1968. **18**: p. 945-958.

248. Koskimaki, D., M.J. Marcinkowski, and A.S. Sastri, *Solid state diffusional transformations in the near-equiatomic Ni-Ti alloys.* Transactions of the Metallurgical Society of AIME, 1969. **245**: p. 1883-1890.

249. Margolin, H., E. Ence, and J.P. Nielsen, *Titanium-nickel phase diagram.* Transactions AIME, 1953(February): p. 243-247.

250. Buehler, W.J., J.V. Gilfrich, and R.C. Wiley, *Effect of low-temperature phase changes on the mechanical properties of alloys near composition TiNi.* Journal of Applied Physics, 1963. **34**(5): p. 1475-1477.

251. Wang, F.E., W.J. Buehler, and S.J. Pickart, *Crystal structure and a unique martensitic transition of TiNi.* Journal of Applied Physics, 1965. **36**(10): p. 3232-3239.

252. Wasilewski, R.J., S.R. Butler, J.E. Hanlon, and D. Worden, *Homogeneity range and the martensitic transformation in TiNi.* Metallurgical Transactions A, 1971. **2**: p. 229-238.

253. Bastin, G.F. and G.D. Rieck, *Diffusion in the titanium-nickel system - I.* Metallurgical Transactions A, 1974. **5**: p. 1817-1826.

254. Hansen, M. and K. Anderko, *Ni-Ti phase diagram in Constitution of binary alloys*. 1958: McGraw-Hill book company, Inc, New York. 1049-1053.

255. Nishida, M., C.M. Wayman, R. Kainuma, and T. Honma, *Further electron microscopy studies of the $Ti_{11}Ni_{14}$ phase in an aged Ti-52at%Ni shape memory alloy.* Scripta Metallurgica, 1986. **20**(6): p. 899-904.

256. Saburi, T., S. Nenno, and T. Fukuda, *Crystal structure and morphology of the metastable X-phase in shape memory alloys.* Journal of Less-Common Metals, 1986. **125**: p. 157-166.

257. Massalski, T.B., H. Okamoto, P.R. Subramanian, and L. Kacprzak, eds. *Binary alloy phase diagrams*. Vol. 3. 1990, ASM International. 2874-2876.

258. Saburi, T., Y. WAtanabe, and S. Nenno, Morphological characteristics of the orthorhombic martensite in a shape memroy titanium-nickel-copper alloy. ISIJ International, 1989. **29**(5): p. 405-411.

259. Mueller, M.H. and H.W. Knott, *The crystal structures of Ti_2Cu, Ti_2Ni, Ti_4Ni_2O and Ti_4Cu_2O.* Transactions of the American Institude of Mining, Metallurgical and Petroleum Engineers, 1963. **227**: p. 674-678.

260. Xie, C.Y., L.c. Zhao, and T.C. Lei, *Effect of Ti_3Ni_4 precipitates on the phase transitions in an aged Ti-51.8% Ni shape memory alloy.* Scripta Metallurgica et Materialia, 1990. **24**: p. 1753-1758.

261. Chen, Q., X.F. Wu, and T. Ko, *The effects of Ti_3Ni_4 precipitates on the R-phase transformation.* Scripta Metallurgica et Materialia, 1993. **29**: p. 49-53.

262. Van-Loo, F.J.J., G.F. Bastin, and A.J.H. Leenen, *Phase relations in the ternary titanium-nickel-copper system at 800 and 870^0C.* Journal of Less-Common Metals, 1978. **57(1)**: p. 111-121.

263. Schetky, L.M. and M.H. Wu. Issues in the further development of nitinol properties and processing for medical device applications. in ASM Materials and Processes for Medical Devices Conference. 2003. Anaheim, CA.

264. Otsuka, K. and C.M. Wayman, eds. *Fabrication of Shape Memory Alloys*. Shape memory alloys. 1998, Cambridge University Press. 133-148.

265. *ASTM Standard Specification F2063-00.* American Society for Testing and Materials, 2000.

266. 60Nitinol Alloys, Report# 75-449, U.S. Naval Ordnance Laboratory, White Oak, MD.

267. Nitinol Alloys, Report# 42-576, U.S. Naval Ordnance Laboratory, White Oak, MD.

268. Miyazaki, S., ed. *Thermal and stress cycling effects and fatigue properties of Ni-Ti alloys*. Engineering aspects of shape memory alloys, ed. T.W. Duerig, K.N. Melton, D. Stockel, and C.M. Wayman. 1990, Butterworth-Heinemann, London. 394-413.

269. Otsuka, K. and X. Ren, *Factors affecting the M_s temperature and its control in shape-memory alloys.* Materials Science Forum, 2002. **394-395**: p. 177-184.

270. Khalil-Allafi, J., A. Dlouhy, and G. Eggeler, Ni_4Ti_3-precipitation during aging of NiTi shape memory alloys and its influence on martensitic phase transformations. Acta Materialia, 2002. **50**: p. 4255-4274.

271. Tang, W., Thermodynamic study of the low temperature phase B19' and the martensitic transformation in near-equiatomic Ti-Ni shape memory alloy. Metallurgical Transactions A, 1997. **28**: p. 537-544.

272. Bozzolo, G., R.D. Noebe, and H.O. Mosca, *Site preference of ternary alloying additions to NiTi: Fe, Pt, Pd, Au, Al, Cu, Zr and Hf.* Journal of Alloys and Compounds, 2005. **389**(1-2): p. 80-94.

273. Bozzolo, G., H.O. Mosca, and R.D. Noebe, Phase structure and site preference ehavior of ternary alloying additions to PdTi and PtTi shape-memory alloys. Intermetallics, 2007. **15**(7): p. 901-911.

274. Noebe, R., T. Biles, and S.A. PadulaII, NiTi-based high-temperature shape-memory alloys: properties, prospects, and potential applications, in Advanced Structural Materials, W.O. Soboyojo, Editor. 2006, CRC Press LLC, Boca Raton, Fla. p. 145-186.

275. Noebe, R., D. Gaydosh, S. PadulaII, A. Garg, T. Biles, and M. Nathal, *Properties and potential of two (Ni,Pt)Ti alloys for use as high-temperature actuator materials.* Proceedings of SPIE-The International Society for Optical Engineering, 2005. **5761 (Active Materials: Behavior and Mechanics)**: p. 364-375.

276. Noebe, R., S. PadulaII, G. Bigelow, O. Rios, A. Garg, and B. Lerch, *Properties of a $Ni_{19.5}Pd_{30}Ti_{50.5}$ high-temperature shape memory alloy in tension and compression.* Proceedings of SPIE-The International Society for Optical Engineering, 2006. **6179 (Active Materials: Behavior and Mechanics)**: p. 617010/1-617010/13.

277. Rios, O., R. Noebe, T. Biles, A. Garg, A. Palczer, D. Scheiman, H.J. Seifert, and M. Kaufman, *Caharacterization of ternary NiTiPt high-temperature shape memory alloys.* Proceedings of SPIE-The International Society for Optical Engineering, 2005. **5761(Active Materials: Behavior and Mechanics)**: p. 376-387.

278. Zhang, J., W. Cai, X. Ren, K. Otsuka, and M. Asai, *The nature of reversible change in M_s temperatures of Ti-Ni alloys with alternating aging.* Materials Transactions, JIM, 1999. **40**(12): p. 1367-1375.

279. Morawiecz, H., D. Stroz, and D. Chrobak, *Effect of deformation and thermal treatment of NiTi alloy on transition sequence.* Journal de Physique IV, 1995. **5-C2**: p. 205-210.

280. Morawiecz, H., D. Stroz, T. Goryczka, and D. Chrobak, *Two-stage martensitic transformation in a deformed and annealed NiTi alloy.* Scripta Materialia, 1996. **35**(4): p. 485-490.

281. Chrobak, D., D. Stroz, and H. Morawiec, Effect of early stages of precipitation and recovery on the multi-step transformation in deformed and annealed near-equiatomic NiTi alloy. Scripta Materialia, 2003. **48**: p. 571-576.

282. Allafi, J.K., X. Ren, and G. Eggeler, The mechanism of multistage martensitic transformations in aged Ni-rich NiTi shape memory alloys. Acta Materialia, 2002. **50**: p. 793-803.

283. Otsuka, K. and X. Ren, *Factors affecting the Ms temperature and its control in shape memory alloys.* Materials Science Forum, 2002. **394-395**: p. 177-184.

284. Liu, Y., H. Yang, and A. Voigt, *Thermal analysis of the effect of aging on the transformation behavior of Ti-50.9at.%Ni.* Materials Science and Engineering A, 2003. **360**: p. 350-355.

285. Stroz, D., TEM studies of the R-phase transformation in a NiTi shape memory alloy after thermo-mechanical treatment. Materials Chemistry and Physics, 2003. **81**: p. 460-462.

286. Carroll, M.C., C. Somsen, and G. Eggeler, *Multiple-step martensitic transformations in Ni-rich NiTi shape memory alloys.* Scripta Materialia, 2004. **50**: p. 187-192.

287. Fan, G., W. Chen, S. Yeng, J. Zhu, X. Ren, and K. Otsuka, Origin of abnormal multi-stage martensitic transformation behavior in aged Ni-rich Ti-Ni shape memory alloys. Acta Materialia, 2004. **52**: p. 4351-4362.

288. Khalil-Allafi, J., G. Eggeler, A. Dlouhy, W.W. Schmahl, and C. Somsen, *On the influence of heterogeneous precipitation on martensitic transformations in a Ni-rich NiTi shape memory alloy.* Materials Science and Engineering A, 2004. **378**: p. 148-151.

289. Michutta, J., M.C. Carroll, A. Yawny, C. Somsen, K. Neuking, and G. Eggeler, *Martensitic phase transformation in Ni-rich NiTi single crystals with one*

family Ni_4Ti_3 precipitates. Materials Science and Engineering A, 2004. **378**: p. 152-156.

290. Johnson, A.J.W., R.F. Hamilton, H. Sehitoglu, G. Biallas, H.J. Maier, Y.I. Chumlyakov, and H.S. Woo, *Analysis of multistep transformations in single-crystal NiTi.* Metallurgical and Materials Transactions A, 2005. **36**: p. 919.

291. Wang, Z.G., X.T. Zu, and Y.Q. Fu, *Study of incomplete transformations of near equiatomic TiNi shape memory alloys by DSC methods.* Materials Science and Engineering A, 2005. **390**: p. 400-403.

292. Khalil-Allafi, J., G. Eggeler, W.W. Schmahl, and D. Sheptyakov, Quantitative phase analysis in microstructures which display multiple step martensitic transformations in Ni-rich NiTi shape memory alloys. Materials Science and Engineering A, 2006. **438-440**: p. 593-596.

293. Michutta, J., C. Somsen, A. Yawny, A. Dlouhy, and G. Eggeler, Elementary martensitic transformation processes in Ni-rich NiTi single crystal with Ni_4Ti_3 precipitates. Acta Materialia, 2006.

294. Chiang, L.J., C.H. Li, Y.F. Hsu, and W.H. Wang, *Age-induced four-stage transformation in Ni-rich NiTi shape memory alloys.* Journal of Alloys and Compounds, 2007. **doi:10.1016/j.jallcom.2007.04.006**.

295. Todoriki, T. and H. Tamura, Trans Jpn Inst Met, 1987. **28**: p. 83.

296. Stroz, D., J. Kwarciak, and H. Morawiec, *Effect of aging on martensitic transformation in nickel-titanium (NiTi) shape memory alloy.* Journal of Materials Science, 1988. **23**(11): p. 4127-4131.

297. Zhu, J.S. and R. Gotthardt, *New phase transition peak in nickel-titanium (NiTi) alloy.* Physics Letters A, 1988. **132**(5): p. 279-282.

298. Favier, D., Y. Liu, and P.G. McCormick, *Three stage transformation behavior in aged nickel-titanium.* Scripta Metallurgica et Materialia, 1993. **28**(6): p. 669-672.

299. Bataillard, L. and R. Gotthardt, Influence of thermal treatment on the appearance of a three step martensitic transformation in NiTi. J. Phys IV, 1995. **5-C8**: p. 647-652.

300. Bataillard, L., J.-E. Bidaux, and R. Gotthardt, Interaction between microstructure and multiple-step transformation in binary NiTi alloys using in-situ tranmission electron microscopy observations. Philosophical Magazine A: Physics of Condensed Matter: Structure, Defects and Mechanical Properties, 1998. **78**(2): p. 327-344.

301. Dlouhy, A., J.K. Allafi, and G. Eggeler, *Multiple-step martensitic transformations in Ni-rich NiTi alloys-an in-situ transmission electron microscopy investigation.* Philosophical Magazine A: Physics of Condensed Matter: Structure, Defects and Mechanical Properties, 2003. **83**(3): p. 339-363.

302. Kim, J.I., Y. Liu, and S. Miyazaki, *Aging induced two stage R-phase transformation in Ti-50.9at.%Ni.* Acta Materialia, 2004. **52**: p. 757.

303. Chrobak, D. and D. Stroz, Two-stage R phase transformation in a cold-rolled and annealed Ti-50.6at.%Ni alloy. Scripta Materialia, 2005. **52**: p. 757-760.

304. Zhou, Y., J. Zhang, G. Fan, X. Ding, J. Sun, X. Ren, and K. Otsuka, *Origin of 2-stage R-phase transformation in low-temperature aged Ni-rich Ti-Ni alloys.* Acta Materialia, 2005. **53**: p. 5365-5377.

305. Chang, S.H., S.K. Wu, and G.H. Chang, Grain size effect on multiple-stage transformation of a cold-rolled and annealed equiatomic TiNi alloy. Scripta Materialia, 2005. **52**(12): p. 1341-1346.

306. Frick, C.P., A.M. Ortega, J. Tyber, A.E.M. Maksound, H.J. Maier, Y. Liu, and K. Gall, *Thermal processing of polycrystalline NiTi shape memory alloys.* Materials Science and Engineering A, 2005. **405**: p. 34-49.

307. Sitepu, H., W.W. Schmahl, J. Khalil-Allafi, G. Eggeler, A. Dlouhy, D.M. Tobbens, and M. Tovar, *Neutron diffraction phase analysis during thermal cycling of a Ni-rich NiTi shape memory alloy using the Rietveld method.* Scripta Materialia, 2002. **46**(7): p. 543-548.

308. Eggeler, G., J. Khalil-Allafi, S. Gollerthan, C. Somsen, W.W. Schmahl, and D. Sheptyakov, *On the effect of aging on martensitic transformation in Ni-rich NiTi shape memory alloys.* Smart Materials and Structures, 2005. **14**(5): p. S186-S191.

309. Liu, Y., Z. Xie, J.V. Humbeeck, L. Delaey, and Y. Liu, *On the deformation of the twinned domain in NiTi shape memory alloys.* Philosophical Magazine A, 2000. **80**(8): p. 1935-1953.

310. Zheng, Q.S. and Y. Liu, *Prediction of the detwinning anisotropy in textured NiTi shape memory alloy.* Philosophical Magazine A, 2002. **82**(4): p. 665-683.

311. Liu, Y. and Z.L. Xie, *Twinning and detwinning of <011> type II twin in shape memory alloy.* Acta Materialia, 2003. **51**: p. 5529-5543.

312. Sehitoglu, H., R. Hamilton, D. Canadinc, X.Y. Zhang, K. Gall, I. Karaman, Y. Chumlyakov, and H. Maier, *Detwinning in NiTi alloys.* Metallurgical and Materials Transactions A, 2003. **34**: p. 5-13.

313. Wayman, C.M. and T.W. Duerig, eds. Engineering aspects of shape memory alloys, ed. T.W. Duerig, K.N. Melton, D. Stockel, and C.M. Wayman. 1990, Butterworth-Heinemann, London. 3-17.

314. Tan, G. and Y. Liu, Comparative study of deformation-induced martensite stabilisation via martensite reorientation and stress-induced martensitic transformation in NiTi. Intermetallics, 2004. **12**: p. 373-381.

315. Plietsch, R. and K. Ehrlich, *Strength Differential effect in pseudoelastic NiTi shape memory alloys.* Acta mater., 1997. **45**(6): p. 2417-2424.

316. Bhattacharya, K. and R.V. Kohn, *Symmetry, texture and recoverable strain of shape-memory polycrystals.* Acta mater., 1996. **44**(2): p. 529-542.

317. Gall, K., T.J. Lim, D.L. McDowell, H. Sehitoglu, and Y.I. Chumlyakov, *The role of intergranular constraint on the stress-induced martensitic transformation in textured polycrystalline NiTi.* International Journal of Plasticity, 2000. **16**(10-11): p. 1189-1214.

318. Saburi, T., M. Yoshida, and S. Nenno, *Deformation behavior of shape memory Ti-Ni alloy crystals.* Scripta Metallurgica, 1984. **18**(4): p. 363-366.

319. Saburi, T., *Mechanical behavior of Ti-Ni alloys*, in *Shape memory materials*, K. Otsuka and C.M. Wayman, Editors. 1998, Cambridge University Press. p. 49-96.

3 EVOLUTION OF MULTIPLE-STAGE TRANSFORMATIONS (MST) IN NICKEL-RICH 50.8-NiTi: EFFECTS OF AGING AND COOLING RATE ON THE SHAPE MEMORY CHARACTERISTICS

3.1 Abstract

Ni-rich 50.8 at.% NiTi has become the workhorse of the Nitinol superelastic applications in the medical industry for either guide-wire applications or superelastic stents. Reversible superelastic strains and mechanical properties of this alloy are typically optimized using a series of thermomechanical treatments [1] during the production and component manufacturing cycles. While the effect of aging heat treatments for short (1-15min), intermediate (0.5-10hrs) and prolonged (24-100hrs) aging times on the transformation temperatures and the superelastic properties of the 50.8-NiTi has been extensively investigated in the past, the influence of cooling rate (at the end of the aging schedule) viz., water quenched (WQ), air cooled (AC), and furnace cooled (FC), on the transformation behavior has not been given sufficient attention, especially in Ni-rich Ni-Ti alloys. The importance of the cooling rate stems from its influence on the multiple-step martensitic (MST) transformations in Ni-rich NiTi alloys and hence on the transformation temperatures. In the present work, it is shown that the cooling rates indeed have sufficient impact not only on the transformation temperatures, but also on the transformation sequence of various phases involved in the martensitic transformations. Thus, a systematic treatment of

the effects of *aging* treatments (300-700^{o}C) and *cooling rate* on the phase transformations is presented. The current work also investigates the *evolution* of MST in 50.8-NiTi alloy under aging at low (300-400^{o}C) and intermediate temperatures (500-700^{o}C) by varying the aging times (0.5, 1, 5hrs). The evolution of the martensitic transformation was accomplished through a series of partial transformation cycles using differential scanning calorimetry (DSC) methods. Finally, the effects of aging temperature, time and the rate of cooling on the *superelastic* properties, such as plateau stress, and on the *mechanical* properties, such as tensile strength and ductility, are examined.

3.2 Introduction

From an engineering point of view NiTi, popularly known as Nitinol, is an advanced functional alloy whose distinctiveness stems from its unique ability to 'memorize' predetermined shape(s): even after severe deformation of several (strain) percent they are capable of returning spontaneously to their original, pre-deformed shape upon certain thermal conditions [2-4]. This phenomenon, termed 'shape memory' (SM) behavior, is both thermal and mechanical in nature. Additionally, the alloy exhibits another remarkable property, namely superelasticity (SE), where the material exhibits an ability to deform to very high strains of 6-10% and recover the original pre-deformed shape spontaneously upon unloading. Unlike the shape memory behavior, materials exhibiting superelasticity do not require any thermal changes to display superelasticity; however, ambient temperature can affect SE. It is now known that the SM effect and SE are unique properties of certain alloy systems

that arise from a (reversible) thermo-elastic behavior of the alloy that has its basis in a temperature-induced diffusionless, solid-solid first-order transformation (high temperature austenite to low-temperature martensite) involving a change in crystalline symmetry [4]. Since the 1990's, the demand for Nitinol products has seen resurgence, especially in the medical community, as a result of the ever growing roster of medical devices and applications [5-9]. To the question, 'what mobilized such a growth?', Duerig *et al.* [6] advance, among many possible reasons, the medical community's drive towards minimally invasive medical procedures [10, 11] and the commercial breakthrough of the stents that revolutionized the medical industry [6, 12-14]. A shift towards minimally invasive medical procedures necessitated the availability of novel medical instruments with unconventional properties, and Nitinol specifically addressed itself to this task. Compared to the cryogenic alloys required in couplings and fasteners [15, 16], or high-M_s alloys necessary in actuator applications [17], the medical applications were based on implants that demanded optimal performance at or around the body temperature (37^oC); this is the temperature window where the Nitinol alloys excelled, in addition to having excellent biocompatibility [18].

The current industry standard Nitinol alloy is the near-equiatomic 50.8 at.% NiTi alloy (henceforth designated as 50.8-NiTi) that has become the workhorse of most superelastic medical applications [1, 19, 20]. It is known that Ni-rich NiTi alloys with Ni composition greater than 50.6 at.% undergo precipitation reactions, where metastable phases such as Ti_3Ni_4, Ti_2Ni_3 and $TiNi_3$ precipitate in seriatim during aging between 300^oC and 800^oC [21-23]. The nature of the phases that precipitate is a strong function of Ni composition and aging parameters (temperature and time) [23,

24]. However, the most important impact of the Ni composition on the usage of a particular Ni-Ti alloy is its influence on the transformation temperatures; it is known that an increase in Ni composition by 1% from 50.5 to 51.5 at.% decreases the M_s (martensite start temperature) to below 100 K (in solution treated condition) [25, 26].

Since the transformation temperatures (especially A_f, the austenite finish temperature) are an important indicator for the type of application of a certain Ni-Ti alloy, several studies [27] on the influence of thermomechanical treatments, specifically, either cold work or aging, or a combination of both, are extant in the literature [15, 22, 28]. While the traditional simplified view of phase transformations occurring in Ni-Ti alloys involves only one-stage cubic austenite (B2) to monoclinic (B19') martensite transformation (transformation strains ~ 6-10%), the influence of cold work, i.e., high density of dislocations [29-31] and the presence of Ni-rich precipitates in Ni-rich (Ni > 50.6at.%) Ni-Ti alloys contribute to a more complex two-stage, three-stage or even four-stage transformations, collectively termed 'multiple stage transformation' (MST) [22, 26, 27, 31-43]. It is now known that the introduction of a dislocation network/substructures or precipitates into the Ni-Ti matrix can act as obstacles to the direct B2-B19' transformation [31, 35, 37, 41]. As a result of this barrier, a competing martensitic transformation, B2→R-phase that involves lower transformation strains (~1-2%), becomes feasible and dominant. Further transformation occurs as R-phase converts to B19', thus leading to a two-step process that is seen as a double peak (two-stage) on the differential scanning calorimetry (DSC) trace. The heating cycle however, involved only one large peak indicating that the B19'→B2 transformation occurred in one step. Yet, it was

observed that aged Ni-rich NiTi alloys exhibited three DSC peaks during cooling from austenitic phase, instead of a two-stage transformation [29, 30, 44-48]. Since the Ni-Ti alloy did not exhibit any competing martensitic transformation, other than to R-phase and B19' phase, there was uncertainty with regards to the correct interpretation of the multiple-stage transformation (MST). Furthermore, according to Carroll *et al.* [35], the DSC peaks evolve from one or two peaks after short aging times to three peaks after intermediate aging times and back again to two peaks or one peak after long term aging, a behavior termed as '2-3-2' transformation by Allafi *et al.* [26].

Bataillard *et al.* [48, 49] cite the influence of local coherency stress fields around the Ni-rich Ti_3Ni_4 precipitates on the transformation sequence in such a way that the B2 matrix initially transforms to R-phase near the regions affected by the coherency stresses followed by the second transformation R-phase→B19'. This second transformation occurs in two steps, one near the precipitate and the other in the Ni-Ti matrix volume unaffected by the coherency. Subsequently, Allafi *et al.* [26] have proposed that the 3-stage transformation was due to localized composition inhomogeneity in the austenite due to the precipitation of Ni-rich Ti_3Ni_4 precipitates that deplete Ni from the surrounding matrix. They implied that since the transformation temperatures depend strongly on the Ni composition of the matrix, the composition (chemical) inhomogeneity in the volume surrounding the precipitates would result in a single B2→R transformation followed by two R→B19' transformations occurring near and away from the precipitates, respectively [35]. Recently, in situ TEM studies [26, 50] of transformations occurring in aged Ni-rich Ni-Ti alloys suggested that, due to the preferential precipitation of lenticular Ti_3Ni_4 at

the grain boundaries, the first DSC peak corresponds to the B2→R-phase transformation near the grain boundary (GB) followed by the R-phse→B19' transformation. Furthermore, the third peak then corresponds to the direct B2→B19' transformation in the precipitate free grain interior (GI) region. Thus, a large scale inhomogeneity in the microstructure due to preferential precipitation of phases near the grain boundary was suggested as the main cause behind the multiple-stage transformations.

All of the above theories, i.e., local-scale inhomogeneity in either coherency stress fields and chemical composition, or the large-scale microstructural inhomogeneity (due to preferential GB precipitation) indicate that the 3-stage transformation is the norm rather than the exception [22]. However, Fan *et al.* [36] point out that, typically, single crystals of Ni-rich NiTi alloys with different Ni compositions and Ni-rich (e.g., 51.5Ni-Ti) polycrystalline alloys exhibit the normal 2-stage transformation, whereas only the near equiatomic polycrystalline alloys capable of undergoing precipitation reactions (e.g., 50.6-NiTi), exhibit 3-stage transformations. Their study suggested that, while the presence of grain boundaries is a necessary condition to create microstructural inhomogeneity due to preferential precipitation, it is not a sufficient condition for the 3-stage transformation. Instead, they invoke that it is the degree of supersaturation, which is high in Ni-rich alloys such as 51.5-NiTi, that governs the nucleation kinetics of the Ti_3Ni_4 precipitation and thus the MST. In particular, if the degree of supersaturation is high, as in the case of 51.5Ni-Ti, the precipitation process is less sensitive to the presence of grain boundaries and thus results in a homogeneous precipitation and thus only 2-stage

transformation. If the degree of supersaturation is low, as in the case of 50.6Ni-Ti, the precipitation is severely affected by the presence of grain boundaries (GB), since the GB nucleation rate is substantially greater than in the grain interior. This leads to large-scale heterogeneity in microstructure and chemical composition between the grain boundaries and the grain interior [36]. Thus, they conclude the two opposing factors, viz., presence of grain boundaries that instigate preferential precipitation due to favorable energetics and the Ni supersaturation level that dictates the nucleation rate, govern the distribution of the precipitates and thus the nature of MST, i.e., 2-stage vs. 3-stage. They also exclude the possibility of 3-stage transformations in single crystals devoid of GBs or in microstructures with small-scale heterogeneities.

More recently, Michutta *et al.* [42] studied the transformations in aged single crystals of 51.3-NiTi and observed that 3-stage transformations can indeed occur in aged Ni-rich single crystals that exhibit homogeneous distribution of the metastable Ti_3Ni_4 precipitates provided that the interparticle spacing is greater than a critical value (~ 200 nm). The three peaks on the DSC trace correspond to the formation and growth of R-phase from all the precipitate/matrix interfaces, followed by the formation and growth of B19' phase along the same interfaces. The final transformation peak corresponds to the B2-B19' transformation. Thus, Michutta *et al.* [42] put forward a general proposal regarding the MST: (a) MST occur in Ni-rich NiTi alloys that exhibit large scale (10μm) microstructural heterogeneities (due to preferential precipitation near GBs in polycrystalline Ni-Ti, differences between the dendritic and interdendritic regions in cast single crystals, heterogeneous distribution of oxide and carbide inclusions and variable grain sizes across the specimen cross

section). (b) MST can also occur in the absence of large-scale microstructural heterogeneities, for example in aged Ni-rich NiTi single crystals with a homogeneous distribution of the precipitates, provided that the interparticle spacing is greater than a threshold value (~ 200 nm).

In the above discussion, whether the microstructure is heterogeneous (due to preferential GB precipitation) or homogeneous (with interparticle spacing greater than 200 nm), the 3-stage transformation was identified as the B2→R phase transformation near the precipitates followed by the R→B19' transformation, and the final peak was identified as B2→B19' transformation in the precipitate free matrix [26, 31, 33, 36, 37, 39, 42, 50]. Additionally, as mentioned earlier, Bataillard *et al.* [49] suggested an alternative sequence for the 3-stage transformation based on the effect of coherency stresses around Ti_3Ni_4 precipitates: the first step consists of B2→R phase transformation nucleating at the precipitate/matrix interfaces and growing into the matrix. The second peak corresponds to the transformation of R→B19' near the precipitate region affected by the coherency stresses followed by the R→B19' peak representing the transformation in the matrix; thus totaling one B2→R and two R→B19' (1R-2M) transformations. More recently, it has also been reported that 3-step transformations in deformed and low-temperature (200^oC-300^oC) aged (i.e., with prior thermomechanical history) 50.6-NiTi alloy may consist of two B2→R phase transformation followed by one R-phase→B19' transformation (2R-1M) [51-53] or even two B2→R-phase and two R→B19' phase transformations (2R, 2M) (in total, 4-stage transformation) [52, 54] that was rationalized by invoking the inhomogeneous distribution of dislocations or grain size.

More recent results have also indicated additional complexity in the transformation sequence: Neutron and X-ray diffractions studies indicated that in some alloys, the first DSC peak corresponds to the formation of both the R-phase and the B19' martensitic transformation; thus a single DSC peak is not necessarily tied to a single martensitic transformation event [55, 56]. In another study of MST in single crystal NiTi alloys with compositions: 50.1, 50.4, 50.8 and 51.5 at.% Ni, Johnson *et al.* [39], first to report the occurrence of an unprecedented MST in 50.1-NiTi alloys and suggest that they are associated with single crystal defects such as dendrites and low-angle boundaries. They observe, in addition to the 2/2-stage B2→R→B19' transformations, the 3/2-stage, 3/3-stage and even 4/4-stage transformations. Furthermore, the presence of the same defects in higher Ni content single crystals does not elicit similar MST.

Thus it can be summarized [35] that the occurrence of MST is governed by local or small-scale inhomogeneity (coherency stress fields, compositional fluctuation, precipitation with a critical interparticle spacing) associated with the precipitation of metastable phases such as Ti_3Ni_4, large-scale inhomogeneity characterized by preferential grain-boundary precipitation and precipitate free matrix, presence of single crystal defects such as dendrites and low-angle boundaries, and the thermomechanical process that cause heterogeneity of both dislocations and precipitate distribution.

The above introduction is not only meant to aid in the analysis of the MST observed in the current work, but also to point out that there exists no uniform description of the causes of MST observed in several Ni-Ti alloys. Furthermore, as

Fan *et al.* point out [36], the sequence of the transformations may vary with composition, aging temperature and time and prior thermomechanical treatment. Carroll *et al.* [35] summarize that it is a challenging task to differentiate between the relative importance or degree of influence of each of the above mechanisms on the multiple phase transformations. In all likelihood, the multiple mechanisms could be concomitantly affecting the MST; but whether the multiple transformations occurring concurrently are synergistic or independent, or if they are interfering with each other is still unclear.

While the effect of aging heat treatments for short (1-15min), intermediate (0.5-10hrs) and prolonged (24-100hrs) aging times on the transformation temperatures and the superelastic properties of the 50.8-NiTi has been extensively investigated in the past [1, 57], the influence of cooling rate (at the end of the aging schedule) viz., water quenched (WQ), air cooled (AC), and furnace cooled (FC), on the transformation behavior has not been given sufficient attention. The few known studies [19, 58] have focused on equiatomic rather than the Ni-rich Ni-Ti alloys. The importance of the cooling rate stems from its influence on the multiple-step martensitic (MST) transformations in Ni-rich NiTi alloys and hence on the transformation temperatures. In the present work, it is shown that the cooling rates indeed have sufficient impact not only on the transformation temperatures, but also on the transformation sequence of various phases involved in the martensitic transformations.

Thus, a systematic treatment of the effects of *aging* treatments (300-700^{o}C) and *cooling rate* on the phase transformations and the superelastic and mechanical

properties is presented. Typical applications of 50.8NiTi involving small geometry parts such as wires or stents may not show much variation in their transformation characteristics with respect to cooling rates between AC and WQ, since the smaller volume parts cool rapidly to the room temperature under both AC and WQ conditions. However, with burgeoning interest in the Ni-Ti alloys for seismic [59-61] and other structural and dynamic impact applications [62-66], which will necessarily entail larger parts and/or intricate geometries, their functional characteristics may certainly be affected by the difference in cooling rates during various cycles of thermomechanical heat treatments. Indeed, as Figure 3.1 indicates (adapted from [67, 68]), the difference in cooling rates affect the hardness of the Ni-rich alloys. Furthermore, recent studies on Ni-rich 55-NiTi alloys [23, 69-72] have shown that by varying the cooling rates, one can produce shape memory or superelastic Nitinol from the same ingot without any additional thermomechanical treatments, indicating a considerable influence of cooling rates on the transformation temperatures. Therefore, as the interest in newer Ni-rich NiTi alloys is seeing resurgence, it is timely that a systematic study of the cooling rate effects is undertaken.

The current work also investigates the *evolution* of MST in 50.8-NiTi alloy under aging at low (300-400^{o}C) and intermediate temperatures (500-700^{o}C) by varying the aging times (0.5, 1, 5hrs). The evolution of the martensitic transformation was accomplished using partial transformation using differential scanning calorimetry (DSC) methods. DSC is the most routinely used method to characterize the phase transformation temperatures occurring in bulk NiTi shape memory alloys. While early DSC traces exhibited only single or double peaks, indicating 1-stage or 2-stage

transformation corresponding to straightforward B2→R and R→B19' transformations, with the discovery of the aforementioned multiple stage transformations, the interpretation of the DSC peaks and the transformation sequence has become non-trivial. Thus, partial DSC cycles are becoming commonplace in elucidating the nature of the MST [33, 36, 40, 43, 47, 73]. Finally, the effects of aging temperature, time and the rate of cooling on the superelastic properties such as plateau stress, and on the mechanical properties (UTS, ductility) are examined here.

3.3 Experimental

3.3.1 Materials and microstructure

The near-equiatomic 50.8 at.% NiTi Nitinol material used in the current work was obtained in the form of 1mm thick sheet from *Johnson Matthey (San Jose, CA)*. The sheet material was obtained in a flat annealed condition (typically aged at ~510–525^{o}C for 5-10 min following a routine 10-30% cold rolling process) that optimizes its superelastic strains. Numerous dog bone tensile specimens of a 25 mm gage length and measuring 6.4 mm width x 1 mm thickness were cut from these sheets and aged between 300±5^{o}C and 700±5^{o}C for 0.5hr, 1hr and 5 hr. At the end of each aging condition (temperature and time), three sample sets were prepared by water quenching (WQ), air-cooling (AC) and furnace cooling (FC) the specimens, respectively. Each of these processes typically involved cooling rate of the order ~ 10^{3} ^{o}C/sec, 1 ^{o}C/sec and 0.01^{o}C/sec, respectively.

Figure 3.2(a, b) shows the optical microstructures of the as-received (AR) and the solution-treated (ST at 800^{o}C, 1hr) 50.8NiTi. Figure 3.2(c) indicates the DSC

curves for AR and ST 50.8-NiTi alloy. The AR sheet material exhibits B2→R→B19' multiple-stage transformation (MST), whereas the ST alloy shows a 1-stage forward B2→B19' and reverse B19'→B2 martensitic transformations, with a hysteresis of ~40^{o}C [37, 41]. The presence of MST and the sequence of martensitic transformations in the AR material are discussed in detail in the following section. Based on the DSC results, the AR material was in superelastic-austenitic condition at room temperature (RT ~ 20^{o}C); the specific transformation temperatures are indicated in Table 3.1. It should be noted that the NiTi sheet material used in the current work is similar to the sheet material studied in a recent investigation by Robertson *et al.* [74, 75], who report that, although the apparent grain size of the sheet NiTi was measured as ~15-20 μm, TEM observations revealed the existence of sub-grain structure of the order ~10nm.

3.3.2 Texture Measurements

Texture measurements of the 50.8-NiTi sheet in as-received and aged conditions were measured with SCINTAG X1 X-ray diffraction (XRD) system with 4-circle goniometer utilizing Cu-K_{α} (λ=1.5405 Å) radiation source (40kV, 20mA). Samples measuring 15mm x 15mm x 1mm were cut from the as-received sheet and were aged at 550^{o}C (10 min) and 800^{o}C (1hr) followed by WQ. The samples were then polished to diamond finish and prepared for optical microscopy examination. The optical micrographs, shown in Figure 3.2, reveal the presence of 'needle' martensite in some grains produced due to the stresses applied during mechanical polishing. Prior to the X-ray texture measurements, the samples were heated above 60^{o}C and gradually cooled back to room temperature (20^{o}C) ensuring that the material

is fully cubic austenite condition. Since 50.8-NiTi is a Ni-rich Nitinol, aging this alloy between 300^{o}C and 600^{o}C leads to the precipitation of Ni-rich metastable phases such as Ti_3Ni_4 and Ti_2Ni_3 [1, 21-24]. However, the precipitation kinetics are such that the precipitation of the Ti_3Ni_4 phase is optimized between 300^{o}C and 500^{o}C, with peak values around 400^{o}C [1, 76] for 50.8-NiTi. Aging between 500^{o}C and 550^{o}C brings about the gradual dissolution of Ti_3Ni_4 along with the activation of recovery processes (dislocation annihilation) [1, 76]; with further aging leading to the formation of the second metastable phase Ti_2Ni_3. Since the aging leads to the precipitation of Ni-rich phases, a concomitant increase in the transformation temperatures (A_f) is observed in the alloy due to the removal of Ni from the matrix [32], thus making the martensitic phase stable at room temperature. However, 50.8-NiTi aged at 550^{o}C for 10min adjusts the matrix Ni concentration such that the alloy is in the austenitic state; thus this aging treatment was chosen to measure the texture evolution of the austenitic phase. Additionally, annealing at 800^{o}C homogenizes the alloy and causes recrystallization and grain growth, evident in Figure 3.2(b); once again producing an austenitic phase.

The crystallographic texture of the austenitic phase was determined from three 'incomplete measured' pole figures of 110, 200 and 211, similar to Robertson *et al.* [75, 77]. The X-ray intensities were background corrected and the orientation distribution function (ODF) was obtained using the popLA (preferred orientation package – Los Alamos) software package. The ODF were then used to calculate the 100, 110 and 111 pole figures (PF) and inverse pole figures (IPF), as shown in Figure 3.3 (equal area projection). As the data indicate, the sheet material exhibited typical

<110>-type rolling texture along with a spread in other minor components (see Table 3.1) similar to the α-fiber texture [75, 77, 78]; the {111} was the strongest normal direction (ND) component. With aging at 550°C and 800°C, the texture evolved by strengthening the {111}<110> component; such strengthening behavior was recently independently reported by Robertson *et al.* [77] and Fernandes *et al.* [78]. Since the texture determines the shape memory characteristics, such as recoverable strains, plateau stresses and anisotropy of mechanical properties (UTS, ductility), this attendant texture variation with aging should be kept in mind during thermomechanical processing.

Table 3.1 Transformation temperatures measured in as-received (AR) NiTi sheet.

Material	Transformation temperatures, °C‡						Grain size (μm)	Texture
50.8-NiTi AR Sheet	R_s (A-R)	R_f (A-R)	M_s (R-M1)	M_f (R-M2)	R'_s (M-R)	A_f (R-A)	10	Major {111}<110> {122}<110> Minor {111}<112>
	15.8	0	-40	<-100	-13.5	15.2		
Solutionized 800°C – 1hr			M_s (A-M)	M_f (A-M)	A_s (M-A)	A_f (M-A)	40	Major {111}<110> (strengthen) Minor {122}<110> {111}<112> {110}<110>
			-23	-7	4	21		

‡ The transformation temperatures are determined by a DSC with R_s, R_f, M_s, M_f and A_s, A_f being the R-phase, martensite and austenite start and finish temperatures. However, as discussed in the Results section, the as-received alloy exhibits {(A→R) + (R→M1) + (R→M2) || (M→R) + (R→A)} forward || reverse transformation sequence.

3.3.3 Experimental Procedure

The phase transformation temperatures were measured using a cryo-differential scanning calorimeter (DSC) (Perkin Elmer Pyris 7 series) in a helium atmosphere. DSC samples typically measuring 90 mg were cut from the aged samples and sealed in Al pans and were heated to 80^{o}C and held for several minutes. Subsequently, complete heating and cooling cycles were performed between 80^{o}C and -110^{o}C at a rate of 20^{o}C/min. In order to identify individual phase transformations (corresponding to different peaks on a DSC chart), partial heating and cooling cycles were performed with different starting and ending temperatures, as was necessary. In all the DSC traces, the top and the bottom curves represent the cooling and heating cycles, respectively.

Quasi-static tension tests were conducted using a servohydraulic load frame at a strain rate of 5 x 10^{-4}/s. The Nitinol samples were sequentially unloaded from strains of 3%, 6% and 10%. Whenever the samples did not recover the loading strains upon unloading, the specimen was heated above 80^{o}C at constant zero load condition using an electric tape-heater wound around the gage length of the specimen. The completion of the reverse transformation was easily noticeable as the extensometer recordings changed from decreasing strain to increasing strain, corresponding to a change from reverse transformation to thermal expansion of the specimen. The specimen was then cooled using forced convection by a fan until the sample temperature returned to the ambient temperature (20^{o}C) and the subsequent loading cycle was initiated.

3.4 Results and Discussion

3.4.1 Phase Transformations: DSC Results

3.4.1.1 As-Received: Transformation sequence

Figure 3.4(I a) indicates the full DSC scan of the AR 50.8-NiTi sheet material. The cooling cycle (top curve) exhibits three peaks 1-2-3, whereas the heating cycle (bottom curve) shows only two peaks, 4-5, thus showing a 3-step/2-step multiple stage transformation (MST). The partial DSC cycles are shown in Figure 3.4(I b-d). The partial cycle (I b) indicates that 1 and 1' are B2→R phase, and its reverse transformation, R→B2, respectively, since its temperature hysteresis is quite small (<10^{o}C) compared to the B2→B19' or R→B19' transformation. The cooling cycle (I c) partially terminates before the end of peak-2 and the heating cycle exhibits an enhancement in the transformation heat (represented by the area under the peak) of peak 1', resembling more closely peak 5 in the full scan. The final partial cooling cycle (I d) now includes a part of the stage-3 transformation and upon heating develops into the peak 4 (only seen as a partially formed shoulder). Furthermore, a full DSC scan between -100^{o}C to -40^{o}C (not shown) indicated the presence of only peak 3 and not peak 2, suggesting that peaks 3-4 belong to a pair of the transformation. Henceforth the cubic B2 austenite, monoclinic B19' martensite, and trigonal R-phase will be denoted as A, M and R, respectively. Since the peaks 1, 2 in the forward transformation correspond to peak 5 and peaks 3 and 4 are a pair, it can be seen that there are two possibilities:

(a) 1, 2 are A→R and R→M1 (martensite-1) transformations and 3 is R→M2 (martensite-2) transformation; and peak 4 represents the reverse M2→R transformation, whereas peak 5 corresponds to an overlap of the M1→R and R→A transformation; or,

(b) 1, 2 are two B2→R-phase (R1, R2) transformations and 3 is one single R-phase→M transformation; and peak 4 corresponds to the reverse M→R-phase and 5 to the R→B2 phase conversion.

Let us first discuss scenario (b): This is supported by Kim *et al.* [51] who consider a solution-treated Ni-rich 50.9-NiTi subjected to both short and long term aging treatment (0 to 3000hrs) at low temperatures (200-300^{o}C), and Chrobak *et al.* [52] who consider a cold-rolled (15% cold-work) 50.6-NiTi aged at 400^{o}C for very short times (0.25-0.5hrs). Kim *et al.* [51] explain the double R-phase transformation based on a modified Bataillard [49] explanation; the first R-phase forms near the precipitate-matrix interface followed by the second peak corresponding to the second R-phase transformation in the matrix (between the precipitates) before finally transforming into the B19' martensite (peak 3). Chrobak *et al.* [52] give an alternate explanation for this 3-stage transformation based on the heterogeneous distribution of dislocations in a cold-rolled NiTi: The first R-phase forms in low dislocation density regions followed by the R-phase in high dislocation density before finally transforming into B19'.

Scenario (a) has been supported by several studies: Moraweic *et al.* [29, 30] who explained the first peak as B2→R followed by R→B19' in two stages due to the interruption of B19' martensite by the dislocation substructures (subgrain boundaries)

that required additional undercooling; Bataillard *et al.* [49] who invoked the influence of coherency stress around the Ti_3Ni_4 precipitates (discussed earlier); Allafi *et al.* [26, 32, 37, 41] who rationalized the MST as governed by the chemical inhomogeneity near the precipitates (Ni-depleted regions near the precipitates transform at higher temperatures than the Ni-rich regions far from the precipitate [32]) and alternatively, by large-scale heterogeneous or preferential grain boundary precipitation [32, 36, 37, 41, 50]; and even through small-scale homogeneous precipitation governed by interparticle spacing [38]. If indeed 1, 2 represent two B2→R phase transformations, then the temperature hysteresis should be $<10^oC$. However, from Figure 3.4(I c,d), the temperature hysteresis is $>50^oC$, suggesting that scenario (a) is the most likely sequence, with the R→M2 (peak-3) transformation completing below -100^oC.

The AR 50.8-NiTi material in this study had undergone a cold-rolling (10-30%) cycle (followed by a short term aging between 510 and 525^oC for 5-15min (depending on the proprietary information of commercial Ni-Ti alloys). Comparing with the observations from: (i) Chrobak *et al.* [31] who study cold-rolled 50.6-NiTi for short aging times between 5-15 min at 400^oC; (ii) Frick *et al.* [73] who investigate cold-rolled (30%) 50.9-NiTi aged at 450^oC and 550^oC for 1.5hr; and (iii) based on the time-temperature-transformation (TTT) diagram for 50.8-NiTi prepared by Pelton *et al.* [1], the likely scenario for the 3-stage/2-stage MST observed for the AR material in the current study is a combined influence of two intertwined processes of dislocation density and precipitate growth. Aging influences both the processes of dislocation annihilation (recovery during annealing) and precipitate growth. Aging heat treatment of a cold-rolled sheet material is likely to produce a complex microstructure

containing relatively large densities of dislocations and precipitates that are interwoven in such a way that precipitation may occur mainly on dislocations, act as obstacles for dislocation movement, and may hinder the recovery process. This scenario is indeed supported by some studies in the literature [31, 52, 73], which showed intricate microstructures containing dislocations decorated with precipitates.

Thus, the heterogeneity of both the dislocations and precipitate distribution leads to the inhomogeneity of Ni composition in the matrix and lead to two R→M (M1, M2) transformations [31]. Also, according to the TTT diagram of (strain annealed) 50.8-NiTi by Pelton *et al.* [1], the metastable Ti_3Ni_4 precipitates begin to dissolve into the matrix between 500^{o}C and 550^{o}C (variable depending on the prior cold-work) with concomitant recovery [52] depending on the aging times. Annealing above 600^{o}C leads to recrystallization and a rapid decrease in dislocation density of cold-worked 50.9-NiTi [73], and beyond 700^{o}C, the material is homogenized (ST), thus affecting the transformation temperatures.

3.4.1.2 Effect of aging Temperature (Aged+WQ): Evolution of MST

Figure 3.5 shows the cooling (top) and heating (bottom) DSC curves of AR 50.8-NiTi aged between 300^{o}C and 700^{o}C for 0.5hr, 1hr and 5hr, respectively, followed by water quenching (WQ). Figure 3.6 shows a comparison of the transformation (DSC traces) in 50.8-NiTi as a function of cooling rate for various aging conditions (300^{o}C-700^{o}C, 0.5-hrm 1-hr, and 5-hrs). Referring to both Figure 3.5 and Figure 3.6, the following observations can be made:

(a) *Aging at 300°C-0.5hr:* The 50.8-NiTi alloy aged at 300°C-0.5hr exhibits a 3-stage/3-stage DSC trace with three peaks in both cooling and heating cycles, 1-2-3 and 3'-2'-1', respectively, in the order of appearance. The partial cooling cycles (not shown) revealed that these peaks correspond to the pairs of transformations, 1↔1', 2↔2' and 3↔3', that represent A↔R, R↔M1 and R↔M2 forward and reverse transformations, respectively. This suggests that the peak 5 in the DSC chart of the AR material that corresponds to an overlap of R→M1 and R→A transformations has split into two separate transformations. This is understandable, since aging 50.8-NiTi at 300°C-0.5hr leads to a single precipitation reaction of Ti_3Ni_4 (also indicated as $Ti_{11}Ni_{14}$ in the literature), which depletes the Ni from the nearby matrix [1]. Since decrease in Ni composition leads to an increase in the transformation temperature [22, 32], it can be seen from Figure 3.5(a) that the A→R transformation temperature (R_s) increases from 16°C (in the AR specimen) to 25°C; correspondingly, the reverse transformation R→A also moves forward in temperature scale. However, since peaks 2 and 3, representing R→M1 and R→M2, respectively, are relatively unchanged (transformation temperatures for these peaks advance only by a few degrees), the reverse transformations also advance by a smaller amount compared to the A↔R transformation (peak 1↔1'). This leads to the separation of peak-5 in Figure 3.4(I-a) into two peaks, 2' and 1'. The reason for a smaller increase in the transformation temperature (TT) of peaks 2 and 3 may be rationalized as follows: Carroll *et al.* [35] posit that in the case of R-phase (smaller transformation strains) the nucleation barrier is small enough that the difference between T_o^R (thermodynamic equilibrium temperature between A and R-phase) and observed R_s (on a DSC chart) is negligible;

whereas, M has a significant nucleation barrier (large transformation strains in addition to barriers such as dislocations and precipitates that resist the large transformation strains) that T_o^M (thermodynamic equilibrium temperature between R-phase and M) and the observed M_s is significant that it requires a certain level of undercooling to induce R→M transformation. Thus, aging at 300°C-0.5hr is not sufficient to influence the peaks 2 and 3 (R→M1, M2) transformations by reducing the degree of undercooling through either annihilating the dislocations or siphoning more Ni from the matrix into the precipitates that may increase the overall transformation temperatures. This, as we will see shortly, occurs at higher temperatures where, aging between 350°C and 450°C, 50.8-NiTi exhibits the highest precipitation rates for Ti_3Ni_4 [1] (corresponding to the peak of the 'c-curve' in the TTT diagram) and the recovery processes (dislocation annihilation) become active at aging temperatures ≥ 500°C [1, 52], with recrystallization occurring at aging temperatures ≥ 600°C [52, 73].

(b) *Aging at 300°C-1 and 5hrs:* Aging at 300°C for longer times of 1-hr and 5-hr present similar observations as in (a) above: the TT for peak-1, i.e., A→R transformation increases steadily to nearly 54°C (see Figure 3.5(b) and Figure 3.6(A-b,c)). Correspondingly, the R→A peak-1' (A_f) also advances on the temperature scale. Furthermore, the transformation heats for these forward (A→R) and reverse transformations are seen to increase with aging time. By contrast, the transformation heats for 2-2'and 3-3' forward and reverse transformations are seen to decrease with aging time. If the increase in R_s (or A_f) transformation temperature is justified on the

grounds of decreased Ni content in the matrix due to the precipitation of Ti_3Ni_4 phase, one may ask why the remaining transformation temperatures are not equally shifted to higher temperaures? The reasons for these observations may be explained as follows. It has been suggested in the literature [52, 79, 80] that the peaks in the DSC thermal measurements are due to three factors: (i) latent heat of transformation (reversible), (ii) internal elastic stored energy (reversible) and (iii) (irreversible) work spent in moving the interfaces through the obstacles. As indicated, (i, ii) are reversible in nature, whereas (iii) corresponds to irreversible energies involved in the transformation (largely frictional work required by the A and M phases). While the (i) latent heat of transformation is dependent on the mass of transformation, (ii) the internal elastic energy and (iii) the irreversible work are influenced by metallurgical conditions (such as dislocation structure and density) of the matrix where the martensitic transformations are taking place [80]. Given that the aging influences the precipitation of Ti_3Ni_4 phases and hence the Ni composition surrounding the precipitate, during longer aging times, the net volume of the matrix near the precipitate that is depleted of Ni is increasing. Thus, this decrease in Ni content not only leads to increasing R_s (or A_f) temperatures for the A↔R transformations, but also the total volume participating in the transformation increases, which in turn increases the transformation heat. Furthermore, aging studies between temperatures 300^{o}C and 500^{o}C have shown that the precipitation of Ti_3Ni_4 phase occurs at dislocations and hinders the dislocation movement [31, 52]; which indicates that 300^{o}C is not a high enough temperature for recovery (dislocation annihilation) that would have altered factors (ii, iii) above. In summary, the two opposing factors of decreasing Ni content (leading to larger

transformation temperatures) and the precipitates hindering the movement of dislocations result in a decrease in the volume of the matrix participating in the 2, 3 (R→M1, R→M2) transformations) (see also [31]). In addition, Chrobak *et al.* [52] show that the A→R phase transformation involves larger elastic energy changes (positive) than the R→M transformation (negative), thus affecting factor (ii) above and hence the overall transformation heat.

(c) *Aging at 400^{o}C-0.5hr and 1hr:* Aging at 400^{o}C for 0.5-hr and 1-hr also shows a 3-stage/3-stage MST: 1-2-3 forward and 3'-2'-1' reverse transformation sequence. As observed for 300^{o}C aging, the peak-5 in AR 50.8-NiTi (that corresponded to a combined M1→R and R→A transformation) splits into 2' and 1' double peak. Furthermore, the transformation heats for 1↔1' (A↔R) transformation increases with aging time compared to the aged 300^{o}C alloys, and this trend is uniform for all aging times (0.5hr-5hr). By contrast, the transformation heats for 2↔2', 3↔3' forward and reverse transformations are seen to decrease with aging time (similar to the observations for 300^{o}C aging cycles). In addition, the transformation temperatures for peaks 2 and 3 (representing R→M1 and R→M2, respectively) increase by nearly 20^{o}C; the first R→M1 transformation (peak-2) begins at -20^{o}C (for 0.5hr and 1hr) compared to -40^{o}C for the as-received (AR) and the 300^{o}C aging (all aging times). This also leads to an increase in the reverse transformation temperatures for peaks-3' and 2' by the same amount for 0.5hr and 1hr aging times.

(d) *Aging at 400°C-5hr:* The critical findings for 400°C aging are, however, observed at 5hr aging period: peak 3'and 2' now overlap in the reverse transformation during the heating cycle (also see Figure 3.6(B-c)), suggesting that the reverse transformation sequence now corresponds to M→R (combination of M1→R and M2→R) followed by R→A. This means that the transformation sequence has evolved from {(A→R) + (R→M1) + (R→M2) || (M2→R) + (M1→A)} for As-Received ⇒ {(A→R) + (R→M1) + (R→M2) || (M2→R) + (M1→R) + (R→A)} for aging at 300°C (0.5hr-5hrs) and 400°C (0.5hr-1hr) ⇒ {(A→R) + (R→M1) + (R→M2) || (M→R) + (R→A)} forward || reverse transformation sequence for aging at 400°C-5hrs.

Furthermore, as the TTT diagram suggests [1], the 50.8-NiTi alloy exhibits its maximum Ti_3Ni_4 precipitation rates, leading to their maximum density, at 400°C. Since maximum density of Ti_3Ni_4 should necessarily correspond to a maximum reduction of Ni from the matrix near the precipitates, the first transformation 1↔1' (A↔R) should also exhibit the maximum transformation temperatures. This is indeed observed for aging at 400°C, where R_s = 46°C and 55°C (or alternative A_f = 50°C and 58°C) for 0.5hr and 5hr aging times. The R→M1 (peak-2) temperature also increases from -20°C to -5°C.

(e) *Aging at 500°C-0.5-hr:* As we will see shortly, aging at 500°C brings about an important transition in the transformation sequence in 50.8-NiTi cold-worked alloy due to the interplay of several phenomenon. As Figure 3.4(II-a) indicates, there is a decrease in the R_s temperature for 0.5-hr (30°C), and 1-hr (22°C) aging, or

equivalently, a decrease in A_f at 0.5-hr age (36^{o}C) and at 1-hr age (32^{o}C) in the 1↔1' (A↔R) transformation temperature compared to the aging at 400^{o}C. This can be rationalized on the basis of the TTT curves for 50.8-NiTi [1]. At 500^{o}C, the Ti_3Ni_4 precipitates begin to dissolve into the matrix with a concomitant increase in the Ni composition in the matrix, thus causing the transformation temperatures to drop. Pelton *et al.* [1] also point out that a second metastable phase Ti_2Ni_3 begins to form at 550^{o}C that requires greater amount of Ni diffusing away from the matrix, thus increasing the transformation temperatures further. However, the aging times used by Pelton *et al.* [1] were between 2 and180 min. (i.e., maximum 3-hrs). It has been suggested by Nishida *et al.* [21] and other workers [23, 24], that long term aging (5-hrs to 1000-hrs) at lower temperatures (500^{o}C) also brings about the precipitation of Ti_2Ni_3. Therefore, the transformation temperatures at 500^{o}C-5-hr aging increases R_s (A_f) = 32^{o}C (45^{o}C).

Figure 3.4(II-a) also indicates a 3-stage/2-stage MST similar to the as-received 50.8-NiTi (forward 1-2-3 || reverse 4-5). However, the difference lies not only in the increase of 1↔1' (A↔R) transformation temperatures, but also of the 2, 3 peak temperatures (R→M1, R→M2) when compared to both as-received or 300^{o}C aged alloy. Also, in contrast to the decreasing heats of the 2 and 3 peaks at a lower temperature aging, here the transformation heats are seen to increase. This can be explained by the fact that temperatures, T ≥ 500^{o}C, is an effective temperature range for recovery (decrease in dislocation density, dislocation rearrangement and formation of subgrains) [1, 52]. Since the density of Ti_3Ni_4 begins to decrease due to the dissolution of the precipitates into the matrix, the precipitates no longer hinder the

movement of dislocations; indeed Chrobak *et al.* [52] have observed well-developed dislocations cells that grow with annealing time and found that the recovery process is no longer disturbed by the precipitates. Thus, the influence of dislocations is reduced. Since sufficient Ti_3Ni_4 still exists in the matrix, the overall temperatures for all the transformations increase. In addition, reduction in the dislocation density may also cause larger volumes of the matrix participating in the R→M1 and R→M2 transformations (since now the elastic energy of the dislocations and the frictional work required by the A-M interfaces decrease), thus explaining the increase in the transformation heats. Therefore, two factors are seen to be crucial in governing the MST at 500°C: the precipitation rate of Ti_3Ni_4 and the recovery processes. Based on the partial DSC runs shown in Figure 3.4(II b-d), the sequence of MST still remains {(A→R) + (R→M1) + (R→M2) || (M2→R) + (M1→A)} with M1→A (peak-5) composed of combined A-R (peak-1) and R-M1 (peak-2) transformations.

(f) *Aging at 500°C-5hr:* Before interpreting the DSC trace for aging at 500°C-1hr, we will first analyze the 500°C-5hr case for reasons that will be clarified shortly. As shown in Figure 3.5(c) and Figure 3.6(C-c), the DSC trace for 50.8-NiTi aged at 500°C-5hr appears to exhibit a 2-stage/1-stage transformation. However, partial DSC scans similar to the partial scans shown in Figure 3.7(II a-d) for a sample air-cooled (AC) from 500°C after aging for 1hr, indicated an important change in the sequence of transformations. Firstly, the partial DSC scans show that the 2-stage/1- stage transformation actually consists of 3-stage/2-peak MST (forward 1-2-3 || reverse 4-5). The first partial scan (see Figure 3.7(II-b)) shows that the 1↔1' is an R↔A

transformation based on the small temperature hysteresis. The second partial DSC scan (see Figure 3.7(II-c)) indicates a second transformation 2↔5 with the reverse peak 5 occurring after 1' during the heating cycle. The third partial cycle (see Figure 3.7(II-d)) scanned from -100^{o}C to 60^{o}C further showed that peak-4 on the heating cycle corresponds to both peaks 1 and 3 during the cooling cycle; indicating that they should be transformations occurring in the same volume of the matrix. As discussed earlier, since the recovery processes are activated at 500^{o}C, aging for 5 hrs may have reduced the dislocation substructures considerably. Additionally, the TTT curve [1] implied that the solvus temperature of the Ti_3Ni_4 is near 500^{o}C. It is known that the precipitation kinetics are controlled by both the thermal energy necessary for diffusion of the Ni and Ti atoms and the nucleation rates; so although there is sufficient thermal energy for rapid diffusion of the atoms, there is little driving force (due to high nucleation barrier). It has been shown by Khalil-Allafi *et al.* [32], who studied MST in 50.7-NiTi polycrystals, that aging at 500^{o}C leads to a heterogeneous microstructure with preferential precipitation of Ti_3Ni_4 near the grain boundary with a relatively precipitate free grain interiors. In other words, aging near the solvus temperature (500^{o}C) leads to preferential precipitation near the grain boundary since the nucleation barrier is greatly reduced there compared to the grain interior (it is only a fraction of that required for a homogeneous precipitation) [36]. This preferential grain boundary precipitation has been invoked [32, 36] to explain the 3-stage/2-peak MST, such that the first peak corresponds to A→R transformation near the grain boundaries (since the decreased Ni content surrounding the grain boundary precipitates raises the A→R

transformation temperature) followed by the A→M1 transformation in the grain interior (second peak) and finally the R→M2 transformation near the grain boundary.

To show that indeed this is the scenario in the current study, the following arguments are invoked: It has been shown that 1↔1' is an A↔R transformation and that in the 2↔5 transformation, peak-5 forms after 1' during the heating cycle. This could mean that peak 2 is either A→M or R→M transformation. However, peak 2 should be A→M for two reasons: Liu *et al.* [33, 81] have demonstrated using a thermodynamic criterion that R-M transformation occurs at a lower temperature than the A→M transformation. Thus, peak-2 is necessarily A→M1 transformation. Moreover, if peak-2 is R→M transformation, peak-5 should correspond to the reverse R→M transformation. This is not feasible since peak-5 forms after peak-1', and hence, has to be the last transformation on heating, which should necessarily reverse to the high-temperature austenite matrix. In addition, since the austenite matrix near the grain boundary has transformed to R-phase (peak-1), peak-2 should correspond to the A→M1 transformation of the grain interior (GI) austenite matrix. Thus, peak-3 will correspond to the R→M2 transformation near the grain boundary (GB). The heating cycle peaks 4 and 5 will thus represent M2→A and M1→A transformations in the grain boundary and the grain interior, respectively. In summary, the transformation sequence has evolved from {(A→R) + (R→M1) + (R→M2) || (M2→R) + (M1→A)} forward || reverse transformation sequence for As-Received $\Rightarrow$ {(A→R) + (R→M1) + (R→M2) || (M2→R) + (M1→R) + (R→A)} for aging at 500^{o}C (0.5hr) $\Rightarrow$ $\{(A\rightarrow R)_{GB} + (A\rightarrow M1)_{GI} + (R\rightarrow M2)_{GB} \parallel (M2\rightarrow A)_{GB} + (M1\rightarrow A)_{GI}\}$ for aging at 500^{o}C-5hrs.

(g) *Aging at 500^{o}C-1hr:* Based on the foregoing discussions, we will now make an attempt to explain the DSC peaks observed in Figure 3.4(III-a). Aging at 500^{o}C-1hr results in a 4-peak/3-peak MST. Partial DSC scans shown in Figure 3.4(III b-e) illustrate that the sequence of the transformations is complex and difficult to identify. However, based on the aging results at 500^{o}C for 0.5hr and 5hr, we can infer that the sequence illustrates a transition from {(A→R) + (R→M1) + (R→M2) || (M2→R) + (M1→R) + (R→A)} mechanism-1 ⇒ {$(A\rightarrow R)_{GB}$ + $(A\rightarrow M1)_{GI}$ + $(R\rightarrow M2)_{GB}$ || $(M2\rightarrow A)_{GB}$ + $(M1\rightarrow A)_{GI}$} mechanism-2. Partial DSC cycle-1 indicates that 1↔1' is an A↔R transformation in either mechanism-1 or -2 (near GB). Partially formed peak-2 during the 2nd partial DSC scan is seen to affect peaks 2' and 6. This may correspond to both R→M1 in mechanism-1 (reverse being peak-6) and $(A\rightarrow M1)_{GI}$ in mechanism-2 (reverse being peak-2') in the grain interior. The 3rd partial DSC scan shown in Figure 3.4(III-d) includes peak-2, as well as part of peak-3 during heating. These transformations seem to affect peaks 5, 6 and 7. It is possible that part of peak-2 may be identified with 2↔6 (R↔M1) in mechanism-1 above, and the rest of part-2 with another component of peak-7 linked to the $(A\leftrightarrow M1)_{GI}$ in mechanism-2 above. Also, peak-3 is likely to correspond to peak-5. However, the 4th low-temperature partial cycle in Figure 3.4(III-e) shows that peaks-3 and 4 affect peak-5 only. It can be hypothesized that peak-3 is likely to be (R→M2) in mechanism-1 and peak-4 $(R\rightarrow M2)_{GB}$ in mechanism-2 or the inverse. Nevertheless, we interpret peak-3 as $(R\text{-}M2)_{GB}$. We reach this conclusion based on the comparison of the DSC scans between WQ and AC samples aged at 500^{o}C-1hr in Figure 3.6(C-b). Since AC from 500^{o}C to room temperature (20^{o}C) takes (500^{o}C-20^{o}C)/(60^{o}C/min) = 8

min, the AC samples differ from the WQ samples in that they may be considered to be aged at intermediate temperatures 350°C-450°C for a few extra minutes. Since this is the window for the high precipitation rates for Ti_3Ni_4, it is possible that this relatively short–term aging may have led to preferential GB precipitation, and thus mechanism-2 above may be operative. Indeed, an analysis of the DSC scan for AC 500°C-1hr specimen using partial DSC cycles (Figure 3.7(II-a)) suggests that mechanism-2 (heterogeneous GB precipitation) is operative. Comparing the DSC scans of WQ and AC samples (500°C-1hr) in Figure 3.6(C-b) shows that peak-3 of AC samples matches with the peak-3 (not peak-4) of the WQ sample. Since peak-3 in the AC sample corresponds to the $(R \rightarrow M2)_{GB}$ transformation, we conclude that peak-3 for the WQ sample indicates the same transformation; thus making peak-4 (WQ) as (R→M2) in mechanism-1. The above sequence has been logically pieced together based on the shorter (0.5hr) and longer (5hr) aging times based on the assumption that it represents a transition between mechanism-1 and -2. The authors recognize that the suggested scenario remains to be confirmed using in-situ neutron diffraction, in-situ TEM studies similar to [37, 41], or X-ray diffraction [51].

(h) *Aging at 600°C and 700°C:* Figure 3.5 and Figure 3.6(D a-c) show the full DSC scans of 50.8-NiTi aged at 600°C for 0.5, 1, and 5-hrs. Frick *et al.* [73] observe that aging the cold-rolled 50.9-NiTi at 600°C annihilates the dislocations as well as recrystallizes the microstructure. Based on the earlier discussion, aging beyond 550°C leads to the precipitation of Ti_2Ni_3 metastable phase that requires a greater depletion of Ni from the matrix. Thus, increasing the aging time from 0.5-hr to 5-hr, increase the

A_f temperature from 15°C to 43°C. Although, the 0.5-hr and 1-hr aged samples show a single A↔M transformation during cooling and heating cycles, the 5hr aged sample shows the formation of additional peaks (seen as a partially developed shoulder). Partial DSC scans {refer to a similar DSC curve for AC 600°C-1hr in Figure 3.7(III-b)} show that there are two transformations 1↔4 and 2↔3 with large hysteresis ~ 50°C. This indicates that there are two A↔M transformations (A↔M1 and A↔M2). We interpret these transformations as occurring near the precipitates (A↔M1) and far from the precipitates (A↔M2), where variation in the Ni composition governs the transformation temperatures. The 700°C aging treatment appears to homogenize the microstructure since the A_f temperature remains constant at 22°C, same as the ST sample at 800°C (see Figure 3.2(c)).

3.4.1.3 Effect of cooling rate

Figure 3.6 shows a comparison of the transformations (DSC traces) in 50.8-NiTi as a function of cooling rate for various aging conditions (300°C-700°C, 0.5-hr, 1-hr, and 5-hrs). The typical cooling rates involved may be assumed as 1000°C/sec for water quenched (WQ), 1°C/sec for air-cooling (AC) and ~10^{-2} °C/sec (actually controlled at 1°C/min) for furnace-cooling (FC) conditions. Water quenching 'freezes' or preserves the aged microstructure at room temperature. During AC, when the samples are removed from the furnace and exposed to room temperature, there is an initial rapid decrease in the temperature (especially when cooled from high temperatures) followed by a more gradual reduction. Air cooling a sample from 600°C to 300°C would typically need ~ 300°C/(1°C/sec) = 5min, spending more time

between 350°C and 450°C, where the precipitation kinetics of Ti_3Ni_4 are rapid. Hence, compared to the WQ samples, the AC samples may be considered as aged for an additional 5-10 min. However, due to slower rates of cooling, furnace cooled samples are aged for longer times than the air-cooled ones. For example, FC between 600°C and 300°C would take 300°C/(1°C/min) = 5 hrs. So, we can expect some of the superelastic/mechanical properties of WQ or AC samples aged for 5hrs to approach the FC samples. It should be noted that the FC samples were soaked at their respective aging temperatures for 0.5 prior to initiating the furnace cooling. Additionally, at the respective temperature under consideration in Figure 3.6, a single FC DSC trace is used for comparison with the WQ and AC samples for all the aging times. Referring to the full DSC scans in Figure 3.6 and the partial DSC cycles in Figure 3.7 and Figure 3.8, the following observations are summarized.

(A) Air-Cooled (AC) specimens

(a) Aging at 300°C and 400°C: 50.8-NiTi samples aged at 300°C for 0.5-hr, 1-hr, or 5-hrs followed by AC exhibit similar behavior in terms of the evolution of the multiple-stage transformation (see Figure 3.6(A, B) in comparison with WQ specimen. The partial DSC scans, Figure 3.7(I a-d), indicated 3-stage/3-stage 1↔1', 2↔2' and 3↔3' pairs of transformations, that represent A↔R, R↔M1 and R↔M2, forward and reverse transformations, respectively, as explained earlier. The general evolution in the peak position and the transformation heats are corresponding well with the WQ samples, with the exception that the transformation temperatures are slightly (a few degrees) higher in the AC samples. As discussed previously, this is due to the

additional aging of the AC (5-10min). However, the precipitation kinetics of Ti_3Ni_4 between 200°C and 300°C is sufficiently sluggish that the few extra minutes of aging does not cause a dramatic increase in A_f.

Aging at 400°C, the temperature with the maximum precipitation rates, the 0.5-hr age + AC samples exhibit nearly the same transformation temperatures (TT) as the WQ sample (A_f temperatures are compared in Figure 3.13(a) for various aging conditions and cooling-rates); however the transformation heats are slightly larger in AC samples. Moreover, 5-hr aged + AC, as well as the WQ and FC (will be discussing shortly) samples exhibit identical DSC scans (all three A_f curves are seen to intersect in the vicinity of 400°C for 5hr aging times in Figure 3.13(a) and show the maximum difference for 1-hr aging (at 400°C). Additionally, the transformation temperatures increase progressively by a greater degree in the WQ, AC and FC samples for 1-hr aging time (before equalizing at 5-hrs) suggesting that the maximum precipitation rates at 400°C are obtained in the vicinity of 1-hr aging time. Indeed, TEM studies of aged 50.6-NiTi by Miyazaki [1, 76] have shown a high density of Ti_3Ni_4 precipitates for 1-hr aging times.

(b) Aging at 500°C: Since the Ti_3Ni_4 precipitates begin to dissolve at this temperature [1, 76], the transformation temperatures decrease for both the AC, as well as the WQ samples, compared to the 400°C aging. With aging from 0.5-hr to 1-hr, the AC samples have already made a transition in the transformation sequence by evolving from mechanism-1 $\{(A\rightarrow R) + (R\rightarrow M1) + (R\rightarrow M2) \parallel (M2\rightarrow R) + (M1\rightarrow R) + (R\rightarrow A)\}$ for aging at 500°C (0.5hr) $\Rightarrow$ mechanism2 $\{(A\rightarrow R)_{GB} + (A\rightarrow M1)_{GI} +$

$(R \rightarrow M2)_{GB} \parallel (M2 \rightarrow A)_{GB} + (M1 \rightarrow A)_{GI}\}$ for aging for 1-hrs at 500°C, as discussed earlier (compare Figure 3.4(II, III) and Figure 3.7(II)). This change in transformation sequence is important because the A_f temperature that is reported, now refers to $(M1 \rightarrow A)_{GI}$ transformation, rather than $(R \rightarrow A)$ in mechanism-1. The $(R \rightarrow A)$ transformation occurs typically in the whole volume of the matrix, whereas $(M1 \rightarrow G)_{GI}$ occurs in the grain interior, away from the grain boundary, where preferential grain boundary precipitation occurs. Therefore, a single A_f temperature doesn't necessarily correspond to the same transformation event in all samples, notwithstanding the practical fact that tailoring it near (or below) the body temperature is of more relevancy for engineering applications. Nevertheless, it is important to understand the physics for any possible advanced application. Moreover, the change in transformation sequence also indicates that the recovery processes have become very effective at these aging conditions. An additional observation is that the A_f curve for the AC sample now falls behind the WQ sample, indicating that the Ni is diffusing back into the matrix at a faster rate around 1-hr aging time. The A_f values begin to climb rapidly for greater aging times, likely due to the precipitation of the second Ni-richer phase.

Aging at higher temperatures for all the aging times, viz., 0.5-hr, 1-hr, or 5-hrs, the AC and the WQ DSC behaviors are very similar, with the slight difference brought about by the fact that the AC samples spend an extra few minutes through the optimal precipitation window '350°C - 450°C', thus affecting the A_f.

(B) Furnace-cooled (FC) specimens:

50.8-NiTi samples aged at 300^{o}C and 400^{o}C followed by furnace cooling (FC) exhibit similar behavior in terms of the evolution of the multiple-stage transformation (see Figure 3.6(A, B) in comparison with the WQ and AC specimen. The partial DSC scans Figure 3.8(I, II a-d) indicate 3-stage/3-stage 1↔1', 2↔2' and 3↔3' pairs of transformations, that represent A↔R, R↔M1 and R↔M2, forward and reverse transformations, respectively, as explained earlier. Here the effect of cooling rate is more evident since the A_f transformation temperatures are much higher in the FC samples than the WQ and the AC specimen aged for 0.5-hr or 1-hr. This is due to the additional aging of the FC (on the order of hours) alloy between 300^{o}C and 400^{o}C that greatly increase the A_f. Unlike the AC and the WQ samples, discussed already, the 500^{o}C FC specimen exhibits mechanism-2 $\{(A\rightarrow R)_{GB} + (A\rightarrow M1)_{GI} + (R\rightarrow M2)_{GB} \parallel (M2\rightarrow A)_{GB} + (M1\rightarrow A)_{GI}\}$ as the transformation sequence (see the partial DSC scans in Figure 3.8(III a-d). The transformation behavior is quite difference for the FC samples aged at 600^{o}C and 700^{o}C in comparison to the WQ and AC conditions. At these high temperatures, the 50.8-NiTi alloy undergoes recovery and recrystallization and upon cooling, the specimen is aged at intermediate temperatures. However, the nature of the precipitation, in terms of its distribution and the final microstructure must be uniform, since the transformation sequence is now the traditional 1↔4, 2↔3$\{(A\rightarrow R) + (R\rightarrow M) \parallel (M\rightarrow R) + (R\rightarrow A)\}$, forward || reverse mechanism (see Figure 3.8 (IV a-d), because the precipitates resist the direct A↔M transformation.

Thus, the effect of cooling rate affects two main properties: With slower cooling rates (WQ→AC→FC), due to the tendency in Ni-rich NiTi alloys to exhibit precipitation reactions, the alloy spends longer times at intermediate temperatures (300^oC-500^oC) that leads to the precipitation of Ni-rich Ti_3Ni_4. This reduces the Ni-content of the surrounding matrix increasing the transformation temperatures (e.g. A_f). The second important difference comes from recognizing the reducing influence of dislocations at aging above 500^oC that lead to heterogeneous microstructures, with preferential precipitation at the grain boundaries compared to the grain interior matrix. This directly influences the mechanism of the multi-stage transformation by changing the transformation sequence as {forward || reverse transformation}:

(i) {(A→R) + (R→M1) + (R→M2) || (M2→R) + (M1→A)} in as-received (AR) 50.8-NiTi ⇒

(ii) {(A→R) + (R→M1) + (R→M2) || (M2→R) + (M1→R) + (R→A)} (aging at $T < 500^oC$) ⇒

(iii) $\{(A\rightarrow R)_{GB} + (A\rightarrow M1)_{GI} + (R\rightarrow M2)_{GB} \parallel (M2\rightarrow A)_{GB} + (M1\rightarrow A)_{GI}\}$ (aging at $T \geq 500^oC$) ⇒

(iv) {(A→R) + (R→M) || (M→R) + (R→A)} (aging at $T \geq 600^oC$, followed by intermediate aging).

This evolution in the sequence of transformation is hastened by slower cooling rates, especially for aging at $T \geq 500^oC$; since the recovery (dislocation annihilation) processes become active beyond 500^oC.

3.4.2 Stress-strain Response of NiTi

3.4.2.1 As-received: Stress-Strain Behavior

Figure 3.9 shows the entire tensile stress-strain curve of the AR 50.8-NiTi that shows ~5% plateau strain and recovery strains of ~ 6%. The inset shows the 'plateau' region and the numbers 1-4 indicate the loading cycle, with 4 being the final cycle, where the specimen is loaded to failure. The plateau stress, UTS and the failure strain are respectively, 400MPa, 1250MPa and 18±2%. Upon unloading from 10% strain, the AR sample recovers only 5% strain (termed pseudoelasticity). The remaining strain was, however, recovered by heating the gage length of the sample using a tape heater above 80^{o}C (< 2 min). It is known that the elastic deformation of austenite (stage I) is followed by the stress-induced martensitic transformation (SIM) (stage II) represented by the flat plateau, subsequently, martensite reorients (stage III) before plastic deformation of martensite begins (stage IV) [82, 83]. From the stress-strain curve, it can be seen that the SIM has been deformed into stage III. In addition, it has been suggested that the reoriented martensite is stabilized due to the grain boundaries in polycrystalline materials that provide resistance to the shape change of the reoriented martensite; this stabilization effect can be reversed through subsequent thermal transformation cycles [82-87]. It has been shown that the stabilization effect in stage III is due to the release of the internal elastic energy stored by the self-accommodating martensite; while in stage IV it is attributed to the frictional forces involved in the plastic deformation [83]. The AR sample was unloaded from stage III region and hence the stabilized martensite recovered upon one thermal cycle beyond

the A_f' (the new austenite finish temperature of the stabilized martensite, note that A_f' > A_f and A_f' increases with increase in deformation level [76]).

3.4.2.2 Effect of Aging Temperature: Aged+WQ

The effects of the aging treatments on the general stress-strain behavior of 50.8-NiTi and the plateau stress, UTS and ductility (aged for 0.5-hr and 5-hrs followed by WQ) are shown in Figure 3.10 and Figure 3.14, respectively. With aging between $300^oC \leq T \leq 400^oC$, there is a systematic decrease of the plateau stress (only the first loading cycle plateau stress is compared) as expected from an increase in A_f [1]. At longer aging times (5-hrs), since the A_f decreases even further, the corresponding plateau stress is also smaller than the 0.5-hr aging times. As the A_f begins to decrease initially at 500^oC corresponding to the decrease in the density of the Ni-rich precipitate, there is an initial increase in the plateau stress level. For longer aging times, however, with the corresponding increase in A_f, the plateau stress reduces. In a similar fashion, the UTS (tensile strength) increase with aging between 300^oC and 400^oC due to effective precipitation hardening. However, long term aging at 500^oC reduces the UTS due to a decrease in both the precipitate density (hence, precipitation hardening) and the initiation of recovery processes (dislocation annihilation), but it is yet un-recrystallized. This is more evident in aged samples at 600^oC, where recovery is completed and recrystallization has begun. Above 700^oC recrystallization and grain growth readily occur, and the UTS is reduced below 900MPa. Ductility variation follows in tandem inversely with the variation in UTS. The ductility is minimum for aging at 400^oC, corresponding to the maximum UTS and precipitate density (refer to

[88] for a more detailed study of the factors affecting the ductility of Ni-Ti alloys as a function of Ni composition and thermomechanical treatment). Aging past 600^{o}C, the ductility of the WQ samples decreases, exhibiting lower failure strains at longer aging times. When one plots the variation of ductility from Figure 3.14 in the manner shown in Figure 3.13(b, c), the data assumes a 'c-curve' character similar to a time-temperature-transformation (TTT) diagram (also observed by Pelton *et al.* [1] for shorter aging times). The 'nose' of the c-curves for various aging times occur in the vicinity of 400^{o}C corresponding to the optimal precipitation rates of Ti_3Ni_4 phase. Additionally, the A_f curves shown in Figure 3.13(a) also exhibit similar but inverted 'c-curve' character, since A_f increases with the increase in precipitation rate.

As shown in Figure 3.10(b, c, f, g), aging below 500^{o}C leads to the formation of a small plateau at 50MPa, corresponding to the R-phase deformation that involves 1-2% transformation strains and low plateau stresses [22]. Upon unloading at 3% (or 4%), these samples exhibit pseudoelasticity (non-linear unloading curve, [89]) and do not recover the loading strains completely, until heated above A_f'. Two of these samples, indicated in Figure 3.10(f, g), aged at 300^{o}C and 400^{o}C for 5-hrs, also exhibit a reduced R-phase plateau at 50MPa upon repeated loading-unloading cycles, until it disappears completely by the 4th loading cycle, indicating the stabilization of martensite. Interestingly, the plateau stress corresponding to the martensite reorientation (occurring between 200MPa and 400MPa) increases slightly from cycle 1 to 3 with a large drop in the 4th cycle where the R-phase plateau vanishes. Two samples (aged for 0.5-hr at 400^{o}C and 500^{o}C, respectively), indicated in Figure 3.10(b, c), were not heated after the unloading cycles at 4% and 8% strain to observe the

hysteresis loop between the unloading and the 2nd loading cycles. The 2nd plateau stress level is slightly lower than the 1st plateau stress level.

Stress-strain curves for samples aged at 500°C, shown in Figure 3.10(c, h), show very little or no R-phase plateau and do not recover 6% loading strains completely. However, the plateau strains are nearly 7%, compared to the as-received material (5%). The increase in the plateau strains and the decrease in the recoverable strains may be rationalized by accounting for two processes: (i) As mentioned previously, aging the samples at 550°C and 800°C led to a strengthening of the {111} <110> texture components that generally improve the recoverable strains (either in SE or SM) [22]. However, since the alloy is under-recovered by aging at 500°C, it becomes easier to introduce slip into the crystal and hence the shape memory characteristics (recovery strains) degrade. This is even more evident for a specimen aged at 600°C or 700°C as shown in Figure 3.10(d, e, i, j). Since recovery and recrystallization have taken place, the shape memory characteristics are less evident, with recovery strains < 5%. Furthermore, in distinct contrast to the lower-temperature aged specimen, the plateau stresses for the subsequent loading cycles are greater than the initial loading plateau, along with larger pseudoelasticity, indicating that the material is work-hardening. In addition, the stress-strain curves show a 'dip' in the plateau region corresponding to the strain level to which the pseudoelastic curve unloads. This suggests that the martensite is being deformed in two types of domains: one where martensite deforms at the plateau stress and a smaller domain (since it involves only few strain %) that not only deforms at lower plateau stress, but also recovers upon unloading.

3.4.2.3 Effect of Cooling rate

The effects of the cooling rate following aging (aged for 0.5-hr or 5-hrs) on the general stress-strain behavior of 50.8-NiTi are shown in Figure 3.10 (WQ), Figure 3.11 (AC), and tFigure 3.12 (FC) and a summary plot of the plateau stresses, UTS and ductility is shown in Figure 3.14. While the general trends in the variation of the plateau stress is similar to the WQ specimen, FC and AC samples exhibit lower and higher plateau stress, respectively, compared with the WQ samples aged between 300^{o}C and 600^{o}C. This trend is reversed for the UTS with AC, WQ, and FC samples exhibiting increased UTS in seriatim. However, the ductility variation for the AC samples is very similar to the FC specimen for shorter aging times, as shown in Figure 3.13 and Figure 3.14. At longer aging times, the AC and the WQ samples have nearly identical UTS, that are lower than the FC material due to intermediate aging for the FC that introduce hardening precipitates. In contrast to lower aging times, the AC and the WQ material aged at 5hrs exhibited nearly the same ductility values. Aging at T $\geq$ 600^{o}C leads to lowering of the ductility and strength in the WQ samples compared to the AC and FC due to solution-treatment of the WQ samples; the AC and FC alloy properties are slightly improved due to intermediate temperature age-hardening. It should be noted that the air-cooling can cause variation of superelastic and mechanical properties between the range observed for WQ and FC material depending on the size and shape of the part, since the component surface cools faster than the interior for large parts. Since NiTi alloys are very sensitive to Ni-composition, processing defects and age hardening, careful processing procedures have to be established for producing uniform properties throughout the product. Since the variation in UTS, plateau stress

and ductility for the AC samples swings between the FC and the WQ samples due to aging for shorter and longer times, respectively, depending on the application design parameters and component sizes, appropriate schedules have to be identified.

The stress-strain behavior as a function of aging is shown in Figure 3.11 for AC samples. The R-phase plateau observed for the WQ alloy at lower aging temperatures (<500^{o}C), are also seen in the FC material (see Figure 3.12), while they are not so prominent in the AC samples. Since in many applications, the presence of the R-phase is undesirable, air-cooling may be effective in eliminating its appearance. At intermediate and higher aging temperatures, the AC and the WQ specimen exhibit similar stress-strain curves in terms of pseudoelastic recovery strains and permanent plastic strains. In contrast, the FC alloys recover most of the shape memory strains, indicating the importance of the presence of precipitates (formed during intermediate temperature aging) in raising the critical stress for slip, thus improving the shape memory characteristics [22].

3.4.3 Discussion

Multiple-stage transformations (MST) observed in Ni-Ti alloys under various conditions have been analyzed critically in the past 10 years, with considerable emphasis on the mechanism and the sequence of transformations involved. Since the first reports in late 1980's [44-46], several reports of MST in various NiTi alloys were reported that exhausted nearly all possible combinations of the three phases, viz., cubic austenite (A), monoclinic martensite (M) and the trigonal R-phase. In many of these findings, several theories have been put forward to explain the individual peaks

or stages of the transformations based on thermodynamic arguments, in-situ TEM, XRD and neutron diffraction observations. More recently, Carroll *et al.* [35] and Michutta *et al.* [42] attempted to summarize various findings on MST observations and suggested additional studies to achieve a more comprehensive fundamental understanding of transformation sequences in complex microstructures of Ni-rich NiTi shape memory alloys. It appears now that several factors, such as dislocation substructures and density, secondary phase particles (precipitates, oxide and carbide particles), both large-scale and small-scale chemical inhomogeneity (due to precipitation of Ni-rich phases, differences between the dendritic and interdendritic regions in cast single crystals), coherency stresses surrounding the precipitates, variable grain sizes, heterogeneous precipitate distribution and even interwoven processes involving both dislocations and precipitates, are all responsible for promulgating MST. In addition to the individual mechanisms discussed just mentioned, the material processing methods such as cold-rolling versus hot-rolling, cast-single crystals versus polycrystalline alloys, cooling rates (and hence component sizes), composition of NiTi alloys, melting practices and thermomechanical history, invoke one or several scenario's discussed above and the particular transformation sequence depends on a combination of several of these factors; the relative importance among various scenario's being difficult to quantify. Combining the evolution of the transformation sequence in the current study with those identified in the literature, the following provides a quick summary of various transformations that are confirmed experimentally. It is not intended to be either comprehensive or conclusive; instead it is aimed to direct the attention to the richness of microstructures observed in these

alloys and their concomitant influence of the phase transformations and hence shape memory characteristics.

(a) 200^{o}C-300^{o}C: {(A→R1) + (A→R2) + (R→M) || (M→R) + (R1→A) + (R2→A)} or (2R-1M)

Observed under low temperature aging in 30% cold-worked + solution treated (ST) 50.9-NiTi aged up to 3600-hrs [51], 50.6- and 51-NiTi polycrystals ST + aged at 250^{o}C (up to 48-hrs) [53], hot-rolled (between 845^{o}C and 955^{o}C) 50.9-NiTi aged at 300^{o}C (1.5-hrs); due to precipitation induced large-scale inhomogeneity of the matrix in terms of both chemical composition and internal stress fields.

(b) 300^{o}C-400^{o}C: {(A→R) + (R→M1) + (R→M2) || (M2→R) + (M1→R) + (R→A)} or (1R-2M)

Observed by Morawiec *et al.* [29, 30] due to the presence of dislocation substructures introduced during thermomechanical processing, Bataillard *et al.* [48, 49] due to the presence of coherency stresses introduced by Ti_3Ni_4 precipitates, Chrobak *et al.* [31] in 10% cold-worked + 400^{o}C aged (up to 4hrs) 50.6-NiTi due to the interaction of dislocation structures decorated with precipitates, Michutta *et al.* [42] due to small-scale heterogeneities introduced by homogeneous precipitation of coherent Ti_3Ni_4 with a critical interparticle spacing and others [73].

(c) 400^{o}C-500^{o}C: $\{(A\rightarrow R)_{GB} + (A\rightarrow M1)_{GI} + (R\rightarrow M2)_{GB} \parallel (M2\rightarrow A)_{GB} + (M1\rightarrow A)_{GI}\}$ or $(1R\text{-}2M)_{GB}$

Observed by several workers: Liu *et al.* [33] in 50.9Ni-Ti, ST + aged at 400^{o}C (0.5hr), Fan *et al.* [36] in 50.6Ni-Ti ST + aged (400^{o}C, 450^{o}C and 500^{o}C, several hrs),

Khalil-Allafi *et al.* [32, 37, 41] in 50.7 and 50.8-NiTi, ST + aged at 400^{o}C, 450^{o}C and 500^{o}C) and in the present study, due to heterogeneous microstructure developed by preferential grain-boundary (GB) precipitation.

(d) 500^{o}C (transition): (1R-2M) $\Rightarrow$ $(1R\text{-}2M)_{GB}$

(i) {(A→R) + (R→M1) + (R→M2) || (M2→R) + (M1→R) + (R→A)} (aging at T < 500^{o}C, 0.5-hr) $\Rightarrow$ $\{(A\rightarrow R)_{GB} + (A\rightarrow M1)_{GI} + (R\rightarrow M2)_{GB} \parallel (M2\rightarrow A)_{GB} + (M1\rightarrow A)_{GI}\}$ (aging at T ≥ 500^{o}C, 5-hrs)

(ii){(A→R1) + (A→R2) + (R1→M1) + (R2→M2) || (M→R) + (R→A)} or (2R-2M)

The transformation (i) was identified in the current study for 50.8-NiTi cold-worked + aged at 500^{o}C with transition occurring for 1hr aging period and the observation of 4-peaks on both cooling and heating, while (ii) was observed in 15% cold-worked 50.6-NiTi alloy aged at 500^{o}C (0.5-hr) [52], due to the interaction of interwoven processes of dislocation annihilation (recovery beginning at 500^{o}C) and heterogeneous grain boundary precipitation.

(e) 500^{o}C-600^{o}C: {(A→R) + (R→M) || (M→R) + (R→A)} or (2-stage/2-stage)

Observed in the current study and others [22], due to recovery and recrystallization along with the homogeneous precipitation of other Ni-rich phases like Ti_2Ni_3. This transformation sequence is also traditionally observed in Ni-Ti alloys with a homogeneous distribution of dislocation substructures and/or precipitates.

(f) 700^{o}C and higher: {(A→M) || (M→A)} or (1-stage/1-stage)

Observed in solution-treated Ni-Ti alloys and is the classical one-step transformation [22].

3.5 Conclusions

In the current study, we investigated the multiple-stage transformations (MST) in Ni-rich 50.8-NiTi which is the most popular commercial Nitinol alloy that is typically cold-worked and aged for optimal superelastic and/or shape memory characteristics. This as-received alloy was aged between 300^{o}C and 700^{o}C for 0.5-hr, 1-hr and 5-hrs followed by WQ. The individual transformations were identified through partial DSC scans and the variation of the A_f transformation temperature quantified as a function of aging. Additionally, the influence of cooling rate on the MST and the transformation sequence was studied through similar aging treatments followed by air-cooling (AC) or furnace-cooling (FC). Finally, the influence of aging and cooling rate on the plateau stresses, UTS and ductility was quantified. The following main conclusions are thus summarized:

(1) As discussed previously, aging between 300^{o}C and 600^{o}C leads to an evolution or transition in the transformation sequence from 3-stage/3-stage mechanism-1 $\{(A\rightarrow R) + (R\rightarrow M1) + (R\rightarrow M2) \parallel (M2\rightarrow R) + (M1\rightarrow R) + (R\rightarrow A)\}$ (aging at $T < 500^{o}C$, 0.5hr) $\Rightarrow$ 3-stage/2-stage mechanism-2 $\{(A\rightarrow R)_{GB} + (A\rightarrow M1)_{GI} + (R\rightarrow M2)_{GB} \parallel (M2\rightarrow A)_{GB} + (M1\rightarrow A)_{GI}\}$ (aging at $T \geq 500^{o}C$, 5hrs), with the transition occurring at 500^{o}C-1-hr aging conditions in the WQ samples. This transition is governed by the initiation of recovery and recrystallization processes at 500^{o}C. Furthermore, reduced cooling rates (AC and FC) hasten this transition.

(2) The variation in the transformation temperatures (especially A_f), plateau stress, UTS and ductility are governed by the precipitation and recovery processes in Ni-rich 50.8-NiTi and in general exhibit typical c-curve variation with temperature, similar to the TTT curves. Additionally, the AC samples behave similar to the FC samples for shorter aging times, while they tend towards WQ properties for longer aging times; therefore, it is important to consider the component size effects that may utilize AC schedules.

(3) The A_f transition temperature corresponds to different transformation mechanisms depending on the aging temperature and time.

(4) The texture of 50.8-NiTi alloys is strengthened with the aging temperatures (particularly {111}<110>) and can greatly influence the shape memory characteristics due to the lattice correspondence between the austenite and martensite phases.

3.6 Acknowledgements

Chapter 3, in full, is a reprint of the material (under preparation) to appear as Raghavendra R. Adharapurapu, Kenneth S. Vecchio, “Evolution of Multiple-Stage Transformations (MST) in Ni-rich 50.8-NiTi: Effects of Aging and Cooling Rate on the Shape Memory Characteristics”. The dissertation author was the primary investigator and author of this paper.

3.7 Figures

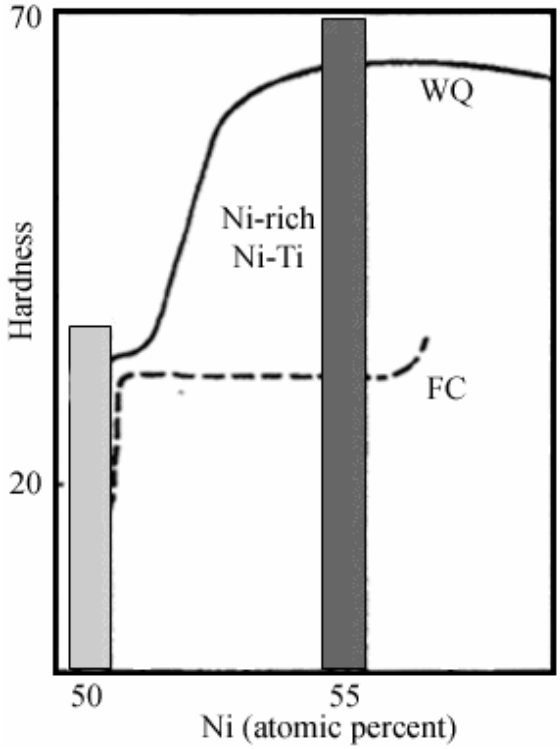

Figure 3.1 Variation of hardness (Rockwell C) in Ni-Ti alloys (cooled from 950°C) as a function of Ni composition under varying cooling rates: water quench (WQ ~ 1000°C/sec) and furnace cool (FC~0.01°C/sec). Intermediate hardness may be obtained by utilizing intermediate cooling rates such as air cooling (AC~1°C/sec). Adapted from [67, 68].

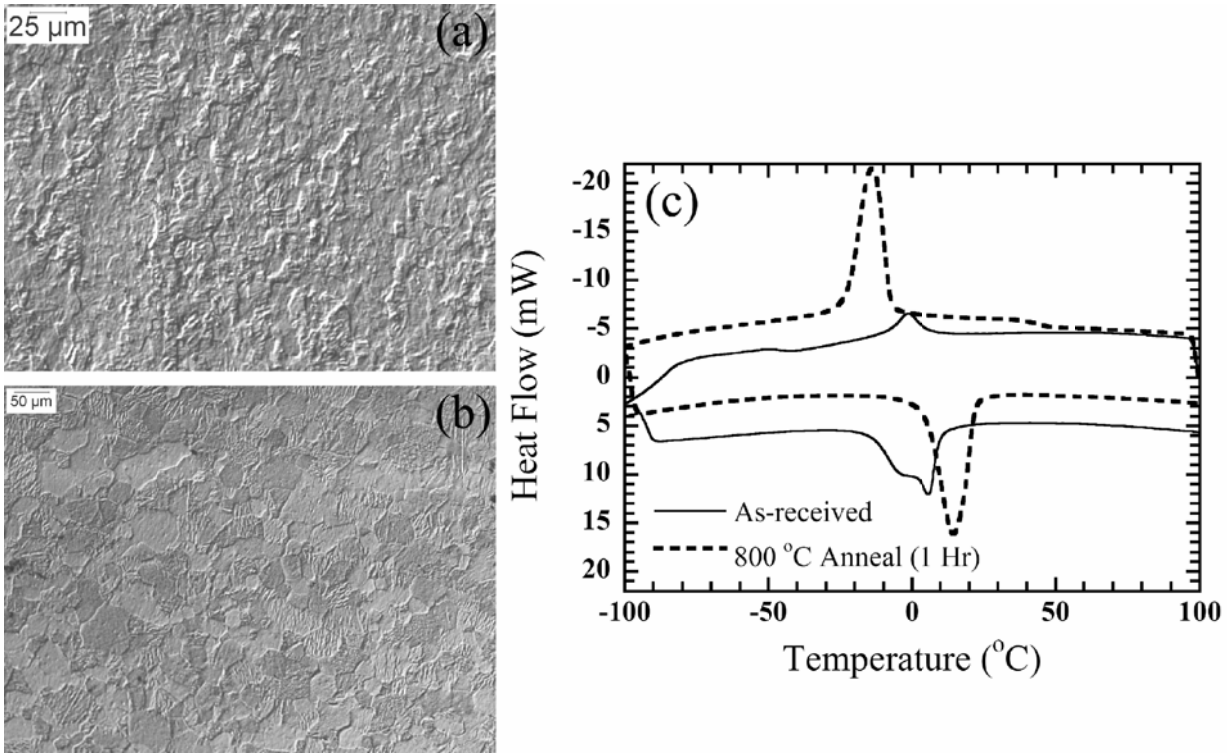

Figure 3.2 Optical micrographs of (a) as-received (AR) 50.8-NiTi sheet, (b) solution-treated (800°C, 1hr). Notice the presence of "needle" martensite in some grains in (a,b) produced due to the stresses applied during mechanical polishing. (c) DSC curves for AR Ni-Ti indicate that the AR sheet exhibits B2→R→B19' multiple-stage transformation, whereas the ST alloy shows a 1-stage forward B2→B19' and reverse B19'→B2 martensitic transformation [37, 41].

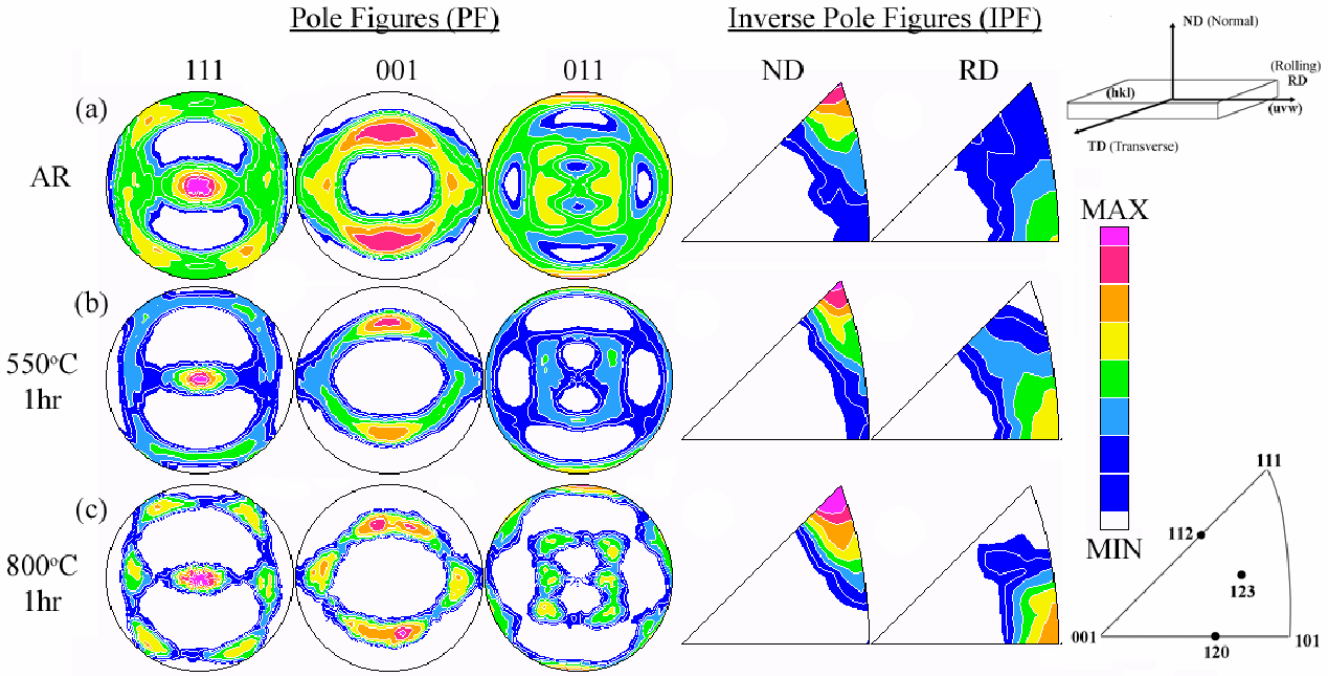

Figure 3.3 Pole figures (PF) and inverse pole figures (IPF) indicating the evolution of austenite texture in cold-rolled 50.8-NiTi sheet as a function of aging: (a) As-received (AR), (b) 550°C-1hr, (c) 800°C-1hr. Note the strengthening of the {111}<110> texture. ND and RD represent normal and rolling directions of the sheet geometry, respectively; the sheet geometry and the IPF triangle are indicated for reference. The data is presented in equal area projection.

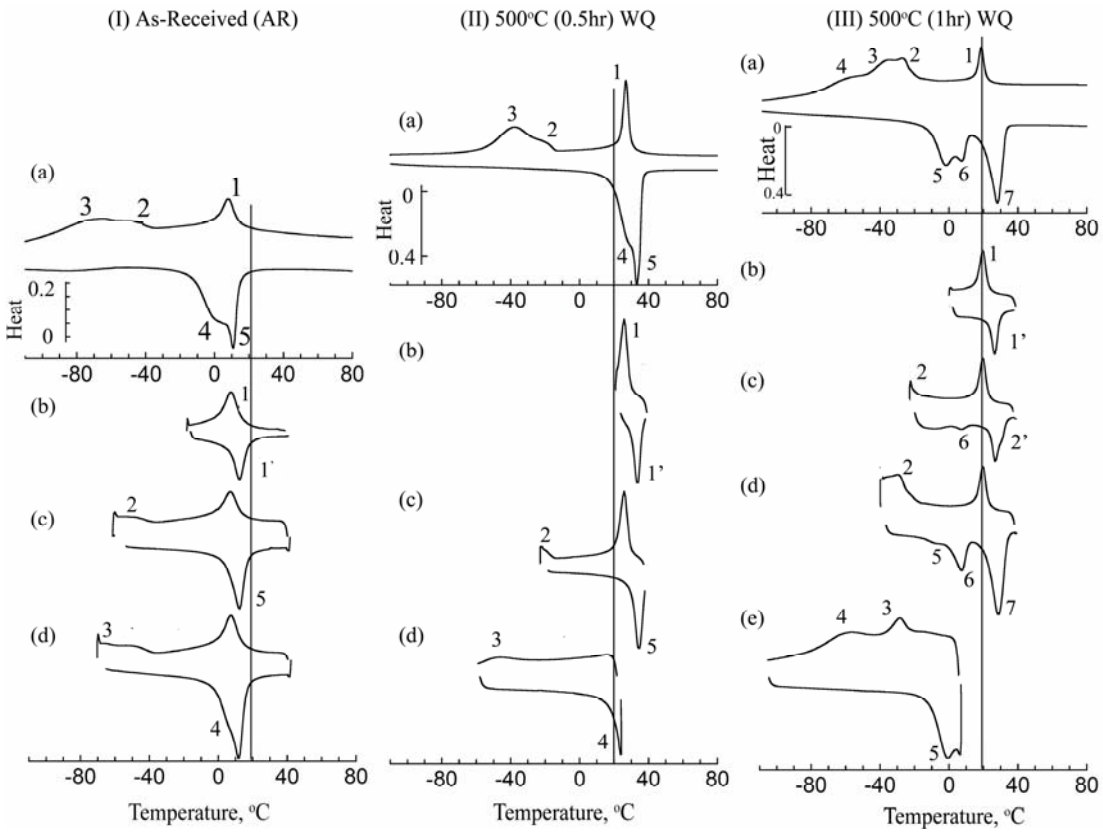

Figure 3.4 Partial DSC scans for (I) as-received (AR), (II) aged 500°C-0.5hr and (III) aged 500°C-1hr, WQ samples.

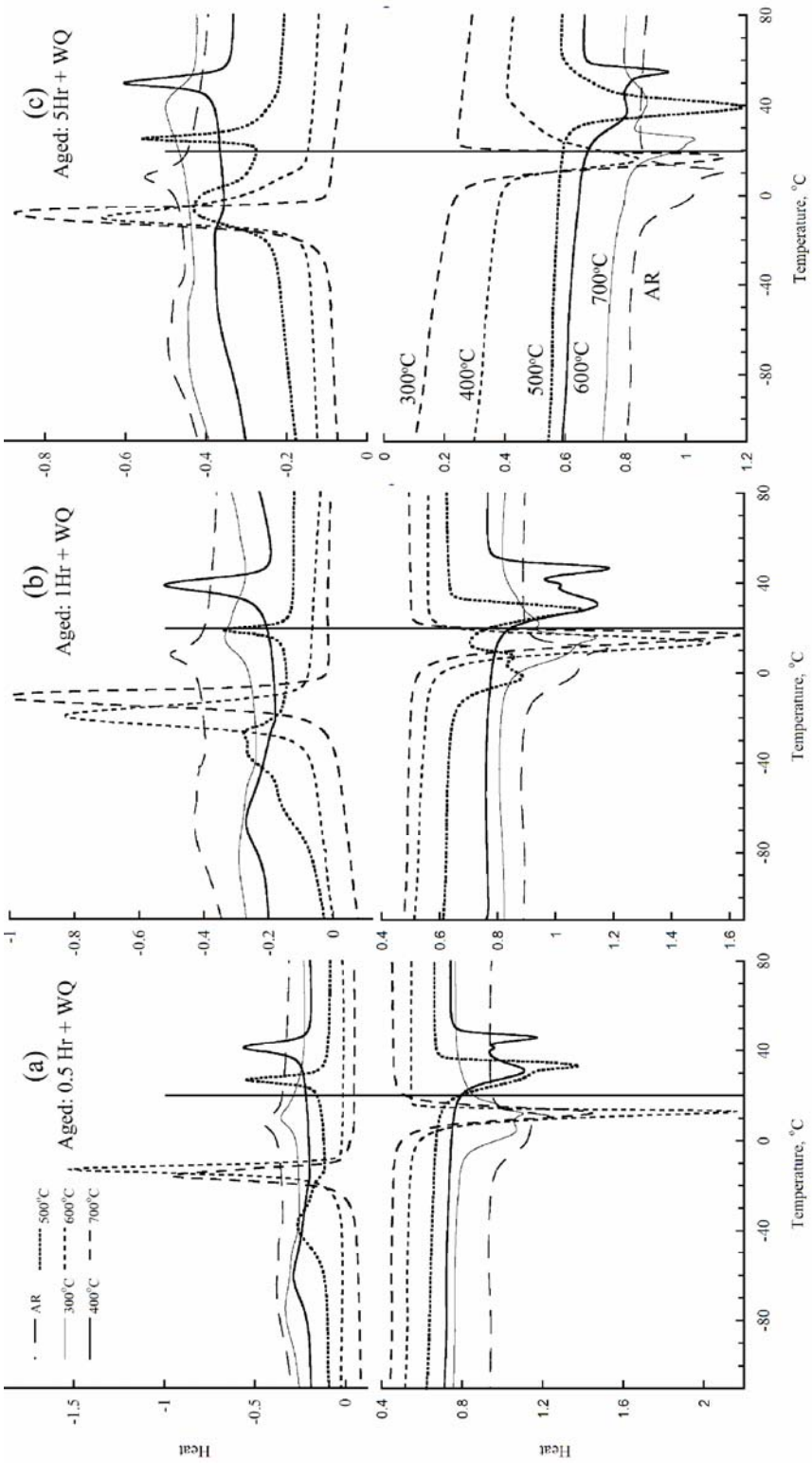

Figure 3.5 DSC scans for 50.8-NiTi aged between 300°C and 700°C for (a) 0.5hr,(b) 1hr and (c) 5hrs.

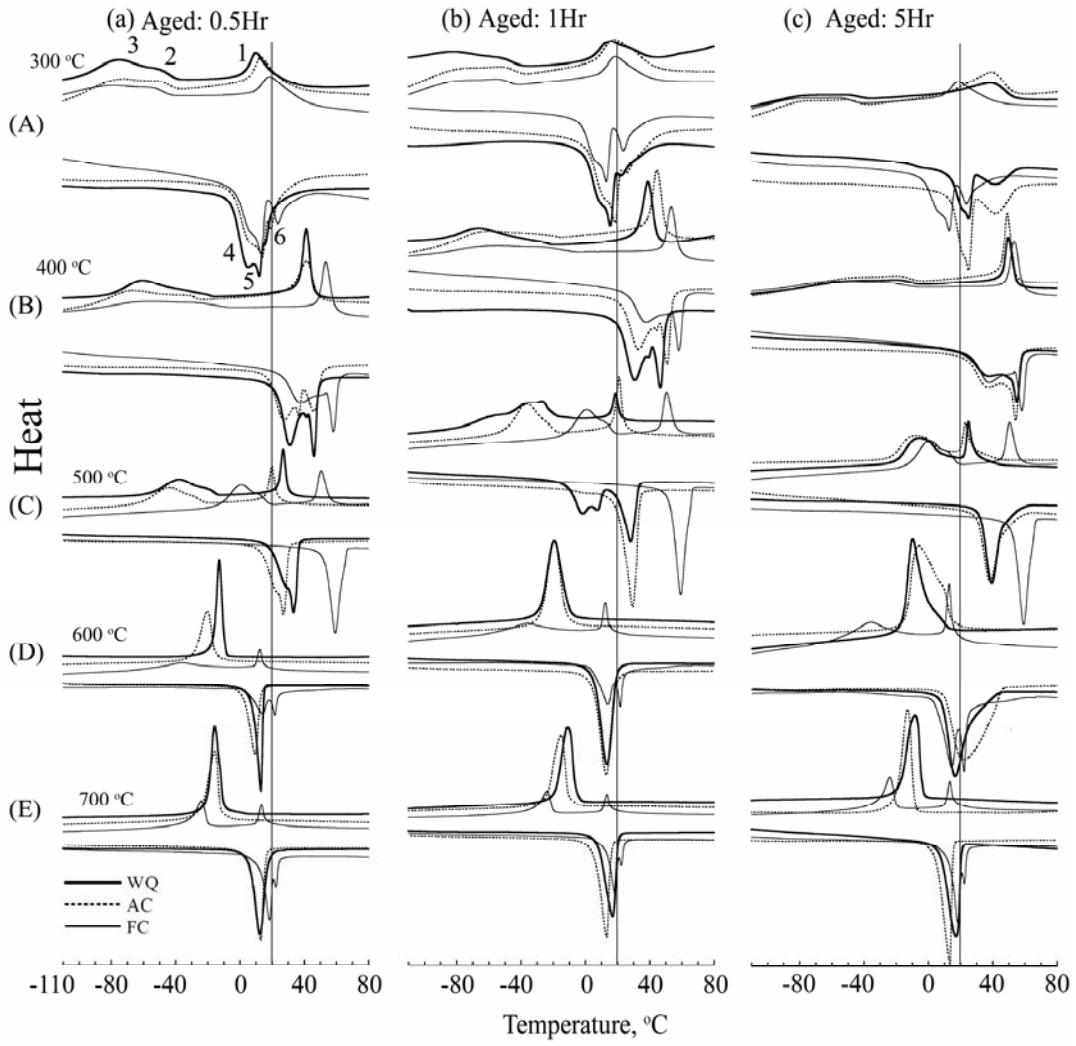

Figure 3.6 Comparison of the DSC scans between WQ, AC and FC 50.8-NiTi aged at (A: a-c) 300°C, (B: a-c) 400°C, (C: a-c) 500°C, (D: a-c) 600°C, (E: a-c) 700°C.

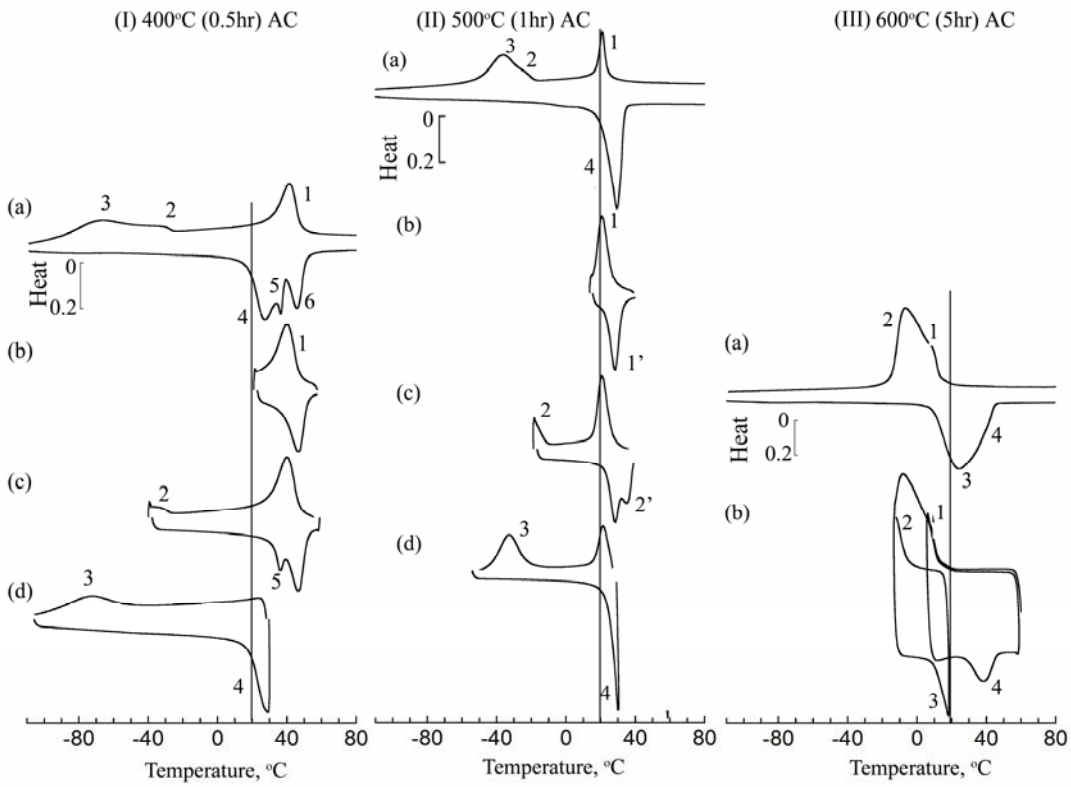

Figure 3.7 Partial DSC scans for AC samples aged at (I) 400°C-0.5hr, (II) 500°C-1hr and (III) 600°C-5hrs.

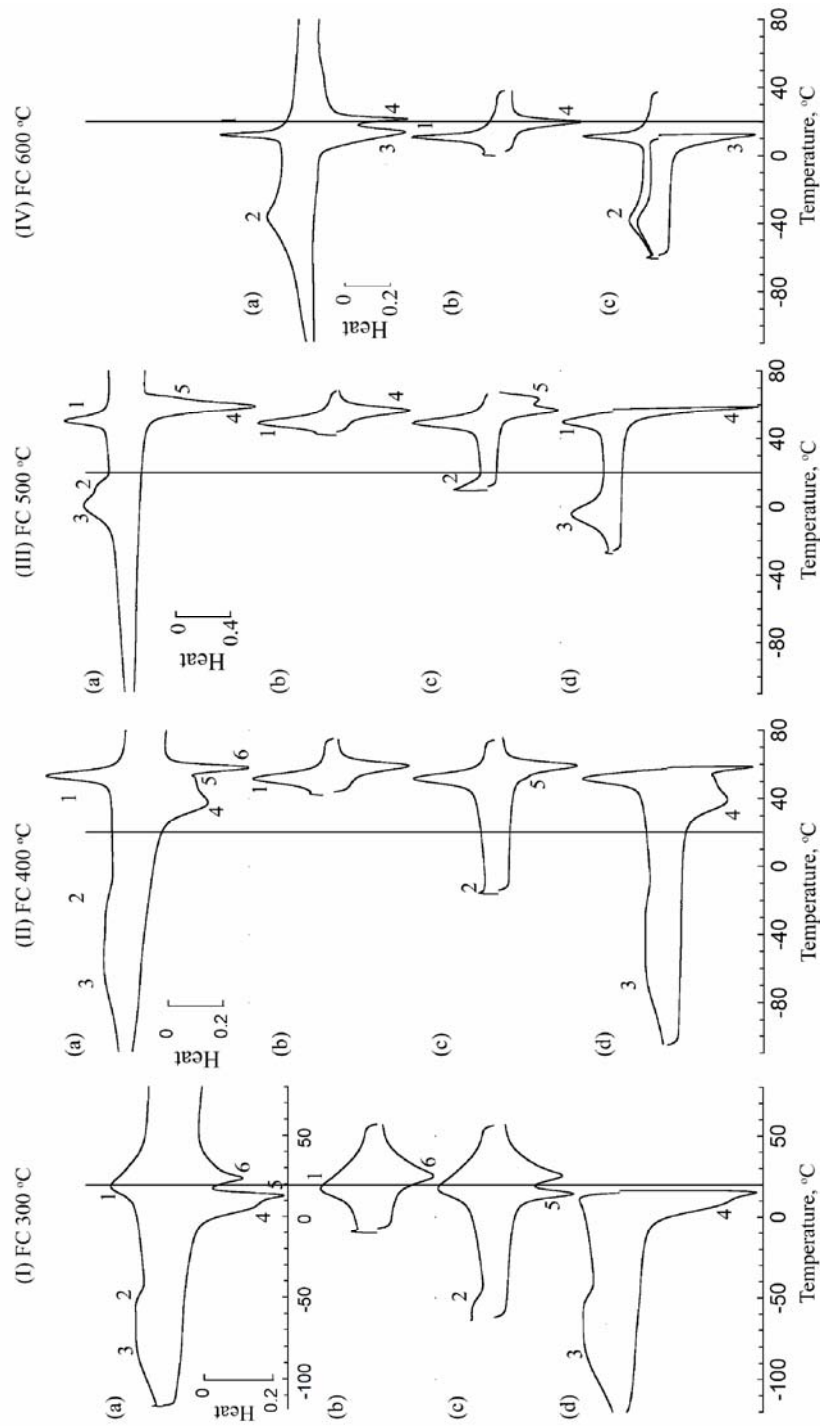

Figure 3.8 Partial DSC scans for FC samples aged at (I) 300°C-0.5hr, (II) 400°C-0.5hr, (III) 500°C-0.5hr and (IV) 600°C-0.5hr.

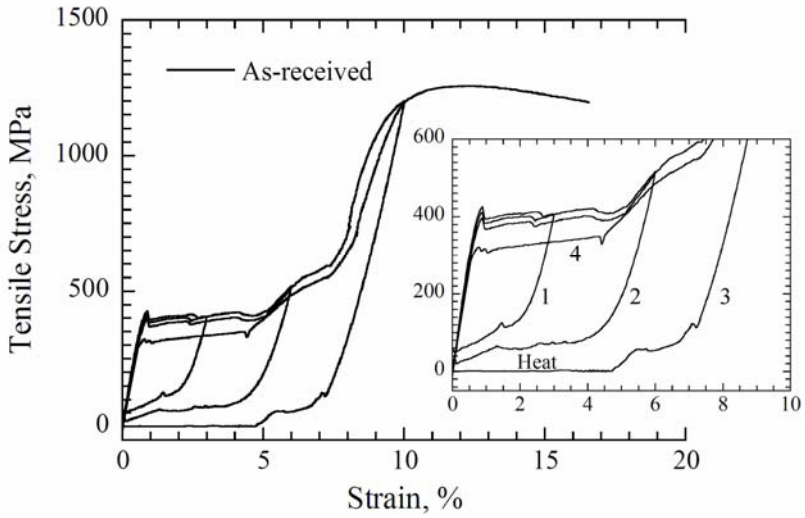

Figure 3.9 Stress-strain curve for as-received 50.8-NiTi sheet specimen. The inset shows the unloading cycles at 3%, 6%, 10% and final cycle 4 loaded to failure.

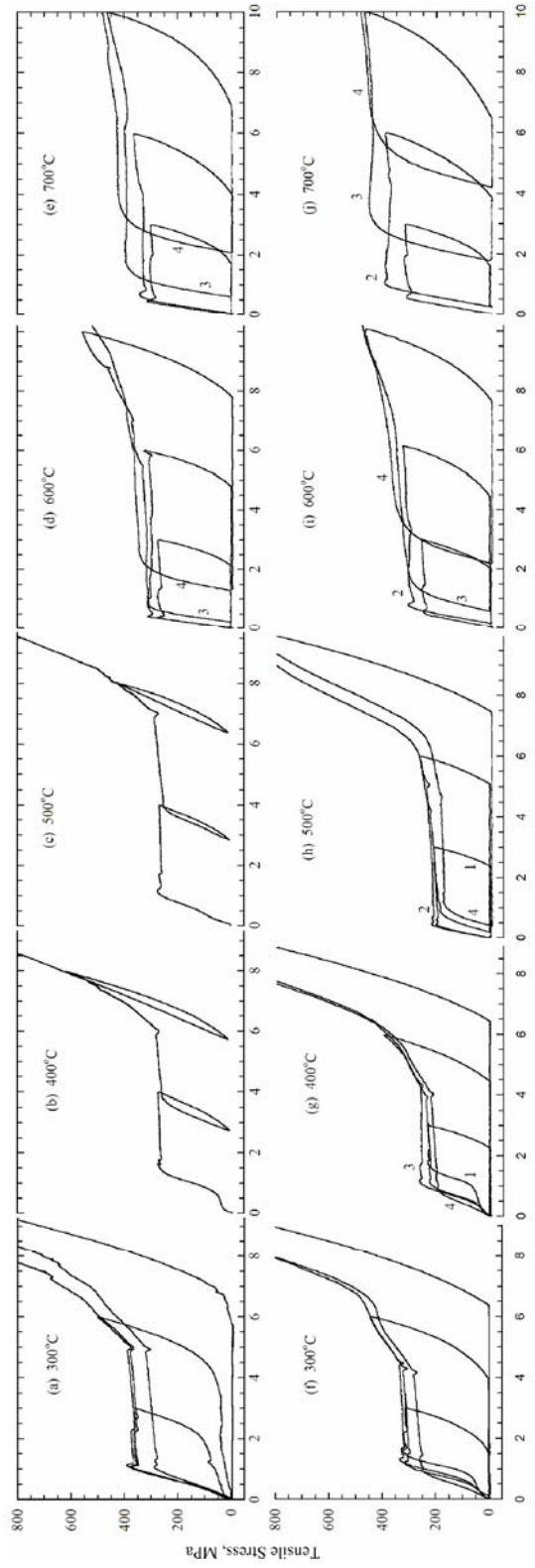

Figure 3.10 Stress-strain curves for WQ samples aged for 0.5hr at (a) 300°C, (b) 400°C, (c) 500°C, (d) 600°C, (e) 700°C; for 5hrs at (f) 300°C, (g) 400°C, (h) 500°C, (i) 600°C, (j) 700°C. The numbers indicate the loading cycle.

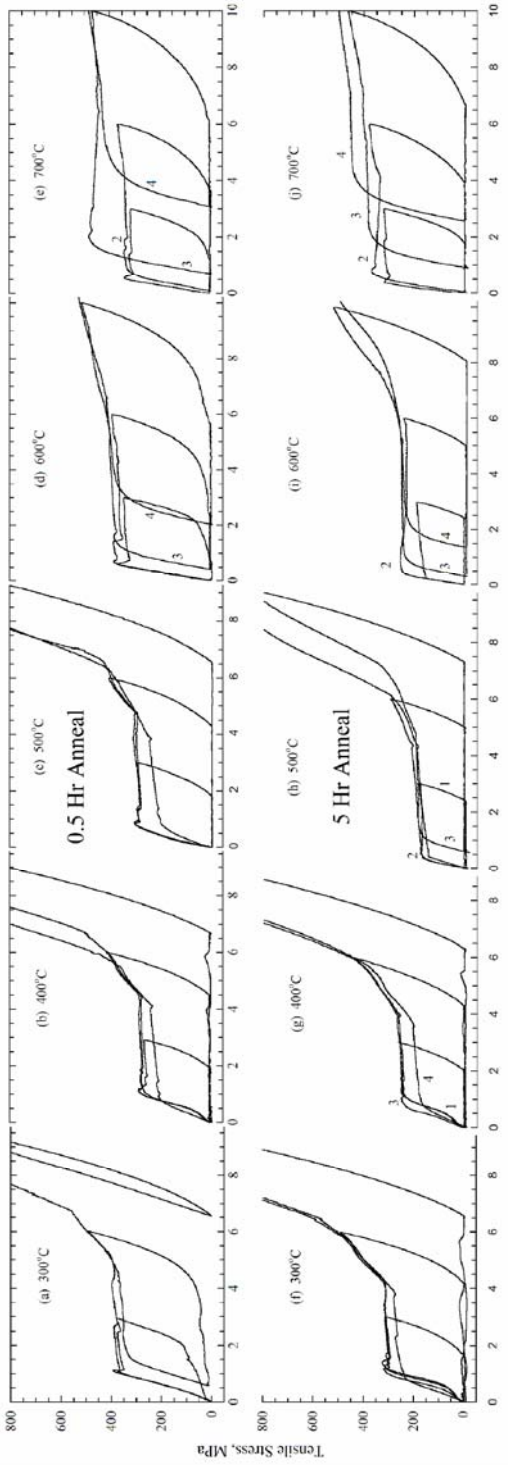

Figure 3.11 Stress-strain curves for AC samples aged for 0.5hr at (a) 300°C, (b) 400°C, (c) 500°C, (d) 600°C, (e) 700°C; for 5hrs at (f) 300°C, (g) 400°C, (h) 500°C, (i) 600°C, (j) 700°C. The numbers indicate the loading cycles.

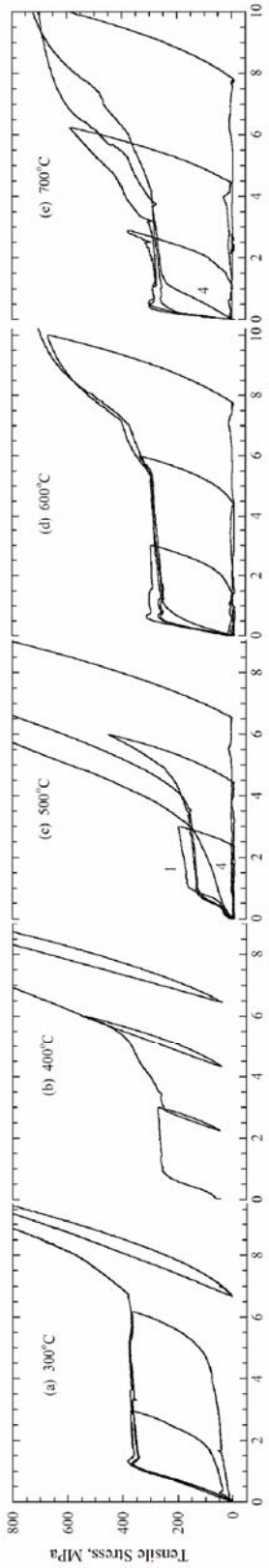

Figure 3.12 Stress-strain curve for FC samples aged for 0.5hr at (a) 300°C, (b) 400°C, (c) 500°C, (d) 600°C, (e) 700°C

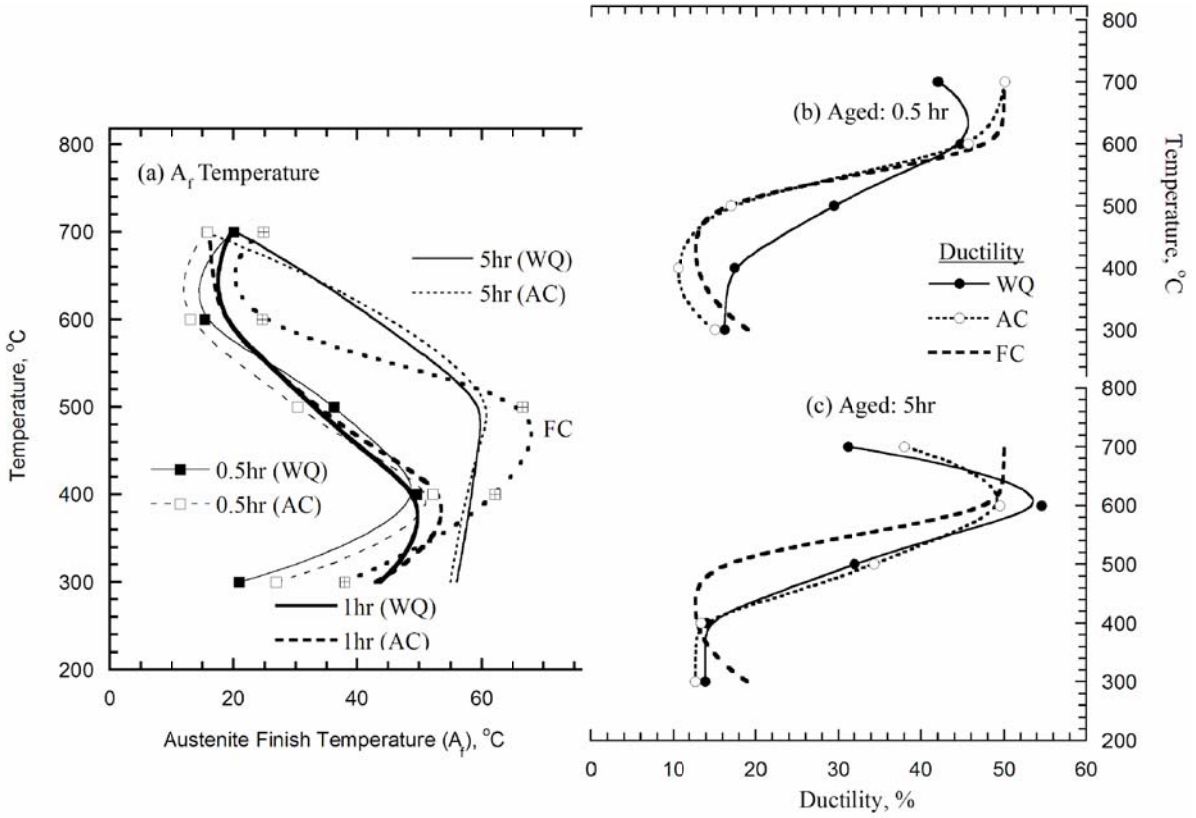

Figure 3.13 Variation of (a) A_f transformation temperature and (b) Ductility (loading cycle 1 and 2) with aging temperature (300°C-700°C), time (0.5hr-1hr-5hrs) and cooling rate (WQ-AC-FC). Note the 'c-curve' characteristics similar to TTT diagram for precipitation.

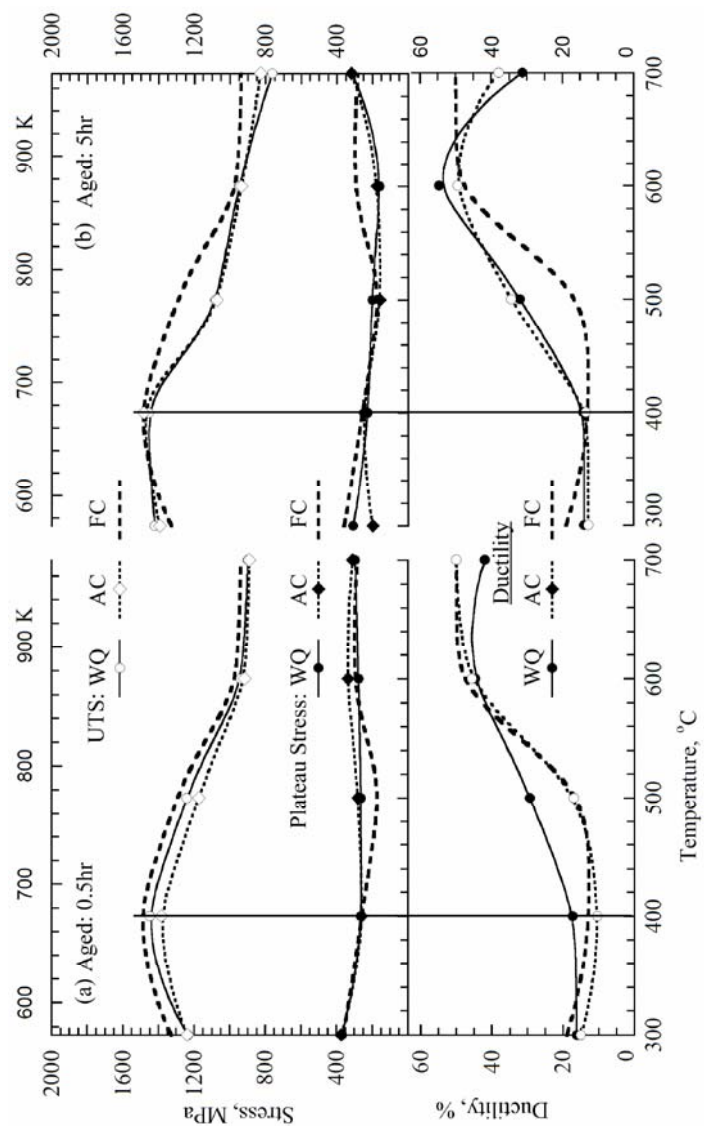

Figure 3.14 Variation of (a) tensile strength (UTS) and (b) ductility with aging temperature (300°C-700°C), time (0.5hr-1hr-5hrs) and cooling rate (WQ-AC-FC).

3.8 References

1. Pelton, A., J. DiCello, and S. Miyazaki. *Optimization of processing and properties of medical-grade nitinol wire*. in *Proceedings of the International Conference on Shape Memory and Superelastic Technologies (SMST)*. 2000. Pacific Grove, CA.

2. Funakubo, H., *Shape memory alloys*. 1987: Gordon & Breach Science Publishers, New York.

3. Otsuka, K. and C.M. Wayman, *Mechanism of shape memory and superelasticity*, in *Shape memory materials*, K. Otsuka and C.M. Wayman, Editors. 1998, Cambridge University Press. p. 27-45.

4. Bhattacharya, K., *Microstructure of martensite: why it forms and how it gives rise to the shape-memory effect*. Oxford series on materials modelling, ed. A.P. Sutton and R.E. Rudd. 2003: Oxford University Press.

5. Duerig, T.W., A.R. Pelton, and D. Stoeckel. *The use of superelasticity in medicine*. in *Metall (Heidelberg)*. 1996: Sonderdruck aus Heft.

6. Duerig, T.W., D. Stoeckel, and A.R. Pelton, *An overview of nitinol medical applications.* Materials Science and Engineering A, 1999. **273-275**: p. 149-160.

7. Pelton, A.R., D. Stoeckel, and T.W. Duerig, *Medical uses of nitinol.* Materials Science Forum, 2000. **327-328**: p. 63-70.

8. Stoeckel, D., *Nitinol medical devices and implants.* Minimally Invasive Therapy and Allied Technologies, 2000. **9**(2): p. 81-88.

9. Pelton, A.R., T.W. Duering, and D. Stockel, *A guide to shape memory and superelasticity in nitinol medical devices.* Minimally Invasive Therapy and Allied Technologies, 2004. **13**(4): p. 218-221.

10. Melzer, A. and D. Stoeckel. *Performance improvement of surgical instrumentation through the use of nitinol materials*. in *The 1st International Conference on shape memory and superelastic technologies*. 1994.

11. Frank, T.G., W. Xu, and A. Cuschieri, *Instruments based on shape memory alloy properties for minimal access surgery: interventional radiology and flexible endoscopy.* Journal of Minimally Invasive Therapy and Allied Technologies (MITAT), 2000. **9**(1).

12. Duerig, T.W. and A.R. Pelton, *An overview of superelastic stent design.* Materials Science Forum, 2002. **394-395**: p. 1-8.

13. Stoeckel, D., C. Bonsignore, and S. Duda, *A survey of stent designs.* Minimally Invasive Therapy and Allied Technologies, 2002. **11**(4): p. 137-147.

14. Stoeckel, D., A. Pelton, and T. Duerig, *Self-expanding nitinol stents : material and design considerations.* European Radiology, 2003(1-12).

15. Duerig, T.W., K.N. Melton, D. Stockel, and C.M. Wayman, *Engineering aspects of shape memory alloys*. 1990: Butterworth-Heinemann, London.

16. Humbeeck, J.V., *Shape memory alloys: A material and a technology.* Advanced Engineering Materials, 2001. **3**(11): p. 837-850.

17. Firstov, G.S., J.V. Humbeeck, and Y.N. Koval, *High-temperature shape memory alloys. Some recent developments.* Materials Science and Engineering A, 2004. **378**: p. 2-10.

18. Ryhanen, J., *Biocompatibility evaluation of nickel-titanium shape memory alloy*, in *Department of Surgery*. 1999, University of Oulu.

19. Yeung, K.W.K., K.M.C. Cheung, W.W. Lu, and C.Y. Chung, *Optimization of thermal treatment parameters to alter austenitic phase transition temperature of NiTi alloy for medical implant.* Materials Science and Engineering A, 2004. **383**: p. 213-218.

20. Favier, D., Y. Liu, L. Orgeas, A. Sandel, L. Debove, and P. Comte-Gaz, *Influence of thermomechanical processing on the superelastic properties of a Ni-rich Nitinol shape memory alloy.* Materials Science and Engineering A, 2006. **429**: p. 130-136.

21. Nishida, M., C.M. Wayman, and T. Honma, *Precipitation processes in near-equiatomic TiNi shape memory alloys.* Metallurgical Transactions A, 1986. **17**: p. 1505-1515.

22. Otsuka, K. and X. Ren, *Physical metallurgy of Ti-Ni based shape memory alloys.* Progress in Materials Science, 2005. **50**: p. 511-678.

23. Adharapurapu, R.R. and K.S. Vecchio, *Microstructure development in Ni-rich 60NiTi (wt.%) alloy: Aging studies on precipitation reactions and shape memory characteristics.* submitted to Metallurgical Transactions A, 2007.

24. Kainuma, R., M. Matsumoto, and T. Honma, *Metallographic study of precipitation processes in Ni-rich TiNi alloys.* Tohoku Daigaku Senko Seiren Kenkyujo iho, 1987. **43**(2): p. 149-158.

25. Tang, W., *Thermodynamic study of the low temperature phase B19' and the martensitic transformation in near-equiatomic Ti-Ni shape memory alloy.* Metallurgical Transactions A, 1997. **28**: p. 537-544.

26. Allafi, J.K., X. Ren, and G. Eggeler, *The mechanism of multistage martensitic transformations in aged Ni-rich NiTi shape memory alloys.* Acta Materialia, 2002. **50**: p. 793-803.

27. Otsuka, K. and X. Ren, *Factors affecting the Ms temperature and its control in shape memory alloys.* Materials Science Forum, 2002. **394-395**: p. 177-184.

28. Otsuka, K. and C.M. Wayman, eds. *Shape memory materials*. 1998, Cambridge University Press.

29. Morawiecz, H., D. Stroz, and D. Chrobak, *Effect of deformation and thermal treatment of NiTi alloy on transition sequence.* Journal de Physique IV, 1995. **5-C2**: p. 205-210.

30. Morawiecz, H., D. Stroz, T. Goryczka, and D. Chrobak, *Two-stage martensitic transformation in a deformed and annealed NiTi alloy.* Scripta Materialia, 1996. **35**(4): p. 485-490.

31. Chrobak, D., D. Stroz, and H. Morawiec, *Effect of early stages of precipitation and recovery on the multi-step transformation in deformed and annealed near-equiatomic NiTi alloy.* Scripta Materialia, 2003. **48**: p. 571-576.

32. Khalil-Allafi, J., A. Dlouhy, and G. Eggeler, *Ni_4Ti_3-precipitation during aging of NiTi shape memory alloys and its influence on martensitic phase transformations.* Acta Materialia, 2002. **50**: p. 4255-4274.

33. Liu, Y., H. Yang, and A. Voigt, *Thermal analysis of the effect of aging on the transformation behavior of Ti-50.9at.%Ni.* Materials Science and Engineering A, 2003. **360**: p. 350-355.

34. Stroz, D., *TEM studies of the R-phase transformation in a NiTi shape memory alloy after thermo-mechanical treatment.* Materials Chemistry and Physics, 2003. **81**: p. 460-462.

35. Carroll, M.C., C. Somsen, and G. Eggeler, *Multiple-step martensitic transformations in Ni-rich NiTi shape memory alloys.* Scripta Materialia, 2004. **50**: p. 187-192.

36. Fan, G., W. Chen, S. Yeng, J. Zhu, X. Ren, and K. Otsuka, *Origin of abnormal multi-stage martensitic transformation behavior in aged Ni-rich Ti-Ni shape memory alloys.* Acta Materialia, 2004. **52**: p. 4351-4362.

37. Khalil-Allafi, J., G. Eggeler, A. Dlouhy, W.W. Schmahl, and C. Somsen, *On the influence of heterogeneous precipitation on martensitic transformations in a Ni-rich NiTi shape memory alloy.* Materials Science and Engineering A, 2004. **378**: p. 148-151.

38. Michutta, J., M.C. Carroll, A. Yawny, C. Somsen, K. Neuking, and G. Eggeler, *Martensitic phase transformation in Ni-rich NiTi single crystals with one family Ni_4Ti_3 precipitates.* Materials Science and Engineering A, 2004. **378**: p. 152-156.

39. Johnson, A.J.W., R.F. Hamilton, H. Sehitoglu, G. Biallas, H.J. Maier, Y.I. Chumlyakov, and H.S. Woo, *Analysis of multistep transformations in single-crystal NiTi.* Metallurgical and Materials Transactions A, 2005. **36**: p. 919.

40. Wang, Z.G., X.T. Zu, and Y.Q. Fu, *Study of incomplete transformations of near equiatomic TiNi shape memory alloys by DSC methods.* Materials Science and Engineering A, 2005. **390**: p. 400-403.

41. Khalil-Allafi, J., G. Eggeler, W.W. Schmahl, and D. Sheptyakov, *Quantitative phase analysis in microstructures which display multiple step martensitic transformations in Ni-rich NiTi shape memory alloys.* Materials Science and Engineering A, 2006. **438-440**: p. 593-596.

42. Michutta, J., C. Somsen, A. Yawny, A. Dlouhy, and G. Eggeler, *Elementary martensitic transformation processes in Ni-rich NiTi single crystal with Ni_4Ti_3 precipitates.* Acta Materialia, 2006.

43. Chiang, L.J., C.H. Li, Y.F. Hsu, and W.H. Wang, *Age-induced four-stage transformation in Ni-rich NiTi shape memory alloys.* Journal of Alloys and Compounds, 2007. **doi:10.1016/j.jallcom.2007.04.006**.

44. Todoriki, T. and H. Tamura, Trans Jpn Inst Met, 1987. **28**: p. 83.

45. Stroz, D., J. Kwarciak, and H. Morawiec, *Effect of aging on martensitic transformation in nickel-titanium (NiTi) shape memory alloy.* Journal of Materials Science, 1988. **23**(11): p. 4127-4131.

46. Zhu, J.S. and R. Gotthardt, *New phase transition peak in nickel-titanium (NiTi) alloy.* Physics Letters A, 1988. **132**(5): p. 279-282.

47. Favier, D., Y. Liu, and P.G. McCormick, Scripta Metall Mater, 1992. **28**: p. 669-672.

48. Bataillard, L. and R. Gotthardt, *Influence of thermal treatment on the appearance of a three step martensitic transformation in NiTi.* J. Phys IV, 1995. **5-C8**: p. 647-652.

49. Bataillard, L., J.-E. Bidaux, and R. Gotthardt, *Interaction between microstructure and multiple-step transformation in binary NiTi alloys using in-situ tranmission electron microscopy observations.* Philosophical Magazine A: Physics of Condensed Matter: Structure, Defects and Mechanical Properties, 1998. **78**(2): p. 327-344.

50. Dlouhy, A., J.K. Allafi, and G. Eggeler, *Multiple-step martensitic transformations in Ni-rich NiTi alloys-an in-situ transmission electron microscopy investigation.* Philosophical Magazine A: Physics of Condensed Matter: Structure, Defects and Mechanical Properties, 2003. **83**(3): p. 339-363.

51. Kim, J.I., Y. Liu, and S. Miyazaki, *Aging induced two stage R-phase transformation in Ti-50.9at.%Ni.* Acta Materialia, 2004. **52**: p. 757.

52. Chrobak, D. and D. Stroz, *Two-stage R phase transformation in a cold-rolled and annealed Ti-50.6at.%Ni alloy.* Scripta Materialia, 2005. **52**: p. 757-760.

53. Zhou, Y., J. Zhang, G. Fan, X. Ding, J. Sun, X. Ren, and K. Otsuka, *Origin of 2-stage R-phase transformation in low-temperature aged Ni-rich Ti-Ni alloys.* Acta Materialia, 2005. **53**: p. 5365-5377.

54. Chang, S.H., S.K. Wu, and G.H. Chang, *Grain size effect on multiple-stage transformation of a cold-rolled and annealed equiatomic TiNi alloy.* Scripta Materialia, 2005. **52**(12): p. 1341-1346.

55. Sitepu, H., W.W. Schmahl, J. Khalil-Allafi, G. Eggeler, A. Dlouhy, D.M. Tobbens, and M. Tovar, *Neutron diffraction phase analysis during thermal cycling of a Ni-rich NiTi shape memory alloy using the Rietveld method.* Scripta Materialia, 2002. **46**(7): p. 543-548.

56. Eggeler, G., J. Khalil-Allafi, S. Gollerthan, C. Somsen, W.W. Schmahl, and D. Sheptyakov, *On the effect of aging on martensitic transformation in Ni-rich NiTi shape memory alloys.* Smart Materials and Structures, 2005. **14**(5): p. S186-S191.

57. Huang, X. and Y. Liu, *Effect of annealing on the transformation behavior and superelasticity of NiTi shape memory alloy.* Scripta Materialia, 2001. **45**: p. 153-160.

58. Jardine, A.P., K.H.G. Ashbee, and M.J. Bassett, *Effects of cooling rate on the shape memory effect thermodynamics of NiTi.* Journal of Materials Science, 1988. **23**: p. 4273-4281.

59. Dolce, M. and D. Cardone, *Mechanical behavior of shape memory alloys for seismic applications. 1. Martensite and austenite NiTi bars subjected to torsion.* International Journal of Mechanical Sciences, 2001. **43**: p. 2631-2656.

60. Dolce, M. and D. Cardone, *Mechanical behavior of shape memory alloys for seismic applications. 2. Austenite NiTi wires subjected to tension.* International Journal of Mechanical Sciences, 2001. **43**: p. 2657-2677.

61. Saadat, S., J. Salichs, M. Noori, Z. Hou, H. Davoodi, I. Bar-on, Y. Suzuki, and A. Masuda, *An overview of vibration and seismic applications of NiTi shape memory alloy.* Smart Materials and Structures, 2002. **11**: p. 218-229.

62. Adharapurapu, R.R., F. Jiang, K.S. Vecchio, and G.T. Gray III, *Response of NiTi shape memory alloy at high strain rate: A systematic investigation of temperature effects on tension-compression asymmetry.* Acta Materialia, 2006. **54**: p. 4609-4620.

63. Chen, W.W., Q. Wu, J.H. Kang, and N.A. Winfree, *Compressive superelastic behavior of a NiTi shape memory alloy at strain rates of 0.001-750 s^{-1}.* International Journal of Solids and Structures, 2001. **38**: p. 8989-8998.

64. Liu, Y., Y. Li, and K.T. Ramesh, *Rate dependence of deformation mechanisms in a shape memory alloy.* Philosophical Magazine A: Physics of Condensed Matter: Structure, Defects and Mechanical Properties, 2002. **82**(12): p. 2461-2473.

65. Liu, Y., Y. Li, K.T. Ramesh, and J.V. Humbeeck, *High strain rate deformation of martensitic NiTi shape memory alloy.* Scripta Materialia, 1999. **41**(1): p. 89-95.

66. Zhao, Y., M. Taya, and H. Izui, *Study on energy absorbing composite structure made of concentric NiTi spring and porous NiTi.* International Journal of Solids and Structures, 2006. **43**: p. 2497-2512.

67. Buehler, W.J. and R.C. Wiley, *The properties of TiNi and associated phases*. 1961, U. S. Naval Ordnance Laboratory. p. 61-75.

68. Buehler, W.J. and F.E. Wang, *A summary of recent research on the Nitinol alloys and their potential application in ocean engineering.* Ocean Engineering, 1968. **1**: p. 105-120.

69. Julien, G.J., *Shape memory parts of 60 Nitinol*, in *US Patent# 7005018*. 2006, Nitinol Technologies, Inc. (Edgewood, WA): United States. p. 1-15.

70. Julien, G.J., *Manufacturing of Nitinol parts and forms*, in *US Patent# 6422010*. 2002, Nitinol Technologies, Inc. (Edgewood, WA): United States. p. 1-15.

71. Clingman, D.J., F.T. Clalkins, and J.P. Smith. *Thermomechanical properties of 60-Nitinol*. in *SPIE Smart Structures and Materials*. 2003. San Diego CA.

72. Adharapurapu, R.R. and K.S. Vecchio, *Superelasticity in a new bioimplant material: Ni-rich 55NiTi alloy.* Experimental Mechanics, 2006. **In Press**.

73. Frick, C.P., A.M. Ortega, J. Tyber, A.E.M. Maksound, H.J. Maier, Y. Liu, and K. Gall, *Thermal processing of polycrystalline NiTi shape memory alloys.* Materials Science and Engineering A, 2005. **405**: p. 34-49.

74. Robertson, S.W., V. Imbeni, H.-R. Wenk, and R.O. Ritchie. *Crystallographic texture in austenitic Nitinol*. in *Proceedings of the International Conference on Shape Memory and Superelastic Technologies (SMST-2004)*. 2004. Baden-Baden German: SMST Society.

75. Robertson, S.W., X.Y. Gong, and R.O. Ritchie, *Effect of product form and heat treatment on the crystallographic texture of austenitic Nitinol.* Journal of Materials Science, 2006. **41**: p. 621-630.

76. Miyazaki, S., *Thermal and stress cycling effects and fatigue properties of Ni-Ti*, in *Engineering asapects of shape memory alloys*, T.W. Duerig, K.N. Melton, D. Stockel, and C.M. Wayman, Editors. 1990, Butterworth Heinemann: London. p. 394-413.

77. Robertson, S.W., V. Imbeni, H.-R. Wenk, and R.O. Ritchie. *Crystallographic texture in austenitic nitinol*. in *Proceedings of the Internatinoal Conference on Shape Memory and Superelastic Technologies (SMST-2004)*. 2004. Baden-Baden German: SMST Society.

78. Fernandes, F.M.B., A.S. Paula, J. Canejo, K.K. Mahesh, R.J.C. Silva, R.M.S. Martins, A.M.A. Cardoso, and N. Schell. *Texture evolution during annealing of NiTi shape memory alloy*. in *Proceedings of the Internatinoal Conference on Shape Memory and Superelastic Technologies (SMST-2004)*. 2004. Baden-Baden German: SMST Society.

79. Ortin, J. and A. Planes, *Thermodynamic analysis of thermal measurements in thermoelastic martensitic transformations.* Acta Metall., 1988. **36**(8): p. 1873-1889.

80. Favier, D. and Y. Liu, *Restoration by rapid overheating of thermally stabilised martensite of NiTi shape memory alloys.* Journal of Alloys and Compounds, 2000. **297**: p. 114-121.

81. Liu, Y. and P.G. McCormick, *Criteria of transformation sequences in NiTi shape memory alloys.* Mater. Trans. JIM, 1996. **37**(4): p. 691-696.

82. Tan, G. and Y. Liu, *Comparative study of deformation-induced martensite stabilisation via martensite reorientation and stress-induced martensitic transformation in NiTi.* Intermetallics, 2004. **12**: p. 373-381.

83. Liu, Y., G. Tan, and S. Miyazaki, *Deformation-induced martensite stabilisation in [100] single-crystalline Ni-Ti.* Materials Science and Engineering A, 2006. **438-440**: p. 612-616.

84. Liu, Y., Y. Liu, and J.V. Humbeeck, *Two-way shape memory effect developed by martensite deformation in NiTi.* Acta Materialia, 1999. **47**(1): p. 199-209.

85. Liu, Y. and D. Favier, *Stabilisation of martensite due to shear deformation via variant reorientation in polycrystalline NiTi.* Acta Materialia, 2000. **48**: p. 3489-3499.

86. Erbstoeszer, B., B. Armstrong, M. Taya, and K. Inoue, *Stabilization of the shape memory effect in NiTi: An experimental investigation.* Scripta Materialia, 2000. **42**: p. 1145-1150.

87. Liu, Y. and G.S. Tan, *Effect of deformation by stress-induced martensitic transformation on the transformation behavior of NiTi.* Intermetallics, 2000. **8**: p. 67-75.

88. Miyazaki, S., Y. Kohiyama, K. Otsuka, and T.W. Duerig, *Effects of several factors on the ductility of Ti-Ni alloy.* Materials Science Forum, 1990. **56-58**: p. 765-770.

89. Duerig, T.W. and T. Zadno, eds. *An engineer's perspective of pseudoelasticity*. Engineering aspects of shape memory alloys, ed. T.W. Duerig, K.N. Melton, D. Stockel, and C.M. Wayman. 1990, Butterworth-Heinemann, London. 394-413.

4 HIGH STRAIN-RATE RESPONSE OF NiTi SHAPE MEMORY ALLOY: A SYSTEMATIC INVESTIGATION OF TEMPERATURE EFFECTS ON TENSION-COMPRESSION ASYMMETRY

Acta Materialia, 2006

4.1 Abstract

A systematic experimental investigation into the effects of temperature on the stress-strain response of NiTi (55.6 wt% Ni) shape memory alloy (SMA) at high strain rate was conducted and compared with the behavior at quasi-static strain rate. Dynamic compression and tension tests, to total strains of 16~24%, were performed at high strain rate (~1200 /s) and under quasi-static conditions at temperatures from –196^{o}C to 400^{o}C. Since the superelastic range for the NiTi alloy used in this work is A_f (2°C) < T < M_d (150°C), it was possible to study the high strain rate deformation of both the austenite phase (where stress-induced martensite – SIM – transformation occurs) at temperatures > 0°C and (thermally-induced) martensite (TIM) phase at lower temperatures. The results indicate differences in the stress-strain response of thermally-induced martensite and stress-induced martensite, in terms of plateau stress characteristics and critical stress (as determined by 0.2% strain offset). The observations illustrate a complex interplay of test temperature, stress state (compression and tension) and martensite type (thermally induced vs. stress induced) that lead to the asymmetry in compression versus tension response of the SMA in both quasi-static and dynamic loading conditions. This asymmetry was captured in the variation of critical stress with temperature that exhibited a three-stage character, with

the critical stress being higher in compression than in tension. These findings have significant implications to the understanding and exploitation of the underlining functional characteristics of shape memory alloys, especially at high strain rates.

4.2 Introduction

Shape memory alloys (SMA) epitomize ‘new age’ material, where the functional characteristics, such as shape memory and superelasticity, are exploited through the interplay of structure and properties. Since the discovery of the shape-memory effect (SME) in Au-Cd alloys more than 50 years ago [1], numerous alloy systems have been reported to exhibit SME behavior [2, 3]. However, after more than a decade of relative dormancy, research on shape memory alloys underwent a revival with the discovery of the SME in NiTi alloys; this alloy promises significant engineering applications. The alloys that exhibit shape memory function can generally be classified into noble metal-based, Fe-based and NiTi-based alloy systems, and non-metallic SMAs [4]. Despite the efforts by the research community to develop SMAs for commercial applications, only a few alloys like NiTi, NiTi-Cu/Nb, Cu-Al-Ni, Fe-Mn-Si, have found a niche in commercial markets. Among these, NiTi is considered to be a favorable shape memory alloy material for practical applications due to its superior memory and structural properties. In fact, it is considered as a promising contender for structural and energy-absorbing applications, including seismic protection of structures [5], supplanting conventional alloys like steel, aluminum, titanium, and Ni-base superalloys.

Shape memory alloys display an intricate non-linear deformation behavior that is dependent on temperature, stress state, strain rate, texture and prior thermo-mechanical deformation history [6]. Unfortunately, the lack of material properties at high strain rates is curtailing its widespread use in a number of aerospace and defense applications. Although, continuum models have been developed to explain why a martensitic microstructure forms [7], a complete reliable theory still evades us. Early experimental studies by Buehler *et al.*[8], Rozner and Wasilewski [9], Wasilewski [10], Miyazaki *et al.* [11], have characterized the macroscopic deformation behavior of NiTi. A later investigation by Shaw and Kyriakides [12] systematically studied and quantified the complex interaction between stress, temperature, deformation and loading rate (quasi-static strain rates). Creep behavior of NiTi alloys has also been studied to understand the effect of creep deformation on shape memory properties [13], and for developing actuators in high-temperature applications based on shape memory alloys [14]. Lin *et al.* [15] investigated the effect of strain rate (quasi-static) and deformation temperatures on the tensile stress-strain response of austenitic NiTi in the superelastic regime. Tobushi *et al.* [16] studied the dependence of stress-induced martensite transformation stress on strain rate and temperature in NiTi SMA. Entemeyer *et al.* [17] examined the physical origin of the (quasi-static) strain rate effect on the superelastic behavior in SMA's, and accordingly described the superelastic behavior of copper-based alloys (CuZnAl and CuAlBe) using a micromechanical model. More recently, Gall *et al.* have studied the tension and compression properties of single and polycrystalline NiTi to understand the asymmetry present in the tension-compression stress-strain curves [18], and to

evaluate the variation of critical stress required for stress-induced martensite with temperature [19].

Dynamic compressive stress-strain curves of Ni-Ti SMA were carried out at room temperature (within superelastic range, $A_f < T < M_d$) by Chen *et al.* [20] to evaluate the variation of transition stress with strain rate. Similar dynamic tensile tests were conducted by Miller *et al.* [21] to study the stress-induced martensitic transformation and subsequent plastic deformation of the martensitic phase. The shock stress, shock velocity and details of the shock wave profile have been measured by Millett *et al.* [22]. An inflection at lower stress was found in the Hugoniot curve (stress-particle velocity) and has been ascribed to the martensitic phase transformation that is characteristic of the shape memory effect in this alloy. In a similar way, the variation of shock velocity with particle velocity was found to be non-linear, contrary to other pure metal and alloy systems. Finally, a break in slope in the rising part of the shock profile has been identified as the Hugoniot Elastic Limit in NiTi. Conversion to the one-dimensional stress equivalent and comparison to quasi-static data indicated that NiTi exhibits significant strain-rate sensitivity.

The mechanical behavior and deformation mechanisms of NiTi shape memory alloys in the martensitic phase were studied by Liu *et al.*, who reported 'Lüders-like' deformation associated with martensite reorientation and detwinning processes [23-26]. Liu *et al.* also studied the asymmetry associated with monotonic tension-compression stress-strain curves for martensitic NiTi at various strain rates [27]. Work on the dynamic properties of NiTi in the martensitic phase by Liu *et al.* [28-30] examined compression stress-strain response at a strain rate of ~3000 s^{-1} and tensile

stress-strain response at ~300 s^{-1}. Although there is growing experimental data on both quasi-static and dynamic stress-strain responses of NiTi, in terms of strain rate or temperature, in the austenitic or martensitic structures, a systematic study of the interplay or interaction between temperature and high strain rate is limited. Depending on the temperature, either thermally-induced or stress-induced martensite phase transformations may occur before or during deformation. As such, both the mechanical response and the deformation mechanisms in NiTi shape memory alloys are more complex than the deformation of typical disordered metals or alloys. Understanding the dynamic response of NiTi is important for its possible use in seismic damping applications, blast mitigation structures and energy absorbing devices. Therefore, the objectives of the present work are:

(1) To conduct accurate high-strain rate tests on NiTi shape memory alloys while achieving constant strain-rate throughout the test, and the same high strain rate in both compression and tension.

(2) To study the stress-induced martensite formation and its relation to the presence/ absence of stress-plateau as a function of strain rate and temperature.

(3) To investigate the role of reverse SIM transformation through unloading.

(4) To investigate the effect of temperature on the evolution of compression-tension asymmetry of NiTi SMA under quasi-static (10-3 /s) and dynamic loading (~1200 /s) conditions.

(5) To compare the variation of critical stress (as defined by 0.2% strain offset) with respect to temperature between quasi-static and dynamic loading conditions.

4.3 Experimental Procedure

4.3.1 Materials and Specimen

The shape memory alloy NiTi (SE508, 55.6 wt.% NiTi) used in this work was purchased from Nitinol Devices and Components in the form of 12.7 mm diameter bar stock that has been cold-rolled. The chemical composition along with the transformation temperatures of NiTi, as measured by differential scanning calorimetry (DSC), are listed in Table 1. Textures were measured at room temperature with electron backscatter diffraction (EBSD) in a scanning electron microscope (SEM) utilizing INCA^{TM} software from Oxford Instruments. The principal texture in the axial direction is a (111)-fiber type texture. However, for the (111) textured grains, the radial direction is distributed primarily near the <101> and <112> orientations. Cylindrical tensile specimens with gauge section dimensions of 3.8*mm* diameter x 11.5*mm* length were used for the tensile tests at high strain rates, whereas, for quasi-static strain rate testing, specimen with dimensions 6.4*mm* diameter x 30*mm* length were utilized. Specimens for compression tests under quasi-static and dynamic strain rates were right, regular cylinders with dimensions 5*mm* diameter × 5*mm* length.

Table 4.1 Material Composition of NiTi SMA

Element		Ni		Ti	O	H	C
wt %		55.6		balance	0.033	0.0009	0.0028
Transformation	A_s	A_f	M_s	M_f	A_s, A_f, austenite start and finish temperature		
Temperature (^oC)	-23	2	-8	-36	M_s, M_f, martensite start and finish temperature		

4.3.2 Testing temperature

Tensile and compressive experiments in this work were performed at low temperatures (-196°C, -100°C, -50°C and 0°C), room temperature (RT, 20°C) and elevated temperatures (100°C, 200°C, 300°C and 400°C). For all the tests, low temperatures were achieved by immersing the entire specimen in a low temperature liquid bath, either a fluorinert electronic liquid (FC-77, 3M Specialty Chemicals Division) cooled by liquid nitrogen or in liquid nitrogen directly (-196°C), for several minutes prior to testing and for the entire duration of the experiment. For high temperature testing at high strain rate, an induction heating system was used to heat the specimen uniformly until the desired temperature set point was attained. Once the set point was attained, the specimen was held at that temperature for ~ 5 minutes to establish equilibrium and a uniform temperature through the entire gage section of the specimen. The temperature of the specimen was monitored by several thermocouples in both the low and high temperature testing, until the start of the test. High temperature low strain rate tension tests were performed using a high-temperature furnace (with feedback control) available with standard Instron servohydraulic load frame. In these tests, the specimen was held at the test temperature for ~ 20min, until the thermocouple readings of the top and bottom portion of the specimen gage length were equalized.

4.3.3 Quasi-static and high strain tests

Quasi-static compression and tension tests were conducted on a servohydraulic load frame at a strain rate of 10^{-3}/s. High strain rate compression and tensile tests, at a

nominal strain rate ~1200/s, were conducted using a split Hopkinson pressure bar (12.7 *mm* diameter) and tensile bar (19.05*mm* diameter), respectively. The incident and the reflected strains are measured by the strain gauges glued at the midpoint of the incident bar, while the transmitted strain is measured by the strain gauges glued at the midpoint of the transmission bar. The dynamic stress, strain and strain rate were calculated using one-dimensional stress wave theory [31]. By the use of a momentum trap in the present Hopkinson bar setup, the specimen is loaded by a single stress pulse without being subjected to any additional reflected pulses. This facilitates a direct correlation between the microstructures and mechanical response of the specimen.

4.3.4 High strain rate compression with pulse shaping

A small quantity of grease or high temperature lubricant was applied over the loading surfaces of the compressive specimen to reduce friction during testing at RT and elevated temperatures. During high temperature testing, tungsten carbide (WC) platens, which were sized to have the same impedance as the Hopkinson bar material (350 Maraging Steel), were sandwiched between the specimen-bars interfaces. The WC inserts have low thermal conductivity and consequently reduce the heating of the Hopkinson bar that are in contact with the specimen. Raising the temperature of the bar interfaces may lead to a decrease in the yield strength and elastic modulus of the bars, thereby invalidating the uniform elastic analysis of the bar data, and also can cause plastic deformation (through indentation) during testing leading to potentially unreliable stress-strain data. Within the range of temperatures examined in this work, the elastic modulus of the bar material does not vary significantly, and therefore the

main use of the WC platens was to eliminate indentation of the bar loading surfaces. Furthermore, it is well known that for a Hopkinson pressure bar test to yield reliable and valid uniaxial-stress, stress-strain responses of the materials under investigation, the specimen should deform at a constant compressive strain rate and remain in stress equilibrium during the duration of loading [32-34]. However, when testing a SMA specimen in a conventional Hopkinson pressure bar test, the normal, square-wave incident pulse cannot provide a constant strain rate due to the non-linear (stress-plateau) behavior exhibited by the material. A typical record of the stress pulses from a conventional Hopkinson pressure bar test on this NiTi material is shown in Figure 4.1a. While a constant amplitude incident stress pulse is generated by the impacting striker, the reflected pulse and therefore strain rate, is not constant (*i.e.* not a square pulse). It should be noted that, as a result of lateral contractions, the tensile specimen is subjected to a nearly constant strain rate during most of the deformation, whereas in the compression test, the strain rate decreases dramatically from a high value (~2900 s^{-1}) to a low value (~500s^{-1}) with increasing strain (see Figure 4.1b). Such a large variation in deformation rate may influence the SMA stress-strain response in a dramatic way. Additionally, high-frequency oscillations can be observed in the pulses from such a conventional Hopkinson pressure bar test [20], (or see Figure 4.1a).

Unlike most conventional metals/alloys, NiTi alloys exhibit a sigmoidal type stress-strain behavior that is the consequence of a phase transformation. Any changes in strain rate and high-frequency oscillations in the incident pulse are therefore highly undesirable since these two effects may influence the apparent transition stress, and hence lead to inaccurate interpretation of the compression-tension asymmetry results.

A tailored incident pulse can be achieved experimentally by placing a deformable material shim (pulse shaper) on the impact surface of the incident bar. As the shim deforms plastically upon loading, it transfers an increasing amount of the incident pulse, such that a tailorable incident pulse shape, with a relative long rise time can be achieved [32-34]. The choice of materials and dimensions for this pulse shaper is strongly dependent upon the desired strain rate and the stress-strain response of the specimen tested. Generally, the pulse shaper materials selected have been low strength, moderate work-hardening materials (e.g. OHFC annealed copper, brass, and 304 stainless steel), having thicknesses of 0.1 to 2 mm. In the present work, a high strength, very high work-hardening rate material, HAYNES B3 alloy (Ni-Mo), with a yield stress ~ 450 MPa and peak compressive strength in excess of 2 GPa was selected to fabricate the pulse-shapers. Optimum dimension of the pulse shaper for different strain rates and specimens was determined by experimental trials to obtain a valid, uniaxial-stress, stress-strain response at a constant strain rate of the SMA. Figure 4.1b shows examples of the strain rate as a function of strain for the dynamic tension test and the dynamic compression test (with and without the use of the pulse shaper). The results show that a constant strain rate was achieved for the tension test and compression test with the pulse shaper out to strains of ~20%. Accurate comparison of compression-tension asymmetry observed at various temperatures (and hence in various crystallographic phases) can be envisaged only when constant strain rate is achieved in all the tests.

4.4 Results and Discussion

4.4.1 Stress-strain response of NiTi at room temperature: Effect of strain rate

The stress-strain curves for the NiTi from quasi-static (0.001 s^{-1}) and dynamic (~1200 s^{-1}) strain rate tests conducted at room temperature (RT), in both tension and compression, are shown in Figure 4.2. The data is plotted in terms of engineering stress and strain, and the same convention is followed throughout this work. Figure 4.2 reveals the superelastic behavior of the SMA associated with the stress-induced martensite (SIM) transformation, in both compression and tension at RT ($>A_f$). Superelasticity is quasi-elastic deformation far beyond the conventional elastic limit of the material, when deformed at a certain temperature above A_f. Lüders-like deformation behavior, as identified by a distinctive stress-plateau in the stress-strain curve, which was observed under quasi-static deformation at room temperature, in both tension and compression, was only barely observed in tension under dynamic loading conditions. Compared to the tensile mode of deformation, compressive stress-strain curve exhibited smaller recoverable strain (note shape of the unloading curves), a steeper transformation stress-strain slope, and a higher critical transformation stress level, in both quasi-static deformation and dynamic deformation.

The stress-strain response of the SMA was found to be asymmetric between tension and compression, a phenomenon termed the Strength Differential Effect (SDE) by Plietsch and Ehrlich [35]. The asymmetry in tension-compression behavior during quasi-static loading has been studied in single crystal and polycrystalline NiTi [18, 27, 36-40]. Orgéas and Favier [38] have proposed several mechanisms to explain this

SDE in NiTi SMA, and based on their investigations, it was concluded that the asymmetric deformation behavior of SMA is an intrinsic property of the SIM transformation. Compression-tension asymmetry in polycrystalline NiTi is caused by asymmetry at the single-crystal level [36]. Indeed, texture imparts additional asymmetry to the compression-tension behavior in polycrystalline NiTi [18]. During the SIM transformation in single crystal NiTi, Plietsch and Ehrlich [35] observed that the maximum transformation strains in tension were twice as high as compressive strains. They further suggested that the SDE is due to the selective formation of different SIM variants between tension and compression, and that the lattice correspondence of martensite variants and the parent lattice leads to the directional dependence of the transformation strains. Liu *et al.* [27] conducted TEM studies on the microstructure of the deformed NiTi SMA in the martensitic phase and observed that dislocation mechanisms were dominant in compression, whereas detwinning (or re-orientation) of martensite variants occurred during the initial process of tensile deformation.

It should be noted that, depending on the transformation temperatures, material composition, and heat treatment, the SMA would be either martensitic or austenitic phase or even possess a two-phase microstructure at room temperature. SIM transformation occurs only during the deformation of the SMA in the parent austenitic phase at temperatures above A_f. Furthermore, when analyzing the deformation mechanisms of martensite, the type of martensite, *i.e.*, thermally-induced or stress-induced, should be clearly distinguished. In the present work, the specimen is in the austenitic state at RT before testing, and the martensite is therefore induced by stress.

The tensile stress-strain curves exhibit a three-stage behavior: elastic deformation of austenite within region I, SIM transformation and Lüders-like deformation behavior of the SIM within region II, and plastic deformation of SIM in region III. In stage II, a clear stress-plateau extends from a strain of ~1.6% to ~6.0.

Very recently, Brinson *et al.* [41] have redefined the meaning of a "full" transformation in a polycrystalline specimen. Using in-situ straining optical microscopy, they demonstrate that the "complete" transformation state of a polycrystalline SMA does not necessarily correspond to 100% martensitic phase, and that the volume fraction of martensite likely lies between 60 to 70%. They explain these observations by a variant locking mechanism within each grain, and thus the variants are unable to achieve full transformation, in contrast to what is generally observed in single crystals. Thus, the residual austenite may influence the stress-strain behavior of SMA, *i.e.*, the deformation mechanisms in stages II and III may be influenced by the untransformed austenite. Similar to the case of NiTi single crystal [39], polycrystalline compressive stress-strain data exhibit three stages during deformation at temperatures above A_s. Sehitoglu *et al.* [39] explain the stages as: Elastic deformation of austenite in stage I followed by a SIM transformation (A $\rightarrow$ M). During the stage II deformation, the stress-strain response of SMA is a consequence of elastic deformation of SIM and some slip in the austenite. Slip is the predominant deformation mechanism of the SIM in stage III.

The high strain rate compressive stress-strain curve shown in Figure 4.2 does not exhibit a clear stress-plateau, while the tension curve displays only a very small one. However, this does not necessarily indicate the absence of a SIM transformation,

it will be shown in later sections that indeed the SIM transformation takes place. The stress-strain response is dependent upon the type of martensite (thermal- or stress-induced) undergoing deformation and upon the rate of deformation. Later in this paper, it will also be shown that, under high strain rates, a stress-plateau behavior of thermally-induced martensite under tensile loading is observed at low temperatures (< M_f), while the SIM transformation at elevated temperatures (> A_f) does not exhibit any clear stress-plateau.

For all the tensile tests in the present work, whether quasi-static or high strain rate, the stress-strain curves did not return to the origin after unloading, *i.e.*, the hysteresis loops are not closed, unlike the loops obtained for small strain under tension. This is because the material has been deformed to a large total strain of ~16 - 24%, well beyond the limit of the materials maximum recoverable inelastic strain (~8-10%) [35].

4.4.2 Dynamic stress-strain response of NiTi at elevated temperatures

Typical stress-strain curves under dynamic and quasi-static compression and tension loading at RT and elevated temperatures are shown in Figure 4.3. Temperature effects on the high strain rate stress-strain response of SMA were found to be different under compression and tension. Overall, in compression, the stress at the same strain decreased with an increase in test temperature from RT to 400°C, with the specimen deformed at RT exhibiting the highest compressive flow stress at maximum strain, see Figure 4.3a. However, during the initial deformation (< 3%), the stress level in specimens deformed at RT was lower than the stresses observed for

samples tested at higher temperatures. In contrast to the compression tests, the relationship between the stress and test temperature was more complex under tensile loading. As shown in Figure 4.3b, the tensile stress did not show a direct or simple correlation with temperature, i.e. the stress-strain curve of SMA tested at RT was lower than the curves obtained at 200°C, 300°C and 400°C, with the behavior at 200°C and 300°C being very similar. The specimen deformed at 200°C exhibited higher stresses overall. Analysis of the quasi-static compression and tension stress-strain curves in Figure 4.3c and 3d, respectively, show that the samples deformed at high temperature show a different behavior compared to the dynamic tests. In quasi-static compression (see Figure 4.3c), during initial deformation (<10%, *i.e.* in stage I and II), the stress at the same strain level increases with test temperature. During stage III deformation, however, the specimens exhibit lower strength levels at higher temperatures compared to RT. In quasi-static tension (see Figure 4.3d), the specimen deformed at 100^{o}C exhibits uniform strain up to 20% without any evidence of necking, with strength levels higher than those observed at RT. On further increase in temperature from 100^{o}C to 400^{o}C, the 0.2% yield strength almost steadily increases (it first decreases slightly at 200^{o}C), which is quite contrary to that observed in conventional alloys. At both 200^{o}C and 300^{o}C, the specimen exhibit uniform strains of about 25%. At higher strains, however, the fracture strength decreases with increase in temperature, with the specimen deformed at 400^{o}C showing the lowest fracture strength. Figure 4.3 also captures the tension-compression asymmetry, wherein the compressive flow stress at the same strain is higher than that in tension in all the specimens tested. This asymmetry is analyzed further in a later section.

Typically, in terms of the conventional temperature-dependence strength theory, the strength of metals or alloys decreases with increases in temperature, under both tension and compression testing. However, for the SMA material, when the test temperature is within the superelastic range, $A_f < T < M_d$, the SIM transformation complicates this trend. As mentioned earlier, the austenite finish temperature, A_f, for the SMA NiTi used in this investigation is 2°C, see Table 1, and M_d, the highest temperature for the SIM transformation, is ~ 150°C [20]. All the high temperature testing (200°C, 300°C and 400°C) was conducted beyond the SIM transformation range (2°C < T < 150°C), and hence the SIM transformation was absent during the deformation of the austenite SMA, at these temperatures. However, testing at RT (~22°C) and 100°C resulted in a SIM transformation, since these temperatures lie within the superelastic range. Since the strength of the SMA is lower in the martensite state than in austenite state, the flow stress is lower at RT and 100°C. As deformation of austenite NiTi is dominated by a dislocation slip mechanism, the stress-strain curves obtained at these temperatures should have followed the conventional trend of strength variation with temperature. It is not clear however, why in both the quasi-static and dynamic tests, this trend is not adhered to consistently.

One common feature in the fractured specimens tested (at high temperatures) at both low and high strain rates is that the geometry of the necked region changes from circular at 200^{o}C to nearly square-type at 400^{o}C. At RT, the fracture region has a small curvature, similar to cup-cone type ductile failure; whereas at 100^{o}C, they exhibit flat fracture with little or almost no necking.

4.4.3 Dynamic stress-strain response of NiTi at low temperature

Having investigated the effect of elevated temperature on the stress-strain response of NiTi SMA, the mechanical behavior at low is now examined. Compression and tension tests were conducted at low temperatures: 0°C, -50°C, -100°C and -196°C; all the tests were performed at a high strain rate of ~1200 /s and quasi-static strain rate of 10^{-3} /s. Taking into account that the martensite finish temperature, M_f, is ~ -36°C, the phenomenon of thermally-induced martensite transformation should be noted, while interpreting the data for the test temperatures -50°C, -100°C and -196°C.

Figure 4.4 shows the stress-strain behavior of NiTi in dynamic and quasi-static compression and tension loading at low temperatures. The stress-strain curves obtained at RT are juxtaposed for comparison. The compressive flow stresses are always higher than the tensile stresses observed at the same strain, similar to the behavior noted at RT and elevated temperatures. However, the contrasting feature is that now a stress-plateau is clearly discernible at low temperatures, especially at -50°C, -100°C and -196°C , where the SMA is in a martensitic phase ($T < M_f$). The plateau slope tends to increase from being flat (0^o) during low strain rate tensile testing to a small finite slope during dynamic tensile testing. The slope tends to be larger during quasi-static compression and increases to more than 45^o under dynamic compression. The plateau stress in both dynamic and quasi-static tensile tests (see Figure 4.4b and 4d) decreases with decrease in temperature from RT to -50^oC, with a slight increase, however, at -100^oC. At -196^oC, the transformation stress is as large as that observed at RT. Fracture strains as large as 40% have been observed at

temperatures -50^{o}C and -100^{o}C under quasi-static testing. All samples failed by flat fracture, with no visible necking, and with the stress-strain curves exhibiting a constant work-hardening until fracture. Under quasi-static and dynamic compression as well, the transformation stress decreases with decrease in temperature from RT to -50^{o}C, with a subsequent increase at -100^{o}C and -196^{o}C. However, the stress levels (at same strain) under dynamic compression were observed to be far greater at -100^{o}C and -196^{o}C than the quasi-static values. In addition, dynamic compression stress-strain curves at -100^{o}C and -196^{o}C exhibit serrations beyond 8% strains. Similar serrations are found only at -196^{o}C for quasi-static compression stress. These serrations may be indicative of either delayed detwinning (discussed immediately below) at higher strain rates or twinning of martensite at higher strains and lower temperatures. Further work is warranted in this regard.

It has been shown that deformation at temperatures below M_f proceeds by martensite variant reorientation and detwinning mechanisms [30, 42]]. Liu *et al.* [30] and Zheng and Liu [43] have suggested two different detwinning mechanisms based on a recent theoretical analysis: (1) domino detwinning and (2) assisted detwinning. They propose that domino detwinning occurs at a constant external load, after its onset in a finite volume. On the other hand, assisted detwinning requires a continuous increase in the external force to advance further deformation and occurs beyond the stress-plateau region. The stress-plateaus obtained in the tensile tests (see Figure 4.4b) are not entirely flat, and have regions of finite, positive slopes, identified in the curves. Another interpretation would lead us to conclude that the stress-plateau exists only for a small strain range. Liu *et al*. [30] also suggest that the end of domino detwinning

corresponds to the stress-plateau termination. When applied to the curves in Figure 4.4b, this means that assisted detwinning sets in early on, i.e., at small total strain during the dynamic deformation.

The phenomenology of the "domino" and/or assisted detwinning appear to exhibit many features in common with previous twinning studies of "autocatalytic" or "polysynthetic" twinning (PST), where twin formation from adjacent existing twins is seen to occur [44-46]. In particular, the spontaneous reversal of elastic twins in geologic materials such as calcite, twinning in metals like antimony, and most recently "PST-like" twinning in intermetallics, pose some intriguing similarities and ideas to pursue. Further, the observation of deformation twins triggering adjacent new twin formation during plastic deformation is also similar to some observations of twinning in body-centered-cubic (BCC) metals [47, 48]. In BCC metals, it can occur where 1/6<111> twinning partials can cross-slip from one {112} plane to another {121} plane containing the twinning vector. In-depth defect analysis to examine the twinning and dislocation mechanisms coincident with the stress plateau in shape memory alloys should help to elucidate this matter.

Although the superelastic range in the present NiTi is A_f (*2*°C) < T < M_d (150°C), it should be noted that the superelastic behavior was seen in the tension and compression curves at 0°C. Similar to the stress-strain curve under quasi-static conditions, the high strain rate compression and tension exhibit the stress-plateau characteristic. This supports that the SIM transformation occurs at 0°C. Since 0°C lies outside the superelastic range, it is prudent to ask why the SIM transformation still occurs. One possibility may be related to the specimen's temperature rise under high

strain rate deformation. Under dynamic deformation conditions and large plastic deformation, the specimen is in a near adiabatic condition, where the heat energy transformed from the plastic deformation is not conducted away due to the limited time available for heat dissipation. Thus, the specimen temperature could increase substantially during the test. For example, Miller *et al.* [21] noted a temperature rise (using a K-type fast response thermocouple) between 22 ~ 48°C for a SMA specimen deformed dynamically at strain rates between 1200-2300/s. Such a large temperature increase may lead to the reverse transformation, M $\rightarrow$ A, and bring the alloy into its superelastic range, even though the specimen is surrounded by the cooling liquid.

4.4.4 Compression–tension asymmetry

Even though the compression-tension asymmetry under quasi-static strain rate has been investigated in single crystal and polycrystalline SMA [7, 18, 27, 35-37, 50-53], to the authors' knowledge, there has been no report on the compression-tension asymmetry under high strain rate loading to date. Compression-tension asymmetry in thermally-induced martensite (TIM), superelastic (SE) austenite and stable austenite has been studied here under low- and high- strain rate deformation, and an effort is made to understand the effect of temperature on this asymmetry. Figure 4.5(a-d) depict typical quasi-static and dynamic stress-strain responses of SMA under compression and tension and illustrate the effect of temperature on the compression-tension asymmetry. The temperature interval between each plot is ~200^{o}C, beginning with -196^{o}C and ending with 400^{o}C.

With increasing test temperature, the asymmetry between compression and tension decreases under both low and high strain rate testing. For example, there is a considerable difference between compression and tension curves at -196°C (see Figure 4.5(a)), while at 400°C (see Figure 4.5(d)), the difference is not substantial, especially during the first 5% strain. However, the magnitude of decrease in compression-tension asymmetry is greater under dynamic conditions than quasi-static strain rate. Moreover, the work hardening rate in both compression and tension does not vary with increase in strain-rate from 10^{-3}/s to 1200/s, *i.e.*, either in compression or tension, the dynamic flow curve is obtained by simply shifting the quasi-static flow curve in a parallel fashion, with the flow stress being higher under dynamic loading. The compression-tension asymmetry is qualitatively analyzed using a critical stress concept, σ_{cr}, which is determined by a stress value of 0.2% strain offset in the stress-strain curve. The critical stress, σ_{cr}, is typically the yield stress of austenite in the high temperature tests, or martensite in the low temperature tests.

When the test temperature is in the superelastic range, $A_f \sim M_d$ (for example, RT and 100°C), stress-induced martensite phase transformation occurs during the deformation and consequently, this critical stress corresponds to the onset of the SIM transformation, *i.e.*, it is the stress required to induce the martensite transformation [36]. Figure 4.6 captures the asymmetry of tension-compression in the variation of critical stress in tension and compression with temperature, at both quasi-static and dynamic strain rates. Under dynamic loading at low temperatures ($T < M_s$), within stage I, the critical stress does not vary significantly. When $T < M_s$, the SMA alloy is in the martensitic phase, and the detwinning mechanism of thermally-induced

martensite is dominant during deformation in this regime [30]. Following stage I is the SIM transformation of stage II (RT and 100°C tests), where the critical stress increases with increasing temperature. At elevated temperatures ($T > M_d$), the specimen is in a fully austenitic phase and deforms by slip, and the critical stress was observed to decrease with increasing temperature in stage III. The critical stress *vs.* temperature trend obtained in both the compression and tension tests exhibits a three-stage characteristic, with the critical stress level being distinctly higher in compression than in tension. It is generally agreed that, under quasi-static deformation rates, the SMA deforms through martensite reorientation (or detwinning) at low temperatures, stress-induced martensite transformation at intermediate temperatures (superelastic range), and finally by slip in austenite at high temperatures [40]. However, there are three striking characteristic differences between the dynamic and quasi-static 0.2% critical stress variation with temperature. First, the slope in the SIM region is ~6 MPa/^{o}C under dynamic loading, while it is nearly half that value, ~3 MPa/^{o}C, under low-strain rate testing. Second, the 0.2% critical stress values under dynamic tension are roughly ~100-200 MPa greater than the quasi-static tension values, whereas, the dynamic compression values are nearly twice as high as the quasi-static compression values, with the largest difference (~600MPa) occurring at 100^{o}C. The third and perhaps the most striking difference is the behavior of 0.2% critical stress in region III. While the yield strength remains nearly temperature independent under quasi-static loading between 100^{o}C – 400^{o}C, it decreases linearly with temperature under dynamic loading. In addition, within the same temperature interval, the small difference in the yield values in compression and tension at low strain rate is observed to be quite large under

dynamic loading. At lower temperatures, where either TIM or SIM formation is possible, it is generally believed that the compression-tension asymmetry is due to the selective formation of different SIM variants between tension and compression, with larger number of variants being available in tension than in compression [35]. If the material exists as a single austenite phase between 200^{o}C to 400^{o}C, it is unclear why there should be such a large asymmetry between compression and tension at higher deformation temperatures.

The unloading portion of the stress-strain curve also provides some interesting insight in the mechanical response of the NiTi SMA. It is pointed out that this unloading curve is influenced by test temperature and stress state (compressive *vs.* tensile). For instance, the compressive unloading curve tends to be perfectly elastic (see Figure 4.5c-d) at elevated temperatures, while it is non-linear at low temperature (e.g., 0^{o}C, see Figure 4.5b). This response reflects the recoverable strain behavior of the SMA. As suggested by Sehitoglu *et al.* [39], the unloading stress-strain response of the SMA is associated with the elastic strain and recoverable strain (both pseudoelastic strain associated with the reverse transformation M $\rightarrow$ A and SME strain obtained by heating at zero stress). When the unloading stress-strain curve is completely linear, only the elastic deformation strain is released and no recoverable strain can be identified from the deformation. If the unloading curve is linear initially and then displays pseudoelastic behavior by unloading to lower strains than suggested by the elastic part of the unloading curve, then it has undergone the reverse transformation, M $\rightarrow$ A. The reverse phase transformation from SIM to austenite in tension is identified by the unloading stress-strain response of the SMA in Figure 4.7

at temperatures 0°C and RT. Moreover, unlike other unloading stress-strain curves obtained at low and elevated temperatures, the curves in Figure 4.7 show a complex stress-strain response at the beginning (overlapping) and at the end (oscillations) of unloading. Hence, as mentioned earlier, a SIM transformation took place in the superelastic temperature range and at 0°C, and the martensite thus formed during the loading process transformed back to the parent austenite during unloading to the stress-free state. The unloading portions of the tensile curves in Figure 4.7 clearly indicated such reverse phase transformation. Further evidence of martensitic transformation was also confirmed by the observation of twins in the post-deformed samples under a TEM. A detailed TEM study of the post-deformed microstructures observed in the current work is currently underway. The SMA was in the austenitic state at 200°C, 300°C and 400°C throughout the loading and unloading process, and hence a reverse phase transformation is never observed upon loading. Similarly, at low temperatures, the SMA was in the (thermally-induced) martensitic state throughout loading and unloading, and therefore, the unloading region of stress-strain does not show this reverse phase transformation.

4.5 Conclusions

Compression and tension tests were performed with a large total strain of up to 16 - 24% at a high strain rate of ~1200/s and low strain rate of 0.001/s at various temperatures. The aim of this work was to investigate the effect of test temperature on the stress-strain response and compression-tension asymmetry of NiTi SMA subjected

to both dynamic and quasi-static loading. The current experimental results support the following conclusions:

(1) In spite of large differences in strength levels occurring due to various transformations, all the dynamic compression tests were successfully conducted at a constant strain rate of ~1200/s for the entire duration of the loading.

(2) The effect of temperature on the stress-strain response of NiTi SMA is strongly dependent upon stress state (compressive *vs.* tensile). The flow stress is much higher in compression than in tension. In compression, the flow stress decreases with increasing temperature at elevated temperatures. In tension, the strength of the SMA is lower at RT and 100^{o}C than at other elevated temperatures due to the SIM transformation. A reverse phase transformation from SIM to austenite was identified by the unloading part of the stress-strain curves at RT and 100°C and corroborated by TEM observations.

(3) The compression-tension asymmetry is strongly dependent upon temperature. The critical stress (determined by 0.2% strain offset) *vs.* temperature exhibits a three-stage characteristic both in compression and tension, with the critical stress being higher in compression than in tension.

(4) The slope in the SIM region is ~6 MPa/^{o}C under dynamic loading, while it is nearly half that value, ~3 MPa/^{o}C, under low-strain rate testing.

(5) The 0.2% critical stress values under dynamic tension are roughly ~100-200 MPa greater than the quasi-static tension values, whereas the dynamic compression values are nearly twice as high as the quasi-static compression values, with the largest difference occurring at 100^{o}C.

(6) The most striking difference is the behavior of the 0.2% critical stress in region III – while the yield strength remains nearly temperature independent under quasi-static loading from 100^{o}C to 400^{o}C; it decreases linearly with temperature under dynamic loading. In addition, the small difference in the yield values in compression and tension at low strain rate is exacerbated under dynamic loading (between 100^{o}C to 400^{o}C).

4.6 Acknowledgements

Chapter 4, in full, is a reprint of the material as it appears in Acta Materialia as Raghavendra R. Adharapurapu, Fengchun Jiang, Kenneth S. Vecchio, George T. Gray III, "Response of NiTi Shape Memory Alloy at High Strain Rate: A Systematic Investigation of Temperature Effects on Tension-Compression Asymmetry", Acta Materialia, Vol. 54, pp. 4609-4620, 2006. The dissertation author was the primary investigator and author of this paper.

4.7 Figures

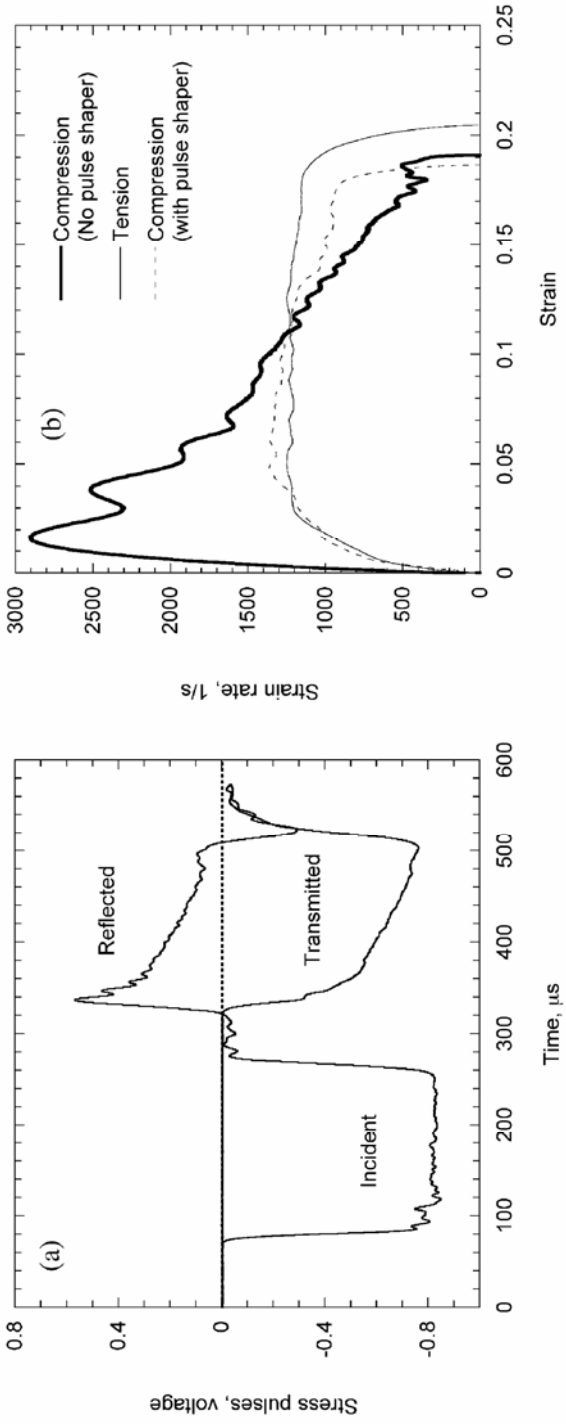

Figure 4.1 (a) Typical stress pulses on SMA in a Hopkinson pressure bar test without pulse shaper. (b) Typical strain rates of SMA specimen as a function of strain under tension and compression (without and with pulse shaper).

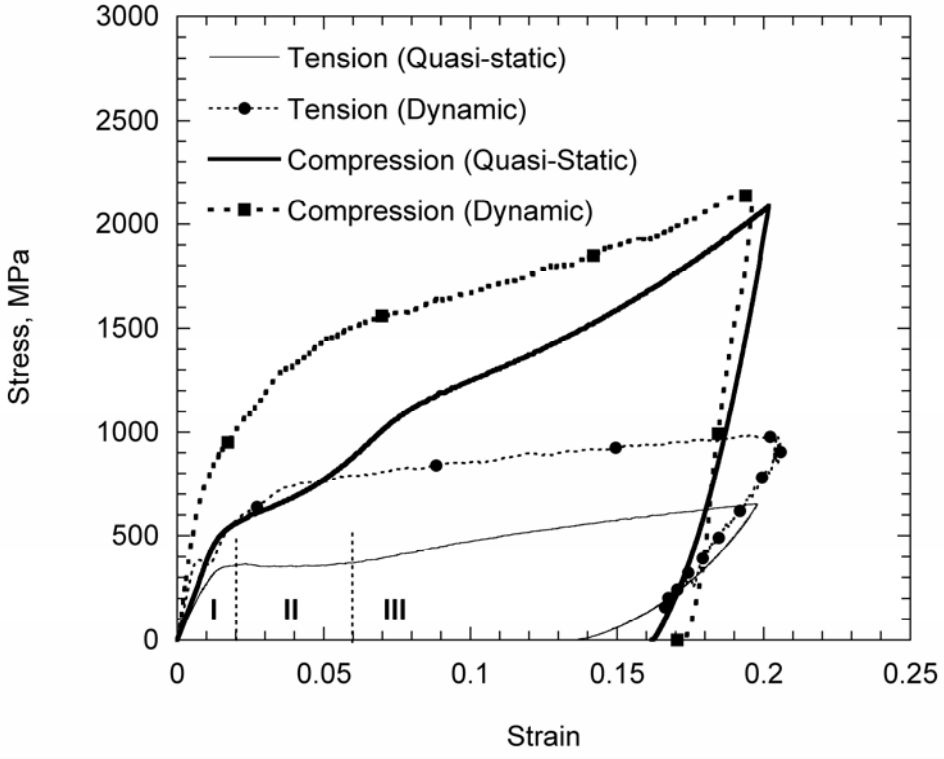

Figure 4.2 Stress-strain curves of compression and tension at room temperature: quasi-static strain rate of 10^{-3}/s, and dynamic (high strain rate of ~1200/s). The figure also shows the stress-strain three-stage characteristic of austenite SMA under (quasi-static) tension and compression.

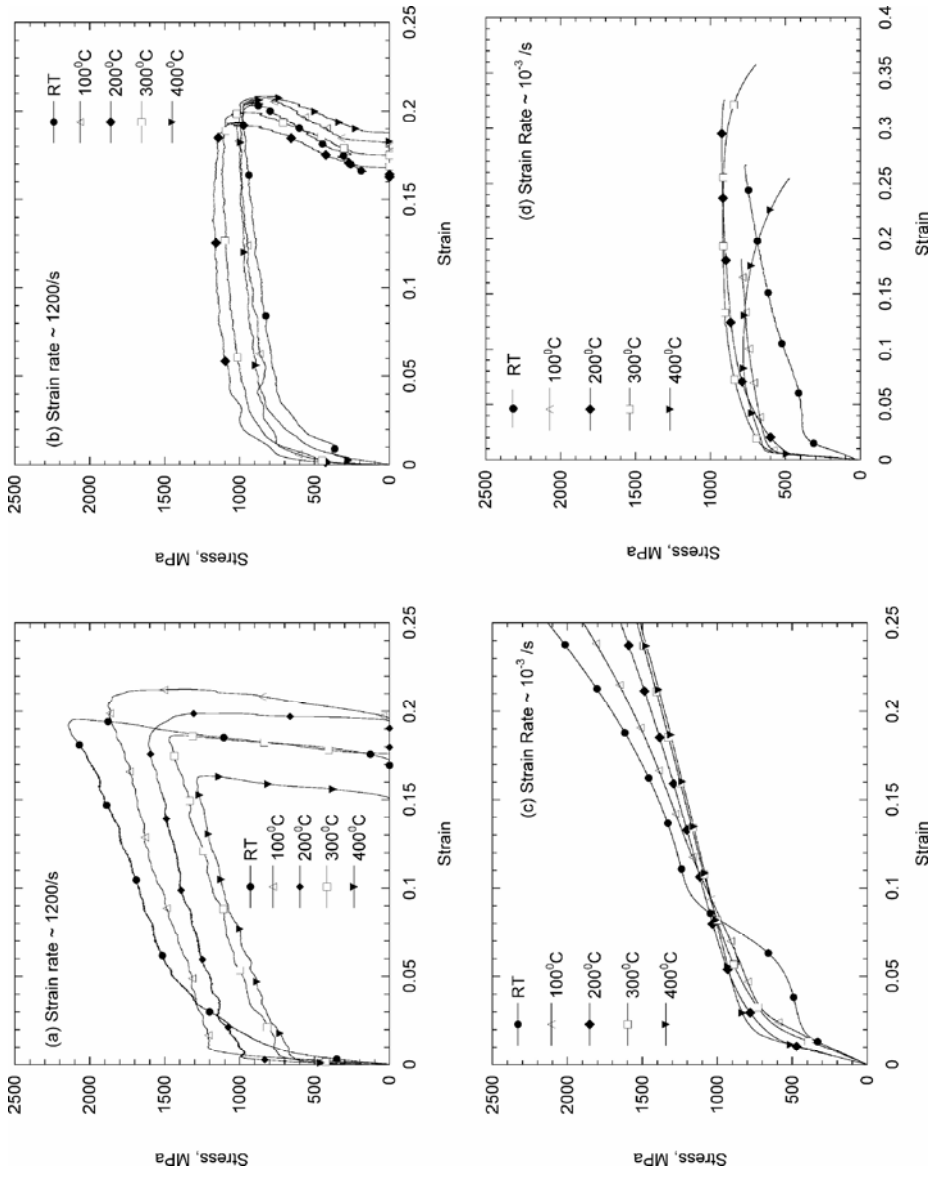

Figure 4.3 Stress-strain curves of NiTi SMA under high temperatures at strain rate ~ 1200/s: (a) compression and (b) tension; at a strain rate of 0.001/s: (c) compression and (d) tension.

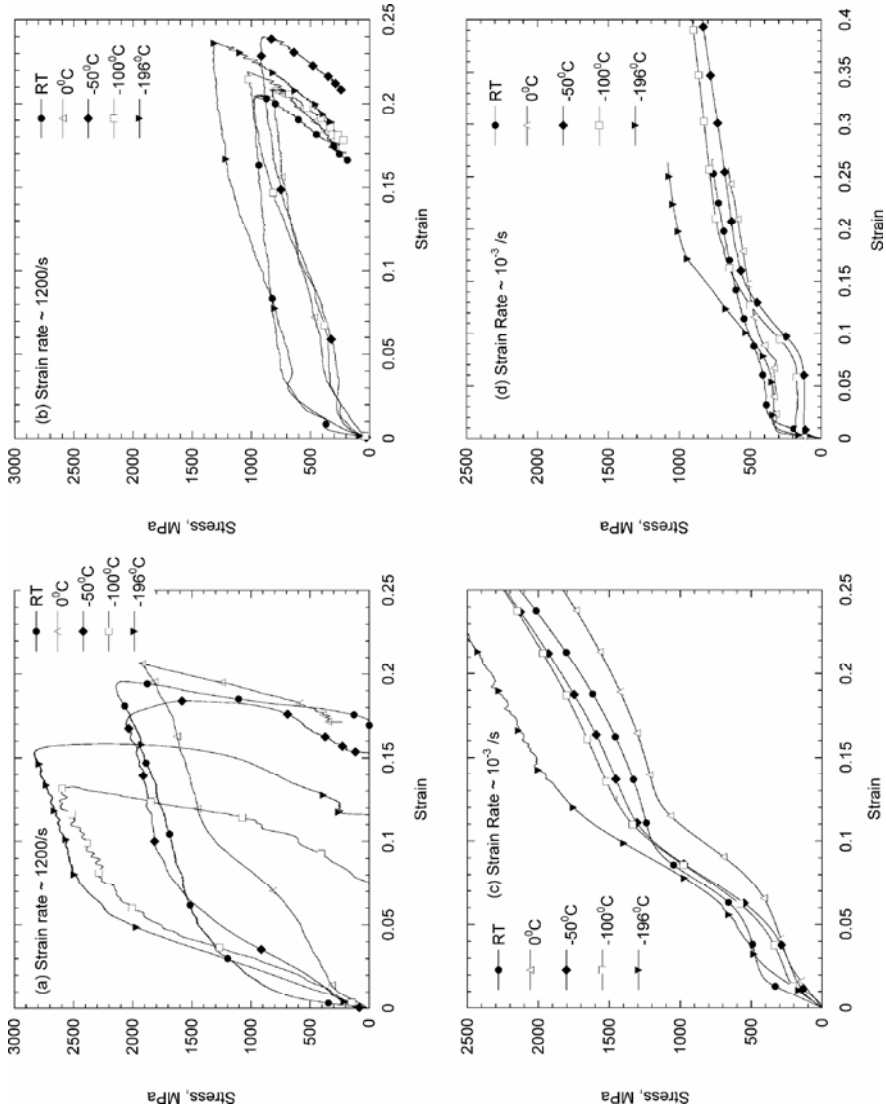

Figure 4.4 Stress-strain curves of NiTi SMA at low temperatures at a strain rate of ~1200/s: (a) compression and (b) tension; at a strain rate of 0.001/s: (c) compression and (d) tension.

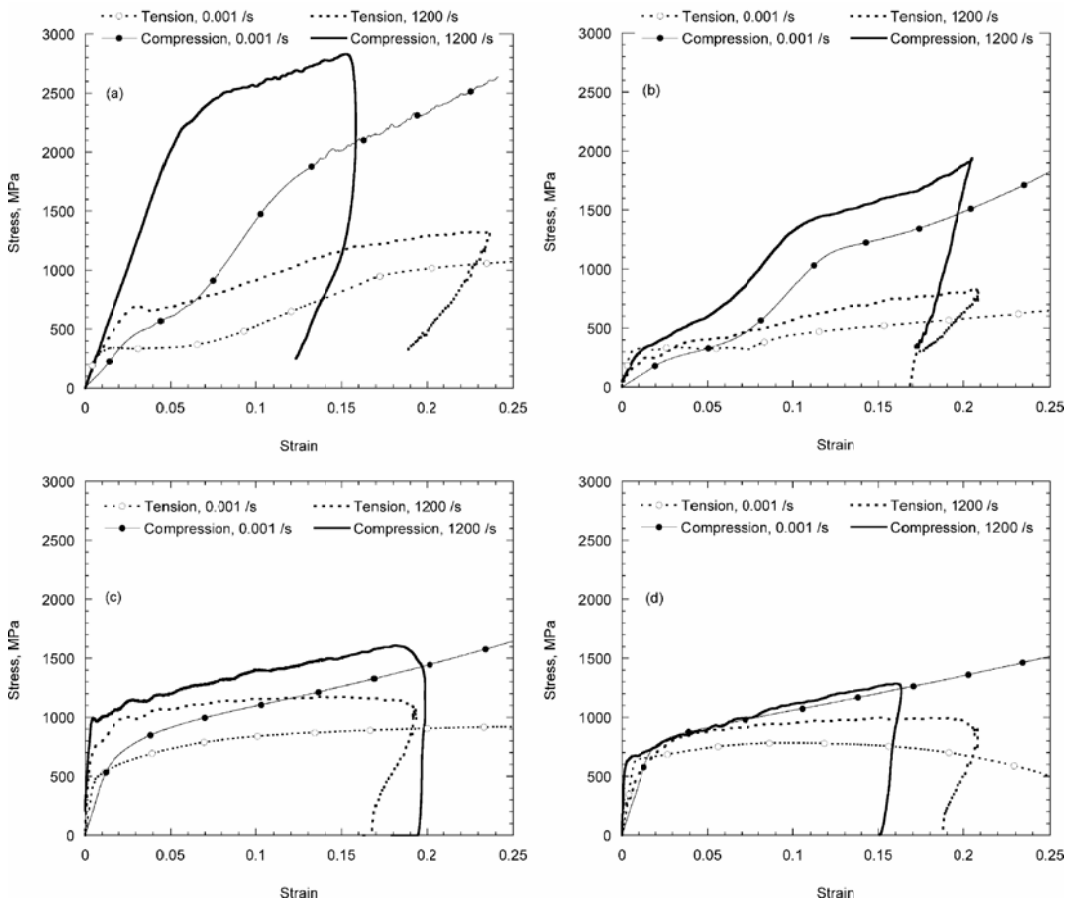

Figure 4.5 Compression and tension stress-strain curves of SMA NiTi, showing the effect of temperature on compression-tension asymmetry at dynamic and quasi-static strain rates. Note the elimination of asymmetry at higher temperature. (a) -196^{o}C (b) 0^{o}C (c) 200^{o}C (d) 400^{o}C

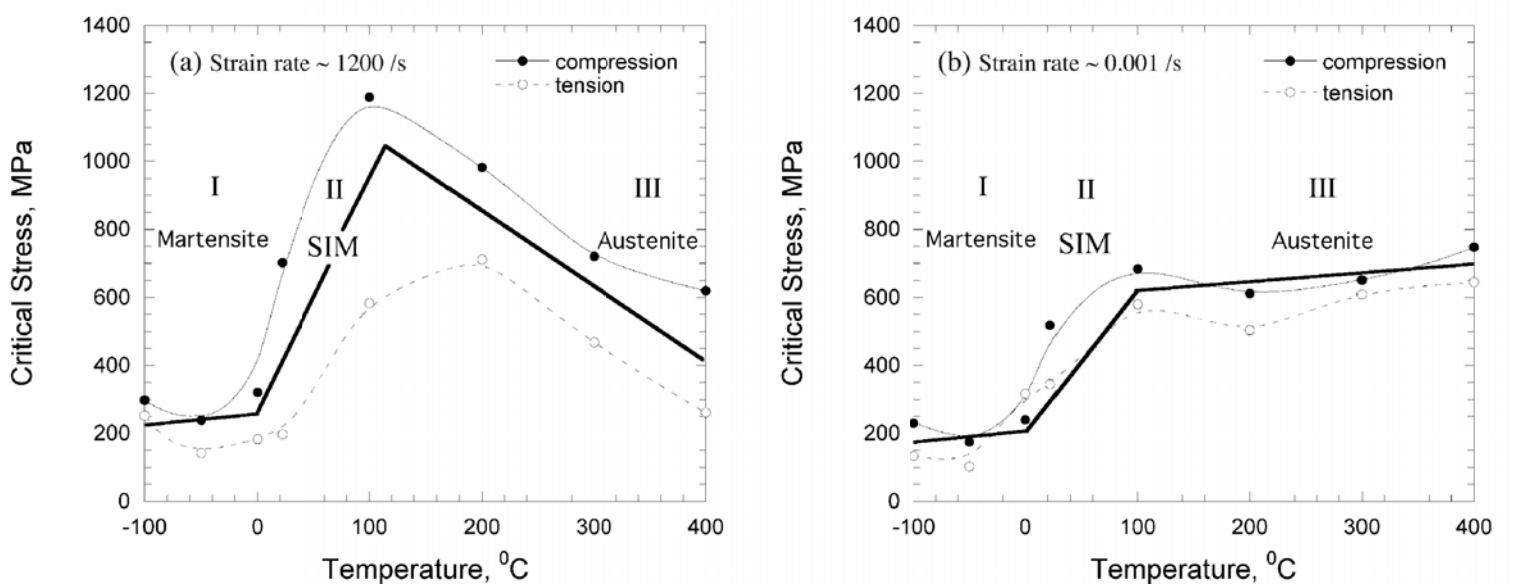

Figure 4.6 Variation of critical stress as a function of test temperature in compression and tension. Critical stress is determined by 0.2% strain offset in stress-strain curve. (a) Dynamic loading rate, (b) quasi-static loading rate.

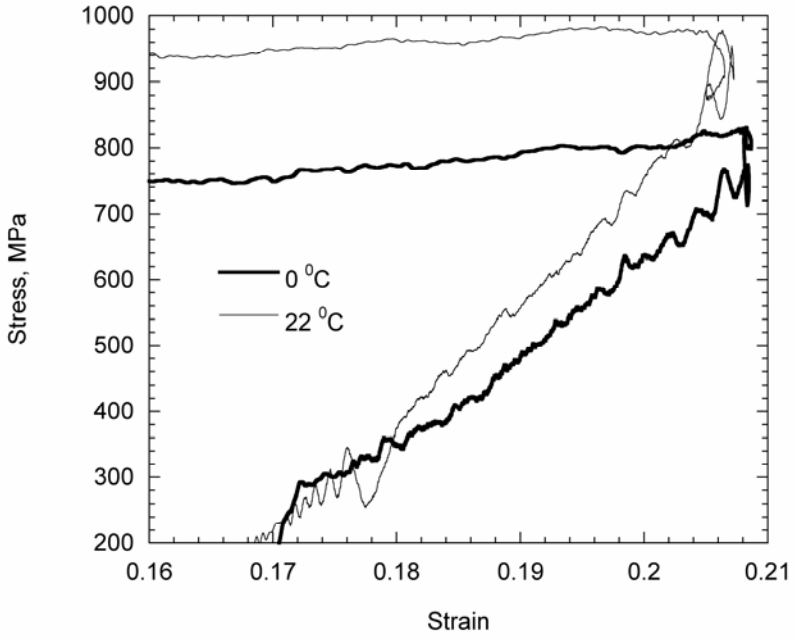

Figure 4.7 Unloading dynamic tensile stress-strain response of SMA, showing a reverse phase transformation from SIM to austenite at 0°C and 22°C.

4.8 References

1. Chang, L.C. and R.A. Read, *Plastic deformation and diffusionless phase changes in metals - The gold-cadmium beta phase.* Trans. AIME, 1951. **189**: p. 47-52.

2. Tadaki, T., K. Otsuka and K. Shimizu, *Shape Memory Alloys.* Ann. Rev. Mater. Sci., 1988. **18**: p. 25-45.

3. Wayman, C.M., *Shape memory and related phenomena.* Progress in Materials Science, 1992. **36**: p. 203-224.

4. Van Humbeeck, J., *Shape memory alloys: A material and a technology.* Advanced Engineering Materials, 2001. **3**(11): p. 837-850.

5. Fugazza, D., *Shape-memory alloy devices in earthquake engineering: Mechanical properties, constitutive modeling and numerical simulations,* in *Earthquake Engineering,* 2003. Universita degli Studi di Pavia: Pavia. p. 141.

6. Otsuka, K. and C.M. Wayman, eds. *Shape memory materials*. 1998, Cambridge University Press.

7. Bhattacharya, K., *Microstructure of martensite: why it forms and how it gives rise to the shape-memory effect*. Oxford series on materials modeling, eds. Adrian P. Sutton and R. E. Rudd. 2003: Oxford University Press.

8. Buehler, W.J., J.V. Gilfrich and R.C. Wiley, *Effect of low-temperature phase changes on the mechanical properties of alloys near composition TiNi.* J. Appl. Phys., 1963. **34**: p. 1475-1477.

9. Rizner, A.G. and R.J. Wasilewski, *Tensile properties of NiAl and NiTi*, J. Inst. Metals, 1966. **94(5)**: p. 169-175

10. Wasilewski, R.J., *The effects of applied stress on the martensitic transformation in NiTi.* Metallurg. Trans., 1971. **2**: p. 2973-2981.

11. Miyazaki, S., K. Otsuka and Y. Suzuki, *Transformation pseudoelasticity and deformation behavior in a Ti-50.6 at% Ni alloy.* Scripta Metall., 1981. **15**: p. 287-292.

12. Shaw, J.A. and S. Kyriakides, *Thermomechanical aspects of NiTi.* Journal of the Mechanics and Physics of Solids, 1995. **43**(8): p. 1243-81.

13. Kobus, E., K. Neuking and G. Eggeler, *Creep behavior of a NiTi alloy and effect of creep pre-deformation on shape memory properties.* Sonderbaende der Praktischen Metallographie, 2000. **31**(Fortschritte in der Metallographie): p. 305-310.

14. Qidwai, A., A. Bhattacharya, I. Vahhi and S. Pulnev. *Initial investigation in actuator design using high-temperature shape memory alloy*. in *Proceedings of SPIE - The International Society for Optical Engineering*. 2003.

15. Lin, P.-H., H. Tobushi, K. Tanaka, T. Hattori and A. Ikai, *Influence of strain rate on deformation properties of TiNi shape memory alloy*. JSME Intl. J, 1996. **39**(1): p. 117-123.

16. Tobushi, J., Y. Shimeno, T. Hachisuka and K. Tanaka, *Influence of strain rate on superelastic properties of TiNi shape memory alloy.* Mech. Maters., 1998. **30**: p. 141-150.

17. Entemeyer, D., E. Patoor, A. Eberhardt and M. Berveiller, *Strain rate sensitivity in superelasticity.* Intl. J. Plasticity, 2000. **16**: p. 1269-1288.

18. Gall, K. and H. Sehitoglu, *The role of texture in tension-compression asymmetry in polycrystalline NiTi.* International Journal of Plasticity, 1999. **15**(1): p. 69-92.

19. Gall, K., H. Sehitoglu, Y.I. Chumlyakov, I.V. Kireeva and H.J. Maier, *The influence of aging on critical transformation stress levels and martensite start*

temperatures in NiTi: part II discussion of experimental results. Trans. ASME, 1999. **1217**(1): p. 28-37.

20. Chen, W.W., Q. Wu, J.H. Kang and N.A. Winfree, *Compressive superelastic behavio of a NiTi shape memory alloy at strain rates of 0.001-750 s^{-1}*. International Journal of Solids and Structures, 2001. **38**: p. 8989-8998.

21. Miller, D.A., W.R. Thissell and D.A.S. Macdougall, *Dynamic tensile plasticity damage evolution in shape-memory Ni-Ti.* J. Phys. IV France, 2000. **10**: p. 341-346.

22. J.C.F. Millet, N.K. Bourne and G.T. Gray III, *Behavior of the Shape Memory Alloy NiTi during One-Dimensional Shock Loading.* J. Appl. Phys., 2002. **92**(6): p. 3107-3110.

23. Liu, Y., Y. Liu and J.V. Humbeeck, *Luuders-like deformation associated with martensite reorientation in NiTi.* Scripta Materialia, 1998. **39**(8): p. 1047-1055.

24. Liu, Y., Z. Xie, J.V. Humbeeck and L. Delaey, *Some results on the detwinning process in NiTi shape memory alloys.* Scripta Materialia, 1999. **41**(12): p. 1273-1281.

25. Liu, Y., Z. Xie, J.V. Humbeeck and L. Delaey, *Deformation of shape memory alloys associated with twinned domain re-configurations.* Materials Science and Engineering A, 1999. **273-275**: p. 679-684.

26. Liu, Y., Z. Xie, J.V. Humbeeck, L. Delaey and Y. Liu, *On the deformation of the twinned domain in NiTi shape memory alloys.* Philosophical Magazine A, 2000. **80**(8): p. 1935-1953.

27. Liu, Y., Z. Xie, J.V. Humbeeck and L. Delaey, *Asymmetry of stress-strain curves under tension and compression for NiTi shape memory alloys.* Acta mater., 1998. **46**(12): p. 4325-4338.

28. Liu, Y., Y. Li, K.T. Ramesh and J.V. Humbeeck, *High strain rate deformation of martensitic NiTi shape memory alloy.* Scripta Materialia, 1999. **41**(1): p. 89-95.

29. Liu, Y., Y. Li and K.T. Ramesh, *Rate dependence of deformation mechanisms in a shape memory alloy.* Philosophical Magazine A: Physics of Condensed Matter: Structure, Defects and Mechanical Properties, 2002. **82**(12): p. 2461-2473.

30. Liu, Y., Y. Li, Z. Xie and K.T. Ramesh, *Dynamic deformation of shape-memory alloys: evidence of domino detwinning?* Philosophical Magazine Letters, 2002. **82**(9): p. 511-517.

31. Boyer, H.E. and T.L. Gall, eds. *Metals Handbook.* 9th ed. 1985, Ameican Society for Metals, Ohio. 190-207.

32. Frew, D.J., M.J. Forrestal and W. Chen, *Puse shaping technique for testing brittle materials with a split Hopkinson pressure bar.* Experimental Mechanics, 2002. **42**: p. 93-106.

33. Gray III, G.T., ed. *Classic Split-Hopkinson Pressure Bar Technique*. ASM-Handbook: Mechanical Testing and Evaluation, ed. H. Kuhn and D. Medlin. Vol. 8. 2000, ASM International: Metals Park, Ohio 44073-0002. 462-476.

34. Follansbee, P.S. and C. Frantz, *Wave propagation in the SHPB.* Trans. ASME: J. Engng. Mater. Technol., 1983. **105**: p. 61-66.

35. Plietsch, R. and K. Ehrlich, *Strength Differential effect in pseudoelastic NiTi shape memory alloys.* Acta mater., 1997. **45**(6): p. 2417-2424.

36. Gall, K., H. Sehitoglu, Y.I. Chumlyakov and I.V. Kireeva, *Tension-compression asymmetry of the stress-strain response in aged single crystal and polycrystalline NiTi.* Acta Mater., 1999. **47**: p. 1203-1217.

37. Orgeas, L. and D. Favier, *Non-symmetric tension-compression behavior of NiTi alloy.* Journal de Physique IV, 1995. **5**(C8, International Conference on Martensitic Transformations, Pt. 2): p. 605-10.

38. Orgeas, L. and D. Favier, *Stress-induced martensite transformation of a NiTi alloy in isothermal shear, tension and compression.* Acta mater., 1998. **46**: p. 5579-5591.

39. Sehitoglu, H., I. Karaman, R. Anderson, X. Zhang, K. Gall, H. J. Maier, and Y. Chumlyakov, *Compressive response of NiTi single crystals.* Acta mater., 2000. **48**: p. 3311-3326.

40. Jacobus, K., H. Sehitoglu and M. Balzer, *Effect of stress state on the stress-induced martensitic transformation in polycryall-T.* Metallurgical and Materials Transactions A, 1996. **27**: p. 3066-3073.

41. Brinson, L.C., I. Schmidt and R. Lammering, *Stress-induced transformation behavior of a polycrystalline NiTi shape memory alloy: micro and macromechanical investigations via in situ optical microscopy.* Journal of the Mechanics and Physics of Solids, 2004. **52**: p. 1549-1571.

42. Huseyin Sehitoglu, R. Hamilton, D. Canadinc, X. Y. Zhang, K. Gall, I. Karaman, Y. Chumlyakov, H. J. Maier, *Detwinning in NiTi Alloys.* Metallurgical and Materials Transactions A, 2003. **34**: p. 5-13

43. Zheng, Q.S. and Y. Liu, *Prediction of the detwinning anisotropy in textured NiTi shape memory alloy.* Philosophical Magazine A: Physics of Condensed Matter: Structure, Defects and Mechanical Properties, 2002. **82**(4): p. 665-683.

44. Klassen-Neklyudova, N. V., *Mechanical Twinning in Crystals*, Plenum Press, NY (1964)

45. Garber, R. I., *Residual Stresses in Plastically Deformed Crystals of Rocksalt*, Zhur. Eksptl. I. Theoret. Fiz., 1938. **8**(6): p. 746-752

46. Christian, J. W., and S. Mahajan, *Deformation Twinning*, Progress in Materials Science, 1995. **39**: p. 1-157

47. Boucher, N. A., and J. W. Christian, *The influence of pre-strain on deformatino twinning in niobium single crystals*, Acta Metallurgica, 1972. **20**: p. 581-591

48. Mahajan, S., *Twin-slip and twin-twin interactions in Mo-35 at.%Re alloy*, Philos. Mag., 1971. **23**: p. 781-794

49. Liu, Y., *On the detwinning mechanism in shape memory alloys*, Solid Mechanics and its Applications (IUTAM Symposium on Mechanics of Martensitic Phase Transformations in Solids, 2001), 2002. **101**: p. 37-44

50. Gao, S. and S. Yi, *Experimental study on the anisotropic behavior of textured NiTi pseudoelastic shape memory alloys.* Journal de Physique IV: Proceedings, 2003. **112**(International Conference on Martensitic Transformations, 2002, Part 2): p. 827-830.

51. Liu, Y., Z.L. Xie, J.V. Humbeeck and L. Delaey, *Effect of texture orientation on the martensite deformation of NiTi shape memory alloy sheet.* Acta Materialia, 1999. **47**(2): p. 645-660.

52. Sittner, P. and V. Novak, *Anisotropy of Cu-Based shape memory alloys in tension/compression thermomechanical loads.* Journal of Engineering Materials and Technology, 1999. **121**(1): p. 48-55.

53. Zheng, Q. and Y. Liu, *Anisotropy of detwinning process in textured NiTi shape memory alloy.* Proceedings of SPIE-The International Society for Optical Engineering, 2000. **3992**(Active Materials: Behavior and Mechanics): p. 560-571.

5 HIGH-STRAIN RATE RESPONSE OF 50.8-NITI: INFLUENCE OF THERMOMECHANICAL TREATMENT AND TEXTURE

5.1 Abstract

There is a growing interest in exploring bulk NiTi alloys for structural and high-strain rate applications, such as energy absorbing structures under impact or seismic loading conditions, where different geometries of NiTi in the form of cylindrical, sheet, tube and even porous geometries may be employed. However, the response of NiTi is dependent on the product form (rod, sheet or tube) through their respective textures and thermomechanical processing history. In the current work, we present the high-strain rate response of 50.8-NiTi in rod and sheet forms between –196°C and 400°C under tensile loading at ~1200/s strain rate. We further compare the dynamic results with corresponding behavior observed at quasi-static strain rates (~10^{-3}/s). To examine the influence of texture, the stress-strain behavior of the sheet is measured parallel and perpendicular to the rolling direction (longitudinal (L) and transverse (T), respectively), and to study the influence of thermomechanical treatment, the properties of cold-worked+annealed sheet material is compared to the solution-treated (ST) rod. Finally, based on the fractography observations, the influence of strain rate on the fracture mechanisms are interpreted.

5.2 Introduction

Development of NiTi in bio-medical applications [1], such as stents and other implants, where its superelastic behavior is of primary importance, and the utilization

of its shape memory property in smart actuators and other non-medical applications [2, 3] has occurred in large strides in the past two decades. As further avenues of "smart" applications are explored, more recent investigations have looked at seismic protection of structures [4-6], and there is a growing interest in the exploitation of Nitinol towards high-strain rate applications such as energy-absorbing structures [7]. The topology of these energy absorbing sandwich structures usually consists of core truss elements in the form of cylindrical pins, tubes or sheets in various complex geometries that optimize performance [8-10]. It is known that the truss members of these sandwich structures typically experience tension or compression loading conditions suggesting that the behavior of the overall structure critically depends on the compressive and tensile behavior of the individual truss elements. However, several studies have shown that Ni-Ti alloys exhibit a pronounced tension-compression asymmetry, particularly, lower recoverable strains, higher 'plateau' or transformation stresses and non-flat plateau behavior under compression, that is a function of texture [11-18]. More recently, this asymmetry in compression-tension behavior was also shown to affected by both temperature and strain-rate [18]. The effect of hydrostatic pressure and the three-dimensional state of stress on the stress-induced transformation in Ni-Ti alloys has also been investigated by several authors, who concluded that larger hydrostatic pressures increase the effective transformation stress [19-23]. Thus, since the optimization of the entire sandwich truss structure is sought and, additionally, depending on the product form (such as rod, sheet or tube), the texture and hence dynamic response may vary significantly, the current work addresses the

difference in dynamic response at high-strain rates for sheet material parallel and perpendicular to the rolling direction (RD).

5.3 Textures in Ni-Ti alloys

Earlier work on texture effects in polycrystalline NiTi alloys [15, 24-39] have shown the strong influence of texture on the shape memory and mechanical properties in different product forms such as rolled plate, sheet, tube and rod stock. Textures typically arise during processing through drawing, rolling, extrusion, solidification and sputtering. Interestingly, Shu and Bhattacharya [28] argue that texture formation is very desirable in Ni-Ti alloys for improving the recoverable strains, whereas detrimental in similar Cu-base shape memory alloys. Some of the common textures observed in bcc materials are indicated in Table 5.1. It has been shown that α-fiber I rolling texture gives the largest uniaxial recoverable strains in the rolling direction (RD) and, transverse direction (TD) (ideal for uniaxial applications) and γ-fiber texture gives uniform in-plane isotropic recoverable strains (thus ideal in multi-axial applications) [27, 28]. Several textures, similar to those observed in rolled and/or recrystallized bcc alloys, have been reported in the literature for NiTi alloys; the important ones are listed below.

1968 De Lange et al. [40] : {111}<110>

1979 Monasevich et al. [24]: {112}<110> (hot-rolled sheet)

1990 Eucken and Hirsch [41] and Mulder et al. [26] : {110}<110>

1990a Li et al. [25] $\{111\}<\bar{1}\,\bar{1}\,2>$ (annealed at 820^{o}C-10min + age 500^{o}C 1.5hrs)

1990b Li et al. [25] {111}<$\bar{2}\,\bar{1}\,3$> (annealed at 820°C-5hrs + age 500°C 1.5hrs)

1993 Mulder et al. [26]: (111}<110>

1996 Inoue et al. [27]: <110>||RD partial fiber and <111>||ND fiber textures, either is strengthened based on thermomechanical treatment. Under special rolling conditions, {112}<110> becomes intense.

1997 Zhao [42]: Combination of {110}<110> and {110}<110> components, relative amount governed by rolling temperature: Cold-rolling (in martensitic phase) produces a dominant {110}<110>, warm-rolling at 300°C (austenite) produced a dominant {111}<110>.

1999 Liu et al. [43]: {110}<110>

2004 Fernandes et al. [44]: α-fiber II <110>||RD texture (annealed below 400°C), above 400°C, {111}<110> component is strengthened.

2004-2006 Robertson et al. [37, 39, 45]: {221}<<122> in tubes, {111}<112>, {221}<110> and {110}<110> in sheet and {110}<110> and {100}<011> in rod geometries.

Thus, it appears that partial α-fiber II and γ fiber texture components are more common in bcc Ni-Ti alloys, with a spread among other possible components observed in bcc rolling and/or recrystallization textures. Due to the lattice correspondence between the austenite and martensite phases, the texture of the martensite phase arising from the parent phase, due to the selection of self-accommodating variants, can be calculated, see Miyazaki *et al.* [46, 47] and Zhao [42].

Table 5.1 Typical texture observed in bcc materials. {hkl}<uvw> indicates that {hkl} planes are parallel to the rolling plane and <uvw> directions are parallel to RD [28, 48].

Texture	{hkl}||Rolling Plane	<uvw>||Rolling Direction	Components
A-fiber I	{11j}, j ≥ 1	<110>||RD	{001}<110> {112}<110> {111}<110>
A-fiber II	{11j}, j ≤ 1	<110>	{111}<110> {110}<110>
γ-fiber	{111}	<11j>	{111}<110> {111}<112>
η-fiber	{0j1}, j ≤ 1	<100>	{001}<100> {011}<100>

It was found that the starting texture triggers different martensite variants at different rates in tension and compression, thus leading to compression-tension asymmetry [15]. Additionally, the texture was also seen to influence the deformation mode of martensitic NiTi shape memory alloy [43]. Despite the apparent significance of texture on the response of NiTi, there have been no studies that compare the high-strain rate response of NiTi with respect to different product forms, such as sheet and drawn rod. The known studies include: (i) [49], in which dynamic response was studied under compression in superelastic NiTi, (ii) [50-52], where high-strain rate response was studied under compression and tension in martensitic NiTi and, (iii) [18], where systematic study of temperature effects on the compression-tension asymmetry at high-strain rate loading was conducted in both martensitic and superelastic NiTi under fully annealed conditions.

Although, the superelastic properties of the NiTi shape memory alloys are very attractive, the alloy's functional properties are sensitive to various parameters such as

alloy chemical composition (specifically, Ni-content) and thermomechanical processing history that affect the transformation temperatures and the mechanical properties. Additionally, superelasticity occurs only between a narrow window of temperatures ($A_f < T < M_d$), with the variation of the superelastic plateau stress with respect to the temperature (also termed stress-rate, $d\sigma/dT$) ranging between 3 and 20MPa/^oC [53]. It is one of the goals of the present study to examine the variation of the stress-rate with respect to texture, heat-treatment (specifically, due to precipitation hardening) and strain-rate. Moreover, the increase in deformation strain-rate not only affects the stress-induced martensite (SIM) in terms of generation of Lüder band phase fronts [54-56] (due to the kinetics of the transformation), but also increases self-heating due to the latent heat involved in the austenite → martensite transformation, combined with the adiabatic (under high strain rate) rather than isothermal conditions [57]. Indeed, studies have indicated an increase in the specimen temperature between 5^{o}C and 50^{o}C for a change in strain-rate between 500/s to 2300/s [58, 59]; a more recent study has observed an increase of 40K for 0.1/s strain rates [57].

Typically, rolled sheet/plate, drawn rod and extruded tube represent the most common products of NiTi alloys, refer to Roberston *et al.* [37]. While, the influence of rolling texture and cold-work on the overall shape memory characteristics, under quasi-static strain rates, have been investigated exhaustively in the past, most of the high-strain rate investigations in the literature have been conducted on solution-treated near-equiatomic NiTi alloys. Consequently, the aim of the present investigation is to study the tensile dynamic response of NiTi (at ~1200/s) in different product forms, specifically, rolled sheet and drawn rod. It is also the objective of this paper to study

the influence of strain rate on the transformation plateau characteristics of both sheet and rod, and accordingly, tensile tests were conducted at quasi-static (0.001/s) and high-strain rates (1200/s). The influence of texture on the dynamic response of Nitinol is studied by testing 50.8-NiTi in the sheet form at low- and high-strain rates along rolling (L) and transverse (T) directions. Furthermore, by conducting the afore-mentioned tests between –196^{o}C and 400^{o}C, the dynamic response of martensitic, superelastic-austenite and stable-austenite are studied. Thus, the objectives are:

1. To conduct accurate (i.e. constant strain rate) high-strain rate tests on 50.8-NiTi SMA in *sheet geometry*.

2. To study the behavior of 50.8-NiTi sheet as a function of temperature (-196^{o}C to 400^{o}C) and strain rate (0.001/s and 1200/s).

3. To investigate the role of texture on the superelastic and shape-memory characteristics by calculating the stress-rate ($d\sigma/dT$) variation for specimen loaded parallel (L) and perpendicular (T) to the sheet rolling direction.

4. To quantify the role of thermomechanical treatment in Ni-rich 50.8-NiTi by comparing the quasi-static and dynamic tensile results between the fully-annealed (ST) 50.8-NiTi and the cold-rolled+annealed 50.8-NiTi sheet as a function of temperature (-196^{o}C to 400^{o}C)

5. To interpret the fracture mechanisms based on fractographic observations

5.4 Experimental

5.4.1 Materials and microstructure

Ni-rich 50.8-NiTi in the form of 12.7 mm drawn rod was obtained from *Nitinol Devices and Components, Inc.* (*NDC, Fremont, CA*). The rod material was obtained in fully annealed condition, i.e., annealed at 800^{o}C for 30-min. This heat treatment recrystallizes the alloy, thus removing any prior cold-work, as well as dissolving the hardening precipitates (Ti_3Ni_4). As indicated in Table 5.2, the austenite finish temperature, A_f = 2^{o}C, indicates that the alloy is in superelastic austenitic condition at room temperature (20^{o}C). Additionally, the differential scanning calorimetry (DSC) scan showed only one transformation peak under cooling and heating, suggesting a direct transformation between B2 austenite (A) ↔ B19' martensite (M).

In addition to the rod stock, 50.8-NiTi was also obtained in the form of rolled sheet of 1-mm thickness from *Johnson Matthey (San Jose, CA)*. The Nitinol sheet was processed through a thermomechanical treatment involving 10-30% cold-work followed by a typical ~510^{o}C-525^{o}C aging treatment for 5-10 minutes that optimizes the superelastic characteristics. Optical micrographs of the as-received material for sheet and rod product are presented in Figure 5.1(a) and (c), respectively, and the specific transformation temperatures are indicated in Table 5.2.

Table 5.2 Transformation temperatures measured in as-received NiTi rod and sheet.

Material	Transformation temperatures, °C*						Grain size, um	Texture
50.8-NiTi AR Sheet	R_s (A-R)	R_f (A-R)	M_s (R-M1)	M_f (R-M2)	R_s' (M-R)	A_f (R-A)	10**	Major {111}<110> {122}<110> Minor {111}<112> {110}<110>
	15.8	0	-40	< -100	-13.5	15.2		
50.8-NiTi Annealed Sheet (800°C, 1-hr)			M_s (A-M)	M_f (A-M)	A_s (M-A)	A_f (M-A)	40	{111}<110> (strengthened)
			-23	-7	4	21		
50.8-NiTi† ST Rod (800°C – 0.5hr)			-8	-36	-23	2	35	(111)-fiber {111}<101> {111}<112>

*The transformation temperatures are determined by a DSC with R_s, R_f, M_s, M_f and A_s, A_f being the R-phase, martensite (M) and austenite (A) start and finish temperatures, respectively. However, as discussed in the Results Section, the as-received alloy exhibits {(A⟶R) + (R⟶M1) + (R⟶M2) || (M⟶R) + (R⟶A)} forward || reverse transformation sequence, compared to the traditional {(A⟶M) || (M⟶A)} transformation.

**TEM observations by Robertson *et al. [39, 45]* revealed the existence of sub-grain structure of the order ~100 nm for similar NiTi sheet material.

† Drawn rod texture is adapted from [18] and the rolled sheet textures are compared with the measurements by Robertson *et al. [39, 45]*.

5.4.2 Starting Textures

Prior to the texture measurements, all the samples were heated above 60^{o}C and gradually cooled back to room temperature (20^{o}C) ensuring that the material is the fully austenitic condition. The texture in drawn NiTi rod (refer to Figure 5.3a for the reference frame) was measured at room temperature with electron back-scattered diffraction (EBSD) in a scanning electron microscope (SEM) utilizing INCA software from Oxford Instruments. The principal texture in the axial direction was measured to be a (111)-fiber type texture with the radial direction distributed primarily near <101> and <112> orientations [18].

Textures in 50.8-NiTi sheet material (refer to Figure 5.3b for the reference frame) were measured using X-ray diffraction method since the microstructure was heavily deformed due to prior thermomechanical treatment, which made it difficult to obtain and/or index the Kikuchi patterns in the EBSD. Thus, textures were measured in As-Received and fully-annealed conditions (800^{o}C-1hr) with a SCINTAG X1 XRD system, with a 4-circle goniometer utilizing Cu-Kα (λ=1.5405 Å) radiation source (40kV, 20mA). Samples measuring 15mm x 15mm x 1mm were cut from the as-received sheet and were aged at 550^{o}C (10-minutes) or 800^{o}C (1-hr) followed by water quenching. The samples were then polished to diamond finish and prepared for optical microscopy examination. The optical micrographs, shown in Figure 5.1, reveal the presence of 'needle' martensite in some grains produced due to the stresses applied during mechanical polishing. Additionally, annealing at 800^{o}C homogenizes the alloy

and causes recrystallization and grain growth, as shown in Figure 5.1(b); this heat-treatment produces an austenitic phase at room temperature.

The crystallographic texture of the austenitic phase was determined from three 'incomplete measured' pole figures of (110), (200) and (211), similar to Robertson *et al.* [37, 39, 45]. The X-ray intensities were background corrected and the orientation distribution function (ODF) was obtained using the popLA (preferred orientation package – Los Alamos) software package. The ODF were then used to calculate the (100), (110) and (111) pole figures (PF) and inverse pole figures (IPF), as shown in Figure 5.4 (equal area projection). As the data indicate, the sheet material exhibited partial <110>-type rolling texture similar to the α-fiber II texture; the {111} was the strongest normal direction (ND) component. With aging at 550^{o}C and 800^{o}C, the texture evolved by strengthening the {111}<110> component; similar strengthening behavior was independently reported by Robertson *et al.* [37, 39, 45] and Fernandes *et al.* [44] recently. The textures measured for both rod and sheet NiTi are summarized in Table 5.2.

5.4.3 DSC measurements

The phase transformation temperatures were measured using a cryo-differential scanning calorimeter (DSC) (Perkin Elmer Pyris 7 series) in a helium atmosphere. DSC samples typically measuring 50 mg were cut from the samples and sealed in Al pans and were heated to 80^{o}C and held for several minutes. Subsequently, complete heating and cooling cycles were performed between 80^{o}C and -110^{o}C at a rate of 10^{o}C/min. In order to identify individual phase transformations

(corresponding to different peaks on a DSC chart), partial heating and cooling cycles were performed with different starting and ending temperatures, as was necessary. In all the DSC scans, the top and the bottom curves represent the cooling and heating cycles, respectively.

5.4.4 Testing temperature

Tensile experiments were performed at low temperatures (-196, -100, -50 and 0°C), room temperature (RT; 20°C) and elevated temperatures (100, 200, 300 and 400°C). For all the tests, low temperatures were achieved by immersing the entire specimen in a low-temperature liquid bath containing methanol cooled by liquid nitrogen or in liquid nitrogen directly (-196°C), for ~20 minutes prior to testing and for the entire duration of the experiment. For high-temperature testing at high strain rate, an induction heating system was used to heat the specimen uniformly until the desired temperature set point was attained. Once the set point was attained, the specimen was held at that temperature for ~5-min to establish equilibrium and a uniform temperature through the entire gage section of the specimen. The temperature of the specimen was monitored by several thermocouples in both the low- and high-temperature testing, until the start of the test. High-temperature, low-strain-rate tension tests were performed using a high-temperature furnace installed on the servohydraulic load frame. In these tests, the specimen was held at the test temperature for ~30 min, until the thermocouple readings of the top and bottom portion of the specimen gage length were equalized.

5.4.5 Quasi-static and high-strain tests

Quasi-static tension tests were conducted using a servohydraulic load frame at a strain rate of 0.001/s. High strain rate tensile tests were conducted using a split Hopkinson tensile bar (19.05 mm diameter) at a nominal strain rate of ~1200/s. The incident and the reflected strain were measured by the strain gages glued at the midpoint of the incident bar, while the transmitted strain was measured by strain gages glued at the midpoint of the transmission bar. The dynamic stress, strain and strain rate were calculated using one-dimensional stress wave theory [60]. By the use of a momentum trap in the present Hopkinson bar setup, the specimen was loaded by a single stress pulse without being subjected to any additional reflected pulses. This facilitates a direct correlation between the microstructures and the mechanical response of the specimen. The specimens used in the tensile testing at quasi-static strain rates measured 6.4 mm diameter x 30 mm length for cylindrical geometry, whereas specimens measuring 30 mm length x 6.4 mm width x 1 mm thickness were machined from NiTi sheet. Cylindrical tensile specimens (from rod stock) with gauge section dimensions of 3.8 mm diameter x 11.5 mm length were used for the tensile tests at high strain rates, whereas the geometry of the sheet specimen used for dynamic testing is shown in Figure 5.5(a).

Thin rolled NiTi sheet, which is one of the most common processing form of the alloys, poses significant experimental challenge for conducting high-strain-rate tensile testing, due to the problems associated with samples small cross-sectional area, difficult gripping, and poor wave signals generally associated with dynamic tension testing. Additionally, difficulty in maintaining constant strain-rate conditions for the

duration of the entire test, including attainment of large strains to failure, represent another serious issue. In the present work, we have successfully overcome all of these challenges, to obtain acceptable dynamic responses for NiTi alloys in tension by modifying the sample gripping area in a split Hopkinson tensile bar as shown in Figure 5.5b. Figure 5.6a show different signal pulses recorded from the strain gages attached to the incident and the transmission bars during the dynamic testing of NiTi sheet at 300°C. The stress-strain curves and the strain rate are plotted as a function of strain, up to 25%, in Figure 5.6b. These curves indicate that constant strain rate of ~1200 /s has been achieved throughout the duration of the test for NiTi sheet, thus allowing an accurate comparison of high strain rate behavior between sheet and cylindrical geometries [18].

5.5 Results and Discussion

5.5.1 DSC measurements

The DSC trace in Figure 5.1(d) indicates that the sheet material is also in superelastic austenitic condition at room temperature; however, it exhibits a 3-stage/2-stage multiple stage transformations (MST) as evidenced by multiple peaks [61]. Figure 5.2(a-d) show in more detail the full and partial DSC scans of the AR 50.8-NiTi sheet material. The cooling cycle (top curve) exhibits three peaks 1-2-3 whereas the heating cycle (bottom curve) shows only two peaks, 4-5, thus showing a 3-stage/2-stage multiple stage transformation (MST). The partial cycle (b) indicates that 1 and 1' are B2→R phase and its reverse transformation, R→B2, respectively, since its temperature hysteresis is quite small (<10^{o}C) compared to the B2→B19' or R→B19'

transformation. The partial cooling cycle (c) partially terminates before the end of peak-2 and the heating cycle exhibits an enhancement in the transformation heat (represented by the area under the peak) of peak-1', resembling more closely to peak-5 in the full scan. The final partial cooling cycle (d) now includes a part of the stage-3 transformation and upon heating develops into the peak 4 (only seen as a partially formed shoulder). Furthermore, a full DSC scan between -100^{o}C to -40^{o}C (not shown) indicated the presence of only peak-3 and not peak-2, suggesting that peak-3 and peak-4 belong to a pair of the transformation. Since the 1 and 2 in the forward transformation correspond to peak-5, and peak-3 and peak-4 are a pair, peak-1 and peak-2 are A→R and R→M1 (martensite-1) transformations, respectively, and peak-3 is R→M2 (martensite-2) transformation. Peak-4 represents the reverse M2→R transformation, whereas peak-5 corresponds to an overlap of the M1→R and R→A transformations. Here A, R, M1 and M2 correspond to austenite, R-phase and martensite phases occurring in two different volumes of the material, see [61] for a detailed analysis of multiple stage transformations.

5.5.2 Tensile Stress-strain response of NiTi at 20^{o}C: sheet vs. rod

The tensile stress-strain curves for NiTi from quasi-static (0.001/s) and dynamic (~1200/s) tests conducted at room temperature (RT) on sheet (Longitudinal (L) and Transverse (T)) are shown in Figure 5.7. Since the specimen is in superelastic (SE) condition, the quasi-static stress-strain curves reveal clear SE plateau regions. Generally, it is agreed that the elastic deformation of austenite (stage I) is followed by the stress-induced martensitic transformation (SIM) (stage II) represented by the flat

plateau. Subsequently, the SIM reorients (stage III) before plastic deformation of martensite begins (stage IV) [62]. The specimen exhibits transformation strains (i.e., strain at the end of the 'plateau' region) of ~ 6.8% in the longitudinal (rolling) direction (L) and 5.2% along the transverse direction (T) (close to the values observed by Liu *et al.* [43]). The 'plateau' region is not entirely flat when deformed at 0.001/s strain rate, however, when tested at 10^{-4}/s deformation rate, the NiTi sheet exhibits a zero-slope plateau up to 7.2% and 5.6% strains in longitudinal and transverse loading directions, respectively. Following Yuan and Yi [29] and Robertson *et al.* [39], the texture influence on the transformation strains may be estimated using: $\varepsilon = \frac{\eta V_m}{M'_{avg}}$, where η =13.08, V_m is the martensite volume fraction (assumed 1 here), and M'_{avg} is the normalized modified Taylor factor calculated by Ono *et al.* [63, 64] based on the discrete texture intensity at a given (hkl) plane. Since the textures measured in the current study are similar to those reported by Robertson *et al.* [39], the transformation strains calculated using their texture components intensity are 4.8% and 6% for loading in L and T directions, respectively. These match reasonably well with the observed values of 5.2% and 6.8%. The ST 50.8Ni-Ti rod material also shows a plateau between 1.6% and 6% [18], however the specimen does not recover the 6% SE strain completely upon unloading, compared to the sheet specimen, under 10^{-3}/s strain rates. It only exhibits pseudoelasticity with a non-linear unloading to 4% and recovering another 2% strain upon heating, indicating the stabilization of martensite during loading cycle [62, 65-67]. The remaining 2% permanent strain is due to the slip introduced into the annealed Ni-Ti matrix. Due to the annealing of the

dislocations and the dissolution of the hardening precipitates at 800^{o}C, the superelastic characteristics of the rod are reduced due to the ease of introducing permanent deformation through slip [68], thus emphasizing the importance of thermomechanical treatment to improve SE in Ni-Ti. Another significant difference is the plateau stress value; the plateau stress is greatest in the TD sheet (average of plateau start and end values, 550 MPa), lowest in the rod (~390 MPa) with the LD value being intermediate (~480 MPa average). The lower plateau stress in the rod has been explained due to the ease of slip in the alloy; the difference in the plateau stress between the transverse and the longitudinal sheet samples may be explained through the texture, and hence the deformation mechanisms that are operating at this temperature. The stress-induced martensitic (SIM) transformation that is responsible for the plateau region, and hence superelasticity, occurs through the formation of martensitic variant(s) [48]. It was suggested that the formation of SIM during uniaxial tension is governed by the variant group(s) that will accommodate the largest tensile strains for a given loading direction [69] and that this variant(s) will then grow during subsequent loading. It is known that the largest recoverable strains in single crystals are possible due to SIM formation when the loading directions are parallel to $<111>_{B2}$ followed by $<110>_{B2}$ and $<100>_{B2}$. Furthermore, different variants recover different transformation strains [42, 70]. For a polycrystalline Ni-Ti with significant texture, only those strains can be recovered that can be accommodated by the rearrangement of martensite variants, noting that each grain may form different set of variant microstructures. Since the sheet texture indicates higher $<110>_{B2}$ components along the rolling direction, it can be reasoned that the formation of martensite variants that accommodate and hence recover larger

strains occurs during loading along the longitudinal than Transverse. This argument may explain the smaller plateau strains in the transverse specimen compared to longitudinal sample. The degree of the role of intergranular constraint on the properties of polycrystalline SMA has also been invoked by several investigators to explain the observed SE strains [31, 42, 48, 70]. Liu *et al.* [43] have offered further analysis on the deformation mechanisms to explain the influence of texture. They studied uniaxial tension along longitudinal and transverse directions and explained the difference in the plateau region as follows. Deformation of the martensite phase along the longitudinal direction resulted in the detwinning of <011> type II twins, whereas, such detwinning was absent in the samples deformed along the transverse direction. Instead, deformation of (001) compound twins and a high density of dislocations were frequently observed in these samples. These observations were rationalized by Liu *et al.* [43] by calculating the shear direction of several twins with respect to the loading directions and found that the rolling direction (L) is more favorable to the shearing of <011> type II martensite twins, while the transverse (T) direction is more favorable to the (001) compound twin shearing. Noting that the strains recoverable by SE are typically the same as those by SM [28], it can be argued that similar triggering of different twins in the longitudinal and transverse directions may be responsible for the observed difference in the plateau strains and stresses for L and T specimens. The stress-strain curves in Figure 5.7a also show that the longitudinal samples exhibit larger ductility (greater by 4-5%) and lower strength (lower by 300MPa) than the transverse samples, understandably due to the deformation across the rolled grain microstructure.

In quite contrast, the dynamic stress-strain curves for the rod and the sheet specimens barely show any plateau region. The 'ringing' in the stress-strain curves observed at the end of the elastic region (Figure 5.7a, for sheet specimen) is due to the oscillations observed in the incident pulse and due to the complex specimen geometry; it is not a material property [59]. Although, this ringing camouflages the plateau region, from Figure 5.7, it is interesting to see that the end of start and end of the 'ringing' corresponds to the beginning and the termination of the plateau region. The average plateau stress follows a similar pattern as that of the quasi-static: the plateau stress is greatest in TD sheet (average of plateau start and end values, 620 MPa), lowest in the rod (~410 MPa) with the LD value being intermediate (~500 MPa average). Miller *et al.* have reported that this plateau start stress, under repeated dynamic loading, decreases with increasing loading cycles and was independent of the level of plastic-strain [59]. This has been ascribed to the martensite stabilization that occurs with increasing loading cycles, similarly observed under quasi-static cyclic loading conditions [71].

Post-plateau deformation in the sheet specimen, however, was different under dynamic deformation compared to the quasi-static rates. The stage III deformation now shows linear strain hardening until failure, with hardening exponent n = 0.3, slightly larger than the rod specimen. It is very likely that under dynamic strain rates, the dislocation generation occurs earlier, possibly during the SIM plateau formation and beyond, thus explaining the strain-hardening region instead of the elastic martensite-reorientation stage. Interestingly, experiments by Miller *et al.* [59] have indicated that, upon cycling, the hardening exponent increases with increasing plastic

strain, whereas it is independent of the cycle number. The failure strains at high-strain rates are nearly twice as large under quasi-static strain rates, with longitudinal specimens exhibiting 4-5% higher ductility than the transverse specimens. Based on the bilinear unloading curve, it has been shown that stress-induced martensite transformation indeed occurs at high deformation rates despite the absence of an obvious plateau region [18, 59]. The higher plateau stresses, thus observed under dynamic loading, may be explained by the following arguments. (a) Due to higher deformation rates, the kinetics of the phase transformation may influence the material response, particularly higher plateau stresses before the SIM transformation begins, (b) due to temperature rise (as a result of the latent heat of transformation) and adiabatic conditions (associated with dynamic deformation), the specimen self-heating may also increase the plateau stresses. Since the stress rate, $d\sigma/dT$, varies between 3 and 20MPa/^{o}C [53], the plateau stress, assuming a stress rate of 5MPa/^{o}C and 10-40^{o}C temperature rise, may be expected to increase ~50-200 MPa which is close to the observed values.

5.5.3 Quasi-static stress-strain response of NiTi: Effect of temperature

The effect of temperature between -196^{o}C and 400^{o}C on the superelastic and overall stress-strain behavior under quasi-static strain rate is shown as a function of texture in Figure 5.8. For the longitudinal samples, with decreasing temperature from 20^{o}C to -50^{o}C, the plateau stress decreases due to the ease of martensite detwinning. However, at -100^{o}C and -196^{o}C, the plateau stress increases due to the low-temperature effects on the material modulus and Peierls stress and also due to the

setting in of irreversible martensite detwinning at $T << M_f$. Although the specimen exhibits $R_f = 0^oC$, the quasi-static stress-strain curves at 0^oC hardly show the R-phase detwinning plateau at low stress levels, and it is completely absent in the dynamic stress-strain data. In addition, they show superelastic 'flat' plateau behavior up to 6% strain. Below -100^oC, the material is entirely martensitic. The transverse specimens also show similar variation of the detwinning plateau stress, although the plateau stress is greater than in the longitudinal samples at any test temperature, with the maximum difference of 150 MPa at -196^oC and minimum of 25 MPa at 50^oC. Additionally, while the longitudinal specimens exhibit 15% ductility at all temperatures, except -50^oC and -100^oC, where they exhibit fracture strains of 20%, the transverse samples show lower ductility of 10-11% at all low temperatures. The tensile strength in the transverse samples is correspondingly greater than the longitudinal oriented samples at each low temperatures by ~ 200-300MPa.

Typically, the thermally-induced martensite in NiTi (formed when cooled below M_f) is made of twinned martensite variants with <011> type II, {11-1} type I and (001) compound twins co-existing in the microstructure; among these the <011> type II twin is more frequently observed [47, 72-76]. The tensile deformation of the twinned martensite proceeds through (a) elastic deformation of the martensite, (b) plateau region corresponding to martensite reorientation and detwinning process, (c) elastic deformation of reoriented martensite and further detwinning, and finally (d) plastic deformation. Liu *et al.* [76] (who studied NiTi bar annealed at 600^oC for 0.5-hr) have shown that during stage (a), the martensite deforms uniformly along the gage length with the inelastic arrangement of some martensite twins and the generation of

dislocations within the (11-1) type I twins. Stage (b), which corresponds to the constant-stress plateau region, involves the martensite reorientation and detwinning of <011> type II twins, following the formation of mobile (100) compound twins between the type-II twins, in addition to the rearrangement of dislocation substructures. During stage (c), further reorientation and detwinning of unfavorably oriented martensite twins occur with increasing stress along with the generation of high density of dislocations [76]; concluding with the plastic deformation of unfavorably oriented martensite plates [76-79]. Zheng and Liu [77] have suggested two detwinning mechanisms, namely, domino and assisted detwinning. They argued that the domino detwinning, once initiated in a finite volume, proceeds at a constant external stress in a self-propagation manner, whereas the assisted detwinning necessitates increasing loading to trigger further detwinning. Furthermore, they suggested that the end of the plateau region corresponds to the cessation of the domino detwinning mechanisms, while assisted detwinning occurs beyond the plateau region. It is observed from Figure 5.8(a,b), that with decreasing temperatures, the plateau region progressively decreases in strain and the slope of the stress-strain curve subsequent to the plateau region increases. This suggests a possible early shift from a domino detwinning to an assisted detwinning mechanisms at lower temperature. In addition, it is possible that dislocation generation occurs concurrently with the assisted detwinning mechanism near the end of the plateau region. The effect of texture through tensile loading along L and T can be accounted for by the difference in twinning deformation. As invoked earlier, Liu *et al.* [43] found that the rolling direction (longitudinal) is more favorable to the shearing of <011> type II martensite

twins, while the transverse directions is more favorable to the (001) compound twin shearing. Since the deformation mechanisms of various martensite twins differs for different twinning systems, it would explain the difference between the martensite deformation in the longitudinal and transverse specimens at low temperatures.

The quasi-static high-temperature response of 50.8Ni-Ti sheet is shown in Figure 5.8(c,d). The sheet material still exhibits superelasticity, based on the discernable 'plateau' for both the longitudinal and transverse specimen, although the plateau now occurs at ~800-900 MPa due to the temperature dependence of the plateau stress in the superelastic condition (through stress-rate, $d\sigma/dT$). Two important observations may be noted for stress-strain curves tested between 100^{o}C and 400^{o}C: (1) the critical stress (calculated by 0.2% strain offset) increases with temperature and (2) the strain hardening coefficient for the transverse specimens is greater than the Longitudinal samples. The second observation can be explained by the deformation perpendicular to the rolling grain direction that is known to increase strength and work-hardening properties. However, the increase in strength with temperature change from 100^{o}C to 400^{o}C seems to be contrary to the typical strength-versus-temperature correlation for bcc alloys; strength is expected to decrease at higher temperatures. However, it can be explained by the fact that Ni-rich NiTi alloys, such as 50.8-NiTi, undergo precipitation reactions upon aging [61, 68, 80-82]. Aging between 200^{o}C and 400^{o}C leads to the precipitation of the Ti_3Ni_4 metastable phase, with maximum density occurring for aging at 400^{o}C. Since the quasi-static specimen were held at these testing temperatures for nearly 20-30 minutes, the alloy was

precipitation hardened (in addition to the initial cold-work+annealing treatment in the as-received samples) and hence exhibited increased strength at high temperatures.

The stress-rate (dσ/dT) variation for different specimens may be calculated by plotting the critical stress (corresponds to the plateau start stress for quasi-static strain rates) as a function of temperature, as shown in Figure 5.11(a, b) for rod and sheet specimens, where the critical stress is calculated by 0.2% strain offset method. The slope, dσ/dT, is calculated between 0^oC and 100^oC, since the highest temperature for superelastic range is ~120^oC-150^oC [18]. Thus the stress rate is calculated as 3.8MPa/^{o}C, 6.1MPa/^{o}C and 6.3MPa/^{o}C for rod and sheet longitudinal and transverse specimens, respectively, at quasi-static strain-rates. It can be seen that the solution-treated rod has lower stress-rate than the cold-worked and aged sheet specimen, although the variation between the longitudinal and transverse specimens is not significant; this suggests that annealing heat treatment above the recrystallization temperature (~600^oC for Ni-Ti alloys) greatly influences the stress-rate. The transformation strain, $\varepsilon^{A\rightarrow M}$, estimated earlier through texture information, may also be calculated using the observed stress-rate values. Typically, the stress rate or the recoverable strains have been calculated by utilizing:

$$\frac{\partial\sigma^{A\rightarrow M}}{\partial T}=\frac{\rho}{\varepsilon_{A\rightarrow M}}\frac{\Delta H^{A\rightarrow M}}{T_o}=\rho\frac{\Delta S^{A\rightarrow M}}{\varepsilon_{A\rightarrow M}}$$

where ΔH and ΔS are the change in molar enthalpy and entropy, respectively, and ρ is the density of Nitinol. $\Delta H^{A\rightarrow M}$ is typically measured using calorimetric methods, where the equation has been corrected for density (ρ=6.45g/cm^3) to maintain consistent units (energy/mass versus energy/volume) [83]. This is the well known

Clausius-Claperyon equation that quantifies the effect of stress on the martensitic transformation for uniaxial stress loading condition [84, 85]. It has been used to calculate the magnitude of reversible strains accompanying the superelastic Nitinol. However, using the T_o values given by [85, 86]:

$$T_o = \frac{M_s + A_s}{2} \quad or \quad T_o = \frac{M_s + A_f}{2}$$

has led to large errors in the calculations. Recently, McKelvey [83] has provided an alternative approach in estimating the reversible transformation strains of a uniaxially loaded specimen in tension using the Clausius Claperyon equation by avoiding the calculation of the equilibrium temperature, T_o. Assuming that at some critical stress (σ_c), the parent austenite will begin to transform to martensite in order to accommodate the strain, this can be represented by the Gibbs-free energy at equilibrium as: $(a) \quad G_A = G_B; \qquad (b) \quad \partial G_A = \partial G_B$

By utilizing the Gibbs-Duhem equation, the partial Gibbs free energies may be rewritten as:

$$\frac{d\sigma}{dT} = \frac{-\Delta S}{\varepsilon^{A\to M}} = \frac{-1}{\varepsilon^{A\to M}} \frac{\Delta H}{T}$$

where S and H are the molar entropy and enthalpy per unit volume, respectively, and $\varepsilon^{A\to M}$ is the strain in either phase and $d\sigma/dT$ is called the *stress rate*, a very important descriptor of SMA and typically varies between 3 to 20 MPa/°C [53], as discussed earlier. This, McKelvey [83] calls an alternative expression for the Clausius-Claperyon equation where the conventional pressure and volume terms are replaced

with the conjugated variables stress and strain. Correcting for the units (for using the enthalpy values from the DSC) and integrating the above expression, we get:

$$\frac{d\sigma}{dT} = \frac{-\rho}{\varepsilon^{A\to M}}\frac{\Delta H}{T} \Rightarrow \sigma_c - \sigma_0 = \frac{-\rho\Delta H}{\varepsilon^{A\to M}}\ln\left(\frac{T}{T_0}\right)$$

where σ_o and T_o are arbitrary stress and temperature parameters, respectively; here we assumed $T_o = 0^oC$ (273K) and $\sigma_o = \sigma(T = 0^oC)$. This linearized equation removes the dependence of the slope on the temperature T_o. Plotting the above equation based on the data shown in Figure 5.11(a, b) for the quasi-static data provides the slopes ($\rho\Delta H/\varepsilon^{A\to M}$) as 1256.3 MPa, 1991.2MPa and 2043MPa for rod, and longitudinal and transverse sheet specimens, respectively. Additionally, using the transformation enthalpies measured by the DSC as 15.6 J/g (rod) and 18 J/g (sheet), the transformation strains may be calculated as 8%, 5.8%, and 5.6% for rod and sheet-L and T specimens. Although, the calculation overestimates the recoverable strain for the rod geometry, the error for the sheet specimen is ~ 10%. A probable reason for the overestimation of the recoverable strain for the rod specimen may be forwarded as follows: the above calculation assumes 100% transformation at the end of the plateau, however, recent studies by Brinson *et al.* [38] have indicated that in polycrystalline shape memory alloys, the volume fraction of the martensite is likely to be ~60%-70%. Additionally, since the solution-treated is more susceptible to slip deformation, the sample may not exhibit optimal SE strains.

5.5.4 Dynamic stress-strain response of NiTi: Effect of temperature

Typical stress-strain response of 50.8Ni-Ti sheet samples under dynamic tensile loading (1200/s) between -196^{o}C and 400^{o}C is shown in Figure 5.9; for

comparison purposes, the room-temperature dynamic response is also shown. The results indicate the presence of the stress-plateau (stage (b) discussed in the previous section associated with the martensite detwinning observed at quasi-static strain rates. Liu *et al.* [50] have observed similar plateau region in the stress-strain response of the martensite phase at a strain rate of 300/s. This suggests that the detwinning 'plateau' mechanisms of the thermally induced martensite (TIM) are still active at 1200/s deformation rates. By contrast the stress-induced martensite 'plateau' of the superelastic austenite phase exhibits greater strain-rate sensitivity, since the plateau is not clearly observed in the current study (see Figure 5.9) and previous reports [59]. The difference perhaps lies in the microstructure: the thermally-induced martensite (at $T < M_f$) microstructure contains several mobile twin interfaces that move upon the application of stress until one favorably oriented variant grows at the expense of the remaining ones. On the other hand, the stress-induced martensite (at $A_f < T < M_d$) needs to form from a sea of austenite matrix, where one specific martensite variant that accommodates the strains optimally, grows into the matrix. Therefore, it is possible to interpret from the observed high-strain rate response of the superelastic austenite and the shape memory martensite, that the kinetics of the austenite-martensite interface(s), and the martensite-martensite interface(s), differs with respect to the influence of strain-rate, as well as, temperature and loading state (i.e. tension vs. compression). The dynamic detwinning plateau, however, is greater than the quasi-static plateau by 50-150 MPa. In both the longitudinal and transverse specimens, the trend in the 'plateau' variation is similar to that observed under quasi-static strain rate, i.e., the plateau decreases with decreasing temperature between 0^oC and -50^oC, before

increasing below -100^{o}C. Additionally, the plateau stress for the longitudinal samples is generally smaller than the transverse specimens due to the influence of texture on the formation of the variants and the deformation of twins, as discussed earlier.

Another major difference between the dynamic and the quasi-static stress-strain response is Stage-c, where dislocation mechanisms are dominant. Instead of the elastic deformation of reoriented martensite and (further) detwinning observed in this region (typically characterized by the martensite elastic modulus), the dynamic stress-strain curves exhibit linear strain-hardening beyond 6% strain. While the strain-hardening coefficient is constant for all the specimens having similar texture, it is slightly larger for the transverse specimens compared to the longitudinal samples. It is possible to interpret these observations as follows. Since the quasi-static Stage-c is accompanied by the further reorientation and detwinning of the less favorably oriented twins, along with a high density of dislocation generation, at high strain-rates, dislocation generation may be the dominant mechanism. Since the detwinning plateau-strains are smaller for the dynamic case, dislocation generation may be forming in tandem or subsequent to the plateau deformation stage. This scenario was also supported by our DSC measurements on the deformed martensite under high strain rates, that exhibited marginally higher A_f temperature, indicating martensite stabilization and two way shape memory effect (TWME) that requires the presence of extensive dislocation networks, as reported in the literature [50]. Finally, the ductility for the longitudinal specimens is typically ~ 25-30%, nearly 5-10% greater than the transverse specimens, under high-strain rate testing.

The SE behavior under dynamic loading between 0^{o}C and 150^{o}C is captured by the 0.2% critical stress variation with temperature in Figure 5.11(b). The stress-rate thus calculated is ~6.9 MPa/^{o}C and 7 MPa/^{o}C for the longitudinal and transverse specimens, respectively, slightly greater than the 6.1 MPa/^{o}C and 6.3 MPa/^{o}C observed under quasi-static strain rate. At higher temperatures, similar to the quasi-static results, (1) the critical stress increases with temperature and (2) the strain hardening coefficient for the transverse specimens is greater than the L samples, due to loading perpendicular to the rolling grain direction. Additionally, the critical stress is greater under dynamic loading compared to the quasi-static strain rates by ~200-300 MPa, as shown in Figure 5.11(b).

5.5.5 Dynamic response of 50.8Ni-Ti: Effect of TM

In order to study the effect of thermomechanical treatment (TM), the quasi-static and dynamic behavior of the cold-worked+annealed sheet 50.8-NiTi is compared to the corresponding behavior of the solution-treated 50.8-NiTi rod, fully-annealed at 800^{o}C for 1-hr. Taking into consideration that the recovery processes (dislocation annihilation) in Ni-rich NiTi alloys become active at 500^{o}C, and recrystallization and grain growth occur at T $\geq$ 600^{o}C, the homogenizing treatment of the rod removes all the work-hardening. Additionally, the time-temperature-transformation (TTT) diagram expressing the precipitation in 50.8-NiTi alloys indicates that annealing at 800^{o}C also dissolves the Ni-rich precipitates, if any, and the microstructure of the solution-treated rod consists of cubic B2 austenite grains [68, 71, 87]. Thus, the solution-treated rod has neither the hardening precipitates nor the work-

hardened matrix; this makes it easier to introduce the slip into the matrix. Therefore, during the deformation of the SE austenite or the thermally-induced martensite, it can be expected that the dislocation mechanisms dominate the deformation processes, which would in turn degrade the superelasticity or shape-memory characteristics, i.e., the recovery strains are lower than the cold-worked and aged Nitinol. The quasi-static and dynamic tensile stress-strain responses of the 50.8-NiTi ST rod are shown in Figure 5.10. The quasi-static low-temperature response between 0^{o}C and -196^{o}C is shown in Figure 5.10a; the plateau detwinning stress decreases from 0^{o}C to -50^{o}C and subsequently increases below -100^{o}C, similar to the sheet specimens. However, the post plateau region shows lower slopes for Stage-c, where elastic accommodation through martensite reorientation and detwinning, and slip are active. Since the linear-hardening observed due to plastic deformation exhibits lower slopes than the 'elastic' deformation processes (such as reorientation and detwinning), and due to the easy of slip in the solution-treated matrix, it is likely that slip is dominant in the detwinning plateau and post-plateau deformation stages. Indeed, at higher strain rates, shown in Figure 5.10b, the slope or the hardening coefficient of the post-plateau region is similar to the quasi-static response; the flow-stress however is increased at higher strain-rates, similar to the strain-rate sensitivity of bcc metals and alloys. The high-strain-rate response is similar to that observed for the sheet, in that the post-plateau region is dominated by slip deformation. This is further corroborated through the high-temperature dynamic response of ST rod (see Figure 5.10d), where the critical stress decreases with increasing temperature, again, typical of the bcc alloy response to increasing temperature. The critical stress (σ_{cr}) variation with temperature in the

ST rod is shown in Figure 5.11a, for the quasi-static and the dynamic strain-rates. The σ_{cr} generally decreases with increasing temperature between -196^{o}C and -50^{o}C, with the $\sigma_{cr}^{dynamic} > \sigma_{cr}^{QS}$. In the SE temperature range $0^{o}C < T < 150^{o}C$, the σ_{cr} increases due to the increase in the stability of the austenite phase. However, between 200^{o}C and 400^{o}C, it can be seen from Figure 5.10c and Figure 5.11a that, $\sigma_{cr}^{QS} > \sigma_{cr}^{dynamic}$. This can be explained by the fact that the quasi-static (QS) specimens were held at the testing temperature for ~30 min leading to aging and hence precipitation hardening; whereas the dynamic specimens were held only for 5 min before testing. At 200^{o}C, the precipitation kinetics are not sufficiently rapid to endow the material with sufficient age hardening, thus at 200^{o}C, the $\sigma_{cr}^{dynamic} > \sigma_{cr}^{QS}$. However, at 300^{o}C and 400^{o}C, even short term aging of 0.5-hr is sufficient to improve the age hardening characteristics [61, 81], thus the $\sigma_{cr}^{QS} > \sigma_{cr}^{dynamic}$. Additionally, the stress-rate in the superelastic range for the solution-treated rod is 3.8 MPa/^{o}C and 4.3 MPa/^{o}C, under low and high-strain rates, respectively; these are nearly half the values observed for the sheet samples with prior thermomechanical treatment. Furthermore, the critical stresses observed for the sheet specimens between 0^{o}C and 100^{o}C are greater than the rod-specimens; thus the thermo-mechanical treatment is effective in improving the resistance to slip deformation and improve the superelastic properties (such as plateau stress and strain).

It can be summarized, therefore, that cold-working and precipitation hardening not only endows the Ni-Ti alloy with higher plateau stress (due to increase in the resistance to slip), but also improves the austenite strength at higher temperatures. Additionally, it also increases the stress-rate sensitivity ($d\sigma/dT$). Additionally,

solution-treatment leads to the domination of slip mechanisms during the detwinning or SIM plateau and post-plateau regions.

5.5.6 Fractography and fracture mechanisms

The fracture surfaces of the ST Nitinol rod failed under tension is shown in Figure 5.12 (a-f). High temperature (200^{o}C-400^{o}C) quasi-static and dynamic specimen exhibited typical ductile void type failure of the austenite phase, as shown in Figure 5.12(c, d). At lower temperatures (0^{o}C to -196^{o}C), as shown in Figure 5.12(a, b), the fracture mechanism was typical of quasi-cleavage failure, with very little cup and cone type failure at all strain-rates. However, the failure mechanism for the superelastic Nitinol was a mixed-mode type failure involving a uniform ductile void growth and cleavage patterns. The mixed-mode type failure mechanism has also been observed by [59] at high strain-rate testing. There are two effects that greatly control the failure mechanism of the SE austenite that is capable of undergoing SIM transformation: (1) triaxial constraint (or hydrostatic stress) affects the SIM, (2) higher strain rates tend to produce mixed-mode (ductile void and cleavage) type failure mechanism [59, 88].

The effect of hydrostatic stress has been confirmed through quasi-static tensile testing of notched specimen and plane-strain fatigue crack growth studies [83, 89], which showed that triaxial stress constraint suppresses SIM transformation. Additionally, high strain rate tensile studies of un-notched specimen in the current study and by Miller *et al.* [59] have shown that the failure mechanism is typically a mixed mode with uniform distribution of void nucleation and growth. Moreover,

high-strain rate tensile tests of notched specimen have shown that increasing triaxiality also decreases the amount of void growth [59]. Recent high-strain rate fracture toughness studies of NiTi under quasi-static and dynamic loading rates [88] have shown that the material exhibits greater tendency to undergo stress-induced martensite transformation near the crack-tip and shows a high amount of ductile void growth (under plane stress conditions), as shown in Figure 12g, even though the quasi-static fracture exhibits only transgranular failure (see Figure 12h). Thus, both stress triaxiality (plane-stress vs. plane strain) and strain-rate influence the fracture mechanisms.

5.6 Conclusions

50.8-NiTi Nitinol is the workhorse of the commercial superelastic Nitinol alloy applications in the biomedical industry [81]. However, a systematic study of the high-strain rate deformation in this alloy has not been thoroughly investigated. Based on the studies of the quasi-static and high-strain rate behavior of 50.8-NiTi as a function of temperature (-196^{o}C to 400^{o}C), microstructure (thermomechanical treatment versus fully-annealed) and texture (parallel (L) and perpendicular (T) to the rolling direction), the follow conclusions are summarized:

(1) The thermomechanically treated sheet Nitinol exhibits multiple-stage transformation (MST) compared to the single austenite (A) ↔ martensite (M) transformation peak observed for the solution-treated rod alloy. This is due to the influence of dislocations and precipitates in the sheet material that interfere with the direct A ↔ M transformation.

(2) The sheet material exhibited <110> || rolling direction (RD)-type texture; the {111} was the strongest normal direction (ND) component. Additionally, the fully annealed drawn rod exhibited a typical γ-fiber texture. The annealing heat-treatment for the sheet leads to the strengthening of the {111}<110> texture components.

(3) Constant high-strain rate tensile tests (1200/s) were successfully demonstrated for the sheet geometry up to large failure strains (~25-30%).

(4) The effect of texture was investigated by studying the tensile stress-strain response of the sheet Nitinol parallel (longitudinal, L) and perpendicular (transverse, T) to the rolling direction. Under low and high strain-rates, the transverse specimens exhibited higher 0.2% critical stress, tensile strength and work hardening and lower ductility than the longitudinal specimens at all temperatures, with the values being greater under dynamic loading compared to the quasi-static strain rates. While the martensite detwinning plateau was observed at low temperatures, the post-plateau deformation under dynamic loading was most likely dominated by slip mechanisms.

(5) The difference in the stress-rate ($d\sigma/dT$) in the superelastic range was only marginally greater for the transverse specimens compared to longitudinal samples. In general, the stress-rate was greater under high-strain rates.

(6) The room temperature ($20^{o}C$) transformation strains were estimated semi-quantitatively using both texture and stress-rate information, and the calculated values were within reasonable limits (~10% error) of the observed strains.

(7) Fracture mechanisms are dominated by quasi-cleavage in low temperature martensite, void growth at high temperature stable austenite and mixed-mode (void + cleavage) in the superelastic austenite at high strain rates. Increasing strain rates

affects the SIM transformation, and thus a transition from cleavage to void type failure is observed.

5.7 Acknowledgements

Chapter 5, in full, is a reprint of the material (under preparation) to appear as Raghavendra R. Adharapurapu, Fengchun Jiang, Kenneth S. Vecchio, John F. Bingert, "High-Strain Rate Response of 50.8-NiTi: Influence of Thermomechanical Treatment and Texture". The dissertation author was the primary investigator and author of this paper.

5.8 Figures

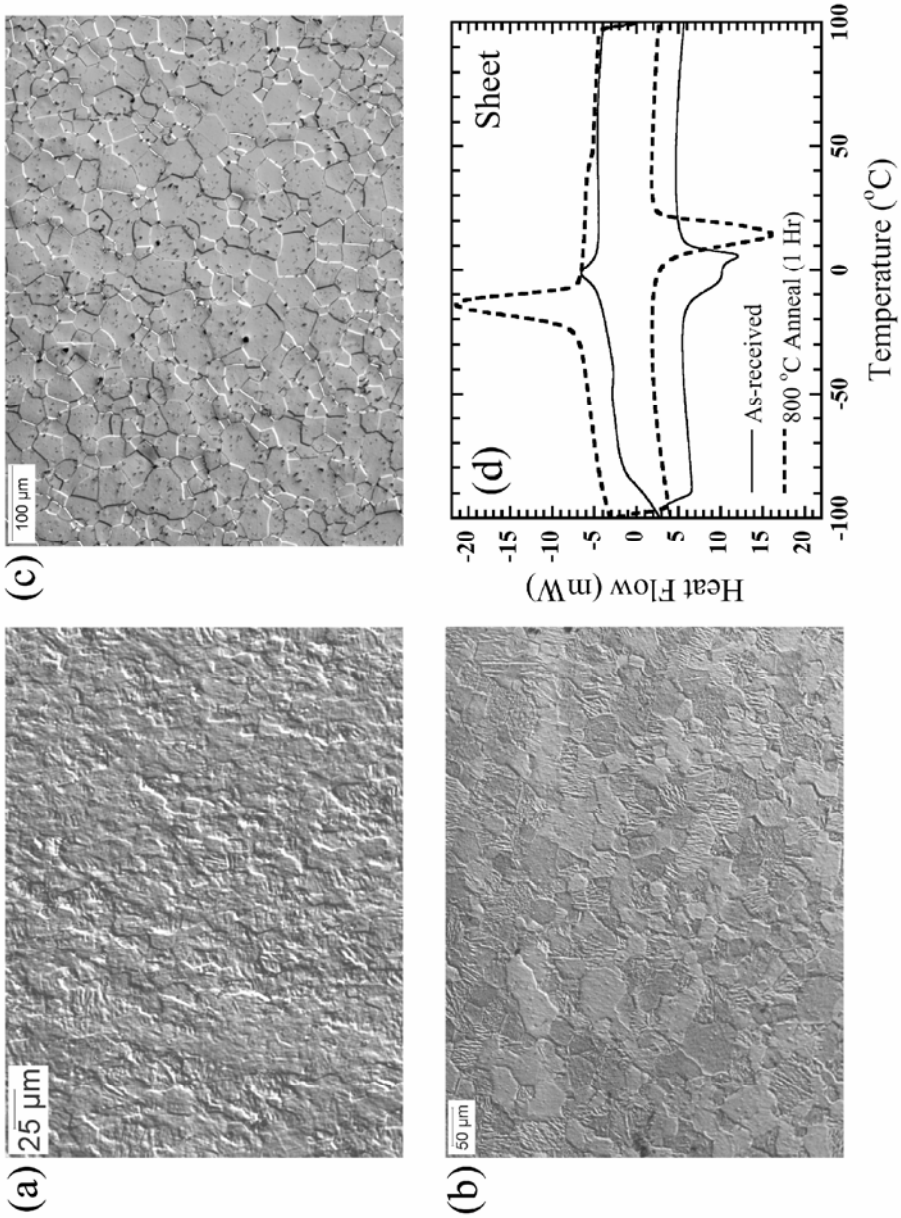

Figure 5.1 Optical micrographs of (a) As-Received (AR) 50.8-NiTi sheet, (b) annealed sheet (800 °C for 1-hr) and (b) 50.8-NiTi drawn rod stock (annealed at 800°C for 0.5-hr). (d) DSC scan of 50.8-NiTi sheet for AR and fully annealed conditions.

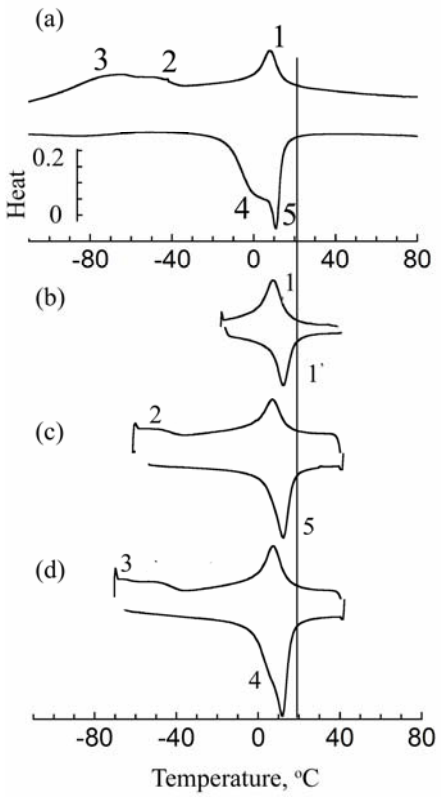

Figure 5.2 Partial DSC scans indicating the transformation sequence in as-received 50.8-NiTi

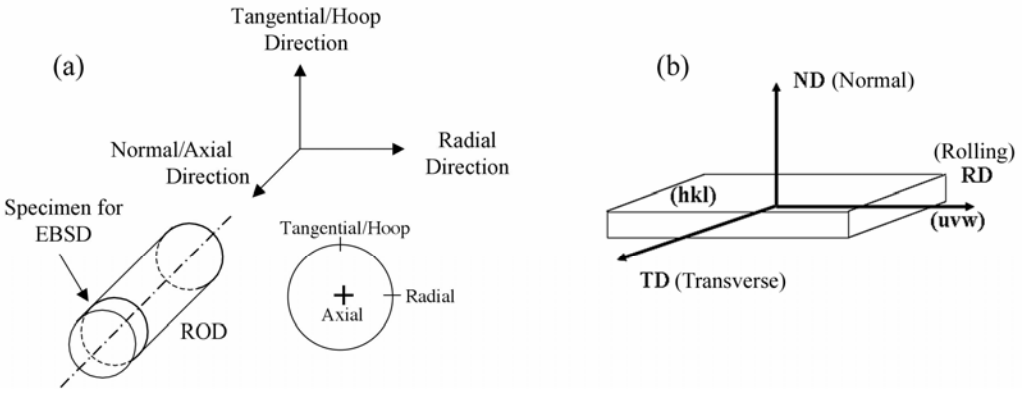

Figure 5.3 The reference frame for texture measurements in (a) Rod and (b) Sheet specimens.

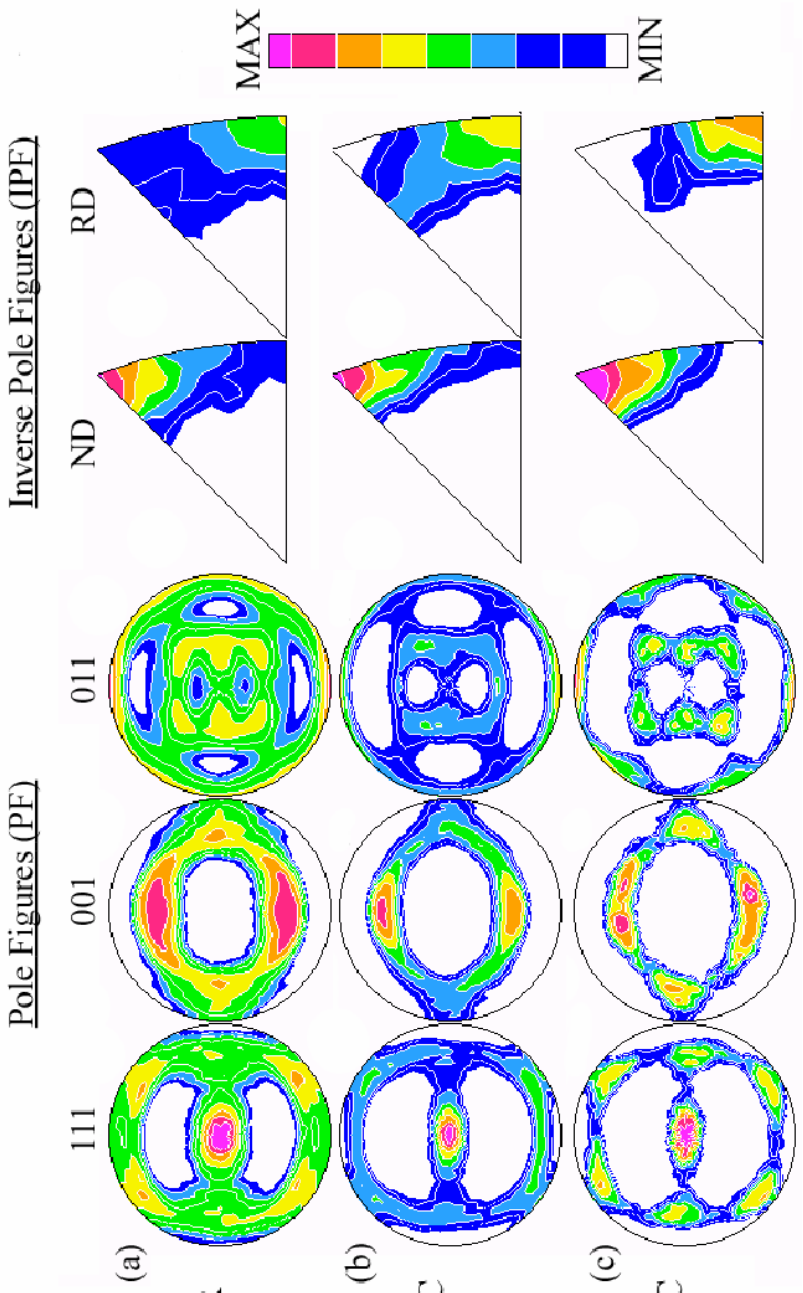

Figure 5.4 Texture evolution of 50.8-NiTi sheet due to aging heat treatments.

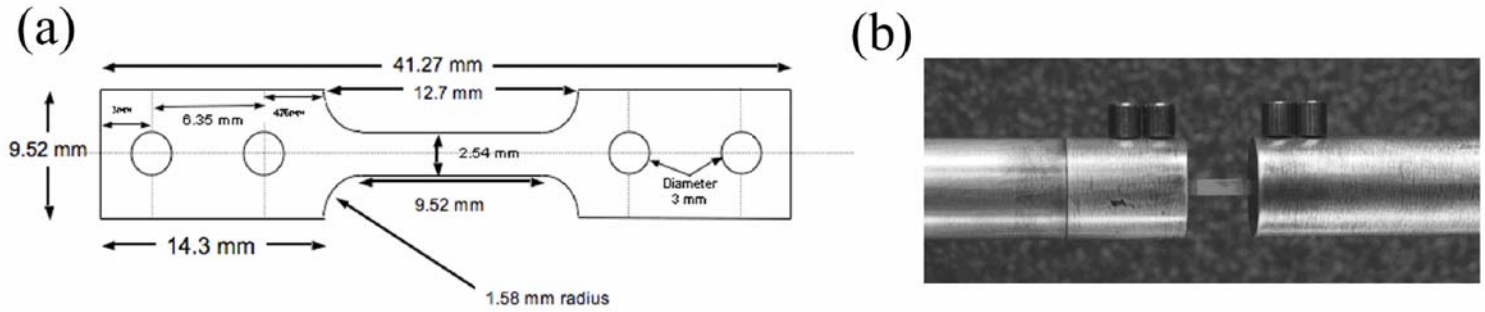

Figure 5.5 (a) Schematic diagram of the tensile specimen used in dynamic testing (1200/s). (b) Details of the gripping area of dynamic tensile sheet specimen in a split-Hopkinson bar. The specimen ends are gripped by high strength steel pins.

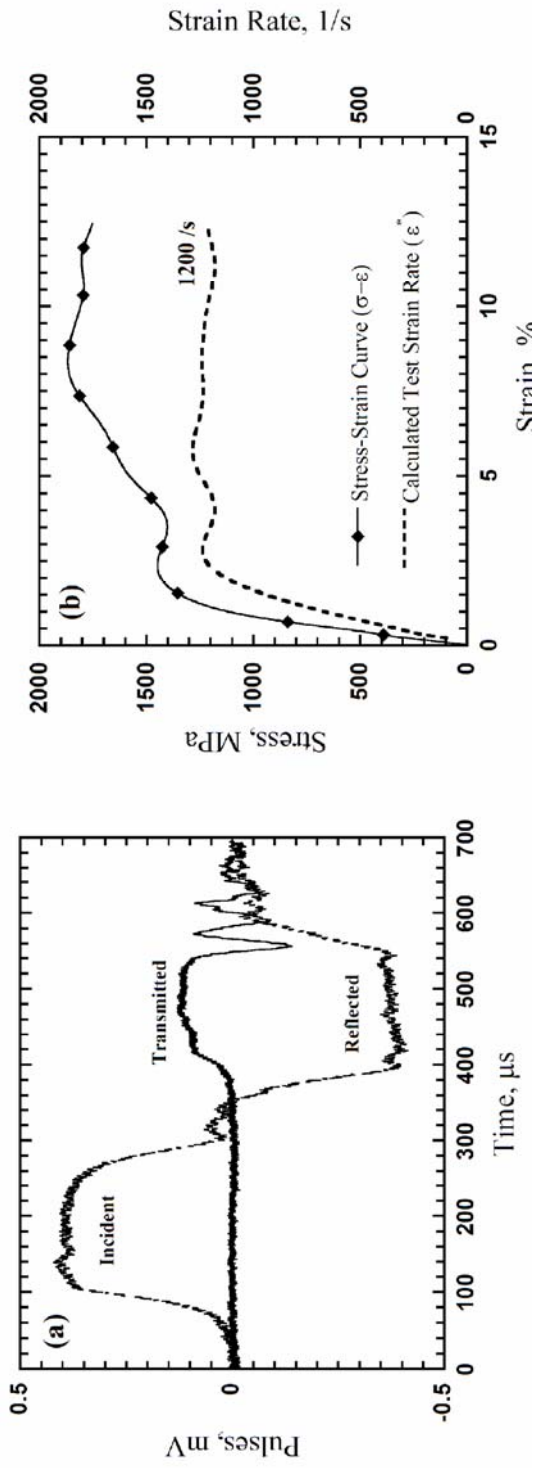

Figure 5.6 (a) Incident, reflected and transmitted pulses recorded during high-strain rate testing of NiTi sheet at 300 °C. (b) Corresponding strain rate and stress-strain curves.

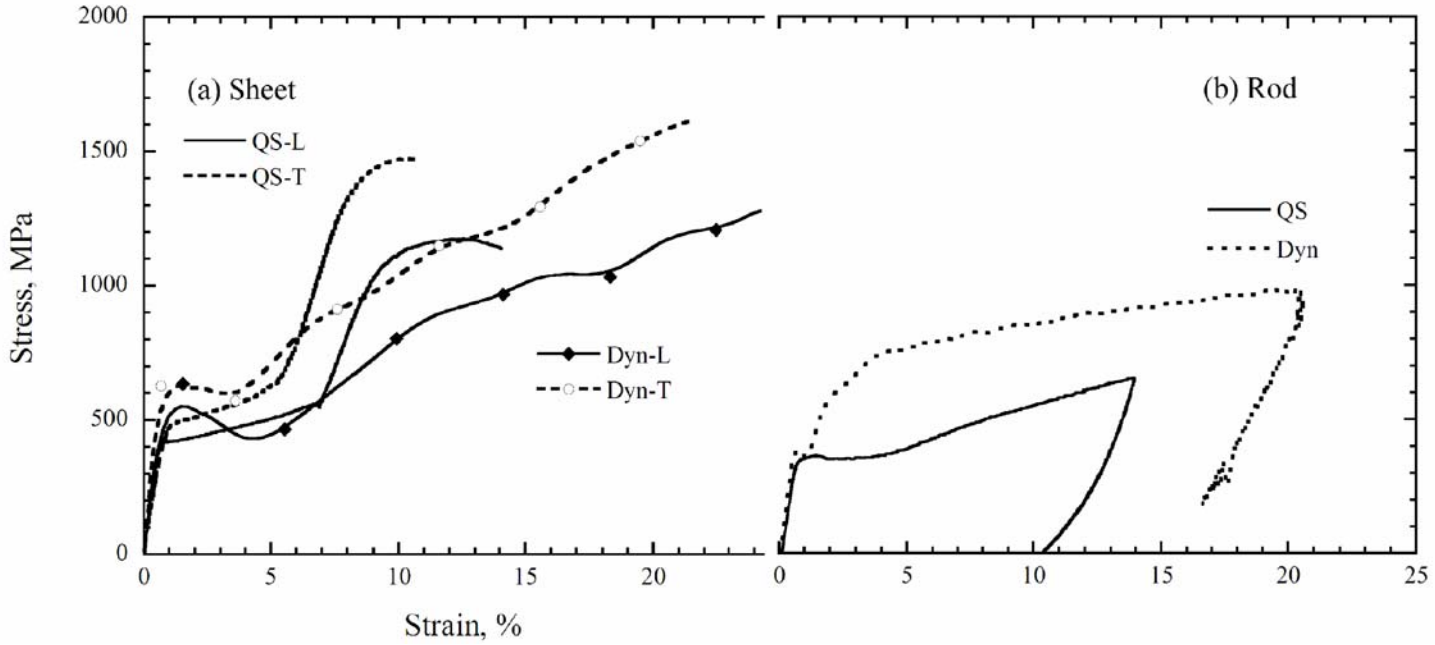

Figure 5.7 Tensile stress-strain behavior of (a) as-received 50.8-NiTi sheet under quasi-static (0.001/s) and dynamic (1200/s) strain-rates in rolling direction (Longitudinal, L) and transverse direction (T), (b) as-received fully annealed 50.8-NiTi Rod.

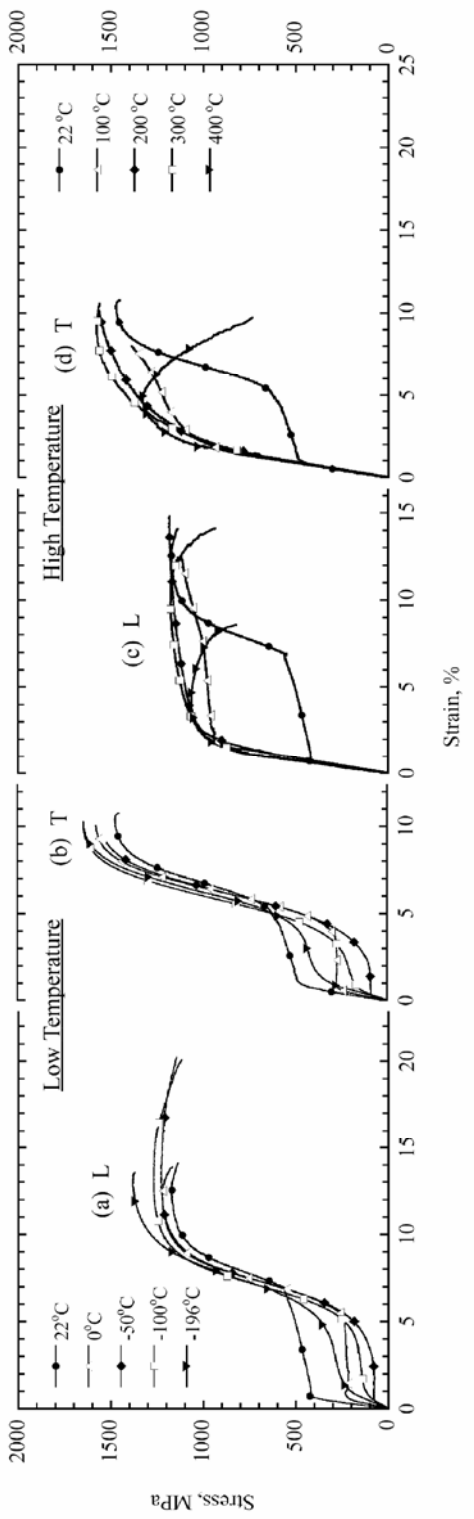

Figure 5.8 Quasi-static tensile stress-strain curves for as-received 50.8Ni-Ti sheet at low temperatures (0 to -196°C) and high temperatures (100 to 400°C) for loading in (a, c) rolling (Longitudinal, L) and (b, d) transverse (T) directions.

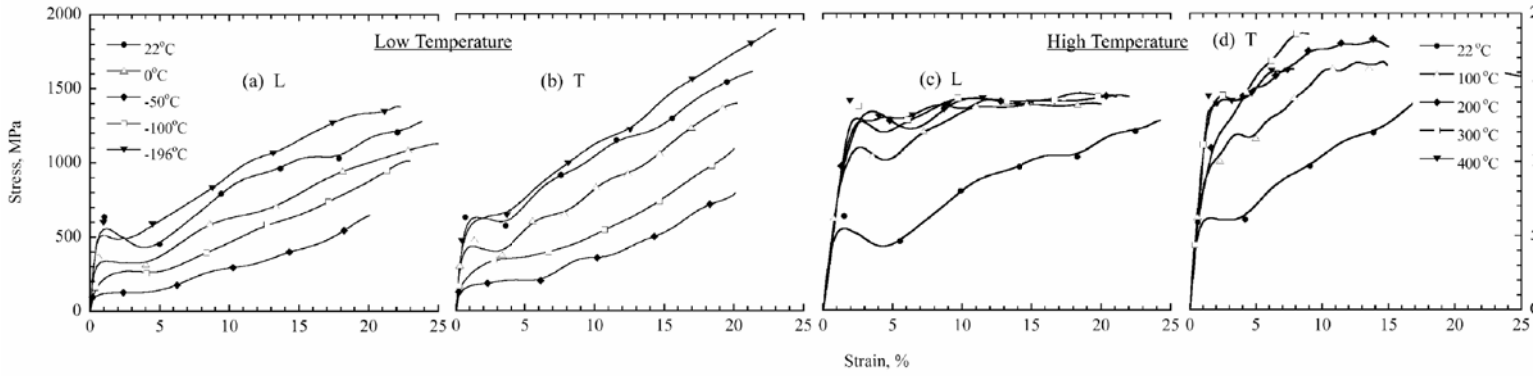

Figure 5.9 Dynamic tensile stress-strain curves for as-received 50.8-NiTi sheet at low temperatures (0 to -196°C) and high temperatures (100 to 400°C) for loading in (a, c) rolling (Longitudinal, L) and (b, d) transverse (T) directions

.

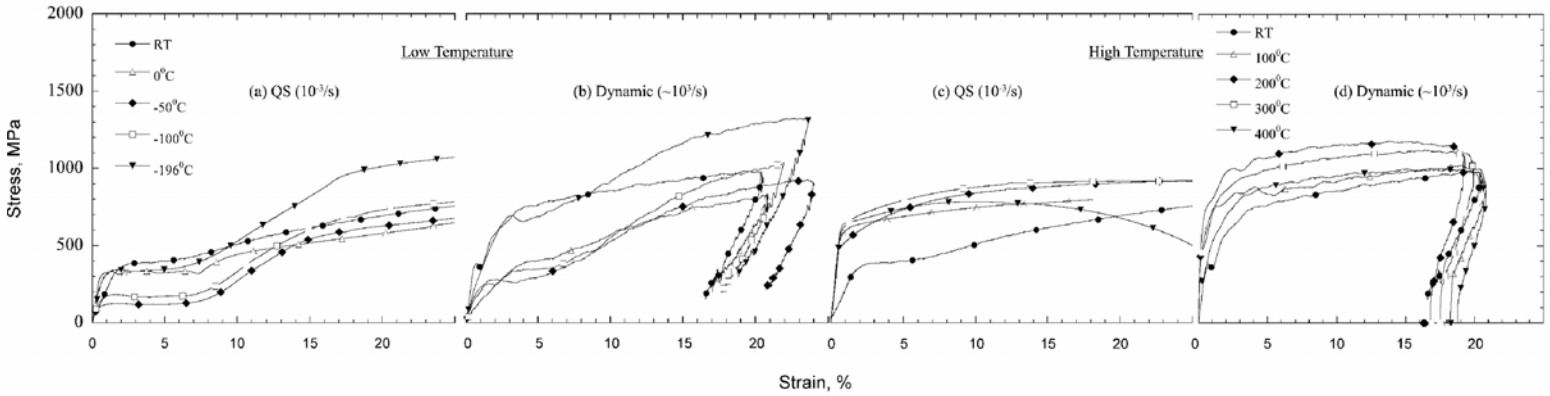

Figure 5.10 Quasi-static and dynamic tensile stress-strain curves for as-received fully-annealed 50.8-NiTi rod at (a, b) low temperatures (0 to -196°C) and (c, d) high temperatures (100 to 400°C), respectively.

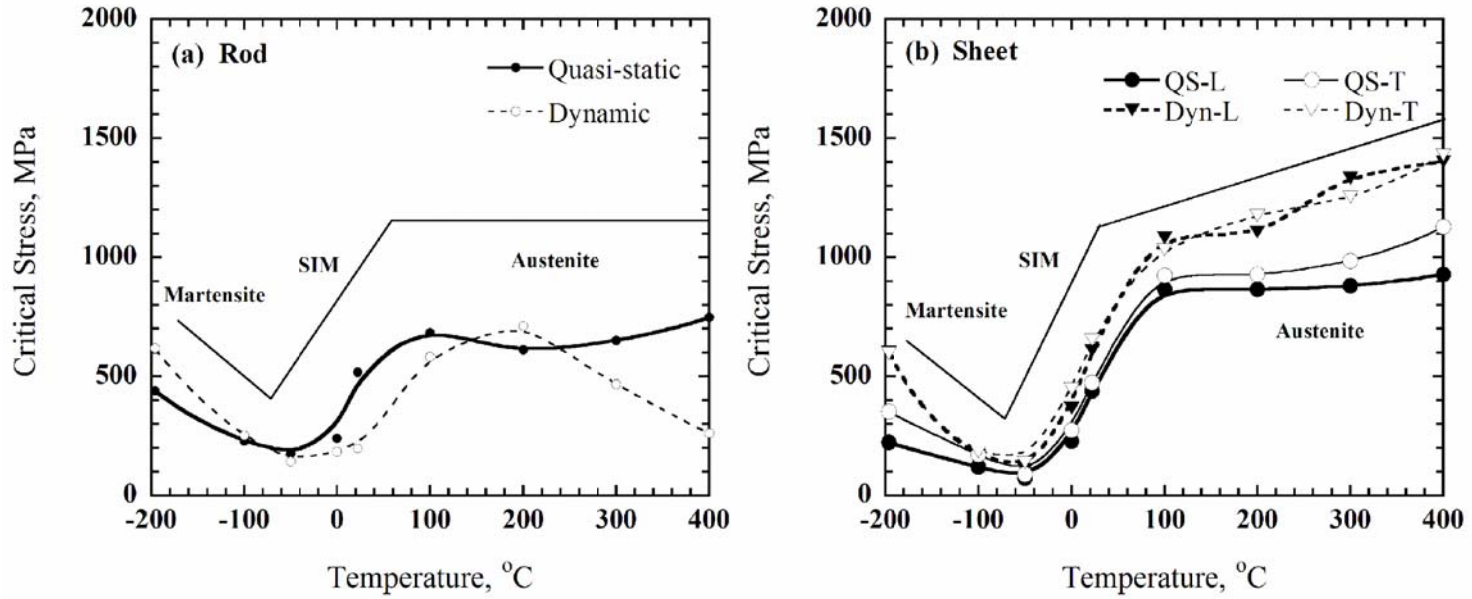

Figure 5.11 Variation of the 0.2% critical stress as a function of strain rate and temperature in (a) ST 50.8-NiTi rod and (b) AR 50.8-NiTi sheet material, in both rolling (L) and transverse (T) directions. The three zones, namely stable martensite (M), superelastic (SE) or stress-induced martensite (SIM) and stable austenite (A), are also identified.

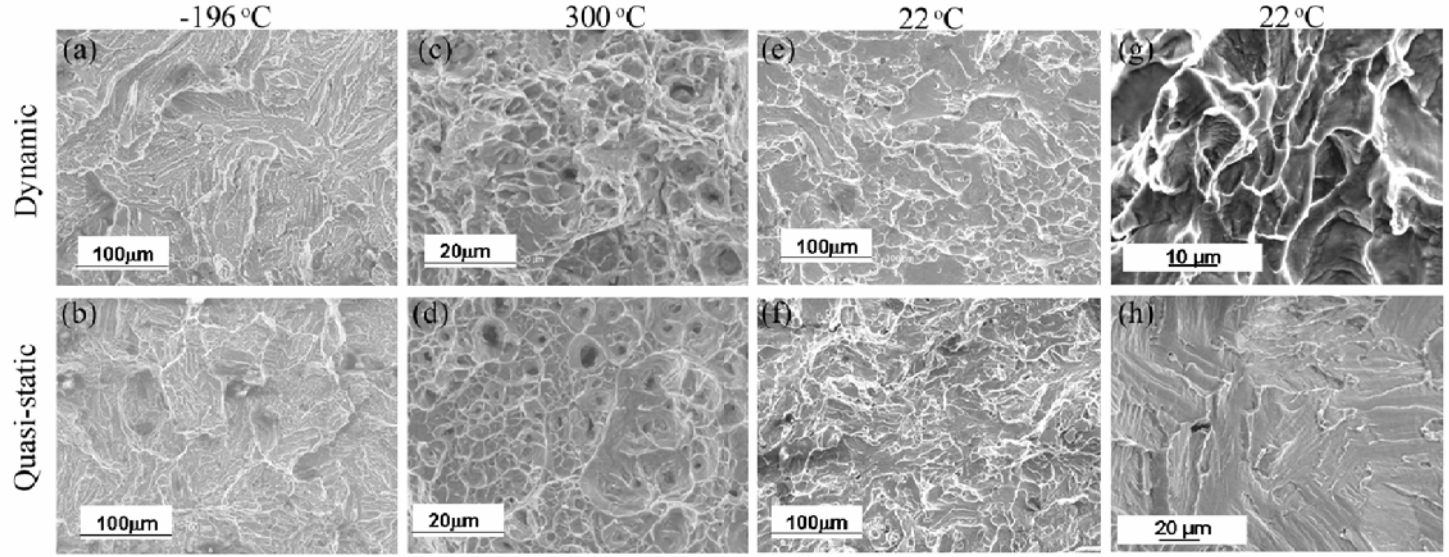

Figure 5.12 Dynamic and quasi-static (respectively) tensile fracture surfaces of ST 50.8-NiTi rod at (a, b) -196^{o}C; (c, d) 300^{o}C, (e, f) 22^{o}C. (g, h) are the fracture surfaces under three-point bend loading under dynamic and quasi-static loading conditions from [88].

5.9 References

1. Duerig, T., A. Pelton, and D. Stockel, *An overview of Nitinol medical applications.* Materials Science and Engineering A, 1999. **273-275**: p. 149-160.

2. Stockel, D., *Shape memory actuators for automotive applications*. Engineering aspects of shape memory alloys, ed. T.W. Duerig, K.N. Melton, D. Stockel, and C.M. Wayman. 1990, London: Butterworth-Heinemann. 283-294.

3. Humbeeck, J.V., *Non-medical applications of shape memory alloys.* Materials Science and Engineering A, 1999. **273-275**: p. 134-148.

4. Liu, Y., Z. Xie, and J.V. Humbeeck, *Cyclic deformation of NiTi shape memory alloys.* Materials Science and Engineering A, 1999. **273-275**: p. 673-678.

5. Dolce, M. and D. Cardone, *Mechanical behavior of shape memory alloys for seismic applications. 1. Martensite and austenite NiTi bars subjected to torsion.* International Journal of Mechanical Sciences, 2001. **43**: p. 2631-2656.

6. Saadat, S., J. Salichs, M. Noori, Z. Hou, H. Davoodi, I. Bar-on, Y. Suzuki, and A. Masuda, *An overview of vibration and seismic applications of NiTi shape memory alloy.* Smart Materials and Structures, 2002. **11**: p. 218-229.

7. Zhao, Y., M. Taya, and H. Izui, *Study on energy absorbing composite structure made of concentric NiTi spring and porous NiTi.* International Journal of Solids and Structures, 2006. **43**: p. 2497-2512.

8. Xue, Z. and J.W. Hutchinson, *Preliminary assessment of sandwich plates subject to blast loads.* International Journal of Mechanical Sciences, 2003. **45**(4): p. 687-705.

9. Xue, Z.Y. and J.W. Hutchinson, *A comparative study of impulse-resistance metal sandwich plates.* International journal of Impact engineering, 2004. **30**: p. 1283-1305.

10. Wicks, N. and J.W. Hutchinson, *Performance of sandwich plates with truss cores.* Mechanics of Materials, 2004. **36**: p. 739-751.

11. Orgeas, L. and D. Favier, *Non-symmetric tension-compression behavior of NiTi alloy.* Journal de Physique IV, 1995. **5**(C8, International Conference on Martensitic Transformations, Pt. 2): p. 605-10.

12. Jacobus, K., H. Sehitoglu, and M. Balzer, *Effect of stress state on the stress-induced martensitic transformation in polycryall-T.* Metallurgical and Materials Transactions A, 1996. **27**: p. 3066-3073.

13. Liu, Y., Z. Xie, J.V. Humbeeck, and L. Delaey, *Asymmetry of stress-strain curves under tension and compression for NiTi shape memory alloys.* Acta mater., 1998. **46**(12): p. 4325-4338.

14. Orgeas, L. and D. Favier, *Stress-induced martensite transformation of a NiTi alloy in isothermal shear, tension and compression.* Acta mater., 1998. **46**: p. 5579-5591.

15. Gall, K. and H. Sehitoglu, *The role of texture in tension-compression asymmetry in polycrystalline NiTi.* International Journal of Plasticity, 1999. **15**(1): p. 69-92.

16. Gall, K., H. Sehitoglu, Y.I. Chumlyakov, and I.V. Kireeva, *Tension-compression asymmetry of the stress-strain response in aged single crystal and polycrystalline NiTi.* Acta Mater., 1999. **47**: p. 1203-1217.

17. Sehitoglu, H., I. Karaman, R. Anderson, and e. al., *Compressive response of NiTi single crystals.* Acta mater., 2000. **48**: p. 3311-3326.

18. Adharapurapu, R.R., F. Jiang, K.S. Vecchio, and G.T. Gray III, *Response of NiTi shape memory alloy at high strain rate: A systematic investigation of temperature effects on tension-compression asymmetry.* Acta Materialia, 2006. **54**: p. 4609-4620.

19. Kakeshita, T., Y. Yoshimura, K.i. Shimizu, S. Endo, Y. Akahama, and F.E. Fujita, *Effect of hydrostatic pressure on martensitic transformation in Cu-Al-Ni shape memory alloys.* Transactions of the Japan Institute of Metals, 1988. **29**(10): p. 781-789.

20. Kakeshita, T., K. Shimizu, S. Nakamichi, R. Tanaka, S. Endo, and F. Ono, *Effect of hydrostatic pressures on thermoelastic martensitic transformation in aged Ti-Ni and ausaged Fe-Ni-Co-Ti shape memory alloys.* Materials Transc, 1992. **33**(1): p. 1-6.

21. Johari, G.P., J.G. McAnanama, and G. Sartor, *Effect of hydrostatic pressure on the thermoelastic transformation of Ni-Ti alloy and the entropy transformation.* Philosophical Magazine B, 1996. **74**(3): p. 243-257.

22. Jacobus, K., H. Sehitoflu, and M. Balzer, *Effect of stress state on the stress-induced martensitic transformation in polycrystalline Ni-Ti alloy.* Metallurgical and Materials Transactions A, 1996. **27**: p. 3066-3073.

23. Daroczi, L., D.L. Beke, C. Lexcellent, and V. Mertinger, *Effect of hydrostatic pressure on the martensitic transformation in near equiatomic Ti-Ni alloys.* Philosophical Magazine B, 2002. **82**(1): p. 105-120.

24. Monasevich, L.A., Y.I. Paskal, V.E. Prib, G.D. Timonin, and D.B. Chernov, *Effect of texture on the shape memory effect in titanium nickelide.* Metal Science and Heat Treatment, 1979. **21**(9): p. 735-737.

25. Li, D.Y., X.F. Wu, and T. Ko, *The texture of titanium-51.5 atomic% nickel rolling plate and its effect on the all-round shape memory effect.* Acta Metallurgica et Materialia, 1990. **38**(1): p. 19-24.

26. Mulder, J.H., P.E. Thoma, and J. Beyer, *Anisotropy of the shape memory effect in tension of cold-rolled 50.8Ti 49.2Ni (at.%) sheet.* Zeitschrift fur Metallkunde, 1993. **84**(7): p. 501-508.

27. Inoue, H., N. Miwa, and N. Inakazu, *Texture and shape memory strain in TiNi alloy sheets.* Acta Materialia, 1996. **44**(12): p. 4825-4834.

28. Shu, Y.C. and K. Bhattacharya, *The influence of texture on the shape-memory effect in polycrystals.* Acta Materialia, 1998. **46**(15): p. 5457-5473.

29. Yuan, W.Q. and S. Yi, *Determination of orientation distribution functions in a TiNi alloy austenite and a TiNiCu alloy martensite.* Scripta Materialia, 1999. **41**(12): p. 1319-1325.

30. Yuan, W.Q. and S. Yi, *Pseudo-elastic strain estimation of texture TiNi shape memory alloys.* Materials Science and Engineering A, 1999. **271**: p. 439-448.

31. Gall, K., T.J. Lim, D.L. McDowell, H. Sehitoglu, and Y.I. Chumlyakov, *The role of intergranular constraint on the stress-induced martensitic transformation in textured polycrystalline NiTi.* International Journal of Plasticity, 2000. **16**(10-11): p. 1189-1214.

32. Gall, K., H. Sehitoglu, R. Anderson, I. Karaman, Y.I. Chumlyakov, and I.V. Kireeva, *On the mechanical behavior of single crystal NiTi shape memory alloys and related polycrystalline phenomenon.* Materials Science & Engineering, A: Structural Materials: Properties, Microstructure and Processing, 2001. **A317**(1-2): p. 85-92.

33. Vaidyanathan, R., M.A.M. Bourke, and D.C. Dunand, *Texture, strain, and phase-fraction measurements during mechanical cycling in superelastic NiTi.* Metallurgical and Materials Transactions A, 2001. **32**(3): p. 777-786.

34. Hornbogen, E., G. Bruckner, and G. Gottstein, *Microstructure and texture of ausformed NiTi.* Zeitschrift fur Metallkunde, 2002. **93**(1): p. 3-6.

35. Gao, S. and S. Yi, *Experimental study on the anisotropic behavior of textured NiTi pseudoelastic shape memory alloys.* Materials Science and Engineering A, 2003. **363**: p. 107-111.

36. McNaney, J.M., V. Imbeni, Y. Jung, P. Papadopoulos, and R.O. Ritchie, *An experimental study of the superelastic effect in a shape-memory Nitinol alloy under biaxial loading.* Mechanics of Materials, 2003. **35**: p. 969-986.

37. Robertson, S.W., V. Imbeni, H.-R. Wenk, and R.O. Ritchie. *Crystallographic texture in austenitic Nitinol*. in *Proceedings of the International Conference on Shape Memory and Superelastic Technologies (SMST-2004)*. 2004. Baden-Baden Germany: SMST Society.

38. Brinson, L.C., I. Schmidt, and R. Lammering, *Stress-induced transformation behavior of a polycrystalline NiTi shape memory alloy: micro and macromechanical investigations via in situ optical microscopy.* Journal of the Mechanics and Physics of Solids, 2004. **52**: p. 1549-1571.

39. Robertson, S.W., X.Y. Gong, and R.O. Ritchie, *Effect of product form and heat treatment on the crystallographic texture of austenitic Nitinol.* Journal of Materials Science, 2006. **41**: p. 621-630.

40. Lange, R.G.D. and J.A. Zijderveld, *Shape memory effect and the martensitic transformation of titanium-nickel.* Journal of Applied Physics, 1968. **39**(5): p. 2195-2200.

41. Eucken, S. and J. Hirsch, *The effect of textures on shape-memory behavior.* Materials Science Forum, 1990. **56-58**(Martensitic Transform., Pt. 2): p. 487-92.

42. Zhao, L., *Texture development and anisotropic behavior in a Ti-45Ni-5Cu (at. %) shape memory alloy*, in *Materials Science and Engineering*. 1997, University of Twente: Enschede, Netherlends.

43. Liu, Y., Z.L. Xie, J.V. Humbeeck, and L. Delaey, *Effect of texture orientation on the martensite deformation of NiTi shape memory alloy sheet.* Acta Materialia, 1999. **47**(2): p. 645-660.

44. Fernandes, F.M.B., A.S. Paula, J. Canejo, K.K. Mahesh, R.J.C. Silva, R.M.S. Martins, A.M.A. Cardoso, and N. Schell. *Texture evolution during annealing of NiTi shape memory alloy*. in *Proceedings of the Internatinoal Conference on Shape Memory and Superelastic Technologies (SMST-2004)*. 2004. Baden-Baden German: SMST Society.

45. Robertson, S.W., V. Imbeni, H.-R. Wenk, and R.O. Ritchie, *Crystallographic texture for tube and plate of superelastic/shape-memory alloy Nitinol used for endovascular stents.* Journal of Biomedical Materials Research Part A, 2004. **72A**(2): p. 190-199.

46. Miyazaki, S., K. Otsuka, and C.M. Wayman, *The shape memory mechanism associate with the martensitic transformation in titanium-nickel alloys - I. Self Accommodation.* Acta Metallurgica, 1989. **37**(7): p. 1873-1884.

47. Miyazaki, S., K. Otsuka, and C.M. Wayman, *The shape memory mechanism associate with the martensitic transformation in titanium-nickel alloys - II. Variant coalescence and shape recovery.* Acta Metallurgica, 1989. **37**(7): p. 1885-1890.

48. Bhattacharya, K., *Microstructure of martensite: why it forms and how it gives rise to the shape-memory effect*. Oxford series on materials modelling, ed. A.P. Sutton and R.E. Rudd. 2003: Oxford University Press.

49. Chen, W.W., Q. Wu, J.H. Kang, and N.A. Winfree, *Compressive superelastic behavior of a NiTi shape memory alloy at strain rates of 0.001-750 s^{-1}.* International Journal of Solids and Structures, 2001. **38**: p. 8989-8998.

50. Liu, Y., Y. Li, and K.T. Ramesh, *Rate dependence of deformation mechanisms in a shape memory alloy.* Philosophical Magazine A: Physics of Condensed Matter: Structure, Defects and Mechanical Properties, 2002. **82**(12): p. 2461-2473.

51. Liu, Y., Y. Li, K.T. Ramesh, and J.V. Humbeeck, *High strain rate deformation of martensitic NiTi shape memory alloy.* Scripta Materialia, 1999. **41**(1): p. 89-95.

52. Liu, Y., Y. Li, Z. Xie, and K.T. Ramesh, *Dynamic deformation of shape-memory alloys: evidence of domino detwinning?* Philosophical Magazine Letters, 2002. **82**(9): p. 511-517.

53. Duerig, T.W. and T. Zadno, eds. *An engineer's perspective of pseudoelasticity*. Engineering aspects of shape memory alloys, ed. T.W. Duerig, K.N. Melton, D. Stockel, and C.M. Wayman. 1990, Butterworth-Heinemann, London. 394-413.

54. Liu, Y., Y. Liu, and J.V. Humbeeck, *Luders-like deformation associated with martensite reorientation in NiTi.* Scripta Materialia, 1998. **39**(8): p. 1047-1055.

55. Tan, G., Y. Liu, P. Sittner, and M. Saunders, *Luders-like deformation associated with stress-induced martensitic transformation in NiTi.* Scripta Materialia, 2005. **50**: p. 193-198.

56. Sittner, P., Y. Liu, and V. Novak, *On the origin of Luders-like deformation of NiTi shape memory alloys.* Journal of the Mechanics and Physics of Solids, 2005. **53**: p. 1719-1746.

57. Pieczyska, E.A., S.P. Gadaj, W.K. Nowacki, and H. Tobushi, *Phase-Transformation Fronts evolution for stress- and strain-controlled tension tests in TiNi shape memory alloy.* Experimental Mechanics, 2006. **46**: p. 531-542.

58. Miller, D.A., W.R. Thissell, and D.A.S. Macdougall, *Dynamic tensile plasticity and damage evolution in shape-memory Ni-Ti.* Journal de Physique IV, 2000. **10**: p. 341-346.

59. Miller, D.A., W.R. Thissell, G.T.G. III, and D.A.S. Macdougall, *Stress-induced martensitic phase transformations in NiTi shape memory alloys during dynamic loading.* Adaptive structures and materials systems (ASME), 2000. **60**: p. 51-63.

60. GrayIII, G.T., ed. *Classic Split-Hopkinson Pressure Bar Technique*. ASM-Handbook: Mechanical Testing and Evaluation, ed. H. Kuhn and D. Medlin. Vol. 8. 2000, ASM International: Metals Park, Ohio 44073-0002. 462-476.

61. Adharapurapu, R.R. and K.S. Vecchio, *Evolution of multiple-stage transformation (MST) in Ni-rich 50.8Ni-Ti: Effects of aging and cooling rate on the shape memory characteristics.* submitted to Journal (?), 2007.

62. Tan, G. and Y. Liu, *Comparative study of deformation-induced martensite stabilisation via martensite reorientation and stress-induced martensitic transformation in NiTi.* Intermetallics, 2004. **12**: p. 373-381.

63. Ono, N. and A. Sato, *Plastic deformation governed by the stress-induced martensitic transformation in polycrystals.* Trans. Jpn. Inst. Metals, 1988. **29**(4): p. 267-273.

64. Ono, N., A. Satoh, and H. Ohta, *A discussion on the mechanical properties of shape memory alloys based on a polycrystal model.* Trans. Jpn. Inst. Metals, 1989. **30**(10): p. 756-764.

65. Liu, Y. and D. Favier, *Stabilisation of martensite due to shear deformation via variant reorientation in polycrystalline NiTi.* Acta Materialia, 2000. **48**: p. 3489-3499.

66. Erbstoeszer, B., B. Armstrong, M. Taya, and K. Inoue, *Stabilization of the shape memory effect in NiTi: An experimental investigation.* Scripta Materialia, 2000. **42**: p. 1145-1150.

67. Liu, Y. and G.S. Tan, *Effect of deformation by stress-induced martensitic transformation on the transformation behavior of NiTi.* Intermetallics, 2000. **8**: p. 67-75.

68. Otsuka, K. and X. Ren, *Physical metallurgy of Ti-Ni based shape memory alloys.* Progress in Materials Science, 2005. **50**: p. 511-678.

69. Plietsch, R. and K. Ehrlich, *Strength Differential effect in pseudoelastic NiTi shape memory alloys.* Acta mater., 1997. **45**(6): p. 2417-2424.

70. Bhattacharya, K. and R.V. Kohn, *Symmetry, texture and recoverable strain of shape-memory polycrystals.* Acta mater., 1996. **44**(2): p. 529-542.

71. Miyazaki, S., *Thermal and stress cycling effects and fatigue properties of Ni-Ti*, in *Engineering asapects of shape memory alloys*, T.W. Duerig, K.N. Melton, D. Stockel, and C.M. Wayman, Editors. 1990, Butterworth Heinemann: London. p. 394-413.

72. Gupta, S.P. and A.A. Johnson, *Morphology and crystallography of β' martensite in TiNi alloys.* Trans. JIM, 1973. **14**: p. 292-302.

73. Knowles, K.M. and D.A. Smith, *The crystallography of the martensitic transformation in equiatomic nickel-titanium.* Acta Metallurgica, 1981. **29**: p. 101-110.

74. Onda, T., Y. Bando, T. Ohba, and K. Otsuka, *Electron-microscopy study of twins in martensite in a Ti-50.0 at. percent Ni alloy.* Mat. Trans. Jap. Inst. Metals, 1992. **33**: p. 354-359.

75. Nishida, M., K. Yamauchi, I. Itai, H. Ohgi, and A. Chiba, *High resolution electron-microscopy studies of twin boundary structures in B19' martensite in the Ti-Ni shape-memory alloy.* Acta Metall. Mater., 1995. **43**: p. 1229-1234.

76. Liu, Y., Z. Xie, J.V. Humbeeck, L. Delaey, and Y. Liu, *On the deformation of the twinned domain in NiTi shape memory alloys.* Philosophical Magazine A, 2000. **80**(8): p. 1935-1953.

77. Zheng, Q.S. and Y. Liu, *Prediction of the detwinning anisotropy in textured NiTi shape memory alloy.* Philosophical Magazine A, 2002. **82**(4): p. 665-683.

78. Liu, Y. and Z.L. Xie, *Twinning and detwinning of <011> type II twin in shape memory alloy.* Acta Materialia, 2003. **51**: p. 5529-5543.

79. Sehitoglu, H., R. Hamilton, D. Canadinc, X.Y. Zhang, K. Gall, I. Karaman, Y. Chumlyakov, and H. Maier, *Detwinning in NiTi alloys.* Metallurgical and Materials Transactions A, 2003. **34**: p. 5-13.

80. Nishida, M., C.M. Wayman, and T. Honma, *Precipitation processes in near-equiatomic TiNi shape memory alloys.* Metallurgical Transactions A, 1986. **17**: p. 1505-1515.

81. Pelton, A., J. DiCello, and S. Miyazaki. *Optimization of processing and properties of medical-grade Nitinol wire*. in *Proceedings of the International*

Conference on Shape Memory and Superelastic Technologies (SMST). 2000. Pacific Grove, CA.

82. Adharapurapu, R.R. and K.S. Vecchio, *Microstructure development in Ni-rich 60NiTi (wt.%) alloy: Aging studies on precipitation reactions and shape memory characteristics.* submitted to Metallurgical Transactions A, 2007.

83. McKelvey, A.L., *Ph.D. Dissertation, Fatigue-crack Propagation behavior in the Shape-Memory and Superelastic Alloy Nitinol*, in *Materials Science and Mineral Engineering*. 1999, Universtiy of California, Bekeley. p. 23-38.

84. Warlimont, H., L. Delaey, R.V. Krishnan, and H. Tas, *Thermoelasticity, pseudoelasticity and the memory effects associated with martensitic transformations. Part 3. Thermodynamics and kinetics.* Journal of Materials Science, 1974. **9**: p. 1545-1555.

85. Melton, K.N. and O. Mercier, *The mechanical properties of nickel-titanium (NiTi)-based shape memory alloys.* Acta Metallurgica, 1981. **29**(2): p. 393-398.

86. Wayman, C.M. and H.C. Tong, *On the equilibrium temperature in thermoelastic martensitic transformations.* Scripta Metallurgica, 1977. **11**(5): p. 341-343.

87. Frick, C.P., A.M. Ortega, J. Tyber, A.E.M. Maksound, H.J. Maier, Y. Liu, and K. Gall, *Thermal processing of polycrystalline NiTi shape memory alloys.* Materials Science and Engineering A, 2005. **405**: p. 34-49.

88. Jiang, F. and K.S. Vecchio, *Fracture of Nitinol under quasi-static and dynamic loading conditions.* submitted to Metallurgical and Materials Transactions A, 2007.

89. McKelvey, A.L. and R.O. Ritchie, *Fatigue-crack growth behavior in the superelastic and shape-memory alloy Nitinol.* Metallurgical and Materials Transactions A, 2001. **32**: p. 731-743.

6 MICROSTRUCTURE DEVELOPMENT IN Ni-RICH 55NiTi ALLOY: AGING STUDIES ON PRECIPITATION REACTIONS AND SHAPE MEMORY CHARACTERISTICS

6.1 Abstract

The current work investigates the influence of aging on the microstructural evolution of a new Ni-rich 60NiTi (weight %). It is demonstrated that this alloy is capable of exhibiting shape memory (SM) and superelasticity (SE). It is known that aging in Ni-rich NiTi alloys leads to the appearance of the metastable Ti_3Ni_4 precipitates which promotes the occurrence of R-phase and hence a multiple transformation path: $B2 \rightarrow R \rightarrow B19'$. Additionally, these precipitates are conducive to the all-round shape memory effect and strengthening of B2 matrix leading to precipitation hardening. Moreover, at higher aging temperatures or, longer aging times, Ti_3Ni_4, Ti_2Ni_3 and $TiNi_3$ precipitates form in seriatim, with $TiNi_3$ being the only stable phase. By varying heat-treatments, a wide range of transformation temperatures may be achieved in these alloys through the control of Ni concentration in the matrix. Since precipitates in Ni-rich NiTi alloys greatly affect the shape memory properties, initial investigations were focused on precipitation studies using conventional metallographic techniques and a TTT (Time-Temperature-Transformation) diagram was obtained for the composition Ti - 55 at. pct or 60 wt. pct Ni. Additionally, the transformation temperatures and the hardness were measured as a function of both aging temperature and time. Combining the upper temperature limits of precipitation

of different phases observed in the present work with the observations from [1, 2], an upper precipitation limit (UPL) phase diagram has been constructed for Ni-Ti alloys system as a function of Ni concentration between 50.6– 56 at pct. Finally, it is shown that recoverable strains between 3-6% may be obtained in SE and SM 55NiTi depending on aging heat-treatments.

6.2 Introduction

The development of novel materials is critical for the advancement of materials engineering and is often the precursor for many progressive and innovative technologies [3-6]. Developed in the 1950's by the Naval Ordnance Laboratory, NiTi 'Nitinol' alloy was found to have very unique properties of shape memory (SM) and superelasticity (SE) at temperatures that proved to be very practical both in common and special engineering applications [7-11]. This has led to the recognition of NiTi as a principal contender among smart materials in a variety of novel applications [11-13].

The early investigations at the NOL by Buehler and his colleagues [9, 14-16] focused on a series of non-magnetic Ni-Ti alloys based on the ductile intermetallic compound NiTi that displayed two distinct sets of properties as a function of Ni composition and heat treatment [16]. This division was initially based upon hardness measurements over a range of Ni composition, viz., 50 to 64 weight pct (remainder being titanium, see Figure 6.1). It can be seen that equiatomic and near-equiatomic (i.e., near 55 weight % Ni) alloys exhibit minimum hardness and are relatively unaffected by cooling rates when cooled from 950°C. In contrast, the alloys composed of Ni in excess of 55 weight pct exhibit increasing hardness under quenched

conditions. A further mark of distinction was revealed in the microstructural differences during metallographic studies. While 55-Nitinol (wt %) was found to be single-phase alloy of NiTi (oxide and nitride impurities were present in minute quantities), Ni-rich NiTi alloys were found to contain $TiNi_3$ phase (in the form of precipitates) in equilibrium with the NiTi matrix phase. It has been shown that a series of thermomechanical treatments, i.e., various combinations of solution-treatments combined with cold work and/or anneal heat-treatments etc., are required to optimize the SE and SM properties of equiatomic NiTi alloys [16-22]. However, departure from the 55-Nitinol (wt pct), i.e. near stoichiometric NiTi, towards the Ni-rich alloys leads to the second group of Nitinol alloys that are also non-magnetic, but are at variance with the former alloys in that the latter group can be thermally hardened by aging heat treatments to high hardness levels, viz., ~60 - 70 R_C [16, 23, 24]. The latter group, i.e., NiTi alloys spanning the composition range from 56 to 62 wt pct Ni (remainder being titanium) were generically designated as 60-Nitinol alloys (designated by wt %) [16]. While both the conventional 55-nitnol and the more recent 60-Nitinol possess common unusual properties such as non-magnetic character, marine corrosion resistance; due to the difference in hardness, microstructural features and the general effect of heat treatment on their properties, 55-Nitinol and 60-Nitinol were considered as separate and distinct alloy types [16]. Furthermore, an additional divergence was seen among the 60-Nitinol alloys, namely, between the ‘quenched’ and ‘furnace cooled’ alloys, as shown in Figure 6.1. While it was pointed out by Buehler and Wang [16] that not only the high hardness ‘quenched’ or low hardness ‘furnace cooled’ 60-Nitinol alloys could be produced, but also indicated the possibility

of attaining alloys with any desired intermediate hardness accomplished by either intermediate cooling rates or by utilizing some sort of ‘overaging’ or pseudo-tempering’ post-quench heat treatment (later investigations by Nitinol Technology Inc., Mountain View, WA, have attributed the SE and SM behavior in 60-nitnol alloys directly resulting from this crucial difference in cooling rate, viz., quenching vs. furnace cooling, respectively [23, 25, 26].

In spite of many promising properties of 60-Nitinol alloys, such as high hardenability, ability to tailor hardness through aging heat-treatments only, high corrosion resistance, low susceptibility to stress corrosion failure, ‘they exhibited the most noteworthy engineering weakness, viz., notch sensitivity’ [16]. Due to the difficulties in forming and hot-working, machining and forming these materials into near-net shapes for practical applications became difficult and impractical [26]. Therefore, 55-Nitinol was eventually preferred over 60-Nitinol, as evidenced by the numerous products in bio-medical and sensor applications. However, since the development of hot rolling methods for 60-Nitinol and special fabrication techniques (by Nitinol Technologies Inc., Mountain View, WA) [23, 25, 26], a number of patents have emerged that exploit some of the afore-mentioned unique properties of the alloys [23, 25, 27, 28]. A decade ago, it was shown that under special heat treatment conditions, both the SM and SE effects could be produced in the alloy from the same ingot without any additional mechanical processing [23, 25, 26]. Since then, the interest in the development of Ni-rich 60-Nitinol alloys has seen a renaissance, although very little work exists on the mechanical properties of these alloys [24, 29-31].

Properties of NiTi shape memory alloys are known to be very sensitive to the Ni composition. For example, a change in Ni content from 50 at.% to 51.5 at.% is known to alter the M_s (martensite start temperature) from above room temperature (22°C) to below -100°C [32]. Moreover, NiTi alloys containing more than 50.6 at.% Ni decompose on aging through the precipitation of Ti_3Ni_4, Ti_2Ni_3 and $TiNi_3$, in seriatim, with Ti_3Ni_4 and Ti_2Ni_3 being metastable phases [1, 2]. Although the phase diagram of NiTi system is very important to understand effects of heat-treatment on the structure-property relationships, the correct phase diagram was established only after three decades of conflicting reports and observations, see [21] for a detailed account of the controversies in this regard. It was the work by Nishida *et al.* [1], and subsequently, Kainuma *et al.* [2] that debunked most of the inconsistencies in various observations and established the TTT (Time-Temperature-Transformation) charts for alloys having compositions (in at.%) Ti-52Ni, Ti-54Ni, Ti-56Ni.

NiTi B2 parent phase $\rightarrow \alpha_1 + Ti_3Ni_4 \rightarrow \alpha_2 + Ti_2Ni_3 \rightarrow \alpha_3 + TiNi_3$,

where α_1, α_2, α_3 are matrices with different Ni concentration.

Previous works have shown that the appearance of Ti_3Ni_4, Ti_2Ni_3 and $TiNi_3$ precipitates depends strongly on the aging parameters, viz., temperature and time [1, 2]. Given that the NiTi alloys are very sensitive to Ni composition, the objective of the present work is to investigate the microstructural evolution of 60NiTi as a function of aging, thus, leading to a TTT chart for 60NiTi based on conventional metallographic studies. These results will then be combined with the observations of Nishida [1] and Kainuma [2] to obtain a comprehensive picture of precipitation processes in Ni-rich NiTi shape memory alloys. In addition to the precipitation processes, the

transformation temperatures (austenite to martensite etc.) and hardness measurements are investigated as a function of aging parameters. Additionally, the SE and SM properties of Ni-rich 60NiTi are demonstrated with an emphasis on recoverable strains and ductility. The motivation for the present work is due to its promising bio-medical and actuator related properties such as high strength, very high hardness, low thermal conductivity and low modulus and the ability to obtain very high surface finish, immunity to most corrosive agents and non-magnetic behavior [23, 24, 26]. Only very recently, interest in the development of 60NiTi has seen a renaissance [24, 26, 29-31], however, very little is known about the aging heat-treatment and microstructure - property relationship for this particular intermetallic alloy system. There is also a drive governed by a growing interest in various defense applications for these materials and hence the present work is a preliminary step in ascertaining the applicability of Ti-55Ni SMA alloys under impact loading conditions.

6.3 Experimental Procedure

Ni-rich Nitinol, 60NiTi alloys were obtained from *Nitinol Technologies, Inc. (Edgewood, WA)* in the form of square cross-section measuring 15mm x 15mm that were hot-rolled at 950°C. Specimen measuring 5mm thick were cut from this stock and were solution-treated (ST) at 1100°C for 1hour in evacuated quartz tubes and then quenched in ice water. They were subsequently aged according the schedule given in Table 6.1. Polished samples were then prepared by mechanical polishing to diamond finish and then etched with $HF+HNO_3$+deionized water for metallographic studies. In addition, 3mm diameter disk specimens measuring 0.1-0.2 μm in thickness were

prepared for TEM studies on a 120kV Philips EM420. Prior to the TEM observation, they were electropolished using the twin jet method that utilized electrolyte of composition 20% H_2SO_4 + 80% Methanol at 10 °C and 15-20V. A Philips XL 20 SEM equipped with both secondary and backscattered imaging capabilities and capable of energy dispersive X-ray (EDX) analysis system (INCA software, Oxford Instruments) and a Rigaku X-ray diffractometer (XRD, rotating anode type and Cu K_α radiation) was utilized for analyzing the matrix and different precipitates.

In addition to the standard metallographic techniques that were used to observe the structural evolution in terms or precipitation sequence and morphology, differential scanning calorimetric (DSC, Perkin Elmer Pyris 7 Series) and (Rockwell C) hardness studies were conducted to measure the variation in the transformation temperatures and hardness values with aging, respectively.

Table 6.1 Aging schedule for Ni-rich (at.%) 55NiTi alloys

Temperature	400°C, 500°C, 600°C, 650°C, 700°C, 750°C, 800°C, 850°C, 900°C, 1000°C
Time (Hours)	0.5 h, 1 h, 2 h, 5 h, 10 h, 24 h, 48 h

6.4 Results and Discussion

6.4.1 As-received material: microstructure

The as-received (AR: hot-rolled) 60NiTi alloy consisted predominantly of $TiNi_3$ in elongated and small blocky morphologies in a matrix of martensitic phase, see Figure 6.2a. Figure 6.2(b, c) show the TEM micrographs of these precipitates, note the extensive line defects within the elongated $TiNi_3$ precipitates (in Figure 6.2b)

accumulated during the hot rolling process at 950°C. As will be shown in a later section, $TiNi_3$ is the only phase that precipitates during aging at 950°C, and this explains its presence in the as-received microstructure. In addition to $TiNi_3$, a small amount of occasional Ti_2Ni_3 lenticular precipitates with preferred orientation(s) were observed in the microstructure, as shown in Figure 6.2d; this may be due to local variations in temperatures during hot-rolling or subsequent cooling that bring down the temperature below 750°C, the temperature at which Ti_2Ni_3 precipitates from the matrix. The 55NiTi AR plate matrix is martensitic based on the DSC observations in Figure 6.3. The multiple peaks observed on the DSC curves are due to the presence of dislocations and/or precipitates [33].

It has been shown in the current work and elsewhere [23-26, 29, 31] that both SE and SM properties of 60NiTi may be obtained from the same ingot without resorting to cold-work or solutionizing treatments of a combination of both, which are usually very expensive. A range of SE and SM properties may be obtained by strictly controlling the microstructure through various aging conditions only: SE may be obtained from as-received (AR – material that has been hot-worked) or solution-treated (ST) alloys by aging them between 600±20°C and 800±20°C between 0.5 and several hours followed by a water-quench (WQ). The AR-aged-WQ 60NiTi exhibits SE with high strength and ductility, 800 - 1000 MPa and 15-20%, respectively [23, 24]; whereas the ST-aged-WQ exhibits very low ductility (typically < 3 % in tension) and hence its SE behavior is severely restricted. SM effect may be achieved in 60NiTi by an isothermal anneal of the AR (with prior hot-worked) or ST material to a

temperature between 600°C and 900°C until thermal equilibrium is attained followed by a controlled furnace cool (~1°C/min, or 10-15 hrs) [23].

6.4.2 Solution-treated and/or Furnace-cooled materials: microstructure

The microstructure of the homogenized (solution-treated + water-quenched: ST-WQ) 60NiTi is shown in Figure 6.4a, while that of solution-treated and furnace cooled (ST-FC) in Figure 6.4b; 60NiTi does not form any martensite upon quenching from 1100°C, whereas lenticular martensite plates are clearly visible in Figure 6.4b within the grains, along with block-shaped $TiNi_3$ precipitates that formed on the grain boundary and in the grain interior where they exhibited long elongated needle morphology of different lengths. The M_s (martensite start temperature) for ST-WQ 60NiTii was found to be below -150^{o}C, measured using a cryo-DSC, and according to [32], the material in solution-treated condition may not show any martensitic transformation even if cooled below 4 K (-269^{o}C). The ST-FC sample however exhibited the following transformation temperatures: M_s = 16°C, M_f = 0°C, A_s = 38°C, A_f = 57°C, indicating a martensitic microstructure at 20^{o}C, see Figure 6.3.

In contrast, ST-WQ 55NiTi (wt.%) (microstructure shown in Figure 6.4c) exhibited a typical twinned martensitic microstructure with evident surface relief, whereas, and upon ST-FC, it forms only cubic austenitic phase. Nishida *et al.* [1] report that they have observed surface relief in ST-FC 55NiTi (wt.%) Nitinol. However, in the current study, the measured transformation temperatures were: A_f = 7°C and M_s < 0°C, which implies that the stable room temperature (RT) phase is austenite. Nishida *et al.* [1] also report the presence of Ti_2Ni_3 and Ti_3Ni_4 precipitates

in ST-FC 52NiTi (at.%) specimen; however, in 60NiTi (wt.%), martensite and $TiNi_3$ precipitates were the only observed phases. The absence of Ti_2Ni_3 and Ti_3Ni_4 precipitates in ST-FC 60NiTi may be due to the insufficient Ni concentration in the grain interior as a result of its depletion from the matrix during the formation of $TiNi_3$ (75 at.% Ni) at high temperatures; the matrix may not contain enough Ni for the precipitation of Ti_2Ni_3 or Ti_3Ni_4 that form during aging at lower temperatures (upper precipitation limit is ~ 780°C and 680°C, respectively). Figure 6.3(a, b) compares the DSC curves for AR and ST-FC 60NiTi; the Ni content in the matrix has been reduced considerably by partitioning it into the $TiNi_3$ precipitates, thus leading to transformation temperatures greater than room temperature (RT). These comparisons between 52NiTi (at.%) and 55NiTi (at.%) or 60NiTi (wt.%) indicate the sensitivity of NiTi alloys' microstructure with respect to Ni concentration. For indexing the XRD patterns of different phases, the crystallographic information was used from the references compiled by Otsuka and Ren [21].

6.4.3 Aging studies: Microstructure of Solution-treated (ST) and Aged 55NiTi

The aging studies of 60NiTi (wt.%) revealed a precipitation sequence, similar to the order observed by Nishida *et al.* [1] and Kainuma *et al.* [2], with a certain upper limit to the precipitation of different phases, viz. Ti_3Ni_4, Ti_2Ni_3 and $TiNi_3$. The sequence, following Nishida *et al.* [1] nomenclature, may be described as follows:

$$\alpha_o \rightarrow \alpha_1 + Ti_3Ni_4 \rightarrow \alpha_2 + Ti_3Ni_4 + Ti_2Ni_3 \rightarrow$$

$$\alpha_3 + Ti_2Ni_3 \rightarrow \alpha_4 + Ti_2Ni_3 + TiNi_3 \rightarrow \alpha_5 + TiNi_3$$

$$450 \pm 10°C \leq T \leq 690 \pm 10°C$$

$$\alpha_o \rightarrow \underline{\alpha'_1 + Ti_2Ni_3} \rightarrow \underline{\alpha'_2 + Ti_2Ni_3 + TiNi_3} \rightarrow \alpha'_3 + TiNi_3$$

$$690 \pm 10°C \leq T \leq 780 \pm 10°C$$

$$\alpha_o \rightarrow \underline{\alpha''_1 + TiNi_3}$$

$$780 \pm 10°C \leq T \leq 1010 \pm 10°C$$

where α_o is the ST-WQ supersaturated 60NiTi (wt.%), α_i (i = 1 to 5) is the matrix (with a Ni composition < 60 at.%) in equilibrium with Ti_3Ni_4 etc. Long term aging studies (t ~ 5000 hours) [1, 2] were considered highly impractical in view of any industrial or practical applications for 60NiTi (wt%), and therefore, in the current study, aging time was varied between 0.5 to 48 hours only. Consequently, only the precipitation reactions underlined above were observed upon aging. The present study, therefore, addresses issues like aging-microstructure-properties (such as transformation temperatures and hardness) in a restricted aging-time window. Since Kainuma *et al.* [2] observed the same sequence of precipitation of different phases for NiTi alloys with Ni concentration > 55 at.% (or 60wt.%), there is no loss of generality in assuming that 60NiTi (wt.%) would not exhibit similar complete precipitation sequence, as indicated above. The microstructural development is divided according to the above sequence and is enunciated in detail subsequently.

6.4.3.1 Aging between 400 °C and 680±10 °C

Figure 6.5 indicates the characteristic optical micrographs of various microstructures observed in 60NiTi (wt.%) when aged between 400°C and 680±10°C. Between nearly 400°C and 450 ±10°C, the XRD peaks corresponding to Ti_3Ni_4 precipitates were barely observable. However, at 500°C, significant peak intensity of

Ti_3Ni_4 phase was easily discernable (see Figure 6.6a), though the optical micrographs do not show any changes in the microstructure. This is largely due to the small size of the precipitates which has been confirmed by [2]. At 600°C, aging at 0.5 h and 1 h produced only Ti_3Ni_4 precipitates (identifiable again through XRD peak identification). However, aging for 5 h revealed the presence of plate like Ti_2Ni_3 precipitates (see Figure 6.5d), which seemed to grow in three crystallographically different directions, and the growth is largely confined within the grain boundaries. With the appearance of Ti_2Ni_3 precipitates (corresponding to the presence of XRD peaks in Figure 6.6b) there is a concomitant drop in the peak intensities of Ti_3Ni_4 precipitates, indicating that they are dissolving back into the matrix and that Ti_2Ni_3 phase is growing at the expense of Ti_3Ni_4. This trend continued with an increase in aging time where, at 48 h aging time, the Ti_3Ni_4 peak intensity is much lower (only a few percent) than the Ti_2Ni_3 peak intensities. Additionally, with increasing aging time, the Ti_2Ni_3 precipitates grew, i.e., elongated until they occupy the entire grain dimension, as clearly evidenced in Figure 6.5(e-i). In Figure 6.5(g-i), the grain boundaries are more clearly visible due to the contrast contributed by a continuous and often blocky Ti_2Ni_3 precipitates that form at the grain boundary. These specimens were macroetched in 49% HF in order to remove the Ni-Ti matrix and expose the Ti_2Ni_3 plate morphology for further spectroscopy (EDS) analysis that confirmed the Ni composition as 40.0±0.12%. Nishida *et al.* [1, 34] have reported similar morphology and distribution of these precipitates in Ti-52Ni (at.%) alloy. They also reported four variants of oval plate-like Ti_3Ni_4 precipitates (trigonal R3 structure [21]) with lenticular cross-section and a $\{111\}_{B2}$ habit plane. It should be noted in

interpreting the microstructure that, in many of the optical micrographs in this work, interference diffraction contract was utilized to accentuate the precipitate morphology that resulted in a surface relief effect for the precipitates.

6.4.3.2 Aging between 680±10 °C and 780±10 °C

Figure 6.9 shows typical microstructures of 60NiTi (wt.%) aged at 700°C and 750°C. Aging at 700°C for as little as 1 h results in the entire matrix being populated by Ti_2Ni_3 and $TiNi_3$ phases. Ti_2Ni_3 precipitate forms within the grain with plate-like morphology (see Figure 6.7), whereas, the $TiNi_3$ phase is in the form of blocky precipitates forming a continuous network along the grain boundary and occasionally appears near the grain boundary too. Furthermore, aging at 700°C leads to the slow dissolution of Ti_2Ni_3 phase into the matrix (as evidenced by a decrease in the corresponding XRD peak intensity, see Figure 6.8) and $TiNi_3$ precipitates start forming within the grain as a small cluster of particles, see Figure 6.9(a-c). This microstructure is typical of the alloy aged at 700°C up to 48 h aging time. Aging at 750°C, the microstructure evolves to a condition where blocky $TiNi_3$ precipitates are prevalent throughout the grain boundary and also within the grain (near the grain boundary) and Ti_2Ni_3 now appears in smaller needle shaped morphology. EDS analysis of the precipitates confirmed the Ni composition of $TiNi_3$ (hexagonal DO_{24} or $P6_3/mmc$ [21]) as 75±0.15 %. Nishida *et al.* [1, 34] report the formation of tetragonal Ti_2Ni_3 that is similar in structure to $Ti_{40}Ni_{56.3}Cu_{3.5}$ alloy and deduce an orientation relationship $(010)_{Ti_2Ni_3} \| (\bar{1}10)_{TiNi}$, $(501)_{Ti_2Ni_3} \| (111)_{TiNi}$ between Ti_2Ni_3 and the parent B2 NiTi matrix. Two phenomena can be seen occurring during isothermal aging at

750°C for longer aging time: the grain boundary $TiNi_3$ precipitates preferentially coarsen and the $TiNi_3$ phase that forms near the grain boundary are smaller, and at many places, a precipitate free zone (PFZ) is developing that widens with aging temperature and time. These PFZ's are more discernable at higher temperature aging and similar to the PFZ's observed in Al-Li alloys [35, 36] and usually develop due to the rapid depletion of excess Ni near the grain boundary. The depletion in Al-Li alloys was established as result of accelerated growth of grain boundary $LiAl_3$ thus leading to a widening PFZ whose thickness varies as a square root of time [35, 36]. It should be mentioned that the presence of PFZ greatly affects the mechanical behavior and the deformation or failure mechanisms in Al-Li [37, 38]; their effect in Ni-rich NiTi is under investigation.

Interestingly, Nishida and Wayman, and Hara *et al.* [34, 39] have observed striated structures in the coarse Ti_2Ni_3 particles formed after very long aging times (100 – 5000 h) and posited that Ti_2Ni_3 itself undergoes a martensitic transformation from the parent tetragonal phase to an orthorhombic intermediate phase characterized by antiphase-like domain structure, and finally to a low temperature monoclinic needle-like morphology.

6.4.3.3 Aging between 780±10 ^{o}C and 1015±10 ^{o}C

Figure 6.10 shows the microstructural changes occurring in 60NiTi (wt.%) during isothermal aging at 800 °C and 850 °C. The Ti_2Ni_3 precipitates no longer form above ~800°C and only $TiNi_3$ precipitates (see Figure 6.8) in the form of small blocky precipitates on the grain boundaries that coarsen with aging time (see Figure 6.10c, e).

$TiNi_3$ also forms as small particles or elongated needles within the grain interior; however, a precipitate free zone develops between the grain boundary and the grain interior (see Figure 6.10e, f). Compared to the Ti-52Ni (at.%) alloy [1], $TiNi_3$ tends to form at lower aging times in 60NiTi (wt.%), perhaps due to the higher Ni concentration in the latter alloy that leads to the acceleration in its nucleation and growth. The smaller $TiNi_3$ particles were seen to dissolve gradually in the matrix, and at their expense, the $TiNi_3$ needles grow in length with increase in aging time. At 900°C and 1000°C the kinetics of nucleation and growth of $TiNi_3$ decreases (see Figure 6.11); although the morphology is similar to the structures observed between 800°C and 850°C, the grain interior is less populated by the precipitates at higher temperature. At isothermal aging for 48 hours at 900°C (see Figure 6.11d), the gain boundary $TiNi_3$ coarsened rapidly, while the grain interior tend to dissolve most of the $TiNi_3$. At 1000°C isothermal aging, the microstructure is nearly devoid of $TiNi_3$ in the grain interior after only 24 h aging time and consists of only moderately coarsened $TiNi_3$ precipitates in the grain boundary. At around 1015 ± 10°C, the specimen is free of any secondary phases, suggesting that the solidus line of NiTi phase in 60NiTi (wt.%) is ~ 1015 ± 10°C, consistent with the NiTi phase diagram [21].

6.4.4 Time-Temperature-Transformation and precipitation limits

The precipitation results obtained above are summarized as a TTT chart in Figure 6.12 using nomenclature similar to [1]. Since aging studies were conducted only until 48 h aging time, a complete precipitation C-curves are not easily evident as observed in [1, 2]. However, the upper temperature limit at which each of the three

precipitate phases, viz., Ti_3Ni_4, Ti_2Ni_3 and $TiNi_3$, form can be still deduced from the TTT chart in Figure 6.12. Combining these upper temperature limit (UTL) observed in the current study with those measured in [1, 2], one can construct a phase-diagram that maps this temperature limit as a function of Ni concentration in Ti-Ni alloys; the resulting graph is shown in Figure 6.13. Based on previous works [1, 2] and the current investigation, it can be concluded that Ti_3Ni_4 and Ti_2Ni_3 are metastable phases that would, at higher aging temperatures or longer aging times, eventually lead to the formation of the $TiNi_3$ as the equilibrium phase. For Ni-Ti alloys with Ni composition between 54 and 56 (at.%), the UTL of precipitation of Ti_3Ni_4 is nearly constant at ~ 680 ± 10°C. However, the UTL of precipitation for Ti_2Ni_3, in Ti-Ni alloys with Ni ≥ 54 at.% reduces rapidly with increase in Ni concentration. Hence, in the current work, it was very difficult to observe the precipitation of only Ti_2Ni_3, and $TiNi_3$ was more likely to form along with Ti_2Ni_3.

6.4.5 Microstructure of Furnace cooled 60NiTi (wt.%)

As indicated earlier, the AR (with prior hot-working) 60NiTi (wt.%) that has been soaked at a temperature between 600^{o}C and 800°C and furnace-cooled (FC) in an oven at a controlled rate of ~1°C/min, produces a microstructure that exhibits shape memory properties, the corresponding micrographs are shown in Figure 6.14. Depending on the starting temperature of the furnace cool, the final microstructure consists of a combination of Ti_3Ni_4 ,Ti_2Ni_3 and $TiNi_3$ in a martensite matrix. Furnace cooling from higher temperatures such as 800^{o}C or 900^{o}C leads to a greater depletion of Ni in the matrix through the formation of $TiNi_3$ and thus, the final microstructure

may contain only $TiNi_3$ phase in martensite microstructure. Otherwise, furnace cooling from between 600^{o}C and 800^{o}C, the specimen spends greater time at intermediate temperatures where Ti_2Ni_3 and $TiNi_3$ are most likely to form.

6.4.6 DSC: Evidence of Shape memory

Due to the removal of Ni from the matrix in the form of precipitates, the overall Ni composition in the matrix reaches near equiatomic level, thus leading to stable shape memory effect between 20^{o}C and 70^{o}C. Figure 6.15 and Figure 6.16 demonstrate the evidence of shape memory behavior through DSC observations for ST-anneal-FC and AR-anneal-FC 60NiTi (wt.%), respectively. While the ST-anneal-FC samples show only one-peak on the DSC curve during cooling or heating, the AR-anneal-FC exhibits multiple peaks, similar to the findings of [33, 40]. The likely reason seems to be that a direct austenite – martensite (B19') is resisted by the precipitates and the extensive line defects that formed during hot rolling procedures, thus leading to a multiple-step transformation, viz., B2-R-B19'. However, the ST-aged-WQ structures possess only the precipitates which do not seem to resist a direct B2-B19' transformation, indicating that the dislocations are the governing factor in the transformations observed in these alloys. All the DSC data point to an austenite start temperature, $A_s > 22°C$, i.e., room temperature. However, the transformation is more pronounced for SM 60NiTi (wt.%) without any prior solution-treatment. These findings indicate that the transformation temperatures may be delicately controlled by heat-treatment alone and any use of prior cold work or solution-treatment processes may be obviated, thus proving economically beneficial.

6.4.7 Hardness

The Hardness of solution-treated 60NiTi (wt.%) was found to be as high as 67 R_C. The variation in hardness with aging temperature and time for the AR+aged and ST+aged 60NiTi (wt.%) is shown in Figure 6.17. The homogenizing heat-treatment at 1100^{o}C completely anneals the sample with further aging leading to several hardening precipitates and, overall, the hardness of the alloy remains high between 70 and 55 R_C. The AR 60NiTi (wt.%) has a martensitic microstructure. Aging above 580^{o}C, the Ni composition in the matrix adjusts to a value such that the matrix is austenitic (see Figure 6.18). This is reflected in the measure hardness values shown in Figure 6.17 where the martensitic structure is softer than the austenitic matrix. Aging between 600^{o}C and 800^{o}C, the hardness steadily increases from 40 to 55 R_C. Beyond 800^{o}C, the AR material is annealed and contains only the stable $TiNi_3$ precipitates; thus the structure is similar to the homogenized and aged material that exhibits a high hardness but brittle behavior. The aging heat treatments of the material that obviate the ST process exhibit reasonable ductility and high strength and also greater SE or SM characteristics [23, 24, 29]. Additionally, the indentation studies used reasonably high loads so that the indentation does not recover in the material even after room temperature aging for several days, therefore these values may be taken as 'real' hardness values.

6.4.8 Superelasticity and Shape Memory in 60NiTi (wt.%)

As shown in Figure 6.18, the DSC curves indicate that the AR material is martensitic and the aged alloy is austenitic. The corresponding shape memory and

superelastic characteristics of 60NiTi (wt.%) are compared with those of 50NiTi (at.%) or 55NiTi (wt.%) in Figure 6.19. In Figure 6.19a, the alloys are loaded to 3% in tension followed by unloading. Subsequently, the specimen is reloaded to 6% followed by unloading. The stress-strain data indicate three important observations:

(1) During the first loading cycle, while the elastic portions of both the alloys coincide up to ~400 MPa, the main difference between 55NiTi (wt.%) and 60NiTi (wt.%) becomes evident in the plateau region. In 55NiTi (wt.%), the plateau corresponds to the austenite $\rightarrow$ martensite stress-induced martensitic (SIM) transformation that begins with the formation of Lüder bands [41] and a concomitant drop in the load (at ~1%). Further transformation occurs at constant stress until the end of the plateau. However, in 55NiTi, there is no indication of load drop and the stress-strain curve monotonically increases beyond the 1% strain value. Since upon unloading, the material recovers the 3% strain, it is reasonable to assume that SIM occurs in 60NiTi (wt.%).

(2) Furthermore, the “plateau” region of 60NiTi (wt.%) has a finite slope indicating that increased stress is necessary to drive the SIM transformation. One can hypothesize that any Lüder bands that may have formed could be ‘locked’ in by the precipitates and to drive the SIM transformation, i.e., to move the Lüder band along the gage length of the specimen, increased stress are necessary. Alternatively, it is possible that an increased stress may be needed to initialize multiple Lüder bands across different regions in the specimen since the earlier bands may have been ‘pinned’ at the precipitates. Further work is needed to confirm these hypotheses.

(3) The unloading stress-strain curve is highly nonlinear unlike the near-flat unloading behavior of 55NiTi (wt.%).

The second loading cycle also reveals some interesting observations:

(1) The elastic portion of the stress-strain (S-S) curves of both the alloys match only up to ~300 MPa. Furthermore, while 55NiTi (wt.%) exhibits the load drop at 1% corresponding to the initiation of the Lüder bands, the 60NiTi (wt.%) S-S curve passes through the lower plateau stress of 55NiTi (wt.%) (at 1% strain) with subsequent loading leading to a non-flat 'plateau' . Since the lower plateau stress corresponds to the initiation of the Lüder bands, it is hypothesized that upon loading 60NiTi (wt.%) in the second cycle, any pinned Lüder bands may be reactivated and the transformation front driven across the gage length. Since it is equally likely that these Lüder band(s) may be intercepted by the precipitates, increased stress are once again necessary to continue the SIM transformation.

(2) 60NiTi (wt.%) recovers only 3.4% when unloaded from 5% total strain compared to the 6% strain recovery in 50NiTi.

It has been shown that by appropriate aging heat treatment cycles, the total superelastic recoverable strains may be optimized to ~ 4-5% [24]. Figure 6.19b shows the S-S response of the shape memory 60NiTi (wt.%) and 55NiTi (wt.%). Similar to case (a), the 60NiTi (wt.%) alloys exhibits a non-flat 'plateau' that corresponds to martensite detwinning [42, 43]. Additionally, upon unloading to zero stress and heating the sample at constant zero load condition, it recovers strains of 2%, 4% and 6% completely; comparable to 55NiTi (wt.%) that also recovers 6% total strain. Furthermore, the specimen also shows similar reloading behavior passing through the

lower stress point on the S-S curve at 1%. However, the third loading cycle retraces the second loading S-S loading curve showing that the S-S curve stabilizes after the initial loading.

6.5 Conclusions

Microstructural evolution and the phase transformations in a new Ni-rich 60NiTi (wt.%) has been investigated with the following conclusions:

(1) Aging the Ni-rich 60NiTi (wt.%) exhibits precipitation reactions with the formation of Ti_3Ni_4, Ti_2Ni_3 and $TiNi_3$ in seriatim. Among these, Ti_3Ni_4, Ti_2Ni_3 are metastable phases and $TiNi_3$ is the only stable phase, since upon aging for longer times or at higher temperatures, the metastable phases eventually transform to $TiNi_3$ phase.

(2) A TTT diagram for 60NiTi (wt.%) was constructed and combining the upper temperature limits of precipitation of different phases observed in the present work with the observations from [1, 2], an upper precipitation limit (UPL) phase diagram has been constructed for Ni-Ti alloys system as a function of Ni concentration between 50.6– 56 at.%.

(3) A wide range of transformation temperatures were achieved through varying aging parameters (temperature and time) leading to both austenitic and martensitic phases at room temperature.

(4) Superelasticity and shape memory characteristics has been successfully demonstrated in Ni-rich 60NiTi (wt.%), thought to be unfeasible, with recoverable strains between 4-6%.

(5) Given the economy in producing acceptable SE and SM in 60NiTi (wt.%) in addition to other attractive properties such as non-magnetic, corrosive resistant, high hardness, wide range of transformation temperatures tunable through controlled aging heat-treatments, it is proposed that 60NiTi (wt.%) has potential for both SE biomedical and shape memory actuator applications [31].

6.6 Acknowledgements

Chapter 6, in full, is a reprint of the material (under preparation) to appear as Raghavendra R. Adharapurapu, Kenneth S. Vecchio, “Microstructure Development in Ni-rich 60NiTi (wt.%) Alloy: Aging Studies on Precipitation Reactions and Shape Memory Characteristics”, submitted to Metallurgical and Materials Transactions. The dissertation author was the primary investigator and author of this paper.

6.7 Figures

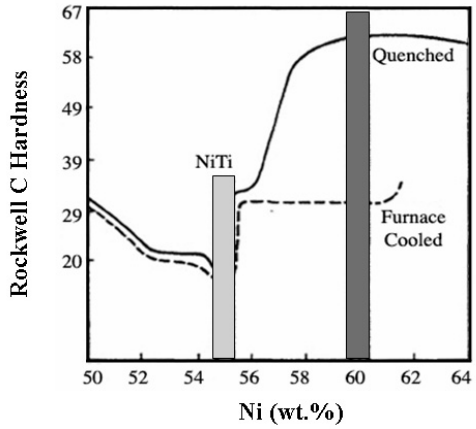

Figure 6.1 Variation of hardness in Ni-Ti alloys as a function of Ni composition in furnace cooled and quenched conditions (from 950°C) [9, 16].

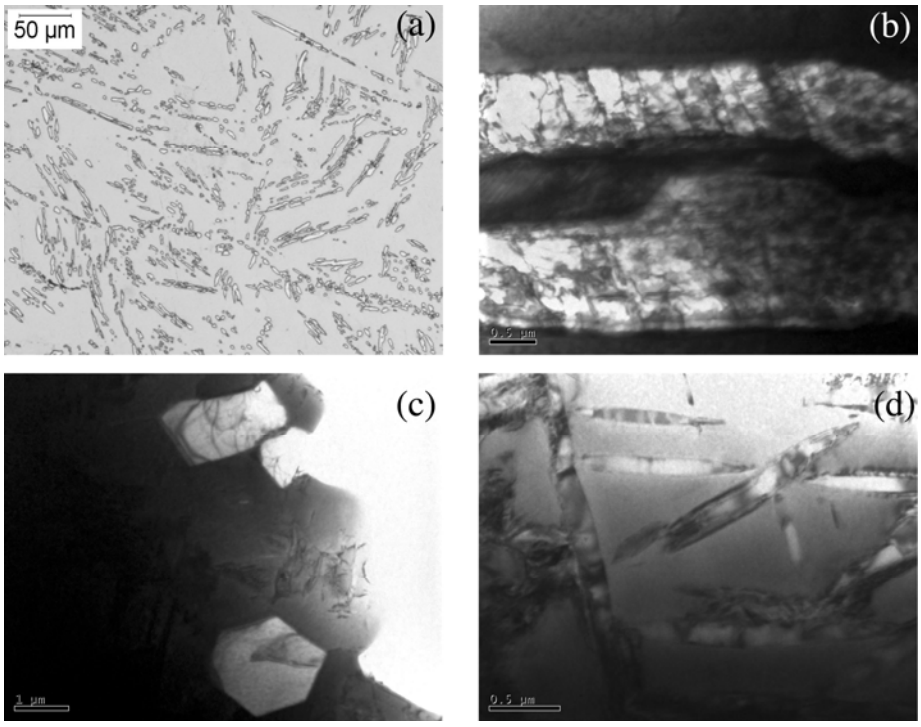

Figure 6.2 (a) Optical micrograph of AR 60NiTi (wt.%). TEM micrographs of (b, c) $TiNi_3$ and (d) Ti_2Ni_3 present in the AR structure. Notice the large deformation evident in $TiNi_3$ precipitates due to initial hot-rolling.

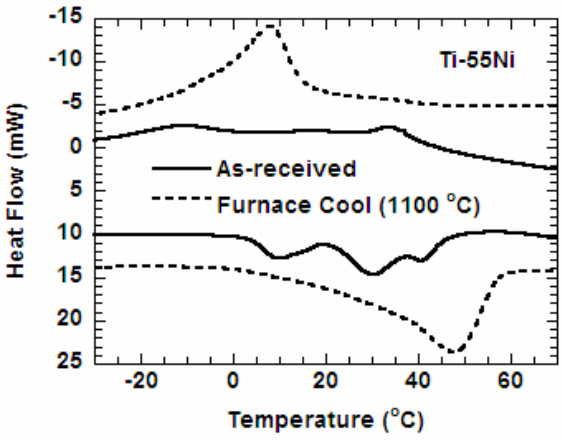

Figure 6.3 DSC curves for as-received (AR) 60NiTi (wt.%) and furnace cooled specimen from 1100°C. The upper curves indicate cooling cycle, whereas the lower curves indicate the heating cycle (10°C/min).

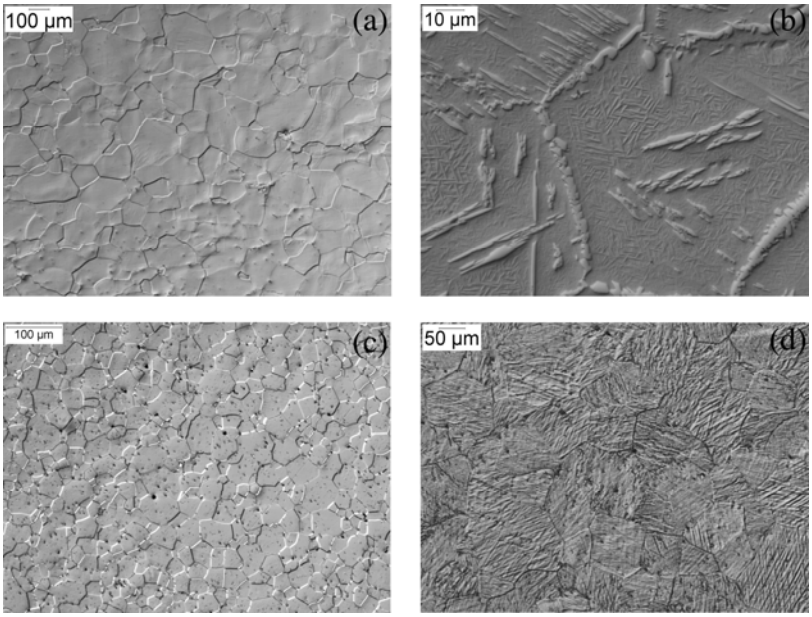

Figure 6.4 Optical micrographs of (a) Solution-annealed (1100°C) and water-quenched 60NiTi (wt.%), (b) solution-annealed (1100°C) and furnace-cooled (1 °C/min) 60NiTi (wt.%); notice the $TiNi_3$ precipitate formation both on the grain boundary and interior (c) as-received (AR) 55NiTi (wt.%) and (d) solution-annealed (1100°C) and water-quenched 55NiTi (wt.%), notice the twinned martensite.

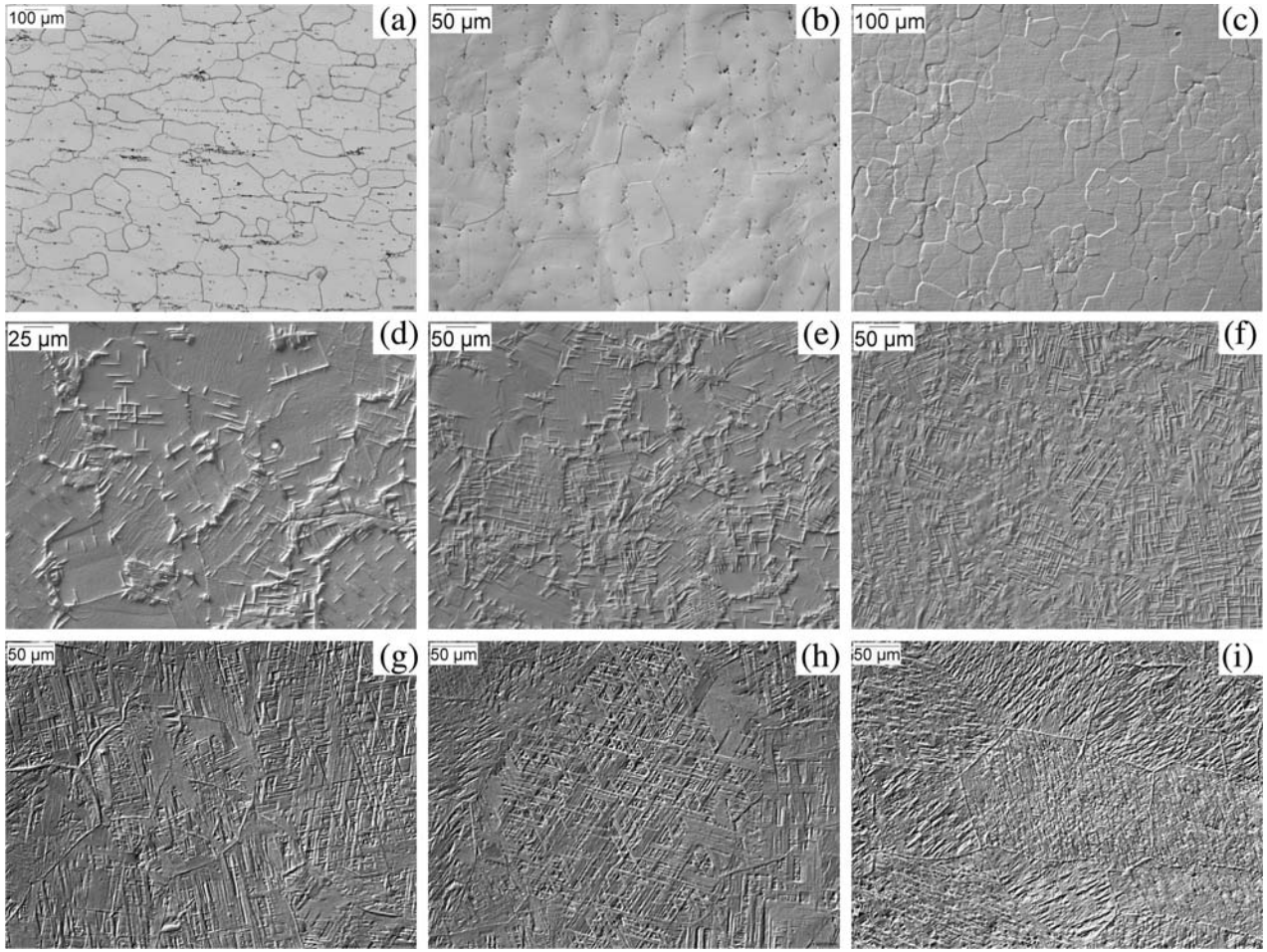

Figure 6.5 Optical micrographs showing the evolution of microstructure as a function of aging time and temperature for 60NiTi (wt.%). (a) 400°C – 24 h, (b) 500°C – 10 h, (c) 600°C – 0.5 h, (d) 600°C – 5 h, (e) 600°C – 10 h, (f) 600°C – 24 h, (g) 650°C – 5 h, (h) 650°C – 10 h, (i) 650°C – 48 h

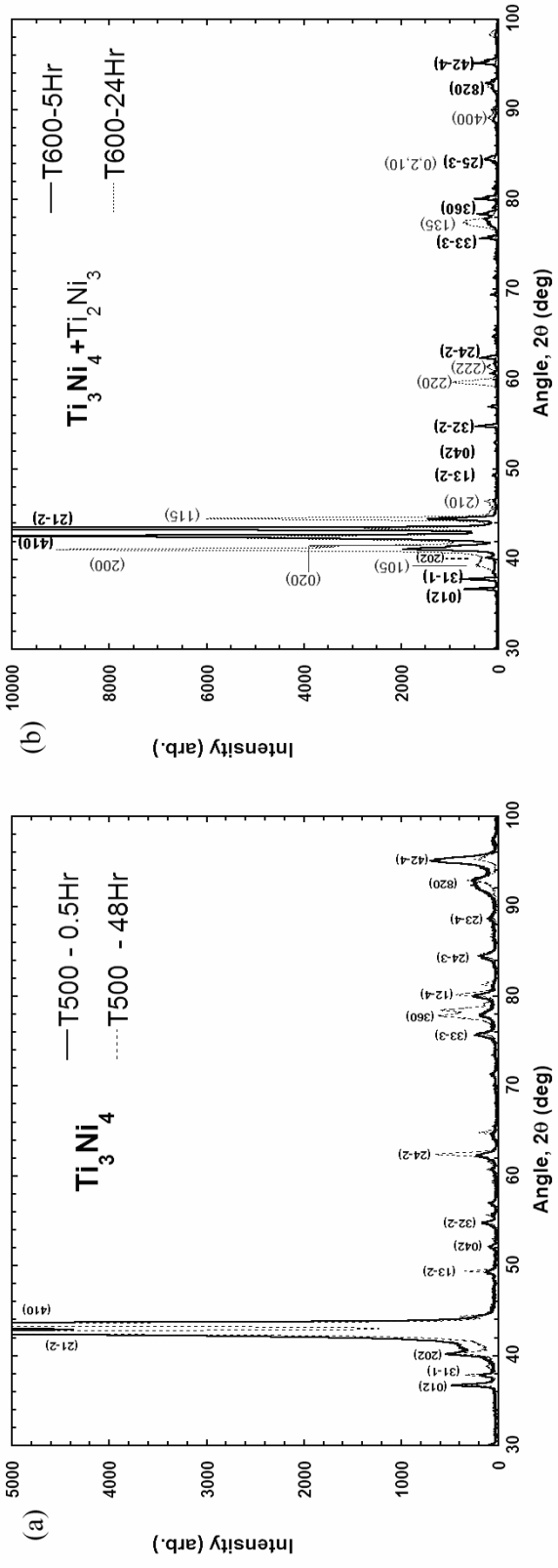

Figure 6.6 Intensity – angle data from XRD of 60NiTi (wt.%) aged at (a) 500°C and (b) 600°C. Note that the maximum intensities of the predominant peaks are nearly 30000 counts in both the cases.

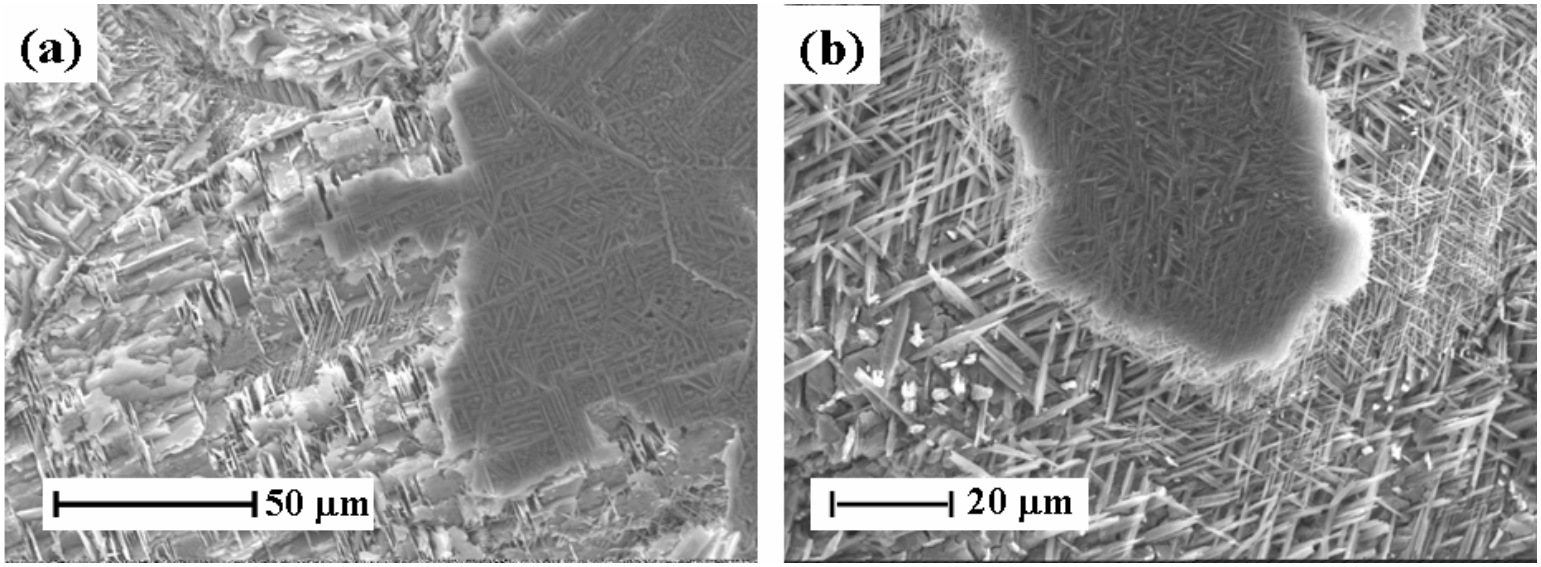

Figure 6.7 SEM images of Ti_2Ni_3 precipitates in 60NiTi (wt.%) aged at (a) 700°C – 1Hr and (b) 750°C – 0.5Hr. The Ti_2Ni_3 precipitates exhibit plate morphology in (a) and needle-like structure in (b). The microstructure was etched with 40% HF and the samples were then ultrsonicated in methanol bath.

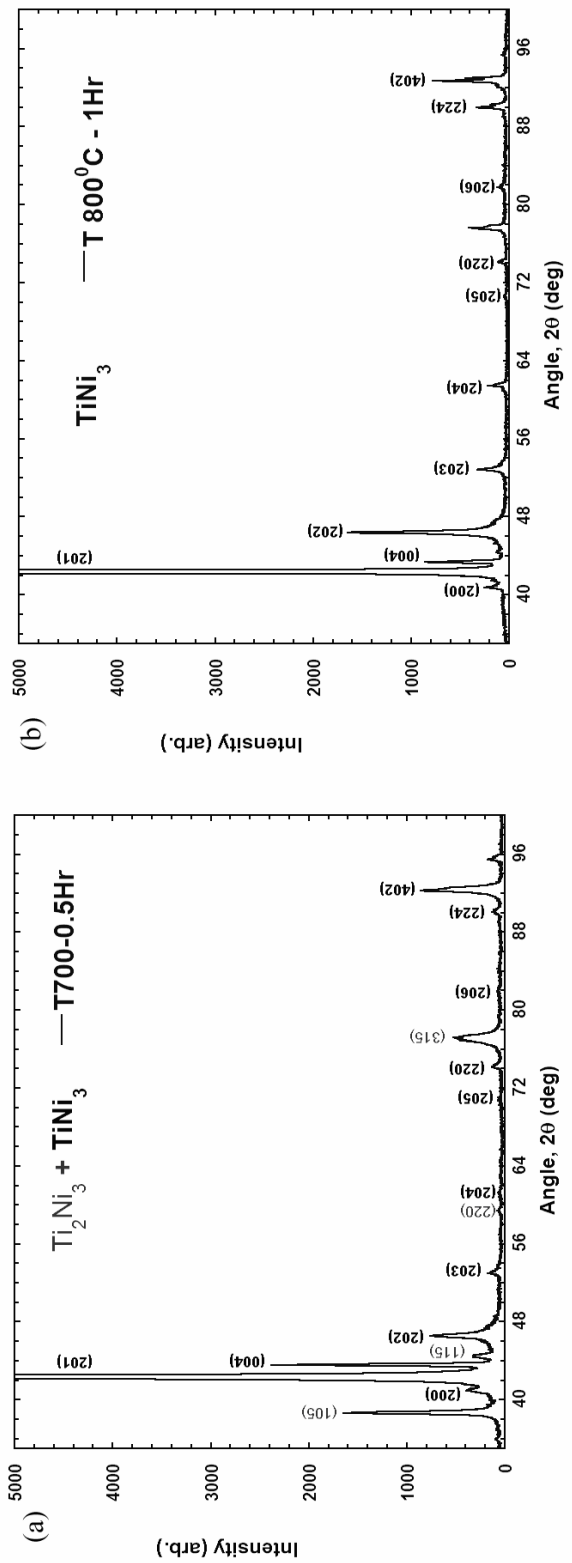

Figure 6.8 Intensity – angle data from XRD of 60NiTi (wt.%) aged at (a) 700°C and (b) 800°C. Note that the maximum intensities of the predominant peaks are nearly 30000 counts in both the cases.

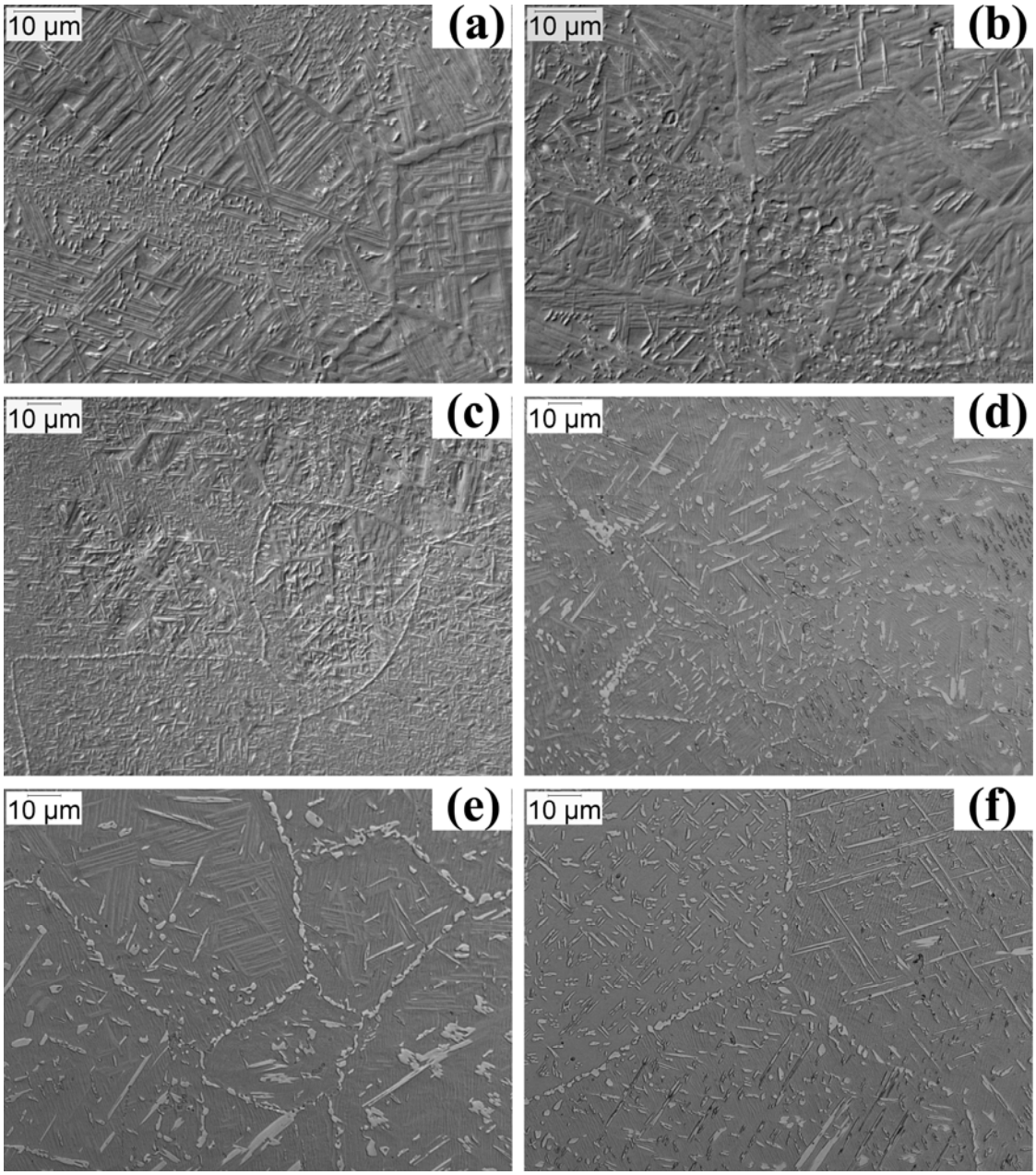

Figure 6.9 Optical micrographs showing the evolution of microstructure as a function of aging parameters (time and temperature) for 60NiTi (wt.%). (a) 700°C – 1 h, (b) 700°C – 10 h, (c) 700°C – 24 h, (d) 750°C – 1 h, (e) 750°C – 24 h, (f) 750°C – 48

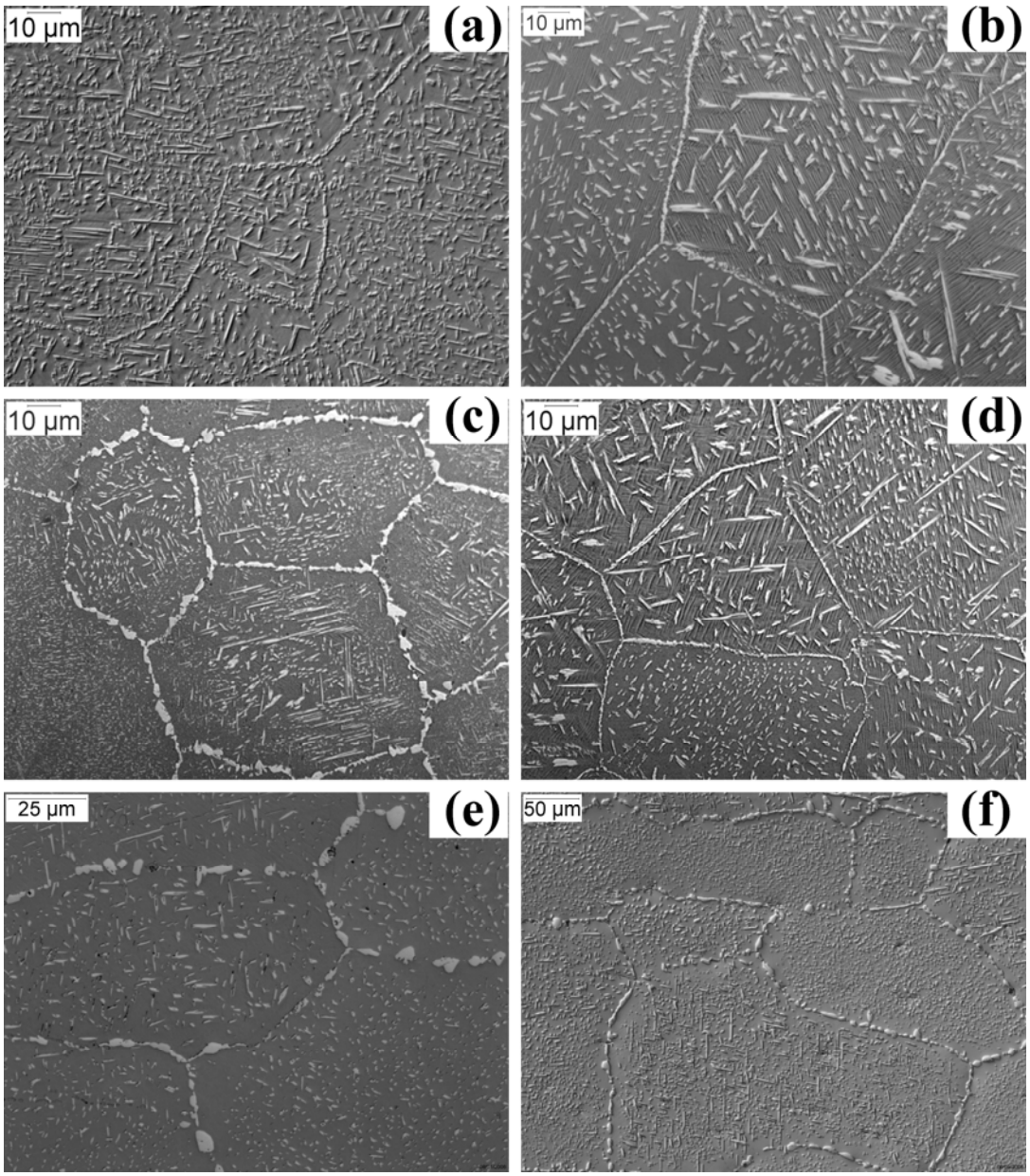

Figure 6.10 Optical micrographs showing the evolution of microstructure as a function of aging parameters (time and temperature) for 60NiTi (wt.%). (a) 800°C – 10 h, (b) 800°C – 24 h, (c) 800°C – 48 h, (d) 850°C – 10 h, (e) 850°C – 24 h, (f) 850°C – 48 h

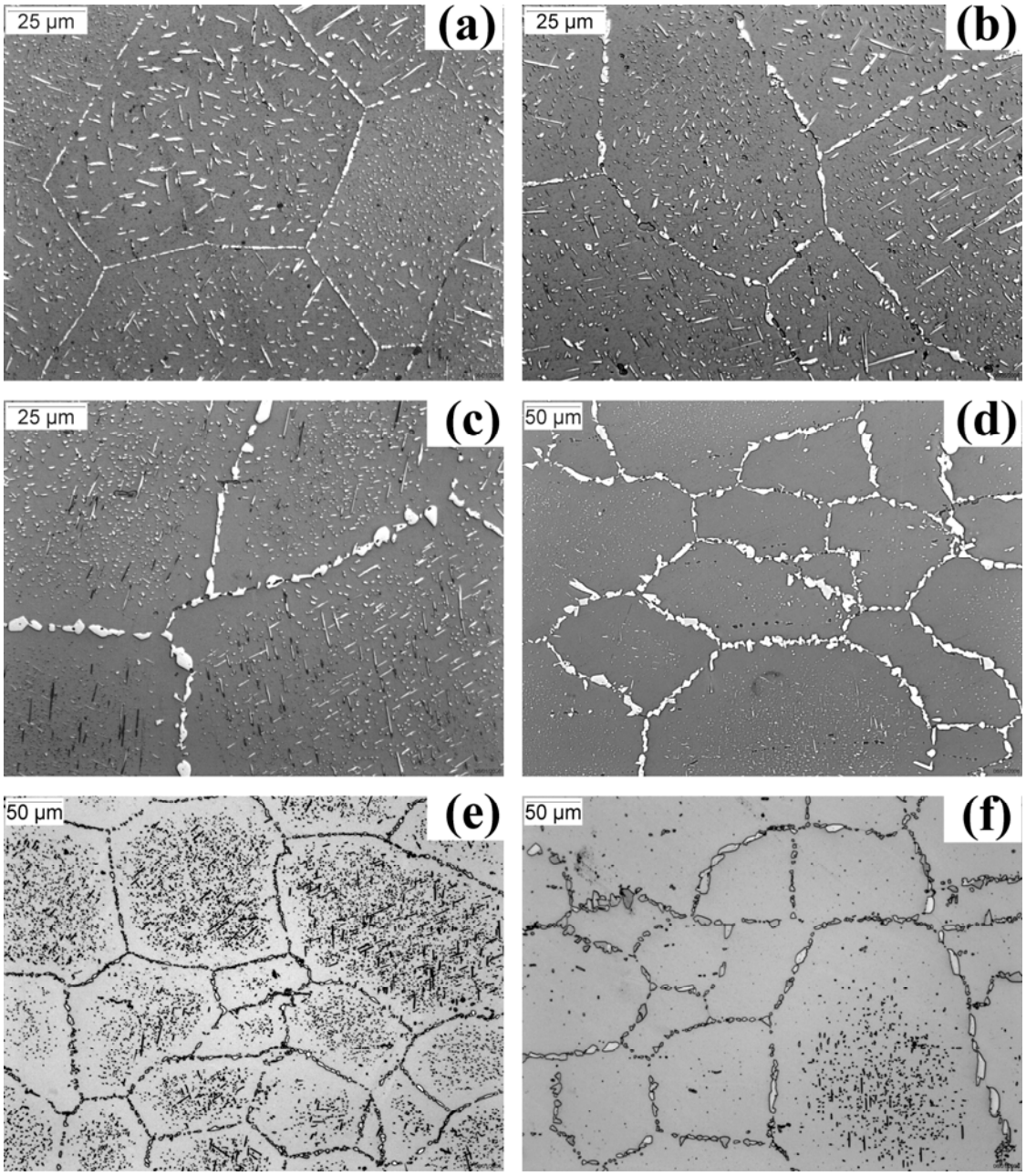

Figure 6.11 Optical micrographs showing the evolution of microstructure as a function of aging parameters (time and temperature) for 60NiTi (wt.%). (a) 900°C – 1 h, (b) 900°C – 5 h, (c) 900°C – 10 h, (d) 900°C – 48 h, (e) 1000°C – 1 h, (f) 1000°C – 24 h

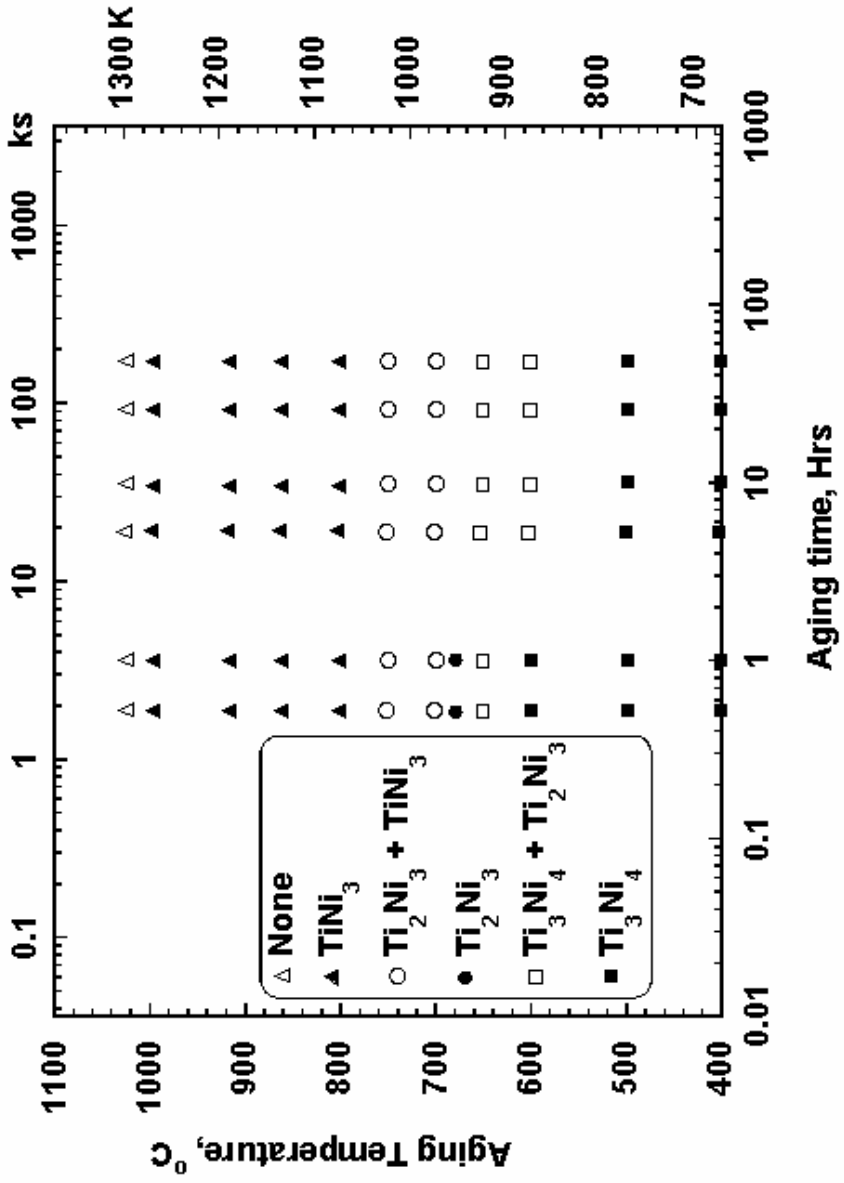

Figure 6.12 Time-Temperature-Transformation data as a function of aging parameters and microstructure for 60NiTi (wt.%).

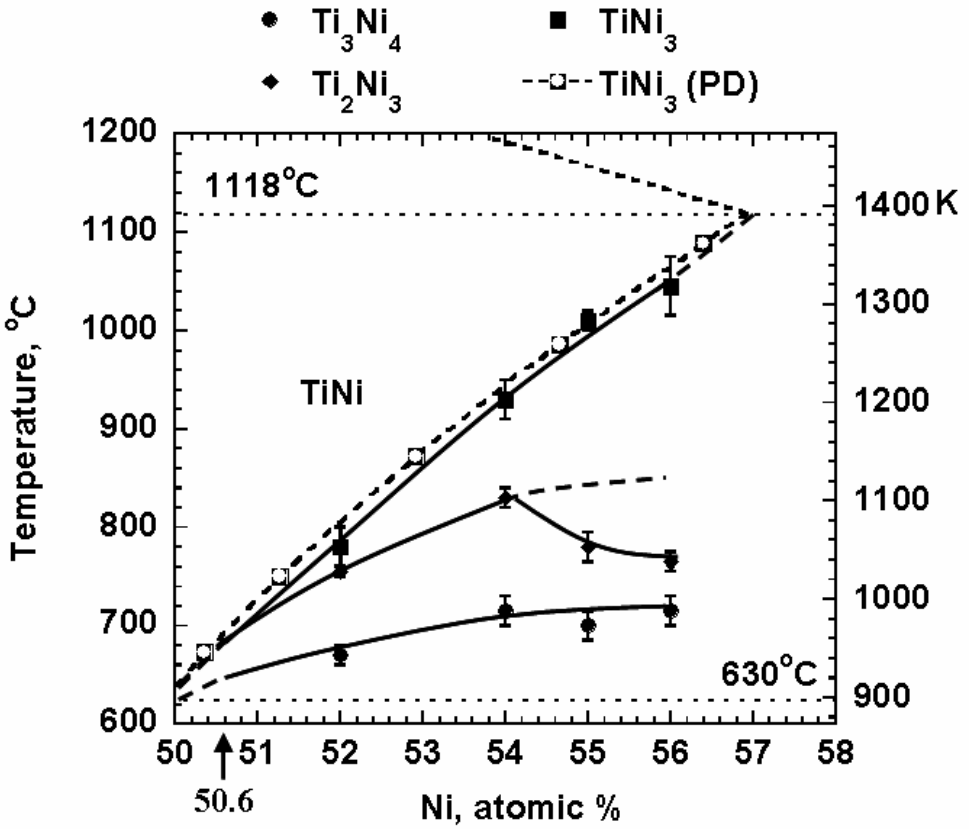

Figure 6.13 Dependence of the maximum temperature of precipitation of different phases, viz., Ti_3Ni_4, Ti_2Ni_3 and $TiNi_3$, on the Ni concentration in the Ti-Ni alloy. While the first two precipitates are metastable, $TiNi_3$ is a stable phase. The solidus boundary for $TiNi_3$ matches well with the established phase diagram (PD) shown in dotted line [21]. The data from the current work is combined with the results from [1, 2] to compute the above plot.

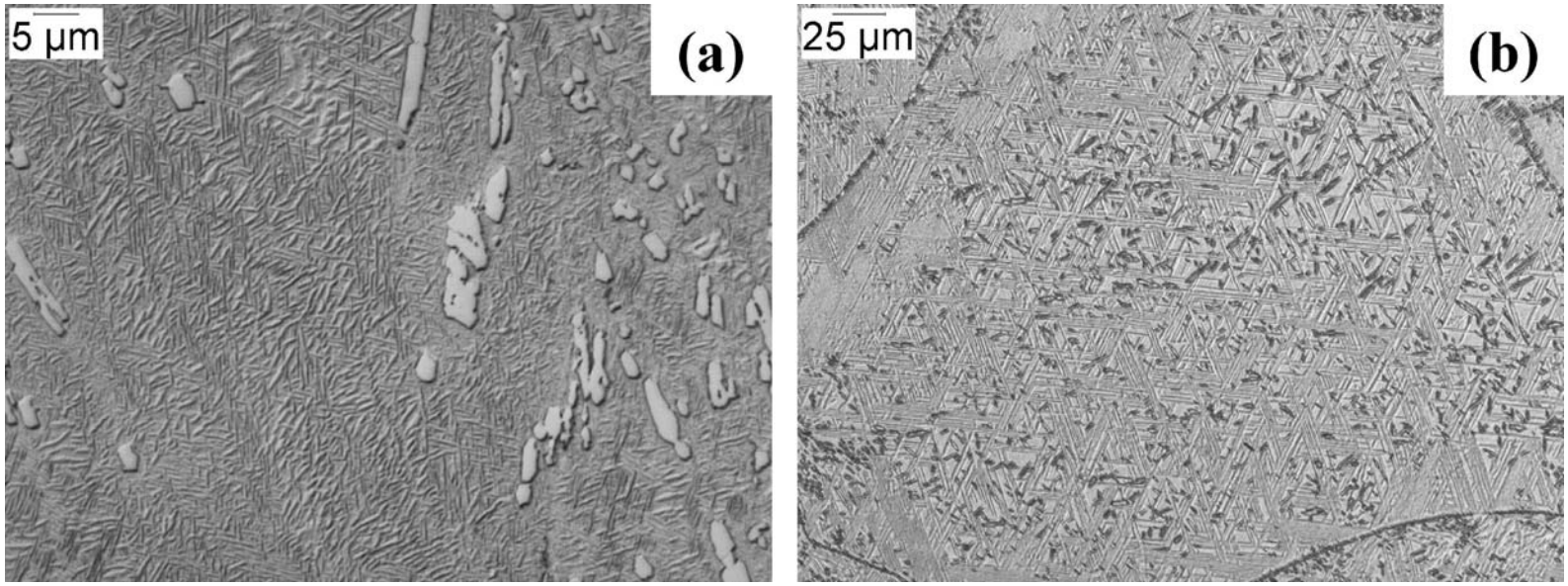

Figure 6.14 Optical micrographs showing the evolution of microstructure as a function of aging parameters (time and temperature) for SM 60NiTi (wt.%). (a) 500°C, (b) 700°C

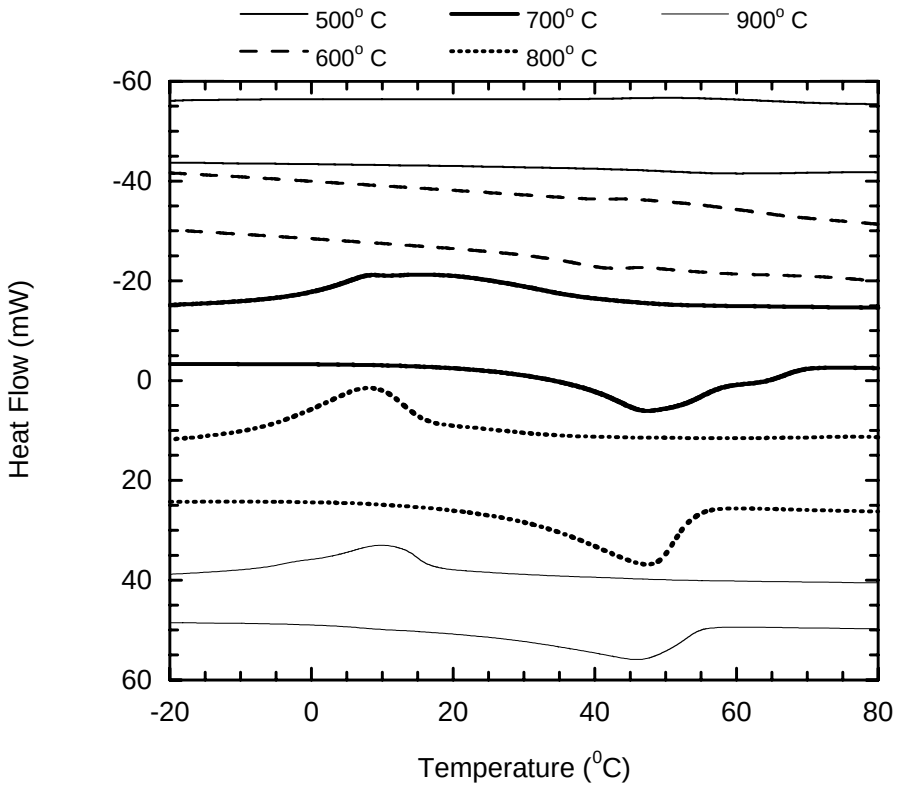

Figure 6.15 DSC data for shape memory (SM) ST-anneal-FC 60NiTi (wt.%) as a function of heat-treatment: Furnace cooled from 500°C - 800°C.

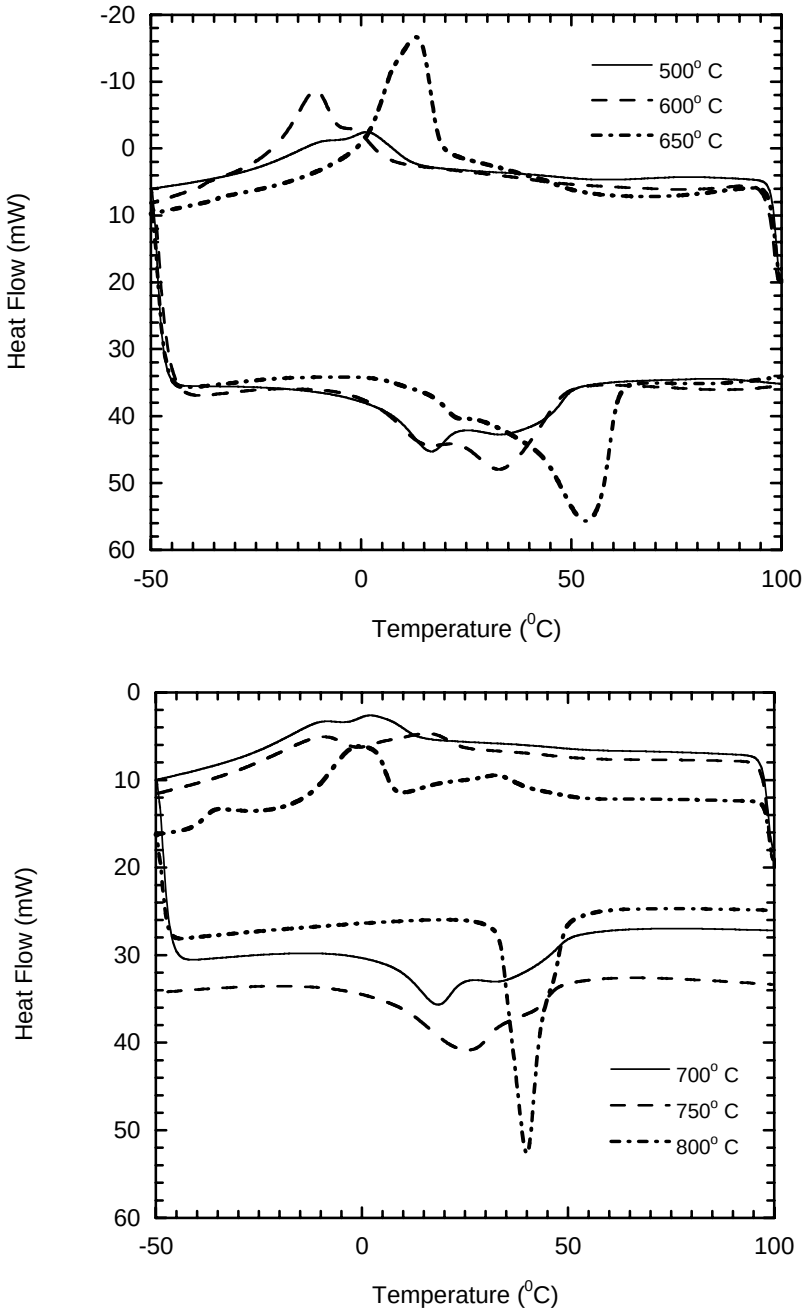

Figure 6.16 DSC data for shape memory (SM) AR-anneal-FC 60NiTi (wt.%) as a function of heat-treatment: Furnace cooled from 500 °C- 800 °C.

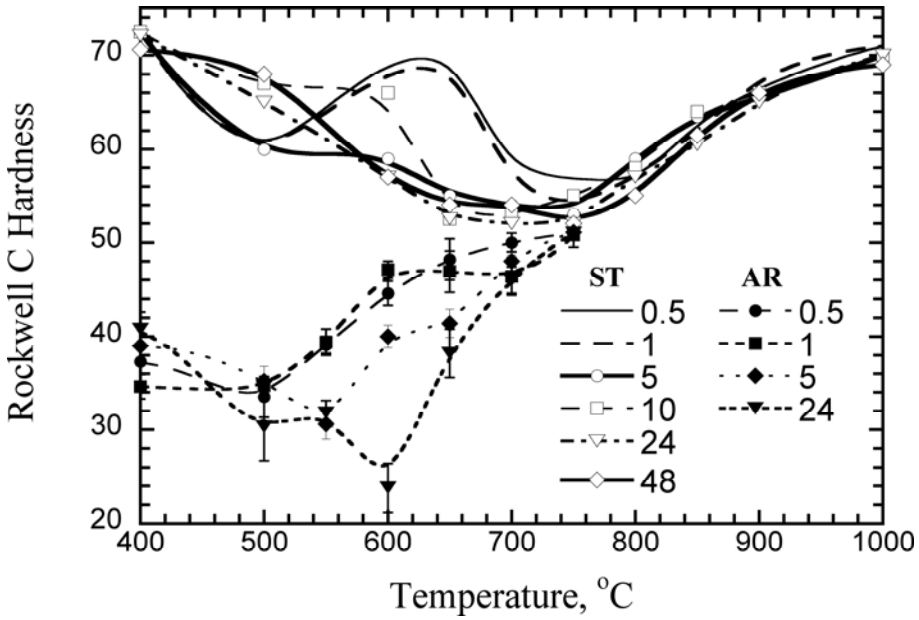

Figure 6.17 Hardness of 60NiTi (wt.%) as a function of aging heat treatment (time in hours) (a) ST-aged-WQ 60NiTi (the hardness values are within ±2 R_C) (b) ST-anneal-FC 60NiTi.

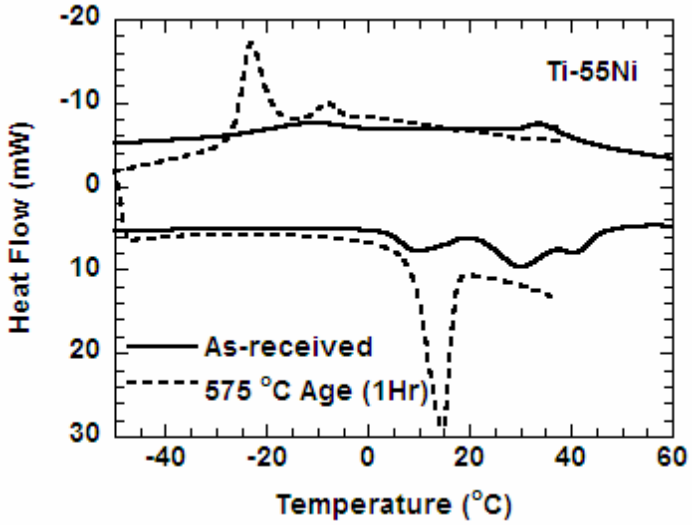

Figure 6.18 DSC curves for as-received (AR) and aged (575°C – 1hr) 60NiTi (wt.%). Notice that the AR material is martensitic (A_f = 45°C) at room temperature whereas the aged material is austenitic (A_f = 20°C).

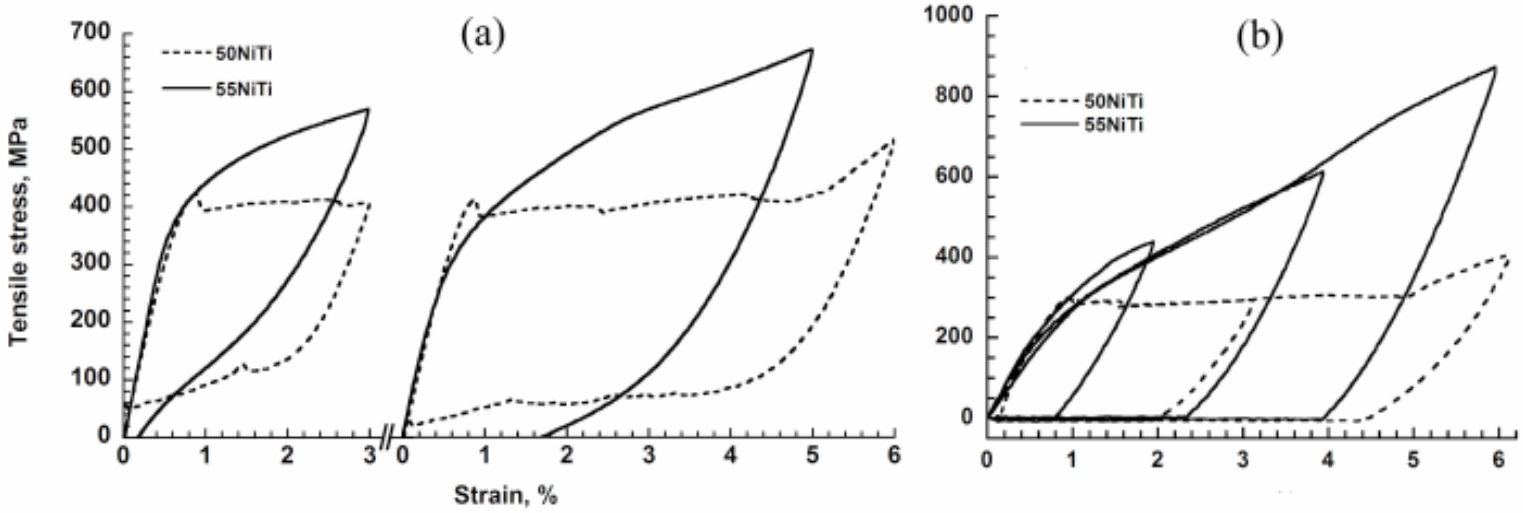

Figure 6.19 Comparison of 55NiTi (wt.%) and 60NiTi (wt.%): (a) Superelasticity (SE) and (b) Shape memory (SM). The specimen in (a) is the aged 60NiTi (wt.%) (575^{o}C – 1hr), while the specimen in (b) is the AR 60NiTi (wt.%).

6.8 References

1. Nishida, M., C.M. Wayman, and T. Honma, *Precipitation processes in near-equiatomic TiNi shape memory alloys.* Metallurgical Transactions A, 1986. **17**: p. 1505-1515.

2. Kainuma, R., M. Matsumoto, and T. Honma, *Metallographic study of precipitation processes in Ni-rich TiNi alloys.* Tohoku Daigaku Senko Seiren Kenkyujo iho, 1987. **43**(2): p. 149-158.

3. Humbeeck, J.V., *Shape memory alloys: A material and a technology.* Advanced Engineering Materials, 2001. **3**(11): p. 837-850.

4. Miyazaki, S. and K. Otsuka, *Development of shape memory alloys.* ISIJ International, 1989. **29**(5): p. 353-377.

5. Tadaki, T., K. Otsuka, and K. Shimizu, *Shape memory alloys.* Ann. Rev. Mater. Sci., 1988. **18**: p. 25-45.

6. Wayman, C.M., *Shape memory and related phenomena.* Progress in Materials Science, 1992. **36**: p. 203-224.

7. Wayman, C.M. and J.D. Harrison, *The origins of the shape memory effect.* The Journal of Minerals, Metals and Materials (JOM), 1989. **41**(9): p. 26-28.

8. Otsuka, K. and K. Shimizu, *Pseudoelasticity and shape memory effects in alloys.* International Metals Reviews, 1986. **31**(3): p. 93-114.

9. Buehler, W.J. and R.C. Wiley, *The properties of TiNi and associated phases.* 1961, U. S. Naval Ordnance Laboratory. p. 61-75.

10. Duerig, T., A. Pelton, and D. Stockel, *An overview of Nitinol medical applications.* Materials Science and Engineering A, 1999. **A272-275**: p. 149-160.

11. Schetky, M.L., *The industrial applications of shape memory alloys in North America.* Materials Science Forum, Proceedings of the International Symposium on Shape Memory Alloys, 2000. **327-328**: p. 9-16.

12. Duerig, T.W. *Applications of shape memory*. in *Materials Science Forum, in Martensitic Transformations II*. 1990.

13. Humbeeck, J.V., *Non-medical applications of shape memory alloys.* Materials Science and Engineering A, 1999. **273-275**: p. 134-148.

14. Buehler, W.J. and R.C. Wiley, *TiNi: Ductile intermetallic compound.* Trans. Quart Am. Soc. Metals., 1962. **55**: p. 269-276.

15. Buehler, W.J., J.V. Gilfrich, and R.C. Wiley, *Effect of low-temperature phase changes on the mechanical properties of alloys near composition TiNi.* Journal of Applied Physics, 1963. **34**(5): p. 1475-1477.

16. Buehler, W.J. and F.E. Wang, *A summary of recent research on the Nitinol alloys and their potential application in ocean engineering.* Ocean Engineering, 1968. **1**: p. 105-120.

17. Saburi, T., T. Tatsumi, and S. Nenno, *Effects of heat treatment on mechanical behavior of titanium-nickel alloys.* Journal de Physique, Colloque, 1982. **C-4**: p. 261-266.

18. Saburi, T., S. Nenno, Y. Nishimoto, and M. Zeniya, *Effects of thermomechanical treatment on the shape-memory effect and pseudoelasticity of Ti-50.2Ni and Ti-47.5Ni-2.5Fe at. pct alloys.* J. Iron and Steel Inst. Japan (Tetsu to Hagane), 1986. **72**(6): p. 571-578.

19. Hornbogen, E., *Microstructure and thermo-mechanical properties of NiTi shape memory alloys.* Materials Science Forum, 2004. **455-456**: p. 335-341.

20. Otsuka, K. and C.M. Wayman, eds. *Shape memory materials*. 1998, Cambridge University Press.

21. Otsuka, K. and X. Ren, *Physical metallurgy of Ti-Ni based shape memory alloys.* Progress in Materials Science, 2005. **50**: p. 511-678.

22. Pelton, A., J. DiCello, and S. Miyazaki. *Optimization of processing and properties of medical-grade Nitinol wire*. in *Proceedings of the International Conference on Shape Memory and Superelastic Technologies (SMST)*. 2000. Pacific Grove, CA.

23. Julien, G.J., *Manufacturing of Nitinol parts and forms*, in *US Patent# 6422010*. 2002, Nitinol Technologies, Inc. (Edgewood, WA): United States. p. 1-15.

24. Adharapurapu, R.R. and K.S. Vecchio, *Superelasticity in a new bioimplant material: Ni-rich 55NiTi alloy.* Experimental Mechanics, 2006. **In Press**.

25. Julien, G.J., *Shape memory parts of 60 Nitinol*, in *US Patent# 7005018*. 2006, Nitinol Technologies, Inc. (Edgewood, WA): United States. p. 1-15.

26. Clingman, D.J., F.T. Clalkins, and J.P. Smith. *Thermomechanical properties of 60-Nitinol*. in *SPIE Smart Structures and Materials*. 2003. San Diego CA.

27. Julien, G.J., *Liquid jet nozzle*, in *US Patent #6715701*. 2004, Nitinol Technologies, Inc. (Edgewood, WA): United States. p. 1-9.

28. Julien, G.J., *Nitinol ball bearing element and process for making*, in *USPTO*. 2005, Nitinol Technologies, Inc. (Edgewood, WA): United States. p. 1-17.

29. Mabe, J.H., R.T. Ruggeri, E. Rosenzweig, and C.-J.M. Yu. *Nitinol performance characterization and rotary actuator design*. in *SPIE 5388-11, Smart Structures and Materials Conference*. 2004. San Diego, CA.

30. Mabe, J.H., R.H. Cabell, and G.W. Butler. *Design and control of amorphing chevron for takeoff and cruise noise reduction*. in *11th AIAA/CEAS Aeroacoustics Conference*. 2005. Monterey, California: AIAA-2005-2889.

31. Calkins, F.T., J.H. Mabe, and G.W. Butler. *Boeing's variable geometry chevron: morphing aerospace structures for jet noise reduction*. in *13th SPIE Smart Structures and Materials Conference*. 2006. San Diego, CA.

32. Tang, W., *Thermodynamic study of the low temperature phase B19' and the martensitic transformation in near-equiatomic Ti-Ni shape memory alloy.* Metallurgical Transactions A, 1997. **28**: p. 537-544.

33. Khalil-Allafi, J., G. Eggeler, A. Dlouhy, W.W. Schmahl, and C. Somsen, *On the influence of heterogeneous precipitation on martensitic transformations in a Ni-rich NiTi shape memory alloy.* Materials Science and Engineering A, 2004. **378**(1-2): p. 148-151.

34. Nishida, M. and C.M. Wayman, *Phase transformation in Ti_2Ni_3 precipitates formed in aged Ti-52 at. pct Ni.* Metallurgical Transactions A, 1987. **18A**: p. 785-799.

35. Jha, S.C., T.H. SandersJr, and M.A. Dayananda, *Grain boundary precipitate free zones in Al-Li alloys.* Acta Metall., 1987. **35**(2): p. 473-482.

36. Jensrud, O. and N. Ryum, *The development of microstructures in Al-Li alloys.* Materials Science and Engineering, 1984. **64**: p. 229-236.

37. Sanders Jr, T.H. and E.A. Starke Jr, *The effect of slip distribution on the monotonic and cyclic ductility of Al-Li binary alloys.* Acta Metall., 1982. **30**: p. 927-939.

38. Pardoen, T., D. Dumont, A. Deschamps, and Y. Brechet, *Grain boundary versus transgranular ductile failure.* Journal of the Mechanics and Physics of Solids, 2003. **51**: p. 637-665.

39. Hara, T., T. Ohba, K. Otsuka, and M. Nishida, *Phase transformation and crystal structures of Ti_2Ni_3 precipitates in Ti-Ni alloys.* Materials Transactions, JIM, 1997. **38**(4): p. 277-284.

40. Allafi, J.K., A. Dlouhy, and G. Eggeler, *Ni_4Ti_3-precipitation during aging of NiTi shape memory alloys and its influence on martensitic phase transformations.* Acta Meterialia, 2002. **50**(17): p. 4255-4274.

41. Sittner, P., Y. Liu, and V. Novak, *On the origin of Lüders-like deformation of NiTi shape memory alloys.* Journal of Mechanics and Physics of Solids, 2005. **53**: p. 1719-1746.

42. Liu, Y., Z.L. Xie, J.V. Humbeeck, and L. Delaey, *Effect of texture orientation on the martensite deformation of NiTi shape memory alloy sheet.* Acta Materialia, 1999. **47**(2): p. 645-660.

43. Liu, Y., Y. Li, Z. Xie, and K.T. Ramesh, *Dynamic deformation of shape-memory alloys: evidence of domino detwinning?* Philosophical Magazine Letters, 2002. **82**(9): p. 511-517.

7 SUPERELASTICITY IN Ni-RICH 55-NiTi ALLOY: MECHANICAL BEHAVIOR

Experimental Mechanics, 2007

7.1 Abstract

With the drive towards minimally invasive procedures, the medical industry is looking towards 'avant-garde' materials, with 50NiTi currently being the prime choice for many critical components/applications. This paper examines a new Ni-rich NiTi alloy that exhibits superelasticity (SE) and shape memory (SM) properties. Superelastic (SE) properties of 55NiTi* are studied here as a function of heat-treatment between 400ºC – 800ºC, and compared with the corresponding response of 50NiTi*, with an aim to develop and optimize thermal treatment procedures to maximize recoverable elastic strains. While optimal tuning of the SE properties in 50NiTi necessitates cold working in conjunction with specific heat treatment/aging, 55NiTi does not require cold work to achieve its optimal SE behavior. Moreover, it can be heat treated to produce strong, stable SE and SM response from the same ingot, with transformation temperatures being a strong function of heat treatment. The main difference between the two alloys is that Ni-Ti alloys with Ni content greater than 50.6 at.% are sensitive to heat treatment; aging in these materials leads to precipitation of several metastable phases. The initial work focuses on SE properties relevant to

*All compositions are quoted in atomic% throughout the paper. The reader should note the following conversions: 50NiTi (at.%) ≈ 55NiTi (wt.%) and 55NiTi (at.%) ≈ 60NiTi (wt.%)

biomedical use, such as: plateau stress, recoverable strains and strength, as a function of heat treatment and microstructure.

7.2 Introduction

The commercial success of 'superelastic' Nitinol was essentially triggered by the medical industry's drive towards minimally invasive procedures that demanded non-conventional materials [1-4]. Nitinol, among many contenders, proved to be the vanguard due to its unique superelastic (SE) properties. Indeed, the success of Nitinol alloys was due to the ability to optimize the superelastic 'window' around the constant body temperature of 37ºC [1, 2]. One of the most important parameter that governs the transformation temperatures in Ni-Ti alloys is the Ni composition. Even an increase in Ni composition by 1%, from 50.5 at.% to 51.5 at.%, decreases the M_S (martensite start temperature) to below 100K (in solution-treated condition) [5]. Such high sensitivity to Ni composition is highly undesirable in many applications. However, changes in both the transformation temperatures and the superelastic properties of NiTi may be achieved through thermo-mechanical treatments, specifically, either through cold work or aging heat treatments or even a combination of both [6, 7]. In near-equiatomic (cold-worked) NiTi alloys, the high density of dislocations constrain the martensitic transformation that distorts the lattice, whereas the resistance in Ni-rich NiTi alloys is provided by the introduction of both dislocations and precipitates. This leads to a variation in the transformation temperatures and hence the variation of superelastic 'window' in which the material can exhibit a stable superelastic effect. Additionally, this resistance also leads to multiple transformation paths, from B2

(austenite) – R-phase – B19' (martensite) phase [6]. Aging leads to the rearrangement of the dislocation networks [6, 8] in 50NiTi or precipitation and grain growth in Ni-rich NiTi alloys [9]. Earlier aging studies done on Ti-50.6Ni indicates that the aging temperature controls the size and distribution of the Ti_3Ni_4 precipitates, which in turn determine the extent of recoverable strains in superelasticity [6]. The combination of both cold-work and aging heat-treatment on Ti-50.6Ni was seen to increase the plateau stress and also the stability of the superelastic curves [6, 10]. The combination of cold work and aging also eliminates the preliminary step of solution treatment, thus being economical in some cases. Moreover, in Ni-rich Nitinol alloys that exhibit precipitation hardening, the Ni content of the matrix is progressively reduced upon aging at higher temperatures and larger times, with excess Ni being partitioned into the Ni-rich precipitates (such as Ti_2Ni_3 or $TiNi_3$), thus providing an excellent handle to control the transformation temperatures [2].

Early studies on Nitinol encompassed alloys with different compositions, ranging between 50-56 at.% NiTi [11, 12]. However, due to difficulty in forming and working with Ni-rich alloys (around 54-56 at.% NiTi) that exhibited extreme brittleness and high notch sensitivity, machining and forming these materials into near-net shapes for practical applications became difficult and impractical [13, 14]. Since the development of hot rolling methods for 55NiTi and special fabrication techniques, a number of patents have emerged that exploit some unique properties of the alloy, such as: high hardness, non magnetic character, immunity against most corrosive agents, high strength and toughness [14, 15]. A decade ago, it was shown that under special heat treatment conditions, both the SM and SE effects could be

produced in the alloy from the same ingot [15], without any additional mechanical processing. Since then, the interest in the development of Ni-rich 55NiTi alloys has seen a resurgence, although very little work exists on the mechanical properties of these alloys [14, 16].

The current work addresses the superelastic properties of 55NiTi that are crucial for any development towards medical device applications. The main difference between 50NiTi and 55NiTi is that Ni-Ti alloys with Ni content greater than 50.6 at.% are sensitive to heat treatment; aging in these materials leads to precipitation of several metastable phases [9]. Therefore, this initial work focuses on SE properties such as plateau stress, recoverable strains and strength as a function of heat treatment and microstructure.

7.3 Experimental procedure

7.3.1 Materials

Equiatomic Nitinol (Ti-50Ni) in the form of 1mm thick rolled sheet was obtained from *Nitinol Devices and Components, Inc. (NDC, Fremont, CA)*. The austenite finish temperature is 14ºC, and therefore, the material was in superelastic-austenitic condition at room temperature (RT ~ 22°C).

Ni-rich Nitinol, Ti-55Ni alloys were obtained from *Nitinol Technologies, Inc. (Edgewood, WA)* in the form of ~3mm plates that were hot-rolled at 950°C. Numerous dog bone tensile specimens of a 25mm gage length and measuring 6.4mm width x 3mm thickness were cut from this stock and aged according to the schedule given in Table 1. For the solution-treatment (ST), the specimen was held at a

temperature of ~1100°C for 1 hour in evacuated quartz tubes and then quenched into water. At least two samples were tested at each test condition, however; only typical stress-strain data are presented for comparison.

7.3.2 Microstructure

The microstructures of as-received 50NiTi and 55NiTi are shown in Figure 7.1(a) and Figure 7.2(a), respectively. The microstructure of 50NiTi sheet was similar to that observed by Robertson *et al.* [17], with an average grain size less than 10μm. The as-received (AR) 55NiTi contained precipitates of Ti_2Ni_3 and $TiNi_3$ in various morphologies. The major secondary phase was the $TiNi_3$ precipitate and was typically in an elongated, needle shape (see Figure 7.1(b)), whereas, Ti_2Ni_3 precipitates occurred in lenticular morphologies and were only occasionally observed, see Figure 7.1(d). It has been known that NiTi alloys containing more than 50.6 at.% Ni decompose on aging through the precipitation of Ti_3Ni_4, Ti_2Ni_3 and $TiNi_3$, in that order, with Ti_3Ni_4 and Ti_2Ni_3 being metastable phases [9, 18]. Typically, Ti_2Ni_3 and subsequently $TiNi_3$ form at higher aging temperatures and times [6]. Ti_3Ni_4 is usually formed at lower aging temperatures (~400-500ºC) and shorter times, with the upper temperature limit for the formation of a particular precipitate being a function of Ni composition in the Nitinol alloys [18]. Due to the hot rolling of 55NiTi, the precipitates have been deformed severely and extensive dislocations in $TiNi_3$ precipitates can be seen in Figure 7.1(b).

Another major difference between 50NiTi and 55NiTi is evident upon observing their microstructure in solution-treated (ST at 1100ºC and water-quenched)

condition. While 50NiTi shows a typical twinned martensitic microstructure (see Figure 7.2(b)), 55NiTi does not exhibit any twinned microstructure, i.e., it formed cubic austenite phase (see Figure 7.2(c)). Moreover, upon furnace cooling (FC) of the materials from 1100°C, 50NiTi formed only the austenitic phase, whereas 55NiTi formed an extensive network of $TiNi_3$ precipitates, as shown in Figure 7.2 (d). The furnace-cooled 55NiTi also exhibited shape-memory characteristics (M_s = 16ºC, M_f = 0ºC, A_s = 38ºC, A_f = 57ºC). $TiNi_3$ precipitate formed both on the grain boundaries that exhibited blocky morphology and in the grain interior in the form of long elongated needles of different lengths. In the grain interior, lenticular martensite was also observed along with the $TiNi_3$ precipitates.

7.3.3 Heat Treatment: Aging schedule

Following the procedure recommended by [15], the as-received (AR) 55NiTi material was aged between 400ºC and 800ºC. Various aging schedules that were followed are summarized in Table 1. While HT-1 and HT-2 were single-step aging at various temperatures for 1 hour and 5 hours respectively, HT-3 consisted of step-aging treatment. Finally, solution-treatment (at 1100ºC) followed by aging between 600ºC – 800ºC for 24 hours was accomplished. To compare the superelastic properties of 55NiTi against the popular 50NiTi, annealing of 50NiTi sheet was accomplished according to the schedule indicated in Table 1.

Table 7.1 Aging Schedule for 50-NiTi and 55-NiTi Alloys

50NiTi: HT-1	400ºC, 500ºC, 600ºC, 700ºC: 1 hour
55NiTi: HT-1	400ºC, 500ºC, 600ºC, 700ºC, 800ºC: 1 hour
55NiTi: HT-2	500ºC, 600ºC, 700ºC: 5 hours
55NiTi: HT-3 (Step aging)	500ºC (5 hours) + 400ºC (1 hr), 600 ºC (5 hrs) + 500ºC (1 hr), 700ºC (5 hours) + 600ºC (1 hour)
55NiTi: HT-4	ST + 600ºC (24 hrs), ST + 700ºC (24 hrs), ST + 800ºC (24 hrs)

7.3.4 Testing and Characterization

Tensile testing of both 50NiTi and 55NiTi and compression testing of 55NiTi was done using a standard servo-hydraulic load frame at a quasi-static strain rate of ~10^{-3}/s. Metallographic studies were done on specimens that were mechanically polished to diamond finish and then etched with HF+HNO_3+deionized water. In addition, 3mm diameter disk specimens measuring 0.1-0.2 μm in thickness were prepared for TEM studies on a 120 kV Philips EM420. Prior to the TEM observation, they were electropolished using the twin jet method that utilized electrolyte of composition 20% H_2SO_4 + 80% Methanol at 10ºC and 15-20V.

7.4 Results and Discussion

7.4.1 As-received (AR) vs. Solution-treated (ST)

The tensile stress-strain curves of as-received (AR) and solution-treated (ST) 50NiTi and 55NiTi are shown in Figure 7.3. The ST material of both compositions are extremely brittle and exhibit strengths of ~350-400 MPa. The AR 50NiTi exhibits

typical superelastic behavior with plateau strains between 1-7% coupled with a ductility of ~25%, whereas, 55NiTi displays a non-flat 'plateau behavior' between 1-4%. The reason for the positive slope of the 'plateau' (strictly speaking, 55NiTi does not exhibit a zero-slope plateau, but for the purpose of comparison, the term 'plateau' will be used in this context throughout the paper) is due to the presence of the precipitates that resist the stress-induced transformation, and as a result, progressively higher stresses are necessary to drive the transformation to completion [19-21]. Similar to the well known compression-tension asymmetry in 50NiTi [22-27], 55NiTi also exhibits a large asymmetry in tension-compression behavior, as shown in Figure 7.3(a). The strength levels in both AR and ST condition for 55NiTi reach nearly ~2500MPa under compression. Additionally, the superelastic 'plateau' is evident in the AR 55NiTi material compression curve, although the slope in compression is greater than the slope in tension.

7.4.2 Heat-treatment (HT-1): Compression and Tension

The compression stress-strain curve for 55NiTi heat-treated according to the HT-1 schedule is shown in Figure 7.4 along with the AR and ST compression data. The variation in the overall stress-strain behavior due to different aging temperatures is not significant. The major observations are that the 'plateau' disappears for the specimens aged at 800°C (1 hour), while only a small portion of the curve for 700ºC exhibited the 'plateau'. Compared to the AR material, however, the ductility and strength levels have increased to about ~30% and 3GPa, respectively.

The tensile stress-strain curves for 55NiTi and 50NiTi for HT-1 aging conditions are shown in Figure 7.5(a) and (b), respectively. Similar to the compression behavior in 55NiTi, the tensile 'plateau' is clearly evident in 55NiTi aged between 400ºC to 600ºC, barely visible at 700ºC, and completely disappears at 800ºC. Additionally the 'plateau' start-stress increases as the aging temperature is increased from 400ºC to 700ºC. Moreover, the typical strain range for the 'plateau' was ~1-5%, with reversible strain up to 3-4%. It may be possible to optimize the reversible elastic-strains up to 6% in these Ni-rich 55NiTi alloys [15]. Another interesting property of these alloys is that they are extremely hard. For example, depending on the aging temperature and time, the hardness of the SE 55NiTi can be varied between 40 – 70 R_C (Rockwell C hardness).

As we will see in the subsequent section, the aging treatment given after solutionizing treatment does not provide enough ductility and the concomitant precipitation hardening is also not enough to provide adequate strength in order to encourage any superelasticity in the matrix for the HT-4 heat-treatment condition. This would suggest that solution treating and cold-working, as necessary parameters to tune the superelasticity, are obviated in comparison to 50NiTi, where they are very crucial. This would render the process of using these alloys very economical, since the essential SE or SM properties can be tuned using aging heat-treatments only (in addition to perhaps additional preliminary hot-rolling steps).

The effect of HT-1 annealing of 50NiTi on its stress-strain behavior is shown in Figure 7.5(b). The first manifestation of annealing is the decrease of plateau stress from ~400 MPa to ~250-300MPa. Additionally, the ductility due to annealing at

600ºC and 700ºC was seen to increase from 25% in the AR condition to nearly 60% (the data in Figure 7.5(b) is shown only until 20%), whereas, the tensile strength drops from 1200MPa to below 1000MPa (see [28]). The plateau strains are essentially unchanged, *i.e.,* between 1 - 6.5%. An interesting observation is that 50NiTi specimens annealed at 400ºC and 500ºC exhibited an early plateau (at a low stress level of ~50MPa) in a very small strain range, indicating the formation of R-phase that was subsequently followed by the larger plateau at ~250MPa, indicating the formation of B19' martensite phase.

7.4.3 Heat-treatment (HT-2, 3, 4): Tension

Aging of the AR 55NiTi was also accomplished for 5 hours single-step and (5 hours + 1 hour) two-step heat-treatments at different temperatures. The corresponding tensile stress-strain results are shown in Figure 7.6(a) and (b), respectively. Aging for longer times typically reduced the 'plateau' start stress and the tensile strength, while an increase in ductility by 2-5% was observed. However, the post-'plateau' work hardening rate was similar to the specimens aged for 1 hour, see Figure 7.6(a). In the two-step aged specimens, while the 'plateau' start stress was reduced, the tensile strength remained nearly the same compared to 5 hours single-step aging (HT-2). Additionally, the slope of the 'plateau' region increased under the two-step heat-treatment; see Figure 7.6(b).

Figure 7.7(a) shows the stress-strain data for compression and tension loading of 55NiTi specimen that were solutionized (solution annealed at 1100ºC for 1 hour and subsequently water quenched) and then aged for 24 hours at 600ºC, 700ºC and 800ºC.

The tensile curves (see the inset in Figure 7.7(a)) indicate that the material is extremely brittle with low strength and hence not preferable for any SE applications. It was, however, in these aging conditions, that the largest asymmetry between tension and compression in 55NiTi was observed. The compression results indicate good ductility of nearly 20% and strength levels in excess of 2GPa. As pointed in the earlier section and also shown elsewhere [9], the precipitation products are dependent on the aging temperature and time. In the case of 55NiTi, aging at 600ºC, 700ºC and 800ºC for 24 hours leads to the precipitation and growth of Ti_3Ni_4 + Ti_2Ni_3, Ti_2Ni_3 + $TiNi_3$, and $TiNi_3$ precipitates respectively. Optical micrographs of 55NiTi, which were solutionized and then aged for 24 hours for 600ºC, 700ºC, and 800ºC are shown in Figure 7.7(b-d), respectively. In Figure 7.7(b) and (c) the precipitates grow to span the whole grain, while in Figure 7.7(c), blocky grain-boundary and needle-like grain-interior $TiNi_3$ precipitates and precipitate-free-zones (PFZ) near these grain boundaries were observed.

7.5 Conclusions

Preliminary studies have shown many promising features of 55NiTi as a candidate for future medical applications. It has been shown that 55NiTi possess some unique properties such as, high strength and very high hardness (can be varied between 25RC – 70RC Rockwell C hardness) along with low thermal conductivity and low modulus [15]. More importantly, 55NiTi allows extremely fine surface finish [15] that is very important for medical devices as the susceptibility of failure in these devices is higher for surface defects that arise due to non-optimal surface finish than

bulk volume defects (such as scratches or pitting during electropolishing). In addition, 55NiTi is non-magnetic and immune to most corrosive agents [15]. Above all, it has been shown in this work and elsewhere [14-16] that both SE and SM properties may be obtained from the same ingot without resorting to cold-work or solutionizing treatments or a combination of both, which are usually very expensive. A range of SE and SM properties may be obtained by strictly controlling the microstructure through various aging conditions only. The lone shortcoming in these alloys is that the range of recoverable superelastic strains is about 60-75% less than conventional 50NiTi due to the presence of large precipitates that typically resist the stress-induced martensitic transformation. However, given the fact that the superelastic window in these alloys can range between –150°C to 600°C [15], and combined with the afore-mentioned properties, this preliminary work encourages further study of 55NiTi for exploitation in critical medical device applications and elsewhere. Currently, work is underway to optimize the SE and SM properties of 55NiTi in order to wheedle maximum reversible strains in these alloys.

7.6 Acknowledgements

Chapter 7, in full, is a reprint of the material as it appears in Experimental Mechanics as Raghavendra R. Adharapurapu, Kenneth S. Vecchio, “Superelasticity in a New BioImplant Material: Ni-rich 55NiTi Alloy”, Experimental Mechanics, Vol. 47, pp.365-371, 2007. The dissertation author was the primary investigator and author of this paper.

7.7 Figures

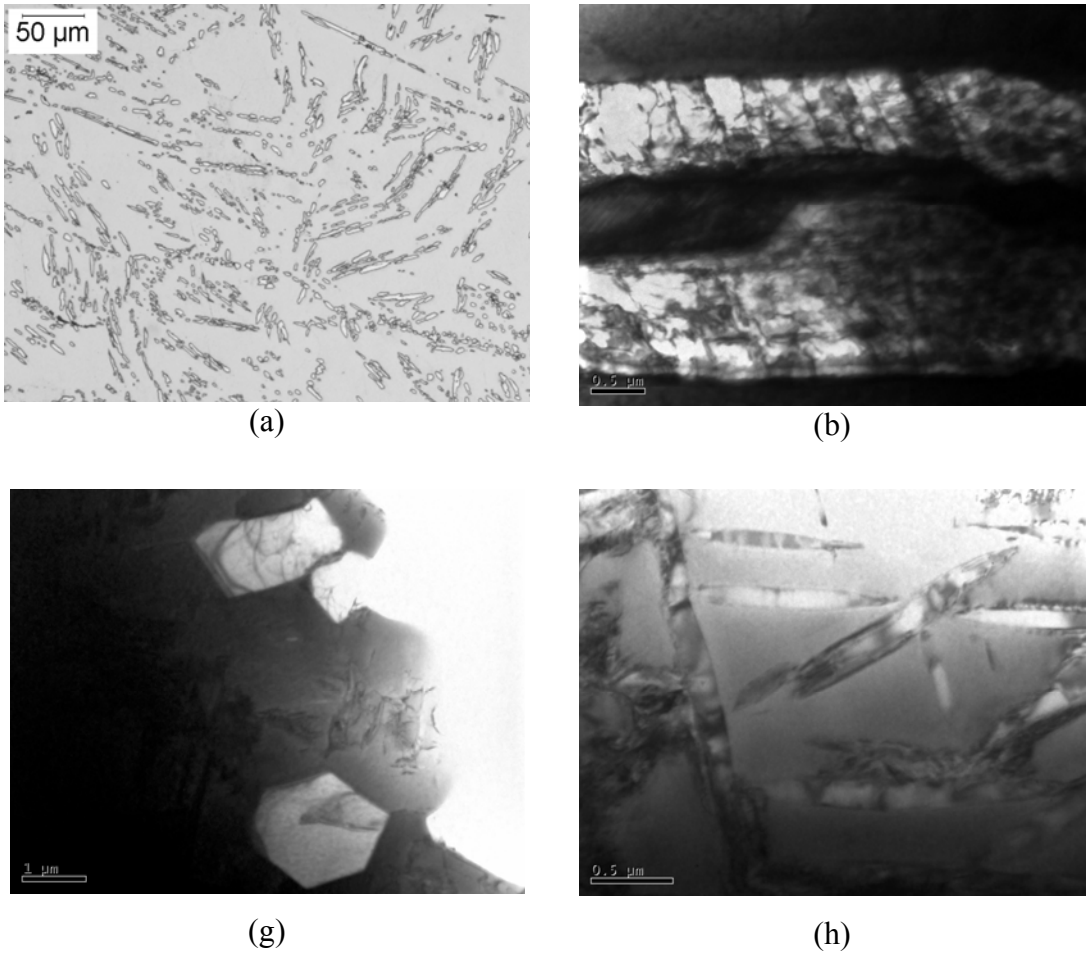

Figure 7.1 (a) Optical micrograph of AR 55NiTi. TEM micrographs of (b) $TiNi_3$ and (c,d) Ti_2Ni_3 present in the AR structure. Notice the large deformation evident in $TiNi_3$ precipitates due to initial hot-rolled plate.

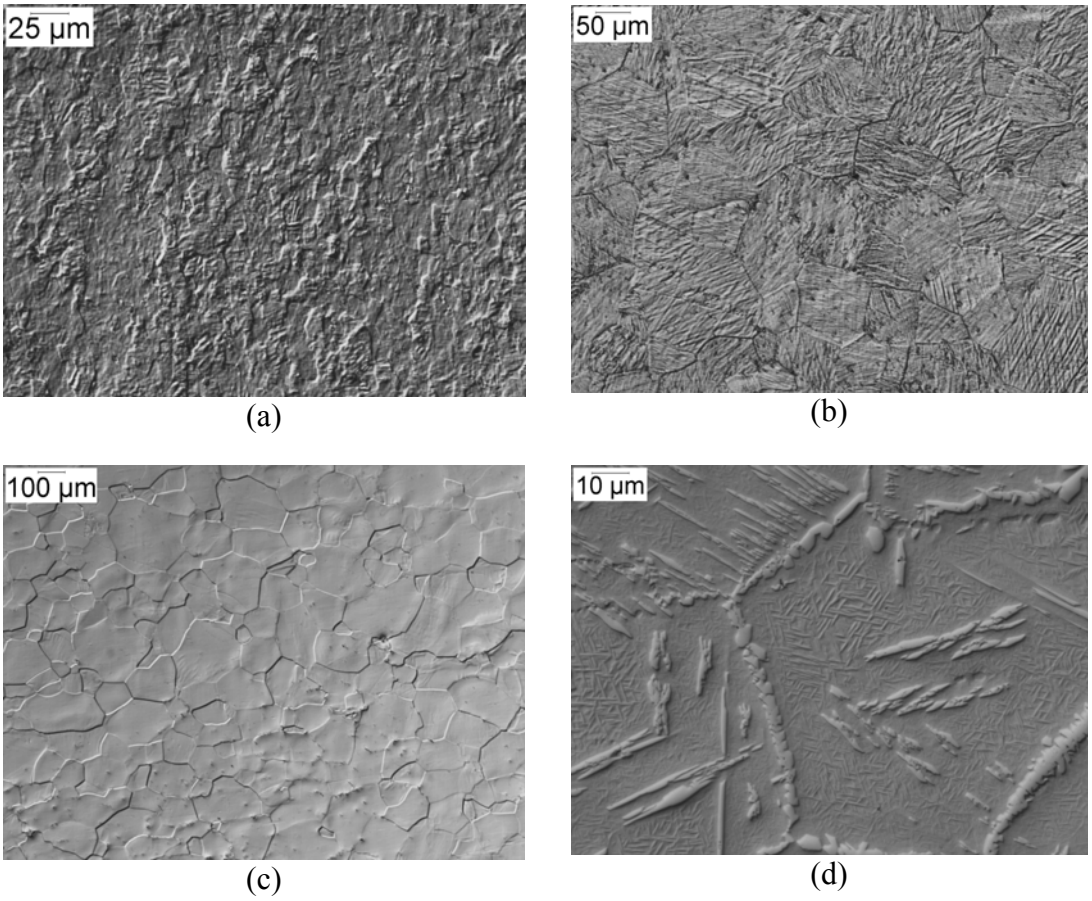

Figure 7.2 Optical micrographs of (a) AR 50NiTi sheet, (b) solution-annealed (1100^{o}C) and water-quenched 50NiTi, notice the twinned martensite microstructure, (c) solution-annealed (1100^{o}C) and water-quenched 55NiTi and (d) solution-annealed (1100^{o}C) and furnace-cooled 55NiTi. Notice the $TiNi_3$ precipitate formation both on the grain boundary and grain interior.

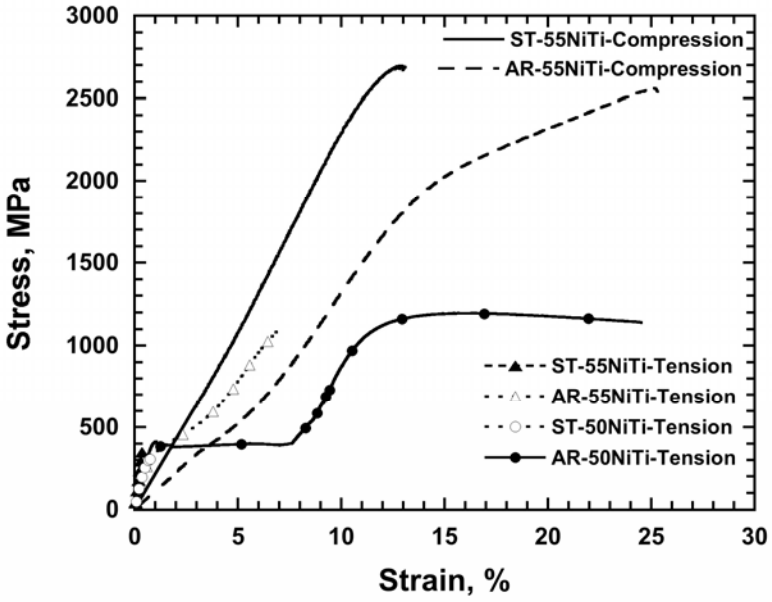

Figure 7.3 Quasi-static tension stress-strain curves for 50NiTi and 55NiTi for AR and ST heat-treatment conditions. Also, Compression curves for AR and ST 55NiTi are included.

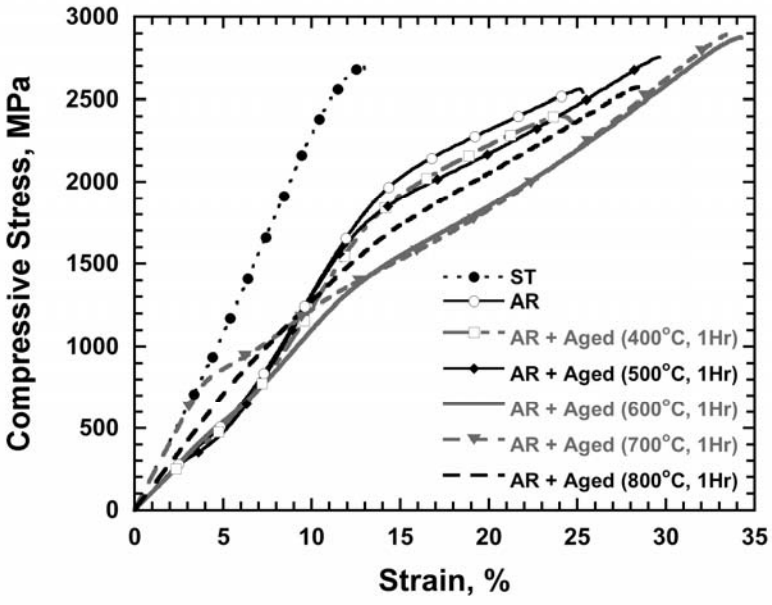

Figure 7.4 Compression stress-strain curves for 55NiTi heat-treated according to the HT-1 schedule indicated in Table 7.1.

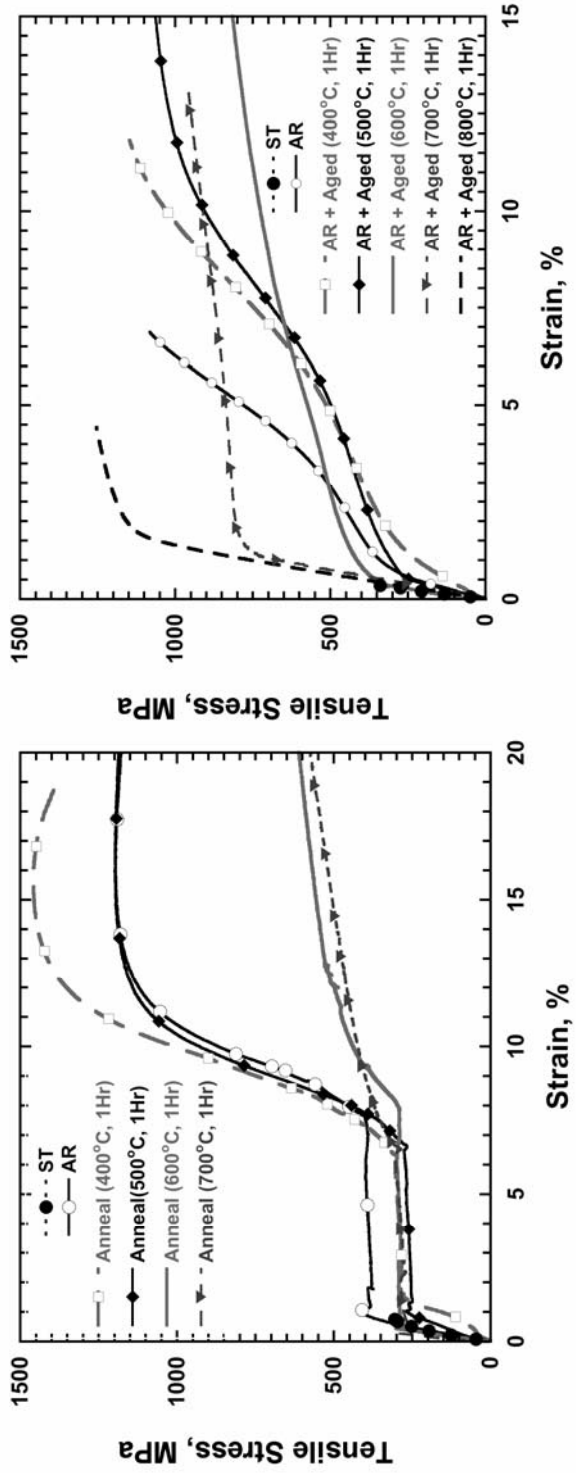

Figure 7.5 Tensile stress-strain curves under HT1 heat-treatment condition for (a) 55NiTi and (b) 50NiTi

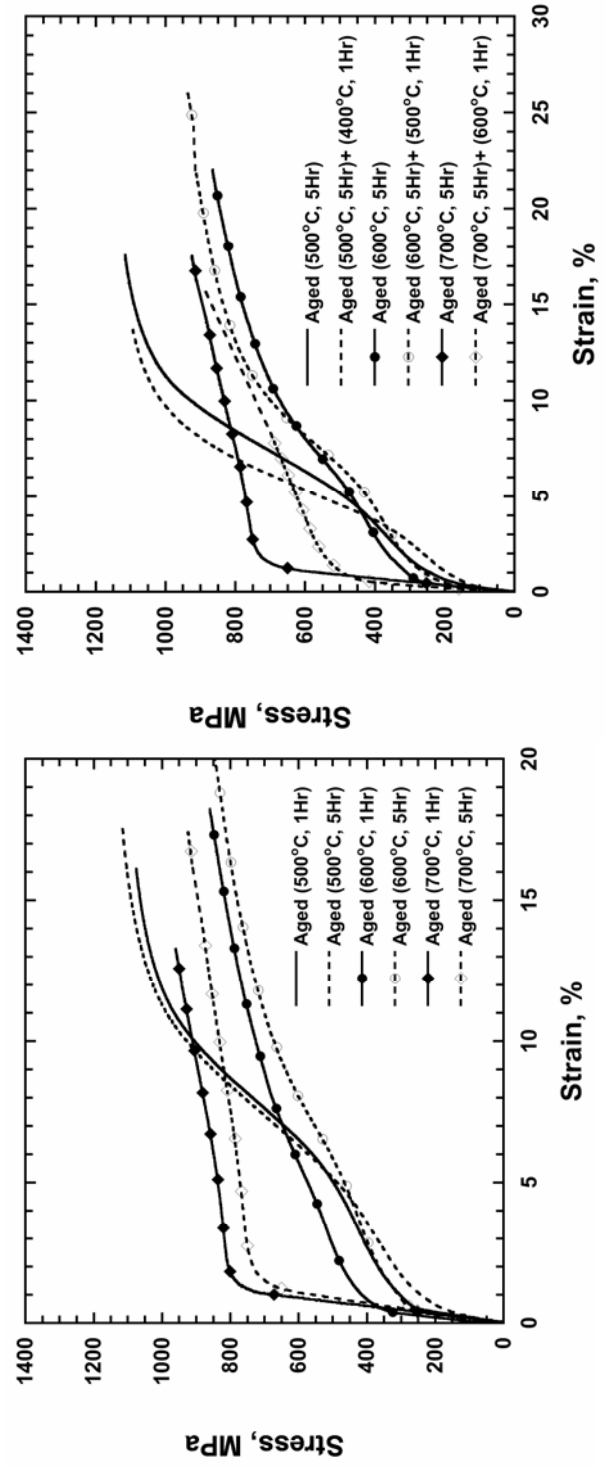

Figure 7.6 Tensile stress-strain curves of 55NiTi aged according to HT-2, 3 heat-treatment conditions (a) Single-step and (b) Two-step HT.

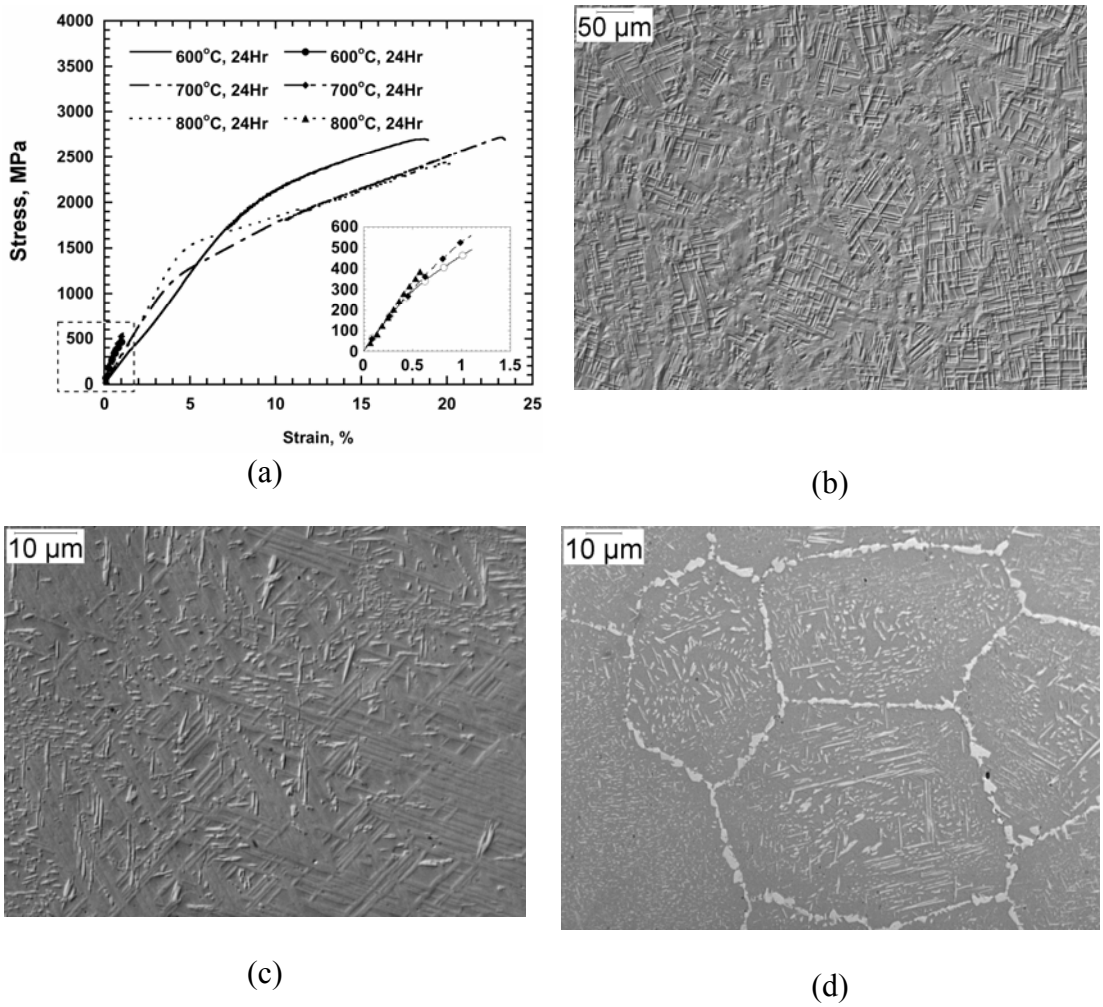

Figure 7.7 Tension and Compression stress-strain curves for solution-treated (ST) + aged (for 24Hrs) 55NiTi. The tension data is enlarged and shown in the inset. Optical Micrographs of 55NiTi that were solutionized and then aged for 24 hours for (b) 600°C, (c) 700°C, (d) 800°C. In (b) and (c), due to the presence of very large precipitates that span the whole grains, differential interference contrast imaging was used to reveal the microstructure. Ti_3Ni_4 and Ti_2Ni_3 precipitates at 600°C (24hr), and Ti_3Ni_4 and Ti_2Ni_3 precipitates at 700°C (24hr) are precipitated on aging. (c) is a regular bright field image. Notice the presence of blocky grain boundary and needle-like grain interior $TiNi_3$ precipitates and precipitate-free-zones (PFZ) near these grain boundaries.

7.8 References

1. Duerig, T., A. Pelton and D. Stockel, An overview of Nitinol medical applications. Materials Science and Engineering A, 1999. **273-275**: p. 149-160.

2. Pelton, A.R., J. DiCello and S. Miyazaki, Optimization of processing and properties of medical grade Nitinol wire. Journal of the Society for Minimally Invasive Therapy and Allied Technology (MITAT), 2000. **9**(1): p. 107-118.

3. Stockel, D., Nitinol medical devices and implants. Journal of the Society for Minimally Invasive Therapy and Allied Technology (MITAT), 2000. **9**(2): p. 81

4. Frank, T.G., W. Xu and A. Cuschieri, Instruments based on shape memory alloy properties for minimal access surgery, interventional radiology and flexible endoscopy. Journal of Minimally Invasive Therapy and Allied Technologies (MITAT), 2000. **9**(2): p. 89-98

5. Tang, W., Thermodynamic study of the low temperature phase B19' and the martensitic transformation in near-equiatomic Ti-Ni shape memory alloy. Metallurgical Transactions A, 1997. **28**: p. 537-544.

6. Otsuka, K. and X. Ren, Physical metallurgy of Ti-Ni based shape memory alloys. Progress in Materials Science, 2005. **50**: p. 511-678.

7. Otsuka, K. and C.M. Wayman, eds. Shape memory materials. 1998, Cambridge University Press. 284.

8. Miyazaki, S., Y. Ohmi, K. Otsuka and Y. Suzuki, Characteristics of deformation and transformation pseudoelasticity in titanium-nickel alloys. Journal de Physique, Colloque (C-4), 1982. p. 255-260.

9. Nishida, M., C.M. Wayman and T. Honma, Precipitation processes in near-equiatomic TiNi shape memory alloys. Metallurgical Transactions A, 1986. **17**: p. 1505-1515.

10. Miyazaki, S., T. Imai, Y. Igo and K. Otsuka, Effect of cyclic deformation on the pseudoelasticity characteristics of titanium-nickel alloys. Metallurgical Transactions A, 1986. **17(1)**: p. 115-120

11. Buehler, W.J. and R.C. Wiley, The properties of TiNi and associated phases. Report NOLTR 61-75 (AD 266607), 1961, U. S. Naval Ordnance Laboratory, White Oak, Silver Spring MD.

12. Jackson, C.M., H.J. Wagner and R.J. Wasilewski, 55-Nitinol - The alloy with a memory: Its physical metallurgy, properties, and applications. 1972, National Aeronautics and Space Administration - SP5110: Washington, D. C.

13. 60-Nitinol Alloys Data Sheet, U. S. Naval Ordnance Laboratory: White Oak, MD.

14. Clingman, D.J., F.T. Clalkins and J.P. Smith. Thermomechanical properties of Ni(60%wt)Ti(40%wt). Proceedings of SPIE-The International Society for Optical Engineering, **5053** (Active Materials: Behavior and Mechanics). 2003: p. 219-229

15. Julien, G. J., Manufacturing of Nitinol parts and forms, U. S. Patent 6422010, 2002.

16. Mabe, J.H., R.T. Ruggeri, E. Rosenzweig and C.-J.M. Yu. Nitinol performance characterization and rotary actuator design. Proceedings of SPIE-The International Society for Optical Engineering **5388** (Industrial and Commercial Applications of Smart Structures Technologies). 2004.: p. 95-109

17. Robertson, S.W., X.Y. Gong and R.O. Ritchie, Effect of product form and heat treatment on the crystallographic texture of austenitic Nitinol. Journal of Materials Science, 2006. **41**: p. 621-630.

18. Kainuma, R., M. Matsumoto and T. Honma, Metallographic study of precipitation processes in Ni-rich TiNi alloys. Tohoku Daigaku Senko Seiren Kenkyujo iho, 1987. **43**(2): p. 149-158.

19. Gall, K., H. Sehitoglu, Y.I. Chumlyakov and I.V. Kireeva, Pseudoelastic cyclic stress-strain response of over-aged single crystal Ti-50.8at.%Ni. Scripta Materialia, 1999. **40**(1): p. 7-12.

20. Gall, K., H. Sehitoglu, Y.I. Chumlyakov, Y.L. Zuev and I. Karaman, The role of coherent precipitates in martensitic transformation in single crystal and polycrystalline Ti-50.8at.%Ni. Scripta Materialia, 1998. **39**(6): p. 699-705.

21. Gall, K. and H.J. Maier, Cyclic deformation mechanisms in precipitated NiTi shape memory alloys. Acta Materialia, 2002. **50**: p. 4463-4657.

22. Orgeas, L. and D. Favier, Non-symmetric tension-compression behavior of NiTi alloy. Journal de Physique IV, 1995. **5**(C8, International Conference on Martensitic Transformations, Pt. 2): p. 605-10.

23. Plietsch, R. and K. Ehrlich, Strength Differential effect in pseudoelastic NiTi shape memory alloys. Acta mater., 1997. **45**(6): p. 2417-2424.

24. Gall, K., H. Sehitoglu, Y.I. Chumlyakov and I.V. Kireeva, Tension-compression asymmetry of the stress-strain response in aged single crystal and polycrystalline NiTi. Acta Mater., 1999. **47**: p. 1203-1217.

25. Gall, K. and H. Sehitoglu, The role of texture in tension-compression asymmetry in polycrystalline NiTi. International Journal of Plasticity, 1999. **15**(1): p. 69-92.

26. Sittner, P., V. Novak, P. Lukas, D. Lugovyy, D. Neov and M. Tovar, Load partition in NiTi shape memory alloy polycrystals investigated by in-situ neutron diffraction and micromechanics modelling. Materials Science Forum, 2002. **404-407**(ECRS 6, Proceedings of the 6th European Conference on Residual Stresses, 2002): p. 829-834.

27. Adharapurapu, R.R., F. Jiang, K.S. Vecchio and G.T. Gray III, Response of NiTi shape memory alloy at high strain rate: A systematic investigation of temperature effects on tension-compression asymmetry. Acta Materialia, 2006, in press.

28. Miyazaki, S., Y. Kohiyama, K. Otsuka and T.W. Duerig, Effects of several factors on the ductility of the Ti-Ni alloy. Materials Science Forum, 1990. **56-58**: p. 765-770.

8 CONCLUSIONS

The current work reports:

(i) The phase-transformation mechanisms in Ni-rich Ni-Ti alloys. These included (a) diffusionless multiple-stage martensitic transformations, and (b) diffusion-based phase transformations that govern the precipitation reactions in Ni-rich alloys and hence the overall time-temperature-transformation (TTT) curves.

(ii) The systematic study of the high-strain rate response of Ni-rich NiTi alloys as a function of temperature (between -196^{o}C and 400^{o}C) and thermomechanical treatment, viz., fully annealed, work-hardened and precipitation hardened conditions.

Two Ni-rich Nitinol alloys, the commercial 50.8-NiTi (at.%) and a new 55-NiTi (at.%) were selected for the study. While the conclusions are delineated at the end of each chapter more elaborately, only the important conclusions are summarized in the following.

I. High-strain rate studies

1. A reverse phase transformation from stress-induced martensite to austenite was identified by the bilinear nature of the unloading part of the stress-strain curves at room temperature (20^{o}C) and 100°C, even though the loading curve did not exhibit any plateau region.

2. In spite of large differences in strength levels occurring due to various transformations, all the dynamic tension and compression tests were successfully conducted at a constant strain rate of ~1200/s for the entire duration of the loading. This was achieved by two modifications to the experimental set-up:

(a) Unique pulse-shaping experiments successfully demonstrated that constant high-strain rate (~1200/s) is achievable in spite of complex sigmoid-type stress-strain curves under compression testing.

(b) Thin rolled NiTi sheet, which posed significant experimental challenge for conducting high-strain-rate tensile testing, due to the problems associated with samples small cross-sectional area, difficult gripping, and poor wave signals generally associated with dynamic tension testing, have been overcome successfully. Acceptable and reliable dynamic responses for NiTi alloys in tension was obtained by modifying the sample gripping area in a split Hopkinson tensile bar that ensured constant high-strain rate during the entire duration of the testing.

3. Since the high-strain rate tests are conducted over a wide range of temperature spanning -196^{o}C and 400^{o}C, the dynamic response of thermally-induced martensite (TIM) at low temperatures ($T < M_f$), superelastic austenite ($A_f < T < M_d$) and stable austenite at high temperatures ($T > M_d$) are studied in a systematic manner. These studies indicated a different strain-rate sensitivity of the austenite-martensite interfaces (during stress-induced martensite) and martensite-martensite interfaces (during the deformation of TIM).

4. Fully annealed NiTi exhibited lowest strength levels compared to the cold-worked material. Precipitation hardened alloys exhibited further improvement in the overall strength levels compared to the work-hardened NiTi alloy.

5. Fracture mechanisms are dominated by quasi-cleavage in low temperature martensite, void growth at high temperature stable austenite and mixed-mode (void + cleavage) in the superelastic austenite at high strain rates. Increasing strain rates

affects the SIM transformation, and thus a transition from cleavage to void type failure is observed.

II. Phase Transformations studies

1. It was observed that the presence of dislocations (through work-hardening) and the presence of Ni-rich precipitates (through age-hardening) contribute to a more complex two-stage or multiple-stage transformations and also improve the overall strength of the NiTi alloy. Based on the microstructural changes, such as recovery, recrystallization and precipitation formation in 50.8-NiTi alloys, the current work uniquely provides a unified and general understanding of the various multiple-stage transformations reported in the literature, specifically providing the transition between two main transformation sequence mechanisms rationalized on the basis of partial differential scanning (DSC) studies. Additionally, the work also identified unusual multiple-stage transformations in 55-NiTi; these were critically different from 50.8-NiTi in terms of the sequence of transformation.

2. Aging in Ni-rich 55NiTi elicited precipitation reactions with the formation of Ti_3Ni_4, Ti_2Ni_3 and $TiNi_3$ in seriatim. A time-temperature-transformation diagram for 55NiTi was constructed, as well as the upper temperature limit of formation for several precipitates has been estimated for Ni-rich NiTi alloys system as a function of Ni concentration between 50.6–56 at.%. Superelasticity and shape memory characteristics have been successfully demonstrated in Ni-rich 55NiTi, thought to be unfeasible, with recoverable strains up to ~4-6%.